The Astrophysical Journal Supplement Series, 283:17 (115pp), 2026 March https://doi.org/10.3847/1538-4365/ae2bdc

The 2025 Evaluation of Experimental Thermonuclear Reaction Rates (ETR25)

Christian Iliadis[1,2], Richard Longland[1,3], Kiana Setoodehnia[1,4], Caleb Marshall[1,2], Peter Mohr[5], and Athanasios Psaltis[1,3]
[1] Triangle Universities Nuclear Laboratory (TUNL), Duke University, Durham, NC 27708, USA; iliadis@unc.edu
[2] Department of Physics & Astronomy, University of North Carolina at Chapel Hill, NC 27599-3255, USA
[3] Department of Physics, North Carolina State University, Raleigh, NC 27695, USA
[4] Department of Physics, Duke University, Durham, NC 27708, USA
[5] HUN-REN Institute for Nuclear Research (Atomki), H-4001 Debrecen, Hungary
Received 2025 August 26; revised 2025 December 9; accepted 2025 December 9; published 2026 February 19

Abstract

This work describes the formalism for estimating thermonuclear reaction rates for astrophysical applications, emphasizing modern statistical approaches such as Monte Carlo sampling and Bayesian models. We discuss related topics including the calculation of resonance energies from nuclear Q values, indirect estimates of particle partial widths, and matching of reaction rates at elevated temperatures to statistical model results. We have evaluated available experimental data on cross sections, resonance energies and strengths, partial widths, lifetimes, spin-parities, and spectroscopic factors. Based on these results, we have estimated numerical values of 78 experimental charged-particle thermonuclear reaction rates for target nuclei in the $A = 2$–40 mass region, for temperatures ranging from 1 MK to 10 GK. For each reaction, three rate values are provided: low, median, and high, corresponding to the 16th, 50th, and 84th percentiles, respectively, of the cumulative reaction rate probability density distribution. Additionally, we present the factor uncertainty of each rate at each temperature grid point. These results enable users to sample the reaction rate probability density in nucleosynthesis calculations, facilitating uncertainty estimates of nuclidic abundances. The rates presented here refer to their laboratory values. For use in stellar model simulations, these values need to be corrected for the effects of thermal excitations of the interacting nuclei. For each reaction, we include graphs that illustrate the fractional contributions to the overall reaction rate along with the associated uncertainty. These visuals are designed to assist both stellar modelers and nuclear experimentalists by identifying the primary sources of rate uncertain=^texttx); ty at specific stellar temperatures. A graphical comparison with earlier Monte Carlo rates is also provided.

Unified Astronomy Thesaurus concepts: Nuclear astrophysics (1129)

1. Introduction

Thermonuclear reaction rates are essential ingredients for predictive modeling of stellar structure, evolution, and explosions, as well as for models of the early Universe. Since nuclear reactions generate the energy that makes stars shine and are responsible for the synthesis of the elements, spectroscopic or photometric astronomical observations cannot be explained without knowing the rates of the thermonuclear reactions. Of particular importance to stellar modelers is the convenient access to state-of-the-art evaluated rates for a large number of relevant nuclear reactions. Previous evaluations of nuclear reaction rates have been given, e.g., by W. A. Fowler et al. (1967), G. R. Caughlan & W. A. Fowler (1988), C. Angulo et al. (1999), C. Iliadis et al. (2001), P. Descouvemont et al. (2004), E. G. Adelberger et al. (2011), and Y. Xu et al. (2013). Most of these reaction rates were based on information derived from nuclear physics experiments and, therefore, are distinct from those estimated from nuclear theory, e.g., Hauser-Feshbach theory (T. Rauscher & F.-K. Thielemann 2000) or the nuclear shell model (H. Herndl et al. 1995).

From a historical perspective, the incorporation of Fowler's rates (W. A. Fowler et al. 1967; G. R. Caughlan & W. A. Fowler 1988) into stellar models established a solid nuclear physics foundation, enabling reasonable estimates of nuclear energy generation and nucleosynthesis. As observations became more quantitative, a major shortcoming of the evaluations mentioned above became apparent: the reported reaction rates had no rigorous statistical meaning, in the sense that they were not derived from probability density functions. With the publication of each evaluation, the nuclear data were updated, but the reaction rates were still computed using techniques developed prior to 1988.

Thermonuclear reaction rates are highly complex quantities derived from a multitude of nuclear physics inputs, painstakingly extracted from laboratory measurements (e.g., resonance energies and strengths, nonresonant cross sections, transfer spectroscopic factors, and so on). Modern techniques to estimate reaction rates from experimental nuclear physics input have employed Monte Carlo sampling methods (R. Longland et al. 2010) and Bayesian techniques (C. Iliadis et al. 2016; D. Odell et al. 2022b). These have a major advantage with respect to earlier results: their recommended values and associated uncertainties[6] can be quantified in terms of probability densities. Some of these methods were used in the 2010 evaluation of Monte Carlo–based experimental

[6] Throughout this work, we use the expression "uncertainty" for a parameter describing the dispersion of a measured value that can, at least in principle, be described by a suitable probability density function. In contradistinction, we use the expression "error" when we think that a mistake has been made.

Table 1
Summary of Reactions with Monte Carlo–based Thermonuclear Rates

Reaction	Q_{nu} (keV)[a]	Table
$D(p,\gamma)^3He$[b]	5493.428[c]	6
$D(d,n)^3He$[b]	3268.862[c]	7
$D(d,p)^3H$[b]	4032.664[c]	8
$^3H(d,n)^4He$[b]	17,589.253[c]	9
$^3He(d,p)^4He$[b]	18,353.054[c]	10
$^3He(^3He,2p)^4He$[b]	12,859.580[c]	11
$^3He(\alpha,\gamma)^7Be$[b]	1586.892 ± 0.070	12
$^7Be(n,p)^7Li$[b]	1644.422 ± 0.071	13
$^7Be(\alpha,\gamma)^{11}C$	7543.943 ± 0.092	14
$^{14}C(p,\gamma)^{15}N$	10,206.975[c]	15
$^{14}C(\alpha,\gamma)^{18}O$	6226.667[c]	16
$^{13}N(\alpha,p)^{16}O$	5217.92 ± 0.26	17
$^{14}N(\alpha,\gamma)^{18}F$	4414.05 ± 0.46	18
$^{15}N(\alpha,\gamma)^{19}F$	4012.630[c]	19
$^{15}O(\alpha,\gamma)^{19}Ne$	3527.09 ± 0.51	20
$^{16}O(p,\gamma)^{17}F$[b]	599.61 ± 0.24	21
$^{16}O(\alpha,\gamma)^{20}Ne$	4728.456[c]	22
$^{17}O(p,\gamma)^{18}F$	5606.43 ± 0.46	23
$^{17}O(p,\alpha)^{14}N$	1192.381[c]	24
$^{18}O(p,\gamma)^{19}F$	7992.938[c]	25
$^{18}O(p,\alpha)^{15}N$	3980.308[c]	26
$^{18}O(\alpha,\gamma)^{22}Ne$	9665.426 ± 0.017	27
$^{18}O(\alpha,n)^{21}Ne$	−698.832 ± 0.038	28
$^{17}F(p,\gamma)^{18}Ne$	3922.28 ± 0.44	29
$^{18}F(p,\gamma)^{19}Ne$	6409.26 ± 0.48	30
$^{18}F(p,\alpha)^{15}O$	2882.16 ± 0.67	31
$^{18}Ne(\alpha,p)^{21}Na$	2637.57 ± 0.36	32
$^{19}Ne(p,\gamma)^{20}Na$	2189.6 ± 1.1	33
$^{20}Ne(p,\gamma)^{21}Na$	2431.004 ± 0.041	34
$^{20}Ne(\alpha,\gamma)^{24}Mg$	9314.702 ± 0.012	35
$^{21}Ne(p,\gamma)^{22}Na$	6737.69 ± 0.14	36
$^{22}Ne(p,\gamma)^{23}Na$	8793.216 ± 0.017	37
$^{22}Ne(\alpha,\gamma)^{26}Mg$	10,612.883 ± 0.033	38
$^{22}Ne(\alpha,n)^{25}Mg$	−480.196 ± 0.049	39
$^{21}Na(p,\gamma)^{22}Mg$	5503.08 ± 0.16	40
$^{22}Na(p,\gamma)^{23}Mg$	7580.24 ± 0.13	41
$^{23}Na(p,\gamma)^{24}Mg$	11,691.681 ± 0.012	42
$^{23}Na(p,\alpha)^{20}Ne$	2376.979[c]	43
$^{22}Mg(p,\gamma)^{23}Al$	139.77 ± 0.38	44
$^{23}Mg(p,\gamma)^{24}Al$	1862.97 ± 0.23	45
$^{24}Mg(p,\gamma)^{25}Al$	2270.226 ± 0.065	46
$^{24}Mg(\alpha,\gamma)^{28}Si$	9981.768 ± 0.012	47
$^{25}Mg(p,\gamma)^{26}Al^t$	6305.187 ± 0.080	48
$^{25}Mg(p,\gamma)^{26}Al^g$	6305.187 ± 0.080	49
$^{25}Mg(p,\gamma)^{26}Al^m$	6305.187 ± 0.080[d]	50
$^{26}Mg(p,\gamma)^{27}Al$	8270.150 ± 0.055	51
$^{23}Al(p,\gamma)^{24}Si$	3281 ± 4[e]	52
$^{24}Al(p,\gamma)^{25}Si$	3412 ± 10	53
$^{25}Al(p,\gamma)^{26}Si$	5512.73 ± 0.12	54
$^{26}Al(p,\gamma)^{27}Si$	7462.06 ± 0.13	55
$^{27}Al(p,\gamma)^{28}Si$	11,583.632 ± 0.046	56
$^{27}Al(p,\alpha)^{24}Mg$	1601.864 ± 0.047	57
$^{26}Si(p,\gamma)^{27}P$	805.6 ± 9.0	58
$^{27}Si(p,\gamma)^{28}P$	2050.9 ± 1.1	59
$^{28}Si(p,\gamma)^{29}P$	2747.62 ± 0.36	60
$^{28}Si(\alpha,\gamma)^{32}S$	6944.7517 ± 0.0014	61
$^{29}Si(p,\gamma)^{30}P$	5593.339 ± 0.064	62
$^{30}Si(p,\gamma)^{31}P$	7295.146 ± 0.021	63
$^{27}P(p,\gamma)^{28}S$	2554 ± 160	64
$^{29}P(p,\gamma)^{30}S$	4393.83 ± 0.41	65
$^{31}P(p,\gamma)^{32}S$	8862.419[c]	66
$^{31}P(p,\alpha)^{28}Si$	1917.667[c]	67
$^{30}S(p,\gamma)^{31}Cl$	262.6 ± 3.4	68
$^{31}S(p,\gamma)^{32}Cl$	1579.46 ± 0.61	69
$^{32}S(p,\gamma)^{33}Cl$	2275.08 ± 0.39	70
$^{33}S(p,\gamma)^{34}Cl$	5141.512 ± 0.048	71
$^{34}S(p,\gamma)^{35}Cl$	6369.127 ± 0.056	72
$^{31}Cl(p,\gamma)^{32}Ar$	2452.9 ± 3.9	73
$^{35}Cl(p,\gamma)^{36}Ar$	8505.149 ± 0.044	74
$^{35}Cl(p,\alpha)^{32}S$	1867.700 ± 0.035	75
$^{34}Ar(p,\gamma)^{35}K$	81.59 ± 0.51	76
$^{35}Ar(p,\gamma)^{36}K$	1656.88 ± 0.75	77
$^{36}Ar(p,\gamma)^{37}K$	1855.650 ± 0.096	78
$^{38}Ar(p,\gamma)^{39}K$	6379.36 ± 0.19	79
$^{35}K(p,\gamma)^{36}Ca$	2597.5 ± 5.6[f]	80
$^{39}K(p,\gamma)^{40}Ca$	8326.046 ± 0.021	81
$^{39}Ca(p,\gamma)^{40}Sc$	527.3 ± 2.8	82
$^{40}Ca(p,\gamma)^{41}Sc$	1082.644 ± 0.076	83

Notes.
[a] Nuclear Q-value, calculated using atomic masses listed in M. Wang et al. (2021) and the total electronic binding energy estimated from Equation (A4) of D. Lunney et al. (2003); see Section 6.1 and C. Iliadis (2019).
[b] Bayesian rate.
[c] Uncertainty less than 5 eV; see M. Wang et al. (2021).
[d] This value is the nuclear proton separation energy used for calculating resonance energies from excitation energies. To calculate the actual Q value, subtract the energy of the first excited state in ^{26}Al ($E_x = 228.305 \pm 0.013$ keV; see M. Basunia & A. Hurst 2016).
[e] Based on the ^{24}Si mass excess from D. Puentes et al. (2022).
[f] Based on the ^{36}Ca mass excess from J. Surbrook et al. (2021).

reaction rates (C. Iliadis et al. 2010a, 2010b, 2010c), hereafter labeled as "ETR10."

We considered the available experimental data for nuclear interactions of protons and α particles with target nuclei in the $A \leqslant 40$ region, and present statistically meaningful estimates of their thermonuclear rates, including uncertainties, following the ideas presented in R. Longland et al. (2010) and C. Iliadis et al. (2016). This information is indispensable for assessing uncertainties of abundances or nuclear energy generation in astrophysical simulations. Table 1 summarizes all reactions for which we present experimental thermonuclear rates, hereafter labeled as "ETR25." Our numerical results are presented on a temperature grid from 1 MK to 10 GK (see Appendix E).

As was the case in previous evaluations, we restrict our considerations to nondegenerate, nonrelativistic circumstances for the interacting nuclei. We also assume that the Maxwell–Boltzmann distribution holds for the relative velocities of the interacting particles. Our reaction rates are appropriate for *bare nuclei in the laboratory*. In other words, when used in astrophysical model simulations, the results presented here need to be corrected, when appropriate, for electron screening at elevated densities, and thermal target excitations at elevated temperatures.

2. Reaction Rate Formalism

The formalism to calculate thermonuclear reaction rates can be found, e.g., in C. Iliadis (2015), and has also been summarized by R. Longland et al. (2010). We are not repeating it here, but will focus on the main results. In the following, all

energies refer to the center-of-mass coordinate system, unless explicitly mentioned otherwise.

The total laboratory thermonuclear rate (in units of $\mathrm{cm^3\,mol^{-1}\,s^{-1}}$) for a reaction involving two nuclei, 0 and 1, in the entrance channel at a given temperature T is given by

$$N_{\rm A}\langle\sigma v\rangle_{01} = \frac{3.7318\cdot 10^{10}}{T_9^{3/2}}\sqrt{\frac{M_0+M_1}{M_0M_1}} \times \int_0^\infty E\;\sigma(E)\;{\rm e}^{-11.605\,E/T_9}\,dE \quad (1)$$

where the center-of-mass energy E is in units of MeV, the temperature T_9 is in GK ($T_9 \equiv T/10^9$ K), the nuclear masses $M_i = m_i/m_u$ are in atomic mass units (u), and the cross section σ is in barns (1 barn $\equiv 10^{-24}\,\mathrm{cm^2}$); $N_{\rm A}$ denotes the Avogadro constant. The reaction rate is determined by the absolute magnitude and the energy dependence of the nuclear reaction cross section, $\sigma(E)$. Based on the energy dependence of $\sigma(E)$, a number of different specialized expressions and procedures can be derived for individual contributions to the total reaction rate.

2.1. Nonresonant Reaction Rates

Nonresonant cross sections vary smoothly with energy and can be converted into the astrophysical S factor, defined by

$$S(E) \equiv E\;e^{2\pi\eta}\;\sigma(E). \quad (2)$$

This definition removes the $1/E$ dependence of nuclear cross sections and the s-wave Coulomb barrier transmission probability, $e^{-2\pi\eta}$ (i.e., the Gamow factor), from the cross section. The astrophysical S factor, therefore, exhibits a much weaker energy dependence. The Sommerfeld parameter, η, is numerically given by

$$2\pi\eta = 0.989510\,Z_0Z_1\sqrt{\frac{M_0M_1}{M_0+M_1}\frac{1}{E}} \quad (3)$$

where Z_i is the charges of nuclei 0 and 1. When the S factor depends weakly on energy, the substitution of Equation (2) into Equation (1) yields an integrand whose energy dependence is dominated on the low-energy side by the penetrability through the Coulomb barrier, and on the high-energy side by the Maxwell–Boltzmann distribution. The integrand is referred to as the Gamow peak and represents the effective energy range of stellar burning for a nonresonant reaction at a given temperature and nuclear masses and charges.

Once the S factor has been estimated over an appropriate range of energies, the thermonuclear reaction rates can be computed by a numerical integration of Equation (1). The energy dependence of the nonresonant S factor can be estimated using microscopic nuclear models, R-matrix theory, potential models, or any other suitable method. For example, in this work, we computed the S factor for direct radiative capture reactions, i.e., for (p,γ) or (α,γ), using the results of a potential model normalized to experimental data, as discussed in Section 9.

2.2. Isolated-resonance Rates

The cross section of an isolated resonance can be described by the one-level Breit–Wigner formula. For the cross section (in units of barns) of a resonance located at a center-of-mass energy E_r, we find

$$\sigma_{\rm BW}(E) = 0.6566\frac{\omega}{E}\frac{M_0+M_1}{M_0M_1} \times \frac{\Gamma_a(E)\Gamma_b(E+Q-E_f)}{(E_r-E)^2+\Gamma(E)^2/4} \quad (4)$$

where all energies and widths are in units of MeV; $\omega \equiv (2J+1)/[(2j_0+1)(2j_1+1)]$ is the spin factor, where J, j_0, and j_1 denote the spins of the resonance, projectile, and target nucleus, respectively; Q is the reaction Q-value, E_f is the energy of the final state in the residual nucleus, and Γ_a, Γ_b, and Γ are the partial widths for the entrance (a) and exit (b) channel, and the total resonance width (i.e., the sum of all partial widths, $\Gamma = \Gamma_a + \Gamma_b + ...$), respectively. In the above expression, and throughout this work, the energy-dependent partial widths denote "observed" rather than "formal" quantities (A. M. Lane & R. G. Thomas 1958). If the partial widths of the resonance have been measured, Equation (4) can be substituted into Equation (1) to compute the reaction rates by numerical integration. Notice that Equation (4) applies equally to subthreshold states, i.e., when $E_r < 0$.

The Breit–Wigner cross section for an isolated resonance, as presented in Equation (4), exhibits slight differences in its energy dependence compared to a comprehensive R-Matrix calculation of a single isolated resonance, as outlined in Section XII of A. M. Lane & R. G. Thomas (1958). Specifically, we employ the "Thomas approximation" (R. G. Thomas 1951), which estimates the level shift using a linear function. Practically, this approximation leads to a minor error when extrapolating the cross section of a broad resonance, since the energy dependence of the level shift is not fully accounted for. However, for low-energy resonances critical in astrophysically significant reactions, the level shift varies only slowly with energy. Our tests with (p,γ) and (α,γ) resonances have indicated that the Thomas approximation introduces an error of less than 10% in the reaction rate for a single isolated resonance.

If the partial widths are not directly known, they may be estimated using experimental nuclear structure information. The particle partial width for a given level, λ, and channel, c, can be written as (A. M. Lane 1960)

$$\Gamma_{\lambda c} = 2P_c\gamma_{\lambda c}^2 = 2P_c\frac{\hbar^2}{\mu R^2}\theta_{\lambda c}^2 \quad (5)$$

where $\gamma_{\lambda c}^2$ and $\theta_{\lambda c}^2$ are the reduced width and dimensionless reduced width, respectively, $\mu = m_0m_1/(m_0+m_1)$ is the reduced mass, R is the channel radius (see later), and P_c is the penetration factor. For a single-nucleon channel, the proton or neutron partial width can be expressed as (C. Iliadis 1997, 2015)

$$\Gamma_{\lambda c} = 2P_c\frac{\hbar^2}{\mu R^2}C^2S\theta_{\rm pc}^2 \quad (6)$$

where C denotes the isospin Clebsch–Gordan coefficient (Appendix B), S is the nucleon spectroscopic factor, and $\theta_{\rm pc}^2$ denotes the dimensionless single-particle reduced width. This expression has the following intuitive meaning. The probability ($\Gamma_{\lambda c}$, in energy units) of decay (or formation) of a

resonance by proton or neutron emission (or absorption) is equal to the product of three probabilities: (i) The probability that the nucleons in the compound nucleus arrange themselves according to a "target + projectile" configuration (C^2S). (ii) The probability that the single nucleon appears at the nuclear surface ($\theta_{\rm pc}^2$). (iii) The probability that the nucleon tunnels through the Coulomb and centripetal barriers (P_c). The partial widths of protons and α particles are strongly energy dependent through the penetration factor, P_c, which is computed from Coulomb wave functions (A. M. Lane & R. G. Thomas 1958).

Equation (6) has not been applied consistently, even in the recent literature. Sometimes, the factor of 2 is replaced by a factor of 3, or the quantity $\theta_{\rm pc}^2$ is set equal to unity. In such cases, unnecessary errors are introduced in the calculation of the particle partial width (for more information, see C. Iliadis 1997). In Table 3, we provide for protons numerical values of $\theta_{\rm pc}^2$ versus bombarding energy and target mass number for orbital angular momenta of $\ell = 0$, 1, 2, and 3. Another source of confusion in the literature arises from the fact that the product C^2S, rather than S, is referred to as the "spectroscopic factor." Unless otherwise specified, we also adopted this terminology, as the product is the key quantity involved in Equation (6).

The above expression provides a versatile way to compute a particle partial width when the spectroscopic factor has been measured in a transfer (stripping) reaction. If the value of C^2S for a level of interest is unknown, but the spectroscopic factor of the mirror state (or, more generally, components of the same isospin multiplet) has been measured, Equation (6) can still be used to estimate the particle partial width (C. Iliadis et al. 1999). See Appendix C.1 for more information. Examples for estimating proton partial widths from spectroscopic factors are given in Appendix A.

For accurate estimates of particle partial widths according to Equation (6), the parameters used to derive C^2S, P_c, and $\theta_{\rm pc}^2$ must be internally consistent. For example, many distorted-wave Born approximation (DWBA) analyses have generated the final-state wave function using a Woods–Saxon nuclear potential radius parameter of $r_0 = 1.25$ fm, a diffuseness of $a = 0.65$ fm, and a Coulomb potential radius parameter of $r_{c0} = 1.25$ fm. The penetration factor is commonly computed using a channel radius of $R = 1.25(A_0^{1/3} + A_1^{1/3})$ fm, where A_0 and A_1 denote the (integer) mass numbers of the projectile and target, respectively. Internal consistency demands that $\theta_{\rm pc}^2$ is computed with exactly the same channel and Woods–Saxon parameters used in the estimation of C^2S and P_c. Otherwise, an additional error is introduced in the derivation of the particle partial width. The uncertainty of indirectly derived particle partial widths will be addressed in Section 8.

2.3. Narrow-resonance Rates

When the partial widths entering in Equation (4) are known, the numerical integration of Equation (1) will provide a reaction rate that takes contributions from all energy regions of the resonance into account. However, for many resonances, neither the cross section has been measured nor the partial widths have been estimated. Instead, all that can be measured is the integrated resonance cross section. This situation is experimentally unavoidable if the total resonance width is much smaller than the resolution of the beam and the thickness of the target. The measured cross section integral is proportional to the resonance strength, defined by

$$\omega\gamma \equiv \frac{2J+1}{(2j_0+1)(2j_1+1)}\frac{\Gamma_a\Gamma_b}{\Gamma}, \tag{7}$$

which can be used to estimate the resonance contribution to the reaction rate. If, for a particular resonance, we can assume that the partial widths in Equation (4) do not vary significantly with energy over the total resonance width, Equation (1) reduces to

$$N_A\langle\sigma v\rangle = \frac{1.5399\cdot 10^{11}}{T_9^{3/2}}\left(\frac{M_0+M_1}{M_0M_1}\right)^{3/2} \times \omega\gamma\, e^{-11.605\, E_r/T_9} \tag{8}$$

where the center-of-mass resonance energy, E_r, and resonance strength, $\omega\gamma$, are both in units of MeV. When the astrophysically important energy range contains more than a single narrow resonance, the combined rate is given by the incoherent sum of their individual rate contributions. According to Equation (8), a given narrow resonance achieves its maximum contribution to the total rate at a temperature of $T_9^{\rm max} = 7.737E_r$, where the resonance energy is in units of MeV. Experimental resonance strengths will be discussed in Section 7.

The price to pay for assuming energy-independent partial widths is that Equation (8) only considers the rate contribution at the resonance energy, E_r. This quantity appears exponentially in the above expression, implying that its experimental value must be accurately known; otherwise, it will significantly contribute to the uncertainty in the reaction rate.

We address now the question, "when can a resonance be considered narrow for the purpose of estimating the reaction rate?" An experimentalist would typically consider a resonance with a total width of, say, 0.15 eV as "narrow." However, for astrophysical purposes, caution is necessary. An example of a resonance with this total width (0.15 eV) is presented in Figure 10 of D. Powell et al. (1999) for the ^{24}Mg(p,γ)^{25}Al reaction. At low temperatures ($\leqslant$30 MK), where the Gamow peak has shifted far below the resonance energy of $E_r = 223$ keV, the contribution of the resonance tail exceeds the rate computed using the approximation of Equation (8) by several orders of magnitude. In practice, the impact of this effect for a given narrow resonance is frequently lessened, because contributions from either other low-energy resonances or nonresonant processes dominate over the tail contribution of the resonance in question. Nevertheless, it is important to assess the impact of the disregarded resonance tail when using Equation (8). We defined a "narrow resonance" as one whose total contribution to the reaction rate is accurately represented by Equation (8), i.e., based solely on the knowledge of its energy, E_r, and strength, $\omega\gamma$.

When a total width has contributions from two channels only (e.g., the proton width, Γ_p, and γ-ray partial width, Γ_γ), at sufficiently low energies, the condition $\Gamma_p \ll \Gamma_\gamma$ (or $\Gamma \approx \Gamma_\gamma$) applies, and the resonance strength becomes $\omega\gamma \approx \omega\Gamma_p$. Conversely, at sufficiently high energies, the proton width typically exceeds the γ-ray partial width significantly, leading to $\omega\gamma \approx \omega\Gamma_\gamma$. These approximations are frequently applicable in practice.

3. Reaction Rates and Modern Statistics

Experimental thermonuclear reaction rates are quantities derived from measured nuclear properties (e.g., cross sections, resonance energies, strengths, and partial widths, excitation energies, spectroscopic factors, etc.) and, therefore, are subject to measurement uncertainties. How does one then estimate the reaction rate uncertainties based on the uncertainties of all measured nuclear input quantities? One answer is analytical error propagation, a path that was first explored in the context of reaction rates by W. J. Thompson & C. Iliadis (1999). Their method worked reasonably well when the uncertainties in the nuclear input were small. However, this approach proved inadequate when the uncertainties of some measured quantities became significant, a common occurrence for many nuclear reactions of astrophysical interest.

When error propagation becomes analytically intractable, a modern approach necessarily resorts to Monte Carlo techniques. This method was introduced for thermonuclear reaction rates in R. Longland et al. (2010) and proved highly successful. The first major advantage of Monte Carlo–based reaction rates is their robustness against the size of nuclear physics input uncertainties. The method remains effective regardless of how large these uncertainties are, as long as there is a physically meaningful probability density function for each nuclear input quantity. The second major advantage of the Monte Carlo method is its fundamental grounding in the central limit theorem of statistics. Measured nuclear quantities can be assigned Gaussian (or lognormal) probability densities when their total uncertainty is determined by a sum (or product) of individual contributions. The central limit theorem also explains why an ensemble of reduced widths is described by a Porter–Thomas probability density distribution; see H. A. Weidenmüller & G. E. Mitchell (2009), R. Longland et al. (2010), and I. Pogrebnyak et al. (2013) for details.

The Monte Carlo method is most useful when the total rate has a significant resonant contribution. In some cases, particularly with light target nuclei, the total cross section within the astrophysically relevant energy range is determined solely by nonresonant contributions. In such cases, other techniques must be employed to estimate statistically rigorous reaction rates, e.g., Bayesian hierarchical models (see Section 4).

The different statistical methods to analyze S factor data, depending on the circumstances, are explained in Figure 1. In each panel, the energy region is divided into three areas. In the energy range to the left (green), no direct S-factor data exist because of the low transmission through the Coulomb barrier. The middle (red) range contains all of the measured data. On the right-hand side (blue), no data are available, e.g., because those energies may not be attainable at low-energy accelerator facilities.

Panel (a) illustrates the scenario for what we term "class I reactions," where resonances are absent, and the total rate is given by nonresonant contributions only. In this case, S-factor data have been measured over a wide energy range. Typically, results are available from different experiments (i.e., depicted by the solid circles and open squares in Figure 1), while statistical and systematic uncertainties are separately reported for all data. The theoretical energy dependence of the S factor may be calculated from a potential model, a microscopic model, or another suitable prescription. For class I reactions, we use reaction rates based on fitting the theoretical S factor to the data using Bayesian hierarchical models (C. Iliadis et al. 2016). As will be explained in Section 4, this method has inherent advantages over the traditional χ^2 fitting technique. An example of the Bayesian analysis of a class I reaction, $D(p,\gamma)^3He$, is provided in J. Moscoso et al. (2021).

Panel (b) depicts the situation for cases where the total rate is dominated by contributions from mostly noninterfering (narrow) resonances ("class II reactions"). In the middle region, two resonances are shaded, indicating that, for those only, the resonance energies and strengths (see Equation (7)) have been measured. Additional, nonresonant, contributions appear between resonances. In the (green) region on the left-hand side, additional low-energy resonances may contribute to the total rate because they correspond to known levels in the compound nucleus. If these states are populated in a proton or α-particle transfer reaction, their experimental spectroscopic factors can be used to calculate the particle partial width according to Equation (6), thereby allowing for the estimation of their contribution to the total rate. For class II reactions, the total rate must be computed from a large body of experimental nuclear physics input: resonance energies, strengths, partial widths, nonresonant contributions, etc. We evaluated the rates of such reactions using the Monte Carlo sampling method (R. Longland et al. 2010; C. Iliadis et al. 2015), as will be explained in Section 5. An example for the Monte Carlo analysis of a class II reaction, $^{29}Si(p,\gamma)^{30}P$, can be found in L. N. Downen et al. (2022b). In the right-hand (blue) region, the contribution of the many unobserved higher-energy resonances must also be estimated. We calculated the rates at these high temperatures by resorting to the statistical (Hauser-Feshbach) nuclear reaction model, and by matching this contribution at a temperature where the total rate is fully determined by the available data (J. R. Newton et al. 2008). This will be discussed in more detail in Section 10.

The most challenging situation, in terms of applying a rigorous statistical technique to the data analysis, is depicted in panel (c). Here, the total rates are dominated by interfering amplitudes from broad resonances and nonresonant processes. We refer to such cases as "class III reactions." Since the amplitudes of different contributions interfere, one cannot simply describe each resonance by the Breit–Wigner formula (Equation (4)) and add their contributions incoherently, as is done for class II reactions. A suitable nuclear model to apply in these situations is the phenomenological R-matrix theory (A. M. Lane & R. G. Thomas 1958; P. Descouvemont & D. Baye 2010). R-matrix fits of the data have been performed so far almost exclusively using traditional (i.e., χ^2) methods. A prominent example for a class III reaction is $^{12}C(\alpha,\gamma)^{16}O$, and its ($\chi^2$) analysis was presented in R. J. deBoer et al. (2017). We predict that class III reactions will be analyzed in the future by implementing R-matrix theory into Bayesian hierarchical models. This has been achieved mostly in the simplest of cases, when the rate is dominated by a single broad resonance (R. S. de Souza et al. 2019a, 2019b; D. Odell et al. 2022a); see also L. Y. Zhang et al. (2022). For the more complex cases, such as $^{12}C(\alpha,\gamma)^{16}O$, $^{12}C(p,\gamma)^{13}N$, or $^{14}N(p,\gamma)^{15}O$, we do not present numerical results in this work, because their reaction rates have not yet been based on rigorous probability density functions.

The above division of reactions into three different classes, based on the complexity of the statistical analysis, is highly idealized. In particular, the meanings of "nonresonant" and "broad-resonance" contributions overlap significantly.

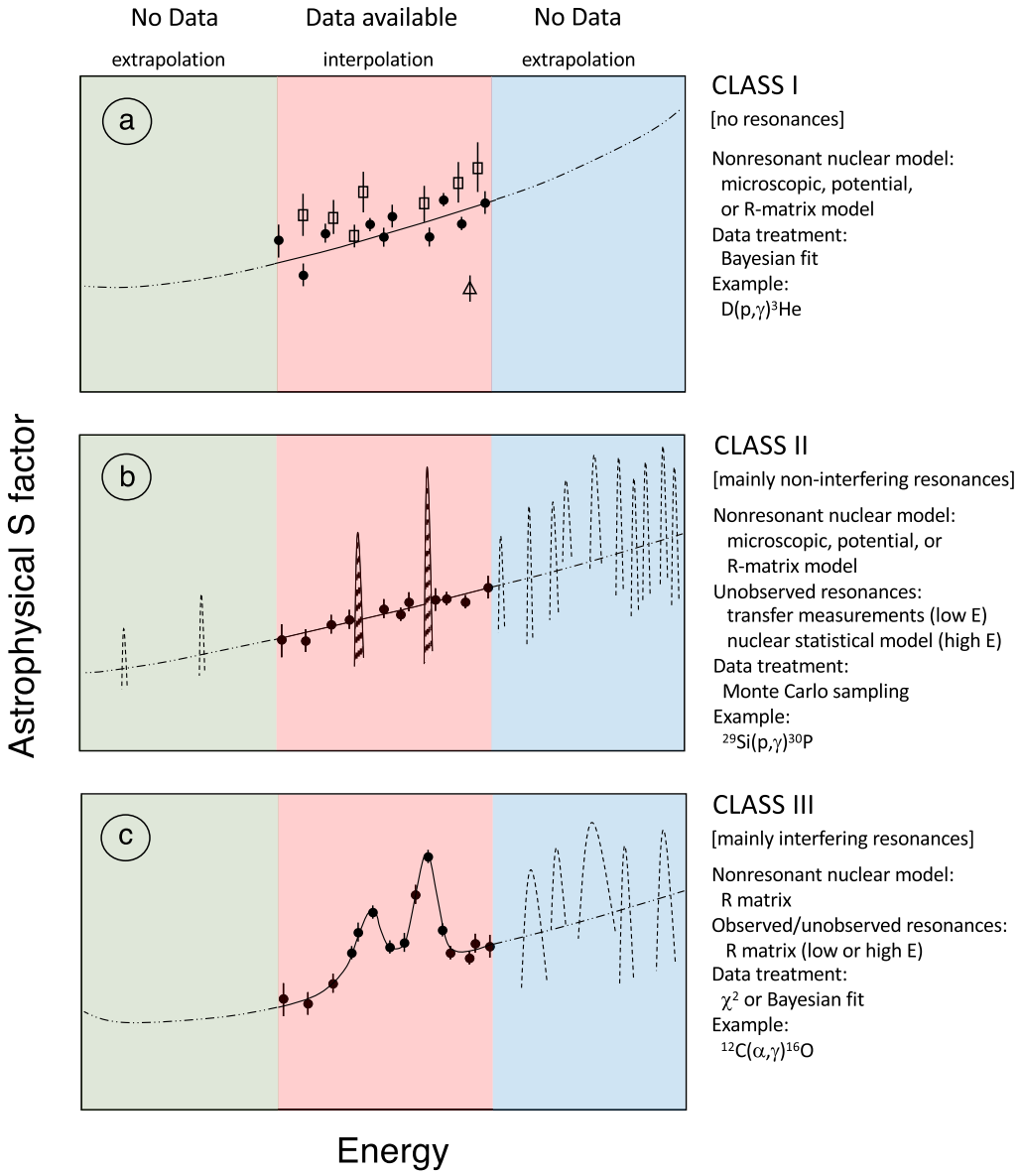

Figure 1. Idealized picture of various *S*-factor contributions to charged-particle reaction rates. In each panel, the energy range is divided into three regions. Green, left: directly measured *S* factor data are not available because of the small transmission through the Coulomb barrier. Red, middle: region where *S* factor data have been obtained in the laboratory. Blue, right: no data are available because of experimental limitations in the attainable beam energy. Three fundamentally different situations are encountered in practice, depending on the nature of contributions in the middle (red) region. (a) Class I reactions: nonresonant *S* factor contributions only. (b) Class II reactions: main contributions from noninterfering (i.e., narrow) resonances. (c) Class III reactions: main contribution from interfering (i.e., broad) resonances. See text.

Nevertheless, Figure 1 demonstrates the key differences. In the following, we focus on Bayesian- and Monte Carlo–based techniques to estimate rigorous thermonuclear reaction rates for class I and II reactions, respectively.

4. Bayesian-based Reaction Rates

4.1. Overview

The first study to present a general Bayesian model for estimating thermonuclear reaction rates was published in C. Iliadis et al. (2016). Bayesian thermonuclear rates have so far been estimated for most of the key Big Bang nucleosynthesis reactions (see C. Iliadis & A. Coc 2020; and references therein).

The Bayesian approach has several advantages over other methods. It allows for a consistent propagation of uncertainties within a well-established statistical framework. Each fitting (model) parameter can be associated with a physically motivated probability density function (e.g., normal, lognormal, Poisson, or uniform distributions), eliminating the need for any implicit approximation by Gaussian probability densities. Bayesian techniques also allow for quantifying the selection of different models used to fit the data. Perhaps most importantly, the interpretation of the results is intuitive, in the sense that all model parameters are random variables (unlike in "frequentist" statistics), and their values can be estimated rigorously for any given coverage probability. The price to be paid is an added layer of complexity: the analysis must resort to numerical techniques (i.e., Markov Chain Monte Carlo, hereafter MCMC, algorithms), and one has to ensure that the results are numerically stable. In the following, we summarize the formalism as it applies to astrophysical *S* factors and

thermonuclear reaction rates. For more information, see C. Iliadis et al. (2016).

When Bayes' theorem is applied to data, represented by the vector y, and model parameters, given by the vector θ, it can be written as (J. M. Hilbe et al. 2017)

$$p(\theta|y) = \frac{\mathcal{L}(y|\theta)\pi(\theta)}{\int \mathcal{L}(y|\theta)\pi(\theta)d\theta}. \quad (9)$$

All factors in this expression serve as probability densities: $\mathcal{L}(y|\theta)$ is the likelihood, i.e., the probability that the data, y, were obtained for given values of the model parameters, θ; $\pi(\theta)$ is the prior, which represents our state of knowledge about each parameter before seeing the data; the product of the likelihood and the prior defines the posterior, $p(\theta|y)$. This quantity is of primary interest because it contains the specific information we seek: the probability of obtaining the values of a specific set of model parameters given the data. The general meaning of Equation (9) is that the availability of new data updates our prior knowledge about the model parameters, and our revised knowledge is fully described by the posterior distribution. Once the posterior is calculated, it can be used to estimate model parameters for any given coverage probability, or to make predictions about physical quantities, such as cross sections or S factors. The normalization factor in the denominator of Equation (9) is irrelevant when a specific Bayesian model is used for parameter estimation or value prediction, but it becomes important when performing Bayesian model selection.

4.2. Likelihoods and Priors

Consider as a simple example an astrophysical S factor subject to statistical uncertainties, $\sigma_{\rm stat}$. If the probability density of each data point is given by a normal (i.e., Gaussian) distribution, the likelihood is given by

$$\mathcal{L}(S^{\rm exp}|\theta) = \prod_{i=1}^{N} \frac{1}{\sigma_{{\rm stat},i}\sqrt{2\pi}} e^{-\frac{[S_i^{\rm exp} - S(\theta)_i]^2}{2\sigma_{{\rm stat},i}^2}} \quad (10)$$

where the product runs over all data points, labeled by the index i. The theoretical S factor, $S(\theta)_i$, is determined by a suitable nuclear reaction model (e.g., a microscopic model, a potential model, or R-matrix theory). The above likelihood represents a product of normal distributions, each with a mean of $S(\theta)_i$, and a standard deviation, $\sigma_{{\rm stat},i}$, given by the experimental statistical uncertainty of the datum i. In symbolic notation, we can rewrite the above expression as

$$S_i^{\rm exp} \sim N(S(\theta)_i, \sigma_{{\rm stat},i}^2) \quad (11)$$

where "N" denotes a normal probability density, and the symbol "$\sim$" means "has the probability distribution of."

Each of the model parameters contained in the vector θ of Equation (9) requires a prior. Priors should be chosen to best represent the physics involved. For example, if all we know about a specific parameter, θ_j, before seeing the data is that its value must lie somewhere in a region between zero and θ_m, we can write the prior as

$$\theta_j \sim U(0, \theta_m) \quad (12)$$

where "U" denotes a uniform (i.e., constant) probability density between the boundaries. If the parameter in question can take values in excess of θ_m, but with a probability inverse to its magnitude, we may choose instead a truncated normal prior

$$\theta_j \sim T(0, \infty)N(0, \theta_m^2), \quad (13)$$

which represents a normal distribution centered at zero with a standard deviation of θ_m, multiplied by a truncation function, T, which suppresses samples outside of the interval defined by its arguments. When the data are of high quality, reasonable choices for the prior, say Equations (12) or (13), will have an insignificant effect on the posterior in Equation (9). We call such priors "noninformative." If the prior impacts the posterior moderately or strongly, we call them "moderately informative" and "highly informative" priors, respectively. In Bayesian analyses, different reasonable choices of prior distributions should always be explored to assess their impact on the posterior inference and parameter estimation. For more information on particular choices of priors, see A. Gelman et al. (2017).

4.3. Systematic Uncertainties

Systematic uncertainties (J. Heinrich & L. Lyons 2007) require careful consideration in the data analysis. We define systematic effects by the following attributes: they do not usually signal their existence by a larger fluctuation of the data; they are not reduced by combining the results from different measurements or by collecting more data; when the experiment is repeated, the presence of systematic effects may not produce different answers. In a nuclear physics experiment, systematic effects impact the overall normalization by shifting all points of a given dataset into the same direction. They are correlated from data point to data point, in the sense that if one happened to know how to correct such an uncertainty for one data point, then one could calculate the correction for all other data points as well. Specifically, a reported systematic uncertainty of, say, 5%, implies a systematic factor uncertainty of $f.u. = 1.05$. The true value of the multiplicative normalization factor, f, is unknown at this stage. However, we can reasonably assume that the expectation value of the normalization factor is unity; otherwise, we would have corrected the data for the systematic effect.

A useful distribution for normalization factors is the lognormal probability density, which is characterized by two quantities: the lognormal location parameter, μ_L, and the spread parameter, σ_L. The median value of the lognormal distribution is given by $x_{\rm med} = e^{\mu_L}$, while the factor uncertainty, for a coverage probability of 68%, is $f.u. = e^{\sigma_L}$. Systematic effects can be included in a hierarchical Bayesian model as a highly informative, lognormal prior with a median of $x_{\rm med} = 1.0$ (or $\mu_L = \ln x_{\rm med} = 0$), and a factor uncertainty given by the systematic uncertainty. In the above example, we would choose $f.u. = 1.05$ (or $\sigma_L = \ln f.u. = \ln(1.05)$). The prior is then explicitly given by

$$\pi(f) = \frac{1}{\ln(f.u.)\sqrt{2\pi}f} e^{-\frac{[\ln f]^2}{2[\ln(f.u.)]^2}} \quad (14)$$

where "ln" represents the natural logarithm. In symbolic notation, this is expressed as

$$f \sim LN(0, [\ln(f.u.)]^2) \quad (15)$$

where "*LN*" denotes a lognormal probability density. The multiplicative normalization factor, f, is applied to the theory prediction, $S(\theta)$. For more information on this prior choice for systematic uncertainties, see C. Iliadis et al. (2016).

In conventional χ^2 fitting, normalization factors are often treated as systematic shifts applied directly to the data. In Bayesian inference, by contrast, the reported data are considered fixed—reflecting observed measurements—and are not adjusted to accommodate model assumptions. Instead, the true (but unknown) S factor is multiplied by the normalization factor, f. This means that, during the fitting, each dataset pulls on the true S factor curve with a strength inversely proportional to the systematic uncertainty: a dataset with a small systematic uncertainty will pull the true S factor curve more strongly toward it compared to one with a large systematic uncertainty. This "pulling" is independent of the dataset size: disregarding statistical uncertainties for a moment, a set consisting of a single datum will have the same weight in the fitting as one containing many data points, if both sets are described by the same factor uncertainty, $f.u.$

4.4. Additional Effects

The Bayesian model should be designed to closely reflect the data-generating processes. For example, in some cases, it is apparent that the observed scatter of the measured data cannot be explained solely by the reported statistical uncertainties. This is illustrated in Figure 1(a), where most of the data points indicated by the black circles miss the best-fit (black solid) line. This indicates the presence of additional sources of statistical uncertainty that were unknown to the experimenter. These have been termed "extrinsic uncertainties" in R. S. de Souza et al. (2019b). Since the observed scatter in the data contains information on the unreported statistical uncertainty, the Bayesian model can predict its magnitude for a given dataset. When both statistical and extrinsic uncertainties are present in a measurement, the overall likelihood is given by a nested (hierarchical) expression. Using again the symbolic notation, we can replace Equation (11) with

$$S'_i \sim N(S(\theta)_i, \sigma^2_{\rm extr}) \quad (16)$$

$$S_i^{\rm exp} \sim N(S'_i, \sigma^2_{{\rm stat};i}). \quad (17)$$

Equations (16) and (17) provide a hierarchical approach for constructing the overall likelihood. First, statistical uncertainties quantified by the standard deviation, $\sigma_{\rm extr}$, of an assumed normal probability density, perturb the true (but unknown) value of the S factor, $S(\theta)_i$, of a data point i, at a given energy to produce a value of S'_i. Second, the latter value is perturbed, in turn, by the reported experimental statistical uncertainty, quantified by the standard deviation, $\sigma_{{\rm stat};i}$, of a normal probability density, to produce the observed value of $S_i^{\rm exp}$. The above example demonstrates how any quantifiable experimental effect impacting the data can be readily incorporated into a hierarchical Bayesian model.

In other cases, individual data points appear outside the range suggested by the bulk of the data ("outliers"; see the open triangle in Figure 1(a)), or all data points of a specific experiment deviate systematically from the results of other experiments ("discrepant data"; see the open squares in Figure 1(a)). A robust algorithm to include such data in the analysis is presented in S. Andreon & B. Weaver (2015). The method treats the complete body of data as a mixture of two populations: one of supposedly correctly measured uncertainties, and another for which the reported uncertainty estimates are too optimistic. The membership to these two populations is described by including additional parameters in the Bayesian model. The algorithm automatically identifies and reduces the weight of data points with overoptimistic uncertainties. Data points contribute more significantly to the posterior the smaller their uncertainty and the higher the probability that the reported uncertainty is accurate. Therefore, all data points are considered in the analysis, and none are discarded subjectively. The algorithm also quantifies the outlier probability of a given datum or experiment. For details, see C. Iliadis et al. (2016).

4.5. Markov Chain Monte Carlo

Except in the simplest cases, the posterior of Equation (9) cannot be computed analytically, necessitating the use of numerical techniques. The implementation, since the late 1980s, of MCMC methods into multiparameter Bayesian hierarchical models is the main reason for the exponential growth in the use of Bayesian inference across many fields (S. E. Fienberg 2006). The MCMC technique allowed for the computation of the posterior and arbitrary functions of the model parameters without the need for approximations. The main idea is, first, to construct a Markov Chain whose stationary distribution is equal to the posterior and, second, to take a sufficiently long random walk by drawing samples from the Markov Chain. Several related algorithms have been devised to solve this problem (e.g., Metropolis-Hastings, Gibbs, Hamiltonian Monte Carlo, etc.; see S. Sharma 2017).

A number of software tools are publicly available and have been successfully used to estimate astrophysical S factors from data. Examples are NIMBLE (P. de Valpine et al. 2017), JAGS (M. Plummer 2003), DREAM (C. J. F. ter Braak & J. A. Vrugt 2008), emcee (D. Foreman-Mackey et al. 2013). All these packages require the user to define the physical model, likelihood, and priors. They also allow for the initialization, adaptation, and monitoring of the Markov Chain. Running a model refers to generating random samples from the posterior distribution of all model parameters. The initial steps of the random walk ("burn-in"), before the Markov Chain has reached convergence, must be discarded. When equilibrium has been achieved, a sufficient number of samples is drawn to ensure that Monte Carlo fluctuations become negligible compared to the statistical, systematic, and extrinsic uncertainties.

The sampling returns the model parameters at each step of the Markov Chain. For each set of parameters, a credible S factor is obtained, from which the reaction rate at all temperatures can be found by a numerical integration of Equations (1) and (2). At a given temperature, the ensemble of rate values found in this manner represents the reaction rate probability density. The recommended rate is estimated by adopting the 50th percentile of the rate probability density, while the rate uncertainty is found from the 16th and 84th percentiles (for a coverage probability of 68%). See R. Longland et al. (2010) and Section 5.

So far, astrophysical S factors and reaction rates estimated using Bayesian hierarchical models have been published for

nine light-ion (class I) reactions: $D(p,\gamma)^3He$, $D(d,n)^3He$, $D(d,p)^3H$, $^3H(d,n)^4He$, $^3He(d,p)^4He$, $^3He(^3He,2p)^4He$, $^3He(\alpha,\gamma)^7Be$, $^7Be(n,p)^7Li$, and $^{16}O(p,\gamma)^{17}F$. These are labeled by table note "b" in Table 1. The rates of some of these reactions were recalculated in the present work (see table notes in Appendix E), because the Bayesian model assumptions have evolved since the original formulation in C. Iliadis et al. (2016), as will be explained below. However, the changes in these rates are very small ($\leqslant$1.5%).

4.6. Practical Considerations

We now address a few issues of practical interest when estimating S factors and thermonuclear rates using Bayesian hierarchical models.

First, for a given reaction, the analysis should start with a collection of data from the entire relevant literature. It is important not to dismiss data simply because they were published some time ago or because they have larger uncertainties than other studies. Unless there is a reason to believe that errors were made in a given publication, all published data should be taken into account in the data analysis.

Second, one should estimate the separate contributions of statistical and systematic uncertainties, when possible. This is particularly important because these enter in a very different manner in the Bayesian model, as discussed above. Sometimes, only the mean values of the S factor or cross section are reported without any uncertainties whatsoever. Such results still provide useful information, but these S-factor data need to be implemented in a different manner in a Bayesian model. Instead of using Equation (14), one can choose to scale the true (unknown) S factor by a factor of 10^g, e.g., using a mildly informative prior of

$$g \sim U(-k, +k) \tag{18}$$

corresponding to a uniform prior between $-k$ and $+k$. In other words, the normalization factor, 10^g, is varied by up to k orders of magnitude up or down during the sampling. Such "relative data" provide only information on the energy dependence of the S factor, but little information on its absolute normalization. This method was applied in the analysis of the $D(p,\gamma)^3He$ reaction rate by J. Moscoso et al. (2021) for experiments that did not report any uncertainties.

Third, a suitable physical model for the true (unknown) S factor must be chosen in the data fitting. Reasonable choices are S factors computed using microscopic models, potential models, or R-matrix theory, because all of these are grounded in nuclear reaction theory. In the simplest case, when microscopic-model S factors are employed in the fitting, only a single physical parameter, i.e., the scale factor of the model S factor used, enters into the Bayesian analysis (see, e.g., A. Gómez Iñesta et al. 2017). A slightly modified strategy was pursued in J. Moscoso et al. (2021), who introduced two fitting parameters: a multiplicative scale factor, a, by which the microscopic-model S factor is multiplied, and an offset, b, according to

$$S_{\rm true}(E) \;=\; aS_{\rm model}(E) + b. \tag{19}$$

The rationale for this choice was that microscopic cross section calculations represent model-based Hamiltonian approaches with a priori difficult-to-quantify uncertainties. A bias in the microscopic-theory S factor may arise from the truncation of the set of basis states used to determine the matrix elements or the exclusion of operators in the Hamiltonian. These issues cannot be entirely disregarded, despite the fact that these types of model calculations are usually tuned to experimental scattering data and binding energies. The Bayesian fit returns estimates of the parameters a and b, which can be used to assess the microscopic-model S-factor prediction (i.e., by checking how much the fit results differ from the values of $a = 1$ and $b = 0$).

Fourth, polynomials are sometimes employed in the data fitting, which has a number of advantages: a simple form, well-known properties, moderate flexibility of shapes, and computational ease of use. However, they also have limitations: poor interpolatory and extrapolatory properties, a poor trade-off between degree and shape, and a disregard of nuclear theory. In extreme cases, these issues may lead to numerically unstable models. The use of polynomials is permissible for several reactions occurring during primordial nucleosynthesis, when the cross section datasets fully cover the astrophysically important energy region (V. Mossa et al. 2020; T.-H. Yeh et al. 2021). In the case of the $D(p,\gamma)^3He$ reaction, a comparison of results obtained with the two assumptions, a microscopic-model prescription versus a polynomial, gave consistent results, both for the derived mean S factor and the associated uncertainties (J. Moscoso et al. 2021). However, the adoption of polynomials as physical model functions should be avoided if the S factor needs to be extrapolated to energy regions devoid of data.

Fifth, choices have to be made for the probability density functions of all likelihoods and priors in Equation (9). Choices of priors have already been discussed above. In most Bayesian hierarchical models, normal (Gaussian) likelihood functions are assumed for describing statistical uncertainties of data points. Lognormal instead of normal likelihoods were adopted in C. Iliadis et al. (2016) and A. Gómez Iñesta et al. (2017). This was justified on the grounds of the central limit theorem: since astrophysical S factors are experimentally determined by products and ratios of several nuclear physics input quantities (e.g., measured signal intensities, incident beam charge, detection efficiencies, number of target nuclei, stopping powers, etc.), the probability density of the derived S factor will tend toward a lognormal distribution. Furthermore, a normal density function predicts a finite probability for negative values of the random variable, which is unphysical for manifestly positive quantities, such as astrophysical S factors. However, it was found that neither the S-factor fit nor the predicted parameters were sensitive to this choice for the reactions studied. Consequently, later publications employed normal likelihood functions (R. S. de Souza et al. 2019a, 2019b, 2020). The reason for this insensitivity is that Gaussian functions closely approximate lognormal densities when the uncertainties are not too large (say, if the standard deviation is $\lesssim$10% of the mean value).

Sixth, the type of numerical sampler needs to be considered carefully, depending on the complexity and magnitude of the parameter space. Suppose one wishes to analyze two independent datasets using a physical model S factor as given by Equation (19). In this case, the data analysis will involve six parameters: two physical model parameters (a and b), two parameters describing the extrinsic scatter in the two datasets, and two additional parameters for the normalization factors.

The computation is relatively simple from a numerical point of view, and can be performed, e.g., with Gibbs samplers (G. Casella & E. I. George 1992) that are implemented in software instruments such as JAGS (M. Plummer 2003) or NIMBLE (P. de Valpine et al. 2017). When the physical model becomes more complex, e.g., an R-matrix expression (see R. S. de Souza et al. 2019a; D. Odell et al. 2022a), several of the parameters may be highly correlated, giving rise to unacceptably slow convergence of the Markov Chains. In such a case, one must resort to more sophisticated samplers designed to handle the parameter correlations (C. J. F. ter Braak & J. A. Vrugt 2008; D. Foreman-Mackey et al. 2013).

5. Monte Carlo–based Reaction Rates

5.1. Overview

For the class II reactions referred to in Section 3, a Monte Carlo technique is used to estimate the reaction rates and associated uncertainties. This method was first described in detail by R. Longland et al. (2010). We provide a short summary here, together with a discussion of improvements made since 2010. The calculations are performed using the computer code RatesMC (R. Longland 2025), which is publicly available (Appendix D) and widely used by many research groups.

The Monte Carlo method relies on assigning probability density distributions to each input variable of the reaction rate calculation (e.g., resonance energies, partial widths, resonance strengths, and spectroscopic factors). Once these have been assigned, a random sample from each probability distribution is drawn. This forms the basis for a single reaction rate sample, which is calculated using Equations (1)–(8). The process of drawing random samples and calculating the reaction rate is repeated many times to obtain an ensemble of reaction rates. This represents the rate probability density, from which the recommended rate and uncertainties can be derived according to rigorously defined probabilities.

The task involves assigning probability distributions to each type of input parameter, with the central limit theorem playing a significant role in guiding these choices. For example, resonance energies are usually derived either from the difference of excitation energy and particle separation energy (Q value) or from an accelerator or magnet calibration. Low-energy resonances, in particular, are often determined using the former method. The central limit theorem states that the *sum* of many random variables is distributed normally, regardless of the form of the individual probability densities. This also implies a finite possibility for sampling a resonance with a negative energy. Such a case is treated consistently in our formalism as a subthreshold resonance, according to Equation (6).

Resonance strengths, partial widths, or nonresonant S factors, on the other hand, are derived from experimental yields. The conversion of a yield to a physical quantity involves the multiplication or division of several quantities (e.g., target thickness, detector efficiency, or beam current). In such cases, the central limit theorem states that the *product* of many random variables is distributed lognormally, regardless of the form of the individual probability densities. Since this probability density is only defined for positive values of the random variable, this choice is also consistent with the fact that these observables are manifestly positive. The lognormal distribution is given by

$$f(x) = \frac{1}{\sigma\sqrt{2\pi}}\frac{1}{x}e^{-(\ln x-\mu)^2/(2\sigma^2)},\ 0 < x < \infty \tag{20}$$

where μ and σ are the lognormal location and shape parameter, respectively, and "ln" denotes the natural logarithm. These parameters are related to the expectation (mean) value, $E[x]$, and variance, $V[x]$, by

$$\mu = \ln(E[x]) - \frac{1}{2}\ln\left(1 + \frac{V[x]}{E[x]^2}\right) \tag{21}$$

$$\sigma = \sqrt{\ln\left(1 + \frac{V[x]}{E[x]^2}\right)} \tag{22}$$

or, equivalently,

$$E[x] = e^{\mu+\sigma^2/2} \tag{23}$$

$$V[x] = e^{2\mu+\sigma^2}(e^{\sigma^2} - 1). \tag{24}$$

The median (50th percentile) of the lognormal distribution is given by $x_{\rm med} = e^{\mu}$, while the factor uncertainty, for a coverage probability of 68%, can be written as $f.u. \equiv e^{\mu+\sigma}/e^{\mu} = e^{\mu}/e^{\mu-\sigma} = e^{\sigma}$.

Reported values and uncertainties (i.e., for a resonance strength, partial width, or nonresonant S factor) can usually be equated with the expectation value, $E[x]$, and square root of the variance, $\sqrt{V[x]}$, respectively. The lognormal parameters are then found from Equations (21) and (22), allowing for random sampling according to Equation (20). In some cases, reported values and uncertainties of a given quantity are presented in the literature as $x_{\rm med}$ and $f.u.$. From these, the lognormal parameters can be determined with $\mu = \ln(x_{\rm med})$ and $\sigma = \ln(f.u.)$.

The Monte Carlo calculation of the reaction rate takes energy correlations explicitly into account. For example, when a narrow-resonance reaction rate is estimated from an energy and particle partial width of a resonance located near the particle threshold, and the resonance energy is sampled according to a normal probability density, the same sampled energy value must be used to estimate the particle partial width.

In this work, we provide a tabulation of the recommended reaction rate for a given temperature, including the median value (50th percentile) of the sampled reaction rate probability density. Additionally, we present "low" and "high" rates, corresponding to the 16th and 84th percentiles, respectively, which together cover a probability range of 68%. It is important to note that these values do not represent strict lower or upper limits, as there remains a 32% chance that the true (but unknown) reaction rate falls outside this interval.

Reaction rates are often (but not always) distributed according to a lognormal distribution, for reasons discussed in detail by R. Longland et al. (2010). If a rate is lognormally distributed, its median value is related to the lognormal location parameter by $x_{\rm med} = e^{\mu}$, and the factor uncertainty of the rate will be given by $f.u. = e^{\sigma}$ (see Section 4.3). Alongside the reaction rates, the tables also include the values of $f.u.$ at each temperature. Unlike the tabulated values for the low, median, and high rates, which are derived from the percentiles of the actual rate probability density, the values of $f.u.$ are based on the lognormal approximation of the reaction rate density.

5.2. Upper Limits of Partial Widths

For many resonances near the particle threshold, the particle partial width is neither known from experiment nor from theory. In such cases, the particle partial width cannot be described by normal or lognormal probability density functions. Instead, a physically motivated probability density can be derived using a fundamental assumption about the Gaussian orthogonal ensemble of random matrix theory. The dimensionless reduced width amplitude, $\theta_{\lambda c}$, appearing in Equation (5), is given by the sum of contributions from many different parts of the nucleon configuration space, with the sign and magnitude of a particular contribution being random from level to level and independent in sign and magnitude from all other parts. According to the central limit theorem, the probability density function of $\theta_{\lambda c}$ will then be approximately Gaussian, with an expectation value of zero. Consequently, the probability density function for $\theta^2_{\lambda c}$, i.e., the square of the amplitude, is given by a chi-squared distribution with 1 degree of freedom.

This probability density function, also known as Porter–Thomas distribution, can be written as (C. E. Porter & R. G. Thomas 1956)

$$f(\theta^2_{\lambda c}) = \frac{1}{\sqrt{2\pi\theta^2_{\lambda c}/\langle\theta^2_{\lambda c}\rangle}} e^{-\theta^2_{\lambda c}/(2\langle\theta^2_{\lambda c}\rangle)}. \quad (25)$$

The mean value, $\langle\theta^2_{\lambda c}\rangle$, may vary with increasing excitation energy because the complexity of the compound nucleus will increase. Therefore, the quantity $\langle\theta^2_{\lambda c}\rangle$ represents the local mean value, applicable to a given region of excitation energy. The above expression implies that the reduced widths for a single reaction channel, i.e., for a given nucleus and set of quantum numbers, vary by several orders of magnitude, with a higher probability for smaller values of the reduced width.

Random sampling and implementation of Equation (25) into the Monte Carlo reaction rate formalism require knowledge of $\langle\theta^2_{\lambda c}\rangle$. This quantity is not predicted by random matrix theory, but values can be obtained by analyzing a large body of data. A preliminary estimate (R. Longland et al. 2010) yielded values of $\langle\theta^2_p\rangle = 0.0045$ and $\langle\theta^2_\alpha\rangle = 0.010$ for protons and α particles, respectively, but disregarded any dependence on excitation energy or spin-parity. These results were used in C. Iliadis et al. (2010a, 2010b, 2010c) without an assigned uncertainty.

Subsequent work by I. Pogrebnyak et al. (2013) analyzed a larger dataset, in the target mass range of $A = 28-67$, using a maximum-likelihood method. They reported values of $\langle\theta^2_{\lambda c}\rangle$, including uncertainties, as a function of target mass and charge, excitation energy, spin-parity, and orbital angular momentum. For α particles, we adopted a global mean value of $\langle\theta^2_\alpha\rangle = 0.017$, with an uncertainty of a factor of 1.7, consistent with the results presented in Figures 2 and 3 of I. Pogrebnyak et al. (2013). For protons, the local mean values reveal a significant scatter, as displayed in their Figures 4 and 5. In the present work, we adopted a global value of $\langle\theta^2_p\rangle = 0.001$, with a factor of 5 uncertainty, which encompasses the reported local mean values. Using these numerical results, we described $\langle\theta^2_{\lambda c}\rangle$ by a lognormal probability density, and sampled values of an unknown reduced width, $\theta^2_{\lambda c}$, according to Equation (25).

It must be emphasized that reduced widths follow a Porter–Thomas distribution only if the nuclear matrix elements have contributions from many different parts of the configuration space. This is clearly not the case for low-lying bound levels of near closed-shell character or α-cluster states, where the matrix elements may be dominated by a few large contributions. However, such states frequently exhibit large values of $\theta^2_{\lambda c}$, and are, thus, likely to be observed in transfer reaction studies. If a level is too weak to be observed in a transfer study, it can be safely assumed that its reduced width can be estimated by sampling from a Porter–Thomas distribution.

When an upper limit of the reduced width of a given level has been determined experimentally, we sample the Porter–Thomas distribution of Equation (25) by truncating it at the experimental upper limit value.[7] For more details, see R. Longland et al. (2010).

5.3. Ambiguous Spins and Parities

The rate contribution of a resonance that has not been directly measured can be found by estimating the involved partial widths (see Equation (4)). If the J^π value of the resonance is not known unambiguously, only a range of orbital angular momenta, ℓ, can be determined. This ambiguity impacts the estimate of the particle partial width, according to Equation (5), through the ℓ-dependence of the penetration factor, P_c. In such cases, we describe the ambiguous spin-parity assignment by a discrete probability distribution, where each allowed J^π (or ℓ) value is assigned a weight reflecting the probability of a given choice. This probability distribution is implemented in the Monte Carlo sampling of the total rate. If such a resonance dominates the total rate, it may result in a multimodal rather than a lognormal rate probability density. In these cases, the tabulated values of the low, median, and high rates, and the factor uncertainty, *f.u.*, need to be interpreted carefully (see Section 5.1).

The method of including ambiguous spin-parity assignments in the Monte Carlo sampling of a total rate was first applied in P. Mohr et al. (2014), to which the reader is referred for details.

5.4. Correlations among Measured Resonance Energies and Strengths

In most experimental studies of nuclear reactions, the measured quantities are expected to be correlated. However, these correlations have not always been quantified in the literature, particularly in older work. Therefore, reasonable assumptions must be made to investigate the impact of such correlations on the total reaction rate. In the present work, we applied the procedures that were first discussed in R. Longland (2017) and R. Longland & N. de Séréville (2020) for resonance strength and resonance energy correlations, respectively. A brief summary is given below.

Resonance strengths and partial widths measured in a given experiment are expected to be correlated through a common normalization uncertainty. This arises from systematic uncertainties in the beam current, target composition, detector efficiency, etc. Frequently, strengths and widths are obtained relative to a well-known reference resonance. This issue will be discussed further in Section 7. It is reasonable to assume that the systematic uncertainties in the strength or partial

[7] Versions of RatesMC between 2013 and 2022 used a rejection sampling technique that favored small values of $\Gamma_{\lambda c}$. Tests revealed that this approach artificially reduced the recommended rate contributions from upper limit resonances by approximately 20%.

widths of this standard (and presumably strong) resonance dominate over the corresponding statistical ones. Furthermore, it can be assumed that the standard resonance has the smallest total uncertainty among the entire ensemble of resonances.

A correlation parameter, ρ_j, for the resonance j with measured strength, $\omega\gamma_j \pm \delta\omega\gamma_j$, can be estimated, according to R. Longland (2017),[8] by

$$\rho_j = \frac{\delta\omega\gamma_r}{\omega\gamma_r}\frac{\omega\gamma_j}{\delta\omega\gamma_j} = \frac{(f.u.)_r - 1}{(f.u.)_j - 1} \quad (26)$$

where the subscript r denotes the reference resonance, and $f.u.$ represents the factor uncertainty in the resonance strength. Since the reference resonance contains the smallest fractional uncertainty of a given dataset, $\rho_j \geqslant 1$.

Given the set of correlation parameters, ρ_j, the procedure to generate correlated Monte Carlo samples of the resonance strengths is as follows: (i) Generate normally distributed, uncorrelated random samples, i, of the strength for each resonance, j, denoted by $y_{j,i}$. (ii) Find the correlated samples, $y'_{j,i}$, according to

$$y'_{j,i} = \rho_j x_{r,i} + y_{j,i}\sqrt{1 - \rho_j^2} \quad (27)$$

where $x_{r,i}$ denotes the samples associated with the reference resonance, r. A visual inspection of this expression shows that, for fully correlated resonances, we find $\rho_j = 1$ and $y'_{j,i} = x_{r,i}$. In other words, the correlated samples for a given resonance are identical to those of the reference resonance. Conversely, if $\rho_j = 0$, then $y'_{j,i} = y_{j,i}$, and the uncorrelated samples remain unchanged. (iii) Calculate the correlated and lognormal samples of a given resonance strength with the factor uncertainty $(f.u.)_j$ from the mean value, $\omega\gamma_j$, by using

$$\omega\gamma_{j,i} = \omega\gamma_j (f.u.)_j^{y'_{j,i}}. \quad (28)$$

This procedure also holds for partial widths when $\omega\gamma$ is replaced by Γ_λ.

Correlated resonance energies can be treated similarly, with some modifications. First, resonance energy uncertainties are described by a normal, not lognormal, probability density (see Section 5.1). For resonance energies, $E_j \pm \delta E_j$, Equations (26) and (28) are replaced with

$$\rho_j = \frac{\delta E_r}{\delta E_j} \quad (29)$$

$$E_{j,i} = E_j + y'_{j,i}\delta E_j. \quad (30)$$

Second, energy correlations must be used to calculate the partial widths, as described in Section 5.1.

The correlations discussed above impact reaction rate uncertainties when multiple resonances contribute significantly to the total rate at a given temperature. When applied to resonance strengths, correlations can increase the rate uncertainties, in some cases by a factor of 3 (R. Longland 2017), compared to the case of uncorrelated strengths. The impact of resonance energy correlations depends not only on how many resonances contribute to the total rate but also on the energy location of these resonances with respect to the Gamow window. For example, R. Longland & N. de Séréville (2020) found that resonance energy correlations in the ^{35}Ar(p,γ)^{36}K reaction slightly decrease the rate uncertainty at 400 MK, but increase it somewhat in the ^{39}Ca(p,γ)^{40}Sc reaction at 30 MK. This effect is generally larger when only a few resonances contribute to the total rate and when they are all located on the same side of the Gamow peak.

The effect of resonance energy and strength correlations needs to be assessed selectively. Resonance strengths measured and scaled to a single reference resonance are expected to be correlated, while those derived from a single-nucleon transfer measurement are not. Such quantities are sensitive to DWBA model uncertainties that are not necessarily correlated, even within a single measurement. See Section 8 for more details.

6. Changes in Policy Compared to ETR10

Compared to the Monte Carlo–based thermonuclear reaction rate evaluation by C. Iliadis et al. (2010a, 2010b, 2010c; ETR10), several policy changes have been implemented. These changes are discussed below.

6.1. Masses and Reaction Q Values

The masses and Q values adopted in ETR10 were sourced from the 2003 Atomic Mass Evaluation (A. Wapstra et al. 2003). Two changes have been made in the present work. First, the *atomic* masses are now based on the 2020 Atomic Mass Evaluation (M. Wang et al. 2021). Second, because the interacting nuclei in a stellar plasma are fully ionized, *nuclear* instead of *atomic* masses are used in our reaction rate calculations. These masses are related by

$$m_{at}(A, Z) = m_{nu}(A, Z) + Zm_e - B_e(Z) \quad (31)$$

where A and Z denote the mass number and atomic number, respectively, m_e is the electron rest mass, and $B_e(Z)$ is the total electron binding energy in the neutral atom of the atomic number Z. We assign a positive sign to the binding energy. It can be approximated by the expression

$$B_e(Z) = 14.4381\, Z^{2.39} + 1.55468 \times 10^{-6} Z^{5.35}\ \text{eV}, \quad (32)$$

which is based on the neutral-atom electron binding energies calculated by K. N. Huang et al. (1976) using the relaxed-orbital relativistic Hartree–Fock–Slater formalism.

As can be seen from the factors involving the projectile and target masses in Equations (1), (4), and (8), the use of nuclear instead of atomic masses causes insignificant changes to the reaction rate (typically less than 0.1%). However, this distinction becomes important when reaction Q values are involved in the calculation. The Q values calculated from nuclear and atomic masses are related by

$$Q_{nu} = Q_{at} + \left(\sum_i B_e^i - \sum_f B_e^f\right) \quad (33)$$

where $\sum B_e^i$ and $\sum B_e^f$ are the sum of the total electron binding energies before and after the nuclear reaction, respectively.

For example, based on Equation (32), the total electron binding energy for Ar and K is 14.4 and 16.4 keV, respectively. This implies that the atomic Q value exceeds the nuclear counterpart by about 2 keV. As a result, when the Q value is derived from nuclear masses, the resonance

[8] Equation (18) of R. Longland (2017) contains an error in the second equality: the correlation parameter is not equal to the ratio of factor uncertainties. Instead, the correct expression is given by Equation (26).

energy—determined by both the energy of the excited state and the Q value—increases by 2 keV. This energy shift is significant because it enters exponentially in the expression, Equation (8), for the narrow-resonance reaction rate. For example, the ^{36}Ar(p,γ)^{37}K reaction rate decreases by ≈40% near 70 MK, when the nuclear instead of atomic Q value is adopted.

For this reason, many of our calculated center-of-mass resonance energies differ from the values adopted in ETR10 by a few keV. For more information on atomic versus nuclear Q values, see C. Iliadis (2019).

6.2. Excitation Energies, J^π Values, and Resonance Energies

In ETR10, level energies and J^π values predominantly relied on the evaluations of P. M. Endt (1990, 1998). In the present study, we primarily adopted the information for these quantities from the Evaluated Nuclear Structure Data File (ENSDF).[9] Notably, some nuclides in the ENSDF compilation have not been updated for over a decade. In such instances, we deemed it essential to take into account results published after the last update of ENSDF. The references, for a given reaction, are provided in the corresponding RatesMC input file (see Appendix D).

We have also modified the determination of resonance energies. The work of P. M. Endt (1990, 1998) often cited resonance energies directly measured from the energy location of thick- or thin-target yield curves. The procedure adopted in ETR10 was then to calculate center-of-mass resonance energies either from excitation energies and Q values or directly from laboratory resonance energies, opting for the method that provided the smaller uncertainty. In the present work, center-of-mass resonance energies, E_r, are always calculated using the expression

$$E_r = E_x - Q_{nu} \tag{34}$$

where E_r, E_x, and Q_{nu} are the center-of-mass resonance energy, excitation energy, and the nuclear Q value, respectively.

When possible, we disregarded resonance energies obtained from yield curves because they are influenced by laboratory electron screening. In contrast, values derived from Equation (34) are not impacted by this effect assuming that the excitation energies were derived from γ-ray spectroscopy. For the ^{27}Al(p,γ)^{28}Si resonance at a laboratory energy of 992 keV (Table 2), the screened energy (i.e., the one measured in the laboratory) is about 1.7 keV lower than the unscreened value (i.e., the one calculated from Equation (34)). Again, it is important to take an energy shift of this magnitude into account because the reaction rate depends exponentially on the resonance energy (see Equation (8)). Laboratory electron screening is discussed in more detail in Appendix C.2.

6.3. S Factor Parameterizations

Nonresonant reaction rates were discussed in Section 2.1. The procedure adopted in ETR10 was to approximate the experimental S factor by a polynomial

$$S(E) \approx S(0) + S'(0)E + \frac{1}{2}S''(0)E^2 \tag{35}$$

where the primes indicate derivatives with respect to the center-of-mass energy, E. The nonresonant reaction rate can then be conveniently calculated using an analytical expression (see Equations (6)–(8) in R. Longland et al. 2010). Furthermore, this expression was multiplied by a cutoff factor, given by (W. A. Fowler et al. 1975)

$$f_{\rm cutoff} = e^{-(T_9/T_{9,\rm cutoff})^2} \tag{36}$$

where $T_{9,\rm cutoff}$ corresponds to the temperature at which the S-factor expansion of Equation (35) becomes inaccurate. This scaling factor was chosen to ensure a smoothly diminishing nonresonant contribution at higher temperatures, but it has no physical significance. The cutoff temperature was found from an energy cutoff, which was typically set equal to the energy of the "first strong and not-too-narrow resonance" (W. A. Fowler et al. 1975).

In the present work, we did not adopt any of these procedures. Instead, we estimated experimental nonresonant S factors by fitting or normalizing the results of nuclear reaction models to data, and then numerically integrating Equation (1). To this end, the experimental nonresonant astrophysical S factor is entered in tabular form in the RatesMC input file.

Numerical tests were performed to assess the error previously introduced by the use of Equations (35) and (36). We found that this error is generally less than 10% in the ideal case of a constant S factor (i.e., $S'(0) = 0$ and $S''(0) = 0$), provided that the cutoff temperature is chosen appropriately. This error is frequently less than the estimated uncertainty in a typical nonresonant reaction rate at low temperatures. Nevertheless, numerical integration of the S factor, as performed in the present work, provides several advantages: (i) It allows for the accurate determination of the nonresonant rate, even in cases where the S factor may be poorly approximated by Equation (35). (ii) The maximum energy limit in the numerical integration can be defined unambiguously rather than by relying on a nonphysical expression such as Equation (36). (iii) It is straightforward to estimate the nonresonant rate uncertainty based on the energy-dependent uncertainty of the nonresonant S factor.

7. Experimental Resonance Strengths

It was mentioned in Section 2.3 that the strength of a narrow resonance, defined by Equation (7), is proportional to the area under the narrow-resonance cross section curve. For most narrow resonances, it is this area, rather than the cross section, that is determined in laboratory experiments. This is a fortunate circumstance, because the energies and strengths are the only parameters required to compute the narrow-resonance reaction rate, as can be seen from Equation (8). We focus in this section on directly measured resonances, as opposed to the indirect estimation of resonance strengths from spectroscopic factors or asymptotic normalization coefficients (see Section 2.2).

A detailed discussion of how to extract a resonance strength from the measured resonance yield of emitted reaction products is given in C. Iliadis (2015). Most experimental resonance strengths have been determined from the plateau height of the thick-target yield assuming an infinitely thick target, $Y^{\rm max}_{\Delta E\to\infty}$, by using

$$\omega\gamma = \frac{2\epsilon_r}{\lambda_r^2} Y^{\rm max}_{\Delta E\to\infty} \tag{37}$$

[9] See https://www.nndc.bnl.gov/ensdf/.

Table 2
Strength Standards of Directly Measured Resonances Adopted in the Present Reaction Rate Evaluation

Reaction	$E_r^{\rm lab}$ (keV)[a]	$\omega\gamma_{c.m.}$ (eV)[b]	Uncertainty	Reference
^{14}N(p,γ)^{15}O	278	$(1.26 \pm 0.03) \times 10^{-2}$	2.4%	c
^{18}O(p,γ)^{19}F	151	$(9.77 \pm 0.35) \times 10^{-4}$	3.6%	d
^{18}O(p,α)^{15}N	151	$(1.67 \pm 0.12) \times 10^{-1}$	7.2%	e
^{22}Ne(p,γ)^{23}Na	479	$(5.06 \pm 0.53) \times 10^{-1}$	11%	f
^{23}Na(p,γ)^{24}Mg	512	$(8.75 \pm 1.20) \times 10^{-2}$	14%	g
^{23}Na(p,α)^{20}Ne	338	$(7.16 \pm 0.29) \times 10^{-2}$	4.1%	h
^{24}Mg(p,γ)^{25}Al	223	$(1.27 \pm 0.09) \times 10^{-2}$	7.1%	i
…	419	$(4.16 \pm 0.26) \times 10^{-2}$	6.3%	j
…	823	$(5.54 \pm 0.53) \times 10^{-1}$	9.6%	k
^{25}Mg(p,γ)^{26}Al	435	$(9.42 \pm 0.65) \times 10^{-2}$	6.9%	j
…	591	$(2.28 \pm 0.17) \times 10^{-1}$	7.5%	l
^{26}Mg(p,γ)^{27}Al	338	$(2.73 \pm 0.16) \times 10^{-1}$	5.9%	j
…	454	$(7.15 \pm 0.41) \times 10^{-1}$	5.7%	j
…	1966	4.96 ± 0.43	8.7%	g
^{27}Al(p,γ)^{28}Si	406	$(8.63 \pm 0.52) \times 10^{-3}$	6.0%	j
…	632	$(2.55 \pm 0.15) \times 10^{-1}$	5.9%	g
…	992	1.84 ± 0.11	6.0%	g
^{28}Si(p,γ)^{29}P	369	$(2.03 \pm 0.24) \times 10^{-3}$	11.8%	n
^{29}Si(p,γ)^{30}P	417	$(2.13 \pm 0.24) \times 10^{-1}$	11.3%	n
^{30}Si(p,γ)^{31}P	620	1.89 ± 0.10	5.3%	g
^{31}P(p,γ)^{32}S	642	$(5.57 \pm 0.48) \times 10^{-2}$	8.6%	g
…	811	$(2.42 \pm 0.19) \times 10^{-1}$	7.9%	g
^{32}S(p,γ)^{33}Cl	588	$(2.91 \pm 0.44) \times 10^{-2}$	15.1%	n
^{34}S(p,γ)^{35}Cl	1211	4.37 ± 0.49	11%	g
^{35}Cl(p,γ)^{36}Ar	860	$(6.81 \pm 0.97) \times 10^{-1}$	14%	g
^{36}Ar(p,γ)^{37}K	918	$(2.58 \pm 0.24) \times 10^{-1}$	9.3%	m
^{37}Cl(p,γ)^{38}Ar	846	$(1.22 \pm 0.16) \times 10^{-1}$	13%	g
^{39}K(p,γ)^{40}Ca	2042	1.74 ± 0.19	11%	g
^{40}Ca(p,γ)^{41}Sc	1842	$(1.36 \pm 0.15) \times 10^{-1}$	11%	g

Notes.
[a] Resonance energy in the laboratory system.
[b] Resonance strength in the center-of-mass system.
[c] From Table IV of S. Daigle et al. (2016).
[d] Weighted average of values listed in Table V of F. R. Pantaleo et al. (2021).
[e] From H. W. Becker et al. (1995).
[f] Weighted average of P. M. Endt (1990), K. J. Kelly et al. (2015), and M. Williams et al. (2020).
[g] From B. Paine & D. Sargood (1979).
[h] From C. Rowland et al. (2002).
[i] From D. Powell et al. (1999).
[j] From D. Powell et al. (1998).
[k] Weighted average of H. P. Trautvetter (1975) and S. Engel et al. (2005).
[l] From M. Anderson et al. (1980).
[m] From P. Mohr et al. (1999).
[n] From Table 1 of D. Sargood (1982), estimated using the absolute value of a resonance strength involving a different isotope of the same element and the resonance strength ratio reported by G. Engelbertink & P. M. Endt (1966).

where ϵ_r is the stopping power, λ_r is the de Broglie wavelength of the projectile, and $Y^{\rm max}_{\Delta E\to\infty}$ denotes the plateau yield for an infinitely thick target. The kinematic quantities, ϵ_r and λ_r, are both evaluated at the resonance energy and refer to the center-of-mass system. Therefore, the quantity $\omega\gamma$ in Equation (37) is the center-of-mass resonance strength.

The maximum yield, $Y_{\rm max}$, is estimated from the number of emitted reaction products, the number of incident projectiles, the detector efficiency, the branching ratios, and the angular correlation effects. It must also be corrected for the finite target thickness used in the measurement.

When the target consists of a compound, X_aY_b, with n_X active nuclei and n_Y inactive nuclei per square centimeter, the quantity ϵ_r must be replaced by the effective stopping power, defined as

$$\epsilon_{\rm eff} \equiv \epsilon_X + \frac{n_Y}{n_X}\epsilon_Y \tag{38}$$

where $n_Y/n_X = b/a$. Note that $\epsilon_{\rm eff}$ is not the same as the total stopping power of a compound (C. Iliadis 2015).

While Equation (37) is useful for determining relative values of the resonance strength, it may not be applicable to estimate absolute resonance strengths. The main issues are as follows:

(i) The dependence of $\omega\gamma$ on the stopping power, ϵ_r, is usually adopted from tabulations[10] or codes, such as SRIM.[11]

[10] See https://physics.nist.gov/PhysRefData/Star/Text/PSTAR-t.html.
[11] See http://www.srim.org.

It is particularly difficult to estimate an uncertainty for these compiled stopping power values. An impression can be obtained from Table 4.3 in C. Iliadis (2015), where estimated stopping power uncertainties for protons and α particles in selected absorbers range from 4% to 8%. Nevertheless, much smaller uncertainties are sometimes adopted in the literature for determining resonance strengths, without any obvious justification.

(ii) In most cases, targets consist of compounds, and stopping powers are estimated using Bragg's (additivity) rule (W. H. Bragg & R. Kleeman 1905), which is implicitly adopted in the above definition of the effective stopping power. Bragg's rule states that the stopping power of a compound can be approximated by taking a weighted average of the stopping powers of its constituent elements, where the weights are usually based on the number of atoms of each element in the compound. The reliability of Bragg's rule is limited because the energy loss of an incident ion to the electrons in the absorber (i.e., the target) depends on the detailed atomic (electronic) structure. Consequently, differences in electron bonding between elemental materials and compounds can lead to inaccuracies in Bragg's rule. The inaccuracies can amount to up to 20% (J. F. Ziegler et al. 2010), depending on the identity and energy of the incident projectile, as well as on the nature of the absorber.

(iii) Corrections for incident beam spread, straggling, and the total resonance width have to be performed carefully to estimate $Y^{\rm max}_{\Delta E\rightarrow\infty}$ in Equation (37) from the measured yield.

The experimental resonance strength can also be found from

$$\omega\gamma \;=\; 2\frac{A_Y}{n\lambda_r^2} \tag{39}$$

where A_Y denotes the area under the resonance yield curve (i.e., the measured yield versus energy). The strength estimated using Equation (39) is independent of beam resolution, straggling, target thickness, stopping power, and resonance width, but requires knowledge of n, the number of (active) target nuclei per square centimeter. The latter quantity can be determined from the measured yield curve by using $n=\Delta E/\epsilon_r$, with ΔE denoting the center-of-mass target thickness in energy units. However, this introduces again a dependence of $\omega\gamma$ on the stopping power.

More reliable, absolute resonance strength values can be determined when the measurement is performed relative to Rutherford scattering (see, e.g., H. P. Trautvetter 1975). Some absolute resonance strengths have been determined by measuring Rutherford scattering *simultaneously* with the reaction of interest (D. Powell et al. 1998; C. Rowland et al. 2002). The results obtained with this technique are independent of the properties of the target (stopping power, stoichiometry, uniformity) and the beam (current integration, straggling). Therefore, they are more reliable than those depending on approximate stopping powers and stoichiometries.

Table 2 provides a set of measured absolute resonance strengths. Most of these values were determined relative to Rutherford scattering. Some of the results have been obtained in inverse-kinematics experiments, again relative to the Rutherford scattering yields. We have adopted these values as standards for normalizing relative resonance strengths (i.e., those obtained from tabulated stopping powers and assumed stoichiometries). A few of the listed values were not measured directly, but were estimated using the absolute value of a resonance strength involving a different isotope of the same element, together with the resonance strength ratio reported by G. Engelbertink & P. M. Endt (1966). The latter ratio was obtained from the ratio of the areas under the respective thin-target yield curves and, therefore, is independent of stopping powers, stoichiometries, beam resolution, straggling, target thickness, or total resonance width.

We address now the confusion in the literature regarding the definition of the resonance strength. First, the modern definition is given by Equation (7). In the older literature, the strength is defined by $S\equiv(2j_0+1)(2j_1+1)\omega\gamma=(2J+1)\Gamma_a\Gamma_b/\Gamma$, where j_0, j_1, and J denote the spin of the projectile, target, and resonance, respectively. The historical definition of the strength, S, is sometimes confused with the modern definition, $\omega\gamma$. Second, we already mentioned that all kinematic quantities in Equations (37) and (39) are given in the center-of-mass system. Since stopping power tabulations, or the code SRIM, provide laboratory values, some authors prefer to express the center-of-mass resonance strength, $\omega\gamma$, in terms of the laboratory stopping power, according to

$$\omega\gamma \;=\; \frac{2}{\lambda_r^2}\frac{M_1}{M_0+M_1}\epsilon_r^{\rm lab}Y^{\rm max}_{\Delta E\rightarrow\infty} \tag{40}$$

where the kinematic factor, $K\equiv M_1/(M_0+M_1)$, takes into account the conversion of the stopping power from the laboratory to the center-of-mass frame. If the center-of-mass de Broglie wavelength is expressed in terms of the laboratory resonance energy, we find

$$\frac{\lambda_r^2}{2} \;=\; \left(\frac{M_0+M_1}{M_1}\right)^2\frac{(\pi\hbar)^2}{M_0E_r^{\rm lab}}. \tag{41}$$

The square of the kinematic factor arises, first, from the definition of the reduced mass, and, second, from the laboratory-to-center-of-mass conversion of the resonance energy. From Equations (37), (40), and (41), we find

$$\omega\gamma \;=\; \left(\frac{M_1}{M_0+M_1}\right)^3\frac{M_0E_r^{\rm lab}}{(\pi\hbar)^2}\epsilon_r^{\rm lab}Y^{\rm max}_{\Delta E\rightarrow\infty}. \tag{42}$$

In the older literature, Equation (42) without the cube of the kinematic factor is sometimes used to define a *laboratory* resonance strength. However, the reported values have been mistakenly interpreted as center-of-mass strengths. This issue is discussed in G. Christian et al. (2013) for the ^{20}Ne(p,γ)^{21}Na reaction, where $K^3=0.86$. In other instances, K instead of K^3 appears mistakenly in the expression of the center-of-mass strength (see, e.g., A. Chafa et al. 2005).

Table 2 also includes a subset of standard resonance strengths based on the work of Sargood and collaborators (B. Paine & D. Sargood 1979; M. Anderson et al. 1980; D. Sargood 1982). Their strengths, which they refer to as "laboratory" values, are defined similarly to Equation (42), but with a kinematic factor of K^2 instead of K^3. This has caused considerable confusion, because their definition of "laboratory" strength differs from that in the older literature, as discussed above. In other words, their reported results must be multiplied by $K=M_1/(M_0+M_1)$ to arrive at the center-of-mass resonance strength, $\omega\gamma$. We have performed this correction for all values listed in Table 2.

8. Indirectly Estimated Particle Partial Widths

Unobserved low-energy resonances (i.e., those in the left-hand region of Figure 1) may completely dominate the total reaction rates at low temperatures. Therefore, the estimation of their contribution by indirect means is of crucial importance. We discuss now the overall uncertainty that can be assigned to a particle partial width, $\Gamma_{\lambda c}$, that is estimated indirectly, using Equation (6), when the spectroscopic factor, C^2S, is extracted from particle transfer data using DWBA theory (N. K. Glendenning 1983). Most of the discussion in this section is related to single-particle transfer reactions and proton partial widths. We will briefly comment on α-particle transfer reactions.

The uncertainty of C^2S will include contributions from both experimental parameters (e.g., counting statistics and the cross section normalization) and theoretical model approximations (e.g., parameters of the optical model for the entrance and exit channel, parameters determining the final-state radial wave function, finite range and nonlocality effects). In addition, except for subthreshold resonances, the levels for which we wish to estimate the partial width according to Equation (6) are unbound. In this case, the radial form factor no longer decays exponentially, but oscillates with a constant amplitude for large distances, causing difficulties in the numerical integration of the DWBA matrix elements. Some DWBA codes, e.g., the version of DWUCK4 extended by J. Comfort, account for this circumstance (C. M. Vincent & H. T. Fortune 1970; S. G. Cooper et al. 1982). With other codes, such as FRESCO (I. J. Thompson 1988), calculations are typically performed by initially assuming that the unbound level is weakly bound. The C^2S value is then estimated by extrapolating the theoretical cross section across the particle threshold to the measured excitation energy. The latter procedure is not rigorous and may contribute to the overall uncertainty. For weakly populated levels, additional sources of uncertainty need to be considered. For example, contributions from multistep (i.e., coupled-channel) processes and compound-nucleus formation can be evaluated quantitatively, but the reliability of such estimated corrections has not always been fully assessed.

Another source of uncertainty originates from specific choices for the total (j) and orbital (ℓ) angular momenta, and the principal quantum number (n), of the transferred particle. For odd-A target nuclei, the calculated DWBA cross section depends on the transferred orbital angular momentum, which may have contributions from two values, ℓ and $\ell + 2$. If the higher component dominates the stripping data, it is especially difficult to extract the C^2S value of the lower component from a two-component fit, even though the latter may dominate the total partial width. Often, both $j = \ell - 1/2$ and $j = \ell + 1/2$ can be added vectorially to the target spin to form the final-state spin (even if the latter is unambiguously known). Which j value to assume in the analysis is usually guided by shell-model arguments, which may be questionable, especially for unbound states. Similarly, it is not always obvious to decide which value of n to assume in the analysis. For example, in the middle of the *sd* shell, $1p$ hole states and $2p$ particle states may occur at about the same excitation energy, leading to the expectation that their configurations might mix.

A systematic evaluation of experimental proton and neutron spectroscopic factors in the $A = 21$–44 region has been reported by P. M. Endt (1977). The overall uncertainty of the experimental values was assessed by calculating ratios of C^2S values for pairs of stripping reactions populating the same level, e.g., (d, n) and (^{3}He, d) for proton transfer, and pairs of reactions exciting mirror states, e.g., (d, p) and (^{3}He, d); see also Appendix C.1. Deviations from unity in these ratios provide an estimate for the experimental uncertainty of individual measurements. P. M. Endt (1977) concluded that "for strong transitions, an error of about 25% should be assigned to measured spectroscopic factors." Considering the values listed in Tables I–X of P. M. Endt (1977), a "strong transition" refers to a C^2S value exceeding 0.1. P. M. Endt (1977) only considered bound states. The above result agrees with the uncertainty of $40\% \pm 24\%$ reported by W. J. Thompson & C. Iliadis (1999), who analyzed neutron spectroscopic factors in the *sd* shell for strong transitions to both bound and unbound levels up to 2.5 MeV excitation.

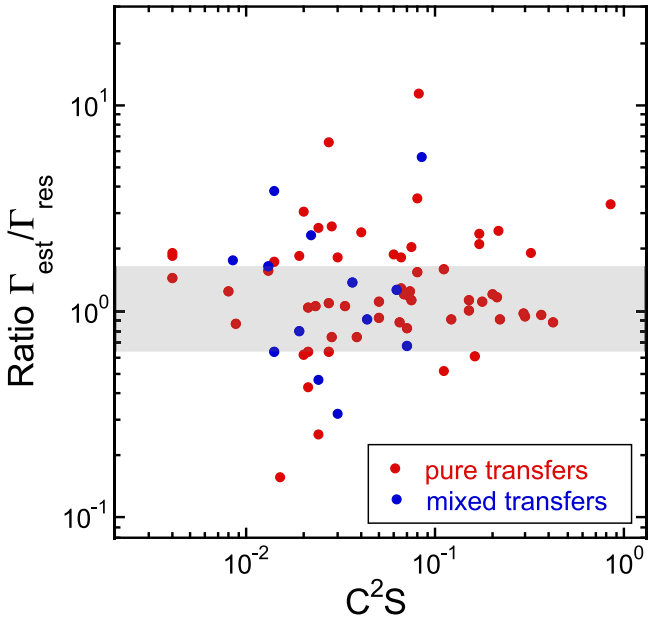

Figure 2. Ratio of proton partial widths estimated from Equation (6) to those measured in resonance reaction studies versus magnitude of the transfer spectroscopic factor, C^2S. The displayed data, courtesy of Art Champagne, form the basis of Figure 7 in S. E. Hale et al. (2004). The red and blue circles refer to pure and mixed transitions, respectively. The gray-shaded area indicates a factor of 1.6 uncertainty band. See text.

In Section 2.2, we pointed out that spectroscopic factors represent only intermediate steps in the calculation of the quantity of primary astrophysical interest, i.e., the particle partial width, $\Gamma_{\lambda c}$. Therefore, a different kind of test was performed in S. E. Hale et al. (2004), who compared proton partial widths estimated from proton-transfer spectroscopic factors (using Equation (6)) with those extracted from resonance reaction studies (i.e., elastic scattering or resonance strength measurements). This information was simultaneously available for 72 levels in $A = 21$–41 compound nuclei. The test included only unbound levels of known spin-parity with center-of-mass resonance energies below 2 MeV. In addition, their sample was limited to levels with total widths of $\Gamma < 20$ keV, and excluded mixed-ℓ transitions, for which the strength of the lower ℓ component could not be extracted from the measured angular distribution. The data are displayed in Figure 2. The red and blue circles denote pure and mixed transitions, respectively. For the whole set, the ratios deviate on average from unity by a factor of 1.6 (gray band), with no significant difference in the scatter of the red or blue circles. We suspect that the average uncertainty of a proton partial

width estimated indirectly using a C^2S value is less than a factor of 1.6, because the above comparison disregarded the uncertainties of the partial widths measured in the resonance reactions. We also emphasize that the results presented in Figure 2 are subject to selection bias, because it is easier in an experiment to populate a single-particle state (with a large C^2S value) than one with a complex nucleon configuration (implying a small C^2S value). In particular, Figure 2 provides no information on uncertainties when the C^2S value is smaller than, say, 0.01. Additional systematic studies of this kind are highly desirable.

In the absence of more information, we adopted the following uncertainties for proton (or neutron) partial widths estimated from reported experimental spectroscopic factors, depending on the magnitude of C^2S: we assumed an uncertainty factor of 1.6, 2, and 3 for $C^2S > 0.1$, $0.1 \geqslant C^2S \geqslant 0.01$, and $C^2S < 0.01$, respectively. When additional information was available, e.g., when authors carefully assessed the impact of the systematic effects mentioned above and obtained smaller uncertainties, we generally adopted their reported values. For example, C. Marshall et al. (2020) performed an MCMC investigation of the ^{70}Zn(d, ^{3}He)^{69}Cu proton pick-up reaction to estimate the uncertainties of spectroscopic factors derived from a DWBA analysis. They found uncertainties ranging from 35% to 108%, depending on the state populated. Additional examples of using statistical methods to quantify uncertainties arising from optical-model potentials can be found in G. B. King et al. (2018), F. Flavigny et al. (2018), and A. E. Lovell et al. (2017).

The above uncertainty factors apply to proton (or neutron) partial widths. The uncertainties are generally larger when estimating α-particle partial widths from α-particle spectroscopic factors. Because systematic studies comparing α-particle transfer and capture are scarce, we determined the uncertainties in our estimated α-particle partial widths on a case-by-case basis. We emphasize again that, for either nucleons or α-particles, the same potential parameters used in the extraction of C^2S values from transfer data must also be employed in the calculation of the partial widths (H. T. Fortune & A. G. Lacaze 2003). See Appendix A.

9. Direct Radiative Capture

For reactions of type (p,γ) or (α,γ), the direct radiative capture process contributes to the nonresonant S factor (R. Christy & I. Duck 1961; C. Rolfs 1973; K. H. Kim et al. 1987; E. Krausmann et al. 1996). We computed this contribution using a single-particle potential model, together with experimental spectroscopic factors.

The potential model assumes a single-step process, where the projectile is directly captured, without formation of a compound nucleus, into a final bound state with the emission of a photon. The electric dipole (E1) part of the total direct-capture cross section usually dominates over the E2 and M1 contributions, except in cases involving α-particle capture on self-conjugate (i.e., $N = Z$) target nuclei, where the E1 contribution is isospin suppressed.

The E1 contribution to the theoretical cross section (in microbarns) for capture from an initial scattering state with the orbital angular momentum ℓ_i to a final bound state with the orbital angular momentum ℓ_f and principal quantum number n (i.e., the number of wave function nodes) is given by (C. Rolfs 1973)

$$\sigma^{DC}(E1, n, \ell_i, \ell_f) = 0.0716\mu^{3/2}\left(\frac{Z_0}{M_0} - \frac{Z_1}{M_1}\right)^2 \times \frac{E_\gamma^3}{E^{3/2}}\frac{(2J_f+1)(2\ell_i+1)}{(2j_0+1)(2j_1+1)(2\ell_f+1)} \times (\ell_i 010|\ell_f 0)^2 R^2_{n\ell_i 1\ell_f} \quad (43)$$

and

$$R_{n\ell_i 1\ell_f} = \int_0^\infty u_s(r)\mathcal{O}_{E1}(r)u_b(r)dr \quad (44)$$

where μ is the reduced mass, Z_0, Z_1 and M_0, M_1 are the charges and nuclear masses (in u), respectively, of the projectile and target; j_0, j_1, J_f are the spins of the projectile, target and final state, respectively; E and E_γ are the center-of-mass energy and the energy of the emitted γ-ray, respectively; $\mathcal{O}_{E1}$ is the radial part of the E1 multipole operator; and u_s and u_b are the radial wave functions of the initial scattering state and final bound state, respectively.

The radial bound-state wave function, with $u_b(r = 0) = 0$ and $\int_0^\infty u_b^2 dr = 1$, was generated using a potential consisting of Woods–Saxon, angular momentum, and Coulomb terms, given by

$$V(r) = \frac{-V_0}{1 + e^{(r-R_{\rm WS})/a}} + \frac{\hbar^2}{2\mu}\frac{\ell_f(\ell_f+1)}{r^2} + V_C(r) \quad (45)$$

where $R_{\rm WS} = r_0 A_1^{1/3}$ and a are the Woods–Saxon potential radius[12] and diffuseness, respectively; A_1 is the mass number of the target nucleus; V_C corresponds to a uniformly charged sphere of the radius $R_{\rm WS}$. The well depth, V_0, was chosen to reproduce the binding energy of the final state. The calculation of the radial scattering wave function will be discussed at the end of this section.

The radial integration in Equation (44) was performed to 500 fm, because for some weakly bound states close to the particle threshold the integrand has a maximum located far beyond the nuclear radius at the lowest center-of-mass energies explored here. For the same reason, and defining $\rho \equiv k_\gamma r$, where $k_\gamma = E_\gamma/\hbar c$ is the wavenumber of the emitted photon, we used the exact expression for the radial part of the E1 operator (G. Bailey et al. 1967)

$$\mathcal{O}_{E1} = \frac{3r}{\rho^3}[(\rho^2 - 2)\sin\rho + 2\rho\cos\rho] \quad (46)$$

instead of its long-wavelength approximation, $\mathcal{O}_{E1} \approx r$, which only applies if $\rho \ll 1$.

The cross section computed using the single-particle potential model described above must be multiplied by the spectroscopic factor to account for the fractional parentage of the initial and final states. When the direct capture to a specific final state can proceed via several values of orbital angular momenta, ℓ_i and ℓ_f, the cross section is given by an

[12] Alternative formulations for the Woods–Saxon potential radius exist, such as: $R_{\rm WS} = r_0(A_0^{1/3} + A_1^{1/3})$ or $R_{\rm WS} = r_0(A_0 + A_1)^{1/3}$.

incoherent sum,

$$\sigma^{DC}_{\rm total} = \sum_k \sum_{\ell_i \ell_f} C^2 S_{k\ell_f} \sigma^{DC}_k(n, \ell_i, \ell_f) \quad (47)$$

with S and C denoting the spectroscopic factor and isospin Clebsch–Gordan coefficient (not to be confused with the ANC discussed below), respectively. The index k runs over all bound states of the final nucleus.

The calculated single-particle cross section, σ^{DC}_{sp}, will depend strongly on the adopted choice of the Woods–Saxon potential radius parameter, r_0, and diffuseness, a. Similar to the discussion in Section 2.2, this means that the bound-state wave functions entering in the calculation of the direct-capture cross section (see Equations (43) and (44)) and the DWBA differential cross section (when the spectroscopic factor is extracted from stripping data) must be generated using the same Woods–Saxon potential parameters to avoid systematic bias.

When the direct capture proceeds at low bombarding energy to a weakly bound final state, the integrand in Equation (44) will peak outside the nuclear radius. For such a peripheral reaction, the single-particle radial bound-state wave function is asymptotically given by (A. M. Mukhamedzhanov et al. 2001)

$$u_{b,\ell_f}(r) \rightarrow b_{\ell_f} W_{-\eta,\ell_f+1/2}(2\kappa r) \quad (48)$$

where b_{ℓ_f} is the single-particle asymptotic normalization coefficient, and W is the Whittaker function (D. Hebbard & B. Robson 1963); κ is the bound-state wavenumber, with $\kappa^2 = 2\mu E_b/\hbar^2$, where μ is the reduced mass, and $E_b = Q - E_x$ is the binding energy of the final state; $\eta = eZ_0Z_1\mu/(\kappa\hbar^2)$ is the bound-state Coulomb parameter.

In a microscopic nuclear model, the capture cross section can be described in terms of the overlap function, I_B, and a many-body wave function for the relative motion. Assuming a single-particle model, the radial dependence of the overlap function, which represents the projection of the bound final state onto the product bound-state wave functions of the target and projectile, can be approximated by

$$I_B(r) \approx \sqrt{C^2 S_{\ell_f}}\, u_{b,\ell_f}(r). \quad (49)$$

At large distances between the target and projectile, the complicated many-body effects will diminish, and the radial dependence of the overlap function becomes asymptotically

$$I_B(r) \rightarrow C_{\ell_f} W_{-\eta,\ell_f+1/2}(2\kappa r) \quad (50)$$

where C_{ℓ_f} is the asymptotic normalization coefficient (ANC). A comparison of Equations (48)–(50) yields the relationship between $C^2S_{\ell_f}$, C_{ℓ_f}, and b_{ℓ_f} (A. M. Mukhamedzhanov et al. 2001)

$$C^2 S_{\ell_f} = \frac{C^2_{\ell_f}}{b^2_{\ell_f}}. \quad (51)$$

In this approach, $C^2_{\ell_f}$ appears as an observable quantity, while both $C^2S_{n\ell_f}$ and $b^2_{\ell_f}$ are derived quantities that depend strongly on the parameters of the adopted single-particle potential model. In other words, for peripheral reactions, the substitution of Equation (51) into Equation (47), and adopting experimental ANCs obtained from transfer reactions, will yield a direct capture cross section that is relatively insensitive to the Woods–Saxon potential parameters. For a comparison of the two methods just discussed, see P. F. Bertone et al. (2002).

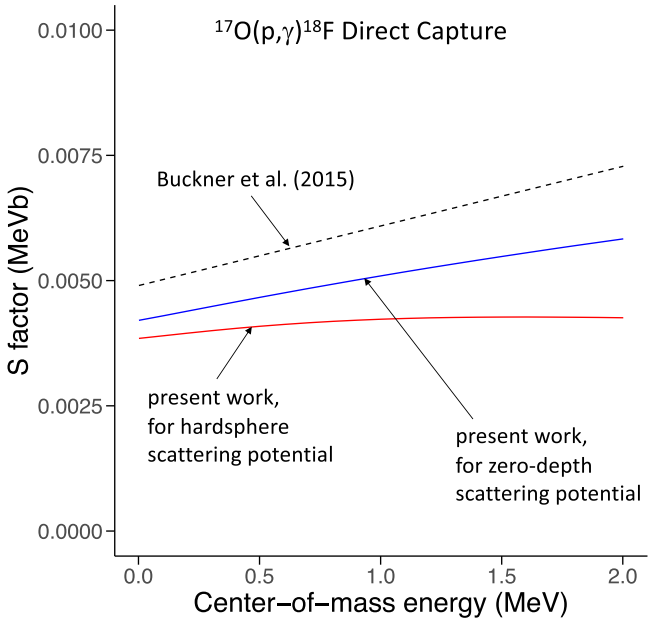

Figure 3. Direct-capture S factor in ^{17}O(p,γ)^{18}F, summed over transitions to 21 levels in ^{18}F. (Blue line) S factor calculated from Equation (47), assuming a zero-depth nuclear potential for the calculation of the radial scattering wave function, u_s. (Red line) S factor calculated from Equation (47), assuming a hard-sphere scattering potential. (Dashed black line) From M. Q. Buckner et al. (2015). Note that the blue and black lines agree within ≈20%. See text for details.

The last ingredient needed to compute the direct capture S factor is the radial scattering wave function (see Equation (44)). Beyond the range of the nuclear potential, it is given by

$$u_s(r) = F_{\ell_i}(r)\cos\delta_{\ell_i} + G_{\ell_i}(r)\sin\delta_{\ell_i} \quad (52)$$

where δ_{ℓ_i} is the nuclear phase shift, and F_{ℓ_i} and G_{ℓ_i} are the regular and irregular Coulomb wave functions, respectively. At low bombarding energies, the scattering phase shifts for the charged-particle reactions of interest in the present work are small and have usually not been measured. Therefore, we have assumed $\delta_{\ell_i} \approx 0$, or $u_s(r) \approx F_{\ell_i}(r)$, corresponding to the assumption that the scattering potential is zero. In the past, hard-sphere scattering phase shifts have been adopted in many low-energy direct capture calculations. This issue was discussed by C. Iliadis & M. Wiescher (2004), who showed that the adoption of a zero-energy instead of a hard-sphere nuclear scattering potential better reproduces the measured direct capture cross section, especially for deeply bound states.

To test the method, Figure 3 presents the total direct capture S factor in the ^{17}O(p,γ)^{18}F reaction, incorporating all contributions from bound final states in ^{18}F. The blue and red lines are derived from Equation (47), assuming zero-depth and hard-sphere scattering potentials, respectively. The experimental spectroscopic factors were adopted from the transfer measurements by L. M. Polsky et al. (1969) and V. Landre et al. (1989). The dashed black line represents the estimate from M. Q. Buckner et al. (2015) using an independent approach. It involved the direct measurement of the ^{17}O(p,γ)^{18}F cross section for the strongest transitions at low bombarding energies (below approximately 300 keV) and the

extraction of the direct components by fitting the measured partial yields. It can be seen that the dashed black and solid blue lines agree within ≈20%, which supports the method employed in this study for estimating the total direct capture S factor using single-particle potential model calculations weighted by experimental spectroscopic factors.

The uncertainties assigned to direct capture cross sections are based on a combination of available experimental data and our judgment. All direct capture uncertainties were determined on a case-by-case basis: in favorable cases, when the results of multiple transfer measurements were consistent, we adopted a 30% uncertainty; in contrast, when data are sparse or of questionable quality, we increased the uncertainty to factors between 3 and 5 (see also the discussion in Section 8).

We will now comment on interference effects between resonant and nonresonant (direct) capture. In principle, such effects need to be considered, depending on the angular momenta involved, when estimating the total cross section from a measured differential one. However, the impact of such interference effects on the total reaction rates is often negligible because the vector coupling coefficients in the interference expression (see, e.g., Equation (A.38) in C. Rolfs 1973) are frequently zero. For example, the Clebsch–Gordan coefficient, $(\ell_R 0 \ell_i 0 | k 0)$, entering the expression for $k = 0$ (i.e., the term impacting the total cross section) vanishes unless the orbital angular momenta of the resonant and direct capture, ℓ_R and ℓ_i, respectively, are equal. Similar arguments apply to the coefficient $(L_R 1 L_D -1 | k 0)$, where L_R and L_D denote the γ-ray multipolarities of the resonant and direct capture process, respectively. As a result, interference effects in the total cross section have been ignored for all reactions evaluated in this work.

We already mentioned that usually the E1 contribution dominates the total direct capture cross section. However, in the case of α-particle capture on self-conjugated target nuclei (i.e., $N = Z$), the E1 component becomes small owing to the factor $(Z_0/M_0 - Z_1/M_1)^2$ in Equation (43). In such cases, the total direct capture cross section is usually dominated by the E2 component. We estimated this contribution along similar lines to what we discussed for the E1 component above. There are two main differences.

First, it is important to accurately account for the number of nodes, N, in the bound-state wave function of the α-particle. This value, along with the orbital angular momentum, L_f, is determined by the Talmi–Moshinsky relation (M. Moshinsky 1959)

$$2N + L_f = \sum_k (2n_k + \ell_{f,k}). \quad (53)$$

Here, n_k and $\ell_{f,k}$ represent the principal quantum number and orbital angular momentum, respectively, of the nucleons involved in the transfer. This equation applies to the three-dimensional harmonic oscillator and ensures the conservation of total oscillator quanta across different coordinate transformations (e.g., from single-particle to relative and center-of-mass coordinates of the α-particle cluster). Consider the example of an α-particle transfer to low-lying bound states of ^{28}Si from ^{24}Mg. For bound states of positive parity, a typical $(sd)^4$ configuration suggests that $2N + L = 8$, while, for configurations where the transferred nucleons are in a $(sd)^3(fp)$ arrangement, $2N + L = 9$.

Second, experimental α-particle spectroscopic factors, often derived from reactions such as (^{6}Li,d) or (^{7}Li,t), exhibit substantially greater uncertainties compared to those of single-particle spectroscopic factors discussed in Section 8. This variation can be substantiated by comparing values obtained from independent DWBA analyses conducted at various bombarding energies. A primary source of uncertainty stems from the choice of optical-model potentials used for both the incoming (e.g., ^{6}Li) and outgoing (e.g., d) scattering channels. In our study, we have assigned a conservative uncertainty factor of 5 to the estimated E2 direct capture component for a transition to a given bound state. As previously emphasized, to reduce bias, it is crucial to consistently use the same bound-state potential parameters and number of nodes, N, in the direct capture calculations as were used in the DWBA analysis of the α-transfer data.

10. Rate Extrapolation to High Temperatures

Previously, we discussed how to estimate statistically meaningful reaction rates based on the available nuclear physics input. However, for a number of reasons, any experiment will have an associated cutoff at some maximum bombarding energy. This cutoff may be dictated by the highest energy attainable by a particle accelerator. Alternatively, measurements may be terminated at an energy where data analysis becomes intractable, possibly because of strongly overlapping resonances that obscure the resonance structure. This implies that the total reaction rate can be computed directly with the methods discussed so far only up to a limiting temperature. Therefore, a method of extrapolation is required to estimate the total rate all the way up to a temperature of 10 GK.

The process of extrapolating a total reaction rate to higher temperatures can be broadly divided into two tasks. First, the lowest temperature at which the available experimental information is no longer sufficient to calculate the reaction rate reliably needs to be estimated. Second, based on this temperature limit, the extrapolation must be performed. In the present work, we follow the procedure detailed in J. R. Newton et al. (2008). At any given temperature, an effective thermonuclear energy range (ETER) is determined, which is based on the experimental distribution of fractional resonant-rate contributions.

Specifically, the ETER for a given temperature is obtained by the following steps: (i) The cumulative distribution of fractional resonant rates is computed, which resembles a step function. (ii) The 50th percentile (i.e., the median) of the cumulative distribution is identified with the energy location, $E(T^{\rm ETER})$, of the ETER. (iii) The 8th and 92nd percentiles of the cumulative distribution define the energy width, $\Delta E(T^{\rm ETER})$, of the ETER. This energy region has generally a significantly different location and width compared to the Gamow peak. See J. R. Newton et al. (2008) for details.

As the temperature increases, the ETER moves to a higher energy and becomes broader. A limiting temperature, $T_{\rm match}^{\rm ETER}$, is eventually reached, where the upper boundary of the ETER coincides with the maximum bombarding energy, $E_{\rm max}^{\rm exp}$, for which experimental information is available. This matching temperature is given by the condition

$$E(T_{\rm match}^{\rm ETER}) + \Delta E(T_{\rm match}^{\rm ETER}) = E_{\rm max}^{\rm exp}. \quad (54)$$

For temperatures beyond $T_{\rm match}^{\rm ETER}$, the total rate must be found by extrapolation.

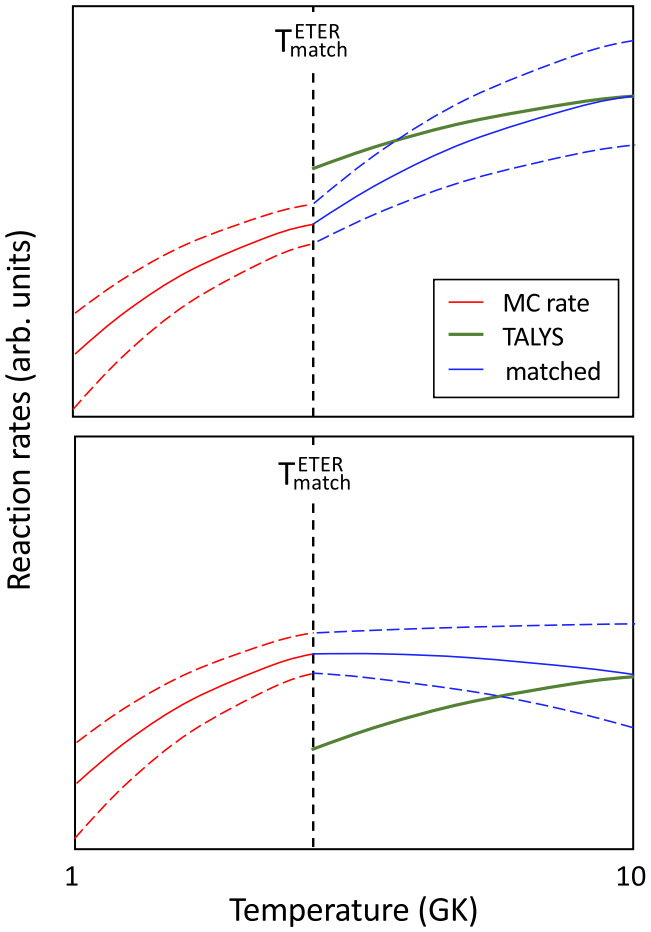

Figure 4. Matching of experimental Monte Carlo rates (red) to TALYS results (green) at high temperatures. The top and bottom panels depict the situation where the TALYS rates at the matching temperature, $T_{\rm match}^{\rm ETER}$ (vertical dashed line), are larger and smaller, respectively, than the median experimental rate. In either case, the TALYS prediction at the highest temperature, 10 GK, is adopted at face value, with an assumed uncertainty of a factor of 10. The matched rates and their uncertainties (blue) beyond $T_{\rm match}^{\rm ETER}$ are found from connecting the experimental rates at $T_{\rm match}^{\rm ETER}$ to the TALYS results at 10 GK, according to Equation (55). All rates depicted here refer to laboratory rates (i.e., assuming that the target is in its ground state).

To perform the rate extrapolation, we adopted theoretical estimates of reaction rates based on the statistical (Hauser-Feshbach) model of nuclear reactions. These have been calculated using TALYS, which is a modern nuclear reaction code that includes many state-of-the-art nuclear models to cover the main reaction mechanisms (A. Koning et al. 2023). In particular, TALYS was updated to estimate nuclear reaction rates of relevance to astrophysics. The uncertainties of the TALYS predictions have mainly two origins: (i) the description of the reaction mechanism, i.e., the model of formation and deexcitation of the compound nucleus, including a possible preequilibrium and direct capture contribution; and (ii) the evaluation of the nuclear quantities entering the calculation of the transmission coefficients for each entrance and exit channel. For more information, see A. L. Sallaska et al. (2013).

As a final step, experimental Monte Carlo–based rates must be matched to the TALYS results at the matching temperature, $T_{\rm match}^{\rm ETER}$. We adopted the procedure depicted in Figure 4. The top and bottom panels correspond to situations where the estimated TALYS rate is larger and smaller, respectively, than the median experimental rate at $T_{\rm match}^{\rm ETER}$ (vertical dashed line). In either case, the TALYS rate at the highest temperature, 10 GK, is adopted at face value, and the matched recommended rate between $T_{\rm match}^{\rm ETER}$ and 10 GK is found from the expression

$$\langle \sigma v \rangle_{\rm rec} = \langle \sigma v \rangle^{\rm TALYS} \times \left[\left(\frac{10 - T_9}{10 - T_{\rm match}^{\rm ETER}} \right) \times \frac{\langle \sigma v \rangle_{\rm match}^{\rm ETER}}{\langle \sigma v \rangle_{\rm match}^{\rm TALYS}} + \left(\frac{T_9 - T_{\rm match}^{\rm ETER}}{10 - T_{\rm match}^{\rm ETER}} \right) \right] \quad (55)$$

where $\langle \sigma v \rangle^{\rm TALYS}$ is the temperature-dependent TALYS rate, and $\langle \sigma v \rangle_{\rm match}^{\rm ETER}$ and $\langle \sigma v \rangle_{\rm match}^{\rm TALYS}$ are the experimental and TALYS rates at the matching temperature, $T_{\rm match}^{\rm ETER}$, respectively, in units of gigakelvin.

The uncertainties of the matched rate are found from a similar procedure. We assumed a factor 10 uncertainty for the TALYS rate at 10 GK. The TALYS high and low bounds are then connected to the high and low experimental rates, respectively, at $T_{\rm match}^{\rm ETER}$ using an expression similar to Equation (55).

The procedure for matching reaction rates at elevated temperatures in the present evaluation differs from that employed in ETR10 (C. Iliadis et al. 2010c). These differences are discussed in detail in Appendix F.

11. Use of Present Reaction Rates in Nucleosynthesis Studies

A number of recent studies have examined how uncertainties in thermonuclear reaction rates affect nucleosynthesis predictions obtained from reaction network simulations. Examples include sensitivity studies of Big Bang nucleosynthesis (C. Iliadis & A. Coc 2020), classical novae (A. Psaltis et al. 2025; E. Wallace et al. 2025), presolar grain isotopic signatures (C. Iliadis et al. 2018; L. Downen et al. 2022a; L. Ward et al. 2025), and abundance anomalies in globular cluster stars (J. R. Dermigny & C. Iliadis 2017). These investigations share two principal goals: (1) to determine realistic final abundance yields and quantify their uncertainties arising from thermonuclear reaction rate uncertainties, and (2) to identify which reaction(s) contribute most strongly to the final abundance uncertainty of a given nuclide.

In contemporary sensitivity studies, Monte Carlo methods are used to vary all reaction rates simultaneously in each network run. Forward and reverse rates associated with the same reaction are not sampled independently; instead, their variations are correlated according to the reciprocity theorem. Previous work has shown that thermonuclear reaction rates are well described by lognormal probability density functions (R. Longland et al. 2010); see also Section 5.1. Accordingly, a sampled rate, x, for a given reaction j at the temperature T is drawn from

$$f[x(T)_j] = \frac{1}{\sigma\sqrt{2\pi}} \frac{1}{x(T)_j} e^{-\frac{[\ln x(T)_j - \mu(T)_j]^2}{2\sigma(T)_j^2}} \quad (56)$$

where the lognormal parameters μ and σ represent the location and spread, respectively.

Sampling is performed using (R. Longland et al. 2012)

$$x(T)_{kj} = x(T)_{{\rm med},j} \, [f.u.(T)]_j^{p(T)_{kj}} \quad (57)$$

where $x_{\rm med}$ is the median rate, and *f.u.* is the tabulated factor uncertainty. The variation exponent p_{kj} is drawn from a standard normal distribution (mean = 0, standard deviation = 1). Importantly, p_{kj} is sampled once per reaction per network run and remains fixed for all temperatures in that run. Repeating the simulation for n Monte Carlo samples produces an ensemble of final abundance yields. For each nuclide, the 50th percentile defines the median abundance $X_{\rm med}$, while the 16th and 84th percentiles give $X_{\rm low}$ and $X_{\rm high}$. The corresponding abundance factor uncertainty is $\Delta f = \sqrt{X_{\rm high}/X_{\rm low}}$ corresponding to a 68% coverage interval.

The influence of a reaction's rate uncertainty on the abundance of a given nuclide is assessed by correlating its variation exponent p_{kj} with the resulting final abundance X_f across the ensemble of Monte Carlo runs. Earlier work used Pearson's linear correlation coefficient r (e.g., A. Coc et al. 2014), or Spearman's rank–order correlation coefficient r_s (C. Iliadis et al. 2015). However, correlations encountered in nucleosynthesis simulations are often neither linear nor monotonic, limiting the usefulness of r and r_s.

A more robust alternative is the mutual information (MI) metric from information theory (E. H. Linfoot 1957; T. M. Cover & J. A. Thomas 2006). MI measures how much knowing one random variable (here, p_{kj}) reduces the uncertainty in another (the final abundance X_f). For random variables Y and Z with values $\{y_i\}$ and $\{z_j\}$, respectively,

$$MI = \sum_y \sum_z P(y, z) \log \left[\frac{P(y, z)}{P(y)\, P(z)} \right] \quad (58)$$

where $P(y)$ and $P(z)$ are the marginal distributions, and $P(y, z)$ is the joint probability distribution. By definition, $MI = 0$ if and only if the variables are statistically independent. MI therefore provides a model-agnostic measure of reaction importance.

The laboratory reaction rates evaluated in this work cover a significant fraction of charged-particle reactions relevant to nucleosynthesis in the Big Bang, classical novae, low–mass and asymptotic giant branch stars, and other astrophysical environments. Before use in nucleosynthesis simulations, these rates must be corrected for the thermal population of target excited states at elevated temperatures.

However, a reaction network may also include reactions for which no Monte Carlo reaction rates are currently available. For such cases (e.g., class III reactions; see Section 3), we recommend that users approximate the rate factor uncertainty by $f.u. = \sqrt{\rm High/Low}$ (Appendix E.2), assuming the rate is lognormally distributed. Here, "high" and "low" denote literature estimates of the upper and lower rate bounds. Unlike the statistically rigorous uncertainties derived in the present work, these values are only approximations and may be adjusted at the discretion of the user when incorporating non–Monte Carlo literature rates into network calculations.

12. Summary

In this work, we have presented a comprehensive analysis of nuclear reaction rates using modern statistical approaches, including Bayesian inference and Monte Carlo methods. We discussed the fundamental reaction rate formalism and outlined the improvements these methods offer in estimating reaction rates more accurately.

Our results highlight the advantages of Bayesian-based reaction rates, particularly in incorporating prior knowledge and systematically accounting for uncertainties. Additionally, we demonstrated how Monte Carlo–based reaction rates provide a robust framework for propagating uncertainties and capturing correlations among nuclear parameters.

Experimental resonance strengths and indirectly estimated partial widths were examined in detail, emphasizing their impact on reaction rate calculations. Furthermore, we discussed direct radiative capture and the extrapolation of reaction rates to high-temperature environments relevant for astrophysical scenarios.

As the main product of this study, we provide in Appendix E a dataset of 78 reaction rates tabulated on a specified temperature grid. For each reaction, we present the fractional contributions to the total rate along with the total rate uncertainties. These experimentally derived rates serve as a valuable resource for nuclear astrophysics applications. We also provide, in Appendix F, a graphical comparison of our new results with previously evaluated Monte Carlo rates.

Importantly, we emphasize that our rates are based on experimental data rather than theoretical models. Additionally, our rates are laboratory based and must be corrected for thermal target excitations before they can be applied in stellar evolution and explosion codes.

To facilitate transparency and reproducibility, all input files and the RatesMC computational code used in this study have been made publicly available on GitHub. This enables researchers to verify our findings, apply our methods to new data, and further improve reaction rate evaluations in the future.

These findings underscore the necessity of applying modern statistical techniques in nuclear reaction rate evaluations to achieve more reliable and precise results. Future work could focus on refining uncertainty quantification, expanding the dataset of measured resonances, and integrating additional constraints from theoretical models and experimental observations.

This study provides a framework for improving nuclear reaction rate predictions, which is crucial for applications in nuclear astrophysics, stellar nucleosynthesis, and thermonuclear processes in astrophysical environments.

Acknowledgments

We would like to thank Stephane Goriely for providing the TALYS results used in the present work for estimating reaction rates at elevated temperatures. The comments of Art Champagne and Robert Janssens are highly appreciated. This work was supported in part by the DOE, Office of Science, Office of Nuclear Physics, under grants DE-FG02-97ER41041 (UNC), DE-FG02-97ER41042 (NCSU), and DE-FG02-97ER41033 (TUNL); P.M. was supported by NKFIH (K134197).

Appendix A
Estimation of Proton Partial Widths

In this section, we explain how to estimate proton partial widths from spectroscopic factors using Equation (6). The penetration factors, P_c, can be readily computed from Coulomb wave functions (see, e.g., the Appendix in A. M. Lane & R. G. Thomas 1958). To assist in these calculations, we provide in Table 3 numerically computed

Table 3
Proton Dimensionless Single-particle Reduced Widths, θ^2_{pc} [a]

Mass A [c]	E (keV)[b]										
	0	100	200	300	400	500	600	700	800	900	1000
$\ell = 0$ [d]	…	…	…	…	…	…	…	…	…	…	…
16	0.61	0.59	0.58	0.55	0.53	0.50	0.45	0.42	0.41	0.40	0.40
22	0.62	0.61	0.61	0.60	0.59	0.58	0.56	0.55	0.52	0.50	0.48
31	0.58	0.58	0.58	0.58	0.58	0.57	0.57	0.57	0.57	0.57	0.57
40	0.52	0.52	0.52	0.53	0.53	0.53	0.54	0.54	0.54	0.54	0.55
50	0.48	0.49	0.49	0.49	0.49	0.50	0.50	0.50	0.51	0.51	0.51
$\ell = 1$ [d]	…	…	…	…	…	…	…	…	…	…	…
16	0.81	0.78	0.77	0.75	0.74	0.73	0.72	0.71	0.71	0.71	0.71
22	0.77	0.77	0.76	0.76	0.75	0.75	0.74	0.73	0.72	0.71	0.70
31	0.71	0.71	0.71	0.71	0.71	0.71	0.71	0.71	0.71	0.70	0.70
40	0.65	0.65	0.65	0.66	0.66	0.66	0.67	0.67	0.67	0.68	0.68
50	0.58	0.58	0.58	0.59	0.59	0.59	0.60	0.60	0.61	0.61	0.62
$\ell = 2$ [d]	…	…	…	…	…	…	…	…	…	…	…
16	0.46	0.46	0.46	0.47	0.47	0.47	0.47	0.47	0.48	0.48	0.48
22	0.42	0.42	0.42	0.42	0.43	0.43	0.43	0.44	0.44	0.44	0.44
31	0.37	0.37	0.37	0.38	0.38	0.38	0.38	0.39	0.39	0.40	0.40
40	0.31	0.31	0.32	0.32	0.32	0.33	0.33	0.34	0.34	0.35	0.35
50	0.28	0.28	0.28	0.29	0.29	0.29	0.29	0.30	0.30	0.30	0.31
$\ell = 3$ [d]	…	…	…	…	…	…	…	…	…	…	…
16	0.47	0.47	0.47	0.47	0.48	0.48	0.48	0.48	0.49	0.49	0.49
22	0.42	0.42	0.42	0.42	0.43	0.43	0.43	0.44	0.44	0.44	0.44
31	0.37	0.37	0.37	0.38	0.38	0.38	0.38	0.39	0.39	0.40	0.40
40	0.31	0.31	0.32	0.32	0.32	0.33	0.33	0.34	0.34	0.35	0.35
50	0.28	0.28	0.28	0.29	0.29	0.29	0.29	0.30	0.30	0.30	0.31

Notes.
[a] Calculated from Equation (9) of C. Iliadis (1997). The parameters used to compute the values listed here (a channel radius parameter of 1.25 fm, and Woods–Saxon parameters of $r_0 = 1.25$ fm, $a = 0.65$ fm, and $r_{c0} = 1.25$ fm) differ somewhat from those reported in C. Iliadis (1997). The present values were adopted because they are commonly encountered in the literature.
[b] Center-of-mass energy.
[c] Target mass number.
[d] The proton is assumed to transfer into the 2s, 2p, 1d, or 1f single-particle orbits.

values of θ^2_{pc} for protons on a grid of energy and orbital angular momentum. These values were obtained for a channel radius of $R = 1.25(A_0^{1/3} + A_1^{1/3})$ fm, where A_0 and A_1 are the (integer) mass numbers of the projectile and target, respectively, and optical-model final-state parameters of $r_0 = 1.25$ fm, $a = 0.65$ fm, and $r_{c0} = 1.25$ fm. When using the θ^2_{pc} values listed in Table 3, the penetration factor, P_c, should be computed at the same channel radius, R, and the spectroscopic factor C^2S should be extracted from the DWBA analysis of stripping data using the same values of the optical-model final-state parameters. See Section 2.2 for additional information.

As an example, consider the s-wave resonance at $E_r^{c.m.} = 34.7$ keV in the ^{22}Ne(p, γ)^{23}Na reaction, corresponding to the level at $E_x = 8827.9$ keV ($1/2^+$) in the ^{23}Na compound nucleus. A spectroscopic factor of $C^2S = 0.020$ was measured by S. E. Hale et al. (2001) using the ^{22}Ne(^{3}He, d)^{23}Na proton-transfer reaction. For $\ell = 0$, we find a penetration factor of 3.98×10^{-20}, and from Table 3, we obtain an interpolated value of $\theta^2_{pc} = 0.62$. The Wigner limit, $\hbar^2/(\mu R^2)$, amounts to 1.918×10^6 eV. The resulting proton partial width from Equation (6) is $\Gamma_p = 1.89 \times 10^{-15}$ eV. Because, in this case, the proton width is so small (and $\omega = 1$); we can assume that $\omega\gamma \approx \Gamma_p$.

Appendix B
Isospin Clebsch–Gordan Coefficients

Results from transfer experiments report spectroscopic factors either in the form of C^2S or as S (see Section 2.2). The isospin Clebsch–Gordan coefficient, C, takes into account that in an actual measurement the transferred nucleon is either a proton or a neutron. For a proton or neutron stripping reaction, e.g., (^{3}He,d), (d,p), etc., this quantity is defined by (P. J. Brussaard & P. W. M. Glaudemans 1977)

$$C = \left(T_i T_{zi} \frac{1}{2} t_z \middle| T_f T_{zf} \right). \quad \text{(B1)}$$

The symbols T_i and T_f denote the isospin of the initial (i.e., of the target) and final state, respectively; T_{zi} and T_{zf} are their respective z-components, with $T_z = (N - Z)/2$, where N and Z are the neutron and proton number, respectively; t_z is the isospin of the transferred nucleon ($t_z = -1/2$ for a proton and $t_z = +1/2$ for a neutron). Values of C^2 are given in Table 4 for proton- and neutron-stripping reactions.

For example, for both proton and neutron transfer to a $N = Z$ target nucleus (e.g., ^{20}Ne, ^{26}Al,...), we find $C^2 = 1$.

Table 4
Square of the Isospin Clebsch–Gordan Coefficient, C^2, for Single-particle Stripping Reactions[a]

	Proton Transfer	Neutron Transfer
$T_f = T_i - \frac{1}{2}$	$\frac{T_i + T_{zi}}{2T_i + 1}$	$\frac{T_i - T_{zi}}{2T_i + 1}$
$T_f = T_i + \frac{1}{2}$	$\frac{T_i - T_{zi} + 1}{2T_i + 1}$	$\frac{T_i + T_{zi} + 1}{2T_i + 1}$

Notes.
[a] The symbols T_i and T_f denote the isospin of the initial (i.e., of the target) and final state, respectively; T_{zi} and T_{zf} are their respective z-components, with $T_z = (N - Z)/2$, where N and Z are the neutron and proton number, respectively.

Appendix C
Common Mistakes

C.1. Spectroscopic Factors from Analog States

Since nuclear forces are approximately charge symmetric, structure information for proton-rich nuclei can be adopted from the corresponding mirror states in the neutron-rich nuclei, and vice versa. This procedure requires reliable mirror state correspondences. When a particle partial width of a resonance needs to be estimated using Equation (6) from a spectroscopic factor, S_a, but the latter quantity has not been measured, one can take advantage of the relationship $S_a \approx S_b$, where S_b is the experimental spectroscopic factor of the corresponding mirror state (Section 8). This procedure is sometimes applied erroneously, as is explained below.

The spectroscopic factor of a stripping reaction is given in the second-quantization formalism by (P. J. Brussaard & P. W. M. Glaudemans 1977)

$$S = \frac{\langle A + 1; J_f T_f || a^{\dagger}_{n\ell j} || A; J_i T_i \rangle^2}{(2J_f + 1)(2T_f + 1)} \quad \text{(C1)}$$

where the final and initial states are labeled by their respective mass numbers (A), spins (J), and isospins (T); $a^{\dagger}_{n\ell j}$ denotes the operator for the creation of a nucleon in the shell-model orbit (n,ℓ,j); and the triple bars in the matrix element stand for reduction in both coordinate and isospin space. It can be seen that the spectroscopic factor represents an overlap integral between an initial state (the target consisting of A nucleons and a single transferred nucleon) and a final state (consisting of $A + 1$ nucleons). Therefore, when the spectroscopic factor of a mirror level, S_b, is adopted instead of S_a in calculating the particle partial width, it is important to ensure that S_b was measured in the *mirror reaction.*

A part of the nuclidic chart is sketched in Figure 5. Suppose one would like to estimate the proton partial width of a resonance in the A_i(p,γ)A_f reaction, but the required S_a value is unknown. Instead, assuming $S_a \approx S_b$, the known value of S_b, measured in the neutron stripping reaction, $B_i \rightarrow B_f$, e.g., (d,p), can be adopted for this purpose. Notice that, in this case, the ground states of the target nuclei, A_i and B_i, are mirror levels, as are the final levels in the nuclei A_f and B_f.

Sometimes, spectroscopic factors measured in pick-up reactions are erroneously used to calculate particle partial widths according to Equation (6). Consider the neutron pick-up reaction $F \rightarrow B_f$, e.g., (p,d), (d,t), or (^{3}He,α). Although A_f and B_f are mirror nuclei, F and A_i are not, and, therefore, a measured spectroscopic factor in a neutron pick-up reaction, $F \rightarrow B_f$, has no relationship to the spectroscopic factor of the A_i(p,γ)A_f reaction, despite the fact that two levels in the nuclei A_f and B_f may be mirror states.

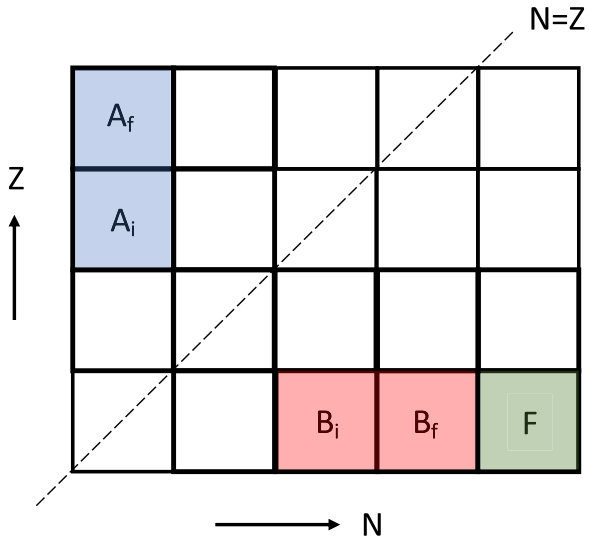

Figure 5. Sketch of the nuclidic chart displaying the number of protons, Z, versus the number of neutrons, N. The $N = Z$ line is depicted as a dashed line. See text.

In addition to charge symmetry, nuclear forces are also approximately charge independent. This implies that, instead of adopting nuclear structure information from only mirror states, we can also take advantage of the information across an isospin-multiplet. For an application of this method, see C. Iliadis et al. (1999).

C.2. Laboratory Electron Screening

We mentioned in Section 1 that the results listed in this work refer to *laboratory* reaction rates. For use in stellar model calculations, these need to be corrected for a number of effects, including the thermal excitation of nuclear levels and electron screening. The former depends on the stellar temperature, while the latter, more precisely referred to as *stellar plasma screening*, depends on both temperature and density. For a review, see M. Aliotta & K. Langanke (2022).

Nuclear reaction measurements are also subject to screening because the reactions proceed in the presence of electrons. Before the laboratory reaction rates can be computed from the nuclear physics input, it is important to apply the necessary corrections for *laboratory electron screening*. Two situations need to be distinguished. The first refers to laboratory screening for a nonresonant reaction cross section, which is particularly noticeable at relatively small bombarding energies. Typically, the measured cross section (or S factor) is fit using an appropriate function that includes a screening correction factor to extract the "bare-nucleus" cross section. The latter is then used to obtain the laboratory reaction rates, as discussed, e.g., in Section 4. This factor can be approximated by

$$f_{nr} \approx e^{\pi\eta(E)\frac{|U_e|}{E}}. \quad \text{(C2)}$$

The quantity $|U_e|$ denotes the electron screening potential and is a fit parameter. For an example, the reader is referred to Figure 4 in R. S. de Souza et al. (2019b), showing the S-factor

of the ^{3}He(d, p)^{4}He reaction, with different fits representing different screening potentials depending on the identities of the target and projectile.

Notice that the screened cross section, at the same bombarding energy, is always larger than the unscreened one because the presence of the electrons reduces the thickness of the effective barrier that the projectile needs to tunnel through. The above procedure is well established, despite the fact that the theory has difficulties in predicting the magnitude of the laboratory screening potential (M. Aliotta & K. Langanke 2022).

Unfortunately, Equation (C2) is frequently applied to the strengths of narrow resonances, as first suggested by H. J. Assenbaum et al. (1987). Several of the reported "corrected" resonance strengths exceed the measured values by up to 25%, depending on the reaction and resonance energy (F. Strieder et al. 2012; M. L. Sergi et al. 2015; R. Depalo et al. 2016; C. G. Bruno et al. 2016). This issue has been discussed in detail by C. Iliadis (2023), who showed that (i) it is incorrect to apply the nonresonant screening correction factor of Equation (C2) to narrow resonances, and (ii) the actual differences between screened and unscreened resonance strengths are negligible (<0.2%).

The reason is that, for a narrow resonance, the presence of electrons causes two effects that nearly compensate each other. The first is the narrowing of the effective barrier, similar to the case of a nonresonant cross section, which increases the magnitude of the screened resonance strength. The second is the lowering of the energy of the resonance level in the compound nucleus, which implies that the energy at which the reaction proceeds is lower than the bare-nucleus resonance energy (Section 6.2). This second effect decreases the magnitude of the screened resonance strength. Therefore, unless it can be demonstrated otherwise, no correction for laboratory electron screening is needed when considering the strengths of narrow resonances. For details, see C. Iliadis (2023).

Appendix D
Online Resources

A majority of the charged-particle-induced thermonuclear reaction rates presented within this work (with the exception of the rates computed using Bayesian methods) are calculated using the RatesMC computer code released under the GNU General Public License v3.0. Installation instructions for RatesMC, which contain information on the necessary software dependencies, can be found within a git repository hosted on GitHub: https://github.com/rlongland/RatesMC. A "training" folder is also included, which provides an example input file and guides users through a comprehensive rate calculation. The release version of the code used for the calculations presented in this work is available on Zenodo (R. Longland 2025).

We also provide the RatesMC input files for all Monte Carlo rates presented in Appendix E, as well as our machine-readable, tabulated reaction rates on Zenodo at doi:10.5281/zenodo.17610211 (C. Iliadis et al. 2025).

Appendix E
Evaluated Thermonuclear Reaction Rates

E.1. General Aspects

For the vast majority of reactions listed in Table 1, the thermonuclear rates, $N_A\langle\sigma v\rangle$, have been evaluated in the present work by taking into account the latest available information on the nuclear physics input. Exceptions are those rates that have been estimated using Bayesian models (Section 4). They are marked in the table with a footnote "b" and have been adopted, with small modifications, from the recent literature.

Results are provided in the following tables and figures. The tables provide numerical values of the total reaction rates. Detailed information on the meaning of the table columns, and the interpretation of the figures, is provided below. The rates presented here refer to their *laboratory* values. This means that, for use in stellar model simulations, the values provided here need to be corrected for the effects of thermal excitations of the interacting nuclei.

The reaction rates (except for the Bayesian ones) have been computed using the code RatesMC (see Section 5.1), using 50,000 rate samples for each reaction. The complete input files to RatesMC for each reaction can be accessed via Github (see Appendix D). These files contain the comprehensive nuclear physics input needed to perform the rate calculations.

The low, median, and high reaction rate values listed in the tables below are directly related to the 16th, 50th, and 84th percentiles, respectively, of the actual rate probability density function. However, the rate factor uncertainty, *f.u.*, is computed under the assumption that the rate probability density has a lognormal shape. In this case, the factor uncertainty is related to the low, median, and high values as explained below. However, if the actual Monte Carlo probability density of the total rate deviates noticeably from a lognormal shape, *f.u.* will no longer be related to the low, median, and high values of the total rate.

C. Iliadis et al. (2010c) provided figures of rate probability densities and numerical values of the Anderson–Darling statistic for assessing how closely the actual rate probability density follows a lognormal shape. We do not provide such details here, but the information can be requested from the authors. The second figure provided below for each reaction can be used to assess approximately the shape of the actual rate probability density at a given temperature. When the rate probability density has a lognormal shape, the normalized rate uncertainty (displayed on a logarithmic scale of the ordinate) will be symmetric about unity.

To illustrate how to interpret the figures, consider Figures 105 and 106. The former displays the fractional contributions to the total ^{28}Si(p,γ)^{29}P reaction rate, while the latter depicts the uncertainty of the total reaction rate versus temperature. At low temperatures (below ≈100 MK), the reaction is dominated by direct capture. As the temperature increases, this contribution gradually decreases, while the narrow resonance at $E_r^{c.m.} = 358$ keV becomes dominant in the range $T \approx 0.1$–2 GK. Notably, Figure 106 shows a dip in the total rate uncertainty near ≈100 MK, where the direct capture and resonance contributions become comparable. In this regime, the independent uncertainties of each component

combine quadratically, leading to a smaller overall uncertainty. At higher temperatures (above ≈2 GK), isolated resonances at $E_r^{c.m.} = 1595$ and 2992 keV begin to contribute significantly. The dotted line denotes the summed contribution from even higher-lying, individually measured resonances. It is also worth noting that the broad resonance at $E_r^{c.m.} = 1595$ keV influences the total rate even at low temperatures ($T \lesssim 100$ MK) through its low-energy tail.

E.2. Explanation of Tables and Figures

Table 5 defines the columns used in the reaction rate tables and the figures that follow.

Table 5
Explanation of the Columns in the Reaction Rate Tables and of the Corresponding Quantities Plotted in the Figures

Item	Description
Table—T (GK)	Stellar temperature in gigakelvin.
Table—Low, Median, High	Experimental reaction rate (i.e., assuming the target is in its ground state) and its uncertainty, calculated using the 16th, 50th, 84th percentiles, respectively, of the rate probability density. Our recommended rate is defined as the median rate, and the "low" and "high" rate values correspond to a coverage probability of 68%. Rates are presented as $N_A\langle\sigma v\rangle$ in units of $cm^3\ mol^{-1}\ s^{-1}$, according to Equation (1). Note that these values are derived from the actual Monte Carlo distribution of the reaction rate, and not from its lognormal approximation. When the computed total rate falls below $10^{-99}\ cm^3\ mol^{-1}\ s^{-1}$, the corresponding tabulated rate is set to zero.
Table—f.u.	Factor uncertainty of the rate, corresponding to 68% coverage of the rate probability density. These values are not directly based on the actual Monte Carlo distribution of the reaction rate, but on its lognormal approximation. The lognormal parameter σ can be calculated using the expression $f.u. = e^{\sigma}$. When the Monte Carlo rate probability density is close to a lognormal approximation, the factor uncertainty can be expressed by percentiles in a number of ways: $$f.u. = \frac{\text{High}}{\text{Median}} = \frac{\text{Median}}{\text{Low}} = \sqrt{\frac{\text{High}}{\text{Low}}}.$$ When the computed total rate falls below $10^{-99}\ cm^3\ mol^{-1}\ s^{-1}$, the associated factor uncertainty is set to unity.
Table notes—Reaction rate	References are provided when the rates are adopted from the published literature. This is the case for the Bayesian rates involving light target nuclei.
Table notes—Observed resonances	Reference(s) for some of the resonance strengths and partial widths for directly observed resonances.
Table notes—Unobserved resonances	Reference(s) for some of the spectroscopic factors or ANCs of bound and unbound levels (i.e., of resonances that have not been observed directly).
Table notes—S factor	Reference(s) with information on recent S-factor data.
Table notes—Normalization	Reference(s) providing information on the absolute normalization of resonance strengths or S factors.
Table notes—High-temperature rates	Comments on the rates at high temperature, if they are normalized to TALYS rates, according to the procedure discussed in Section 10. These estimated rates are listed in parentheses in the tables below.
Table notes—Previous rates	Reference(s) with *numerical* values of previous reaction rates. In particular, we do not provide references when the rate has previously only been displayed in a figure.
Table notes—Other	Other comments.
Figure—Individual Reaction rate contributions	Fractional contributions (including uncertainties) of each component to the total reaction rate, normalized to unity. Only contributions $\geqslant$5% of the total rate ($\geqslant$10% in rare cases) are displayed individually; all smaller contributions are combined and shown as a dotted black line. "DC" denotes direct capture, and resonance energies (in keV) refer to the center-of-mass frame. The vertical placement of resonance labels indicates their relative importance. For temperatures above the matching temperature, where the table lists rates in parentheses, possible contributions from higher-lying, unmeasured resonances are not included in the plots; corrected rates that account for these contributions are provided in the table.
Figure—Reaction rate uncertainties	Uncertainty as a function of stellar temperature, expressed as ratios normalized to our recommended (median) rate in the accompanying table. Shaded blue bands represent the 68%, 90%, and 98% coverage probabilities. For temperatures above the matching temperature, where the table lists rates in parentheses, possible contributions from higher-lying, unmeasured resonances are not included in the plotted uncertainties. Corrected rates that account for these contributions are provided in the table.

E.3. Tables and Figures of Experimental Reaction Rates

This appendix lists the reaction rate tables (Tables 6–83) and figures (Figures 6–152) presented in this work.

Table 6
Total Laboratory Reaction Rates for $D(p,\gamma)^3He$

T (GK)	Low	Median	High	*f.u.*	T (GK)	Low	Median	High	*f.u.*
0.001	1.399E-11	1.454E-11	1.508E-11	1.038E+00	0.140	1.205E+01	1.232E+01	1.261E+01	1.023E+00
0.002	1.933E-08	2.007E-08	2.080E-08	1.038E+00	0.150	1.396E+01	1.428E+01	1.460E+01	1.023E+00
0.003	6.257E-07	6.494E-07	6.728E-07	1.037E+00	0.160	1.599E+01	1.635E+01	1.672E+01	1.022E+00
0.004	5.533E-06	5.741E-06	5.946E-06	1.037E+00	0.180	2.036E+01	2.081E+01	2.127E+01	1.022E+00
0.005	2.588E-05	2.684E-05	2.779E-05	1.037E+00	0.200	2.511E+01	2.566E+01	2.622E+01	1.022E+00
0.006	8.359E-05	8.666E-05	8.969E-05	1.036E+00	0.250	3.844E+01	3.926E+01	4.010E+01	1.021E+00
0.007	2.124E-04	2.202E-04	2.278E-04	1.036E+00	0.300	5.353E+01	5.466E+01	5.582E+01	1.021E+00
0.008	4.577E-04	4.743E-04	4.906E-04	1.036E+00	0.350	7.006E+01	7.155E+01	7.306E+01	1.021E+00
0.009	8.745E-04	9.058E-04	9.367E-04	1.035E+00	0.400	8.781E+01	8.968E+01	9.158E+01	1.021E+00
0.010	1.525E-03	1.579E-03	1.633E-03	1.035E+00	0.450	1.066E+02	1.088E+02	1.112E+02	1.021E+00
0.011	2.478E-03	2.566E-03	2.652E-03	1.035E+00	0.500	1.262E+02	1.290E+02	1.317E+02	1.021E+00
0.012	3.807E-03	3.940E-03	4.072E-03	1.034E+00	0.600	1.679E+02	1.716E+02	1.753E+02	1.021E+00
0.013	5.586E-03	5.779E-03	5.971E-03	1.034E+00	0.700	2.121E+02	2.168E+02	2.215E+02	1.021E+00
0.014	7.889E-03	8.160E-03	8.430E-03	1.034E+00	0.800	2.584E+02	2.642E+02	2.700E+02	1.022E+00
0.015	1.079E-02	1.116E-02	1.152E-02	1.034E+00	0.900	3.064E+02	3.133E+02	3.203E+02	1.022E+00
0.016	1.437E-02	1.485E-02	1.534E-02	1.033E+00	1.000	3.559E+02	3.640E+02	3.722E+02	1.022E+00
0.018	2.383E-02	2.463E-02	2.542E-02	1.033E+00	1.250	4.849E+02	4.961E+02	5.075E+02	1.022E+00
0.020	3.683E-02	3.805E-02	3.925E-02	1.033E+00	1.500	6.198E+02	6.343E+02	6.491E+02	1.023E+00
0.025	8.797E-02	9.077E-02	9.357E-02	1.032E+00	1.750	7.592E+02	7.772E+02	7.955E+02	1.023E+00
0.030	1.706E-01	1.759E-01	1.812E-01	1.031E+00	2.000	9.020E+02	9.235E+02	9.454E+02	1.023E+00
0.040	4.480E-01	4.612E-01	4.743E-01	1.029E+00	2.500	1.192E+03	1.221E+03	1.250E+03	1.024E+00
0.050	8.901E-01	9.153E-01	9.403E-01	1.028E+00	3.000	1.479E+03	1.516E+03	1.553E+03	1.024E+00
0.060	1.504E+00	1.545E+00	1.586E+00	1.027E+00	3.500	1.752E+03	1.795E+03	1.839E+03	1.024E+00
0.070	2.289E+00	2.350E+00	2.410E+00	1.026E+00	4.000	2.000E+03	2.049E+03	2.100E+03	1.024E+00
0.080	3.241E+00	3.324E+00	3.408E+00	1.025E+00	5.000	(2.793E+03)	(2.905E+03)	(3.021E+03)	(1.040E+00)
0.090	4.352E+00	4.462E+00	4.571E+00	1.025E+00	6.000	(3.414E+03)	(3.557E+03)	(3.706E+03)	(1.042E+00)
0.100	5.617E+00	5.755E+00	5.893E+00	1.024E+00	7.000	(4.017E+03)	(4.194E+03)	(4.378E+03)	(1.044E+00)
0.110	7.026E+00	7.195E+00	7.366E+00	1.024E+00	8.000	(4.600E+03)	(4.812E+03)	(5.033E+03)	(1.046E+00)
0.120	8.574E+00	8.776E+00	8.981E+00	1.023E+00	9.000	(5.167E+03)	(5.410E+03)	(5.664E+03)	(1.047E+00)
0.130	1.025E+01	1.048E+01	1.073E+01	1.023E+00	10.000	(5.708E+03)	(5.988E+03)	(6.281E+03)	(1.049E+00)

Note. Reaction rate: J. Moscoso et al. (2021). *S* factor: see column 2 in Table 1 and Appendix A in J. Moscoso et al. (2021). Normalization: J. B. Warren et al. (1963), L. Ma et al. (1997), G. J. Schmid et al. (1995), C. Casella et al. (2002), I. Tišma et al. (2019), V. Mossa et al. (2020), and S. Turkat et al. (2021). High-temperature rates (in parentheses): A. Coc et al. (2015). Previous rates: C. Iliadis et al. (2016), T.-H. Yeh et al. (2021), and O. Pisanti et al. (2021). Other: Bayesian rate.

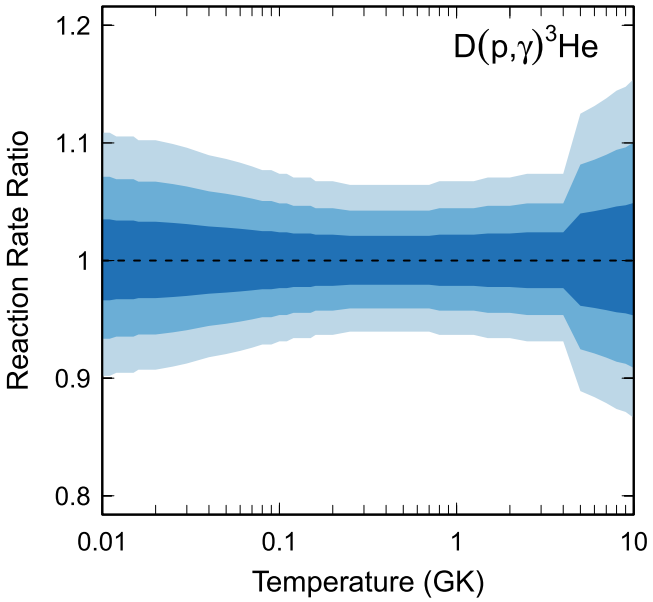

Figure 6. Reaction rate uncertainties versus temperature. The three different shades refer to coverage probabilities of 68%, 90%, and 98%.

Table 7
Total Laboratory Reaction Rates for $D(d,n)^3He$

T (GK)	Low	Median	High	*f.u.*	T (GK)	Low	Median	High	*f.u.*
0.001	1.308E-08	1.323E-08	1.336E-08	1.011E+00	0.140	5.579E+05	5.642E+05	5.700E+05	1.011E+00
0.002	5.431E-05	5.493E-05	5.549E-05	1.011E+00	0.150	6.506E+05	6.580E+05	6.647E+05	1.011E+00
0.003	2.993E-03	3.027E-03	3.058E-03	1.011E+00	0.160	7.488E+05	7.573E+05	7.650E+05	1.011E+00
0.004	3.697E-02	3.739E-02	3.778E-02	1.011E+00	0.180	9.599E+05	9.708E+05	9.808E+05	1.011E+00
0.005	2.191E-01	2.216E-01	2.239E-01	1.011E+00	0.200	1.189E+06	1.202E+06	1.215E+06	1.011E+00
0.006	8.466E-01	8.562E-01	8.650E-01	1.011E+00	0.250	1.824E+06	1.845E+06	1.864E+06	1.011E+00
0.007	2.482E+00	2.510E+00	2.536E+00	1.011E+00	0.300	2.529E+06	2.557E+06	2.583E+06	1.011E+00
0.008	6.010E+00	6.078E+00	6.140E+00	1.011E+00	0.350	3.283E+06	3.321E+06	3.355E+06	1.011E+00
0.009	1.266E+01	1.281E+01	1.294E+01	1.011E+00	0.400	4.074E+06	4.121E+06	4.163E+06	1.011E+00
0.010	2.402E+01	2.429E+01	2.454E+01	1.011E+00	0.450	4.892E+06	4.947E+06	4.998E+06	1.011E+00
0.011	4.197E+01	4.245E+01	4.288E+01	1.011E+00	0.500	5.727E+06	5.792E+06	5.851E+06	1.011E+00
0.012	6.872E+01	6.949E+01	7.021E+01	1.011E+00	0.600	7.431E+06	7.515E+06	7.592E+06	1.011E+00
0.013	1.067E+02	1.079E+02	1.090E+02	1.011E+00	0.700	9.153E+06	9.257E+06	9.352E+06	1.011E+00
0.014	1.585E+02	1.603E+02	1.619E+02	1.011E+00	0.800	1.087E+07	1.100E+07	1.111E+07	1.011E+00
0.015	2.269E+02	2.295E+02	2.318E+02	1.011E+00	0.900	1.257E+07	1.272E+07	1.285E+07	1.011E+00
0.016	3.149E+02	3.185E+02	3.217E+02	1.011E+00	1.000	1.425E+07	1.441E+07	1.456E+07	1.011E+00
0.018	5.614E+02	5.678E+02	5.736E+02	1.011E+00	1.250	1.830E+07	1.851E+07	1.870E+07	1.011E+00
0.020	9.223E+02	9.327E+02	9.423E+02	1.011E+00	1.500	2.213E+07	2.238E+07	2.261E+07	1.011E+00
0.025	2.481E+03	2.509E+03	2.535E+03	1.011E+00	1.750	2.571E+07	2.601E+07	2.627E+07	1.011E+00
0.030	5.251E+03	5.311E+03	5.365E+03	1.011E+00	2.000	2.907E+07	2.940E+07	2.971E+07	1.011E+00
0.040	1.553E+04	1.571E+04	1.587E+04	1.011E+00	2.500	(3.500E+07)	(3.546E+07)	(3.592E+07)	(1.013E+00)
0.050	3.337E+04	3.375E+04	3.409E+04	1.011E+00	3.000	(4.036E+07)	(4.093E+07)	(4.150E+07)	(1.014E+00)
0.060	5.957E+04	6.024E+04	6.086E+04	1.011E+00	3.500	(4.522E+07)	(4.585E+07)	(4.649E+07)	(1.014E+00)
0.070	9.438E+04	9.545E+04	9.643E+04	1.011E+00	4.000	(4.957E+07)	(5.031E+07)	(5.106E+07)	(1.015E+00)
0.080	1.377E+05	1.393E+05	1.407E+05	1.011E+00	5.000	(5.724E+07)	(5.816E+07)	(5.909E+07)	(1.016E+00)
0.090	1.894E+05	1.915E+05	1.935E+05	1.011E+00	6.000	(6.379E+07)	(6.488E+07)	(6.598E+07)	(1.017E+00)
0.100	2.490E+05	2.518E+05	2.544E+05	1.011E+00	7.000	(6.947E+07)	(7.072E+07)	(7.199E+07)	(1.018E+00)
0.110	3.160E+05	3.196E+05	3.229E+05	1.011E+00	8.000	(7.449E+07)	(7.583E+07)	(7.719E+07)	(1.018E+00)
0.120	3.902E+05	3.946E+05	3.986E+05	1.011E+00	9.000	(7.895E+07)	(8.037E+07)	(8.182E+07)	(1.018E+00)
0.130	4.709E+05	4.762E+05	4.811E+05	1.011E+00	10.000	(8.280E+07)	(8.437E+07)	(8.597E+07)	(1.019E+00)

Note. Reaction rate: A. Gómez Iñesta et al. (2017). *S* factor: see Table 2 and Figure 1 in A. Gómez Iñesta et al. (2017). Normalization: see Table 2 of A. Gómez Iñesta et al. (2017). High-temperature rates (in parentheses): A. Coc et al. (2015). Previous rates: A. Coc et al. (2015) and O. Pisanti et al. (2021). Other: the rates listed in the table have been recalculated using a modified Bayesian model compared to A. Gómez Iñesta et al. (2017), as discussed in Section 4.

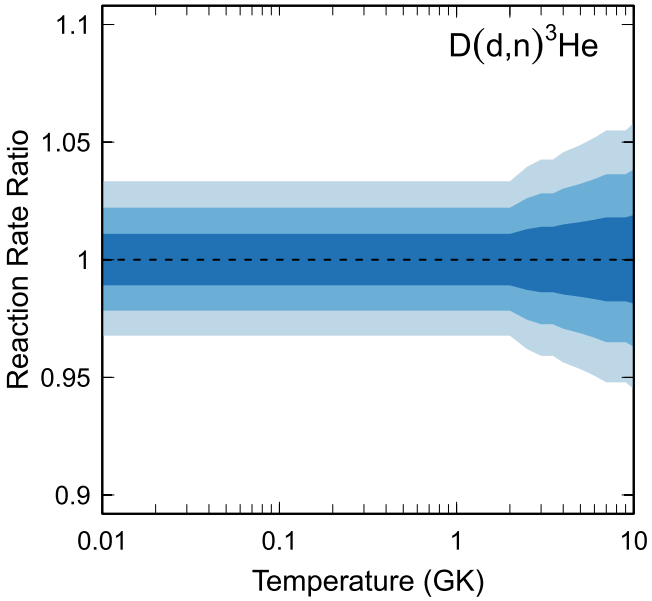

Figure 7. Reaction rate uncertainties versus temperature. The three different shades refer to coverage probabilities of 68%, 90%, and 98%.

Table 8
Total Laboratory Reaction Rates for $D(d,p)^3H$

T (GK)	Low	Median	High	*f.u.*	T (GK)	Low	Median	High	*f.u.*
0.001	1.344E-08	1.361E-08	1.381E-08	1.013E+00	0.140	5.257E+05	5.325E+05	5.401E+05	1.013E+00
0.002	5.572E-05	5.644E-05	5.724E-05	1.013E+00	0.150	6.110E+05	6.189E+05	6.277E+05	1.013E+00
0.003	3.065E-03	3.104E-03	3.149E-03	1.013E+00	0.160	7.009E+05	7.099E+05	7.201E+05	1.013E+00
0.004	3.779E-02	3.828E-02	3.883E-02	1.013E+00	0.180	8.930E+05	9.046E+05	9.175E+05	1.013E+00
0.005	2.236E-01	2.265E-01	2.298E-01	1.013E+00	0.200	1.100E+06	1.114E+06	1.130E+06	1.013E+00
0.006	8.629E-01	8.740E-01	8.865E-01	1.013E+00	0.250	1.667E+06	1.688E+06	1.713E+06	1.013E+00
0.007	2.526E+00	2.559E+00	2.595E+00	1.013E+00	0.300	2.288E+06	2.317E+06	2.350E+06	1.013E+00
0.008	6.109E+00	6.188E+00	6.276E+00	1.013E+00	0.350	2.945E+06	2.983E+06	3.026E+06	1.013E+00
0.009	1.286E+01	1.302E+01	1.321E+01	1.013E+00	0.400	3.628E+06	3.675E+06	3.728E+06	1.013E+00
0.010	2.436E+01	2.467E+01	2.502E+01	1.013E+00	0.450	4.328E+06	4.384E+06	4.447E+06	1.013E+00
0.011	4.252E+01	4.307E+01	4.368E+01	1.013E+00	0.500	5.039E+06	5.104E+06	5.177E+06	1.013E+00
0.012	6.953E+01	7.043E+01	7.144E+01	1.013E+00	0.600	6.478E+06	6.562E+06	6.655E+06	1.013E+00
0.013	1.078E+02	1.092E+02	1.108E+02	1.013E+00	0.700	7.920E+06	8.023E+06	8.137E+06	1.013E+00
0.014	1.600E+02	1.621E+02	1.644E+02	1.013E+00	0.800	9.352E+06	9.473E+06	9.609E+06	1.013E+00
0.015	2.289E+02	2.319E+02	2.352E+02	1.013E+00	0.900	1.077E+07	1.090E+07	1.106E+07	1.013E+00
0.016	3.173E+02	3.214E+02	3.260E+02	1.013E+00	1.000	1.215E+07	1.231E+07	1.249E+07	1.013E+00
0.018	5.647E+02	5.720E+02	5.802E+02	1.013E+00	1.250	1.550E+07	1.570E+07	1.592E+07	1.013E+00
0.020	9.260E+02	9.379E+02	9.513E+02	1.013E+00	1.500	1.865E+07	1.889E+07	1.916E+07	1.013E+00
0.025	2.480E+03	2.512E+03	2.548E+03	1.013E+00	1.750	2.162E+07	2.190E+07	2.221E+07	1.013E+00
0.030	5.229E+03	5.296E+03	5.372E+03	1.013E+00	2.000	2.441E+07	2.472E+07	2.508E+07	1.013E+00
0.040	1.535E+04	1.555E+04	1.577E+04	1.013E+00	2.500	(2.938E+07)	(2.976E+07)	(3.015E+07)	(1.013E+00)
0.050	3.277E+04	3.320E+04	3.367E+04	1.013E+00	3.000	(3.392E+07)	(3.440E+07)	(3.488E+07)	(1.014E+00)
0.060	5.815E+04	5.890E+04	5.975E+04	1.013E+00	3.500	(3.813E+07)	(3.863E+07)	(3.921E+07)	(1.014E+00)
0.070	9.164E+04	9.282E+04	9.415E+04	1.013E+00	4.000	(4.188E+07)	(4.251E+07)	(4.315E+07)	(1.015E+00)
0.080	1.331E+05	1.348E+05	1.367E+05	1.013E+00	5.000	(4.868E+07)	(4.946E+07)	(5.025E+07)	(1.016E+00)
0.090	1.821E+05	1.844E+05	1.871E+05	1.013E+00	6.000	(5.459E+07)	(5.552E+07)	(5.646E+07)	(1.017E+00)
0.100	2.383E+05	2.414E+05	2.448E+05	1.013E+00	7.000	(5.969E+07)	(6.077E+07)	(6.186E+07)	(1.018E+00)
0.110	3.012E+05	3.051E+05	3.095E+05	1.013E+00	8.000	(6.413E+07)	(6.529E+07)	(6.646E+07)	(1.018E+00)
0.120	3.704E+05	3.752E+05	3.805E+05	1.013E+00	9.000	(6.790E+07)	(6.912E+07)	(7.036E+07)	(1.018E+00)
0.130	4.453E+05	4.511E+05	4.575E+05	1.013E+00	10.000	(7.093E+07)	(7.228E+07)	(7.365E+07)	(1.019E+00)

Note. Reaction rate: A. Gómez Iñesta et al. (2017). *S* factor: see Table 2 and Figure 2 in A. Gómez Iñesta et al. (2017). Normalization: see Table 2 of A. Gómez Iñesta et al. (2017). High-temperature rates (in parentheses): A. Coc et al. (2015). Previous rates: A. Coc et al. (2015) and O. Pisanti et al. (2021). Other: the rates listed in the table have been recalculated using a modified Bayesian model compared to A. Gómez Iñesta et al. (2017), as discussed in Section 4.

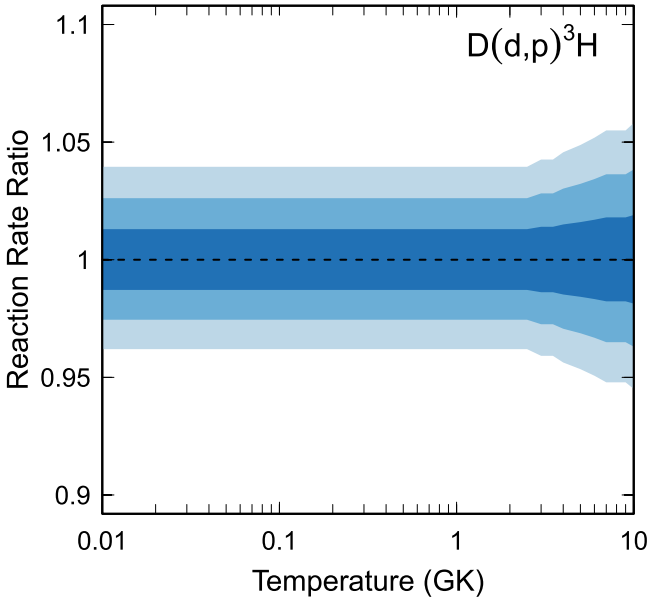

Figure 8. Reaction rate uncertainties versus temperature. The three different shades refer to coverage probabilities of 68%, 90%, and 98%.

Table 9
Total Laboratory Reaction Rates for $^{3}H(d,n)^{4}He$

T (GK)	Low	Median	High	*f.u.*	T (GK)	Low	Median	High	*f.u.*
0.001	1.986E-07	1.998E-07	2.010E-07	1.006E+00	0.140	1.047E+08	1.050E+08	1.053E+08	1.003E+00
0.002	1.437E-03	1.445E-03	1.454E-03	1.006E+00	0.150	1.214E+08	1.218E+08	1.221E+08	1.003E+00
0.003	1.040E-01	1.046E-01	1.052E-01	1.006E+00	0.160	1.384E+08	1.388E+08	1.392E+08	1.003E+00
0.004	1.530E+00	1.539E+00	1.548E+00	1.006E+00	0.180	1.727E+08	1.732E+08	1.736E+08	1.003E+00
0.005	1.028E+01	1.034E+01	1.040E+01	1.006E+00	0.200	2.064E+08	2.069E+08	2.074E+08	1.003E+00
0.006	4.380E+01	4.405E+01	4.430E+01	1.006E+00	0.250	2.836E+08	2.843E+08	2.850E+08	1.002E+00
0.007	1.389E+02	1.397E+02	1.405E+02	1.006E+00	0.300	3.475E+08	3.483E+08	3.492E+08	1.002E+00
0.008	3.594E+02	3.614E+02	3.635E+02	1.006E+00	0.350	3.979E+08	3.988E+08	3.998E+08	1.002E+00
0.009	8.015E+02	8.060E+02	8.104E+02	1.006E+00	0.400	4.364E+08	4.375E+08	4.386E+08	1.002E+00
0.010	1.598E+03	1.606E+03	1.615E+03	1.006E+00	0.450	4.651E+08	4.663E+08	4.675E+08	1.002E+00
0.011	2.918E+03	2.934E+03	2.950E+03	1.006E+00	0.500	4.860E+08	4.873E+08	4.885E+08	1.003E+00
0.012	4.971E+03	4.998E+03	5.025E+03	1.005E+00	0.600	5.105E+08	5.119E+08	5.132E+08	1.003E+00
0.013	8.001E+03	8.044E+03	8.088E+03	1.005E+00	0.700	5.196E+08	5.210E+08	5.224E+08	1.003E+00
0.014	1.229E+04	1.235E+04	1.242E+04	1.005E+00	0.800	5.192E+08	5.206E+08	5.220E+08	1.003E+00
0.015	1.814E+04	1.824E+04	1.834E+04	1.005E+00	0.900	5.131E+08	5.145E+08	5.160E+08	1.003E+00
0.016	2.591E+04	2.604E+04	2.618E+04	1.005E+00	1.000	5.036E+08	5.051E+08	5.065E+08	1.003E+00
0.018	4.865E+04	4.891E+04	4.917E+04	1.005E+00	1.250	(4.596E+08)	(4.624E+08)	(4.652E+08)	(1.006E+00)
0.020	8.372E+04	8.416E+04	8.461E+04	1.005E+00	1.500	(4.295E+08)	(4.325E+08)	(4.355E+08)	(1.007E+00)
0.025	2.486E+05	2.499E+05	2.512E+05	1.005E+00	1.750	(4.016E+08)	(4.044E+08)	(4.072E+08)	(1.007E+00)
0.030	5.714E+05	5.743E+05	5.772E+05	1.005E+00	2.000	(3.762E+08)	(3.792E+08)	(3.822E+08)	(1.008E+00)
0.040	1.932E+06	1.942E+06	1.951E+06	1.005E+00	2.500	(3.342E+08)	(3.369E+08)	(3.396E+08)	(1.008E+00)
0.050	4.617E+06	4.638E+06	4.660E+06	1.005E+00	3.000	(3.012E+08)	(3.039E+08)	(3.066E+08)	(1.009E+00)
0.060	8.974E+06	9.013E+06	9.052E+06	1.004E+00	3.500	(2.751E+08)	(2.776E+08)	(2.801E+08)	(1.009E+00)
0.070	1.521E+07	1.527E+07	1.534E+07	1.004E+00	4.000	(2.539E+08)	(2.564E+08)	(2.590E+08)	(1.010E+00)
0.080	2.339E+07	2.348E+07	2.357E+07	1.004E+00	5.000	(2.222E+08)	(2.244E+08)	(2.266E+08)	(1.010E+00)
0.090	3.344E+07	3.356E+07	3.369E+07	1.004E+00	6.000	(1.995E+08)	(2.017E+08)	(2.039E+08)	(1.011E+00)
0.100	4.521E+07	4.536E+07	4.552E+07	1.004E+00	7.000	(1.827E+08)	(1.847E+08)	(1.867E+08)	(1.011E+00)
0.110	5.847E+07	5.866E+07	5.886E+07	1.003E+00	8.000	(1.696E+08)	(1.716E+08)	(1.737E+08)	(1.012E+00)
0.120	7.297E+07	7.320E+07	7.344E+07	1.003E+00	9.000	(1.593E+08)	(1.612E+08)	(1.631E+08)	(1.012E+00)
0.130	8.845E+07	8.873E+07	8.900E+07	1.003E+00	10.000	(1.507E+08)	(1.527E+08)	(1.547E+08)	(1.013E+00)

Note. Reaction rate: R. S. de Souza et al. (2019a). *S* factor: see Figure 1 and Appendix in R. S. de Souza et al. (2019a). Observed resonances: see Table 1 in R. S. de Souza et al. (2019a). Normalization: see Figure 1 in R. S. de Souza et al. (2019a), except R. E. Brown et al. (1987), who did not determine absolute cross sections. High-temperature rates (in parentheses): P. Descouvemont et al. (2004). Previous rates: P. Descouvemont et al. (2004) and H. S. Bosch & G. Hale (1993). Other: Bayesian rate.

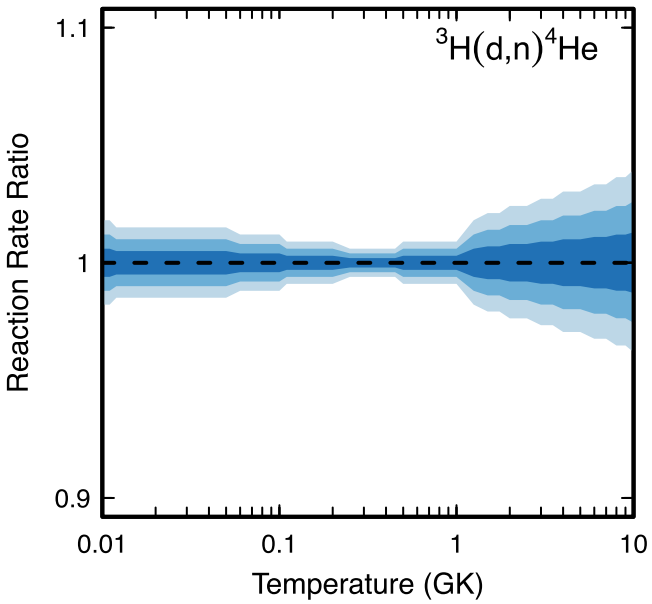

Figure 9. Reaction rate uncertainties versus temperature. The three different shades refer to coverage probabilities of 68%, 90%, and 98%.

Table 10
Total Laboratory Reaction Rates for ^{3}He(d,p)^{4}He

T (GK)	Low	Median	High	*f.u.*	T (GK)	Low	Median	High	*f.u.*
0.001	3.437E-19	3.496E-19	3.555E-19	1.017E+00	0.140	2.961E+05	3.000E+05	3.039E+05	1.013E+00
0.002	5.934E-13	6.035E-13	6.138E-13	1.017E+00	0.150	3.967E+05	4.019E+05	4.071E+05	1.013E+00
0.003	6.150E-10	6.248E-10	6.348E-10	1.016E+00	0.160	5.193E+05	5.255E+05	5.318E+05	1.012E+00
0.004	4.848E-08	4.926E-08	5.005E-08	1.016E+00	0.180	8.362E+05	8.462E+05	8.564E+05	1.012E+00
0.005	1.076E-06	1.093E-06	1.111E-06	1.016E+00	0.200	1.263E+06	1.278E+06	1.293E+06	1.012E+00
0.006	1.140E-05	1.158E-05	1.176E-05	1.016E+00	0.250	2.894E+06	2.926E+06	2.958E+06	1.011E+00
0.007	7.480E-05	7.600E-05	7.722E-05	1.016E+00	0.300	5.434E+06	5.493E+06	5.554E+06	1.011E+00
0.008	3.525E-04	3.581E-04	3.638E-04	1.016E+00	0.350	8.923E+06	9.021E+06	9.120E+06	1.011E+00
0.009	1.304E-03	1.325E-03	1.347E-03	1.016E+00	0.400	1.330E+07	1.345E+07	1.360E+07	1.011E+00
0.010	4.020E-03	4.085E-03	4.150E-03	1.016E+00	0.450	1.845E+07	1.865E+07	1.886E+07	1.011E+00
0.011	1.075E-02	1.092E-02	1.109E-02	1.016E+00	0.500	2.421E+07	2.448E+07	2.475E+07	1.011E+00
0.012	2.563E-02	2.604E-02	2.646E-02	1.016E+00	0.600	3.694E+07	3.735E+07	3.776E+07	1.011E+00
0.013	5.572E-02	5.661E-02	5.752E-02	1.016E+00	0.700	5.025E+07	5.086E+07	5.147E+07	1.012E+00
0.014	1.122E-01	1.140E-01	1.158E-01	1.016E+00	0.800	6.337E+07	6.413E+07	6.490E+07	1.012E+00
0.015	2.118E-01	2.151E-01	2.186E-01	1.016E+00	0.900	7.571E+07	7.662E+07	7.754E+07	1.012E+00
0.016	3.784E-01	3.844E-01	3.906E-01	1.016E+00	1.000	8.695E+07	8.799E+07	8.904E+07	1.012E+00
0.018	1.056E+00	1.073E+00	1.090E+00	1.016E+00	1.250	(1.073E+08)	(1.101E+08)	(1.130E+08)	(1.026E+00)
0.020	2.552E+00	2.593E+00	2.634E+00	1.016E+00	1.500	(1.241E+08)	(1.275E+08)	(1.309E+08)	(1.027E+00)
0.025	1.491E+01	1.515E+01	1.539E+01	1.016E+00	1.750	(1.361E+08)	(1.399E+08)	(1.438E+08)	(1.028E+00)
0.030	5.717E+01	5.802E+01	5.889E+01	1.015E+00	2.000	(1.443E+08)	(1.486E+08)	(1.531E+08)	(1.030E+00)
0.040	4.029E+02	4.090E+02	4.151E+02	1.015E+00	2.500	(1.541E+08)	(1.590E+08)	(1.641E+08)	(1.032E+00)
0.050	1.611E+03	1.635E+03	1.660E+03	1.015E+00	3.000	(1.584E+08)	(1.639E+08)	(1.696E+08)	(1.035E+00)
0.060	4.633E+03	4.703E+03	4.773E+03	1.015E+00	3.500	(1.600E+08)	(1.661E+08)	(1.724E+08)	(1.038E+00)
0.070	1.078E+04	1.093E+04	1.109E+04	1.014E+00	4.000	(1.604E+08)	(1.670E+08)	(1.738E+08)	(1.041E+00)
0.080	2.163E+04	2.194E+04	2.224E+04	1.014E+00	5.000	(1.596E+08)	(1.669E+08)	(1.746E+08)	(1.046E+00)
0.090	3.901E+04	3.956E+04	4.011E+04	1.014E+00	6.000	(1.584E+08)	(1.662E+08)	(1.743E+08)	(1.049E+00)
0.100	6.487E+04	6.578E+04	6.670E+04	1.014E+00	7.000	(1.572E+08)	(1.654E+08)	(1.740E+08)	(1.052E+00)
0.110	1.014E+05	1.027E+05	1.041E+05	1.013E+00	8.000	(1.561E+08)	(1.647E+08)	(1.738E+08)	(1.055E+00)
0.120	1.506E+05	1.526E+05	1.546E+05	1.013E+00	9.000	(1.554E+08)	(1.641E+08)	(1.733E+08)	(1.056E+00)
0.130	2.148E+05	2.176E+05	2.204E+05	1.013E+00	10.000	(1.546E+08)	(1.636E+08)	(1.731E+08)	(1.058E+00)

Note. Reaction rate: R. S. de Souza et al. (2019b). *S* factor: see Figure 4 and Appendix in R. S. de Souza et al. (2019b). Observed resonances: see Table 2 in R. S. de Souza et al. (2019b). Normalization: see Figure 4 and Appendix in R. S. de Souza et al. (2019b). High-temperature rates (in parentheses): P. Descouvemont et al. (2004). Previous rates: P. Descouvemont et al. (2004). Other: Bayesian rate.

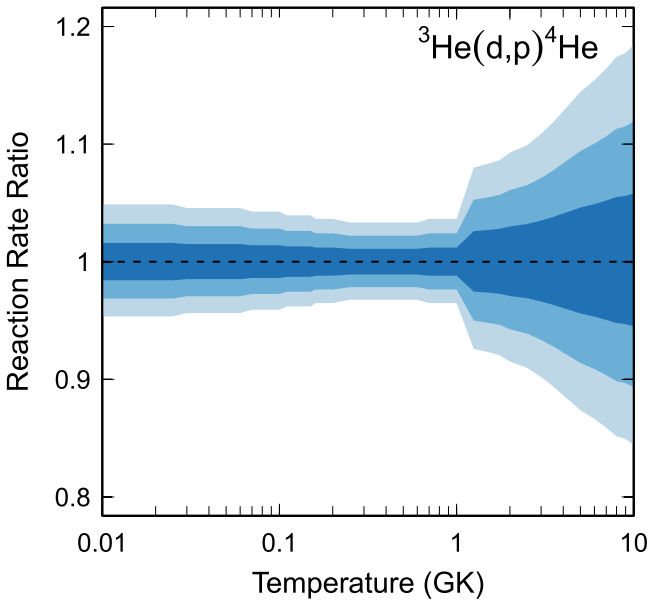

Figure 10. Reaction rate uncertainties versus temperature. The three different shades refer to coverage probabilities of 68%, 90%, and 98%.

Table 11
Total Laboratory Reaction Rates for ^{3}He(^{3}He,2p)^{4}He

T (GK)	Low	Median	High	*f.u.*	T (GK)	Low	Median	High	*f.u.*
0.001	2.660E-41	2.740E-41	2.830E-41	1.031E+00	0.140	1.058E+01	1.084E+01	1.115E+01	1.027E+00
0.002	1.669E-30	1.719E-30	1.776E-30	1.031E+00	0.150	1.725E+01	1.769E+01	1.819E+01	1.027E+00
0.003	2.846E-25	2.932E-25	3.028E-25	1.031E+00	0.160	2.696E+01	2.764E+01	2.842E+01	1.027E+00
0.004	5.636E-22	5.804E-22	5.994E-22	1.031E+00	0.180	5.928E+01	6.078E+01	6.246E+01	1.026E+00
0.005	1.241E-19	1.278E-19	1.319E-19	1.031E+00	0.200	1.165E+02	1.195E+02	1.228E+02	1.026E+00
0.006	7.570E-18	7.794E-18	8.049E-18	1.031E+00	0.250	4.476E+02	4.589E+02	4.712E+02	1.026E+00
0.007	2.013E-16	2.072E-16	2.140E-16	1.031E+00	0.300	1.238E+03	1.270E+03	1.304E+03	1.026E+00
0.008	3.008E-15	3.096E-15	3.198E-15	1.031E+00	0.350	2.774E+03	2.845E+03	2.921E+03	1.026E+00
0.009	2.954E-14	3.040E-14	3.139E-14	1.031E+00	0.400	5.371E+03	5.510E+03	5.658E+03	1.026E+00
0.010	2.110E-13	2.171E-13	2.242E-13	1.030E+00	0.450	9.348E+03	9.597E+03	9.856E+03	1.026E+00
0.011	1.176E-12	1.210E-12	1.249E-12	1.030E+00	0.500	1.502E+04	1.543E+04	1.585E+04	1.027E+00
0.012	5.374E-12	5.529E-12	5.708E-12	1.030E+00	0.600	3.259E+04	3.352E+04	3.446E+04	1.027E+00
0.013	2.090E-11	2.150E-11	2.219E-11	1.030E+00	0.700	6.008E+04	6.183E+04	6.361E+04	1.028E+00
0.014	7.107E-11	7.312E-11	7.548E-11	1.030E+00	0.800	9.896E+04	1.020E+05	1.049E+05	1.029E+00
0.015	2.160E-10	2.222E-10	2.294E-10	1.030E+00	0.900	1.503E+05	1.550E+05	1.595E+05	1.030E+00
0.016	5.967E-10	6.138E-10	6.336E-10	1.030E+00	1.000	2.146E+05	2.215E+05	2.280E+05	1.030E+00
0.018	3.597E-09	3.699E-09	3.819E-09	1.030E+00	1.250	4.326E+05	4.473E+05	4.611E+05	1.032E+00
0.020	1.688E-08	1.735E-08	1.791E-08	1.030E+00	1.500	(7.390E+05)	(7.960E+05)	(8.560E+05)	(1.076E+00)
0.025	3.714E-07	3.819E-07	3.941E-07	1.030E+00	1.750	(1.120E+06)	(1.210E+06)	(1.300E+06)	(1.077E+00)
0.030	3.905E-06	4.013E-06	4.141E-06	1.029E+00	2.000	(1.580E+06)	(1.700E+06)	(1.840E+06)	(1.079E+00)
0.040	1.191E-04	1.224E-04	1.262E-04	1.029E+00	2.500	(2.680E+06)	(2.900E+06)	(3.130E+06)	(1.081E+00)
0.050	1.342E-03	1.378E-03	1.421E-03	1.029E+00	3.000	(3.990E+06)	(4.320E+06)	(4.670E+06)	(1.082E+00)
0.060	8.454E-03	8.679E-03	8.945E-03	1.028E+00	3.500	(5.490E+06)	(5.950E+06)	(6.420E+06)	(1.081E+00)
0.070	3.659E-02	3.756E-02	3.869E-02	1.028E+00	4.000	(7.150E+06)	(7.750E+06)	(8.360E+06)	(1.081E+00)
0.080	1.221E-01	1.253E-01	1.291E-01	1.028E+00	5.000	(1.090E+07)	(1.180E+07)	(1.270E+07)	(1.079E+00)
0.090	3.373E-01	3.461E-01	3.563E-01	1.028E+00	6.000	(1.510E+07)	(1.630E+07)	(1.750E+07)	(1.077E+00)
0.100	8.073E-01	8.280E-01	8.524E-01	1.027E+00	7.000	(1.970E+07)	(2.120E+07)	(2.270E+07)	(1.073E+00)
0.110	1.728E+00	1.772E+00	1.824E+00	1.027E+00	8.000	(2.460E+07)	(2.630E+07)	(2.810E+07)	(1.069E+00)
0.120	3.385E+00	3.471E+00	3.571E+00	1.027E+00	9.000	(2.950E+07)	(3.150E+07)	(3.360E+07)	(1.067E+00)
0.130	6.166E+00	6.321E+00	6.503E+00	1.027E+00	10.000	(3.460E+07)	(3.680E+07)	(3.910E+07)	(1.063E+00)

Note. Reaction rate: C. Iliadis et al. (2016). *S* factor: see Table 2 and Appendix C in C. Iliadis et al. (2016). Normalization: see Table 2 of C. Iliadis et al. (2016). High-temperature rates (in parentheses): C. Angulo et al. (1999). Previous rates: E. G. Adelberger et al. (2011). Other: the rates listed in the table have been recalculated using a modified Bayesian model compared to C. Iliadis et al. (2016), as discussed in Section 4.

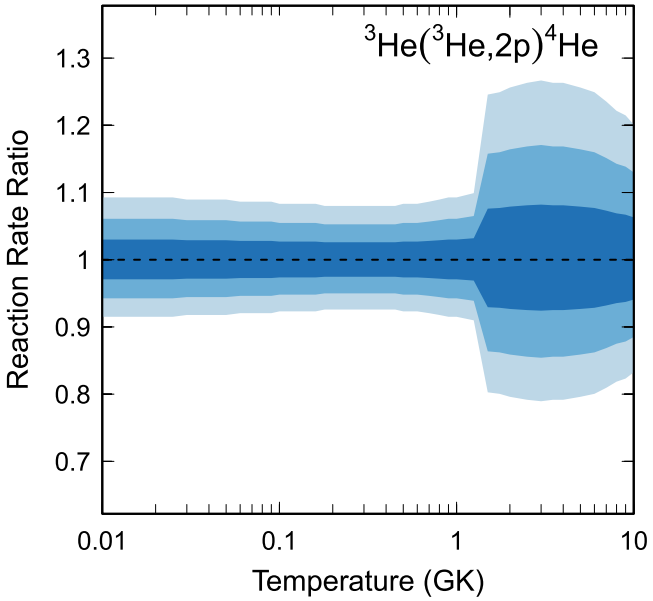

Figure 11. Reaction rate uncertainties versus temperature. The three different shades refer to coverage probabilities of 68%, 90%, and 98%.

Table 12
Total Laboratory Reaction Rates for $^{3}He(\alpha,\gamma)^{7}Be$

T (GK)	Low	Median	High	*f.u.*	T (GK)	Low	Median	High	*f.u.*
0.001	1.148E-47	1.178E-47	1.199E-47	1.021E+00	0.140	3.811E-04	3.911E-04	3.982E-04	1.021E+00
0.002	2.240E-36	2.299E-36	2.341E-36	1.021E+00	0.150	6.360E-04	6.527E-04	6.646E-04	1.021E+00
0.003	6.633E-31	6.808E-31	6.932E-31	1.021E+00	0.160	1.015E-03	1.041E-03	1.060E-03	1.021E+00
0.004	1.861E-27	1.910E-27	1.945E-27	1.021E+00	0.180	2.314E-03	2.375E-03	2.418E-03	1.021E+00
0.005	5.251E-25	5.389E-25	5.487E-25	1.021E+00	0.200	4.692E-03	4.816E-03	4.903E-03	1.021E+00
0.006	3.872E-23	3.974E-23	4.046E-23	1.021E+00	0.250	1.916E-02	1.967E-02	2.003E-02	1.021E+00
0.007	1.198E-21	1.229E-21	1.252E-21	1.021E+00	0.300	5.549E-02	5.695E-02	5.799E-02	1.021E+00
0.008	2.028E-20	2.082E-20	2.119E-20	1.021E+00	0.350	1.287E-01	1.321E-01	1.345E-01	1.021E+00
0.009	2.213E-19	2.272E-19	2.313E-19	1.021E+00	0.400	2.563E-01	2.630E-01	2.678E-01	1.021E+00
0.010	1.732E-18	1.778E-18	1.810E-18	1.021E+00	0.450	4.565E-01	4.685E-01	4.770E-01	1.021E+00
0.011	1.045E-17	1.073E-17	1.092E-17	1.021E+00	0.500	7.477E-01	7.674E-01	7.813E-01	1.021E+00
0.012	5.129E-17	5.264E-17	5.360E-17	1.021E+00	0.600	1.672E+00	1.716E+00	1.748E+00	1.021E+00
0.013	2.125E-16	2.181E-16	2.221E-16	1.021E+00	0.700	3.155E+00	3.238E+00	3.297E+00	1.021E+00
0.014	7.654E-16	7.855E-16	7.998E-16	1.021E+00	0.800	5.293E+00	5.432E+00	5.531E+00	1.021E+00
0.015	2.451E-15	2.515E-15	2.561E-15	1.021E+00	0.900	8.161E+00	8.376E+00	8.528E+00	1.021E+00
0.016	7.101E-15	7.288E-15	7.420E-15	1.021E+00	1.000	1.181E+01	1.212E+01	1.234E+01	1.021E+00
0.018	4.658E-14	4.780E-14	4.867E-14	1.021E+00	1.250	2.453E+01	2.517E+01	2.563E+01	1.021E+00
0.020	2.350E-13	2.412E-13	2.455E-13	1.021E+00	1.500	4.246E+01	4.358E+01	4.437E+01	1.021E+00
0.025	5.981E-12	6.138E-12	6.250E-12	1.021E+00	1.750	6.542E+01	6.714E+01	6.836E+01	1.021E+00
0.030	7.021E-11	7.205E-11	7.336E-11	1.021E+00	2.000	9.290E+01	9.535E+01	9.708E+01	1.021E+00
0.040	2.514E-09	2.581E-09	2.627E-09	1.021E+00	2.500	(1.647E+02)	(1.705E+02)	(1.765E+02)	(1.035E+00)
0.050	3.173E-08	3.257E-08	3.316E-08	1.021E+00	3.000	(2.497E+02)	(2.585E+02)	(2.675E+02)	(1.035E+00)
0.060	2.180E-07	2.237E-07	2.278E-07	1.021E+00	3.500	(3.480E+02)	(3.602E+02)	(3.728E+02)	(1.035E+00)
0.070	1.011E-06	1.037E-06	1.056E-06	1.021E+00	4.000	(4.582E+02)	(4.742E+02)	(4.908E+02)	(1.035E+00)
0.080	3.571E-06	3.664E-06	3.731E-06	1.021E+00	5.000	(7.102E+02)	(7.351E+02)	(7.608E+02)	(1.035E+00)
0.090	1.034E-05	1.062E-05	1.081E-05	1.021E+00	6.000	(1.000E+03)	(1.035E+03)	(1.071E+03)	(1.035E+00)
0.100	2.579E-05	2.647E-05	2.695E-05	1.021E+00	7.000	(1.324E+03)	(1.370E+03)	(1.418E+03)	(1.035E+00)
0.110	5.722E-05	5.873E-05	5.980E-05	1.021E+00	8.000	(1.679E+03)	(1.738E+03)	(1.799E+03)	(1.035E+00)
0.120	1.156E-04	1.187E-04	1.208E-04	1.021E+00	9.000	(2.063E+03)	(2.135E+03)	(2.210E+03)	(1.035E+00)
0.130	2.166E-04	2.223E-04	2.264E-04	1.021E+00	10.000	(2.471E+03)	(2.558E+03)	(2.647E+03)	(1.035E+00)

Note. Reaction rate: C. Iliadis et al. (2016). *S* factor: see Table 3 and Appendix C in C. Iliadis et al. (2016). Normalization: see Table 3 of C. Iliadis et al. (2016). High-temperature rates (in parentheses): A. Kontos et al. (2013). Previous rates: A. Kontos et al. (2013), R. J. deBoer et al. (2014), and X. Zhang et al. (2020). Other: for three energies (126.5, 147.7, and 168.9 keV), the statistical *S*-factor uncertainties listed in Table 2 of H. Costantini et al. (2008) are erroneous, as pointed out in V. Zerkin & B. Pritychenko (2018; EXFOR). The erroneous values were used by C. Iliadis et al. (2016). The Bayesian rate listed above was obtained using the corrected values.

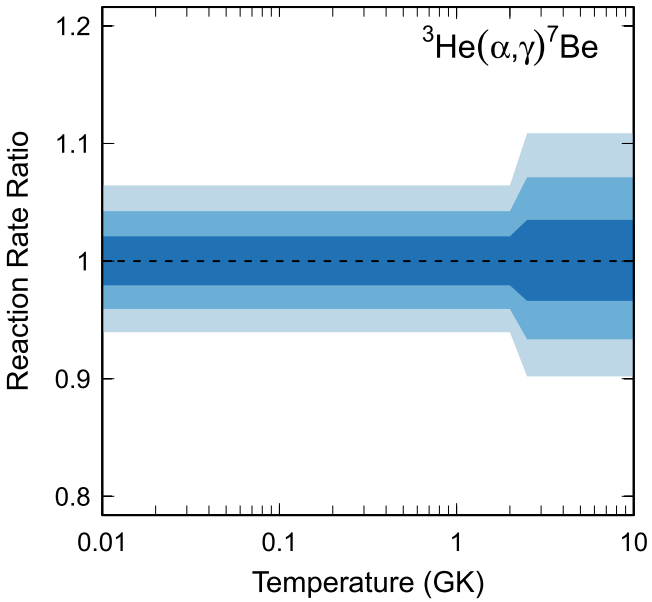

Figure 12. Reaction rate uncertainties versus temperature. The three different shades refer to coverage probabilities of 68%, 90%, and 98%.

Table 13
Total Laboratory Reaction Rates for ^{7}Be(n,p)^{7}Li

T (GK)	Low	Median	High	*f.u.*	T (GK)	Low	Median	High	*f.u.*
0.001	5.076E+09	5.156E+09	5.237E+09	1.015E+00	0.140	2.892E+09	2.944E+09	2.997E+09	1.018E+00
0.002	4.948E+09	5.025E+09	5.103E+09	1.015E+00	0.150	2.839E+09	2.890E+09	2.943E+09	1.018E+00
0.003	4.853E+09	4.928E+09	5.004E+09	1.015E+00	0.160	2.788E+09	2.839E+09	2.891E+09	1.018E+00
0.004	4.775E+09	4.848E+09	4.922E+09	1.015E+00	0.180	2.697E+09	2.747E+09	2.798E+09	1.018E+00
0.005	4.709E+09	4.780E+09	4.853E+09	1.015E+00	0.200	2.613E+09	2.662E+09	2.712E+09	1.018E+00
0.006	4.650E+09	4.721E+09	4.793E+09	1.015E+00	0.250	2.439E+09	2.486E+09	2.533E+09	1.019E+00
0.007	4.597E+09	4.666E+09	4.737E+09	1.015E+00	0.300	2.298E+09	2.342E+09	2.388E+09	1.019E+00
0.008	4.548E+09	4.617E+09	4.687E+09	1.015E+00	0.350	2.182E+09	2.225E+09	2.268E+09	1.019E+00
0.009	4.504E+09	4.572E+09	4.641E+09	1.015E+00	0.400	2.085E+09	2.126E+09	2.168E+09	1.019E+00
0.010	4.462E+09	4.530E+09	4.599E+09	1.015E+00	0.450	2.002E+09	2.042E+09	2.083E+09	1.019E+00
0.011	4.424E+09	4.491E+09	4.559E+09	1.015E+00	0.500	1.932E+09	1.971E+09	2.010E+09	1.020E+00
0.012	4.387E+09	4.453E+09	4.521E+09	1.015E+00	0.600	1.820E+09	1.857E+09	1.894E+09	1.020E+00
0.013	4.352E+09	4.418E+09	4.485E+09	1.015E+00	0.700	1.735E+09	1.771E+09	1.807E+09	1.020E+00
0.014	4.320E+09	4.385E+09	4.452E+09	1.015E+00	0.800	1.671E+09	1.705E+09	1.740E+09	1.020E+00
0.015	4.288E+09	4.353E+09	4.419E+09	1.015E+00	0.900	1.620E+09	1.653E+09	1.687E+09	1.020E+00
0.016	4.258E+09	4.323E+09	4.388E+09	1.015E+00	1.000	1.578E+09	1.611E+09	1.644E+09	1.020E+00
0.018	4.202E+09	4.266E+09	4.330E+09	1.015E+00	1.250	(1.486E+09)	(1.531E+09)	(1.576E+09)	(1.030E+00)
0.020	4.149E+09	4.212E+09	4.277E+09	1.015E+00	1.500	(1.431E+09)	(1.474E+09)	(1.518E+09)	(1.030E+00)
0.025	4.034E+09	4.096E+09	4.159E+09	1.015E+00	1.750	(1.384E+09)	(1.426E+09)	(1.468E+09)	(1.030E+00)
0.030	3.932E+09	3.993E+09	4.055E+09	1.015E+00	2.000	(1.341E+09)	(1.382E+09)	(1.423E+09)	(1.030E+00)
0.040	3.763E+09	3.823E+09	3.883E+09	1.015E+00	2.500	(1.265E+09)	(1.303E+09)	(1.342E+09)	(1.030E+00)
0.050	3.623E+09	3.682E+09	3.741E+09	1.016E+00	3.000	(1.197E+09)	(1.233E+09)	(1.270E+09)	(1.030E+00)
0.060	3.504E+09	3.561E+09	3.620E+09	1.016E+00	3.500	(1.137E+09)	(1.172E+09)	(1.207E+09)	(1.030E+00)
0.070	3.400E+09	3.457E+09	3.514E+09	1.016E+00	4.000	(1.086E+09)	(1.119E+09)	(1.152E+09)	(1.030E+00)
0.080	3.306E+09	3.362E+09	3.419E+09	1.016E+00	5.000	(1.001E+09)	(1.032E+09)	(1.063E+09)	(1.030E+00)
0.090	3.222E+09	3.277E+09	3.333E+09	1.017E+00	6.000	(9.364E+08)	(9.645E+08)	(9.934E+08)	(1.030E+00)
0.100	3.145E+09	3.199E+09	3.255E+09	1.017E+00	7.000	(8.859E+08)	(9.125E+08)	(9.398E+08)	(1.030E+00)
0.110	3.074E+09	3.128E+09	3.183E+09	1.017E+00	8.000	(8.462E+08)	(8.716E+08)	(8.977E+08)	(1.030E+00)
0.120	3.009E+09	3.062E+09	3.117E+09	1.017E+00	9.000	(8.149E+08)	(8.394E+08)	(8.645E+08)	(1.035E+00)
0.130	2.948E+09	3.001E+09	3.055E+09	1.017E+00	10.000	(7.910E+08)	(8.148E+08)	(8.392E+08)	(1.050E+00)

Note. Reaction rate: R. S. de Souza et al. (2020). *S* factor: see Figure 3 and Appendix in R. S. de Souza et al. (2020). Normalization: see Figure 2 and Section 2 in R. S. de Souza et al. (2020). High-temperature rates (in parentheses): P. Descouvemont et al. (2004). Previous rates: P. Descouvemont et al. (2004) and L. Damone et al. (2018). Other: Bayesian rate. Although we adopt at the highest temperatures ($T \geqslant 1.25$ GK) the values of P. Descouvemont et al. (2004), their rate uncertainties are unrealistically small over almost their entire temperature range. Therefore, we adopted a more realistic estimate of 3% rate uncertainty for $T = 1.25-8.0$ GK and their published rate uncertainties for $T = 9.0 - 10.0$ GK.

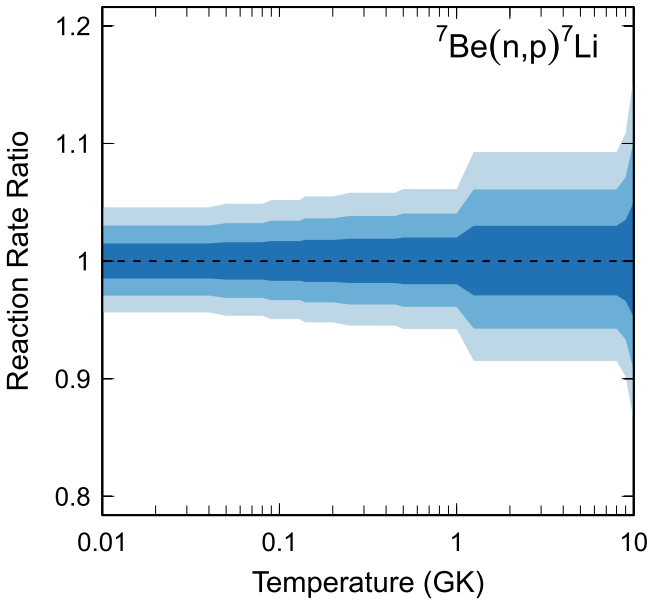

Figure 13. Reaction rate uncertainties versus temperature. The three different shades refer to coverage probabilities of 68%, 90%, and 98%.

Table 14
Total Laboratory Reaction Rates for ^{7}Be(α,γ)^{11}C

T (GK)	Low	Median	High	*f.u.*	T (GK)	Low	Median	High	*f.u.*
0.001	5.381E-92	1.598E-91	4.752E-91	2.999E+00	0.140	6.715E-11	3.514E-10	3.050E-09	6.483E+00
0.002	2.125E-71	6.311E-71	1.877E-70	2.999E+00	0.150	1.700E-10	8.697E-10	7.487E-09	6.394E+00
0.003	2.115E-61	6.281E-61	1.868E-60	2.999E+00	0.160	3.981E-10	1.989E-09	1.698E-08	6.307E+00
0.004	4.301E-55	1.277E-54	3.798E-54	2.999E+00	0.180	1.823E-09	8.600E-09	7.174E-08	6.095E+00
0.005	1.322E-50	3.925E-50	1.168E-49	2.999E+00	0.200	7.567E-09	3.103E-08	2.475E-07	5.593E+00
0.006	3.505E-47	1.041E-46	3.095E-46	2.999E+00	0.250	5.869E-07	8.779E-07	3.365E-06	2.900E+00
0.007	1.475E-42	1.268E-41	1.220E-40	8.680E+00	0.300	2.794E-05	3.314E-05	4.808E-05	1.694E+00
0.008	2.505E-40	2.141E-39	2.060E-38	8.639E+00	0.350	4.692E-04	5.397E-04	6.434E-04	1.347E+00
0.009	1.913E-38	1.626E-37	1.563E-36	8.600E+00	0.400	3.864E-03	4.401E-03	5.079E-03	1.229E+00
0.010	7.980E-37	6.741E-36	6.480E-35	8.563E+00	0.450	1.965E-02	2.227E-02	2.542E-02	1.182E+00
0.011	2.078E-35	1.744E-34	1.676E-33	8.527E+00	0.500	7.133E-02	8.059E-02	9.150E-02	1.160E+00
0.012	3.715E-34	3.094E-33	2.971E-32	8.492E+00	0.600	4.830E-01	5.429E-01	6.123E-01	1.141E+00
0.013	4.878E-33	4.037E-32	3.874E-31	8.459E+00	0.700	1.872E+00	2.093E+00	2.347E+00	1.131E+00
0.014	4.962E-32	4.086E-31	3.919E-30	8.426E+00	0.800	5.186E+00	5.761E+00	6.420E+00	1.123E+00
0.015	4.080E-31	3.341E-30	3.200E-29	8.395E+00	0.900	1.155E+01	1.275E+01	1.412E+01	1.116E+00
0.016	2.795E-30	2.277E-29	2.181E-28	8.364E+00	1.000	2.215E+01	2.430E+01	2.676E+01	1.110E+00
0.018	8.394E-29	6.763E-28	6.471E-27	8.305E+00	1.250	7.380E+01	8.019E+01	8.736E+01	1.100E+00
0.020	1.564E-27	1.247E-26	1.193E-25	8.248E+00	1.500	1.684E+02	1.823E+02	1.979E+02	1.099E+00
0.025	5.400E-25	4.214E-24	4.020E-23	8.117E+00	1.750	3.051E+02	3.303E+02	3.591E+02	1.104E+00
0.030	4.591E-23	3.512E-22	3.338E-21	7.997E+00	2.000	4.756E+02	5.159E+02	5.624E+02	1.112E+00
0.040	2.933E-20	2.140E-19	2.017E-18	7.783E+00	2.500	8.732E+02	9.516E+02	1.046E+03	1.140E+00
0.050	2.840E-18	1.987E-17	1.859E-16	7.596E+00	3.000	1.284E+03	1.408E+03	1.567E+03	1.178E+00
0.060	9.180E-17	6.177E-16	5.725E-15	7.429E+00	3.500	1.666E+03	1.838E+03	2.084E+03	1.224E+00
0.070	1.465E-15	9.476E-15	8.710E-14	7.277E+00	4.000	1.999E+03	2.224E+03	2.588E+03	1.276E+00
0.080	1.430E-14	8.939E-14	8.140E-13	7.138E+00	5.000	2.519E+03	2.857E+03	3.577E+03	1.381E+00
0.090	9.761E-14	5.905E-13	5.340E-12	7.009E+00	6.000	2.864E+03	3.327E+03	4.532E+03	1.480E+00
0.100	5.100E-13	2.980E-12	2.678E-11	6.890E+00	7.000	3.084E+03	3.672E+03	5.400E+03	1.566E+00
0.110	2.162E-12	1.224E-11	1.090E-10	6.779E+00	8.000	3.209E+03	3.924E+03	6.157E+03	1.640E+00
0.120	7.725E-12	4.255E-11	3.757E-10	6.674E+00	9.000	3.269E+03	4.098E+03	6.785E+03	1.703E+00
0.130	2.408E-11	1.295E-10	1.132E-09	6.576E+00	10.000	3.285E+03	4.215E+03	7.290E+03	1.756E+00

Note. Observed resonances: M. Wiescher et al. (1983), G. Hardie et al. (1984), M. Freer et al. (2012), A. Psaltis et al. (2022a), and A. Psaltis et al. (2022b). Unobserved resonances: M. Hartos et al. (2018) for the subsubthreshold resonance. High-temperature rates (in parentheses): no matching to statistical model rates is needed over the listed temperature range. Previous rates: Y. Xu et al. (2013) and A. Psaltis et al. (2022b). Other: prescription of M. Hartos et al. (2018) was used for $E_r^{c.m.} = -44$ keV; Γ_α and Γ_p were adopted from M. Freer et al. (2012) for resonances with $E_r^{c.m.} > 1500$ keV; values of Γ_γ were assumed to be 1 eV, with a factor of 10 uncertainty when no value was provided in the literature.

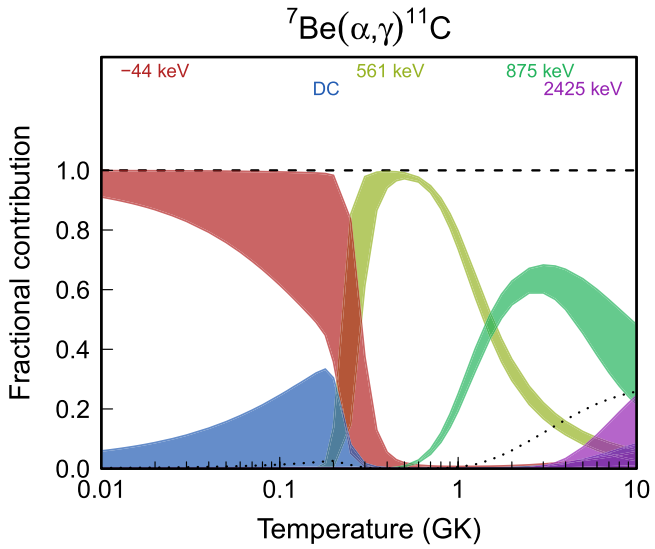

Figure 14. Fractional contributions to the total rate. "DC" refers to direct radiative capture. Resonance energies are given in the center-of-mass frame.

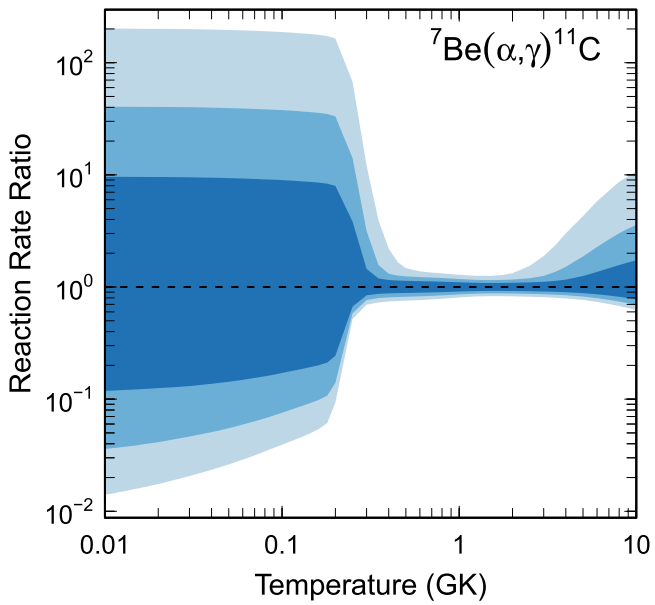

Figure 15. Reaction rate uncertainties versus temperature. The three different shades refer to coverage probabilities of 68%, 90%, and 98%.

Table 15
Total Laboratory Reaction Rates for $^{14}C(p,\gamma)^{15}N$

T (GK)	Low	Median	High	*f.u.*	T (GK)	Low	Median	High	*f.u.*
0.001	1.743E-50	2.489E-50	3.611E-50	1.440E+00	0.140	1.021E-03	1.450E-03	2.096E-03	1.434E+00
0.002	2.251E-38	3.214E-38	4.664E-38	1.440E+00	0.150	1.786E-03	2.534E-03	3.660E-03	1.432E+00
0.003	1.673E-32	2.388E-32	3.464E-32	1.440E+00	0.160	2.980E-03	4.224E-03	6.095E-03	1.431E+00
0.004	8.395E-29	1.198E-28	1.738E-28	1.440E+00	0.180	7.416E-03	1.047E-02	1.505E-02	1.425E+00
0.005	3.585E-26	5.117E-26	7.423E-26	1.440E+00	0.200	1.649E-02	2.310E-02	3.300E-02	1.415E+00
0.006	3.629E-24	5.179E-24	7.513E-24	1.440E+00	0.250	9.046E-02	1.212E-01	1.673E-01	1.361E+00
0.007	1.446E-22	2.064E-22	2.994E-22	1.440E+00	0.300	3.785E-01	4.790E-01	6.278E-01	1.291E+00
0.008	3.020E-21	4.309E-21	6.250E-21	1.440E+00	0.350	1.262E+00	1.530E+00	1.911E+00	1.237E+00
0.009	3.934E-20	5.614E-20	8.142E-20	1.440E+00	0.400	3.436E+00	4.055E+00	4.901E+00	1.200E+00
0.010	3.586E-19	5.117E-19	7.421E-19	1.440E+00	0.450	7.957E+00	9.230E+00	1.090E+01	1.175E+00
0.011	2.474E-18	3.530E-18	5.119E-18	1.440E+00	0.500	1.626E+01	1.861E+01	2.159E+01	1.157E+00
0.012	1.366E-17	1.949E-17	2.826E-17	1.440E+00	0.600	5.125E+01	5.747E+01	6.516E+01	1.131E+00
0.013	6.291E-17	8.976E-17	1.302E-16	1.439E+00	0.700	1.227E+02	1.360E+02	1.521E+02	1.117E+00
0.014	2.493E-16	3.557E-16	5.157E-16	1.439E+00	0.800	2.416E+02	2.665E+02	2.959E+02	1.110E+00
0.015	8.706E-16	1.242E-15	1.801E-15	1.439E+00	0.900	4.131E+02	4.546E+02	5.031E+02	1.106E+00
0.016	2.731E-15	3.896E-15	5.648E-15	1.439E+00	1.000	6.364E+02	6.998E+02	7.740E+02	1.106E+00
0.018	2.062E-14	2.941E-14	4.264E-14	1.439E+00	1.250	1.387E+03	1.527E+03	1.693E+03	1.108E+00
0.020	1.175E-13	1.675E-13	2.429E-13	1.439E+00	1.500	2.338E+03	2.580E+03	2.877E+03	1.113E+00
0.025	3.818E-12	5.445E-12	7.892E-12	1.439E+00	1.750	3.424E+03	3.790E+03	4.258E+03	1.120E+00
0.030	5.408E-11	7.711E-11	1.117E-10	1.439E+00	2.000	4.616E+03	5.125E+03	5.812E+03	1.127E+00
0.040	2.553E-09	3.638E-09	5.271E-09	1.438E+00	2.500	(7.184E+03)	(8.115E+03)	(1.003E+04)	(1.183E+00)
0.050	3.928E-08	5.596E-08	8.106E-08	1.438E+00	3.000	(9.164E+03)	(1.100E+04)	(2.003E+04)	(1.511E+00)
0.060	3.143E-07	4.477E-07	6.483E-07	1.437E+00	3.500	(1.070E+04)	(1.371E+04)	(3.296E+04)	(1.843E+00)
0.070	1.648E-06	2.347E-06	3.398E-06	1.437E+00	4.000	(1.180E+04)	(1.620E+04)	(4.842E+04)	(2.181E+00)
0.080	6.450E-06	9.180E-06	1.329E-05	1.436E+00	5.000	(1.288E+04)	(2.066E+04)	(8.590E+04)	(2.881E+00)
0.090	2.039E-05	2.901E-05	4.198E-05	1.436E+00	6.000	(1.275E+04)	(2.458E+04)	(1.309E+05)	(3.627E+00)
0.100	5.485E-05	7.802E-05	1.129E-04	1.436E+00	7.000	(1.166E+04)	(2.815E+04)	(1.828E+05)	(4.455E+00)
0.110	1.301E-04	1.850E-04	2.676E-04	1.435E+00	8.000	(9.752E+03)	(3.152E+04)	(2.415E+05)	(5.447E+00)
0.120	2.792E-04	3.969E-04	5.740E-04	1.435E+00	9.000	(7.124E+03)	(3.480E+04)	(3.073E+05)	(6.858E+00)
0.130	5.522E-04	7.846E-04	1.134E-03	1.434E+00	10.000	(3.806E+03)	(3.806E+04)	(3.806E+05)	(1.000E+01)

Note. Observed resonances: J. Görres et al. (1990), T. Szücs & P. Mohr (2015), and P. Torres-Sánchez et al. (2023). Normalization: none. Unobserved resonances: none. High-temperature rates (in parentheses): matching to statistical model rate above $T = 2.4$ GK. Previous rates: C. Iliadis et al. (2010c). Other: the direct-capture S factor has been calculated using experimental spectroscopic factors from J. Bommer et al. (1975), R. Sercely et al. (1979), and E. T. Ruziev et al. (2024).

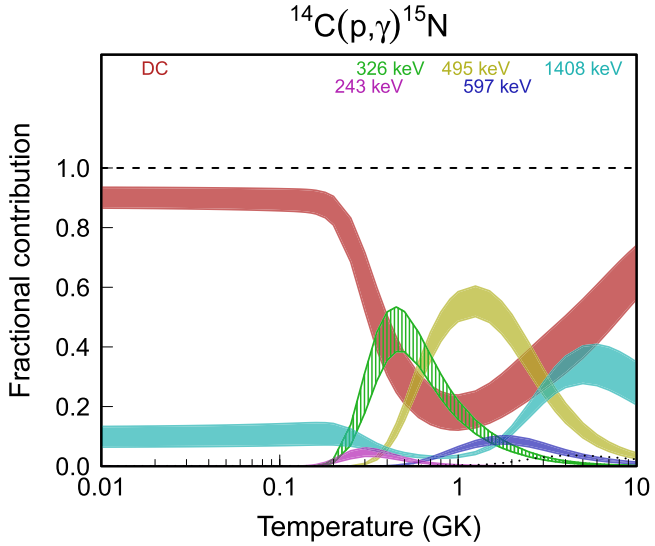

Figure 16. Fractional contributions to the total rate. "DC" refers to direct radiative capture. Resonance energies are given in the center-of-mass frame.

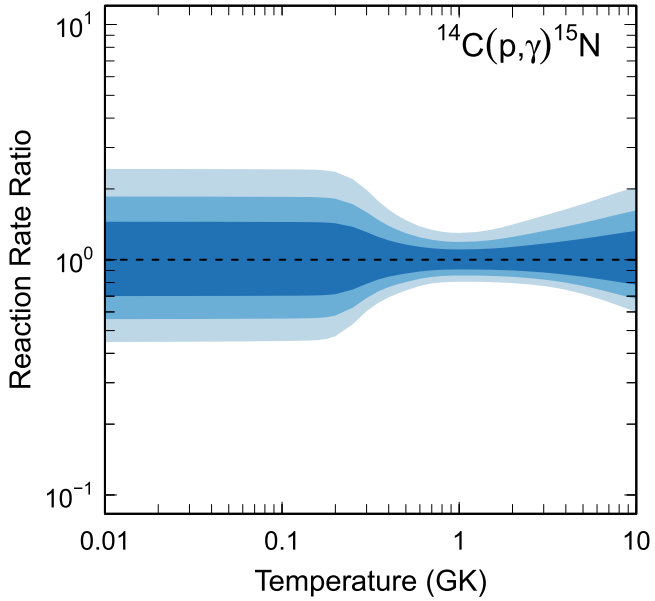

Figure 17. Reaction rate uncertainties versus temperature. The three different shades refer to coverage probabilities of 68%, 90%, and 98%.

Table 16
Total Laboratory Reaction Rates for $^{14}C(\alpha,\gamma)^{18}O$

T (GK)	Low	Median	High	*f.u.*	T (GK)	Low	Median	High	*f.u.*
0.001	0.000E+00	0.000E+00	0.000E+00	1.000E+00	0.140	4.220E-15	4.769E-14	2.317E-13	8.138E+00
0.002	0.000E+00	0.000E+00	0.000E+00	1.000E+00	0.150	1.028E-14	1.146E-13	5.561E-13	7.827E+00
0.003	5.185E-87	1.536E-86	4.587E-86	2.977E+00	0.160	2.246E-14	2.448E-13	1.186E-12	7.480E+00
0.004	3.838E-78	1.136E-77	3.387E-77	2.973E+00	0.180	8.625E-14	8.599E-13	4.137E-12	6.700E+00
0.005	7.869E-72	2.325E-71	6.925E-71	2.969E+00	0.200	2.764E-13	2.347E-12	1.110E-11	5.853E+00
0.006	5.153E-67	1.521E-66	4.525E-66	2.966E+00	0.250	3.955E-12	1.643E-11	6.519E-11	3.796E+00
0.007	9.573E-63	1.888E-62	4.112E-62	2.118E+00	0.300	1.262E-10	1.892E-10	3.539E-10	1.703E+00
0.008	1.362E-59	2.709E-59	5.986E-59	2.141E+00	0.350	9.030E-09	1.038E-08	1.198E-08	1.155E+00
0.009	6.293E-57	1.263E-56	2.834E-56	2.162E+00	0.400	2.788E-07	3.188E-07	3.650E-07	1.146E+00
0.010	1.242E-54	2.511E-54	5.703E-54	2.182E+00	0.450	4.073E-06	4.657E-06	5.330E-06	1.145E+00
0.011	1.260E-52	2.567E-52	5.894E-52	2.200E+00	0.500	3.439E-05	3.932E-05	4.498E-05	1.145E+00
0.012	7.520E-51	1.545E-50	3.575E-50	2.218E+00	0.600	8.156E-04	9.319E-04	1.065E-03	1.144E+00
0.013	2.907E-49	6.017E-49	1.405E-48	2.234E+00	0.700	7.561E-03	8.635E-03	9.861E-03	1.143E+00
0.014	7.857E-48	1.637E-47	3.853E-47	2.249E+00	0.800	3.915E-02	4.468E-02	5.100E-02	1.143E+00
0.015	1.569E-46	3.293E-46	7.824E-46	2.264E+00	0.900	1.379E-01	1.573E-01	1.795E-01	1.142E+00
0.016	2.429E-45	5.127E-45	1.227E-44	2.278E+00	1.000	3.724E-01	4.245E-01	4.838E-01	1.141E+00
0.018	3.089E-43	6.596E-43	1.601E-42	2.303E+00	1.250	2.145E+00	2.438E+00	2.772E+00	1.138E+00
0.020	2.004E-41	4.328E-41	1.063E-40	2.326E+00	1.500	(6.584E+00)	(7.524E+00)	(9.177E+00)	(1.181E+00)
0.025	8.553E-38	1.890E-37	4.749E-37	2.374E+00	1.750	(1.283E+01)	(1.505E+01)	(2.224E+01)	(1.326E+00)
0.030	5.515E-35	1.196E-34	2.960E-34	2.332E+00	2.000	(2.465E+01)	(2.972E+01)	(5.161E+01)	(1.471E+00)
0.040	5.462E-30	4.002E-29	1.885E-28	5.376E+00	2.500	(5.683E+01)	(7.251E+01)	(1.633E+02)	(1.764E+00)
0.050	6.977E-26	7.753E-25	3.793E-24	8.108E+00	3.000	(1.009E+02)	(1.366E+02)	(3.784E+02)	(2.062E+00)
0.060	4.861E-23	5.517E-22	2.688E-21	8.850E+00	3.500	(1.524E+02)	(2.201E+02)	(7.231E+02)	(2.365E+00)
0.070	5.088E-21	5.791E-20	2.822E-19	9.070E+00	4.000	(2.071E+02)	(3.201E+02)	(1.217E+03)	(2.674E+00)
0.080	1.625E-19	1.854E-18	9.022E-18	9.114E+00	5.000	(3.110E+02)	(5.594E+02)	(2.705E+03)	(3.317E+00)
0.090	2.359E-18	2.689E-17	1.304E-16	9.073E+00	6.000	(3.908E+02)	(8.410E+02)	(4.935E+03)	(4.010E+00)
0.100	1.963E-17	2.247E-16	1.090E-15	8.974E+00	7.000	(4.345E+02)	(1.163E+03)	(8.027E+03)	(4.789E+00)
0.110	1.100E-16	1.256E-15	6.105E-15	8.829E+00	8.000	(4.323E+02)	(1.531E+03)	(1.215E+04)	(5.738E+00)
0.120	4.576E-16	5.217E-15	2.536E-14	8.640E+00	9.000	(3.740E+02)	(1.956E+03)	(1.754E+04)	(7.099E+00)
0.130	1.517E-15	1.724E-14	8.386E-14	8.409E+00	10.000	(2.459E+02)	(2.459E+03)	(2.459E+04)	(1.000E+01)

Note. Observed resonances: J. Görres et al. (1992), M. Gai et al. (1987), and M. Gai (1992). Normalization: none. Unobserved resonances: the reduced widths were adopted from α transfer work (A. Cunsolo et al. 1981). High-temperature rates (in parentheses): matching to statistical model rate above $T = 1.42$ GK. Previous rates: M. A. Hashimoto et al. (1986), L. Buchmann et al. (1988), C. Funck & K. Langanke (1989), M. Lugaro et al. (2004), and C. Iliadis et al. (2010c). Other: the direct-capture S factor (including tails of higher-lying resonances) was adopted from J. Görres et al. (1992).

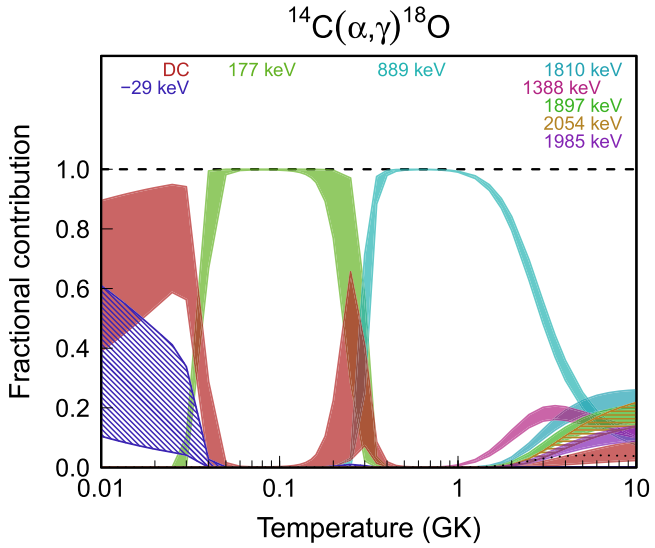

Figure 18. Fractional contributions to the total rate. "DC" refers to direct radiative capture. Resonance energies are given in the center-of-mass frame.

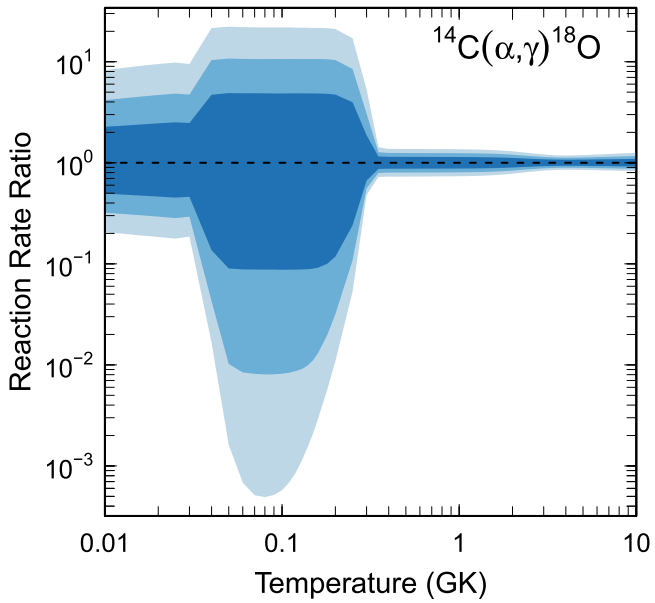

Figure 19. Reaction rate uncertainties versus temperature. The three different shades refer to coverage probabilities of 68%, 90%, and 98%.

Table 17
Total Laboratory Reaction Rates for $^{13}N(\alpha,p)^{16}O$

T (GK)	Low	Median	High	*f.u.*	T (GK)	Low	Median	High	*f.u.*
0.001	0.000E+00	0.000E+00	0.000E+00	1.000E+00	0.140	7.303E-13	1.614E-12	3.794E-12	2.275E+00
0.002	0.000E+00	0.000E+00	0.000E+00	1.000E+00	0.150	2.692E-12	5.742E-12	1.327E-11	2.219E+00
0.003	0.000E+00	0.000E+00	0.000E+00	1.000E+00	0.160	8.839E-12	1.812E-11	4.070E-11	2.152E+00
0.004	0.000E+00	0.000E+00	0.000E+00	1.000E+00	0.180	7.395E-11	1.400E-10	2.919E-10	2.003E+00
0.005	0.000E+00	0.000E+00	0.000E+00	1.000E+00	0.200	4.878E-10	8.605E-10	1.646E-09	1.865E+00
0.006	0.000E+00	0.000E+00	0.000E+00	1.000E+00	0.250	2.578E-08	4.236E-08	7.338E-08	1.710E+00
0.007	3.793E-64	6.139E-64	1.058E-63	1.697E+00	0.300	6.619E-07	1.097E-06	1.946E-06	1.744E+00
0.008	1.223E-60	1.986E-60	3.427E-60	1.702E+00	0.350	1.140E-05	1.919E-05	3.435E-05	1.766E+00
0.009	1.134E-57	1.846E-57	3.193E-57	1.706E+00	0.400	1.571E-04	2.686E-04	4.698E-04	1.748E+00
0.010	4.091E-55	6.671E-55	1.158E-54	1.711E+00	0.450	1.632E-03	2.885E-03	5.100E-03	1.769E+00
0.011	7.059E-53	1.154E-52	2.009E-52	1.716E+00	0.500	1.229E-02	2.252E-02	4.068E-02	1.813E+00
0.012	6.752E-51	1.107E-50	1.933E-50	1.720E+00	0.600	2.978E-01	5.720E-01	1.066E+00	1.880E+00
0.013	4.000E-49	6.568E-49	1.151E-48	1.725E+00	0.700	3.068E+00	6.038E+00	1.136E+01	1.909E+00
0.014	1.589E-47	2.617E-47	4.600E-47	1.731E+00	0.800	1.776E+01	3.539E+01	6.649E+01	1.917E+00
0.015	4.518E-46	7.457E-46	1.315E-45	1.736E+00	0.900	6.981E+01	1.390E+02	2.606E+02	1.912E+00
0.016	9.670E-45	1.600E-44	2.830E-44	1.741E+00	1.000	2.086E+02	4.128E+02	7.690E+02	1.898E+00
0.018	2.196E-42	3.648E-42	6.490E-42	1.752E+00	1.250	1.532E+03	2.904E+03	5.277E+03	1.826E+00
0.020	2.358E-40	3.943E-40	7.061E-40	1.764E+00	1.500	6.145E+03	1.083E+04	1.891E+04	1.726E+00
0.025	2.826E-36	4.786E-36	8.753E-36	1.797E+00	1.750	1.761E+04	2.875E+04	4.756E+04	1.623E+00
0.030	3.743E-33	6.450E-33	1.212E-32	1.836E+00	2.000	4.067E+04	6.214E+04	9.711E+04	1.534E+00
0.040	1.452E-28	2.625E-28	5.271E-28	1.942E+00	2.500	1.418E+05	1.999E+05	2.831E+05	1.412E+00
0.050	3.206E-25	6.345E-25	1.421E-24	2.121E+00	3.000	3.464E+05	4.684E+05	6.276E+05	1.350E+00
0.060	1.495E-22	3.329E-22	8.110E-22	2.323E+00	3.500	6.778E+05	8.986E+05	1.173E+06	1.321E+00
0.070	2.317E-20	5.454E-20	1.347E-19	2.404E+00	4.000	1.151E+06	1.509E+06	1.952E+06	1.309E+00
0.080	1.363E-18	3.228E-18	7.895E-18	2.406E+00	5.000	2.571E+06	3.329E+06	4.300E+06	1.299E+00
0.090	3.631E-17	8.576E-17	2.086E-16	2.392E+00	6.000	4.674E+06	6.034E+06	7.821E+06	1.298E+00
0.100	5.320E-16	1.254E-15	3.027E-15	2.379E+00	7.000	7.478E+06	9.659E+06	1.258E+07	1.301E+00
0.110	4.962E-15	1.163E-14	2.805E-14	2.366E+00	8.000	1.090E+07	1.414E+07	1.848E+07	1.308E+00
0.120	3.313E-14	7.654E-14	1.840E-13	2.347E+00	9.000	1.483E+07	1.929E+07	2.537E+07	1.314E+00
0.130	1.716E-13	3.884E-13	9.266E-13	2.318E+00	10.000	1.910E+07	2.496E+07	3.301E+07	1.320E+00

Note. Observed resonances: S. R. Salisbury et al. (1962) and S. R. Salisbury & H. T. Richards (1962); cross section data for $E_r^{c.m} = 3.26-6.02$ MeV were taken from H. Jayatissa et al. (2022). Unobserved resonances: A. Meyer et al. (2020), using the $^{13}C(^7Li, t)^{17}O$ reaction for mirror states. Previous rates: G. R. Caughlan & W. A. Fowler (1988) and A. Meyer et al. (2020). High-temperature rates (in parentheses): no matching to statistical model rates is needed over the listed temperature range. Other: values for Γ_α were assumed to have a factor uncertainty of 2.5; Γ_p was assumed to have a 20% uncertainty when no value was provided in the literature.

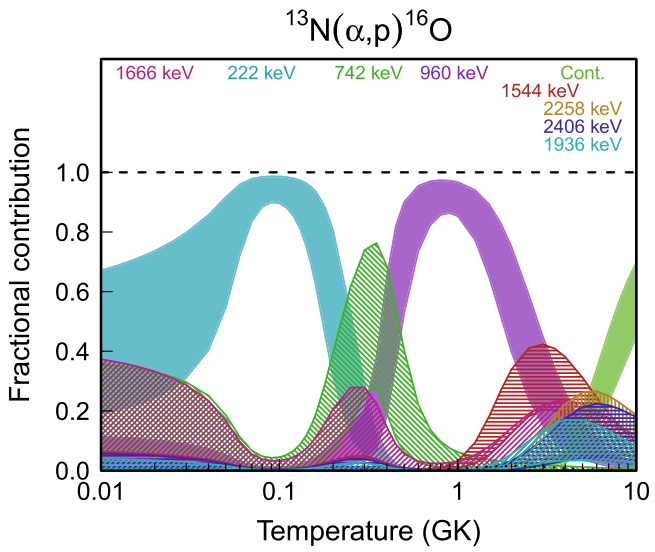

Figure 20. Fractional contributions to the total rate. "Cont." refers to the continuum of higher-lying, unresolved resonances. Resonance energies are given in the center-of-mass frame.

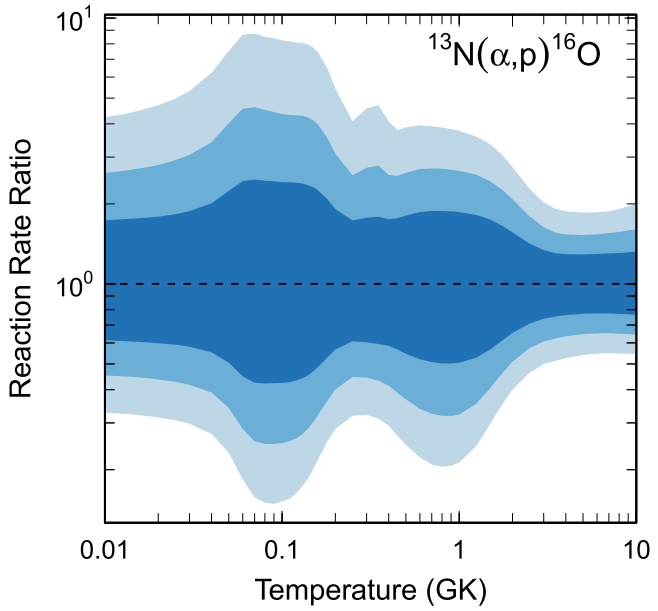

Figure 21. Reaction rate uncertainties versus temperature. The three different shades refer to coverage probabilities of 68%, 90%, and 98%.

Table 18
Total Laboratory Reaction Rates for $^{14}N(\alpha,\gamma)^{18}F$

T (GK)	Low	Median	High	*f.u.*	T (GK)	Low	Median	High	*f.u.*
0.001	0.000E+00	0.000E+00	0.000E+00	1.000E+00	0.140	2.286E-15	2.534E-15	2.803E-15	1.108E+00
0.002	0.000E+00	0.000E+00	0.000E+00	1.000E+00	0.150	2.446E-14	2.687E-14	2.945E-14	1.098E+00
0.003	4.392E-99	2.148E-98	1.057E-97	4.974E+00	0.160	1.933E-13	2.107E-13	2.292E-13	1.089E+00
0.004	3.026E-89	1.480E-88	7.285E-88	4.974E+00	0.180	5.961E-12	6.420E-12	6.908E-12	1.077E+00
0.005	3.039E-82	1.487E-81	7.318E-81	4.974E+00	0.200	9.095E-11	9.718E-11	1.038E-10	1.068E+00
0.006	6.700E-77	3.277E-76	1.613E-75	4.974E+00	0.250	1.161E-08	1.229E-08	1.300E-08	1.058E+00
0.007	1.244E-72	6.085E-72	2.995E-71	4.974E+00	0.300	2.787E-07	2.946E-07	3.113E-07	1.057E+00
0.008	1.908E-68	6.458E-68	2.079E-67	3.279E+00	0.350	2.598E-06	2.749E-06	2.909E-06	1.058E+00
0.009	1.768E-65	5.950E-65	1.916E-64	3.274E+00	0.400	1.348E-05	1.430E-05	1.517E-05	1.061E+00
0.010	6.341E-63	2.126E-62	6.825E-62	3.270E+00	0.450	4.770E-05	5.071E-05	5.392E-05	1.064E+00
0.011	1.088E-60	3.629E-60	1.165E-59	3.266E+00	0.500	1.302E-04	1.386E-04	1.476E-04	1.065E+00
0.012	1.033E-58	3.429E-58	1.101E-57	3.263E+00	0.600	6.096E-04	6.501E-04	6.933E-04	1.067E+00
0.013	6.057E-57	2.007E-56	6.425E-56	3.261E+00	0.700	2.177E-03	2.335E-03	2.506E-03	1.074E+00
0.014	2.381E-55	7.860E-55	2.519E-54	3.259E+00	0.800	7.457E-03	8.082E-03	8.787E-03	1.087E+00
0.015	6.699E-54	2.199E-53	7.043E-53	3.257E+00	0.900	2.484E-02	2.709E-02	2.963E-02	1.093E+00
0.016	1.414E-52	4.637E-52	1.484E-51	3.255E+00	1.000	7.475E-02	8.169E-02	8.934E-02	1.094E+00
0.018	3.126E-50	1.019E-49	3.266E-49	3.253E+00	1.250	6.506E-01	7.103E-01	7.760E-01	1.093E+00
0.020	3.270E-48	1.059E-47	3.390E-47	3.252E+00	1.500	2.883E+00	3.151E+00	3.446E+00	1.094E+00
0.025	3.620E-44	1.159E-43	3.742E-43	3.250E+00	1.750	8.331E+00	9.106E+00	9.962E+00	1.094E+00
0.030	4.413E-41	1.391E-40	4.519E-40	3.250E+00	2.000	1.830E+01	1.999E+01	2.187E+01	1.094E+00
0.040	1.374E-36	4.269E-36	1.410E-35	3.248E+00	2.500	5.384E+01	5.874E+01	6.416E+01	1.092E+00
0.050	2.347E-33	6.997E-33	2.304E-32	3.185E+00	3.000	1.082E+02	1.179E+02	1.286E+02	1.091E+00
0.060	8.722E-31	2.694E-30	9.772E-30	3.511E+00	3.500	1.753E+02	1.909E+02	2.082E+02	1.090E+00
0.070	1.083E-28	3.809E-28	1.933E-27	4.588E+00	4.000	2.483E+02	2.706E+02	2.953E+02	1.091E+00
0.080	1.111E-26	2.854E-26	1.652E-25	4.326E+00	5.000	3.927E+02	4.289E+02	4.687E+02	1.093E+00
0.090	5.590E-24	7.130E-24	1.192E-23	2.022E+00	6.000	5.167E+02	5.654E+02	6.199E+02	1.096E+00
0.100	1.388E-21	1.647E-21	1.984E-21	1.316E+00	7.000	6.131E+02	6.725E+02	7.401E+02	1.101E+00
0.110	1.328E-19	1.535E-19	1.773E-19	1.169E+00	8.000	6.832E+02	7.512E+02	8.298E+02	1.106E+00
0.120	5.944E-18	6.752E-18	7.654E-18	1.136E+00	9.000	7.313E+02	8.061E+02	8.938E+02	1.112E+00
0.130	1.472E-16	1.650E-16	1.845E-16	1.120E+00	10.000	7.617E+02	8.413E+02	9.363E+02	1.119E+00

Note. Observed resonances: P. D. Parker (1968), R. Couch et al. (1971), C. Rolfs et al. (1973a, 1973b, 1973c), H. W. Becker et al. (1982), and J. Görres et al. (2000). Normalization: H. W. Becker et al. (1982). Unobserved resonances: S. Gorodetzky et al. (1967) and S. G. Cooper (1986). High-temperature rates (in parentheses): no matching to statistical model rates is needed over the listed temperature range. Previous rates: J. Görres et al. (2000). Other: for the $E_r^{c.m.} = 238$ keV resonance, the upper-limit on Γ_α was deduced from the upper limit given by R. Couch et al. (1971). Since the isospin of this state is $T = 1$, we assumed for $\langle\theta_\alpha^2\rangle$ a value of 1×10^{-5} with a factor of 10 uncertainty.

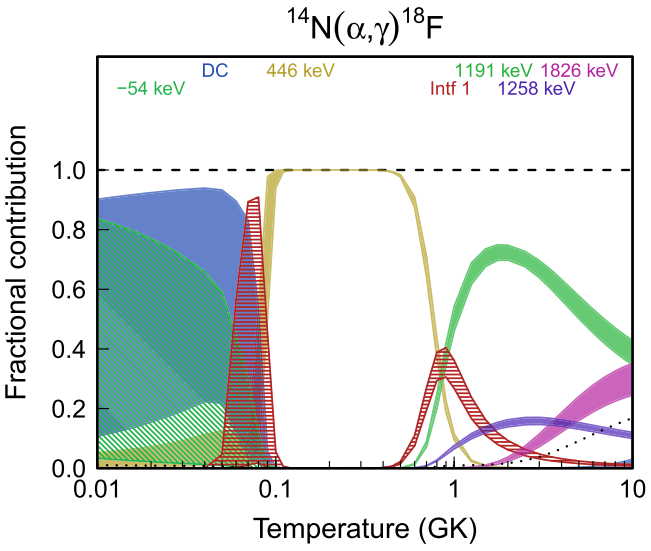

Figure 22. Fractional contributions to the total rate. "DC" refers to direct radiative capture. Resonance energies are given in the center-of-mass frame. "Intf 1" labels the combined contribution of the two interfering 4^+ resonances at $E_r^{c.m.} = 238$ and 884 keV.

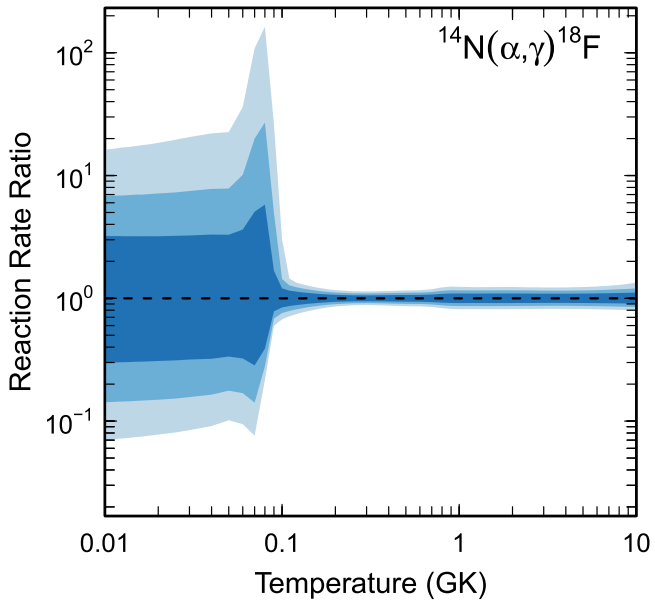

Figure 23. Reaction rate uncertainties versus temperature. The three different shades refer to coverage probabilities of 68%, 90%, and 98%.

Table 19
Total Laboratory Reaction Rates for $^{15}N(\alpha,\gamma)^{19}F$

T (GK)	Low	Median	High	*f.u.*	T (GK)	Low	Median	High	*f.u.*
0.001	0.000E+00	0.000E+00	0.000E+00	1.000E+00	0.140	6.370E-17	1.858E-16	5.508E-16	2.929E+00
0.002	0.000E+00	0.000E+00	0.000E+00	1.000E+00	0.150	4.568E-16	1.284E-15	3.759E-15	2.839E+00
0.003	8.113E-98	2.400E-97	7.179E-97	2.995E+00	0.160	2.703E-15	7.082E-15	2.020E-14	2.687E+00
0.004	6.251E-88	1.849E-87	5.531E-87	2.995E+00	0.180	6.690E-14	1.366E-13	3.449E-13	2.249E+00
0.005	6.796E-81	2.011E-80	6.014E-80	2.995E+00	0.200	1.197E-12	1.832E-12	3.702E-12	1.812E+00
0.006	1.591E-75	4.707E-75	1.408E-74	2.995E+00	0.250	3.539E-10	4.093E-10	5.048E-10	1.253E+00
0.007	3.099E-71	9.168E-71	2.742E-70	2.995E+00	0.300	1.934E-08	2.135E-08	2.380E-08	1.119E+00
0.008	2.096E-67	4.206E-67	1.054E-66	2.231E+00	0.350	3.765E-07	4.081E-07	4.434E-07	1.087E+00
0.009	2.060E-64	4.138E-64	1.037E-63	2.231E+00	0.400	3.714E-06	3.993E-06	4.298E-06	1.076E+00
0.010	7.811E-62	1.568E-61	3.926E-61	2.229E+00	0.450	2.269E-05	2.435E-05	2.612E-05	1.073E+00
0.011	1.407E-59	2.820E-59	7.057E-59	2.228E+00	0.500	9.774E-05	1.050E-04	1.126E-04	1.074E+00
0.012	1.397E-57	2.796E-57	6.992E-57	2.226E+00	0.600	8.797E-04	9.468E-04	1.018E-03	1.076E+00
0.013	8.531E-56	1.706E-55	4.262E-55	2.224E+00	0.700	4.208E-03	4.535E-03	4.888E-03	1.078E+00
0.014	3.484E-54	6.958E-54	1.737E-53	2.222E+00	0.800	1.369E-02	1.475E-02	1.590E-02	1.078E+00
0.015	1.014E-52	2.023E-52	5.047E-52	2.220E+00	0.900	3.549E-02	3.809E-02	4.093E-02	1.074E+00
0.016	2.214E-51	4.411E-51	1.100E-50	2.218E+00	1.000	8.168E-02	8.698E-02	9.278E-02	1.066E+00
0.018	5.191E-49	1.032E-48	2.568E-48	2.214E+00	1.250	5.296E-01	5.519E-01	5.759E-01	1.043E+00
0.020	5.715E-47	1.133E-46	2.814E-46	2.210E+00	1.500	2.535E+00	2.634E+00	2.738E+00	1.039E+00
0.025	7.064E-43	1.391E-42	3.441E-42	2.201E+00	1.750	8.594E+00	8.945E+00	9.317E+00	1.041E+00
0.030	9.355E-40	1.830E-39	4.511E-39	2.192E+00	2.000	2.199E+01	2.293E+01	2.391E+01	1.043E+00
0.040	3.330E-35	6.439E-35	1.576E-34	2.174E+00	2.500	8.226E+01	8.590E+01	8.970E+01	1.045E+00
0.050	5.763E-32	1.103E-31	2.680E-31	2.158E+00	3.000	1.963E+02	2.052E+02	2.144E+02	1.046E+00
0.060	1.704E-29	3.230E-29	7.789E-29	2.142E+00	3.500	3.627E+02	3.793E+02	3.967E+02	1.046E+00
0.070	1.673E-27	3.083E-27	7.278E-27	2.100E+00	4.000	5.721E+02	5.989E+02	6.268E+02	1.047E+00
0.080	1.198E-25	2.237E-25	4.649E-25	1.978E+00	5.000	1.076E+03	1.128E+03	1.184E+03	1.049E+00
0.090	9.728E-24	2.270E-23	5.855E-23	2.460E+00	6.000	1.629E+03	1.713E+03	1.803E+03	1.053E+00
0.100	6.308E-22	1.751E-21	5.093E-21	2.830E+00	7.000	2.181E+03	2.299E+03	2.428E+03	1.057E+00
0.110	2.364E-20	6.930E-20	2.058E-19	2.946E+00	8.000	2.701E+03	2.855E+03	3.025E+03	1.061E+00
0.120	5.049E-19	1.498E-18	4.464E-18	2.975E+00	9.000	3.177E+03	3.365E+03	3.578E+03	1.066E+00
0.130	6.788E-18	2.010E-17	5.988E-17	2.969E+00	10.000	3.601E+03	3.822E+03	4.077E+03	1.070E+00

Note. Observed resonances: H. Smotrich et al. (1961), J. Aitken et al. (1969), J. H. Aitken et al. (1970), W. R. Dixon et al. (1971), D. W. O. Rogers et al. (1972a, 1972b, 1973), B. Underwood et al. (1974), D. W. O. Rogers et al. (1976), W. Dixon & R. Storey (1977), T. J. M. Symons et al. (1978), S. Wilmes et al. (2002), A. Di Leva et al. (2017), A. Volya et al. (2022), and R. Fang et al. (2024). Normalization: J. H. Aitken et al. (1970), W. R. Dixon & R. S. Storey (1971), S. Wilmes et al. (2002), A. Di Leva et al. (2017), and R. Fang et al. (2024). Unobserved resonances: F. de Oliveira et al. (1996), Z. Q. Mao et al. (1996), H. T. Fortune & A. G. Lacaze (2003), H. T. Fortune (2003), and H. T. Fortune et al. (2010). High-temperature rates (in parentheses): no matching to statistical model rates is needed over the listed temperature range. Previous rates: C. Iliadis et al. (2010a). Other: the resonance strength values for the $E_r^{c.m.} = 1324$ keV resonance from W. R. Dixon & R. S. Storey (1971) and J. H. Aitken et al. (1970) were adjusted using an updated value of the $E_r^{c.m.} = 1258$ keV resonance in $^{14}N(\alpha,\gamma)^{18}F$ (H. W. Becker et al. 1982).

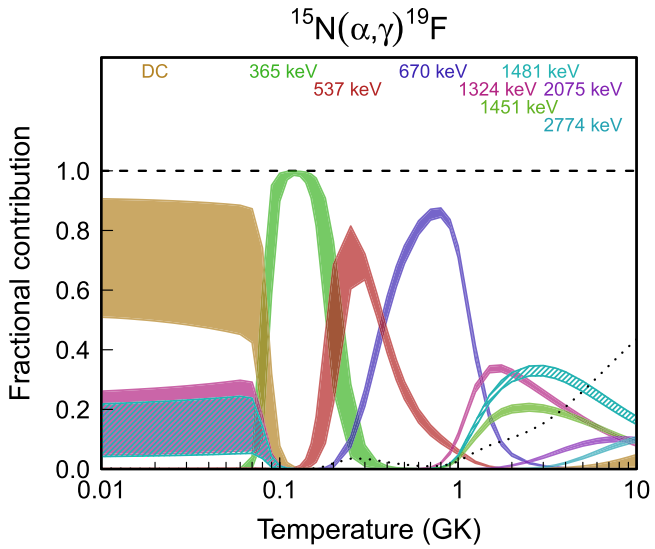

Figure 24. Fractional contributions to the total rate. "DC" refers to direct radiative capture. Resonance energies are given in the center-of-mass frame.

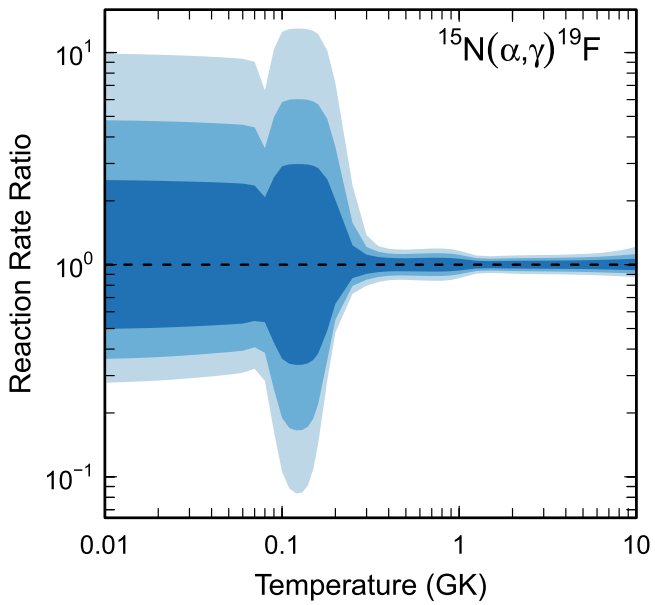

Figure 25. Reaction rate uncertainties versus temperature. The three different shades refer to coverage probabilities of 68%, 90%, and 98%.

Table 20
Total Laboratory Reaction Rates for $^{15}O(\alpha,\gamma)^{19}Ne$

T (GK)	Low	Median	High	*f.u.*	*T* (GK)	Low	Median	High	*f.u.*
0.001	0.000E+00	0.000E+00	0.000E+00	1.000E+00	0.140	4.481E-19	4.261E-18	4.268E-17	9.731E+00
0.002	0.000E+00	0.000E+00	0.000E+00	1.000E+00	0.150	6.614E-18	6.329E-17	6.354E-16	9.794E+00
0.003	0.000E+00	0.000E+00	0.000E+00	1.000E+00	0.160	6.994E-17	6.672E-16	6.712E-15	9.783E+00
0.004	5.833E-97	5.763E-96	5.723E-95	9.960E+00	0.180	3.548E-15	3.338E-14	3.358E-13	9.663E+00
0.005	2.950E-89	2.915E-88	2.895E-87	9.960E+00	0.200	8.223E-14	7.528E-13	7.558E-12	9.472E+00
0.006	2.240E-83	2.213E-82	2.198E-81	9.960E+00	0.250	2.416E-11	1.996E-10	1.952E-09	8.849E+00
0.007	1.119E-78	1.106E-77	1.098E-76	9.960E+00	0.300	1.101E-09	8.163E-09	7.562E-08	8.171E+00
0.008	1.166E-74	9.316E-74	8.464E-73	8.436E+00	0.350	1.751E-08	1.164E-07	1.007E-06	7.522E+00
0.009	2.223E-71	1.774E-70	1.611E-69	8.431E+00	0.400	1.451E-07	8.671E-07	6.920E-06	6.921E+00
0.010	1.489E-68	1.188E-67	1.078E-66	8.427E+00	0.450	7.781E-07	4.216E-06	3.075E-05	6.362E+00
0.011	4.404E-66	3.515E-65	3.186E-64	8.421E+00	0.500	3.132E-06	1.538E-05	1.022E-04	5.824E+00
0.012	6.783E-64	5.402E-63	4.894E-62	8.414E+00	0.600	2.957E-05	1.155E-04	6.454E-04	4.747E+00
0.013	6.127E-62	4.874E-61	4.409E-60	8.406E+00	0.700	1.951E-04	5.545E-04	2.602E-03	3.762E+00
0.014	3.557E-60	2.827E-59	2.557E-58	8.398E+00	0.800	1.007E-03	2.118E-03	7.875E-03	3.016E+00
0.015	1.425E-58	1.132E-57	1.022E-56	8.388E+00	0.900	3.955E-03	6.953E-03	2.004E-02	2.511E+00
0.016	4.165E-57	3.304E-56	2.978E-55	8.379E+00	1.000	1.231E-02	1.960E-02	4.519E-02	2.182E+00
0.018	1.634E-54	1.293E-53	1.164E-52	8.361E+00	1.250	9.948E-02	1.449E-01	2.407E-01	1.764E+00
0.020	2.806E-52	2.214E-51	1.990E-50	8.343E+00	1.500	4.066E-01	5.718E-01	8.549E-01	1.591E+00
0.025	8.446E-48	6.616E-47	5.929E-46	8.298E+00	1.750	1.113E+00	1.532E+00	2.194E+00	1.504E+00
0.030	2.212E-44	1.716E-43	1.534E-42	8.255E+00	2.000	2.359E+00	3.204E+00	4.491E+00	1.454E+00
0.040	2.136E-39	1.633E-38	1.444E-37	8.169E+00	2.500	6.646E+00	8.890E+00	1.218E+01	1.405E+00
0.050	7.548E-36	5.695E-35	4.975E-34	8.084E+00	3.000	1.300E+01	1.730E+01	2.349E+01	1.398E+00
0.060	3.859E-33	2.877E-32	2.485E-31	7.999E+00	3.500	2.063E+01	2.744E+01	3.739E+01	1.422E+00
0.070	5.652E-31	4.155E-30	3.549E-29	7.911E+00	4.000	(2.897E+01)	(3.878E+01)	(5.428E+01)	(1.369E+00)
0.080	3.527E-29	2.536E-28	2.137E-27	7.787E+00	5.000	(7.422E+01)	(1.161E+02)	(3.290E+02)	(2.199E+00)
0.090	1.838E-27	1.154E-26	8.170E-26	6.795E+00	6.000	(1.304E+02)	(2.454E+02)	(1.047E+03)	(3.074E+00)
0.100	1.569E-25	9.217E-25	6.110E-24	6.403E+00	7.000	(1.826E+02)	(4.311E+02)	(2.457E+03)	(4.031E+00)
0.110	1.160E-23	8.122E-23	6.860E-22	7.755E+00	8.000	(2.133E+02)	(6.757E+02)	(4.820E+03)	(5.151E+00)
0.120	6.115E-22	5.062E-21	4.899E-20	8.931E+00	9.000	(2.036E+02)	(9.797E+02)	(8.393E+03)	(6.689E+00)
0.130	2.060E-20	1.887E-19	1.880E-18	9.508E+00	10.000	(1.344E+02)	(1.344E+03)	(1.344E+04)	(1.000E+01)

Note. Observed resonances: none. Normalization: none. Unobserved resonances: spectroscopic factors used to deduce the proton partial widths were taken from F. de Oliveira et al. (1996). High-temperature rates (in parentheses): matching to statistical model rate above $T = 4.0$ GK. Previous rates: K. I. Hahn et al. (1996), W. P. Tan et al. (2009), C. Iliadis et al. (2010c), and B. Davids et al. (2011). Other: the γ-ray partial widths were scaled from those of the mirror states, except for the 850 keV resonance, where we adopted the partial width from B. Davids et al. (2003). See also B. Davids et al. (2011). The direct-capture *S* factor has been calculated using experimental spectroscopic factors from Z. Q. Mao et al. (1996). For the α-particle partial widths of resonances with $E_r^{c.m.} > 1$ MeV, see P. V. Magnus et al. (1990), A. M. Laird et al. (2002), A. N. Ostrowski et al. (2002), B. Davids et al. (2003), D. W. Visser et al. (2004), and W. P. Tan et al. (2009).

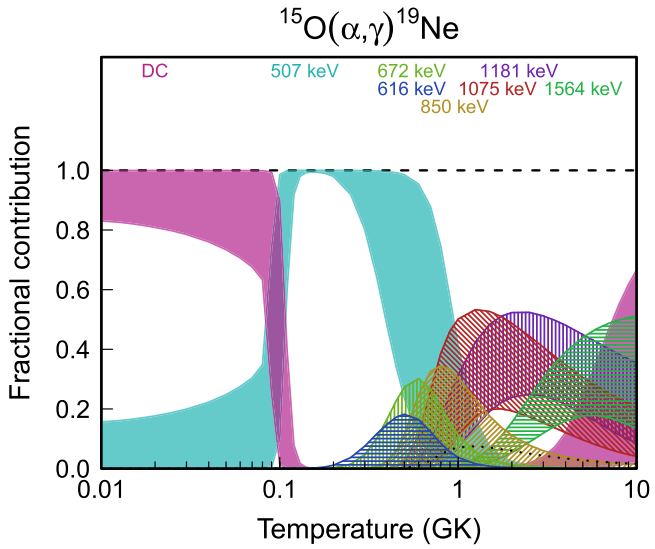

Figure 26. Fractional contributions to the total rate. "DC" refers to direct radiative capture. Resonance energies are given in the center-of-mass frame.

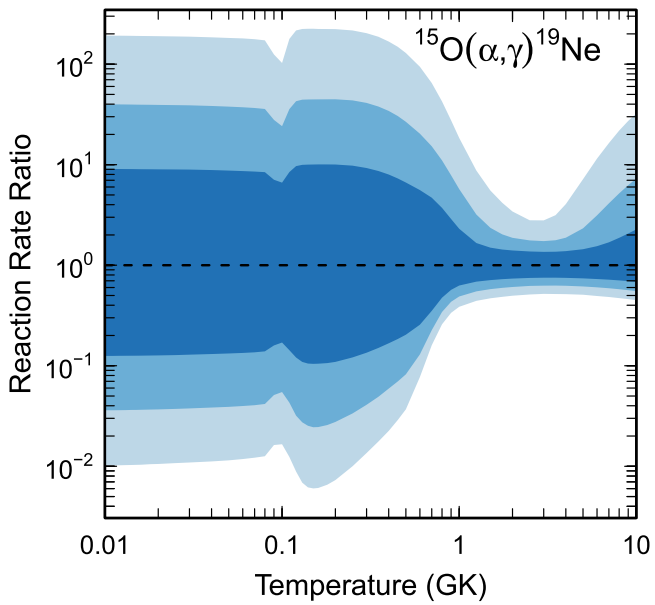

Figure 27. Reaction rate uncertainties versus temperature. The three different shades refer to coverage probabilities of 68%, 90%, and 98%.

Table 21
Total Laboratory Reaction Rates for $^{16}O(p,\gamma)^{17}F$

T (GK)	Low	Median	High	*f.u.*	T (GK)	Low	Median	High	*f.u.*
0.001	5.229E-63	5.435E-63	5.650E-63	1.042E+00	0.140	4.472E-06	4.659E-06	4.851E-06	1.042E+00
0.002	2.935E-48	3.051E-48	3.172E-48	1.042E+00	0.150	8.764E-06	9.131E-06	9.507E-06	1.042E+00
0.003	4.164E-41	4.338E-41	4.517E-41	1.042E+00	0.160	1.620E-05	1.688E-05	1.757E-05	1.042E+00
0.004	1.343E-36	1.399E-36	1.457E-36	1.042E+00	0.180	4.791E-05	4.991E-05	5.197E-05	1.042E+00
0.005	2.154E-33	2.244E-33	2.336E-33	1.042E+00	0.200	1.216E-04	1.266E-04	1.319E-04	1.042E+00
0.006	5.980E-31	6.230E-31	6.486E-31	1.042E+00	0.250	7.781E-04	8.106E-04	8.440E-04	1.042E+00
0.007	5.332E-29	5.555E-29	5.783E-29	1.042E+00	0.300	3.176E-03	3.309E-03	3.446E-03	1.042E+00
0.008	2.162E-27	2.253E-27	2.345E-27	1.042E+00	0.350	9.703E-03	1.011E-02	1.053E-02	1.042E+00
0.009	4.935E-26	5.142E-26	5.353E-26	1.042E+00	0.400	2.426E-02	2.528E-02	2.632E-02	1.042E+00
0.010	7.290E-25	7.595E-25	7.907E-25	1.042E+00	0.450	5.244E-02	5.464E-02	5.689E-02	1.042E+00
0.011	7.668E-24	7.988E-24	8.317E-24	1.042E+00	0.500	1.016E-01	1.058E-01	1.102E-01	1.042E+00
0.012	6.148E-23	6.405E-23	6.669E-23	1.042E+00	0.600	3.000E-01	3.126E-01	3.255E-01	1.042E+00
0.013	3.951E-22	4.117E-22	4.286E-22	1.042E+00	0.700	7.083E-01	7.381E-01	7.683E-01	1.042E+00
0.014	2.114E-21	2.203E-21	2.293E-21	1.042E+00	0.800	1.432E+00	1.493E+00	1.554E+00	1.042E+00
0.015	9.699E-21	1.010E-20	1.052E-20	1.042E+00	0.900	2.590E+00	2.699E+00	2.809E+00	1.042E+00
0.016	3.903E-20	4.067E-20	4.234E-20	1.042E+00	1.000	4.301E+00	4.482E+00	4.666E+00	1.042E+00
0.018	4.578E-19	4.770E-19	4.966E-19	1.042E+00	1.250	1.180E+01	1.229E+01	1.280E+01	1.042E+00
0.020	3.809E-18	3.968E-18	4.131E-18	1.042E+00	1.500	2.526E+01	2.632E+01	2.740E+01	1.042E+00
0.025	2.639E-16	2.749E-16	2.862E-16	1.042E+00	1.750	4.612E+01	4.806E+01	5.005E+01	1.042E+00
0.030	6.641E-15	6.919E-15	7.204E-15	1.042E+00	2.000	7.545E+01	7.863E+01	8.188E+01	1.042E+00
0.040	7.211E-13	7.513E-13	7.822E-13	1.042E+00	2.500	1.618E+02	1.686E+02	1.755E+02	1.042E+00
0.050	1.998E-11	2.082E-11	2.167E-11	1.042E+00	3.000	2.851E+02	2.971E+02	3.093E+02	1.042E+00
0.060	2.497E-10	2.601E-10	2.708E-10	1.042E+00	3.500	4.406E+02	4.591E+02	4.779E+02	1.042E+00
0.070	1.865E-09	1.943E-09	2.023E-09	1.042E+00	4.000	(6.842E+02)	(7.129E+02)	(7.428E+02)	(1.042E+00)
0.080	9.751E-09	1.016E-08	1.058E-08	1.042E+00	5.000	(1.256E+03)	(1.309E+03)	(1.364E+03)	(1.042E+00)
0.090	3.933E-08	4.098E-08	4.267E-08	1.042E+00	6.000	(1.983E+03)	(2.066E+03)	(2.153E+03)	(1.042E+00)
0.100	1.304E-07	1.359E-07	1.414E-07	1.042E+00	7.000	(2.841E+03)	(2.960E+03)	(3.084E+03)	(1.042E+00)
0.110	3.709E-07	3.865E-07	4.024E-07	1.042E+00	8.000	(3.807E+03)	(3.967E+03)	(4.133E+03)	(1.042E+00)
0.120	9.340E-07	9.731E-07	1.013E-06	1.042E+00	9.000	(4.862E+03)	(5.066E+03)	(5.279E+03)	(1.042E+00)
0.130	2.129E-06	2.219E-06	2.310E-06	1.042E+00	10.000	(5.986E+03)	(6.237E+03)	(6.499E+03)	(1.042E+00)

Note. Reaction rate: C. Iliadis et al. (2022). *S* factor: see Table 2 of C. Iliadis et al. (2022). Observed resonances: the two resonances at $E_r^{c.m.} = 2.50$ and 3.26 MeV (D. Tilley et al. 1993) are negligible for the total rate. Normalization: see Table 3 of C. Iliadis et al. (2022). High-temperature rates (in parentheses): for temperatures of $T \geqslant 4$ GK, the rates were calculated assuming a constant S-factor of 4.0×10^{-3} MeVb (see Figure 2 of C. Iliadis et al. 2008). Previous rates: C. Iliadis et al. (2008). Other: Bayesian rate.

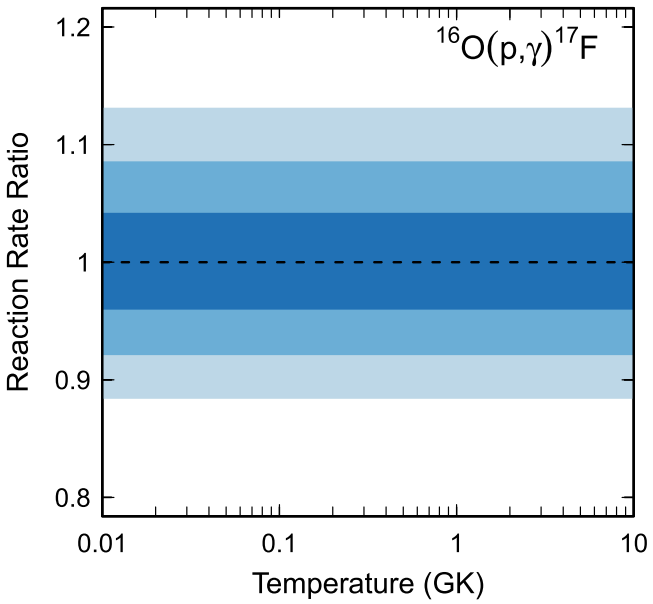

Figure 28. Reaction rate uncertainties versus temperature. The three different shades refer to coverage probabilities of 68%, 90%, and 98%.

Table 22
Total Laboratory Reaction Rates for $^{16}O(\alpha,\gamma)^{20}Ne$

T (GK)	Low	Median	High	*f.u.*	T (GK)	Low	Median	High	*f.u.*
0.001	0.000E+00	0.000E+00	0.000E+00	1.000E+00	0.140	3.624E-23	7.445E-23	1.587E-22	2.082E+00
0.002	0.000E+00	0.000E+00	0.000E+00	1.000E+00	0.150	1.983E-22	4.058E-22	8.628E-22	2.075E+00
0.003	0.000E+00	0.000E+00	0.000E+00	1.000E+00	0.160	9.392E-22	1.913E-21	4.057E-21	2.067E+00
0.004	1.024E-97	2.315E-97	5.223E-97	2.267E+00	0.180	1.480E-20	2.980E-20	6.281E-20	2.048E+00
0.005	5.537E-90	1.251E-89	2.822E-89	2.266E+00	0.200	1.755E-19	3.338E-19	6.808E-19	1.956E+00
0.006	4.414E-84	9.972E-84	2.248E-83	2.265E+00	0.250	3.754E-16	4.317E-16	4.989E-16	1.158E+00
0.007	2.289E-79	5.170E-79	1.165E-78	2.265E+00	0.300	2.618E-13	2.964E-13	3.357E-13	1.133E+00
0.008	1.920E-75	4.164E-75	9.201E-75	2.184E+00	0.350	2.935E-11	3.304E-11	3.721E-11	1.126E+00
0.009	3.745E-72	8.117E-72	1.793E-71	2.183E+00	0.400	1.010E-09	1.129E-09	1.263E-09	1.118E+00
0.010	2.559E-69	5.543E-69	1.224E-68	2.181E+00	0.450	1.587E-08	1.761E-08	1.957E-08	1.111E+00
0.011	7.709E-67	1.669E-66	3.683E-66	2.180E+00	0.500	1.445E-07	1.593E-07	1.759E-07	1.104E+00
0.012	1.207E-64	2.611E-64	5.759E-64	2.179E+00	0.600	4.029E-06	4.397E-06	4.804E-06	1.092E+00
0.013	1.108E-62	2.395E-62	5.280E-62	2.178E+00	0.700	4.397E-05	4.769E-05	5.173E-05	1.085E+00
0.014	6.531E-61	1.411E-60	3.111E-60	2.177E+00	0.800	2.651E-04	2.865E-04	3.095E-04	1.081E+00
0.015	2.655E-59	5.735E-59	1.263E-58	2.176E+00	0.900	1.070E-03	1.154E-03	1.245E-03	1.079E+00
0.016	7.866E-58	1.698E-57	3.739E-57	2.174E+00	1.000	3.250E-03	3.506E-03	3.780E-03	1.079E+00
0.018	3.164E-55	6.824E-55	1.501E-54	2.172E+00	1.250	2.346E-02	2.533E-02	2.734E-02	1.080E+00
0.020	5.546E-53	1.195E-52	2.626E-52	2.170E+00	1.500	8.494E-02	9.180E-02	9.927E-02	1.082E+00
0.025	1.739E-48	3.736E-48	8.198E-48	2.165E+00	1.750	2.078E-01	2.248E-01	2.435E-01	1.083E+00
0.030	4.680E-45	1.004E-44	2.198E-44	2.161E+00	2.000	3.997E-01	4.326E-01	4.688E-01	1.083E+00
0.040	4.676E-40	9.985E-40	2.180E-39	2.152E+00	2.500	9.761E-01	1.055E+00	1.143E+00	1.082E+00
0.050	1.683E-36	3.578E-36	7.791E-36	2.144E+00	3.000	1.768E+00	1.904E+00	2.053E+00	1.078E+00
0.060	8.678E-34	1.838E-33	3.991E-33	2.137E+00	3.500	2.762E+00	2.956E+00	3.169E+00	1.071E+00
0.070	1.271E-31	2.683E-31	5.812E-31	2.129E+00	4.000	4.008E+00	4.257E+00	4.530E+00	1.063E+00
0.080	7.781E-30	1.636E-29	3.536E-29	2.122E+00	5.000	7.777E+00	8.141E+00	8.531E+00	1.048E+00
0.090	2.519E-28	5.278E-28	1.138E-27	2.116E+00	6.000	1.473E+01	1.530E+01	1.591E+01	1.040E+00
0.100	5.037E-27	1.051E-26	2.261E-26	2.109E+00	7.000	2.708E+01	2.821E+01	2.949E+01	1.044E+00
0.110	6.913E-26	1.437E-25	3.084E-25	2.102E+00	8.000	(5.142E+01)	(7.279E+01)	(2.677E+02)	(2.547E+00)
0.120	7.022E-25	1.454E-24	3.114E-24	2.096E+00	9.000	(5.872E+01)	(1.456E+02)	(9.960E+02)	(4.660E+00)
0.130	5.583E-24	1.152E-23	2.461E-23	2.089E+00	10.000	(2.503E+01)	(2.503E+02)	(2.503E+03)	(1.000E+01)

Note. Observed resonances: from the compilation of D. Tilley et al. (1998), complemented by more recent experimental data (H. Knee 1995; A. Mayer 2001; H. Costantini et al. 2010; U. Hager et al. 2011, 2012). The resonance strengths for ^{20}Ne production were corrected for the α-particle decay of higher-lying states in ^{20}Ne. Normalization: none. Unobserved resonances: none. High-temperature rates (in parentheses): matching to statistical model rate above $T = 7.2$ GK. Previous rates: C. Angulo et al. (1999), C. Iliadis et al. (2010c), and H. Costantini et al. (2010). Other: the direct-capture S factor was recalculated and adjusted to U. Hager et al. (2011, 2012); the results are close to previous calculations (K. Langanke 1984; M. Dufour et al. 1994; P. Mohr 2005).

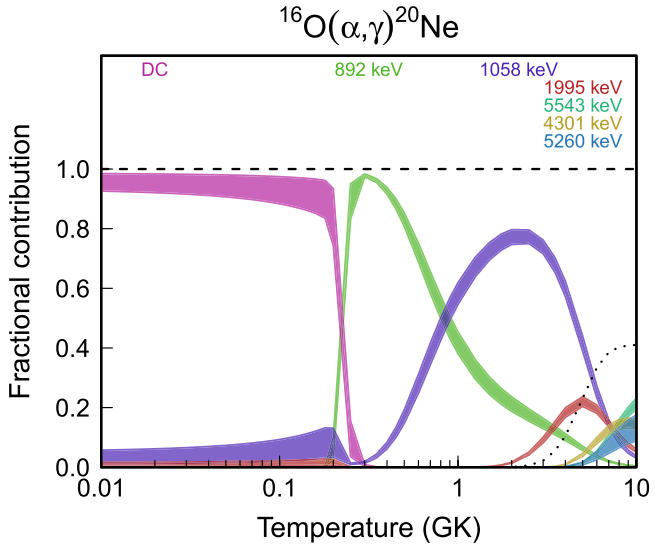

Figure 29. Fractional contributions to the total rate. "DC" refers to direct radiative capture. Resonance energies are given in the center-of-mass frame.

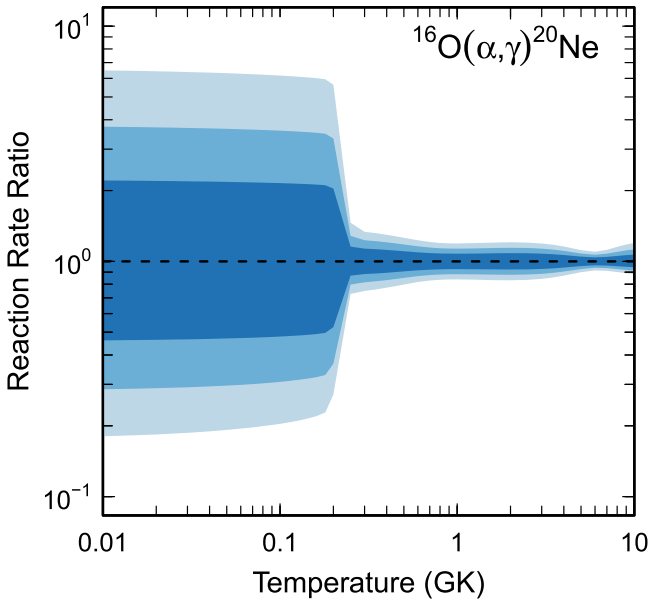

Figure 30. Reaction rate uncertainties versus temperature. The three different shades refer to coverage probabilities of 68%, 90%, and 98%.

Table 23
Total Laboratory Reaction Rates for $^{17}O(p,\gamma)^{18}F$

T (GK)	Low	Median	High	*f.u.*	T (GK)	Low	Median	High	*f.u.*
0.001	2.033E-63	2.485E-63	3.577E-63	1.402E+00	0.140	4.511E-06	4.999E-06	5.575E-06	1.113E+00
0.002	1.138E-48	1.365E-48	1.744E-48	1.271E+00	0.150	9.552E-06	1.053E-05	1.168E-05	1.107E+00
0.003	1.623E-41	1.932E-41	2.377E-41	1.225E+00	0.160	1.893E-05	2.079E-05	2.295E-05	1.102E+00
0.004	5.277E-37	6.252E-37	7.568E-37	1.203E+00	0.180	6.220E-05	6.791E-05	7.451E-05	1.095E+00
0.005	8.534E-34	1.008E-33	1.209E-33	1.193E+00	0.200	1.674E-04	1.823E-04	1.996E-04	1.093E+00
0.006	2.390E-31	2.816E-31	3.354E-31	1.186E+00	0.250	1.102E-03	1.201E-03	1.317E-03	1.094E+00
0.007	2.149E-29	2.530E-29	3.001E-29	1.183E+00	0.300	4.673E-03	5.096E-03	5.590E-03	1.095E+00
0.008	8.789E-28	1.033E-27	1.223E-27	1.181E+00	0.350	1.846E-02	2.003E-02	2.180E-02	1.088E+00
0.009	2.023E-26	2.376E-26	2.809E-26	1.179E+00	0.400	7.413E-02	8.062E-02	8.785E-02	1.089E+00
0.010	3.012E-25	3.536E-25	4.175E-25	1.178E+00	0.450	2.702E-01	2.957E-01	3.245E-01	1.097E+00
0.011	3.193E-24	3.746E-24	4.419E-24	1.177E+00	0.500	8.333E-01	9.154E-01	1.009E+00	1.101E+00
0.012	2.579E-23	3.025E-23	3.566E-23	1.177E+00	0.600	4.889E+00	5.379E+00	5.937E+00	1.103E+00
0.013	1.670E-22	1.958E-22	2.308E-22	1.176E+00	0.700	1.768E+01	1.941E+01	2.139E+01	1.101E+00
0.014	9.005E-22	1.055E-21	1.243E-21	1.176E+00	0.800	4.626E+01	5.068E+01	5.568E+01	1.098E+00
0.015	4.161E-21	4.873E-21	5.741E-21	1.176E+00	0.900	9.708E+01	1.061E+02	1.162E+02	1.095E+00
0.016	1.686E-20	1.975E-20	2.326E-20	1.176E+00	1.000	1.743E+02	1.901E+02	2.077E+02	1.092E+00
0.018	2.010E-19	2.353E-19	2.769E-19	1.175E+00	1.250	4.861E+02	5.281E+02	5.742E+02	1.087E+00
0.020	1.724E-18	2.012E-18	2.362E-18	1.172E+00	1.500	9.348E+02	1.012E+03	1.097E+03	1.084E+00
0.025	1.621E-16	1.876E-16	2.175E-16	1.160E+00	1.750	1.460E+03	1.577E+03	1.703E+03	1.081E+00
0.030	7.340E-15	8.888E-15	1.092E-14	1.224E+00	2.000	2.008E+03	2.163E+03	2.332E+03	1.078E+00
0.040	1.753E-12	2.248E-12	2.916E-12	1.297E+00	2.500	3.052E+03	3.276E+03	3.517E+03	1.074E+00
0.050	5.402E-11	6.952E-11	9.044E-11	1.301E+00	3.000	3.954E+03	4.232E+03	4.530E+03	1.071E+00
0.060	5.528E-10	7.007E-10	9.002E-10	1.282E+00	3.500	4.721E+03	5.045E+03	5.388E+03	1.069E+00
0.070	3.097E-09	3.827E-09	4.804E-09	1.250E+00	4.000	5.390E+03	5.758E+03	6.152E+03	1.069E+00
0.080	1.234E-08	1.482E-08	1.804E-08	1.212E+00	5.000	6.581E+03	7.067E+03	7.602E+03	1.076E+00
0.090	4.048E-08	4.739E-08	5.590E-08	1.178E+00	6.000	7.749E+03	8.410E+03	9.173E+03	1.089E+00
0.100	1.184E-07	1.360E-07	1.569E-07	1.153E+00	7.000	8.988E+03	9.889E+03	1.096E+04	1.105E+00
0.110	3.217E-07	3.648E-07	4.152E-07	1.138E+00	8.000	1.032E+04	1.150E+04	1.293E+04	1.120E+00
0.120	8.245E-07	9.258E-07	1.047E-06	1.128E+00	9.000	1.170E+04	1.319E+04	1.500E+04	1.133E+00
0.130	1.992E-06	2.220E-06	2.493E-06	1.120E+00	10.000	1.308E+04	1.489E+04	1.708E+04	1.144E+00

Note. Observed resonances: C. Rolfs et al. (1973b), A. Chafa et al. (2007), A. Kontos et al. (2012), A. Di Leva et al. (2014), and M. Q. Buckner et al. (2015). Normalization: C. Fox et al. (2005) and M. Q. Buckner et al. (2015). Unobserved resonances: H.-B. Mak et al. (1980) and V. Landre et al. (1989). High-temperature rates (in parentheses): no corrections for missing high-energy resonances are necessary up to $T = 10$ GK. Previous rates: D. Rapagnani et al. (2025). Other: the two interfering 1^- resonances at $E_r^{c.m.} = -1.6$ and 65 keV were sampled with a random interference sign.

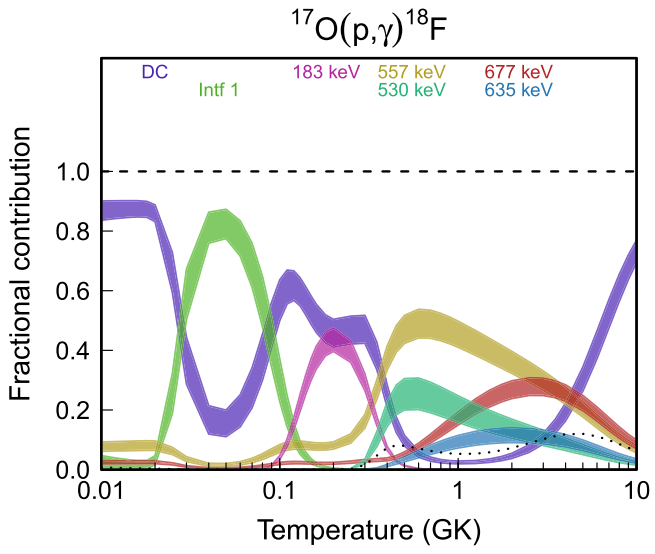

Figure 31. Fractional contributions to the total rate. "DC" refers to direct radiative capture. Resonance energies are given in the center-of-mass frame. "Intf 1" labels the combined contribution of the two interfering 1^- resonances at $E_r^{c.m.}$=−1.6 and 65 keV.

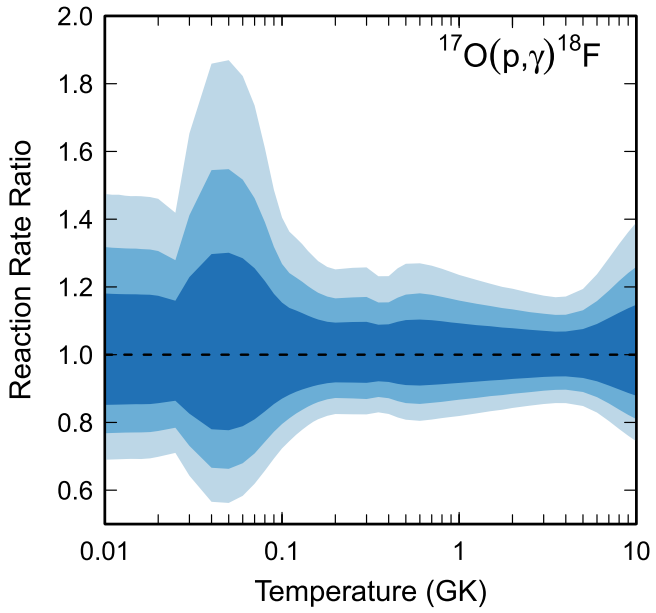

Figure 32. Reaction rate uncertainties versus temperature. The three different shades refer to coverage probabilities of 68%, 90%, and 98%.

Table 24
Total Laboratory Reaction Rates for $^{17}O(p,\alpha)^{14}N$

T (GK)	Low	Median	High	*f.u.*	T (GK)	Low	Median	High	*f.u.*
0.001	1.414E-62	2.359E-62	6.670E-62	2.199E+00	0.140	1.302E-03	1.407E-03	1.522E-03	1.081E+00
0.002	4.903E-48	7.856E-48	2.046E-47	2.084E+00	0.150	3.158E-03	3.413E-03	3.689E-03	1.081E+00
0.003	5.195E-41	8.128E-41	2.015E-40	2.017E+00	0.160	6.877E-03	7.429E-03	8.029E-03	1.081E+00
0.004	1.373E-36	2.113E-36	5.040E-36	1.967E+00	0.180	2.501E-02	2.700E-02	2.918E-02	1.081E+00
0.005	1.908E-33	2.891E-33	6.691E-33	1.926E+00	0.200	6.941E-02	7.494E-02	8.096E-02	1.080E+00
0.006	4.764E-31	7.116E-31	1.597E-30	1.891E+00	0.250	4.239E-01	4.569E-01	4.930E-01	1.079E+00
0.007	3.912E-29	5.795E-29	1.266E-28	1.861E+00	0.300	1.570E+00	1.679E+00	1.797E+00	1.070E+00
0.008	1.490E-27	2.195E-27	4.687E-27	1.834E+00	0.350	5.839E+00	6.278E+00	6.749E+00	1.076E+00
0.009	3.246E-26	4.756E-26	9.955E-26	1.811E+00	0.400	2.317E+01	2.546E+01	2.802E+01	1.100E+00
0.010	4.632E-25	6.778E-25	1.389E-24	1.790E+00	0.450	8.204E+01	9.115E+01	1.014E+02	1.112E+00
0.011	4.751E-24	6.954E-24	1.399E-23	1.772E+00	0.500	2.404E+02	2.677E+02	2.985E+02	1.115E+00
0.012	3.751E-23	5.507E-23	1.084E-22	1.756E+00	0.600	1.259E+03	1.397E+03	1.552E+03	1.111E+00
0.013	2.396E-22	3.533E-22	6.822E-22	1.742E+00	0.700	4.167E+03	4.593E+03	5.069E+03	1.104E+00
0.014	1.285E-21	1.909E-21	3.624E-21	1.729E+00	0.800	1.030E+04	1.127E+04	1.236E+04	1.096E+00
0.015	5.994E-21	8.976E-21	1.665E-20	1.714E+00	0.900	2.099E+04	2.281E+04	2.484E+04	1.088E+00
0.016	2.539E-20	3.809E-20	6.875E-20	1.689E+00	1.000	3.749E+04	4.048E+04	4.379E+04	1.081E+00
0.018	4.587E-19	6.537E-19	1.051E-18	1.550E+00	1.250	1.120E+05	1.192E+05	1.272E+05	1.066E+00
0.020	1.040E-17	1.444E-17	2.060E-17	1.413E+00	1.500	2.503E+05	2.637E+05	2.784E+05	1.055E+00
0.025	9.739E-15	1.342E-14	1.845E-14	1.420E+00	1.750	(4.467E+05)	(4.735E+05)	(5.444E+05)	(1.105E+00)
0.030	1.121E-12	1.532E-12	2.091E-12	1.438E+00	2.000	(7.015E+05)	(7.643E+05)	(1.084E+06)	(1.254E+00)
0.040	3.974E-10	5.385E-10	7.311E-10	1.454E+00	2.500	(1.354E+06)	(1.562E+06)	(3.053E+06)	(1.554E+00)
0.050	1.251E-08	1.692E-08	2.297E-08	1.454E+00	3.000	(2.240E+06)	(2.747E+06)	(6.842E+06)	(1.858E+00)
0.060	1.186E-07	1.606E-07	2.181E-07	1.445E+00	3.500	(3.333E+06)	(4.360E+06)	(1.320E+07)	(2.168E+00)
0.070	5.724E-07	7.749E-07	1.053E-06	1.423E+00	4.000	(4.581E+06)	(6.422E+06)	(2.288E+07)	(2.483E+00)
0.080	1.846E-06	2.490E-06	3.373E-06	1.387E+00	5.000	(7.269E+06)	(1.189E+07)	(5.515E+07)	(3.136E+00)
0.090	4.924E-06	6.479E-06	8.615E-06	1.337E+00	6.000	(9.707E+06)	(1.907E+07)	(1.089E+08)	(3.837E+00)
0.100	1.378E-05	1.692E-05	2.120E-05	1.246E+00	7.000	(1.129E+07)	(2.776E+07)	(1.882E+08)	(4.620E+00)
0.110	4.528E-05	5.134E-05	5.916E-05	1.147E+00	8.000	(1.149E+07)	(3.774E+07)	(2.964E+08)	(5.570E+00)
0.120	1.534E-04	1.677E-04	1.841E-04	1.096E+00	9.000	(9.867E+06)	(4.879E+07)	(4.356E+08)	(6.936E+00)
0.130	4.754E-04	5.148E-04	5.577E-04	1.083E+00	10.000	(6.077E+06)	(6.077E+07)	(6.077E+08)	(1.000E+01)

Note. Observed resonances: W. Kieser et al. (1979), J. C. Blackmon et al. (1995), A. Kontos et al. (2012), M. L. Sergi et al. (2015), and C. G. Bruno et al. (2016). Normalization: we adopted a Bayesian weighted average of the $E_r^{c.m.} = 65$ keV resonance strength values reported by J. C. Blackmon et al. (1995), M. L. Sergi et al. (2015), and C. G. Bruno et al. (2016). Unobserved resonances: H.-B. Mak et al. (1980) and V. Landre et al. (1989). High-temperature rates (in parentheses): matching to statistical model rate above $T = 1.7$ GK. Previous rates: D. Rapagnani et al. (2025). Other: the two interfering 1^- resonances at $E_r^{c.m.} = -1.6$ and 65 keV were sampled with a random interference sign.

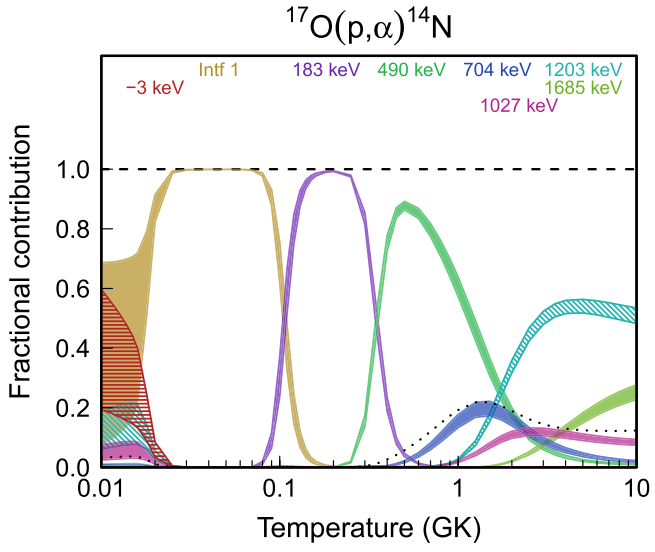

Figure 33. Fractional contributions to the total rate. Resonance energies are given in the center-of-mass frame. "Intf 1" labels the combined contribution of the two interfering 1^- resonances at $E_r^{c.m.}$=−1.6 and 65 keV.

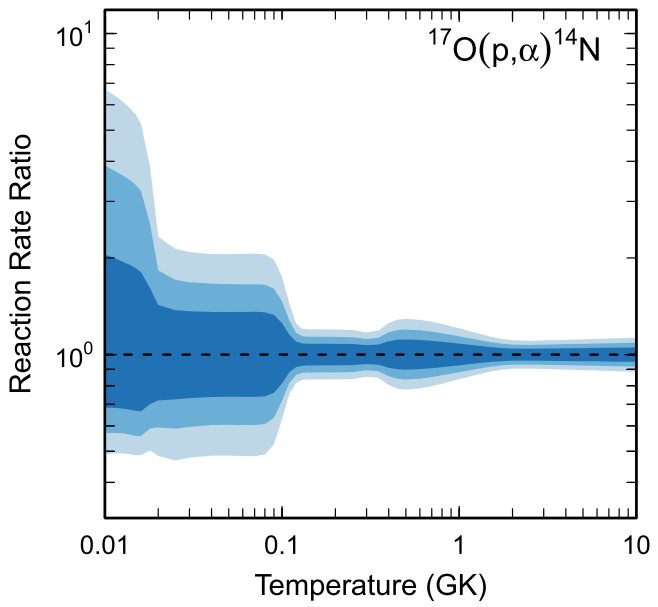

Figure 34. Reaction rate uncertainties versus temperature. The three different shades refer to coverage probabilities of 68%, 90%, and 98%.

Table 25
Total Laboratory Reaction Rates for $^{18}O(p,\gamma)^{19}F$

T (GK)	Low	Median	High	*f.u.*	T (GK)	Low	Median	High	*f.u.*
0.001	4.119E-63	5.203E-63	6.704E-63	1.277E+00	0.140	1.604E-02	1.863E-02	2.159E-02	1.161E+00
0.002	2.615E-48	3.289E-48	4.216E-48	1.272E+00	0.150	3.221E-02	3.740E-02	4.333E-02	1.161E+00
0.003	4.061E-41	5.090E-41	6.498E-41	1.267E+00	0.160	5.889E-02	6.837E-02	7.920E-02	1.160E+00
0.004	1.448E-36	1.817E-36	2.320E-36	1.268E+00	0.180	1.587E-01	1.840E-01	2.133E-01	1.160E+00
0.005	2.729E-33	3.503E-33	4.668E-33	1.325E+00	0.200	3.445E-01	3.998E-01	4.637E-01	1.161E+00
0.006	9.710E-31	1.336E-30	2.040E-30	1.486E+00	0.250	1.324E+00	1.538E+00	1.787E+00	1.163E+00
0.007	1.111E-28	1.661E-28	2.828E-28	1.620E+00	0.300	3.094E+00	3.598E+00	4.184E+00	1.164E+00
0.008	5.256E-27	8.226E-27	1.456E-26	1.678E+00	0.350	5.487E+00	6.388E+00	7.440E+00	1.166E+00
0.009	1.252E-25	1.971E-25	3.473E-25	1.681E+00	0.400	8.247E+00	9.603E+00	1.119E+01	1.166E+00
0.010	1.780E-24	2.751E-24	4.747E-24	1.651E+00	0.450	1.116E+01	1.299E+01	1.512E+01	1.166E+00
0.011	1.732E-23	2.579E-23	4.297E-23	1.597E+00	0.500	1.410E+01	1.638E+01	1.906E+01	1.164E+00
0.012	1.269E-22	1.811E-22	2.872E-22	1.531E+00	0.600	2.002E+01	2.314E+01	2.679E+01	1.158E+00
0.013	7.481E-22	1.023E-21	1.538E-21	1.462E+00	0.700	2.678E+01	3.071E+01	3.529E+01	1.149E+00
0.014	3.717E-21	4.914E-21	6.973E-21	1.398E+00	0.800	3.624E+01	4.123E+01	4.720E+01	1.143E+00
0.015	1.606E-20	2.067E-20	2.807E-20	1.344E+00	0.900	5.079E+01	5.761E+01	6.621E+01	1.148E+00
0.016	6.164E-20	7.796E-20	1.022E-19	1.303E+00	1.000	7.315E+01	8.320E+01	9.667E+01	1.160E+00
0.018	6.815E-19	8.441E-19	1.067E-18	1.257E+00	1.250	1.808E+02	2.080E+02	2.452E+02	1.177E+00
0.020	5.529E-18	6.785E-18	8.480E-18	1.241E+00	1.500	3.820E+02	4.411E+02	5.184E+02	1.174E+00
0.025	3.897E-16	4.744E-16	5.898E-16	1.233E+00	1.750	6.791E+02	7.833E+02	9.146E+02	1.167E+00
0.030	1.041E-14	1.261E-14	1.558E-14	1.226E+00	2.000	1.059E+03	1.218E+03	1.416E+03	1.161E+00
0.040	1.337E-12	1.595E-12	1.936E-12	1.207E+00	2.500	2.000E+03	2.293E+03	2.643E+03	1.152E+00
0.050	7.697E-11	9.022E-11	1.062E-10	1.176E+00	3.000	3.099E+03	3.548E+03	4.082E+03	1.150E+00
0.060	6.845E-09	8.317E-09	1.012E-08	1.216E+00	3.500	4.292E+03	4.922E+03	5.688E+03	1.154E+00
0.070	2.754E-07	3.312E-07	3.987E-07	1.204E+00	4.000	5.550E+03	6.400E+03	7.454E+03	1.162E+00
0.080	4.509E-06	5.363E-06	6.380E-06	1.190E+00	5.000	8.181E+03	9.598E+03	1.144E+04	1.185E+00
0.090	3.911E-05	4.615E-05	5.440E-05	1.179E+00	6.000	(1.042E+04)	(1.364E+04)	(2.909E+04)	(1.721E+00)
0.100	2.169E-04	2.544E-04	2.978E-04	1.172E+00	7.000	(1.117E+04)	(1.868E+04)	(7.658E+04)	(2.886E+00)
0.110	8.688E-04	1.015E-03	1.183E-03	1.168E+00	8.000	(1.037E+04)	(2.401E+04)	(1.456E+05)	(4.190E+00)
0.120	2.728E-03	3.178E-03	3.694E-03	1.164E+00	9.000	(7.845E+03)	(2.949E+04)	(2.369E+05)	(5.896E+00)
0.130	7.113E-03	8.271E-03	9.596E-03	1.163E+00	10.000	(3.503E+03)	(3.503E+04)	(3.503E+05)	(1.000E+01)

Note. Observed resonances: M. Wiescher et al. (1980), R. B. Vogelaar et al. (1990), J. Dermigny et al. (2016), A. Best et al. (2019), and F. R. Pantaleo et al. (2021). Normalization: F. R. Pantaleo et al. (2021). Unobserved resonances: A. Champagne & M. Pitt (1986) and M. La Cognata et al. (2008). High-temperature rates (in parentheses): matching to statistical model rate above $T = 5.5$ GK. Previous rates: M. Q. Buckner et al. (2012). Other: none.

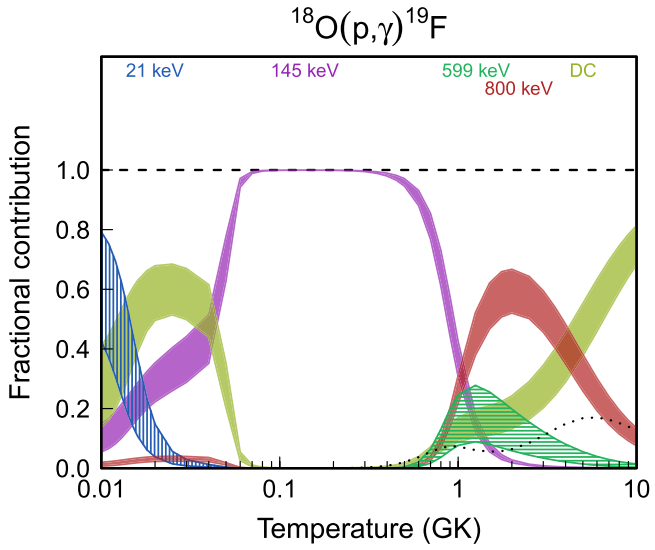

Figure 35. Fractional contributions to the total rate. "DC" refers to direct radiative capture. Resonance energies are given in the center-of-mass frame.

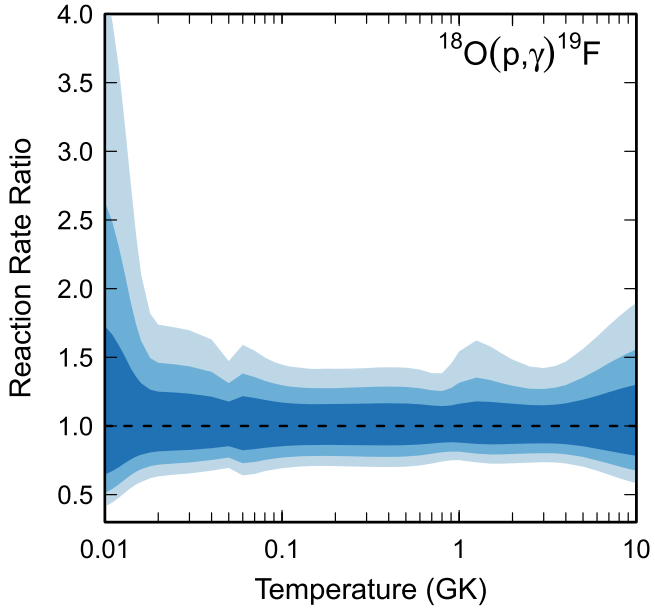

Figure 36. Reaction rate uncertainties versus temperature. The three different shades refer to coverage probabilities of 68%, 90%, and 98%.

Table 26
Total Laboratory Reaction Rates for $^{18}O(p,\alpha)^{15}N$

T (GK)	Low	Median	High	*f.u.*	T (GK)	Low	Median	High	*f.u.*
0.001	9.242E-60	1.285E-59	1.796E-59	1.398E+00	0.140	2.999E+00	3.226E+00	3.467E+00	1.075E+00
0.002	5.774E-45	8.013E-45	1.118E-44	1.395E+00	0.150	6.039E+00	6.489E+00	6.963E+00	1.074E+00
0.003	8.783E-38	1.215E-37	1.691E-37	1.391E+00	0.160	1.107E+01	1.189E+01	1.275E+01	1.073E+00
0.004	3.048E-33	4.186E-33	5.796E-33	1.382E+00	0.180	2.998E+01	3.220E+01	3.453E+01	1.073E+00
0.005	5.526E-30	7.511E-30	1.028E-29	1.367E+00	0.200	6.555E+01	7.046E+01	7.560E+01	1.074E+00
0.006	1.890E-27	2.552E-27	3.466E-27	1.358E+00	0.250	2.589E+02	2.792E+02	3.003E+02	1.077E+00
0.007	2.109E-25	2.835E-25	3.845E-25	1.356E+00	0.300	6.384E+02	6.910E+02	7.467E+02	1.082E+00
0.008	9.846E-24	1.322E-23	1.786E-23	1.351E+00	0.350	1.249E+03	1.362E+03	1.487E+03	1.093E+00
0.009	2.338E-22	3.133E-22	4.212E-22	1.346E+00	0.400	2.208E+03	2.451E+03	2.741E+03	1.116E+00
0.010	3.332E-21	4.460E-21	5.984E-21	1.344E+00	0.450	3.840E+03	4.380E+03	5.058E+03	1.150E+00
0.011	3.253E-20	4.349E-20	5.832E-20	1.342E+00	0.500	6.844E+03	8.031E+03	9.548E+03	1.183E+00
0.012	2.391E-19	3.198E-19	4.293E-19	1.342E+00	0.600	2.269E+04	2.746E+04	3.350E+04	1.217E+00
0.013	1.414E-18	1.896E-18	2.548E-18	1.345E+00	0.700	6.828E+04	8.295E+04	1.014E+05	1.220E+00
0.014	7.051E-18	9.494E-18	1.280E-17	1.351E+00	0.800	1.728E+05	2.089E+05	2.541E+05	1.214E+00
0.015	3.052E-17	4.136E-17	5.612E-17	1.359E+00	0.900	3.718E+05	4.470E+05	5.396E+05	1.207E+00
0.016	1.177E-16	1.603E-16	2.193E-16	1.368E+00	1.000	7.004E+05	8.368E+05	1.004E+06	1.199E+00
0.018	1.309E-15	1.803E-15	2.499E-15	1.385E+00	1.250	2.250E+06	2.652E+06	3.138E+06	1.183E+00
0.020	1.065E-14	1.480E-14	2.066E-14	1.396E+00	1.500	4.906E+06	5.730E+06	6.711E+06	1.171E+00
0.025	7.347E-13	1.034E-12	1.458E-12	1.412E+00	1.750	8.468E+06	9.831E+06	1.144E+07	1.164E+00
0.030	1.883E-11	2.663E-11	3.772E-11	1.419E+00	2.000	1.259E+07	1.455E+07	1.685E+07	1.158E+00
0.040	2.126E-09	3.028E-09	4.307E-09	1.426E+00	2.500	2.124E+07	2.444E+07	2.814E+07	1.152E+00
0.050	6.721E-08	9.315E-08	1.303E-07	1.395E+00	3.000	2.918E+07	3.348E+07	3.841E+07	1.148E+00
0.060	2.012E-06	2.399E-06	2.911E-06	1.207E+00	3.500	3.584E+07	4.102E+07	4.695E+07	1.145E+00
0.070	5.629E-05	6.375E-05	7.220E-05	1.134E+00	4.000	4.123E+07	4.707E+07	5.377E+07	1.142E+00
0.080	8.515E-04	9.504E-04	1.061E-03	1.117E+00	5.000	4.920E+07	5.585E+07	6.350E+07	1.137E+00
0.090	7.269E-03	8.019E-03	8.848E-03	1.104E+00	6.000	5.521E+07	6.226E+07	7.033E+07	1.129E+00
0.100	4.022E-02	4.394E-02	4.802E-02	1.094E+00	7.000	6.077E+07	6.793E+07	7.620E+07	1.120E+00
0.110	1.613E-01	1.751E-01	1.900E-01	1.086E+00	8.000	6.667E+07	7.384E+07	8.208E+07	1.110E+00
0.120	5.078E-01	5.486E-01	5.927E-01	1.081E+00	9.000	7.318E+07	8.031E+07	8.851E+07	1.100E+00
0.130	1.327E+00	1.430E+00	1.540E+00	1.078E+00	10.000	8.031E+07	8.741E+07	9.554E+07	1.091E+00

Note. Observed resonances: see for this reaction the reference list in C. Iliadis et al. (2010c). Normalization: H. Lorenz-Wirzba et al. (1979) and H. W. Becker et al. (1995). Unobserved resonances: A. Champagne & M. Pitt (1986) and M. La Cognata et al. (2008). High-temperature rates (in parentheses): no corrections for missing high-energy resonances are necessary up to $T = 10$ GK. Previous rates: M. La Cognata et al. (2010) and C. Iliadis et al. (2010c). Other: the two interfering $1/2^+$ resonances at $E_r^{c.m.} = 145$ and 628 keV were sampled assuming destructive (constructive) interference outside (between) both resonances (H. Lorenz-Wirzba et al. 1979; H. W. Becker et al. 1995).

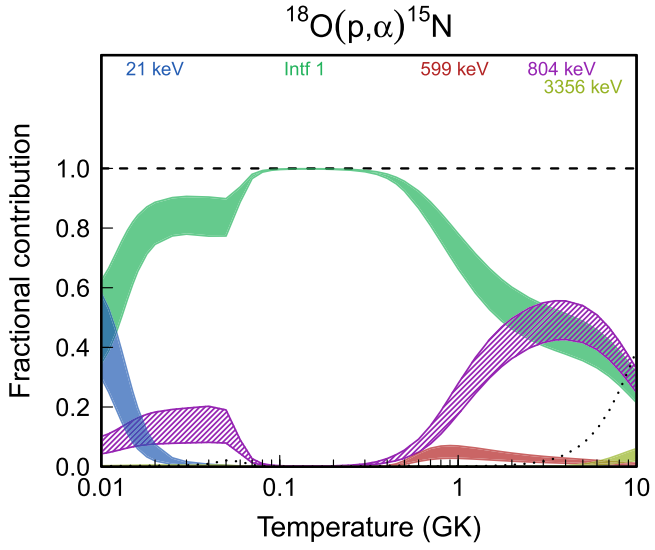

Figure 37. Fractional contributions to the total rate. Resonance energies are given in the center-of-mass frame. "Intf 1" labels the combined contribution of the two interfering $1/2^+$ resonances at $E_r^{c.m.} = 145$ and 628 keV.

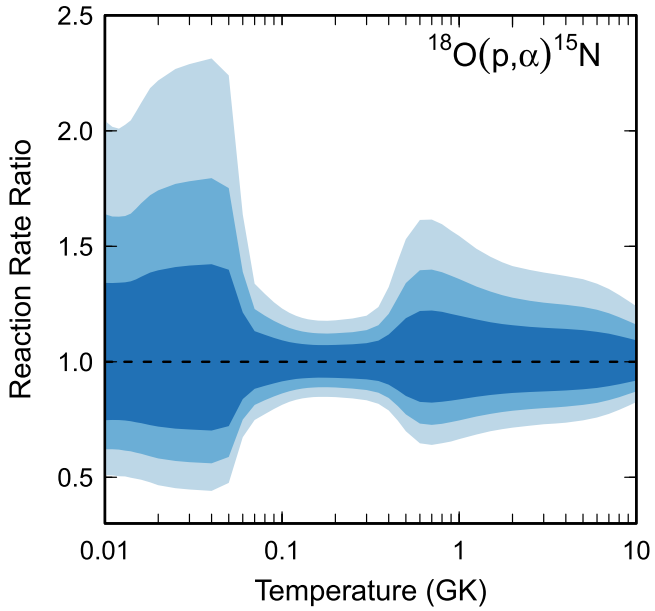

Figure 38. Reaction rate uncertainties versus temperature. The three different shades refer to coverage probabilities of 68%, 90%, and 98%.

Table 27
Total Laboratory Reaction Rates for $^{18}O(\alpha,\gamma)^{22}Ne$

T (GK)	Low	Median	High	*f.u.*	T (GK)	Low	Median	High	*f.u.*
0.001	0.000E+00	0.000E+00	0.000E+00	1.000E+00	0.140	1.121E-15	1.369E-15	1.670E-15	1.224E+00
0.002	0.000E+00	0.000E+00	0.000E+00	1.000E+00	0.150	8.645E-15	1.049E-14	1.271E-14	1.214E+00
0.003	0.000E+00	0.000E+00	0.000E+00	1.000E+00	0.160	5.176E-14	6.247E-14	7.528E-14	1.207E+00
0.004	3.050E-97	6.114E-97	1.215E-96	2.002E+00	0.180	1.036E-12	1.235E-12	1.471E-12	1.193E+00
0.005	1.884E-89	3.775E-89	7.503E-89	2.002E+00	0.200	1.187E-11	1.392E-11	1.634E-11	1.174E+00
0.006	1.661E-83	3.329E-83	6.617E-83	2.002E+00	0.250	1.321E-09	1.469E-09	1.637E-09	1.114E+00
0.007	1.016E-78	2.194E-78	7.897E-78	5.437E+00	0.300	4.599E-08	4.969E-08	5.370E-08	1.081E+00
0.008	3.966E-72	7.964E-70	2.307E-68	5.326E+01	0.350	7.007E-07	7.516E-07	8.055E-07	1.073E+00
0.009	1.312E-67	7.145E-66	8.376E-65	2.762E+01	0.400	5.769E-06	6.174E-06	6.604E-06	1.071E+00
0.010	5.487E-64	1.033E-62	8.138E-62	1.561E+01	0.450	3.034E-05	3.245E-05	3.467E-05	1.070E+00
0.011	3.765E-61	4.331E-60	2.899E-59	1.180E+01	0.500	1.150E-04	1.229E-04	1.314E-04	1.069E+00
0.012	7.202E-59	7.293E-58	4.751E-57	1.188E+01	0.600	8.439E-04	9.013E-04	9.630E-04	1.069E+00
0.013	5.088E-57	6.133E-56	4.119E-55	1.414E+01	0.700	3.449E-03	3.683E-03	3.935E-03	1.069E+00
0.014	1.632E-55	2.849E-54	2.102E-53	1.783E+01	0.800	9.771E-03	1.043E-02	1.114E-02	1.068E+00
0.015	2.800E-54	8.051E-53	6.882E-52	2.240E+01	0.900	2.175E-02	2.321E-02	2.478E-02	1.068E+00
0.016	3.120E-53	1.496E-51	1.566E-50	2.724E+01	1.000	4.107E-02	4.381E-02	4.672E-02	1.067E+00
0.018	1.910E-51	1.782E-49	3.123E-48	3.515E+01	1.250	1.318E-01	1.399E-01	1.485E-01	1.062E+00
0.020	8.341E-50	7.764E-48	2.263E-46	3.773E+01	1.500	3.142E-01	3.319E-01	3.508E-01	1.057E+00
0.025	1.422E-45	2.070E-44	5.703E-43	1.791E+01	1.750	6.690E-01	7.128E-01	7.647E-01	1.072E+00
0.030	7.019E-41	5.764E-40	4.604E-39	8.166E+00	2.000	1.343E+00	1.473E+00	1.656E+00	1.116E+00
0.040	9.450E-34	5.544E-33	3.255E-32	5.912E+00	2.500	(4.113E+00)	(4.782E+00)	(7.909E+00)	(1.408E+00)
0.050	1.882E-29	9.599E-29	4.894E-28	5.143E+00	3.000	(1.086E+01)	(1.342E+01)	(2.966E+01)	(1.723E+00)
0.060	1.234E-26	6.098E-26	3.037E-25	5.017E+00	3.500	(2.449E+01)	(3.228E+01)	(8.930E+01)	(2.042E+00)
0.070	1.165E-24	5.974E-24	3.004E-23	5.110E+00	4.000	(4.759E+01)	(6.720E+01)	(2.233E+02)	(2.368E+00)
0.080	3.429E-23	1.803E-22	9.343E-22	5.259E+00	5.000	(1.258E+02)	(2.073E+02)	(9.197E+02)	(3.042E+00)
0.090	5.036E-22	2.547E-21	1.350E-20	4.998E+00	6.000	(2.355E+02)	(4.659E+02)	(2.585E+03)	(3.764E+00)
0.100	9.589E-21	2.624E-20	1.181E-19	3.450E+00	7.000	(3.440E+02)	(8.514E+02)	(5.672E+03)	(4.568E+00)
0.110	3.089E-19	4.374E-19	9.465E-19	2.004E+00	8.000	(4.089E+02)	(1.351E+03)	(1.050E+04)	(5.539E+00)
0.120	7.086E-18	8.977E-18	1.199E-17	1.416E+00	9.000	(3.901E+02)	(1.937E+03)	(1.722E+04)	(6.927E+00)
0.130	1.071E-16	1.320E-16	1.637E-16	1.256E+00	10.000	(2.577E+02)	(2.577E+03)	(2.577E+04)	(1.000E+01)

Note. Observed resonances: J. Graff et al. (1968), G. Chouraqui et al. (1970), H. P. Trautvetter et al. (1978), S. Dababneh et al. (2003), A. C. Dombos et al. (2022), and L. Wang et al. (2023). Unobserved resonances: none. High-temperature rates (in parentheses): matching to statistical model rate above $T = 2.03$ GK. Previous rates: C. Angulo et al. (1999), S. Dababneh et al. (2003), C. Iliadis et al. (2010c), and L. Wang et al. (2023). Other: the direct-capture contribution has been estimated using α-spectroscopic factors reported in N. Anantaraman et al. (1979). The resonances at $E_r^{c.m.} = 388$, 472, 542, 615, and 630 keV are assumed to have correlated resonance strengths. See the discussion in C. Iliadis et al. (2010c) for the $E_r^{c.m.} = 60$ and 174 keV resonances.

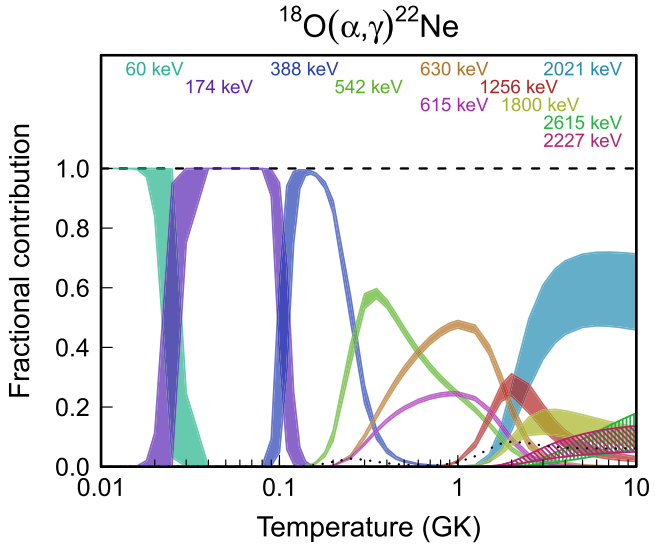

Figure 39. Fractional contributions to the total rate. Resonance energies are given in the center-of-mass frame.

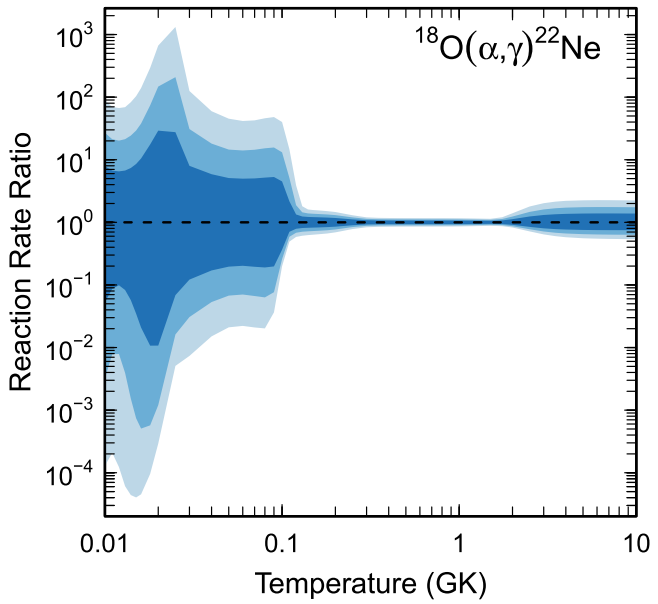

Figure 40. Reaction rate uncertainties versus temperature. The three different shades refer to coverage probabilities of 68%, 90%, and 98%.

Table 28
Total Laboratory Reaction Rates for $^{18}O(\alpha,n)^{21}Ne$

T (GK)	Low	Median	High	*f.u.*	T (GK)	Low	Median	High	*f.u.*
0.001	0.000E+00	0.000E+00	0.000E+00	1.000E+00	0.140	2.450E-26	2.970E-26	3.645E-26	1.245E+00
0.002	0.000E+00	0.000E+00	0.000E+00	1.000E+00	0.150	1.776E-24	2.144E-24	2.606E-24	1.227E+00
0.003	0.000E+00	0.000E+00	0.000E+00	1.000E+00	0.160	7.544E-23	9.079E-23	1.097E-22	1.217E+00
0.004	0.000E+00	0.000E+00	0.000E+00	1.000E+00	0.180	3.910E-20	4.692E-20	5.636E-20	1.207E+00
0.005	0.000E+00	0.000E+00	0.000E+00	1.000E+00	0.200	5.847E-18	7.021E-18	8.460E-18	1.210E+00
0.006	0.000E+00	0.000E+00	0.000E+00	1.000E+00	0.250	5.031E-14	6.238E-14	8.317E-14	1.345E+00
0.007	0.000E+00	0.000E+00	0.000E+00	1.000E+00	0.300	2.280E-11	3.142E-11	5.372E-11	1.615E+00
0.008	0.000E+00	0.000E+00	0.000E+00	1.000E+00	0.350	2.017E-09	3.221E-09	6.604E-09	1.862E+00
0.009	0.000E+00	0.000E+00	0.000E+00	1.000E+00	0.400	6.584E-08	1.172E-07	2.600E-07	2.016E+00
0.010	0.000E+00	0.000E+00	0.000E+00	1.000E+00	0.450	1.098E-06	2.060E-06	4.637E-06	2.079E+00
0.011	0.000E+00	0.000E+00	0.000E+00	1.000E+00	0.500	1.121E-05	2.134E-05	4.731E-05	2.081E+00
0.012	0.000E+00	0.000E+00	0.000E+00	1.000E+00	0.600	4.104E-04	7.694E-04	1.609E-03	2.011E+00
0.013	0.000E+00	0.000E+00	0.000E+00	1.000E+00	0.700	5.827E-03	1.064E-02	2.103E-02	1.931E+00
0.014	0.000E+00	0.000E+00	0.000E+00	1.000E+00	0.800	4.457E-02	7.942E-02	1.520E-01	1.873E+00
0.015	0.000E+00	0.000E+00	0.000E+00	1.000E+00	0.900	2.242E-01	3.914E-01	7.339E-01	1.831E+00
0.016	0.000E+00	0.000E+00	0.000E+00	1.000E+00	1.000	8.460E-01	1.449E+00	2.656E+00	1.795E+00
0.018	0.000E+00	0.000E+00	0.000E+00	1.000E+00	1.250	1.071E+01	1.729E+01	3.004E+01	1.710E+00
0.020	0.000E+00	0.000E+00	0.000E+00	1.000E+00	1.500	6.698E+01	1.049E+02	1.746E+02	1.647E+00
0.025	0.000E+00	0.000E+00	0.000E+00	1.000E+00	1.750	2.683E+02	4.174E+02	6.827E+02	1.621E+00
0.030	0.000E+00	0.000E+00	0.000E+00	1.000E+00	2.000	7.868E+02	1.234E+03	2.017E+03	1.623E+00
0.040	3.897E-91	9.811E-91	2.691E-90	2.686E+00	2.500	3.705E+03	5.963E+03	9.982E+03	1.656E+00
0.050	1.721E-73	4.291E-73	1.167E-72	2.662E+00	3.000	1.096E+04	1.798E+04	3.060E+04	1.690E+00
0.060	1.037E-61	2.566E-61	6.928E-61	2.640E+00	3.500	2.521E+04	4.211E+04	7.358E+04	1.740E+00
0.070	2.916E-53	6.944E-53	1.853E-52	2.567E+00	4.000	4.953E+04	8.532E+04	1.572E+05	1.840E+00
0.080	7.806E-47	1.639E-46	4.104E-46	2.335E+00	5.000	1.415E+05	2.684E+05	5.975E+05	2.183E+00
0.090	1.110E-41	1.848E-41	3.964E-41	1.973E+00	6.000	3.153E+05	6.687E+05	1.863E+06	2.571E+00
0.100	1.918E-37	2.657E-37	4.568E-37	1.657E+00	7.000	5.994E+05	1.421E+06	4.665E+06	2.905E+00
0.110	6.273E-34	8.019E-34	1.145E-33	1.454E+00	8.000	1.019E+06	2.653E+06	9.702E+06	3.164E+00
0.120	5.546E-31	6.864E-31	8.927E-31	1.339E+00	9.000	1.592E+06	4.463E+06	1.749E+07	3.356E+00
0.130	1.754E-28	2.140E-28	2.674E-28	1.278E+00	10.000	2.327E+06	6.886E+06	2.818E+07	3.497E+00

Note. Observed resonances: J. K. Bair & H. B. Willard (1962), J. K. Bair & F. X. Haas (1973), and A. Best et al. (2013). Unobserved resonances: none. High-temperature rates (in parentheses): no matching to statistical model rates is needed over the listed temperature range. Previous rates: C. Angulo et al. (1999). Other: high-energy cross sections are taken from L. F. Hansen et al. (1967). Values of J^{π} are adopted from the R-matrix fit of A. Best et al. (2013) for resonances with $E_r^{c.m.} > 900$ keV. For ambiguous J^{π} values, we assigned equal probability to the possible choices and normalized Γ_{α} so that $\omega\Gamma_{\alpha}$ is constant. For the calculation of Γ_n, we have summed the neutron partial widths ($\Gamma_{n0} + \Gamma_{n1}$) reported in A. Best et al. (2013).

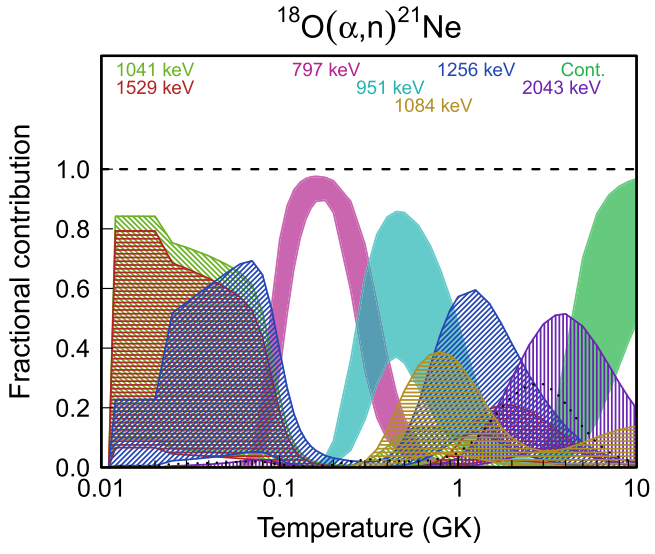

Figure 41. Fractional contributions to the total rate. "Cont." refers to the continuum of unresolved resonances. Resonance energies are given in the center-of-mass frame.

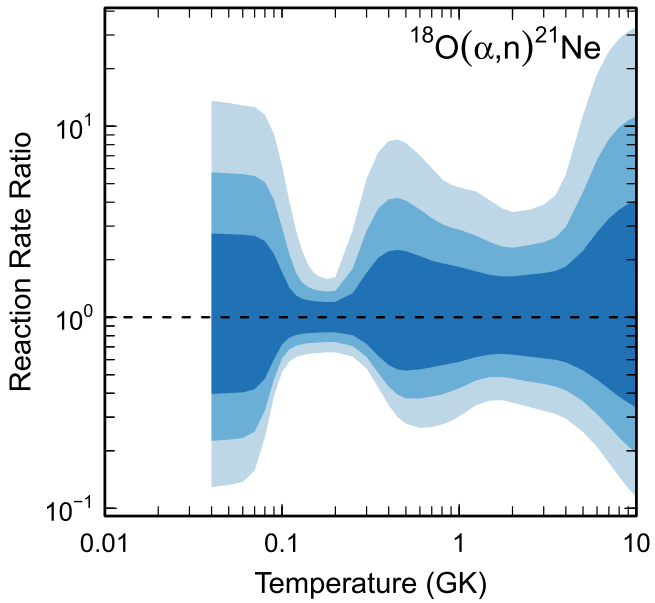

Figure 42. Reaction rate uncertainties versus temperature. The three different shades refer to coverage probabilities of 68%, 90%, and 98%.

Table 29
Total Laboratory Reaction Rates for $^{17}F(p,\gamma)^{18}Ne$

T (GK)	Low	Median	High	*f.u.*	T (GK)	Low	Median	High	*f.u.*
0.001	1.173E-69	1.513E-69	1.957E-69	1.293E+00	0.140	1.004E-07	1.288E-07	1.660E-07	1.287E+00
0.002	1.160E-53	1.497E-53	1.936E-53	1.293E+00	0.150	2.113E-07	2.710E-07	3.492E-07	1.287E+00
0.003	6.673E-46	8.607E-46	1.113E-45	1.293E+00	0.160	4.173E-07	5.351E-07	6.892E-07	1.286E+00
0.004	5.225E-41	6.739E-41	8.714E-41	1.293E+00	0.180	1.390E-06	1.781E-06	2.292E-06	1.285E+00
0.005	1.579E-37	2.036E-37	2.632E-37	1.293E+00	0.200	3.911E-06	5.011E-06	6.446E-06	1.285E+00
0.006	7.116E-35	9.177E-35	1.187E-34	1.293E+00	0.250	3.112E-05	3.982E-05	5.113E-05	1.282E+00
0.007	9.358E-33	1.207E-32	1.560E-32	1.293E+00	0.300	1.542E-04	1.969E-04	2.521E-04	1.278E+00
0.008	5.234E-31	6.749E-31	8.724E-31	1.292E+00	0.350	5.930E-04	7.554E-04	9.641E-04	1.275E+00
0.009	1.569E-29	2.023E-29	2.615E-29	1.292E+00	0.400	1.999E-03	2.572E-03	3.341E-03	1.300E+00
0.010	2.932E-28	3.781E-28	4.888E-28	1.292E+00	0.450	6.088E-03	8.068E-03	1.105E-02	1.361E+00
0.011	3.791E-27	4.888E-27	6.319E-27	1.292E+00	0.500	1.665E-02	2.293E-02	3.331E-02	1.429E+00
0.012	3.651E-26	4.707E-26	6.084E-26	1.292E+00	0.600	8.908E-02	1.310E-01	2.044E-01	1.524E+00
0.013	2.765E-25	3.565E-25	4.607E-25	1.292E+00	0.700	3.210E-01	4.885E-01	7.843E-01	1.570E+00
0.014	1.716E-24	2.212E-24	2.860E-24	1.292E+00	0.800	8.548E-01	1.323E+00	2.151E+00	1.591E+00
0.015	9.013E-24	1.162E-23	1.502E-23	1.292E+00	0.900	1.835E+00	2.858E+00	4.675E+00	1.601E+00
0.016	4.105E-23	5.291E-23	6.839E-23	1.292E+00	1.000	3.369E+00	5.256E+00	8.614E+00	1.604E+00
0.018	5.999E-22	7.732E-22	9.994E-22	1.292E+00	1.250	9.906E+00	1.536E+01	2.507E+01	1.595E+00
0.020	6.036E-21	7.779E-21	1.005E-20	1.292E+00	1.500	2.016E+01	3.075E+01	4.956E+01	1.573E+00
0.025	6.136E-19	7.906E-19	1.021E-18	1.292E+00	1.750	3.362E+01	5.013E+01	7.933E+01	1.542E+00
0.030	2.074E-17	2.672E-17	3.452E-17	1.291E+00	2.000	4.989E+01	7.248E+01	1.122E+02	1.507E+00
0.040	3.477E-15	4.477E-15	5.781E-15	1.291E+00	2.500	9.057E+01	1.247E+02	1.828E+02	1.434E+00
0.050	1.317E-13	1.695E-13	2.189E-13	1.291E+00	3.000	1.421E+02	1.876E+02	2.605E+02	1.368E+00
0.060	2.095E-12	2.695E-12	3.479E-12	1.290E+00	3.500	2.048E+02	2.631E+02	3.484E+02	1.318E+00
0.070	1.901E-11	2.445E-11	3.155E-11	1.290E+00	4.000	2.784E+02	3.513E+02	4.517E+02	1.284E+00
0.080	1.170E-10	1.504E-10	1.941E-10	1.290E+00	5.000	4.547E+02	5.661E+02	7.112E+02	1.253E+00
0.090	5.424E-10	6.970E-10	8.993E-10	1.289E+00	6.000	6.603E+02	8.216E+02	1.028E+03	1.248E+00
0.100	2.029E-09	2.607E-09	3.363E-09	1.289E+00	7.000	8.807E+02	1.099E+03	1.381E+03	1.252E+00
0.110	6.422E-09	8.249E-09	1.064E-08	1.288E+00	8.000	1.102E+03	1.381E+03	1.743E+03	1.257E+00
0.120	1.779E-08	2.284E-08	2.945E-08	1.288E+00	9.000	1.313E+03	1.651E+03	2.090E+03	1.262E+00
0.130	4.420E-08	5.673E-08	7.313E-08	1.288E+00	10.000	1.505E+03	1.900E+03	2.411E+03	1.266E+00

Note. Observed resonances: D. W. Bardayan et al. (2000), Y. Parpottas et al. (2005), and K. A. Chipps et al. (2009). Normalization: none. Unobserved resonances: T. K. Li et al. (1976; for mirror states) and S. A. Kuvin et al. (2017). High-temperature rates (in parentheses): no corrections for missing high-energy resonances are necessary up to $T = 10$ GK. Previous rates: A. García et al. (1991), D. W. Bardayan et al. (2000), and C. Iliadis et al. (2010c). See also S. A. Kuvin et al. (2017) for the direct-capture contribution. Other: the γ-ray partial widths were adopted from the mirror states, except for the resonance at $E_r^{c.m.} = 601.7$ keV. The Γ_γ value for this resonance was deduced from the measured resonance strength and proton width (D. W. Bardayan et al. 2000; Y. Parpottas et al. 2005; K. A. Chipps et al. 2009).

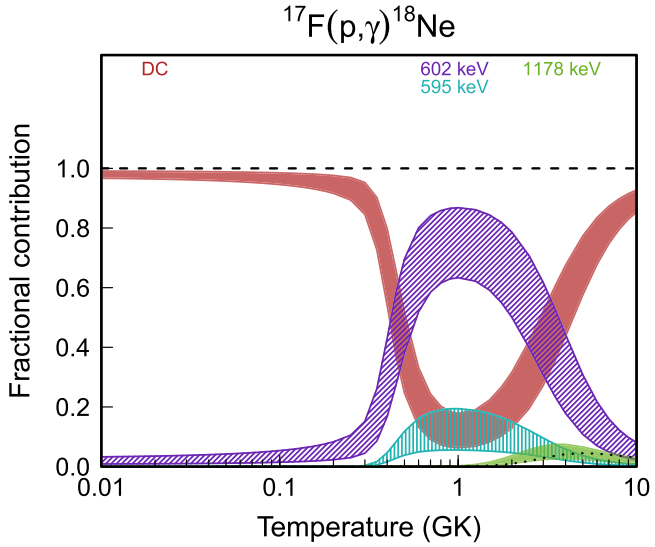

Figure 43. Fractional contributions to the total rate. "DC" refers to direct radiative capture. Resonance energies are given in the center-of-mass frame.

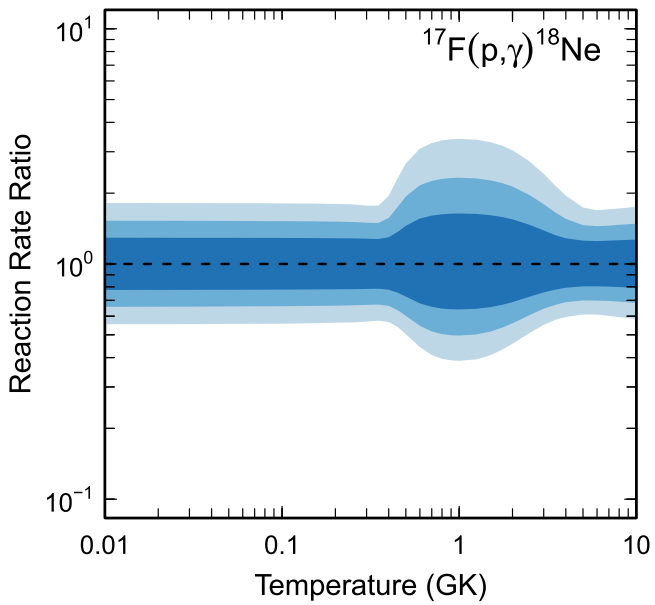

Figure 44. Reaction rate uncertainties versus temperature. The three different shades refer to coverage probabilities of 68%, 90%, and 98%.

Table 30
Total Laboratory Reaction Rates for $^{18}F(p,\gamma)^{19}Ne$

T (GK)	Low	Median	High	*f.u.*	T (GK)	Low	Median	High	*f.u.*
0.001	3.308E-68	1.410E-67	5.817E-67	5.115E+00	0.140	5.393E-07	9.692E-07	1.964E-06	1.921E+00
0.002	1.124E-51	6.639E-51	6.248E-50	7.163E+00	0.150	1.164E-06	2.017E-06	3.920E-06	1.860E+00
0.003	1.307E-43	7.766E-43	4.919E-42	6.189E+00	0.160	2.409E-06	4.035E-06	7.501E-06	1.799E+00
0.004	6.199E-39	3.849E-38	2.511E-37	6.473E+00	0.180	9.445E-06	1.508E-05	2.583E-05	1.693E+00
0.005	8.574E-36	7.210E-35	4.094E-34	6.566E+00	0.200	3.306E-05	5.228E-05	8.678E-05	1.653E+00
0.006	2.128E-33	2.903E-32	2.435E-31	9.679E+00	0.250	4.529E-04	7.690E-04	1.402E-03	1.783E+00
0.007	1.916E-31	4.759E-30	1.524E-28	2.248E+01	0.300	3.225E-03	5.938E-03	1.174E-02	1.917E+00
0.008	8.344E-30	3.931E-28	4.488E-26	5.016E+01	0.350	1.407E-02	2.700E-02	5.521E-02	1.985E+00
0.009	2.097E-28	1.831E-26	4.015E-24	9.117E+01	0.400	4.322E-02	8.438E-02	1.747E-01	2.015E+00
0.010	3.454E-27	5.068E-25	1.479E-22	1.370E+02	0.450	1.038E-01	2.038E-01	4.241E-01	2.024E+00
0.011	4.068E-26	8.643E-24	2.899E-21	1.776E+02	0.500	2.097E-01	4.098E-01	8.528E-01	2.019E+00
0.012	3.639E-25	1.170E-22	3.488E-20	2.067E+02	0.600	6.071E-01	1.158E+00	2.379E+00	1.981E+00
0.013	2.594E-24	7.528E-22	2.832E-19	2.223E+02	0.700	1.334E+00	2.440E+00	4.872E+00	1.916E+00
0.014	1.534E-23	3.367E-21	1.685E-18	2.259E+02	0.800	2.508E+00	4.346E+00	8.327E+00	1.834E+00
0.015	7.739E-23	1.608E-20	7.974E-18	2.202E+02	0.900	4.275E+00	7.000E+00	1.274E+01	1.747E+00
0.016	3.407E-22	5.760E-20	3.095E-17	2.082E+02	1.000	6.797E+00	1.059E+01	1.827E+01	1.665E+00
0.018	4.716E-21	5.447E-19	2.959E-16	1.751E+02	1.250	1.750E+01	2.510E+01	3.861E+01	1.514E+00
0.020	4.561E-20	3.872E-18	1.787E-15	1.404E+02	1.500	3.636E+01	5.017E+01	7.226E+01	1.438E+00
0.025	4.305E-18	1.251E-16	4.431E-14	7.516E+01	1.750	6.527E+01	8.850E+01	1.243E+02	1.406E+00
0.030	1.381E-16	2.159E-15	3.681E-13	4.066E+01	2.000	1.056E+02	1.425E+02	1.978E+02	1.394E+00
0.040	2.154E-14	1.591E-13	5.283E-12	1.448E+01	2.500	2.238E+02	3.010E+02	4.163E+02	1.386E+00
0.050	7.792E-13	3.605E-12	3.502E-11	6.922E+00	3.000	3.917E+02	5.298E+02	7.302E+02	1.383E+00
0.060	1.203E-11	4.183E-11	2.128E-10	4.274E+00	3.500	6.065E+02	8.252E+02	1.137E+03	1.383E+00
0.070	1.068E-10	3.101E-10	1.141E-09	3.185E+00	4.000	(8.424E+02)	(1.163E+03)	(1.723E+03)	(1.431E+00)
0.080	6.466E-10	1.651E-09	5.015E-09	2.676E+00	5.000	(1.047E+03)	(1.688E+03)	(4.898E+03)	(2.257E+00)
0.090	2.957E-09	6.870E-09	1.848E-08	2.408E+00	6.000	(1.154E+03)	(2.236E+03)	(9.663E+03)	(3.129E+00)
0.100	1.095E-08	2.360E-08	5.844E-08	2.247E+00	7.000	(1.162E+03)	(2.819E+03)	(1.618E+04)	(4.084E+00)
0.110	3.435E-08	7.002E-08	1.625E-07	2.136E+00	8.000	(1.063E+03)	(3.449E+03)	(2.470E+04)	(5.203E+00)
0.120	9.464E-08	1.837E-07	4.053E-07	2.053E+00	9.000	(8.443E+02)	(4.138E+03)	(3.550E+04)	(6.740E+00)
0.130	2.352E-07	4.386E-07	9.254E-07	1.984E+00	10.000	(4.888E+02)	(4.888E+03)	(4.888E+04)	(1.000E+01)

Note. Observed resonances: C. Akers et al. (2016). Normalization: none. Unobserved resonances: A. S. Adekola et al. (2011, 2012) and R. L. Kozub et al. (2005, 2006) for mirror levels. High-temperature rates (in parentheses): matching to statistical model rate above $T = 3.9$ GK. Previous rates: C. Iliadis et al. (2010c) and C. Akers et al. (2016). Other: the particle partial widths for higher-energy resonances were adopted from D. J. Mountford et al. (2012). For the properties of other resonances and bound states, see K. Setoodehnia et al. (2025). For the six two-level interferences (Figure 45), we included both constructive and destructive interference in the sampling of the total rate.

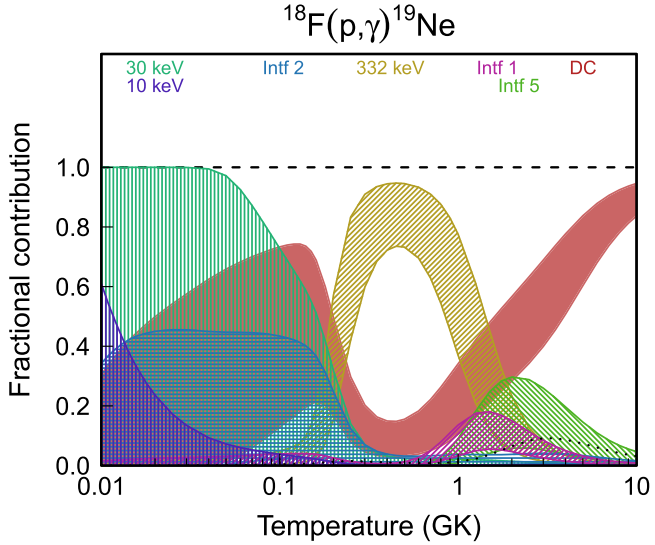

Figure 45. Fractional contributions to the total rate. "DC" refers to direct radiative capture. Resonance energies are given in the center-of-mass frame. Other labels refer to the interference of two resonances: $3/2^+$ resonances at $E_r^{c.m.} = -277$ and 663 keV (Intf 1); $1/2^+$ resonances at -127 and 1392 keV (Intf 2); and $3/2^+$ resonances at 833 and 1161 keV (Intf 5).

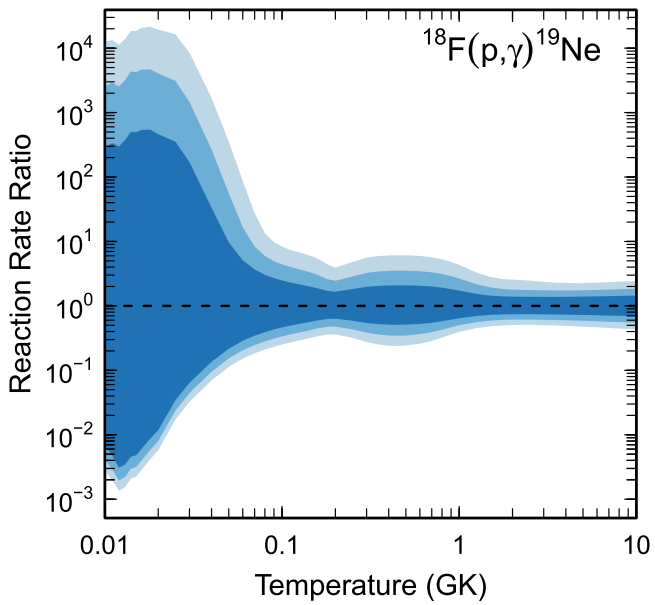

Figure 46. Reaction rate uncertainties versus temperature. The three different shades refer to coverage probabilities of 68%, 90%, and 98%.

Table 31
Total Laboratory Reaction Rates for $^{18}F(p,\alpha)^{15}O$

T (GK)	Low	Median	High	*f.u.*	T (GK)	Low	Median	High	*f.u.*
0.001	2.964E-64	1.006E-63	4.632E-63	4.020E+00	0.140	4.532E-03	1.726E-02	7.503E-02	3.895E+00
0.002	7.269E-48	3.821E-47	1.590E-46	4.218E+00	0.150	9.359E-03	3.516E-02	1.522E-01	3.858E+00
0.003	8.029E-40	3.673E-39	1.001E-38	3.491E+00	0.160	1.826E-02	6.737E-02	2.903E-01	3.812E+00
0.004	3.709E-35	1.872E-34	5.865E-34	3.729E+00	0.180	6.091E-02	2.135E-01	9.071E-01	3.689E+00
0.005	7.021E-32	2.833E-31	1.091E-30	3.663E+00	0.200	1.795E-01	5.822E-01	2.414E+00	3.521E+00
0.006	2.785E-29	9.083E-29	3.224E-28	3.288E+00	0.250	1.825E+00	4.592E+00	1.719E+01	3.031E+00
0.007	5.023E-27	1.560E-26	4.982E-26	3.146E+00	0.300	1.155E+01	2.382E+01	7.741E+01	2.647E+00
0.008	5.704E-25	1.852E-24	5.958E-24	3.257E+00	0.350	5.004E+01	9.089E+01	2.584E+02	2.386E+00
0.009	4.022E-23	1.302E-22	3.826E-22	3.121E+00	0.400	1.698E+02	2.802E+02	7.066E+02	2.181E+00
0.010	1.619E-21	4.634E-21	1.182E-20	2.828E+00	0.450	5.067E+02	7.593E+02	1.689E+03	1.989E+00
0.011	3.575E-20	8.968E-20	2.039E-19	2.581E+00	0.500	1.388E+03	1.911E+03	3.719E+03	1.810E+00
0.012	4.677E-19	1.065E-18	2.263E-18	2.428E+00	0.600	8.023E+03	9.948E+03	1.527E+04	1.539E+00
0.013	3.999E-18	8.703E-18	1.789E-17	2.359E+00	0.700	3.213E+04	3.819E+04	5.090E+04	1.385E+00
0.014	2.451E-17	5.274E-17	1.072E-16	2.347E+00	0.800	9.474E+04	1.105E+05	1.375E+05	1.300E+00
0.015	1.151E-16	2.516E-16	5.186E-16	2.373E+00	0.900	2.220E+05	2.564E+05	3.086E+05	1.252E+00
0.016	4.369E-16	9.900E-16	2.079E-15	2.420E+00	1.000	4.395E+05	5.042E+05	5.972E+05	1.222E+00
0.018	3.980E-15	9.698E-15	2.147E-14	2.534E+00	1.250	1.491E+06	1.699E+06	1.979E+06	1.187E+00
0.020	2.333E-14	6.075E-14	1.427E-13	2.635E+00	1.500	3.334E+06	3.794E+06	4.400E+06	1.174E+00
0.025	6.679E-13	1.855E-12	4.778E-12	2.746E+00	1.750	(5.311E+06)	(6.188E+06)	(8.617E+06)	(1.279E+00)
0.030	8.678E-12	2.417E-11	6.554E-11	2.809E+00	2.000	(8.332E+06)	(9.974E+06)	(1.649E+07)	(1.425E+00)
0.040	4.722E-10	1.423E-09	4.980E-09	3.290E+00	2.500	(1.471E+07)	(1.864E+07)	(4.054E+07)	(1.721E+00)
0.050	1.099E-08	3.850E-08	1.590E-07	3.739E+00	3.000	(2.155E+07)	(2.898E+07)	(7.816E+07)	(2.021E+00)
0.060	1.432E-07	5.407E-07	2.331E-06	3.926E+00	3.500	(2.798E+07)	(4.012E+07)	(1.291E+08)	(2.326E+00)
0.070	1.165E-06	4.549E-06	1.981E-05	3.988E+00	4.000	(3.347E+07)	(5.138E+07)	(1.922E+08)	(2.638E+00)
0.080	6.657E-06	2.632E-05	1.149E-04	4.005E+00	5.000	(4.028E+07)	(7.199E+07)	(3.444E+08)	(3.285E+00)
0.090	2.913E-05	1.155E-04	5.051E-04	4.004E+00	6.000	(4.107E+07)	(8.781E+07)	(5.117E+08)	(3.983E+00)
0.100	1.041E-04	4.112E-04	1.799E-03	3.993E+00	7.000	(3.657E+07)	(9.732E+07)	(6.686E+08)	(4.766E+00)
0.110	3.165E-04	1.243E-03	5.433E-03	3.975E+00	8.000	(2.840E+07)	(1.001E+08)	(7.918E+08)	(5.718E+00)
0.120	8.485E-04	3.300E-03	1.440E-02	3.953E+00	9.000	(1.845E+07)	(9.615E+07)	(8.612E+08)	(7.084E+00)
0.130	2.048E-03	7.882E-03	3.435E-02	3.927E+00	10.000	(8.603E+06)	(8.603E+07)	(8.603E+08)	(1.000E+01)

Note. Observed resonances: R. Coszach et al. (1995), J. S. Graulich et al. (1997), D. W. Bardayan et al. (2002), A. S. J. Murphy et al. (2009), and D. J. Mountford et al. (2012). Normalization: none. Unobserved resonances: A. S. Adekola et al. (2011, 2012) and R. L. Kozub et al. (2005, 2006) for mirror levels. High-temperature rates (in parentheses): matching to statistical model rate above $T = 1.5$ GK. Previous rates: C. Iliadis et al. (2010c), M. R. Hall et al. (2020), and D. Kahl et al. (2021). Other: the particle partial widths for higher-energy resonances were adopted from D. J. Mountford et al. (2012). For the properties of other resonances and bound states, see K. Setoodehnia et al. (2025). For the six two-level interferences (Figure 47), we included both constructive and destructive interference in the sampling of the total rate.

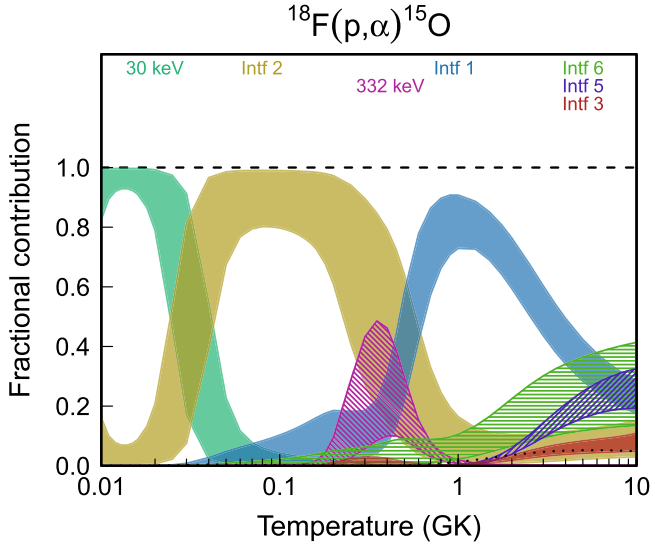

Figure 47. Fractional contributions to the total rate. Resonance energies are given in the center-of-mass frame. Other labels refer to the combined contribution of two interfering resonances: $3/2^+$ resonances at $E_r^{c.m.} = -277$ and 663 keV (Intf 1); $1/2^+$ resonances at -127 and 1392 keV (Intf 2); $5/2^+$ resonances at 291 and 1091 keV (Intf 3); $3/2^+$ resonances at 1201 and 1343 keV (Intf 5); and $1/2^+$ resonances at 1022 and 1426 keV (Intf 6).

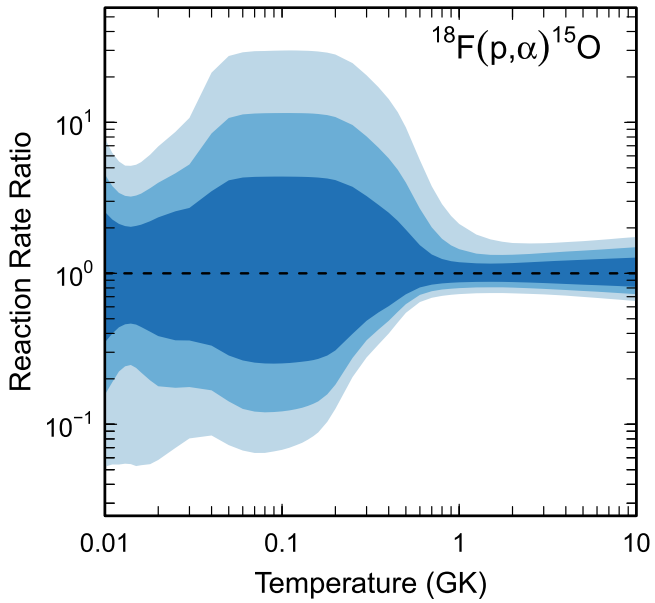

Figure 48. Reaction rate uncertainties versus temperature. The three different shades refer to coverage probabilities of 68%, 90%, and 98%.

Table 32
Total Laboratory Reaction Rates for ^{18}Ne(α,p)^{21}Na

T (GK)	Low	Median	High	*f.u.*	T (GK)	Low	Median	High	*f.u.*
0.001	0.000E+00	0.000E+00	0.000E+00	1.000E+00	0.140	5.377E-22	1.314E-21	3.278E-21	2.510E+00
0.002	0.000E+00	0.000E+00	0.000E+00	1.000E+00	0.150	4.967E-21	1.193E-20	2.862E-20	2.421E+00
0.003	0.000E+00	0.000E+00	0.000E+00	1.000E+00	0.160	3.723E-20	8.926E-20	2.101E-19	2.382E+00
0.004	0.000E+00	0.000E+00	0.000E+00	1.000E+00	0.180	1.333E-18	3.199E-18	7.639E-18	2.409E+00
0.005	2.203E-99	2.614E-98	1.269E-97	1.003E+01	0.200	2.957E-17	7.477E-17	1.802E-16	2.493E+00
0.006	5.313E-93	6.898E-92	3.875E-91	1.096E+01	0.250	1.355E-14	3.748E-14	8.864E-14	2.600E+00
0.007	1.717E-88	2.519E-87	1.767E-86	1.280E+01	0.300	1.296E-12	3.176E-12	7.349E-12	2.406E+00
0.008	3.800E-85	6.486E-84	5.581E-83	1.500E+01	0.350	5.055E-11	1.101E-10	2.336E-10	2.176E+00
0.009	1.441E-82	2.852E-81	2.964E-80	1.733E+01	0.400	9.905E-10	2.115E-09	4.478E-09	2.153E+00
0.010	1.640E-80	3.660E-79	4.459E-78	1.966E+01	0.450	1.161E-08	2.497E-08	5.603E-08	2.237E+00
0.011	7.755E-79	1.913E-77	2.669E-76	2.195E+01	0.500	9.466E-08	2.028E-07	4.797E-07	2.287E+00
0.012	1.888E-77	5.096E-76	8.048E-75	2.414E+01	0.600	3.341E-06	6.519E-06	1.453E-05	2.124E+00
0.013	2.794E-76	8.176E-75	1.423E-73	2.624E+01	0.700	6.729E-05	1.194E-04	2.277E-04	1.871E+00
0.014	2.774E-75	8.738E-74	1.656E-72	2.824E+01	0.800	8.218E-04	1.388E-03	2.443E-03	1.748E+00
0.015	2.004E-74	6.793E-73	1.385E-71	3.012E+01	0.900	6.482E-03	1.074E-02	1.846E-02	1.709E+00
0.016	1.135E-73	4.056E-72	8.844E-71	3.190E+01	1.000	3.583E-02	5.905E-02	1.002E-01	1.691E+00
0.018	1.967E-72	7.797E-71	1.898E-69	3.517E+01	1.250	8.675E-01	1.394E+00	2.295E+00	1.639E+00
0.020	1.914E-71	8.220E-70	2.177E-68	3.807E+01	1.500	7.886E+00	1.211E+01	1.917E+01	1.569E+00
0.025	1.087E-69	5.412E-68	1.675E-66	4.404E+01	1.750	4.124E+01	6.018E+01	9.050E+01	1.494E+00
0.030	1.568E-68	8.359E-67	2.884E-65	3.949E+01	2.000	1.541E+02	2.155E+02	3.087E+02	1.426E+00
0.040	2.086E-55	7.170E-55	2.468E-54	3.451E+00	2.500	1.177E+03	1.578E+03	2.144E+03	1.354E+00
0.050	4.982E-46	1.621E-45	5.312E-45	3.281E+00	3.000	5.452E+03	7.302E+03	9.908E+03	1.352E+00
0.060	8.429E-40	2.659E-39	8.451E-39	3.188E+00	3.500	1.835E+04	2.487E+04	3.420E+04	1.370E+00
0.070	2.274E-35	7.049E-35	2.204E-34	3.130E+00	4.000	4.917E+04	6.749E+04	9.434E+04	1.392E+00
0.080	4.677E-32	1.427E-31	4.408E-31	3.087E+00	5.000	2.150E+05	3.066E+05	4.474E+05	1.451E+00
0.090	1.736E-29	5.227E-29	1.596E-28	3.047E+00	6.000	5.974E+05	9.009E+05	1.398E+06	1.540E+00
0.100	1.962E-27	5.821E-27	1.755E-26	2.996E+00	7.000	1.236E+06	2.005E+06	3.350E+06	1.659E+00
0.110	9.555E-26	2.738E-25	8.135E-25	2.915E+00	8.000	2.095E+06	3.702E+06	6.688E+06	1.800E+00
0.120	2.561E-24	6.905E-24	1.989E-23	2.792E+00	9.000	3.084E+06	5.989E+06	1.170E+07	1.959E+00
0.130	4.413E-23	1.119E-22	3.017E-22	2.644E+00	10.000	4.088E+06	8.798E+06	1.853E+07	2.140E+00

Note. Observed resonances: P. Mohr (2014). Normalization: none. Unobserved resonances: P. Mohr et al. (2014). High-temperature rates (in parentheses): no corrections for missing high-energy resonances are necessary up to $T = 10$ GK. Previous rates: P. Mohr et al. (2014) and L. Y. Zhang et al. (2014). Other: the rate for ^{18}Ne(α,p)^{21}Na was calculated from the (total) experimental ^{18}Ne + α rate (i.e., including the p and $2p$ exit channels) using the calculated branching ratio for the (α,p) channel from TALYS, which deviates from unity by less than 10% up to $T = 2$ GK.

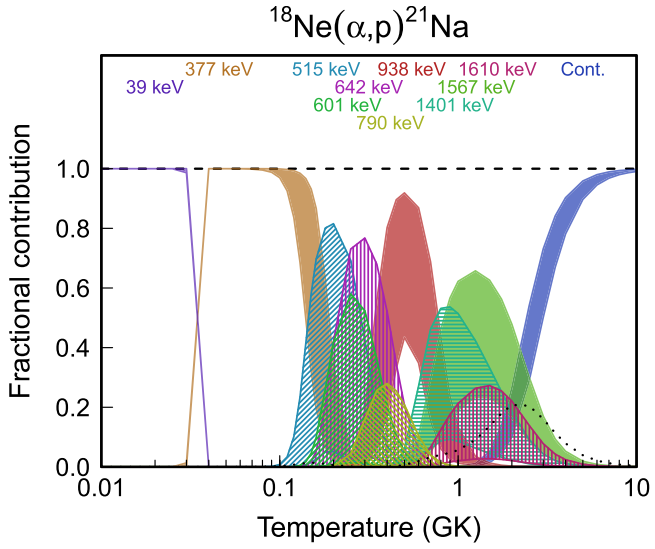

Figure 49. Fractional contributions to the total rate. "Cont." refers to the continuum of higher-lying, unresolved resonances. Resonance energies are given in the center-of-mass frame.

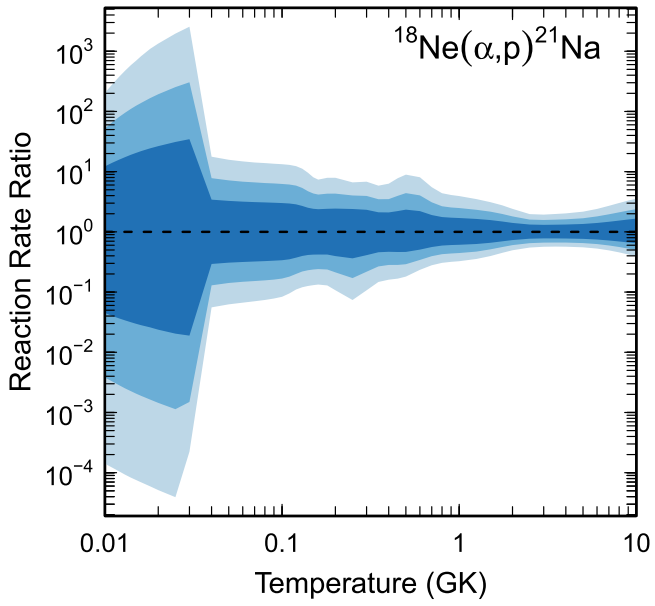

Figure 50. Reaction rate uncertainties versus temperature. The three different shades refer to coverage probabilities of 68%, 90%, and 98%.

Table 33
Total Laboratory Reaction Rates for ^{19}Ne(p,γ)^{20}Na

T (GK)	Low	Median	High	*f.u.*	T (GK)	Low	Median	High	*f.u.*
0.001	3.144E-76	4.617E-76	6.812E-76	1.477E+00	0.140	1.754E-09	2.548E-09	3.721E-09	1.462E+00
0.002	5.094E-59	7.479E-59	1.103E-58	1.477E+00	0.150	3.964E-09	5.745E-09	8.378E-09	1.459E+00
0.003	1.142E-50	1.677E-50	2.474E-50	1.477E+00	0.160	8.466E-09	1.219E-08	1.771E-08	1.451E+00
0.004	2.116E-45	3.106E-45	4.581E-45	1.476E+00	0.180	3.675E-08	5.085E-08	7.159E-08	1.401E+00
0.005	1.181E-41	1.733E-41	2.556E-41	1.476E+00	0.200	1.772E-07	2.388E-07	3.239E-07	1.355E+00
0.006	8.508E-39	1.249E-38	1.841E-38	1.476E+00	0.250	9.591E-06	1.449E-05	2.228E-05	1.528E+00
0.007	1.628E-36	2.390E-36	3.523E-36	1.476E+00	0.300	2.217E-04	3.461E-04	5.452E-04	1.571E+00
0.008	1.242E-34	1.823E-34	2.687E-34	1.476E+00	0.350	2.149E-03	3.371E-03	5.312E-03	1.575E+00
0.009	4.841E-33	7.104E-33	1.047E-32	1.476E+00	0.400	1.163E-02	1.822E-02	2.867E-02	1.573E+00
0.010	1.135E-31	1.665E-31	2.454E-31	1.475E+00	0.450	4.260E-02	6.652E-02	1.044E-01	1.568E+00
0.011	1.789E-30	2.625E-30	3.868E-30	1.475E+00	0.500	1.189E-01	1.849E-01	2.893E-01	1.563E+00
0.012	2.054E-29	3.013E-29	4.440E-29	1.475E+00	0.600	5.408E-01	8.335E-01	1.295E+00	1.550E+00
0.013	1.821E-28	2.671E-28	3.935E-28	1.475E+00	0.700	1.567E+00	2.386E+00	3.674E+00	1.534E+00
0.014	1.303E-27	1.911E-27	2.815E-27	1.475E+00	0.800	(3.354E+00)	(5.054E+00)	(7.771E+00)	(1.522E+00)
0.015	7.787E-27	1.142E-26	1.682E-26	1.475E+00	0.900	(5.142E+00)	(7.819E+00)	(1.274E+01)	(1.575E+00)
0.016	3.994E-26	5.855E-26	8.625E-26	1.475E+00	1.000	(7.306E+00)	(1.121E+01)	(1.931E+01)	(1.628E+00)
0.018	7.200E-25	1.055E-24	1.554E-24	1.474E+00	1.250	(1.306E+01)	(2.053E+01)	(4.007E+01)	(1.762E+00)
0.020	8.685E-24	1.273E-23	1.874E-23	1.474E+00	1.500	(2.211E+01)	(3.562E+01)	(7.771E+01)	(1.896E+00)
0.025	1.272E-21	1.863E-21	2.742E-21	1.474E+00	1.750	(2.997E+01)	(4.950E+01)	(1.194E+02)	(2.032E+00)
0.030	5.685E-20	8.327E-20	1.225E-19	1.473E+00	2.000	(3.959E+01)	(6.707E+01)	(1.772E+02)	(2.168E+00)
0.040	1.438E-17	2.104E-17	3.094E-17	1.472E+00	2.500	(5.650E+01)	(1.010E+02)	(3.132E+02)	(2.444E+00)
0.050	7.320E-16	1.070E-15	1.573E-15	1.471E+00	3.000	(7.162E+01)	(1.354E+02)	(4.823E+02)	(2.726E+00)
0.060	1.463E-14	2.137E-14	3.138E-14	1.470E+00	3.500	(8.464E+01)	(1.699E+02)	(6.831E+02)	(3.014E+00)
0.070	1.595E-13	2.328E-13	3.416E-13	1.469E+00	4.000	(9.554E+01)	(2.043E+02)	(9.155E+02)	(3.310E+00)
0.080	1.143E-12	1.667E-12	2.445E-12	1.468E+00	5.000	(1.115E+02)	(2.743E+02)	(1.481E+03)	(3.931E+00)
0.090	6.030E-12	8.793E-12	1.289E-11	1.467E+00	6.000	(1.200E+02)	(3.479E+02)	(2.199E+03)	(4.609E+00)
0.100	2.525E-11	3.678E-11	5.389E-11	1.466E+00	7.000	(1.215E+02)	(4.282E+02)	(3.100E+03)	(5.382E+00)
0.110	8.823E-11	1.285E-10	1.881E-10	1.465E+00	8.000	(1.156E+02)	(5.193E+02)	(4.237E+03)	(6.327E+00)
0.120	2.669E-10	3.884E-10	5.681E-10	1.464E+00	9.000	(1.009E+02)	(6.256E+02)	(5.680E+03)	(7.640E+00)
0.130	7.181E-10	1.044E-09	1.526E-09	1.463E+00	10.000	(7.528E+01)	(7.528E+02)	(7.528E+03)	(1.000E+01)

Note. Observed resonances: R. Wilkinson et al. (2017). Normalization: none. Unobserved resonances: H. T. Fortune & R. R. Betts (1974) and C. A. Mosley & H. T. Fortune (1977). High-temperature rates (in parentheses): matching to statistical model rate above $T = 0.79$ GK. Previous rates: C. Iliadis et al. (2010c). Other: the γ-ray partial widths were adopted from the mirror states. The total widths for the 797 and 889 keV resonances were measured by R. Coszach et al. (1994).

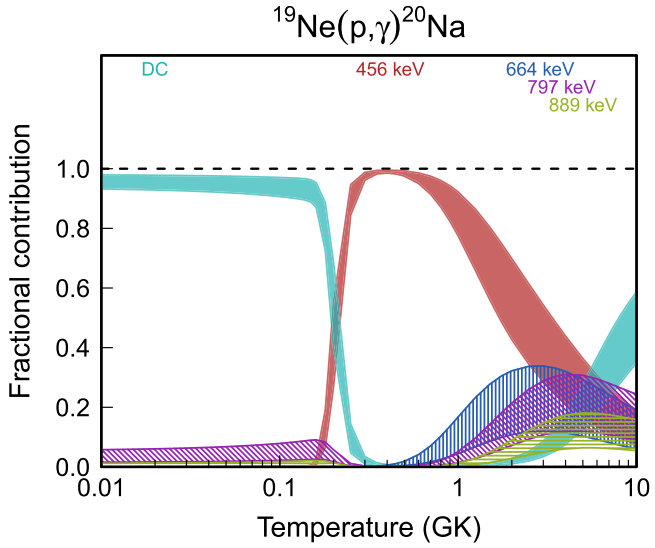

Figure 51. Fractional contributions to the total rate. "DC" refers to direct radiative capture. Resonance energies are given in the center-of-mass frame.

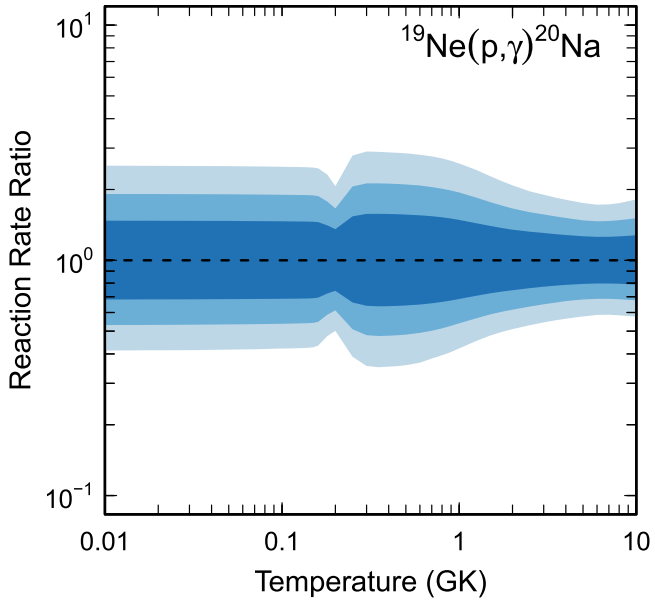

Figure 52. Reaction rate uncertainties versus temperature. The three different shades refer to coverage probabilities of 68%, 90%, and 98%.

Table 34
Total Laboratory Reaction Rates for ^{20}Ne(p,γ)^{21}Na

T (GK)	Low	Median	High	*f.u.*	T (GK)	Low	Median	High	*f.u.*
0.001	9.418E-73	1.312E-72	1.825E-72	1.392E+00	0.140	1.077E-07	1.282E-07	1.537E-07	1.198E+00
0.002	1.019E-55	1.409E-55	1.950E-55	1.384E+00	0.150	2.306E-07	2.741E-07	3.277E-07	1.195E+00
0.003	1.723E-47	2.369E-47	3.268E-47	1.377E+00	0.160	4.626E-07	5.488E-07	6.547E-07	1.192E+00
0.004	2.564E-42	3.510E-42	4.824E-42	1.372E+00	0.180	1.590E-06	1.877E-06	2.230E-06	1.187E+00
0.005	1.196E-38	1.631E-38	2.234E-38	1.367E+00	0.200	4.646E-06	5.462E-06	6.456E-06	1.180E+00
0.006	7.405E-36	1.006E-35	1.374E-35	1.362E+00	0.250	4.340E-05	4.997E-05	5.789E-05	1.156E+00
0.007	1.243E-33	1.682E-33	2.291E-33	1.358E+00	0.300	2.661E-04	2.993E-04	3.385E-04	1.129E+00
0.008	8.437E-32	1.139E-31	1.547E-31	1.354E+00	0.350	1.159E-03	1.284E-03	1.429E-03	1.111E+00
0.009	2.965E-30	3.990E-30	5.405E-30	1.350E+00	0.400	3.777E-03	4.156E-03	4.584E-03	1.103E+00
0.010	6.332E-29	8.493E-29	1.148E-28	1.347E+00	0.450	9.810E-03	1.076E-02	1.183E-02	1.099E+00
0.011	9.165E-28	1.226E-27	1.653E-27	1.343E+00	0.500	2.145E-02	2.351E-02	2.581E-02	1.098E+00
0.012	9.730E-27	1.298E-26	1.746E-26	1.340E+00	0.600	7.189E-02	7.888E-02	8.679E-02	1.100E+00
0.013	8.026E-26	1.068E-25	1.433E-25	1.337E+00	0.700	1.788E-01	1.969E-01	2.175E-01	1.104E+00
0.014	5.373E-25	7.124E-25	9.543E-25	1.334E+00	0.800	3.794E-01	4.190E-01	4.646E-01	1.107E+00
0.015	3.017E-24	3.991E-24	5.333E-24	1.330E+00	0.900	7.514E-01	8.286E-01	9.183E-01	1.106E+00
0.016	1.459E-23	1.925E-23	2.567E-23	1.328E+00	1.000	1.450E+00	1.589E+00	1.750E+00	1.099E+00
0.018	2.366E-22	3.106E-22	4.125E-22	1.322E+00	1.250	6.624E+00	7.093E+00	7.637E+00	1.075E+00
0.020	2.594E-21	3.390E-21	4.486E-21	1.317E+00	1.500	2.241E+01	2.368E+01	2.513E+01	1.060E+00
0.025	3.107E-19	4.023E-19	5.272E-19	1.304E+00	1.750	5.663E+01	5.952E+01	6.272E+01	1.053E+00
0.030	1.182E-17	1.517E-17	1.972E-17	1.294E+00	2.000	1.154E+02	1.210E+02	1.271E+02	1.050E+00
0.040	2.328E-15	2.943E-15	3.773E-15	1.275E+00	2.500	(3.087E+02)	(3.247E+02)	(3.504E+02)	(1.065E+00)
0.050	9.823E-14	1.227E-13	1.553E-13	1.261E+00	3.000	(3.855E+02)	(4.312E+02)	(7.217E+02)	(1.396E+00)
0.060	1.690E-12	2.092E-12	2.620E-12	1.248E+00	3.500	(4.536E+02)	(5.417E+02)	(1.229E+03)	(1.731E+00)
0.070	1.631E-11	2.002E-11	2.486E-11	1.238E+00	4.000	(5.118E+02)	(6.556E+02)	(1.877E+03)	(2.072E+00)
0.080	1.055E-10	1.287E-10	1.585E-10	1.229E+00	5.000	(5.930E+02)	(8.888E+02)	(3.602E+03)	(2.776E+00)
0.090	5.099E-10	6.186E-10	7.564E-10	1.222E+00	6.000	(6.245E+02)	(1.128E+03)	(5.911E+03)	(3.524E+00)
0.100	1.975E-09	2.385E-09	2.901E-09	1.215E+00	7.000	(6.033E+02)	(1.370E+03)	(8.811E+03)	(4.351E+00)
0.110	6.444E-09	7.746E-09	9.377E-09	1.210E+00	8.000	(5.297E+02)	(1.620E+03)	(1.235E+04)	(5.340E+00)
0.120	1.831E-08	2.193E-08	2.645E-08	1.205E+00	9.000	(4.021E+02)	(1.884E+03)	(1.660E+04)	(6.748E+00)
0.130	4.649E-08	5.554E-08	6.675E-08	1.201E+00	10.000	(2.170E+02)	(2.170E+03)	(2.170E+04)	(1.000E+01)

Note. Observed resonances: P. M. Endt & C. van der Leun (1978) and E. Masha et al. (2023). Normalization: S. Lyons et al. (2018) and E. Masha et al. (2023). High-temperature rates (in parentheses): matching to statistical model rate above $T = 2.5$ GK. Previous rates: S. Lyons et al. (2018). Other: comparison of S factors at zero energy: $S(0) = 3500$ keVb (C. Rolfs et al. 1975), 6300 keVb (S. Lyons et al. 2018), 5900 keVb (A. M. Mukhamedzhanov et al. 2006), 6250 keVb (present).

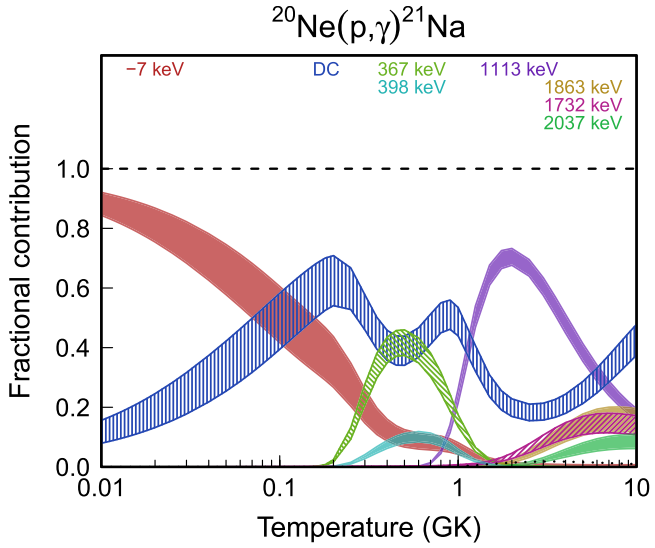

Figure 53. Fractional contributions to the total rate. "DC" refers to direct radiative capture. Resonance energies are given in the center-of-mass frame.

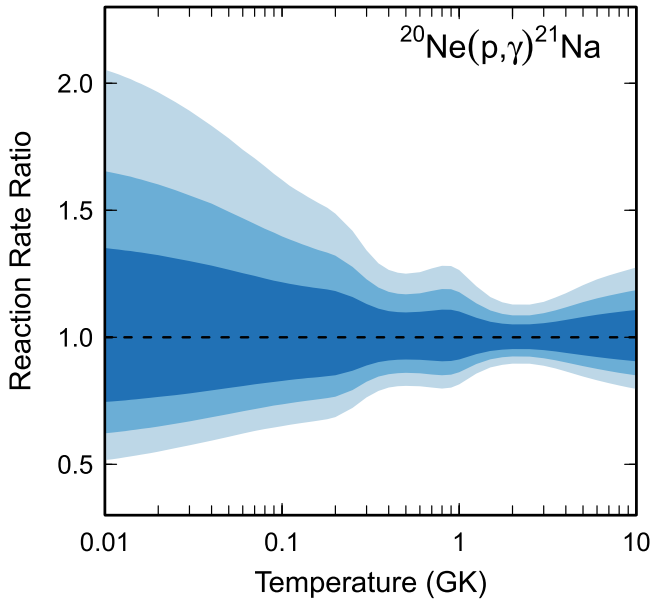

Figure 54. Reaction rate uncertainties versus temperature. The three different shades refer to coverage probabilities of 68%, 90%, and 98%.

Table 35
Total Laboratory Reaction Rates for $^{20}Ne(\alpha,\gamma)^{24}Mg$

T (GK)	Low	Median	High	*f.u.*	T (GK)	Low	Median	High	*f.u.*
0.001	0.000E+00	0.000E+00	0.000E+00	1.000E+00	0.140	1.007E-24	1.036E-23	4.956E-23	6.875E+00
0.002	0.000E+00	0.000E+00	0.000E+00	1.000E+00	0.150	3.743E-24	3.189E-23	1.498E-22	5.641E+00
0.003	0.000E+00	0.000E+00	0.000E+00	1.000E+00	0.160	2.724E-23	1.043E-22	4.104E-22	3.507E+00
0.004	0.000E+00	0.000E+00	0.000E+00	1.000E+00	0.180	4.948E-21	7.454E-21	1.320E-20	1.650E+00
0.005	0.000E+00	0.000E+00	0.000E+00	1.000E+00	0.200	6.099E-19	8.634E-19	1.416E-18	1.560E+00
0.006	4.803E-99	2.382E-98	1.175E-97	5.011E+00	0.250	4.247E-15	5.757E-15	8.282E-15	1.421E+00
0.007	1.717E-93	8.515E-93	4.202E-92	5.011E+00	0.300	1.485E-12	1.977E-12	2.700E-12	1.360E+00
0.008	9.657E-89	3.619E-88	1.646E-87	4.099E+00	0.350	9.431E-11	1.242E-10	1.656E-10	1.331E+00
0.009	7.113E-85	2.693E-84	1.233E-83	4.126E+00	0.400	2.072E-09	2.710E-09	3.559E-09	1.315E+00
0.010	1.528E-81	5.837E-81	2.688E-80	4.149E+00	0.450	2.248E-08	2.929E-08	3.814E-08	1.306E+00
0.011	1.254E-78	4.831E-78	2.235E-77	4.169E+00	0.500	1.495E-07	1.940E-07	2.511E-07	1.299E+00
0.012	4.774E-76	1.851E-75	8.595E-75	4.185E+00	0.600	2.519E-06	3.249E-06	4.170E-06	1.289E+00
0.013	9.703E-74	3.786E-73	1.763E-72	4.199E+00	0.700	1.930E-05	2.466E-05	3.135E-05	1.276E+00
0.014	1.172E-71	4.600E-71	2.147E-70	4.211E+00	0.800	9.734E-05	1.225E-04	1.535E-04	1.257E+00
0.015	9.169E-70	3.612E-69	1.688E-68	4.220E+00	0.900	4.015E-04	4.960E-04	6.108E-04	1.235E+00
0.016	4.946E-68	1.953E-67	9.143E-67	4.228E+00	1.000	1.479E-03	1.804E-03	2.199E-03	1.221E+00
0.018	5.752E-65	2.282E-64	1.070E-63	4.239E+00	1.250	2.337E-02	2.829E-02	3.435E-02	1.214E+00
0.020	2.521E-62	1.004E-61	4.709E-61	4.244E+00	1.500	1.788E-01	2.168E-01	2.631E-01	1.215E+00
0.025	5.661E-57	2.068E-56	9.420E-56	4.028E+00	1.750	7.958E-01	9.643E-01	1.171E+00	1.215E+00
0.030	1.239E-51	4.228E-51	1.209E-50	3.220E+00	2.000	2.453E+00	2.970E+00	3.606E+00	1.214E+00
0.040	3.702E-43	2.002E-42	8.110E-42	4.964E+00	2.500	1.179E+01	1.425E+01	1.729E+01	1.213E+00
0.050	5.691E-38	3.879E-37	1.758E-36	5.745E+00	3.000	3.327E+01	4.020E+01	4.874E+01	1.212E+00
0.060	1.621E-34	1.306E-33	6.107E-33	6.282E+00	3.500	6.955E+01	8.404E+01	1.018E+02	1.211E+00
0.070	4.700E-32	4.214E-31	1.994E-30	6.659E+00	4.000	1.211E+02	1.463E+02	1.770E+02	1.210E+00
0.080	3.296E-30	3.135E-29	1.494E-28	6.931E+00	5.000	2.654E+02	3.210E+02	3.882E+02	1.210E+00
0.090	8.833E-29	8.786E-28	4.202E-27	7.127E+00	6.000	4.514E+02	5.474E+02	6.634E+02	1.213E+00
0.100	1.214E-27	1.245E-26	5.961E-26	7.263E+00	7.000	6.628E+02	8.061E+02	9.797E+02	1.218E+00
0.110	1.030E-26	1.075E-25	5.151E-25	7.337E+00	8.000	8.849E+02	1.079E+03	1.316E+03	1.222E+00
0.120	6.059E-26	6.408E-25	3.072E-24	7.337E+00	9.000	1.104E+03	1.350E+03	1.654E+03	1.226E+00
0.130	2.719E-25	2.877E-24	1.379E-23	7.234E+00	10.000	1.313E+03	1.609E+03	1.978E+03	1.230E+00

Note. Observed resonances: P. Smulders (1965), G. Highland & T. Thwaites (1968), and P. Schmalbrock et al. (1983). Normalization: P. Smulders (1965) and P. Schmalbrock et al. (1983). Unobserved resonances: N. Anantaraman et al. (1977), normalized to T. A. Carey et al. (1984) and Z. Q. Mao et al. (1996). High-temperature rates (in parentheses): no matching to statistical model rates is needed over the listed temperature range. Previous rates: C. Iliadis et al. (2010c). Other: an upper limit value of twice the Wigner limit was used for all unobserved resonances below 744 keV.

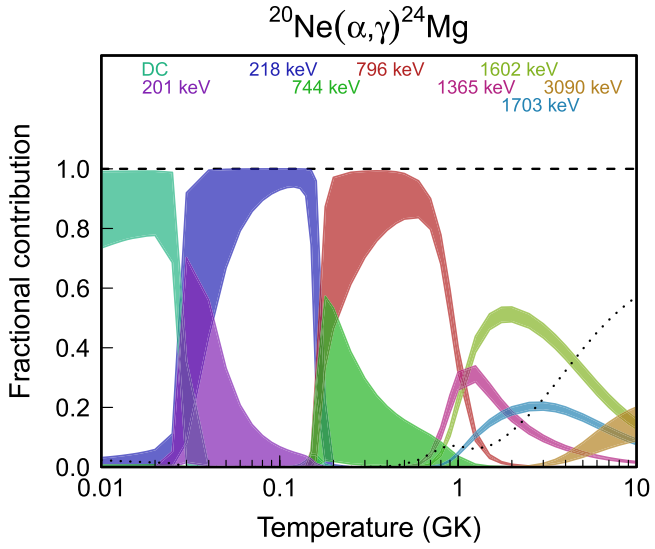

Figure 55. Fractional contributions to the total rate. "DC" refers to direct radiative capture. Resonance energies are given in the center-of-mass frame.

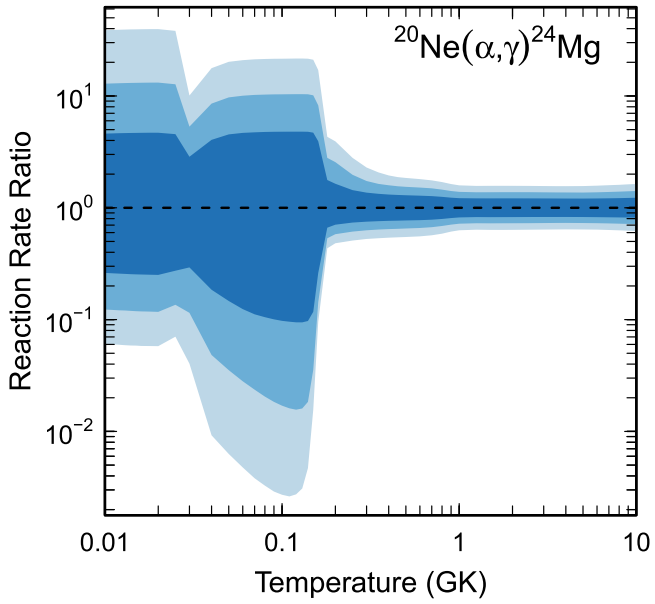

Figure 56. Reaction rate uncertainties versus temperature. The three different shades refer to coverage probabilities of 68%, 90%, and 98%.

Table 36
Total Laboratory Reaction Rates for ^{21}Ne(p,γ)^{22}Na

T (GK)	Low	Median	High	*f.u.*	T (GK)	Low	Median	High	*f.u.*
0.001	7.473E-75	1.068E-74	1.626E-74	7.260E+00	0.140	4.031E-03	4.925E-03	6.019E-03	1.223E+00
0.002	1.391E-57	2.187E-57	5.254E-55	4.135E+01	0.150	7.327E-03	8.924E-03	1.088E-02	1.219E+00
0.003	3.950E-49	5.314E-48	1.003E-44	1.022E+02	0.160	1.258E-02	1.525E-02	1.851E-02	1.214E+00
0.004	1.271E-43	8.102E-41	6.024E-39	8.827E+01	0.180	3.361E-02	4.031E-02	4.834E-02	1.199E+00
0.005	5.661E-39	1.847E-36	5.293E-35	6.043E+01	0.200	8.495E-02	1.005E-01	1.189E-01	1.184E+00
0.006	9.654E-36	1.930E-33	4.346E-32	5.348E+01	0.250	6.830E-01	7.960E-01	9.274E-01	1.166E+00
0.007	1.068E-33	3.361E-31	7.621E-30	5.817E+01	0.300	3.366E+00	3.914E+00	4.551E+00	1.163E+00
0.008	2.488E-32	1.742E-29	4.727E-28	6.605E+01	0.350	1.083E+01	1.259E+01	1.463E+01	1.163E+00
0.009	3.903E-31	3.628E-28	1.335E-26	7.191E+01	0.400	2.594E+01	3.013E+01	3.503E+01	1.163E+00
0.010	6.738E-30	4.008E-27	2.140E-25	7.353E+01	0.450	5.084E+01	5.909E+01	6.866E+01	1.163E+00
0.011	9.139E-29	2.748E-26	2.148E-24	7.097E+01	0.500	8.690E+01	1.010E+02	1.174E+02	1.162E+00
0.012	9.515E-28	1.313E-25	1.476E-23	6.538E+01	0.600	1.960E+02	2.277E+02	2.643E+02	1.162E+00
0.013	7.884E-27	4.881E-25	7.645E-23	5.816E+01	0.700	3.602E+02	4.177E+02	4.843E+02	1.160E+00
0.014	5.360E-26	1.492E-24	3.108E-22	5.046E+01	0.800	5.888E+02	6.809E+02	7.878E+02	1.157E+00
0.015	3.068E-25	3.939E-24	1.051E-21	4.304E+01	0.900	8.923E+02	1.029E+03	1.186E+03	1.153E+00
0.016	1.514E-24	9.795E-24	3.017E-21	3.630E+01	1.000	1.279E+03	1.469E+03	1.686E+03	1.149E+00
0.018	2.579E-23	6.649E-23	1.758E-20	2.546E+01	1.250	2.611E+03	2.980E+03	3.399E+03	1.142E+00
0.020	2.984E-22	5.817E-22	6.965E-20	1.789E+01	1.500	4.387E+03	4.993E+03	5.680E+03	1.139E+00
0.025	4.198E-20	6.699E-20	8.585E-19	8.096E+00	1.750	6.440E+03	7.329E+03	8.342E+03	1.139E+00
0.030	5.856E-18	7.767E-18	1.382E-17	3.283E+00	2.000	8.614E+03	9.812E+03	1.119E+04	1.141E+00
0.040	2.797E-13	3.624E-13	4.719E-13	1.313E+00	2.500	1.291E+04	1.473E+04	1.685E+04	1.144E+00
0.050	2.346E-10	2.979E-10	3.790E-10	1.273E+00	3.000	1.680E+04	1.919E+04	2.201E+04	1.147E+00
0.060	1.991E-08	2.499E-08	3.136E-08	1.257E+00	3.500	2.012E+04	2.302E+04	2.646E+04	1.148E+00
0.070	4.583E-07	5.707E-07	7.112E-07	1.247E+00	4.000	2.291E+04	2.623E+04	3.017E+04	1.149E+00
0.080	4.686E-06	5.803E-06	7.199E-06	1.240E+00	5.000	2.709E+04	3.103E+04	3.572E+04	1.150E+00
0.090	2.797E-05	3.452E-05	4.268E-05	1.236E+00	6.000	2.988E+04	3.424E+04	3.941E+04	1.150E+00
0.100	1.149E-04	1.415E-04	1.743E-04	1.232E+00	7.000	3.173E+04	3.639E+04	4.191E+04	1.150E+00
0.110	3.601E-04	4.426E-04	5.443E-04	1.230E+00	8.000	3.295E+04	3.784E+04	4.363E+04	1.151E+00
0.120	9.242E-04	1.134E-03	1.392E-03	1.228E+00	9.000	(2.947E+04)	(3.701E+04)	(7.373E+04)	(1.624E+00)
0.130	2.042E-03	2.501E-03	3.064E-03	1.225E+00	10.000	(1.897E+03)	(1.897E+04)	(1.897E+05)	(1.000E+01)

Note. Observed resonances: P. M. Endt (1990), P. M. Endt (1998), and references therein. Normalization: J. Keinonen et al. (1977) and J. Görres et al. (1983). Unobserved resonances: P. Neogy et al. (1972). High-temperature rates (in parentheses): matching to statistical model rate above $T = 8.9$ GK. Previous rates: C. Iliadis et al. (2010c). Other: none.

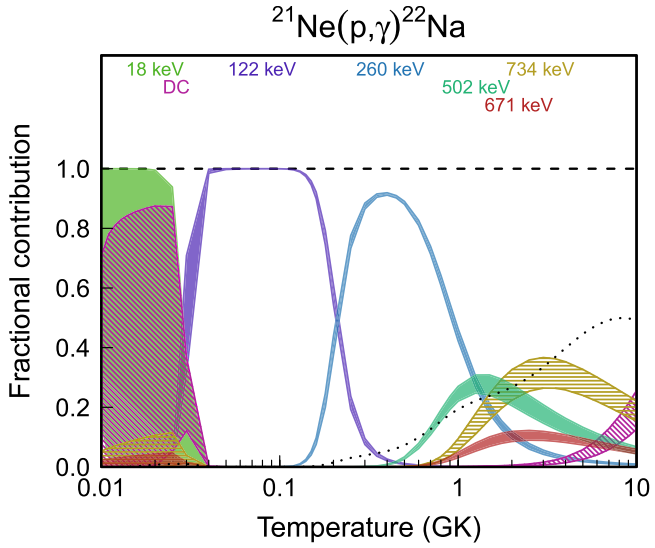

Figure 57. Fractional contributions to the total rate. "DC" refers to direct radiative capture. Resonance energies are given in the center-of-mass frame.

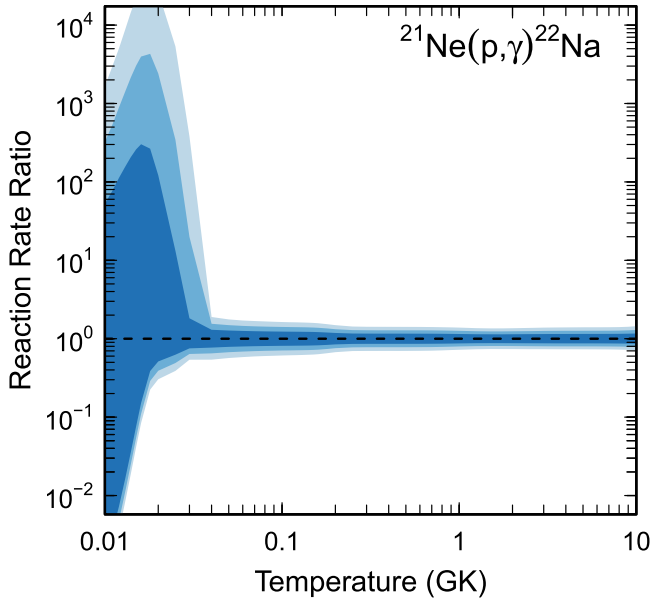

Figure 58. Reaction rate uncertainties versus temperature. The three different shades refer to coverage probabilities of 68%, 90%, and 98%.

Table 37
Total Laboratory Reaction Rates for ^{22}Ne(p,γ)^{23}Na

T (GK)	Low	Median	High	*f.u.*	T (GK)	Low	Median	High	*f.u.*
0.001	8.567E-72	1.599E-70	8.256E-70	9.990E+00	0.140	4.515E-06	4.887E-06	5.319E-06	1.086E+00
0.002	2.891E-56	5.337E-56	5.196E-55	5.117E+00	0.150	1.028E-05	1.110E-05	1.203E-05	1.082E+00
0.003	6.017E-48	8.946E-48	1.467E-47	1.629E+00	0.160	2.119E-05	2.282E-05	2.466E-05	1.079E+00
0.004	1.234E-42	1.883E-42	3.183E-42	1.632E+00	0.180	7.152E-05	7.668E-05	8.248E-05	1.074E+00
0.005	7.884E-39	1.255E-38	2.226E-38	1.702E+00	0.200	1.951E-04	2.082E-04	2.228E-04	1.069E+00
0.006	8.837E-36	1.743E-35	4.069E-35	2.193E+00	0.250	1.860E-03	1.959E-03	2.065E-03	1.054E+00
0.007	1.812E-32	5.844E-32	1.849E-31	3.182E+00	0.300	2.028E-02	2.168E-02	2.320E-02	1.070E+00
0.008	2.096E-29	6.001E-29	1.639E-28	2.815E+00	0.350	1.611E-01	1.735E-01	1.868E-01	1.077E+00
0.009	5.334E-27	1.339E-26	3.248E-26	2.493E+00	0.400	8.193E-01	8.830E-01	9.507E-01	1.078E+00
0.010	4.347E-25	9.960E-25	2.238E-24	2.290E+00	0.450	2.949E+00	3.174E+00	3.413E+00	1.076E+00
0.011	1.549E-23	3.351E-23	7.117E-23	2.162E+00	0.500	8.270E+00	8.883E+00	9.534E+00	1.074E+00
0.012	2.977E-22	6.182E-22	1.273E-21	2.084E+00	0.600	3.942E+01	4.215E+01	4.506E+01	1.069E+00
0.013	3.559E-21	7.236E-21	1.461E-20	2.038E+00	0.700	1.225E+02	1.305E+02	1.390E+02	1.065E+00
0.014	2.946E-20	5.903E-20	1.184E-19	2.013E+00	0.800	2.919E+02	3.101E+02	3.296E+02	1.063E+00
0.015	1.810E-19	3.625E-19	7.229E-19	2.004E+00	0.900	5.821E+02	6.181E+02	6.567E+02	1.063E+00
0.016	8.814E-19	1.765E-18	3.512E-18	2.004E+00	1.000	1.024E+03	1.088E+03	1.158E+03	1.064E+00
0.018	1.196E-17	2.423E-17	4.868E-17	2.023E+00	1.250	2.929E+03	3.131E+03	3.363E+03	1.073E+00
0.020	9.417E-17	1.939E-16	3.953E-16	2.054E+00	1.500	6.092E+03	6.559E+03	7.112E+03	1.082E+00
0.025	3.629E-15	7.801E-15	1.649E-14	2.146E+00	1.750	1.047E+04	1.133E+04	1.237E+04	1.089E+00
0.030	3.885E-14	8.724E-14	1.918E-13	2.232E+00	2.000	1.587E+04	1.721E+04	1.887E+04	1.093E+00
0.040	6.866E-13	1.633E-12	3.796E-12	2.358E+00	2.500	2.873E+04	3.121E+04	3.428E+04	1.095E+00
0.050	3.771E-12	9.016E-12	2.151E-11	2.387E+00	3.000	4.284E+04	4.645E+04	5.090E+04	1.092E+00
0.060	1.471E-11	3.093E-11	7.004E-11	2.164E+00	3.500	5.681E+04	6.139E+04	6.700E+04	1.088E+00
0.070	8.539E-11	1.255E-10	2.168E-10	1.628E+00	4.000	6.979E+04	7.517E+04	8.173E+04	1.084E+00
0.080	7.629E-10	9.030E-10	1.121E-09	1.242E+00	5.000	(7.808E+04)	(9.511E+04)	(2.146E+05)	(1.737E+00)
0.090	6.055E-09	6.832E-09	7.770E-09	1.137E+00	6.000	(7.368E+04)	(1.089E+05)	(4.143E+05)	(2.641E+00)
0.100	3.608E-08	4.010E-08	4.478E-08	1.115E+00	7.000	(6.295E+04)	(1.182E+05)	(6.328E+05)	(3.616E+00)
0.110	1.633E-07	1.797E-07	1.989E-07	1.105E+00	8.000	(4.809E+04)	(1.238E+05)	(8.548E+05)	(4.739E+00)
0.120	5.873E-07	6.419E-07	7.060E-07	1.097E+00	9.000	(3.091E+04)	(1.266E+05)	(1.070E+06)	(6.273E+00)
0.130	1.755E-06	1.907E-06	2.086E-06	1.091E+00	10.000	(1.271E+04)	(1.271E+05)	(1.271E+06)	(1.000E+01)

Note. Observed resonances: P. M. Endt (1990), K. J. Kelly et al. (2017), F. Ferraro et al. (2018), and M. Williams et al. (2020). Normalization: see Table 2. Unobserved resonances: S. E. Hale et al. (2001). High-temperature rates (in parentheses): matching to statistical model rate above $T = 4.2$ GK. Previous rates: M. Williams et al. (2020). Other: the levels at $E_x = 8862$, 8894, and 9000 keV, tentatively assigned by J. R. Powers et al. (1971), have been disregarded since no evidence for their existence has been observed in the dedicated study of S. E. Hale et al. (2001).

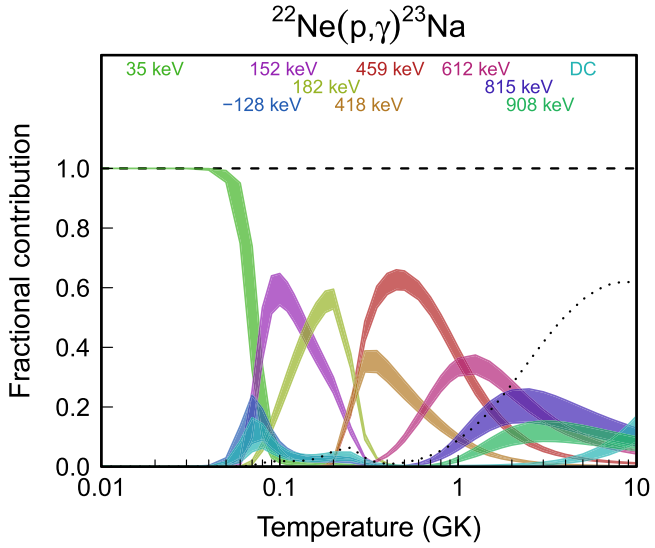

Figure 59. Fractional contributions to the total rate. "DC" refers to direct radiative capture. Resonance energies are given in the center-of-mass frame.

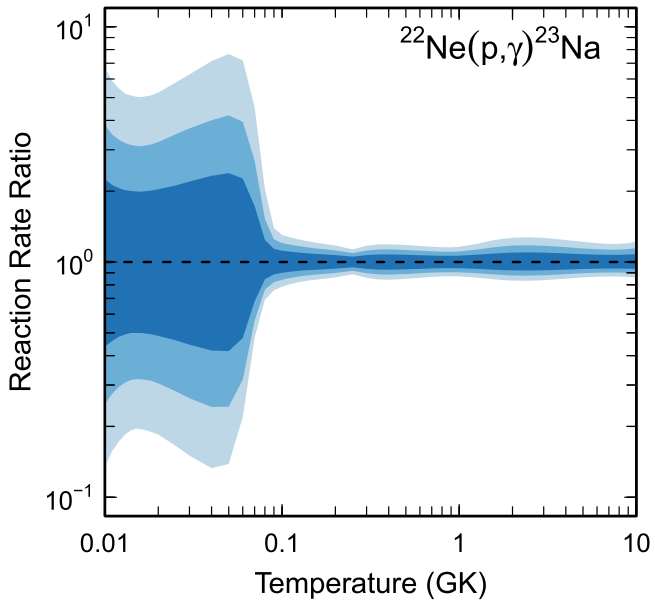

Figure 60. Reaction rate uncertainties versus temperature. The three different shades refer to coverage probabilities of 68%, 90%, and 98%.

Table 38
Total Laboratory Reaction Rates for $^{22}Ne(\alpha,\gamma)^{26}Mg$

T (GK)	Low	Median	High	*f.u.*	T (GK)	Low	Median	High	*f.u.*
0.001	0.000E+00	0.000E+00	0.000E+00	1.000E+00	0.140	4.364E-20	1.569E-19	6.632E-19	3.920E+00
0.002	0.000E+00	0.000E+00	0.000E+00	1.000E+00	0.150	3.034E-19	1.031E-18	4.054E-18	3.710E+00
0.003	0.000E+00	0.000E+00	0.000E+00	1.000E+00	0.160	1.726E-18	5.644E-18	2.071E-17	3.528E+00
0.004	0.000E+00	0.000E+00	0.000E+00	1.000E+00	0.180	3.514E-17	1.082E-16	3.672E-16	3.278E+00
0.005	0.000E+00	0.000E+00	0.000E+00	1.000E+00	0.200	4.609E-16	1.326E-15	4.289E-15	3.099E+00
0.006	0.000E+00	0.000E+00	0.000E+00	1.000E+00	0.250	1.149E-13	2.198E-13	5.674E-13	2.343E+00
0.007	1.644E-99	4.197E-98	6.766E-97	2.349E+01	0.300	1.144E-11	1.555E-11	2.609E-11	1.662E+00
0.008	4.063E-87	1.114E-86	3.390E-86	2.960E+00	0.350	3.777E-10	4.613E-10	6.271E-10	1.367E+00
0.009	2.418E-82	9.182E-82	4.263E-81	4.219E+00	0.400	5.337E-09	6.305E-09	7.942E-09	1.257E+00
0.010	7.919E-78	3.279E-77	1.465E-76	4.388E+00	0.450	4.177E-08	4.865E-08	5.945E-08	1.219E+00
0.011	5.237E-74	2.028E-73	8.146E-73	4.077E+00	0.500	2.148E-07	2.483E-07	2.995E-07	1.204E+00
0.012	8.305E-71	3.090E-70	1.129E-69	3.822E+00	0.600	2.449E-06	2.808E-06	3.355E-06	1.194E+00
0.013	4.341E-68	1.580E-67	5.448E-67	3.667E+00	0.700	1.373E-05	1.565E-05	1.858E-05	1.187E+00
0.014	9.341E-66	3.417E-65	1.131E-64	3.599E+00	0.800	5.079E-05	5.745E-05	6.753E-05	1.176E+00
0.015	9.833E-64	3.697E-63	1.221E-62	3.600E+00	0.900	1.476E-04	1.649E-04	1.908E-04	1.159E+00
0.016	5.781E-62	2.263E-61	7.493E-61	3.654E+00	1.000	3.733E-04	4.103E-04	4.647E-04	1.135E+00
0.018	5.219E-59	2.222E-58	7.612E-58	3.864E+00	1.250	(2.943E-03)	(3.223E-03)	(4.002E-03)	(1.168E+00)
0.020	1.195E-56	5.555E-56	2.037E-55	4.143E+00	1.500	(2.591E-02)	(2.911E-02)	(4.344E-02)	(1.308E+00)
0.025	2.321E-52	1.199E-51	5.056E-51	4.559E+00	1.750	(1.165E-01)	(1.344E-01)	(2.342E-01)	(1.448E+00)
0.030	4.455E-48	1.687E-47	7.062E-47	4.060E+00	2.000	(5.230E-01)	(6.200E-01)	(1.235E+00)	(1.589E+00)
0.040	2.351E-40	1.152E-39	5.601E-39	4.856E+00	2.500	(4.517E+00)	(5.667E+00)	(1.413E+01)	(1.874E+00)
0.050	1.344E-35	6.139E-35	2.942E-34	4.655E+00	3.000	(2.172E+01)	(2.893E+01)	(8.661E+01)	(2.163E+00)
0.060	2.027E-32	8.466E-32	3.940E-31	4.422E+00	3.500	(6.980E+01)	(9.914E+01)	(3.464E+02)	(2.457E+00)
0.070	4.661E-30	1.613E-29	6.713E-29	3.848E+00	4.000	(1.691E+02)	(2.571E+02)	(1.027E+03)	(2.758E+00)
0.080	4.927E-28	1.450E-27	4.806E-27	3.178E+00	5.000	(5.633E+02)	(9.976E+02)	(4.983E+03)	(3.383E+00)
0.090	3.037E-26	9.272E-26	3.333E-25	3.386E+00	6.000	(1.138E+03)	(2.412E+03)	(1.446E+04)	(4.058E+00)
0.100	1.128E-24	3.988E-24	1.713E-23	3.915E+00	7.000	(1.616E+03)	(4.265E+03)	(2.984E+04)	(4.818E+00)
0.110	2.689E-23	1.050E-22	4.838E-22	4.217E+00	8.000	(1.683E+03)	(5.886E+03)	(4.708E+04)	(5.748E+00)
0.120	4.338E-22	1.714E-21	7.939E-21	4.252E+00	9.000	(1.206E+03)	(6.250E+03)	(5.625E+04)	(7.091E+00)
0.130	5.024E-21	1.895E-20	8.505E-20	4.122E+00	10.000	(4.198E+02)	(4.198E+03)	(4.198E+04)	(1.000E+01)

Note. Observed resonances: K. Wolke et al. (1989), S. Hunt et al. (2019), and G. J. Shahina et al. (2022). Normalization: none. Unobserved resonances: U. Giesen et al. (1993), C. Ugalde et al. (2007), R. Talwar et al. (2016), and H. Jayatissa et al. (2020). Relative spectroscopic factors were normalized to the 703 keV resonance. High-temperature rates (in parentheses): matching to statistical model rate above $T = 1.1$ GK. Previous rates: R. Longland et al. (2012), P. Adsley et al. (2021a), and M. Wiescher et al. (2023). Other: energies, J^{π} values, neutron, and γ-ray partial widths were adopted from E. W. Lees et al. (1974), C. E. Moss (1976), H. Weigmann et al. (1976), U. E. P. Berg et al. (1984), J. J. Kraushaar et al. (1986), F. Glatz et al. (1986), G. M. Crawley et al. (1989), M. Yasue et al. (1990), T. A. Walkiewicz et al. (1992), P. E. Koehler (2002), R. Longland et al. (2009), R. J. deBoer et al. (2010), C. Massimi et al. (2012), P. Adsley et al. (2018), G. Lotay et al. (2019), P. Adsley et al. (2021b), and Y. Chen et al. (2021).

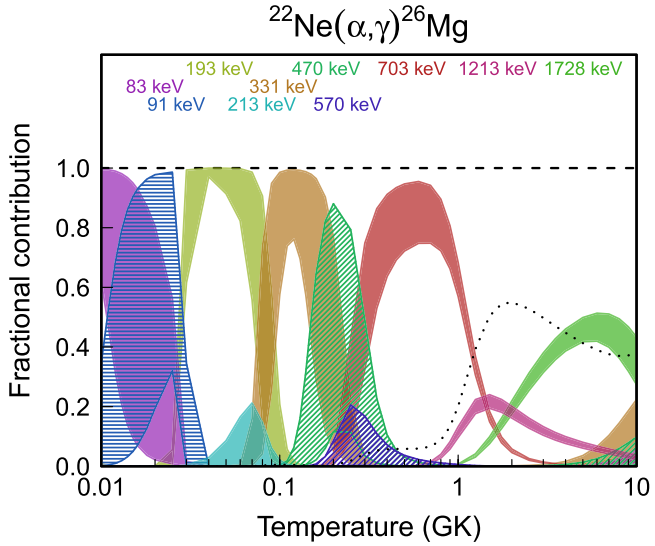

Figure 61. Fractional contributions to the total rate. Resonance energies are given in the center-of-mass frame.

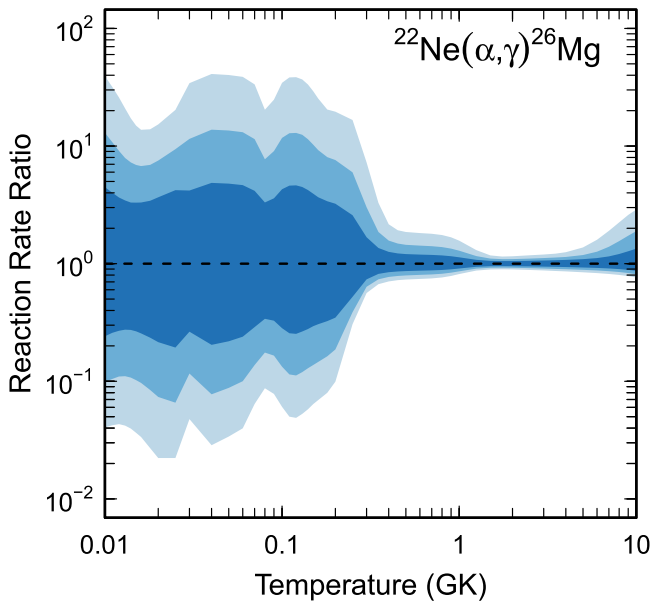

Figure 62. Reaction rate uncertainties versus temperature. The three different shades refer to coverage probabilities of 68%, 90%, and 98%.

Table 39
Total Laboratory Reaction Rates for ^{22}Ne(α,n)^{25}Mg

T (GK)	Low	Median	High	*f.u.*	T (GK)	Low	Median	High	*f.u.*
0.001	0.000E+00	0.000E+00	0.000E+00	1.000E+00	0.140	6.414E-23	2.422E-22	8.312E-22	3.501E+00
0.002	0.000E+00	0.000E+00	0.000E+00	1.000E+00	0.150	1.226E-21	4.092E-21	1.269E-20	3.124E+00
0.003	0.000E+00	0.000E+00	0.000E+00	1.000E+00	0.160	1.739E-20	5.031E-20	1.427E-19	2.764E+00
0.004	0.000E+00	0.000E+00	0.000E+00	1.000E+00	0.180	1.821E-18	3.824E-18	8.822E-18	2.142E+00
0.005	0.000E+00	0.000E+00	0.000E+00	1.000E+00	0.200	9.672E-17	1.533E-16	2.837E-16	1.709E+00
0.006	0.000E+00	0.000E+00	0.000E+00	1.000E+00	0.250	1.761E-13	2.106E-13	2.709E-13	1.265E+00
0.007	0.000E+00	0.000E+00	0.000E+00	1.000E+00	0.300	2.879E-11	3.279E-11	3.825E-11	1.165E+00
0.008	0.000E+00	0.000E+00	0.000E+00	1.000E+00	0.350	1.115E-09	1.251E-09	1.418E-09	1.135E+00
0.009	0.000E+00	0.000E+00	0.000E+00	1.000E+00	0.400	1.754E-08	1.947E-08	2.177E-08	1.120E+00
0.010	0.000E+00	0.000E+00	0.000E+00	1.000E+00	0.450	1.533E-07	1.685E-07	1.865E-07	1.108E+00
0.011	0.000E+00	0.000E+00	0.000E+00	1.000E+00	0.500	9.106E-07	9.898E-07	1.083E-06	1.095E+00
0.012	0.000E+00	0.000E+00	0.000E+00	1.000E+00	0.600	1.699E-05	1.800E-05	1.918E-05	1.065E+00
0.013	0.000E+00	0.000E+00	0.000E+00	1.000E+00	0.700	2.077E-04	2.184E-04	2.305E-04	1.054E+00
0.014	0.000E+00	0.000E+00	0.000E+00	1.000E+00	0.800	1.835E-03	1.933E-03	2.044E-03	1.056E+00
0.015	0.000E+00	0.000E+00	0.000E+00	1.000E+00	0.900	1.170E-02	1.231E-02	1.299E-02	1.054E+00
0.016	0.000E+00	0.000E+00	0.000E+00	1.000E+00	1.000	5.585E-02	5.855E-02	6.152E-02	1.050E+00
0.018	0.000E+00	0.000E+00	0.000E+00	1.000E+00	1.250	1.090E+00	1.136E+00	1.185E+00	1.043E+00
0.020	0.000E+00	0.000E+00	0.000E+00	1.000E+00	1.500	(1.038E+01)	(1.106E+01)	(1.402E+01)	(1.167E+00)
0.025	0.000E+00	0.000E+00	0.000E+00	1.000E+00	1.750	(5.324E+01)	(5.827E+01)	(8.884E+01)	(1.310E+00)
0.030	5.310E-88	5.484E-87	2.614E-86	7.045E+00	2.000	(2.729E+02)	(3.069E+02)	(5.468E+02)	(1.453E+00)
0.040	1.627E-67	1.720E-66	8.238E-66	7.433E+00	2.500	(2.532E+03)	(3.016E+03)	(6.921E+03)	(1.743E+00)
0.050	3.578E-55	3.823E-54	1.835E-53	7.623E+00	3.000	(1.278E+04)	(1.616E+04)	(4.540E+04)	(2.037E+00)
0.060	6.157E-47	6.524E-46	3.136E-45	7.620E+00	3.500	(4.342E+04)	(5.859E+04)	(1.947E+05)	(2.336E+00)
0.070	4.674E-41	4.879E-40	2.342E-39	7.330E+00	4.000	(1.124E+05)	(1.624E+05)	(6.230E+05)	(2.641E+00)
0.080	1.230E-36	1.223E-35	5.846E-35	6.771E+00	5.000	(4.355E+05)	(7.342E+05)	(3.571E+06)	(3.275E+00)
0.090	3.661E-33	3.213E-32	1.515E-31	6.096E+00	6.000	(1.044E+06)	(2.111E+06)	(1.244E+07)	(3.956E+00)
0.100	2.414E-30	1.750E-29	8.071E-29	5.433E+00	7.000	(1.804E+06)	(4.555E+06)	(3.152E+07)	(4.722E+00)
0.110	5.207E-28	3.086E-27	1.366E-26	4.843E+00	8.000	(2.391E+06)	(8.044E+06)	(6.391E+07)	(5.655E+00)
0.120	4.805E-26	2.380E-25	9.822E-25	4.338E+00	9.000	(2.418E+06)	(1.218E+07)	(1.092E+08)	(7.003E+00)
0.130	2.270E-24	9.776E-24	3.670E-23	3.899E+00	10.000	(1.623E+06)	(1.623E+07)	(1.623E+08)	(1.000E+01)

Note. Observed resonances: K. Wolke et al. (1989), V. Harms et al. (1991), H. W. Drotleff et al. (1993), and M. Jaeger et al. (2001). Unobserved resonances: U. Giesen et al. (1993), C. Ugalde et al. (2007), R. Talwar et al. (2016), and H. Jayatissa et al. (2020). Relative spectroscopic factors have been normalized to the 703 keV resonance. High-temperature rates (in parentheses): matching to statistical model rate above $T = 1.28$ GK. Previous rates: R. Longland et al. (2012), P. Adsley et al. (2021a), and M. Wiescher et al. (2023). Other: energies, J^{π} values, neutron, and γ-ray partial widths were adopted from E. W. Lees et al. (1974), C. E. Moss (1976), H. Weigmann et al. (1976), U. E. P. Berg et al. (1984), J. J. Kraushaar et al. (1986), F. Glatz et al. (1986), G. M. Crawley et al. (1989), M. Yasue et al. (1990), T. A. Walkiewicz et al. (1992), P. E. Koehler (2002), R. Longland et al. (2009), R. J. deBoer et al. (2010), C. Massimi et al. (2012), P. Adsley et al. (2018), G. Lotay et al. (2019), P. Adsley et al. (2021b), and Y. Chen et al. (2021).

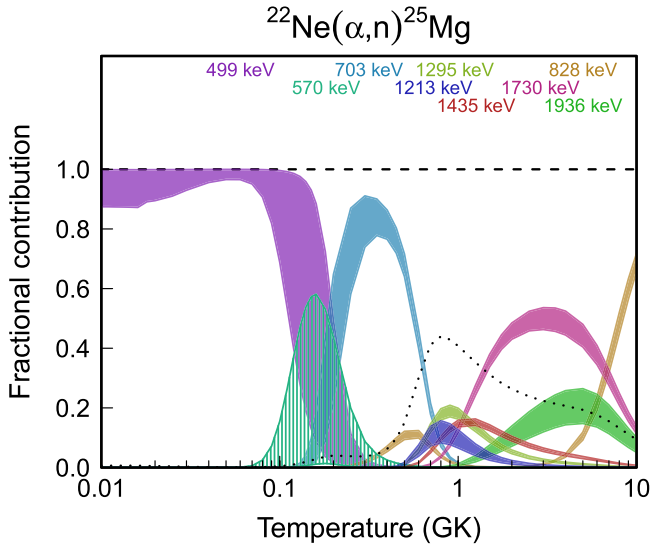

Figure 63. Fractional contributions to the total rate. Resonance energies are given in the center-of-mass frame.

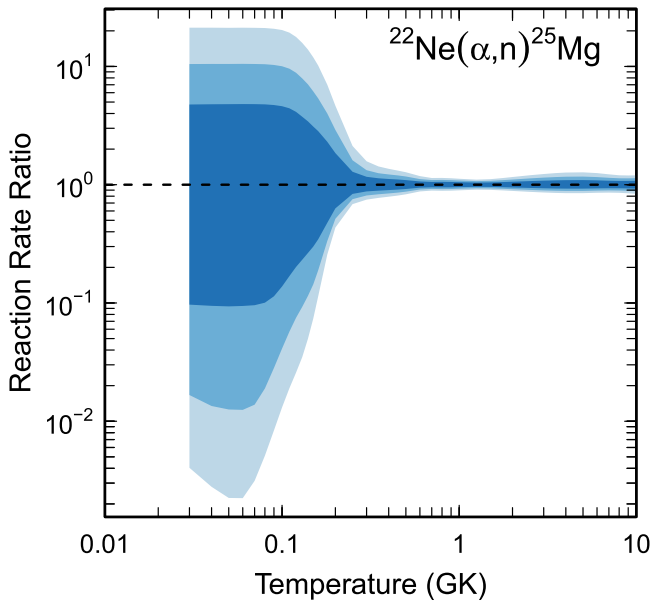

Figure 64. Reaction rate uncertainties versus temperature. The three different shades refer to coverage probabilities of 68%, 90%, and 98%.

Table 40
Total Laboratory Reaction Rates for ^{21}Na(p,γ)^{22}Mg

T (GK)	Low	Median	High	*f.u.*	T (GK)	Low	Median	High	*f.u.*
0.001	8.471E-81	1.845E-80	4.332E-80	2.245E+00	0.140	7.673E-05	9.952E-05	1.293E-04	1.300E+00
0.002	2.035E-62	4.427E-62	1.038E-61	2.243E+00	0.150	2.202E-04	2.838E-04	3.666E-04	1.291E+00
0.003	1.693E-53	3.679E-53	8.626E-53	2.241E+00	0.160	5.501E-04	7.055E-04	9.056E-04	1.283E+00
0.004	7.177E-48	1.558E-47	3.651E-47	2.239E+00	0.180	2.493E-03	3.168E-03	4.031E-03	1.272E+00
0.005	7.220E-44	1.566E-43	3.668E-43	2.238E+00	0.200	8.204E-03	1.036E-02	1.309E-02	1.263E+00
0.006	8.157E-41	1.768E-40	4.140E-40	2.236E+00	0.250	6.661E-02	8.316E-02	1.040E-01	1.249E+00
0.007	2.236E-38	4.843E-38	1.133E-37	2.235E+00	0.300	2.555E-01	3.173E-01	3.940E-01	1.242E+00
0.008	2.295E-36	4.965E-36	1.162E-35	2.233E+00	0.350	6.439E-01	7.966E-01	9.852E-01	1.237E+00
0.009	1.150E-34	2.485E-34	5.812E-34	2.232E+00	0.400	1.255E+00	1.548E+00	1.910E+00	1.234E+00
0.010	3.345E-33	7.226E-33	1.689E-32	2.231E+00	0.450	2.068E+00	2.546E+00	3.133E+00	1.231E+00
0.011	6.371E-32	1.375E-31	3.213E-31	2.230E+00	0.500	3.046E+00	3.741E+00	4.591E+00	1.228E+00
0.012	8.646E-31	1.865E-30	4.356E-30	2.228E+00	0.600	5.380E+00	6.554E+00	7.991E+00	1.219E+00
0.013	8.902E-30	1.919E-29	4.480E-29	2.227E+00	0.700	8.302E+00	9.960E+00	1.198E+01	1.201E+00
0.014	7.290E-29	1.570E-28	3.665E-28	2.226E+00	0.800	1.246E+01	1.456E+01	1.710E+01	1.171E+00
0.015	4.925E-28	1.060E-27	2.474E-27	2.225E+00	0.900	1.906E+01	2.158E+01	2.460E+01	1.137E+00
0.016	2.825E-27	6.077E-27	1.418E-26	2.224E+00	1.000	2.955E+01	3.260E+01	3.620E+01	1.107E+00
0.018	6.212E-26	1.334E-25	3.111E-25	2.222E+00	1.250	8.109E+01	8.746E+01	9.448E+01	1.080E+00
0.020	8.892E-25	1.907E-24	4.443E-24	2.219E+00	1.500	1.773E+02	1.914E+02	2.069E+02	1.081E+00
0.025	1.833E-22	3.919E-22	9.117E-22	2.214E+00	1.750	3.174E+02	3.435E+02	3.723E+02	1.084E+00
0.030	1.064E-20	2.268E-20	5.269E-20	2.209E+00	2.000	4.905E+02	5.317E+02	5.774E+02	1.086E+00
0.040	3.934E-18	8.339E-18	1.931E-17	2.200E+00	2.500	(8.443E+02)	(9.253E+02)	(1.087E+03)	(1.135E+00)
0.050	2.791E-16	5.704E-16	1.294E-15	2.139E+00	3.000	(9.630E+02)	(1.122E+03)	(1.978E+03)	(1.464E+00)
0.060	3.598E-14	5.319E-14	8.068E-14	1.514E+00	3.500	(1.039E+03)	(1.291E+03)	(3.036E+03)	(1.797E+00)
0.070	6.303E-12	9.168E-12	1.339E-11	1.462E+00	4.000	(1.082E+03)	(1.443E+03)	(4.243E+03)	(2.136E+00)
0.080	3.865E-10	5.491E-10	7.801E-10	1.424E+00	5.000	(1.098E+03)	(1.711E+03)	(7.045E+03)	(2.837E+00)
0.090	9.505E-09	1.319E-08	1.828E-08	1.389E+00	6.000	(1.049E+03)	(1.966E+03)	(1.041E+04)	(3.584E+00)
0.100	1.214E-07	1.650E-07	2.244E-07	1.362E+00	7.000	(9.519E+02)	(2.240E+03)	(1.449E+04)	(4.411E+00)
0.110	9.620E-07	1.287E-06	1.726E-06	1.340E+00	8.000	(8.134E+02)	(2.569E+03)	(1.964E+04)	(5.402E+00)
0.120	5.335E-06	7.053E-06	9.335E-06	1.324E+00	9.000	(6.257E+02)	(3.004E+03)	(2.650E+04)	(6.812E+00)
0.130	2.251E-05	2.947E-05	3.863E-05	1.310E+00	10.000	(3.599E+02)	(3.599E+03)	(3.599E+04)	(1.000E+01)

Note. Observed resonances: J. M. D'Auria et al. (2004). Normalization: none. Unobserved resonances: none. High-temperature rates (in parentheses): matching to statistical model rate above $T = 2.4$ GK. Previous rates: C. Iliadis et al. (2010c). Other: the resonance energies were derived from the excitation energies listed in ENSDF 2015, assuming inflated uncertainties based on the scatter of the values reported in the original literature.

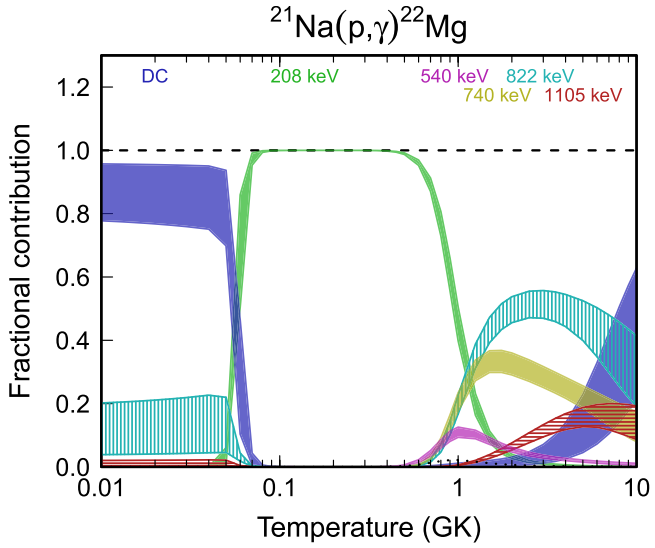

Figure 65. Fractional contributions to the total rate. "DC" refers to direct radiative capture. Resonance energies are given in the center-of-mass frame.

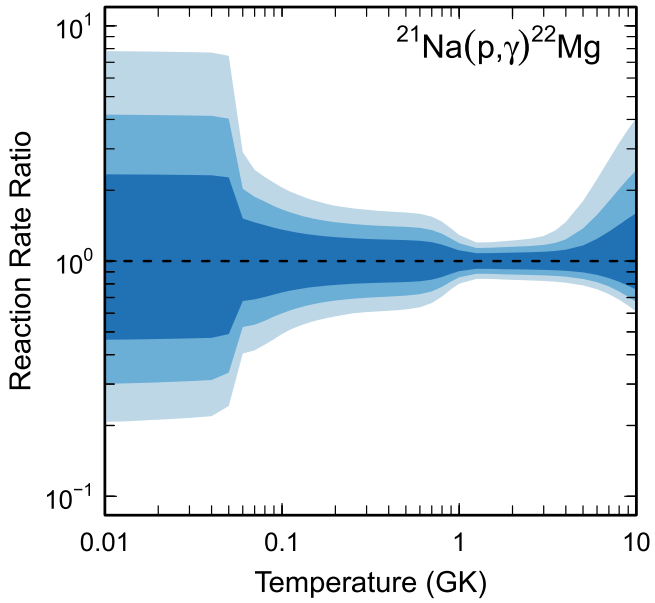

Figure 66. Reaction rate uncertainties versus temperature. The three different shades refer to coverage probabilities of 68%, 90%, and 98%.

Table 41
Total Laboratory Reaction Rates for ^{22}Na(p,γ)^{23}Mg

T (GK)	Low	Median	High	*f.u.*	T (GK)	Low	Median	High	*f.u.*
0.001	1.910E-80	1.153E-79	1.552E-76	8.091E+01	0.140	6.558E-05	2.194E-04	9.462E-04	3.793E+00
0.002	4.503E-62	2.405E-61	3.345E-58	7.470E+01	0.150	1.964E-04	6.240E-04	2.653E-03	3.680E+00
0.003	3.285E-53	1.394E-52	2.429E-50	4.602E+01	0.160	5.196E-04	1.562E-03	6.511E-03	3.563E+00
0.004	1.268E-47	4.767E-47	6.747E-46	2.527E+01	0.180	2.716E-03	7.297E-03	2.886E-02	3.334E+00
0.005	1.200E-43	4.170E-43	2.566E-42	1.467E+01	0.200	1.036E-02	2.565E-02	9.428E-02	3.129E+00
0.006	1.314E-40	4.322E-40	1.948E-39	9.434E+00	0.250	1.188E-01	2.593E-01	7.887E-01	2.743E+00
0.007	3.660E-38	1.125E-37	4.328E-37	6.630E+00	0.300	6.093E-01	1.261E+00	3.268E+00	2.497E+00
0.008	8.344E-36	1.944E-35	5.182E-35	4.153E+00	0.350	1.949E+00	3.900E+00	9.156E+00	2.331E+00
0.009	2.725E-33	6.315E-33	1.534E-32	2.876E+00	0.400	4.697E+00	9.097E+00	1.993E+01	2.206E+00
0.010	5.731E-31	1.346E-30	3.196E-30	2.477E+00	0.450	9.388E+00	1.757E+01	3.676E+01	2.102E+00
0.011	5.293E-29	1.202E-28	2.714E-28	2.289E+00	0.500	1.660E+01	2.990E+01	6.010E+01	2.010E+00
0.012	2.328E-27	5.090E-27	1.108E-26	2.187E+00	0.600	4.074E+01	6.801E+01	1.264E+02	1.850E+00
0.013	5.689E-26	1.207E-25	2.550E-25	2.122E+00	0.700	8.104E+01	1.263E+02	2.182E+02	1.716E+00
0.014	8.691E-25	1.805E-24	3.750E-24	2.079E+00	0.800	1.408E+02	2.072E+02	3.349E+02	1.610E+00
0.015	9.148E-24	1.874E-23	3.834E-23	2.050E+00	0.900	2.211E+02	3.124E+02	4.756E+02	1.527E+00
0.016	7.114E-23	1.443E-22	2.925E-22	2.029E+00	1.000	3.214E+02	4.403E+02	6.405E+02	1.464E+00
0.018	2.143E-21	4.298E-21	8.553E-21	2.001E+00	1.250	(6.346E+02)	(8.476E+02)	(1.230E+03)	(1.393E+00)
0.020	3.269E-20	6.478E-20	1.282E-19	1.982E+00	1.500	(1.102E+03)	(1.509E+03)	(2.558E+03)	(1.533E+00)
0.025	4.900E-18	9.526E-18	1.874E-17	1.978E+00	1.750	(1.464E+03)	(2.058E+03)	(3.992E+03)	(1.672E+00)
0.030	1.737E-16	3.474E-16	7.415E-16	2.138E+00	2.000	(1.945E+03)	(2.806E+03)	(6.129E+03)	(1.813E+00)
0.040	2.663E-14	6.224E-14	1.643E-13	2.502E+00	2.500	(2.731E+03)	(4.164E+03)	(1.113E+04)	(2.098E+00)
0.050	7.966E-13	1.950E-12	4.983E-12	2.502E+00	3.000	(3.400E+03)	(5.493E+03)	(1.736E+04)	(2.388E+00)
0.060	8.682E-12	2.022E-11	4.817E-11	2.359E+00	3.500	(3.936E+03)	(6.765E+03)	(2.469E+04)	(2.684E+00)
0.070	7.591E-11	1.607E-10	3.563E-10	2.219E+00	4.000	(4.345E+03)	(7.975E+03)	(3.300E+04)	(2.987E+00)
0.080	8.121E-10	2.129E-09	7.230E-09	3.108E+00	5.000	(4.826E+03)	(1.025E+04)	(5.245E+04)	(3.620E+00)
0.090	1.019E-08	3.647E-08	1.514E-07	3.857E+00	6.000	(4.918E+03)	(1.240E+04)	(7.555E+04)	(4.307E+00)
0.100	1.097E-07	4.146E-07	1.780E-06	4.048E+00	7.000	(4.681E+03)	(1.452E+04)	(1.026E+05)	(5.085E+00)
0.110	8.143E-07	3.056E-06	1.330E-05	4.046E+00	8.000	(4.149E+03)	(1.671E+04)	(1.345E+05)	(6.037E+00)
0.120	4.432E-06	1.614E-05	7.045E-05	3.986E+00	9.000	(3.318E+03)	(1.905E+04)	(1.719E+05)	(7.383E+00)
0.130	1.877E-05	6.586E-05	2.865E-04	3.898E+00	10.000	(2.165E+03)	(2.165E+04)	(2.165E+05)	(1.000E+01)

Note. Observed resonances: S. Seuthe et al. (1990), F. Stegmüller et al. (1996), A. L. Sallaska et al. (2011), and C. Fougères et al. (2023). Normalization: the resonance strength values in the above references disagree. We increased the uncertainties to encompass all strength values. Unobserved resonances: S. Schmidt et al. (1995). High-temperature rates (in parentheses): matching to statistical model rate above $T = 1.2$ GK. Previous rates: A. L. Sallaska et al. (2013). Other: insufficient information on C^2S values for bound levels in ^{23}Mg is available to calculate the direct-capture S factor according to the formalism discussed in Section 9. Therefore, we assumed a constant value of 20 keVb, with an uncertainty of a factor of 3. This choice encompasses the S factors in this target mass range.

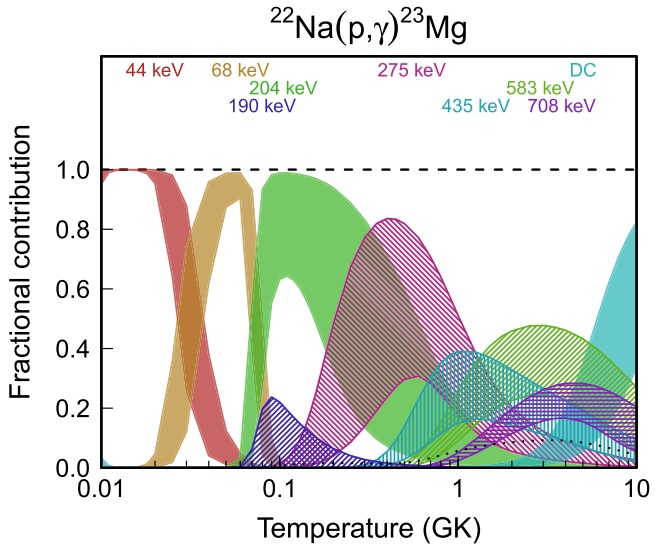

Figure 67. Fractional contributions to the total rate. "DC" refers to direct radiative capture. Resonance energies are given in the center-of-mass frame.

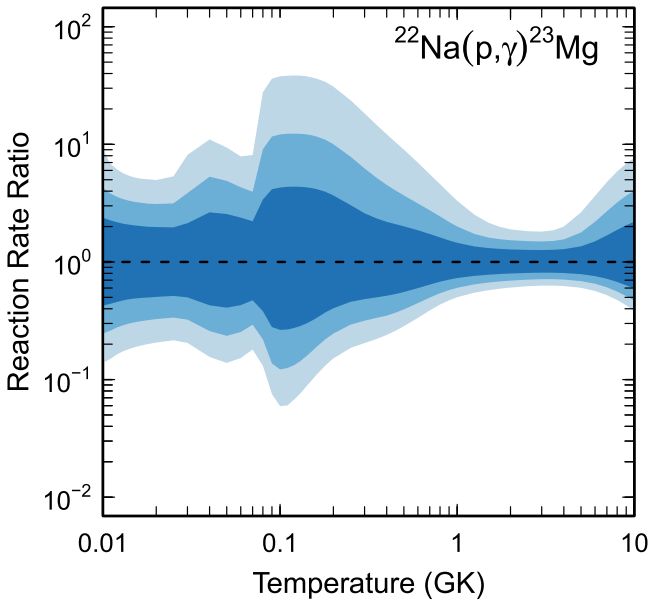

Figure 68. Reaction rate uncertainties versus temperature. The three different shades refer to coverage probabilities of 68%, 90%, and 98%.

Table 42
Total Laboratory Reaction Rates for ^{23}Na(p,γ)^{24}Mg

T (GK)	Low	Median	High	*f.u.*	T (GK)	Low	Median	High	*f.u.*
0.001	2.406E-80	3.862E-80	2.760E-78	1.146E+01	0.140	9.123E-06	9.970E-06	1.090E-05	1.094E+00
0.002	5.741E-62	9.010E-62	7.483E-61	7.728E+00	0.150	3.852E-05	4.219E-05	4.628E-05	1.096E+00
0.003	4.716E-53	7.199E-53	1.288E-52	4.549E+00	0.160	1.373E-04	1.507E-04	1.658E-04	1.100E+00
0.004	1.989E-47	2.987E-47	4.786E-47	2.897E+00	0.180	1.154E-03	1.274E-03	1.407E-03	1.105E+00
0.005	1.996E-43	2.977E-43	4.585E-43	2.125E+00	0.200	6.359E-03	7.042E-03	7.808E-03	1.109E+00
0.006	2.256E-40	3.351E-40	5.074E-40	1.762E+00	0.250	1.347E-01	1.498E-01	1.668E-01	1.114E+00
0.007	6.197E-38	9.177E-38	1.379E-37	1.597E+00	0.300	9.956E-01	1.110E+00	1.238E+00	1.116E+00
0.008	6.376E-36	9.423E-36	1.407E-35	1.529E+00	0.350	4.031E+00	4.497E+00	5.022E+00	1.117E+00
0.009	3.202E-34	4.730E-34	7.047E-34	1.502E+00	0.400	1.123E+01	1.253E+01	1.401E+01	1.117E+00
0.010	9.343E-33	1.380E-32	2.054E-32	1.492E+00	0.450	2.446E+01	2.730E+01	3.052E+01	1.118E+00
0.011	1.783E-31	2.635E-31	3.921E-31	1.489E+00	0.500	4.496E+01	5.018E+01	5.609E+01	1.117E+00
0.012	2.426E-30	3.585E-30	5.333E-30	1.487E+00	0.600	1.092E+02	1.217E+02	1.359E+02	1.116E+00
0.013	2.504E-29	3.700E-29	5.504E-29	1.487E+00	0.700	2.022E+02	2.249E+02	2.504E+02	1.113E+00
0.014	2.055E-28	3.037E-28	4.518E-28	1.487E+00	0.800	3.200E+02	3.547E+02	3.935E+02	1.109E+00
0.015	1.391E-27	2.057E-27	3.059E-27	1.487E+00	0.900	4.600E+02	5.077E+02	5.608E+02	1.105E+00
0.016	7.992E-27	1.182E-26	1.758E-26	1.487E+00	1.000	6.206E+02	6.830E+02	7.514E+02	1.101E+00
0.018	1.763E-25	2.606E-25	3.879E-25	1.487E+00	1.250	1.116E+03	1.224E+03	1.342E+03	1.097E+00
0.020	2.529E-24	3.740E-24	5.568E-24	1.487E+00	1.500	1.753E+03	1.930E+03	2.127E+03	1.102E+00
0.025	5.243E-22	7.754E-22	1.154E-21	1.487E+00	1.750	2.539E+03	2.818E+03	3.133E+03	1.111E+00
0.030	3.056E-20	4.520E-20	6.725E-20	1.487E+00	2.000	3.473E+03	3.882E+03	4.353E+03	1.120E+00
0.040	1.176E-17	1.725E-17	2.550E-17	1.475E+00	2.500	5.710E+03	6.454E+03	7.314E+03	1.132E+00
0.050	1.175E-15	1.715E-15	2.563E-15	1.493E+00	3.000	8.248E+03	9.382E+03	1.070E+04	1.139E+00
0.060	6.115E-14	9.840E-14	1.699E-13	1.682E+00	3.500	1.084E+04	1.238E+04	1.416E+04	1.143E+00
0.070	1.597E-12	2.682E-12	4.705E-12	1.718E+00	4.000	1.334E+04	1.526E+04	1.748E+04	1.145E+00
0.080	2.298E-11	3.669E-11	6.082E-11	1.625E+00	5.000	1.769E+04	2.027E+04	2.324E+04	1.146E+00
0.090	2.633E-10	3.605E-10	5.229E-10	1.412E+00	6.000	2.110E+04	2.416E+04	2.771E+04	1.146E+00
0.100	3.108E-09	3.639E-09	4.398E-09	1.199E+00	7.000	2.367E+04	2.712E+04	3.109E+04	1.146E+00
0.110	3.272E-08	3.622E-08	4.024E-08	1.110E+00	8.000	2.558E+04	2.934E+04	3.363E+04	1.147E+00
0.120	2.729E-07	2.979E-07	3.256E-07	1.094E+00	9.000	(2.161E+04)	(3.192E+04)	(1.078E+05)	(2.427E+00)
0.130	1.770E-06	1.931E-06	2.108E-06	1.092E+00	10.000	(3.662E+03)	(3.662E+04)	(3.662E+05)	(1.000E+01)

Note. Observed resonances: Z. E. Switkowski et al. (1975), J. Görres et al. (1989), J. M. Cesaratto et al. (2013), and A. Boeltzig et al. (2019). Normalization: the resonance strengths reported in Z. E. Switkowski et al. (1975) have been normalized to B. Paine & D. Sargood (1979; see Table 2). Unobserved resonances: C. Marshall et al. (2023). High-temperature rates (in parentheses): matching to statistical model rate above $T = 8.7$ GK. Previous rates: A. Boeltzig et al. (2019). Other: the C^2S values for direct capture were taken from J. D. Garrett et al. (1978), S. E. Hale et al. (2004), and C. Marshall et al. (2023). All of these values were assumed to have a 50% uncertainty based on the findings of A. Boeltzig et al. (2022). The adopted resonance energies are weighted averages of M. S. Basunia & A. Chakraborty (2022) and C. Marshall et al. (2023), with uncertainties adjusted if large disagreements were present as in the case of the $E_r^{c.m.} = 136$ keV resonance.

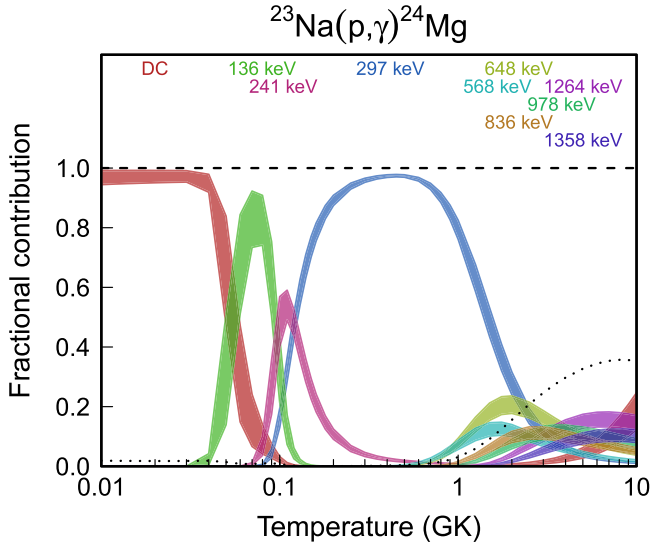

Figure 69. Fractional contributions to the total rate. "DC" refers to direct radiative capture. Resonance energies are given in the center-of-mass frame.

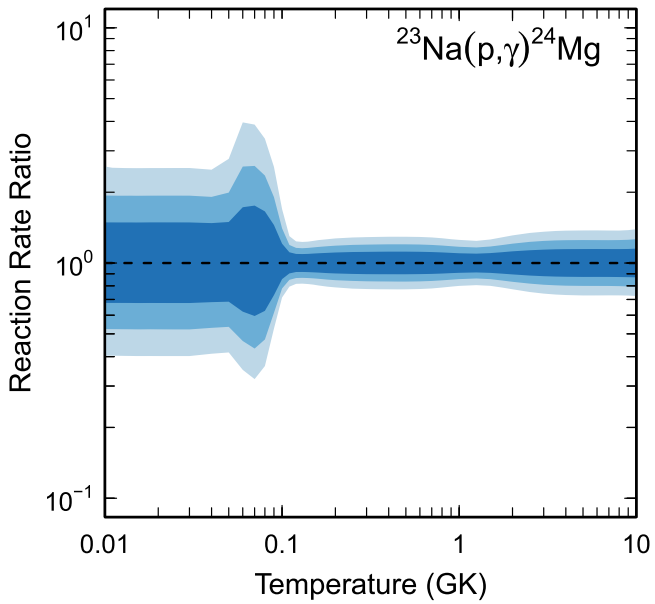

Figure 70. Reaction rate uncertainties versus temperature. The three different shades refer to coverage probabilities of 68%, 90%, and 98%.

Table 43
Total Laboratory Reaction Rates for ^{23}Na(p,α)^{20}Ne

T (GK)	Low	Median	High	*f.u.*	T (GK)	Low	Median	High	*f.u.*
0.001	1.133E-78	2.927E-78	3.773E-77	7.171E+00	0.140	5.539E-05	6.585E-05	7.928E-05	1.199E+00
0.002	2.674E-60	6.795E-60	2.482E-59	5.391E+00	0.150	1.626E-04	1.880E-04	2.199E-04	1.165E+00
0.003	2.130E-51	5.279E-51	1.249E-50	3.799E+00	0.160	4.410E-04	4.984E-04	5.681E-04	1.137E+00
0.004	8.780E-46	2.167E-45	4.556E-45	3.002E+00	0.180	2.587E-03	2.847E-03	3.142E-03	1.103E+00
0.005	8.755E-42	2.151E-41	4.316E-41	2.650E+00	0.200	1.149E-02	1.251E-02	1.365E-02	1.091E+00
0.006	9.886E-39	2.434E-38	4.763E-38	2.494E+00	0.250	1.861E-01	2.013E-01	2.182E-01	1.083E+00
0.007	2.725E-36	6.709E-36	1.294E-35	2.416E+00	0.300	1.236E+00	1.330E+00	1.436E+00	1.078E+00
0.008	2.828E-34	6.942E-34	1.325E-33	2.366E+00	0.350	4.880E+00	5.225E+00	5.608E+00	1.072E+00
0.009	1.447E-32	3.526E-32	6.664E-32	2.322E+00	0.400	1.436E+01	1.526E+01	1.626E+01	1.065E+00
0.010	4.320E-31	1.044E-30	1.952E-30	2.279E+00	0.450	3.598E+01	3.798E+01	4.015E+01	1.057E+00
0.011	8.485E-30	2.025E-29	3.746E-29	2.239E+00	0.500	8.184E+01	8.608E+01	9.057E+01	1.052E+00
0.012	1.187E-28	2.798E-28	5.134E-28	2.203E+00	0.600	3.384E+02	3.571E+02	3.768E+02	1.056E+00
0.013	1.254E-27	2.933E-27	5.331E-27	2.174E+00	0.700	1.061E+03	1.126E+03	1.195E+03	1.062E+00
0.014	1.050E-26	2.437E-26	4.395E-26	2.153E+00	0.800	2.634E+03	2.804E+03	2.986E+03	1.065E+00
0.015	7.216E-26	1.663E-25	2.980E-25	2.138E+00	0.900	5.478E+03	5.839E+03	6.227E+03	1.067E+00
0.016	4.173E-25	9.618E-25	1.715E-24	2.129E+00	1.000	1.002E+04	1.069E+04	1.141E+04	1.067E+00
0.018	9.175E-24	2.137E-23	3.788E-23	2.121E+00	1.250	3.171E+04	3.398E+04	3.652E+04	1.074E+00
0.020	1.306E-22	3.079E-22	5.435E-22	2.120E+00	1.500	7.377E+04	7.976E+04	8.686E+04	1.087E+00
0.025	2.715E-20	6.528E-20	1.140E-19	2.111E+00	1.750	1.425E+05	1.555E+05	1.716E+05	1.100E+00
0.030	1.659E-18	3.980E-18	6.833E-18	2.072E+00	2.000	2.423E+05	2.658E+05	2.963E+05	1.110E+00
0.040	7.632E-16	1.706E-15	2.819E-15	1.936E+00	2.500	5.390E+05	5.944E+05	6.665E+05	1.116E+00
0.050	7.338E-14	1.442E-13	2.272E-13	1.755E+00	3.000	9.565E+05	1.052E+06	1.176E+06	1.113E+00
0.060	3.710E-12	5.877E-12	8.583E-12	1.514E+00	3.500	1.471E+06	1.609E+06	1.788E+06	1.106E+00
0.070	1.286E-10	1.781E-10	2.429E-10	1.378E+00	4.000	2.053E+06	2.234E+06	2.464E+06	1.099E+00
0.080	2.539E-09	3.402E-09	4.544E-09	1.342E+00	5.000	(3.948E+06)	(4.989E+06)	(1.244E+07)	(1.879E+00)
0.090	2.905E-08	3.838E-08	5.066E-08	1.324E+00	6.000	(6.180E+06)	(9.462E+06)	(3.781E+07)	(2.763E+00)
0.100	2.142E-07	2.794E-07	3.647E-07	1.308E+00	7.000	(8.126E+06)	(1.578E+07)	(8.675E+07)	(3.719E+00)
0.110	1.140E-06	1.464E-06	1.885E-06	1.289E+00	8.000	(9.043E+06)	(2.402E+07)	(1.681E+08)	(4.827E+00)
0.120	4.802E-06	6.048E-06	7.652E-06	1.265E+00	9.000	(8.138E+06)	(3.415E+07)	(2.902E+08)	(6.348E+00)
0.130	1.724E-05	2.115E-05	2.618E-05	1.234E+00	10.000	(4.613E+06)	(4.613E+07)	(4.613E+08)	(1.000E+01)

Note. Observed resonances: F. C. Flack et al. (1954), T. R. Fisher & W. Whaling (1963), J. Kuperus et al. (1963), A. Luukko et al. (1970), J. Zyskind et al. (1981), J. R. Vanhoy et al. (1987), J. Görres et al. (1989), and C. Rowland et al. (2002). Normalization: C. Rowland et al. (2002; see Table 2). Unobserved resonances: E. Goldberg et al. (1954), P. Glaudemans & P. M. Endt (1962), P. Schmalbrock et al. (1983), W. Vermeer et al. (1988), S. E. Hale et al. (2004), and C. Marshall et al. (2023). High-temperature rates (in parentheses): matching to statistical model rate above $T = 4.1$ GK. Previous rates: C. Iliadis et al. (2010c). Other: subthreshold and low-energy resonance parameters were derived from the proton partial widths of C. Marshall et al. (2023), the γ-ray branching ratios of W. Vermeer et al. (1988), $\omega\gamma_{\alpha\gamma}$ of P. Schmalbrock et al. (1983), and the total widths of P. Schmalbrock et al. (1983) and E. Goldberg et al. (1954).

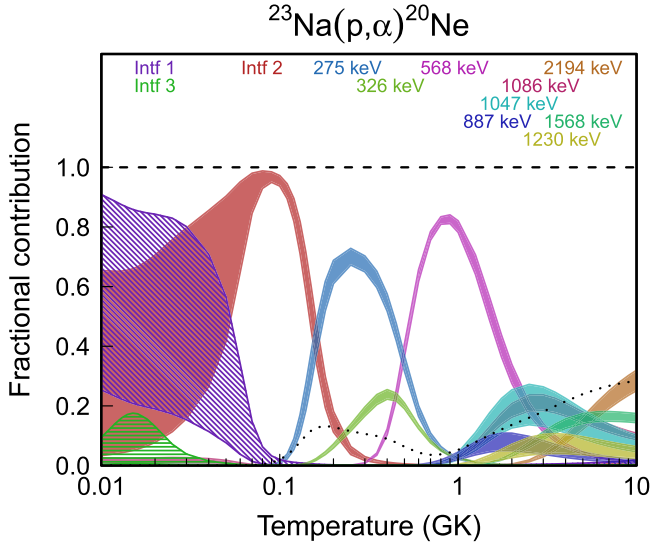

Figure 71. Fractional contributions to the total rate. Resonance energies are given in the center-of-mass frame. "Inf1" refers to the combined contribution of the two interfering 1^- resonances at -303 and 170.2 keV. "Inf2" stands for for the two interfering 2^+ resonances at -170.4 and -239 keV. "Inf3" denotes the two interfering 0^+ resonances at -235 and 38 keV.

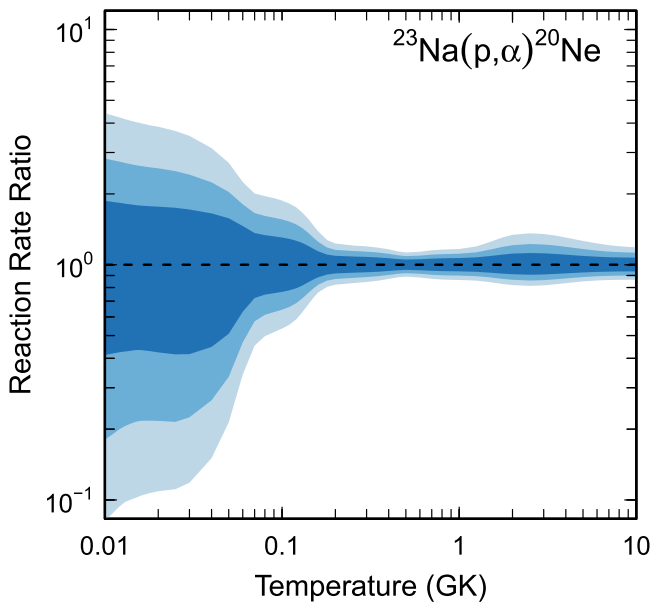

Figure 72. Reaction rate uncertainties versus temperature. The three different shades refer to coverage probabilities of 68%, 90%, and 98%.

Table 44
Total Laboratory Reaction Rates for ^{22}Mg(p,γ)^{23}Al

T (GK)	Low	Median	High	*f.u.*	T (GK) (GK)	Low	Median	High	*f.u.*
0.001	1.508E-87	3.008E-87	6.013E-87	2.000E+00	0.140	7.503E-12	1.497E-11	2.985E-11	1.997E+00
0.002	4.811E-68	9.595E-68	1.918E-67	2.000E+00	0.150	1.898E-11	3.776E-11	7.520E-11	1.995E+00
0.003	1.408E-58	2.808E-58	5.614E-58	2.000E+00	0.160	4.451E-11	8.843E-11	1.760E-10	1.995E+00
0.004	1.321E-52	2.635E-52	5.267E-52	2.000E+00	0.180	2.057E-10	4.069E-10	8.114E-10	2.014E+00
0.005	2.340E-48	4.668E-48	9.332E-48	2.000E+00	0.200	7.846E-10	1.558E-09	3.151E-09	2.082E+00
0.006	4.074E-45	8.125E-45	1.624E-44	2.000E+00	0.250	1.204E-08	2.471E-08	5.680E-08	2.451E+00
0.007	1.577E-42	3.146E-42	6.289E-42	2.000E+00	0.300	9.729E-08	2.094E-07	5.684E-07	2.855E+00
0.008	2.152E-40	4.293E-40	8.582E-40	2.000E+00	0.350	5.036E-07	1.127E-06	3.518E-06	3.126E+00
0.009	1.372E-38	2.737E-38	5.471E-38	2.000E+00	0.400	1.898E-06	4.332E-06	1.457E-05	3.257E+00
0.010	4.914E-37	9.802E-37	1.959E-36	2.000E+00	0.450	5.702E-06	1.304E-05	4.495E-05	3.286E+00
0.011	1.122E-35	2.239E-35	4.475E-35	2.000E+00	0.500	1.443E-05	3.286E-05	1.110E-04	3.247E+00
0.012	1.789E-34	3.568E-34	7.133E-34	2.000E+00	0.600	6.500E-05	1.440E-04	4.441E-04	3.063E+00
0.013	2.127E-33	4.242E-33	8.480E-33	2.000E+00	0.700	2.180E-04	4.663E-04	1.277E-03	2.823E+00
0.014	1.983E-32	3.955E-32	7.907E-32	2.000E+00	0.800	6.129E-04	1.286E-03	3.239E-03	2.627E+00
0.015	1.508E-31	3.007E-31	6.011E-31	2.000E+00	0.900	1.533E-03	3.217E-03	8.060E-03	2.567E+00
0.016	9.634E-31	1.922E-30	3.841E-30	2.000E+00	1.000	3.505E-03	7.404E-03	1.968E-02	2.656E+00
0.018	2.564E-29	5.114E-29	1.022E-28	2.000E+00	1.250	1.979E-02	4.556E-02	1.594E-01	3.189E+00
0.020	4.325E-28	8.626E-28	1.724E-27	2.000E+00	1.500	7.630E-02	1.978E-01	8.776E-01	3.683E+00
0.025	1.240E-25	2.473E-25	4.943E-25	2.000E+00	1.750	(1.634E-01)	(4.429E-01)	(2.096E+00)	(3.722E+00)
0.030	9.251E-24	1.845E-23	3.689E-23	2.000E+00	2.000	(2.872E-01)	(7.961E-01)	(3.895E+00)	(3.832E+00)
0.040	4.932E-21	9.837E-21	1.966E-20	2.000E+00	2.500	(6.450E-01)	(1.872E+00)	(9.758E+00)	(4.057E+00)
0.050	4.266E-19	8.508E-19	1.701E-18	2.000E+00	3.000	(1.171E+00)	(3.569E+00)	(1.974E+01)	(4.289E+00)
0.060	1.277E-17	2.546E-17	5.090E-17	2.000E+00	3.500	(1.858E+00)	(5.957E+00)	(3.485E+01)	(4.528E+00)
0.070	1.924E-16	3.837E-16	7.670E-16	2.000E+00	4.000	(2.685E+00)	(9.082E+00)	(5.603E+01)	(4.776E+00)
0.080	1.801E-15	3.592E-15	7.180E-15	2.000E+00	5.000	(4.656E+00)	(1.770E+01)	(1.205E+02)	(5.305E+00)
0.090	1.191E-14	2.376E-14	4.750E-14	2.000E+00	6.000	(6.925E+00)	(3.006E+01)	(2.238E+02)	(5.893E+00)
0.100	6.059E-14	1.208E-13	2.416E-13	2.000E+00	7.000	(9.430E+00)	(4.767E+01)	(3.854E+02)	(6.570E+00)
0.110	2.510E-13	5.006E-13	1.001E-12	2.000E+00	8.000	(1.217E+01)	(7.368E+01)	(6.427E+02)	(7.388E+00)
0.120	8.826E-13	1.761E-12	3.519E-12	2.000E+00	9.000	(1.503E+01)	(1.133E+02)	(1.061E+03)	(8.452E+00)
0.130	2.716E-12	5.421E-12	1.083E-11	1.999E+00	10.000	(1.745E+01)	(1.745E+02)	(1.745E+03)	(1.000E+01)

Note. Observed resonances: none. Normalization: none. Unobserved resonances: P. M. Endt (1977), P. M. Endt & C. van der Leun (1978), and J. A. Caggiano et al. (2001). High-temperature rates (in parentheses): matching to statistical model rate above $T = 1.6$ GK. Previous rates: C. Iliadis et al. (2010c). Other: the direct-capture S factor for the ground state was estimated using C^2S= 0.24 of the mirror state in ^{23}Ne (P. M. Endt 1977).

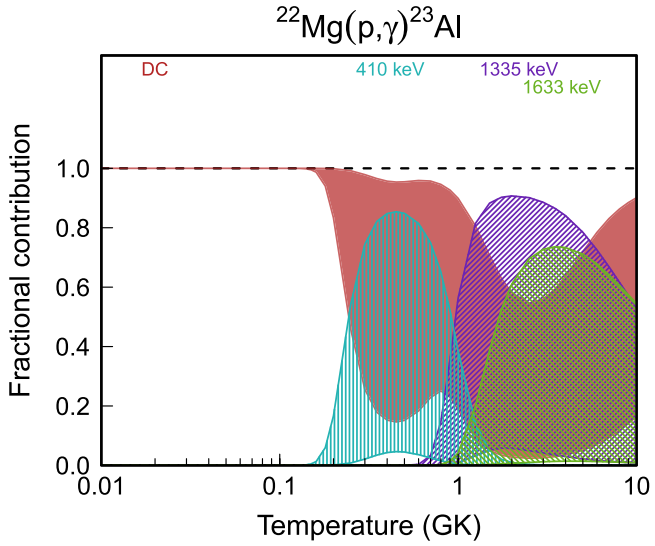

Figure 73. Fractional contributions to the total rate. "DC" refers to direct radiative capture. Resonance energies are given in the center-of-mass frame.

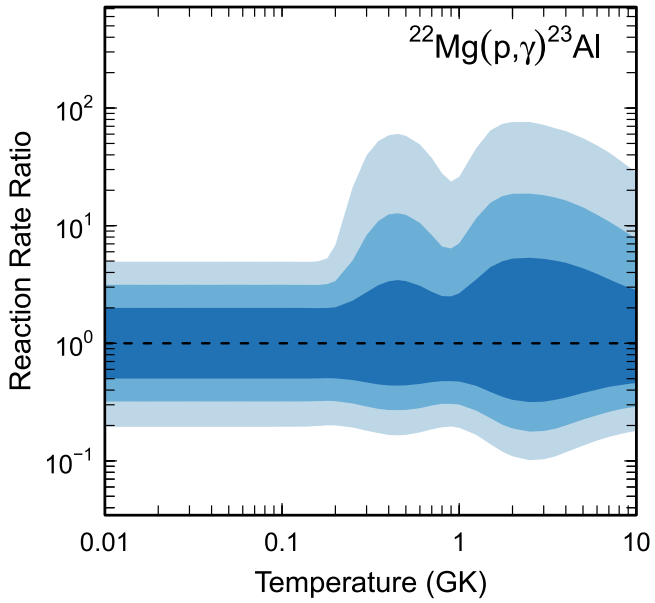

Figure 74. Reaction rate uncertainties versus temperature. The three different shades refer to coverage probabilities of 68%, 90%, and 98%.

Table 45
Total Laboratory Reaction Rates for ^{23}Mg(p,γ)^{24}Al

T (GK)	Low	Median	High	*f.u.*	T (GK)	Low	Median	High	*f.u.*
0.001	3.574E-86	7.122E-86	1.428E-85	2.005E+00	0.140	1.802E-10	3.563E-10	7.126E-10	1.994E+00
0.002	1.171E-66	2.334E-66	4.680E-66	2.005E+00	0.150	4.544E-10	8.937E-10	1.782E-09	1.984E+00
0.003	3.470E-57	6.914E-57	1.387E-56	2.005E+00	0.160	1.093E-09	2.104E-09	4.152E-09	1.951E+00
0.004	3.279E-51	6.535E-51	1.310E-50	2.005E+00	0.180	6.759E-09	1.149E-08	2.051E-08	1.752E+00
0.005	5.839E-47	1.164E-46	2.333E-46	2.005E+00	0.200	4.974E-08	7.867E-08	1.231E-07	1.584E+00
0.006	1.020E-43	2.032E-43	4.076E-43	2.005E+00	0.250	4.822E-06	8.297E-06	1.408E-05	1.714E+00
0.007	4.002E-41	7.926E-41	1.586E-40	1.996E+00	0.300	1.410E-04	2.505E-04	4.323E-04	1.758E+00
0.008	5.472E-39	1.084E-38	2.169E-38	1.996E+00	0.350	1.592E-03	2.841E-03	4.909E-03	1.762E+00
0.009	3.494E-37	6.919E-37	1.385E-36	1.996E+00	0.400	9.690E-03	1.724E-02	2.969E-02	1.756E+00
0.010	1.253E-35	2.481E-35	4.966E-35	1.996E+00	0.450	3.903E-02	6.896E-02	1.183E-01	1.746E+00
0.011	2.864E-34	5.672E-34	1.135E-33	1.996E+00	0.500	1.180E-01	2.068E-01	3.528E-01	1.733E+00
0.012	4.569E-33	9.048E-33	1.811E-32	1.996E+00	0.600	6.143E-01	1.051E+00	1.770E+00	1.702E+00
0.013	5.435E-32	1.076E-31	2.154E-31	1.996E+00	0.700	1.974E+00	3.301E+00	5.467E+00	1.670E+00
0.014	5.070E-31	1.004E-30	2.010E-30	1.996E+00	0.800	4.691E+00	7.701E+00	1.253E+01	1.641E+00
0.015	3.856E-30	7.636E-30	1.528E-29	1.996E+00	0.900	(7.385E+00)	(1.216E+01)	(2.050E+01)	(1.666E+00)
0.016	2.464E-29	4.881E-29	9.768E-29	1.996E+00	1.000	(9.923E+00)	(1.649E+01)	(2.930E+01)	(1.719E+00)
0.018	6.560E-28	1.299E-27	2.600E-27	1.996E+00	1.250	(1.582E+01)	(2.690E+01)	(5.395E+01)	(1.853E+00)
0.020	1.107E-26	2.192E-26	4.387E-26	1.996E+00	1.500	(2.518E+01)	(4.386E+01)	(9.800E+01)	(1.988E+00)
0.025	3.170E-24	6.280E-24	1.257E-23	1.996E+00	1.750	(3.226E+01)	(5.760E+01)	(1.418E+02)	(2.124E+00)
0.030	2.364E-22	4.682E-22	9.369E-22	1.996E+00	2.000	(4.131E+01)	(7.563E+01)	(2.035E+02)	(2.261E+00)
0.040	1.256E-19	2.488E-19	4.978E-19	1.996E+00	2.500	(5.619E+01)	(1.084E+02)	(3.413E+02)	(2.539E+00)
0.050	1.082E-17	2.143E-17	4.288E-17	1.996E+00	3.000	(6.935E+01)	(1.414E+02)	(5.097E+02)	(2.822E+00)
0.060	3.221E-16	6.382E-16	1.277E-15	1.996E+00	3.500	(8.077E+01)	(1.746E+02)	(7.093E+02)	(3.112E+00)
0.070	4.827E-15	9.563E-15	1.913E-14	1.996E+00	4.000	(9.057E+01)	(2.084E+02)	(9.416E+02)	(3.410E+00)
0.080	4.491E-14	8.899E-14	1.781E-13	1.996E+00	5.000	(1.057E+02)	(2.791E+02)	(1.516E+03)	(4.036E+00)
0.090	2.953E-13	5.851E-13	1.171E-12	1.996E+00	6.000	(1.149E+02)	(3.557E+02)	(2.257E+03)	(4.720E+00)
0.100	1.492E-12	2.957E-12	5.917E-12	1.996E+00	7.000	(1.176E+02)	(4.401E+02)	(3.195E+03)	(5.500E+00)
0.110	6.144E-12	1.217E-11	2.436E-11	1.996E+00	8.000	(1.131E+02)	(5.344E+02)	(4.368E+03)	(6.450E+00)
0.120	2.147E-11	4.253E-11	8.511E-11	1.996E+00	9.000	(9.998E+01)	(6.418E+02)	(5.832E+03)	(7.753E+00)
0.130	6.566E-11	1.300E-10	2.602E-10	1.996E+00	10.000	(7.660E+01)	(7.660E+02)	(7.660E+03)	(1.000E+01)

Note. Observed resonances: none. Normalization: none. Unobserved resonances: D. W. Visser et al. (2007, 2008), I. Tomandl et al. (2004), and G. Lotay et al. (2008). High-temperature rates (in parentheses): matching to statistical model rate above $T = 0.83$ GK. Previous rates: L. Erikson et al. (2010) and C. Iliadis et al. (2010c). Other: the ^{24}Al–^{24}Na mirror state assignments were adopted from H. Herndl et al. (1998) and G. Lotay et al. (2008).

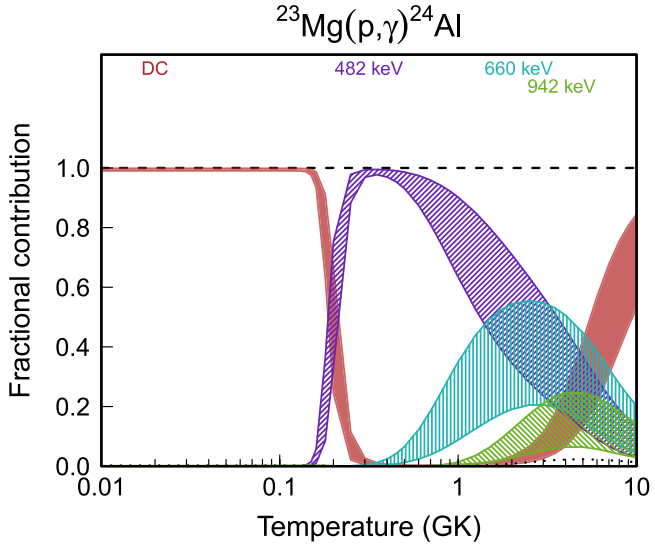

Figure 75. Fractional contributions to the total rate. "DC" refers to direct radiative capture. Resonance energies are given in the center-of-mass frame.

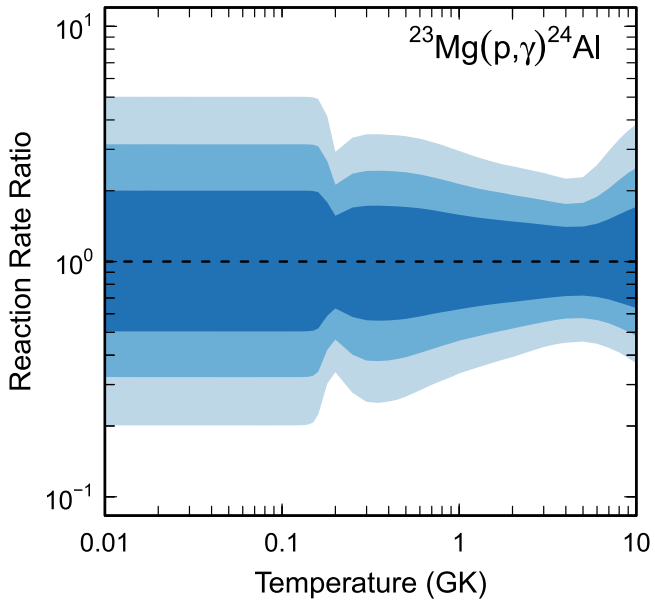

Figure 76. Reaction rate uncertainties versus temperature. The three different shades refer to coverage probabilities of 68%, 90%, and 98%.

Table 46
Total Laboratory Reaction Rates for ^{24}Mg(p,γ)^{25}Al

T (GK)	Low	Median	High	*f.u.*	T (GK)	Low	Median	High	*f.u.*
0.001	8.139E-86	1.059E-85	1.376E-85	1.301E+00	0.140	6.345E-04	6.973E-04	7.640E-04	1.098E+00
0.002	2.744E-66	3.569E-66	4.638E-66	1.301E+00	0.150	1.881E-03	2.064E-03	2.258E-03	1.097E+00
0.003	8.251E-57	1.073E-56	1.394E-56	1.301E+00	0.160	4.836E-03	5.300E-03	5.795E-03	1.096E+00
0.004	7.875E-51	1.024E-50	1.331E-50	1.301E+00	0.180	2.297E-02	2.514E-02	2.747E-02	1.095E+00
0.005	1.413E-46	1.837E-46	2.387E-46	1.301E+00	0.200	7.854E-02	8.591E-02	9.381E-02	1.094E+00
0.006	2.482E-43	3.228E-43	4.194E-43	1.301E+00	0.250	6.824E-01	7.463E-01	8.149E-01	1.094E+00
0.007	1.094E-40	1.391E-40	1.772E-40	1.273E+00	0.300	2.745E+00	3.003E+00	3.282E+00	1.094E+00
0.008	1.507E-38	1.914E-38	2.438E-38	1.273E+00	0.350	7.178E+00	7.854E+00	8.591E+00	1.095E+00
0.009	9.688E-37	1.230E-36	1.566E-36	1.272E+00	0.400	1.444E+01	1.580E+01	1.729E+01	1.095E+00
0.010	3.495E-35	4.437E-35	5.648E-35	1.272E+00	0.450	2.450E+01	2.680E+01	2.931E+01	1.095E+00
0.011	8.039E-34	1.020E-33	1.298E-33	1.271E+00	0.500	3.704E+01	4.048E+01	4.424E+01	1.094E+00
0.012	1.290E-32	1.636E-32	2.080E-32	1.271E+00	0.600	6.779E+01	7.390E+01	8.055E+01	1.091E+00
0.013	1.542E-31	1.956E-31	2.487E-31	1.270E+00	0.700	1.035E+02	1.123E+02	1.220E+02	1.086E+00
0.014	1.447E-30	1.834E-30	2.331E-30	1.270E+00	0.800	1.418E+02	1.533E+02	1.657E+02	1.082E+00
0.015	1.106E-29	1.402E-29	1.780E-29	1.270E+00	0.900	1.817E+02	1.955E+02	2.104E+02	1.077E+00
0.016	7.104E-29	9.003E-29	1.143E-28	1.269E+00	1.000	2.229E+02	2.386E+02	2.556E+02	1.072E+00
0.018	1.911E-27	2.419E-27	3.068E-27	1.268E+00	1.250	3.329E+02	3.527E+02	3.739E+02	1.060E+00
0.020	3.256E-26	4.118E-26	5.220E-26	1.267E+00	1.500	4.568E+02	4.805E+02	5.059E+02	1.053E+00
0.025	9.558E-24	1.207E-23	1.527E-23	1.265E+00	1.750	5.935E+02	6.234E+02	6.550E+02	1.051E+00
0.030	7.296E-22	9.200E-22	1.163E-21	1.263E+00	2.000	7.390E+02	7.782E+02	8.193E+02	1.053E+00
0.040	4.084E-19	5.131E-19	6.465E-19	1.259E+00	2.500	1.045E+03	1.108E+03	1.176E+03	1.061E+00
0.050	7.253E-17	8.517E-17	9.997E-17	1.174E+00	3.000	1.356E+03	1.448E+03	1.548E+03	1.069E+00
0.060	1.022E-13	1.192E-13	1.387E-13	1.166E+00	3.500	1.666E+03	1.791E+03	1.928E+03	1.076E+00
0.070	3.108E-11	3.561E-11	4.071E-11	1.145E+00	4.000	1.975E+03	2.133E+03	2.312E+03	1.082E+00
0.080	2.222E-09	2.513E-09	2.835E-09	1.130E+00	5.000	2.575E+03	2.811E+03	3.083E+03	1.095E+00
0.090	6.020E-08	6.747E-08	7.542E-08	1.120E+00	6.000	3.144E+03	3.466E+03	3.846E+03	1.107E+00
0.100	8.289E-07	9.225E-07	1.024E-06	1.112E+00	7.000	3.667E+03	4.083E+03	4.575E+03	1.119E+00
0.110	6.987E-06	7.739E-06	8.548E-06	1.107E+00	8.000	(2.464E+03)	(3.772E+03)	(1.448E+04)	(2.684E+00)
0.120	4.077E-05	4.501E-05	4.954E-05	1.103E+00	9.000	(1.174E+03)	(3.117E+03)	(2.157E+04)	(4.787E+00)
0.130	1.796E-04	1.977E-04	2.170E-04	1.100E+00	10.000	(2.231E+02)	(2.231E+03)	(2.231E+04)	(1.000E+01)

Note. Observed resonances: P. M. Endt & C. van dèr Leun (1973), H. P. Trautvetter & C. Rolfs (1975), D. Powell et al. (1998, 1999), and S. Engel et al. (2005). Normalization: low-energy resonances were normalized to D. Powell et al. (1998, 1999), high-energy ones to H. P. Trautvetter (1975) and S. Engel et al. (2005); see Table 2. Unobserved resonances: none. High-temperature rates (in parentheses): matching to statistical model rate above $T = 7.1$ GK. Previous rates: C. Iliadis et al. (2001, 2010c). Other: our adopted strength of the $E_r^{c.m.} = 215$ keV resonance agrees with the results of B. Limata et al. (2010) and H. Zhang et al. (2021).

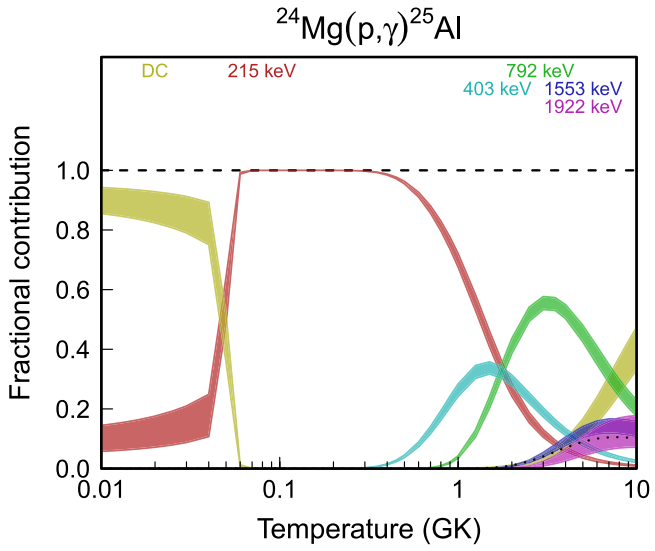

Figure 77. Fractional contributions to the total rate. "DC" refers to direct radiative capture. Resonance energies are given in the center-of-mass frame.

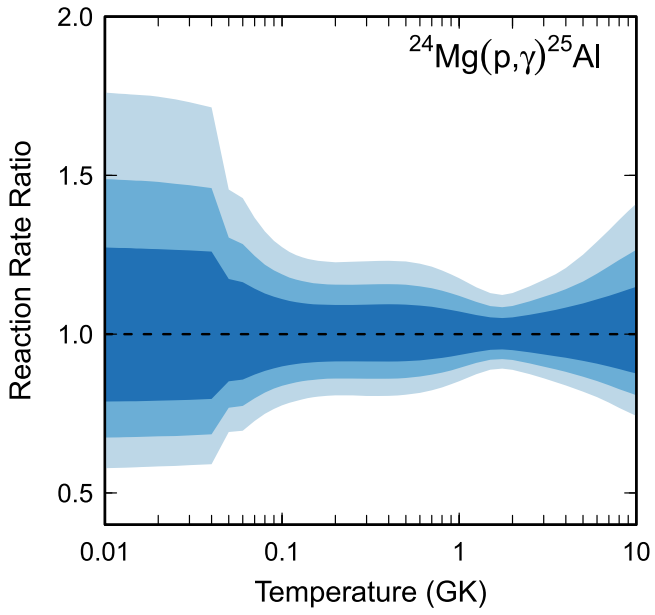

Figure 78. Reaction rate uncertainties versus temperature. The three different shades refer to coverage probabilities of 68%, 90%, and 98%.

Table 47
Total Laboratory Reaction Rates for $^{24}Mg(\alpha,\gamma)^{28}Si$

T (GK)	Low	Median	High	*f.u.*	T (GK)	Low	Median	High	*f.u.*
0.001	0.000E+00	0.000E+00	0.000E+00	1.000E+00	0.140	8.722E-28	5.879E-27	7.518E-26	9.242E+00
0.002	0.000E+00	0.000E+00	0.000E+00	1.000E+00	0.150	1.010E-26	9.165E-26	1.317E-24	1.071E+01
0.003	0.000E+00	0.000E+00	0.000E+00	1.000E+00	0.160	1.096E-25	1.151E-24	1.609E-23	1.119E+01
0.004	0.000E+00	0.000E+00	0.000E+00	1.000E+00	0.180	9.991E-24	8.902E-23	1.053E-21	9.947E+00
0.005	0.000E+00	0.000E+00	0.000E+00	1.000E+00	0.200	4.875E-22	3.450E-21	3.196E-20	8.120E+00
0.006	0.000E+00	0.000E+00	0.000E+00	1.000E+00	0.250	9.946E-19	4.827E-18	3.020E-17	5.457E+00
0.007	0.000E+00	0.000E+00	0.000E+00	1.000E+00	0.300	5.305E-16	1.402E-15	8.016E-15	4.115E+00
0.008	0.000E+00	0.000E+00	0.000E+00	1.000E+00	0.350	9.222E-14	1.599E-13	7.517E-13	3.290E+00
0.009	3.826E-97	1.896E-96	9.304E-96	4.910E+00	0.400	5.260E-12	7.731E-12	2.704E-11	2.740E+00
0.010	2.472E-93	1.225E-92	6.011E-92	4.909E+00	0.450	1.330E-10	1.779E-10	4.724E-10	2.356E+00
0.011	5.315E-90	2.633E-89	1.292E-88	4.909E+00	0.500	1.885E-09	2.354E-09	4.977E-09	2.075E+00
0.012	4.742E-87	2.349E-86	1.153E-85	4.908E+00	0.600	1.163E-07	1.333E-07	2.017E-07	1.700E+00
0.013	2.065E-84	1.023E-83	5.020E-83	4.908E+00	0.700	2.481E-06	2.740E-06	3.436E-06	1.480E+00
0.014	4.963E-82	2.458E-81	1.206E-80	4.907E+00	0.800	2.600E-05	2.833E-05	3.261E-05	1.348E+00
0.015	7.235E-80	3.583E-79	1.758E-78	4.907E+00	0.900	1.663E-04	1.801E-04	2.007E-04	1.265E+00
0.016	6.893E-78	3.413E-77	1.675E-76	4.906E+00	1.000	7.452E-04	8.044E-04	8.835E-04	1.211E+00
0.018	2.193E-74	1.086E-73	5.330E-73	4.905E+00	1.250	1.150E-02	1.234E-02	1.335E-02	1.138E+00
0.020	2.285E-71	1.131E-70	5.550E-70	4.903E+00	1.500	7.354E-02	7.857E-02	8.439E-02	1.104E+00
0.025	6.318E-65	2.086E-64	7.373E-64	3.562E+00	1.750	2.827E-01	3.014E-01	3.225E-01	1.087E+00
0.030	3.952E-59	1.732E-58	6.225E-58	4.065E+00	2.000	7.921E-01	8.426E-01	8.993E-01	1.077E+00
0.040	6.149E-51	3.152E-50	1.232E-49	4.797E+00	2.500	3.550E+00	3.759E+00	3.997E+00	1.066E+00
0.050	9.906E-46	3.566E-45	1.229E-44	3.886E+00	3.000	1.035E+01	1.092E+01	1.155E+01	1.059E+00
0.060	6.819E-42	2.601E-41	8.776E-41	3.709E+00	3.500	2.347E+01	2.467E+01	2.601E+01	1.054E+00
0.070	5.394E-39	3.473E-38	1.535E-37	5.088E+00	4.000	4.490E+01	4.718E+01	4.966E+01	1.053E+00
0.080	1.188E-36	1.047E-35	4.944E-35	6.115E+00	5.000	1.170E+02	1.232E+02	1.301E+02	1.058E+00
0.090	1.029E-34	9.356E-34	4.471E-33	6.261E+00	6.000	(2.110E+02)	(2.519E+02)	(5.591E+02)	(1.707E+00)
0.100	5.050E-33	3.718E-32	1.692E-31	5.630E+00	7.000	(2.885E+02)	(4.416E+02)	(1.839E+03)	(2.848E+00)
0.110	1.639E-31	9.924E-31	4.147E-30	5.126E+00	8.000	(3.223E+02)	(6.874E+02)	(4.200E+03)	(4.121E+00)
0.120	3.762E-30	2.058E-29	9.745E-29	5.676E+00	9.000	(2.810E+02)	(9.879E+02)	(7.957E+03)	(5.785E+00)
0.130	6.460E-29	3.566E-28	2.871E-27	7.280E+00	10.000	(1.342E+02)	(1.342E+03)	(1.342E+04)	(1.000E+01)

Note. Observed resonances: P. M. Endt (1990) and E. Strandberg et al. (2008). Normalization: none. Unobserved resonances: T. Tanabe et al. (1983). High-temperature rates (in parentheses): matching to statistical model rate above $T = 5.4$ GK. Previous rates: P. Adsley et al. (2020). Other: the dominating E2 direct-capture contribution to bound levels in ^{28}Si has been estimated using α-particle spectroscopic factors reported in T. Tanabe et al. (1983).

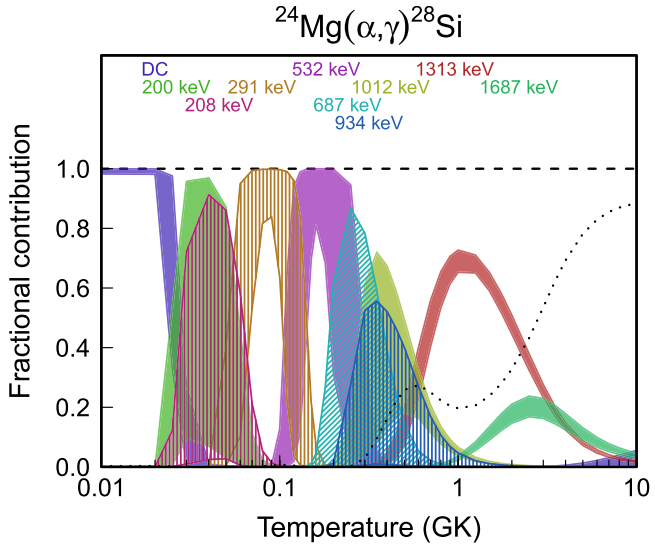

Figure 79. Fractional contributions to the total rate. "DC" refers to direct radiative capture. Resonance energies are given in the center-of-mass frame.

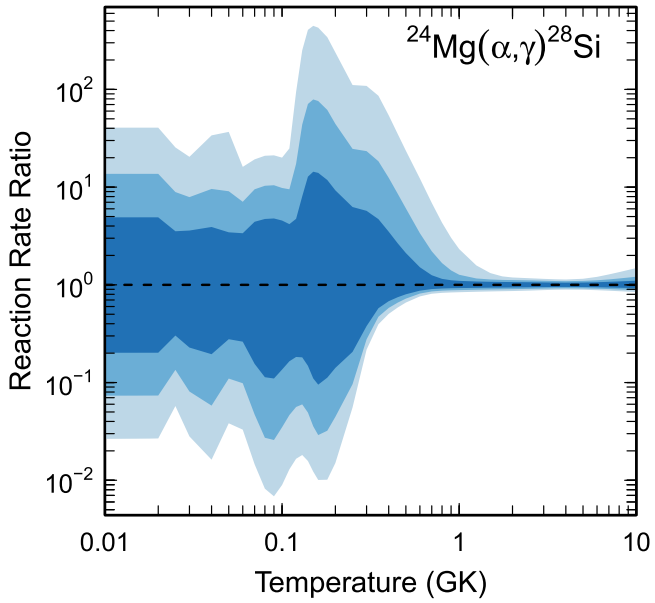

Figure 80. Reaction rate uncertainties versus temperature. The three different shades refer to coverage probabilities of 68%, 90%, and 98%.

Table 48
Total Laboratory Reaction Rates for ^{25}Mg(p,γ)^{26}Al^{t} (Population of Both the Ground and Isomeric State)

T (GK)	Low	Median	High	*f.u.*	T (GK)	Low	Median	High	*f.u.*
0.001	1.684E-85	2.185E-85	2.835E-85	1.300E+00	0.140	1.644E-06	1.834E-06	2.080E-06	1.129E+00
0.002	5.820E-66	7.550E-66	9.798E-66	1.300E+00	0.150	5.867E-06	6.436E-06	7.088E-06	1.100E+00
0.003	1.771E-56	2.298E-56	2.982E-56	1.300E+00	0.160	1.995E-05	2.196E-05	2.422E-05	1.102E+00
0.004	1.703E-50	2.210E-50	2.868E-50	1.300E+00	0.180	1.751E-04	1.943E-04	2.159E-04	1.111E+00
0.005	3.072E-46	3.985E-46	5.172E-46	1.300E+00	0.200	1.046E-03	1.163E-03	1.295E-03	1.113E+00
0.006	5.483E-43	7.097E-43	9.193E-43	1.298E+00	0.250	2.674E-02	2.963E-02	3.291E-02	1.110E+00
0.007	2.949E-40	4.097E-40	6.358E-40	1.538E+00	0.300	2.327E-01	2.562E-01	2.827E-01	1.103E+00
0.008	1.230E-37	2.917E-37	7.904E-37	2.492E+00	0.350	1.097E+00	1.199E+00	1.314E+00	1.095E+00
0.009	3.632E-35	1.037E-34	3.028E-34	2.867E+00	0.400	3.543E+00	3.843E+00	4.181E+00	1.087E+00
0.010	4.324E-33	1.233E-32	3.593E-32	2.864E+00	0.450	8.902E+00	9.596E+00	1.037E+01	1.079E+00
0.011	2.940E-31	6.991E-31	1.858E-30	2.509E+00	0.500	1.879E+01	2.014E+01	2.162E+01	1.073E+00
0.012	1.643E-29	3.155E-29	6.455E-29	2.022E+00	0.600	5.902E+01	6.265E+01	6.656E+01	1.062E+00
0.013	6.823E-28	1.245E-27	2.310E-27	1.847E+00	0.700	1.369E+02	1.444E+02	1.524E+02	1.055E+00
0.014	2.007E-26	3.732E-26	7.091E-26	1.889E+00	0.800	2.613E+02	2.748E+02	2.891E+02	1.052E+00
0.015	4.160E-25	7.989E-25	1.562E-24	1.944E+00	0.900	4.370E+02	4.588E+02	4.823E+02	1.051E+00
0.016	6.213E-24	1.214E-23	2.399E-23	1.972E+00	1.000	6.644E+02	6.978E+02	7.335E+02	1.051E+00
0.018	5.818E-22	1.148E-21	2.281E-21	1.989E+00	1.250	1.443E+03	1.521E+03	1.606E+03	1.055E+00
0.020	2.193E-20	4.331E-20	8.622E-20	1.992E+00	1.500	2.478E+03	2.623E+03	2.779E+03	1.059E+00
0.025	1.441E-17	2.848E-17	5.670E-17	1.993E+00	1.750	3.711E+03	3.942E+03	4.192E+03	1.063E+00
0.030	1.038E-15	2.052E-15	4.079E-15	1.992E+00	2.000	5.095E+03	5.428E+03	5.786E+03	1.066E+00
0.040	2.105E-13	4.048E-13	7.929E-13	1.945E+00	2.500	8.151E+03	8.715E+03	9.321E+03	1.070E+00
0.050	6.224E-12	1.052E-11	1.894E-11	1.752E+00	3.000	1.136E+04	1.218E+04	1.305E+04	1.072E+00
0.060	8.116E-11	1.210E-10	1.874E-10	1.537E+00	3.500	(1.321E+04)	(1.486E+04)	(2.283E+04)	(1.330E+00)
0.070	5.939E-10	8.488E-10	1.219E-09	1.441E+00	4.000	(1.403E+04)	(1.694E+04)	(3.706E+04)	(1.697E+00)
0.080	2.805E-09	3.991E-09	5.668E-09	1.425E+00	5.000	(1.424E+04)	(2.014E+04)	(7.029E+04)	(2.452E+00)
0.090	9.706E-09	1.383E-08	1.970E-08	1.429E+00	6.000	(1.301E+04)	(2.222E+04)	(1.065E+05)	(3.250E+00)
0.100	2.709E-08	3.838E-08	5.482E-08	1.426E+00	7.000	(1.086E+04)	(2.339E+04)	(1.425E+05)	(4.124E+00)
0.110	6.718E-08	9.301E-08	1.310E-07	1.398E+00	8.000	(8.149E+03)	(2.377E+04)	(1.758E+05)	(5.156E+00)
0.120	1.674E-07	2.187E-07	2.943E-07	1.329E+00	9.000	(5.196E+03)	(2.347E+04)	(2.041E+05)	(6.607E+00)
0.130	4.822E-07	5.755E-07	7.108E-07	1.219E+00	10.000	(2.256E+03)	(2.256E+04)	(2.256E+05)	(1.000E+01)

Note. Observed resonances: M. Anderson et al. (1980), P. M. Endt (1990), C. Iliadis et al. (1990), D. Powell et al. (1998), F. Strieder et al. (2012), J. Dermigny et al. (2016), and H. Zhang et al. (2023). Normalization: see Table 2. Unobserved resonances: C. Iliadis et al. (1996), and references therein. High-temperature rates (in parentheses): matching to statistical model rate above $T = 3.1$ GK. Previous rates: H. Zhang et al. (2023). Other: the results given in this table and Figures 81 and 82 correspond to the rates for populating all final states in ^{26}Al.

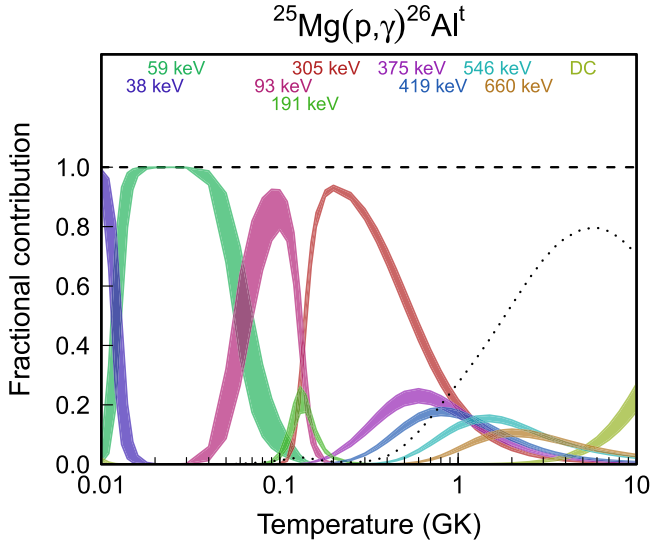

Figure 81. Fractional contributions to the total rate. "DC" refers to direct radiative capture. Resonance energies are given in the center-of-mass frame.

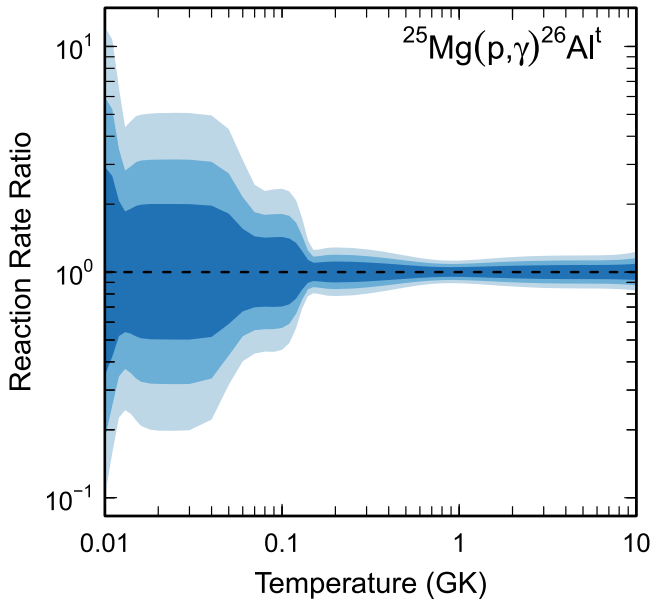

Figure 82. Reaction rate uncertainties versus temperature. The three different shades refer to coverage probabilities of 68%, 90%, and 98%.

Table 49
Total Laboratory Reaction Rates for ^{25}Mg(p,γ)^{26}Al^{g} (Population of the Ground State Only)

T (GK)	Low	Median	High	*f.u.*	T (GK)	Low	Median	High	*f.u.*
0.001	1.303E-85	1.693E-85	2.197E-85	1.300E+00	0.140	1.352E-06	1.506E-06	1.697E-06	1.125E+00
0.002	4.503E-66	5.849E-66	7.592E-66	1.300E+00	0.150	4.937E-06	5.426E-06	5.972E-06	1.101E+00
0.003	1.370E-56	1.780E-56	2.310E-56	1.300E+00	0.160	1.704E-05	1.880E-05	2.076E-05	1.104E+00
0.004	1.318E-50	1.711E-50	2.222E-50	1.300E+00	0.180	1.514E-04	1.683E-04	1.871E-04	1.112E+00
0.005	2.377E-46	3.087E-46	4.007E-46	1.300E+00	0.200	9.066E-04	1.009E-03	1.124E-03	1.114E+00
0.006	4.236E-43	5.488E-43	7.116E-43	1.298E+00	0.250	2.305E-02	2.559E-02	2.843E-02	1.111E+00
0.007	2.232E-40	3.061E-40	4.628E-40	1.510E+00	0.300	1.987E-01	2.193E-01	2.423E-01	1.105E+00
0.008	8.808E-38	2.009E-37	5.400E-37	2.449E+00	0.350	9.284E-01	1.017E+00	1.116E+00	1.097E+00
0.009	2.507E-35	7.021E-35	2.054E-34	2.845E+00	0.400	2.969E+00	3.230E+00	3.521E+00	1.089E+00
0.010	2.986E-33	8.354E-33	2.441E-32	2.843E+00	0.450	7.392E+00	7.987E+00	8.648E+00	1.082E+00
0.011	2.101E-31	4.846E-31	1.268E-30	2.474E+00	0.500	1.546E+01	1.660E+01	1.786E+01	1.075E+00
0.012	1.199E-29	2.295E-29	4.599E-29	2.002E+00	0.600	4.762E+01	5.064E+01	5.391E+01	1.064E+00
0.013	5.104E-28	9.326E-28	1.735E-27	1.856E+00	0.700	1.084E+02	1.145E+02	1.209E+02	1.057E+00
0.014	1.518E-26	2.847E-26	5.470E-26	1.906E+00	0.800	2.033E+02	2.139E+02	2.250E+02	1.052E+00
0.015	3.180E-25	6.149E-25	1.215E-24	1.959E+00	0.900	3.348E+02	3.514E+02	3.689E+02	1.050E+00
0.016	4.778E-24	9.366E-24	1.870E-23	1.985E+00	1.000	5.021E+02	5.267E+02	5.528E+02	1.050E+00
0.018	4.479E-22	8.879E-22	1.780E-21	2.001E+00	1.250	1.060E+03	1.115E+03	1.174E+03	1.052E+00
0.020	1.686E-20	3.352E-20	6.729E-20	2.003E+00	1.500	1.783E+03	1.882E+03	1.989E+03	1.057E+00
0.025	1.109E-17	2.202E-17	4.419E-17	2.004E+00	1.750	2.630E+03	2.786E+03	2.955E+03	1.061E+00
0.030	7.986E-16	1.586E-15	3.178E-15	2.002E+00	2.000	3.569E+03	3.793E+03	4.035E+03	1.064E+00
0.040	1.620E-13	3.131E-13	6.178E-13	1.955E+00	2.500	5.632E+03	6.011E+03	6.420E+03	1.068E+00
0.050	4.793E-12	8.141E-12	1.476E-11	1.760E+00	3.000	7.807E+03	8.350E+03	8.942E+03	1.071E+00
0.060	6.260E-11	9.356E-11	1.454E-10	1.543E+00	3.500	(9.103E+03)	(1.020E+04)	(1.554E+04)	(1.322E+00)
0.070	4.566E-10	6.545E-10	9.442E-10	1.444E+00	4.000	(9.677E+03)	(1.164E+04)	(2.532E+04)	(1.689E+00)
0.080	2.159E-09	3.078E-09	4.381E-09	1.427E+00	5.000	(9.837E+03)	(1.387E+04)	(4.824E+04)	(2.444E+00)
0.090	7.467E-09	1.065E-08	1.518E-08	1.430E+00	6.000	(9.008E+03)	(1.533E+04)	(7.333E+04)	(3.243E+00)
0.100	2.080E-08	2.955E-08	4.214E-08	1.427E+00	7.000	(7.532E+03)	(1.618E+04)	(9.847E+04)	(4.117E+00)
0.110	5.164E-08	7.152E-08	1.006E-07	1.399E+00	8.000	(5.671E+03)	(1.650E+04)	(1.219E+05)	(5.150E+00)
0.120	1.299E-07	1.692E-07	2.272E-07	1.327E+00	9.000	(3.628E+03)	(1.635E+04)	(1.422E+05)	(6.601E+00)
0.130	3.841E-07	4.562E-07	5.600E-07	1.214E+00	10.000	(1.579E+03)	(1.579E+04)	(1.579E+05)	(1.000E+01)

Note. Observed resonances: M. Anderson et al. (1980), P. M. Endt (1990), C. Iliadis et al. (1990), D. Powell et al. (1998), F. Strieder et al. (2012), J. Dermigny et al. (2016), and H. Zhang et al. (2023). Normalization: see Table 2. Unobserved resonances: C. Iliadis et al. (1996), and references therein. High-temperature rates (in parentheses): matching to statistical model rate above $T = 3.1$ GK. Previous rates: H. Zhang et al. (2023). Other: the results given in this table and Figures 83 and 84 correspond to the rates for populating the ground state (J^{π}=5^{+}) of ^{26}Al.

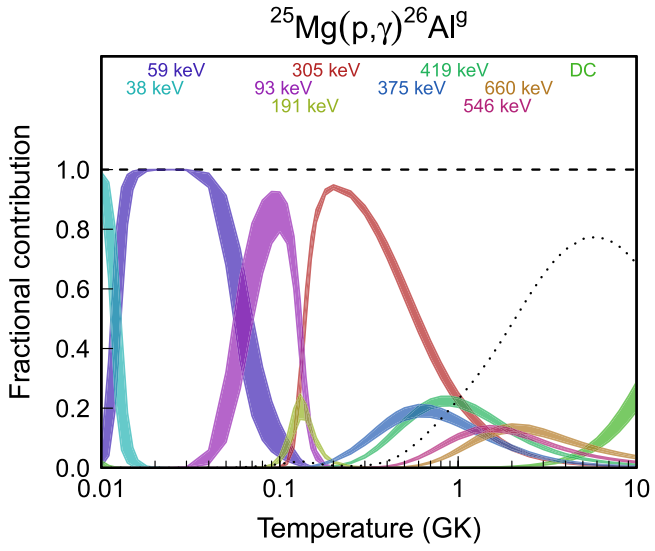

Figure 83. Fractional contributions to the total rate. "DC" refers to direct radiative capture. Resonance energies are given in the center-of-mass frame.

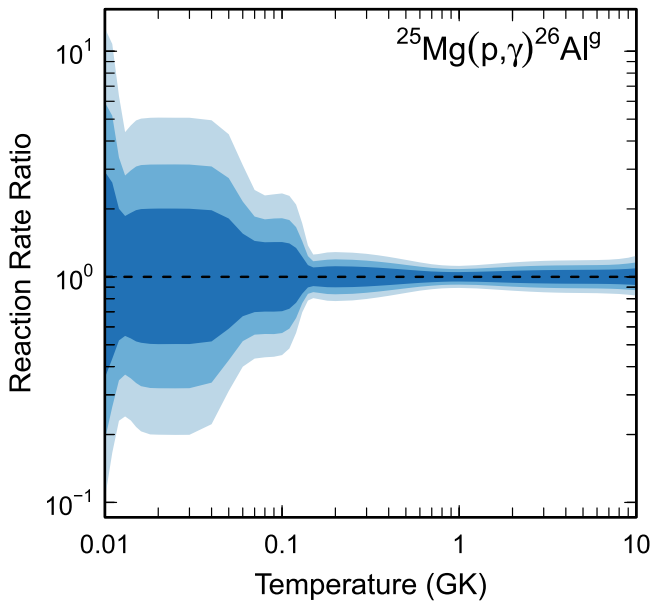

Figure 84. Reaction rate uncertainties versus temperature. The three different shades refer to coverage probabilities of 68%, 90%, and 98%.

Table 50
Total Laboratory Reaction Rates for ^{25}Mg(p,γ)^{26}Al^{m} (Population of the Isomeric State Only)

T (GK)	Low	Median	High	*f.u.*	T (GK)	Low	Median	High	*f.u.*
0.001	3.813E-86	4.961E-86	6.441E-86	1.302E+00	0.140	2.740E-07	3.273E-07	4.294E-07	1.279E+00
0.002	1.318E-66	1.715E-66	2.226E-66	1.302E+00	0.150	8.980E-07	1.005E-06	1.168E-06	1.160E+00
0.003	4.011E-57	5.219E-57	6.775E-57	1.302E+00	0.160	2.853E-06	3.137E-06	3.479E-06	1.109E+00
0.004	3.858E-51	5.020E-51	6.517E-51	1.302E+00	0.180	2.324E-05	2.553E-05	2.811E-05	1.100E+00
0.005	6.959E-47	9.054E-47	1.175E-46	1.302E+00	0.200	1.365E-04	1.504E-04	1.658E-04	1.102E+00
0.006	1.247E-43	1.619E-43	2.096E-43	1.298E+00	0.250	3.614E-03	3.963E-03	4.352E-03	1.097E+00
0.007	7.185E-41	1.029E-40	1.719E-40	1.626E+00	0.300	3.326E-02	3.620E-02	3.946E-02	1.090E+00
0.008	3.534E-38	8.891E-38	2.454E-37	2.595E+00	0.350	1.656E-01	1.793E-01	1.941E-01	1.083E+00
0.009	1.116E-35	3.258E-35	9.513E-35	2.905E+00	0.400	5.627E-01	6.062E-01	6.528E-01	1.077E+00
0.010	1.326E-33	3.869E-33	1.129E-32	2.903E+00	0.450	1.483E+00	1.592E+00	1.707E+00	1.073E+00
0.011	8.410E-32	2.104E-31	5.758E-31	2.604E+00	0.500	3.281E+00	3.506E+00	3.746E+00	1.069E+00
0.012	4.295E-30	8.468E-30	1.825E-29	2.112E+00	0.600	1.124E+01	1.195E+01	1.270E+01	1.063E+00
0.013	1.678E-28	3.054E-28	5.695E-28	1.862E+00	0.700	2.813E+01	2.985E+01	3.165E+01	1.061E+00
0.014	4.701E-27	8.650E-27	1.630E-26	1.873E+00	0.800	5.733E+01	6.081E+01	6.449E+01	1.061E+00
0.015	9.486E-26	1.801E-25	3.501E-25	1.932E+00	0.900	1.012E+02	1.075E+02	1.141E+02	1.062E+00
0.016	1.394E-24	2.704E-24	5.344E-24	1.968E+00	1.000	1.610E+02	1.713E+02	1.821E+02	1.064E+00
0.018	1.291E-22	2.547E-22	5.070E-22	1.992E+00	1.250	3.809E+02	4.068E+02	4.342E+02	1.068E+00
0.020	4.863E-21	9.600E-21	1.915E-20	1.996E+00	1.500	6.926E+02	7.416E+02	7.942E+02	1.071E+00
0.025	3.196E-18	6.308E-18	1.260E-17	1.997E+00	1.750	1.079E+03	1.158E+03	1.243E+03	1.073E+00
0.030	2.304E-16	4.537E-16	9.066E-16	1.995E+00	2.000	1.524E+03	1.637E+03	1.759E+03	1.075E+00
0.040	4.720E-14	9.023E-14	1.765E-13	1.941E+00	2.500	2.517E+03	2.708E+03	2.915E+03	1.076E+00
0.050	1.412E-12	2.451E-12	4.350E-12	1.770E+00	3.000	3.555E+03	3.828E+03	4.123E+03	1.077E+00
0.060	1.738E-11	2.871E-11	4.797E-11	1.668E+00	3.500	4.554E+03	4.907E+03	5.288E+03	1.078E+00
0.070	1.184E-10	1.979E-10	3.379E-10	1.699E+00	4.000	(5.012E+03)	(5.676E+03)	(8.875E+03)	(1.348E+00)
0.080	5.351E-10	9.218E-10	1.639E-09	1.764E+00	5.000	(5.026E+03)	(6.679E+03)	(1.983E+04)	(2.149E+00)
0.090	1.808E-09	3.185E-09	5.841E-09	1.808E+00	6.000	(4.527E+03)	(7.278E+03)	(3.185E+04)	(2.992E+00)
0.100	5.032E-09	8.870E-09	1.640E-08	1.813E+00	7.000	(3.708E+03)	(7.545E+03)	(4.363E+04)	(3.908E+00)
0.110	1.265E-08	2.148E-08	3.904E-08	1.759E+00	8.000	(2.718E+03)	(7.530E+03)	(5.412E+04)	(4.979E+00)
0.120	3.179E-08	4.937E-08	8.442E-08	1.635E+00	9.000	(1.674E+03)	(7.261E+03)	(6.240E+04)	(6.466E+00)
0.130	8.785E-08	1.192E-07	1.815E-07	1.456E+00	10.000	(6.768E+02)	(6.768E+03)	(6.768E+04)	(1.000E+01)

Note. Observed resonances: M. Anderson et al. (1980), P. M. Endt (1990), C. Iliadis et al. (1990), D. Powell et al. (1998), F. Strieder et al. (2012), J. Dermigny et al. (2016), and H. Zhang et al. (2023). Normalization: see Table 2. Unobserved resonances: C. Iliadis et al. (1996), and references therein. High-temperature rates (in parentheses): matching to statistical model rate above $T = 3.6$ GK. Previous rates: H. Zhang et al. (2023). Other: the results given in this table and Figures 85 and 86 correspond to the rates for populating the isomeric state at E_x= 228 keV (J^{π}=0^{+}) in ^{26}Al.

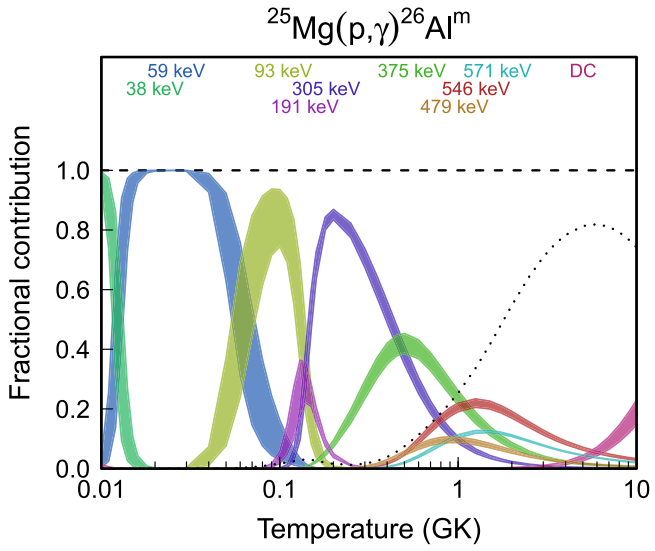

Figure 85. Fractional contributions to the total rate. "DC" refers to direct radiative capture. Resonance energies are given in the center-of-mass frame.

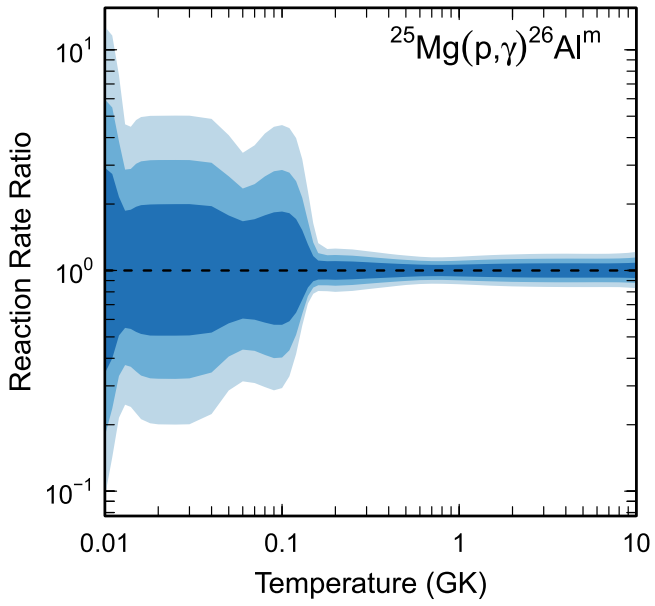

Figure 86. Reaction rate uncertainties versus temperature. The three different shades refer to coverage probabilities of 68%, 90%, and 98%.

Table 51
Total Laboratory Reaction Rates for ^{26}Mg(p,γ)^{27}Al

T (GK)	Low	Median	High	*f.u.*	T (GK)	Low	Median	High	*f.u.*
0.001	1.961E-85	2.926E-85	4.374E-85	1.498E+00	0.140	5.605E-06	6.649E-06	8.430E-06	1.252E+00
0.002	6.934E-66	1.034E-65	1.546E-65	1.498E+00	0.150	2.081E-05	2.319E-05	2.662E-05	1.147E+00
0.003	2.135E-56	3.184E-56	4.760E-56	1.498E+00	0.160	7.104E-05	7.675E-05	8.384E-05	1.092E+00
0.004	2.071E-50	3.087E-50	4.613E-50	1.497E+00	0.180	6.203E-04	6.564E-04	6.952E-04	1.059E+00
0.005	3.752E-46	5.594E-46	8.362E-46	1.498E+00	0.200	3.765E-03	3.967E-03	4.183E-03	1.054E+00
0.006	6.640E-43	9.903E-43	1.480E-42	1.498E+00	0.250	1.035E-01	1.090E-01	1.149E-01	1.054E+00
0.007	2.606E-40	3.888E-40	5.813E-40	1.498E+00	0.300	9.498E-01	1.000E+00	1.054E+00	1.054E+00
0.008	3.600E-38	5.369E-38	8.025E-38	1.498E+00	0.350	4.593E+00	4.835E+00	5.090E+00	1.053E+00
0.009	2.362E-36	3.512E-36	5.234E-36	1.494E+00	0.400	1.488E+01	1.564E+01	1.645E+01	1.051E+00
0.010	9.582E-35	1.487E-34	2.437E-34	1.666E+00	0.450	3.694E+01	3.877E+01	4.072E+01	1.050E+00
0.011	2.630E-33	5.071E-33	1.952E-32	2.771E+00	0.500	7.618E+01	7.983E+01	8.372E+01	1.048E+00
0.012	5.634E-32	1.745E-31	1.633E-30	4.785E+00	0.600	2.238E+02	2.339E+02	2.446E+02	1.046E+00
0.013	1.082E-30	6.574E-30	7.574E-29	6.792E+00	0.700	4.795E+02	5.000E+02	5.216E+02	1.043E+00
0.014	1.936E-29	1.728E-28	2.044E-27	8.070E+00	0.800	8.445E+02	8.793E+02	9.158E+02	1.042E+00
0.015	2.904E-28	3.016E-27	3.553E-26	8.672E+00	0.900	1.307E+03	1.360E+03	1.414E+03	1.040E+00
0.016	3.363E-27	3.711E-26	4.280E-25	8.902E+00	1.000	1.852E+03	1.924E+03	2.000E+03	1.039E+00
0.018	2.123E-25	2.367E-24	2.684E-23	8.959E+00	1.250	3.476E+03	3.607E+03	3.744E+03	1.038E+00
0.020	5.887E-24	6.560E-23	7.257E-22	8.886E+00	1.500	5.351E+03	5.553E+03	5.765E+03	1.038E+00
0.025	2.307E-21	2.663E-20	2.819E-19	8.868E+00	1.750	7.399E+03	7.683E+03	7.984E+03	1.039E+00
0.030	1.399E-19	1.789E-18	2.091E-17	1.000E+01	2.000	9.601E+03	9.980E+03	1.038E+04	1.040E+00
0.040	7.615E-17	1.668E-15	2.314E-14	1.359E+01	2.500	1.452E+04	1.512E+04	1.576E+04	1.042E+00
0.050	1.660E-14	2.240E-13	3.407E-12	1.130E+01	3.000	2.030E+04	2.116E+04	2.208E+04	1.043E+00
0.060	1.096E-12	8.087E-12	1.018E-10	8.032E+00	3.500	2.704E+04	2.823E+04	2.948E+04	1.044E+00
0.070	2.850E-11	1.228E-10	1.192E-09	5.630E+00	4.000	3.471E+04	3.627E+04	3.790E+04	1.045E+00
0.080	3.740E-10	1.179E-09	7.672E-09	4.102E+00	5.000	(4.928E+04)	(5.796E+04)	(1.250E+05)	(1.667E+00)
0.090	3.015E-09	7.811E-09	3.362E-08	3.148E+00	6.000	(5.944E+04)	(8.490E+04)	(3.163E+05)	(2.577E+00)
0.100	1.745E-08	3.814E-08	1.155E-07	2.514E+00	7.000	(6.321E+04)	(1.149E+05)	(6.083E+05)	(3.556E+00)
0.110	8.232E-08	1.515E-07	3.462E-07	2.052E+00	8.000	(5.892E+04)	(1.473E+05)	(1.011E+06)	(4.681E+00)
0.120	3.495E-07	5.401E-07	9.743E-07	1.698E+00	9.000	(4.527E+04)	(1.811E+05)	(1.527E+06)	(6.215E+00)
0.130	1.423E-06	1.883E-06	2.790E-06	1.432E+00	10.000	(2.160E+04)	(2.160E+05)	(2.160E+06)	(1.000E+01)

Note. Observed resonances: C. Iliadis et al. (1990), B. Limata et al. (2010), and H. Zhang et al. (2021). Normalization: see Table 2. Unobserved resonances: A. Champagne et al. (1990). High-temperature rates (in parentheses): matching to statistical model rate above $T = 4.3$ GK. Previous rates: C. Iliadis et al. (2001, 2010c). Other: the proton widths of threshold levels were obtained by reanalyzing the ^{26}Mg(^{3}He,d) data of A. Champagne et al. (1990).

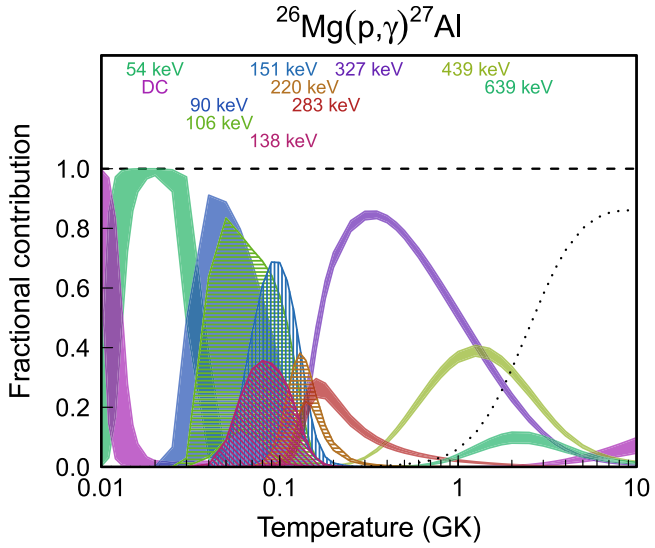

Figure 87. Fractional contributions to the total rate. "DC" refers to direct radiative capture. Resonance energies are given in the center-of-mass frame.

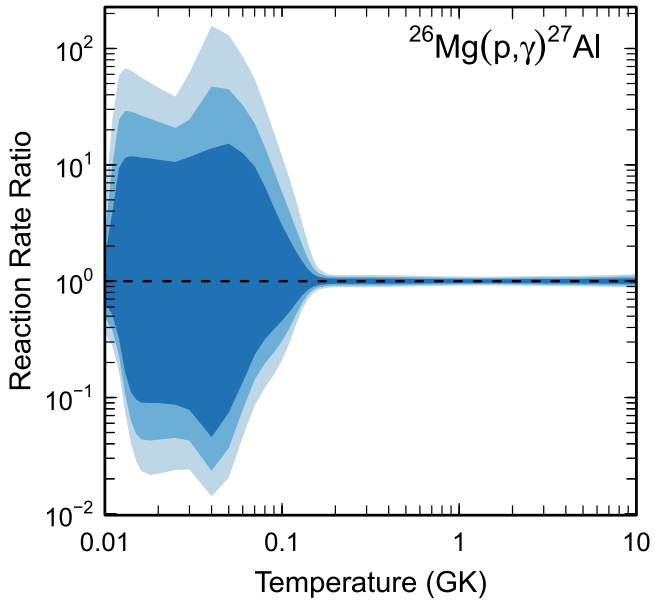

Figure 88. Reaction rate uncertainties versus temperature. The three different shades refer to coverage probabilities of 68%, 90%, and 98%.

Table 52
Total Laboratory Reaction Rates for ^{23}Al(p,γ)^{24}Si

T (GK)	Low	Median	High	*f.u.*	T (GK)	Low	Median	High	*f.u.*
0.001	1.061E-91	1.377E-91	1.788E-91	1.301E+00	0.140	1.562E-04	2.476E-04	3.940E-04	1.595E+00
0.002	6.125E-71	7.956E-71	1.033E-70	1.301E+00	0.150	3.472E-04	5.533E-04	8.841E-04	1.604E+00
0.003	6.198E-61	8.050E-61	1.045E-60	1.301E+00	0.160	6.921E-04	1.111E-03	1.787E-03	1.615E+00
0.004	1.260E-54	1.637E-54	2.125E-54	1.301E+00	0.180	2.147E-03	3.499E-03	5.712E-03	1.639E+00
0.005	3.874E-50	5.032E-50	6.532E-50	1.301E+00	0.200	5.210E-03	8.608E-03	1.426E-02	1.663E+00
0.006	1.027E-46	1.334E-46	1.731E-46	1.301E+00	0.250	2.418E-02	4.146E-02	7.071E-02	1.717E+00
0.007	6.622E-44	8.934E-44	1.297E-43	1.505E+00	0.300	6.396E-02	1.126E-01	1.964E-01	1.760E+00
0.008	1.198E-41	1.619E-41	2.367E-41	1.514E+00	0.350	1.231E-01	2.214E-01	3.939E-01	1.794E+00
0.009	9.699E-40	1.313E-39	1.934E-39	1.523E+00	0.400	1.960E-01	3.583E-01	6.470E-01	1.822E+00
0.010	4.272E-38	5.795E-38	8.591E-38	1.533E+00	0.450	2.756E-01	5.100E-01	9.323E-01	1.844E+00
0.011	1.170E-36	1.589E-36	2.372E-36	1.542E+00	0.500	3.562E-01	6.655E-01	1.228E+00	1.862E+00
0.012	2.190E-35	2.982E-35	4.481E-35	1.552E+00	0.600	5.041E-01	9.568E-01	1.790E+00	1.890E+00
0.013	3.008E-34	4.105E-34	6.209E-34	1.561E+00	0.700	6.234E-01	1.197E+00	2.262E+00	1.911E+00
0.014	3.196E-33	4.371E-33	6.660E-33	1.571E+00	0.800	7.130E-01	1.380E+00	2.625E+00	1.925E+00
0.015	2.739E-32	3.752E-32	5.758E-32	1.581E+00	0.900	7.778E-01	1.511E+00	2.890E+00	1.933E+00
0.016	1.953E-31	2.681E-31	4.149E-31	1.592E+00	1.000	(9.010E-01)	(1.758E+00)	(3.419E+00)	(1.948E+00)
0.018	6.322E-30	8.702E-30	1.370E-29	1.613E+00	1.250	(1.671E+00)	(3.334E+00)	(7.231E+00)	(2.082E+00)
0.020	1.264E-28	1.748E-28	2.803E-28	1.634E+00	1.500	(3.030E+00)	(6.187E+00)	(1.480E+01)	(2.217E+00)
0.025	5.117E-26	7.180E-26	1.212E-25	1.694E+00	1.750	(4.300E+00)	(8.990E+00)	(2.352E+01)	(2.354E+00)
0.030	5.698E-24	8.553E-24	1.712E-23	1.875E+00	2.000	(6.020E+00)	(1.290E+01)	(3.663E+01)	(2.491E+00)
0.040	8.069E-19	2.865E-18	9.991E-18	3.524E+00	2.500	(9.406E+00)	(2.119E+01)	(6.967E+01)	(2.770E+00)
0.050	1.060E-14	2.766E-14	7.049E-14	2.588E+00	3.000	(1.288E+01)	(3.060E+01)	(1.143E+02)	(3.055E+00)
0.060	5.575E-12	1.196E-11	2.508E-11	2.132E+00	3.500	(1.627E+01)	(4.089E+01)	(1.710E+02)	(3.348E+00)
0.070	4.642E-10	8.808E-10	1.638E-09	1.885E+00	4.000	(1.948E+01)	(5.194E+01)	(2.405E+02)	(3.648E+00)
0.080	1.230E-08	2.153E-08	3.719E-08	1.745E+00	5.000	(2.514E+01)	(7.634E+01)	(4.218E+02)	(4.281E+00)
0.090	1.522E-07	2.530E-07	4.193E-07	1.664E+00	6.000	(2.951E+01)	(1.041E+02)	(6.684E+02)	(4.974E+00)
0.100	1.109E-06	1.785E-06	2.890E-06	1.620E+00	7.000	(3.228E+01)	(1.359E+02)	(9.939E+02)	(5.762E+00)
0.110	5.495E-06	8.737E-06	1.391E-05	1.597E+00	8.000	(3.305E+01)	(1.724E+02)	(1.415E+03)	(6.713E+00)
0.120	2.049E-05	3.240E-05	5.133E-05	1.589E+00	9.000	(3.135E+01)	(2.149E+02)	(1.957E+03)	(7.981E+00)
0.130	6.159E-05	9.723E-05	1.541E-04	1.589E+00	10.000	(2.658E+01)	(2.658E+02)	(2.658E+03)	(1.000E+01)

Note. Observed resonances: none. Normalization: none. Unobserved resonances: A. Banu et al. (2011), C. Wolf et al. (2019), and G. Lotay et al. (2022). High-temperature rates (in parentheses): matching to statistical model rate above $T = 0.97$ GK. Previous rates: H. Herndl et al. (1995) and A. Banu et al. (2011) Other: excitation energies were adopted from M. S. Basunia & A. Chakraborty (2022).

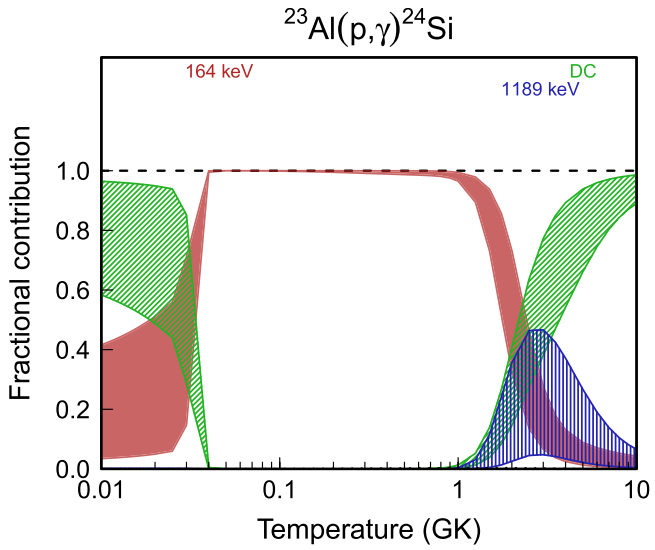

Figure 89. Fractional contributions to the total rate. "DC" refers to direct radiative capture. Resonance energies are given in the center-of-mass frame.

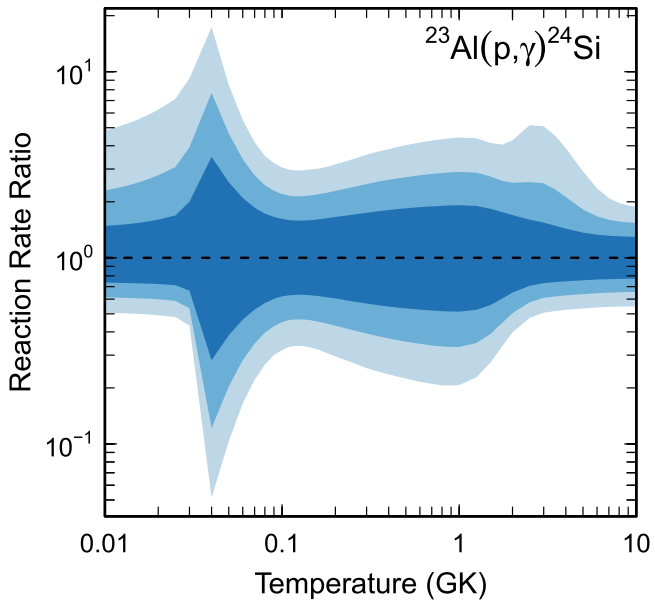

Figure 90. Reaction rate uncertainties versus temperature. The three different shades refer to coverage probabilities of 68%, 90%, and 98%.

Table 53
Total Laboratory Reaction Rates for ^{24}Al(p,γ)^{25}Si

T (GK)	Low	Median	High	*f.u.*	T (GK)	Low	Median	High	*f.u.*
0.001	1.619E-91	8.197E-91	4.036E-90	5.068E+00	0.140	3.609E-08	2.920E-07	2.103E-06	7.883E+00
0.002	6.588E-71	3.335E-70	1.642E-69	5.068E+00	0.150	1.522E-07	1.186E-06	7.907E-06	7.352E+00
0.003	6.652E-61	3.367E-60	1.658E-59	5.068E+00	0.160	5.346E-07	4.053E-06	2.551E-05	6.949E+00
0.004	1.365E-54	6.910E-54	3.403E-53	5.068E+00	0.180	4.322E-06	3.084E-05	1.762E-04	6.373E+00
0.005	4.224E-50	2.138E-49	1.053E-48	5.068E+00	0.200	2.312E-05	1.558E-04	8.262E-04	5.962E+00
0.006	1.126E-46	5.698E-46	2.806E-45	5.068E+00	0.250	4.749E-04	2.814E-03	1.339E-02	5.238E+00
0.007	6.323E-44	3.165E-43	1.597E-42	5.982E+00	0.300	3.701E-03	1.925E-02	8.455E-02	4.718E+00
0.008	1.143E-41	5.734E-41	2.903E-40	6.091E+00	0.350	1.656E-02	7.655E-02	3.115E-01	4.318E+00
0.009	9.265E-40	4.643E-39	2.359E-38	6.198E+00	0.400	5.150E-02	2.158E-01	8.256E-01	4.005E+00
0.010	4.079E-38	2.047E-37	1.043E-36	6.306E+00	0.450	1.265E-01	4.870E-01	1.754E+00	3.755E+00
0.011	1.116E-36	5.609E-36	2.869E-35	6.417E+00	0.500	(2.595E-01)	(9.354E-01)	(3.212E+00)	(3.519E+00)
0.012	2.089E-35	1.051E-34	5.396E-34	6.533E+00	0.600	(6.873E-01)	(2.494E+00)	(8.737E+00)	(3.566E+00)
0.013	2.867E-34	1.444E-33	7.453E-33	6.653E+00	0.700	(1.411E+00)	(5.156E+00)	(1.842E+01)	(3.613E+00)
0.014	3.046E-33	1.535E-32	7.953E-32	6.778E+00	0.800	(2.456E+00)	(9.035E+00)	(3.290E+01)	(3.660E+00)
0.015	2.608E-32	1.315E-31	6.875E-31	6.911E+00	0.900	(3.813E+00)	(1.413E+01)	(5.241E+01)	(3.707E+00)
0.016	1.858E-31	9.393E-31	4.921E-30	7.051E+00	1.000	(5.459E+00)	(2.036E+01)	(7.696E+01)	(3.755E+00)
0.018	6.003E-30	3.040E-29	1.613E-28	7.351E+00	1.250	(9.523E+00)	(3.615E+01)	(1.429E+02)	(3.874E+00)
0.020	1.196E-28	6.083E-28	3.259E-27	7.674E+00	1.500	(1.661E+01)	(6.419E+01)	(2.648E+02)	(3.995E+00)
0.025	4.794E-26	2.462E-25	1.354E-24	8.566E+00	1.750	(2.212E+01)	(8.707E+01)	(3.742E+02)	(4.117E+00)
0.030	4.650E-24	2.400E-23	1.375E-22	9.523E+00	2.000	(2.944E+01)	(1.181E+02)	(5.278E+02)	(4.240E+00)
0.040	3.670E-21	1.937E-20	1.208E-19	1.177E+01	2.500	(4.145E+01)	(1.727E+02)	(8.316E+02)	(4.491E+00)
0.050	4.276E-19	2.319E-18	1.663E-17	1.455E+01	3.000	(5.183E+01)	(2.247E+02)	(1.160E+03)	(4.748E+00)
0.060	1.693E-17	9.307E-17	8.117E-16	1.768E+01	3.500	(6.056E+01)	(2.735E+02)	(1.506E+03)	(5.012E+00)
0.070	4.751E-16	2.401E-15	2.445E-14	1.913E+01	4.000	(6.789E+01)	(3.202E+02)	(1.874E+03)	(5.284E+00)
0.080	1.358E-14	7.328E-14	1.082E-12	1.802E+01	5.000	(7.961E+01)	(4.117E+02)	(2.694E+03)	(5.858E+00)
0.090	3.473E-13	2.445E-12	4.056E-11	1.569E+01	6.000	(8.940E+01)	(5.117E+02)	(3.703E+03)	(6.480E+00)
0.100	6.903E-12	5.973E-11	8.141E-10	1.317E+01	7.000	(9.889E+01)	(6.338E+02)	(5.024E+03)	(7.168E+00)
0.110	9.840E-11	8.890E-10	9.815E-09	1.112E+01	8.000	(1.088E+02)	(7.920E+02)	(6.825E+03)	(7.949E+00)
0.120	9.714E-10	8.485E-09	7.878E-08	9.641E+00	9.000	(1.187E+02)	(1.000E+03)	(9.310E+03)	(8.868E+00)
0.130	6.804E-09	5.700E-08	4.622E-07	8.612E+00	10.000	(1.271E+02)	(1.271E+03)	(1.271E+04)	(1.000E+01)

Note. Observed resonances: none. Normalization: none. Unobserved resonances: B. Longfellow et al. (2018). High-temperature rates (in parentheses): matching to statistical model rate above $T = 0.50$ GK. Previous rates: H. Herndl et al. (1995). Other: with the exception of the 281 keV resonance, all C^2S values were taken from H. Herndl et al. (1995) and assigned to states observed by B. Longfellow et al. (2018). The C^2S value of the 281 keV resonance was adopted from B. Longfellow et al. (2018).

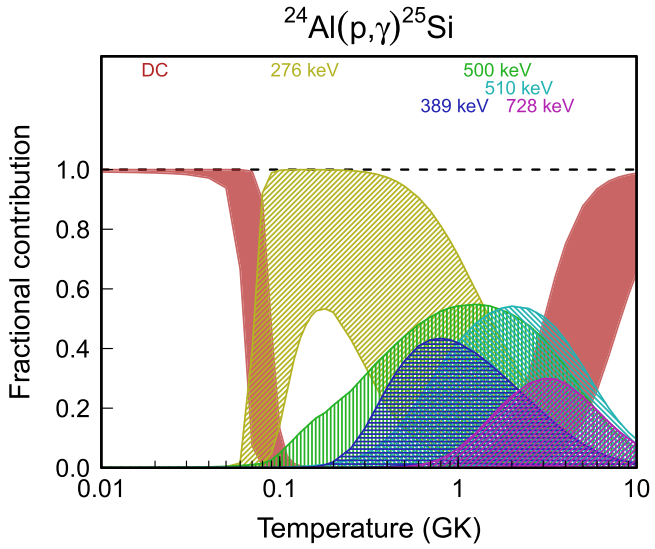

Figure 91. Fractional contributions to the total rate. "DC" refers to direct radiative capture. Resonance energies are given in the center-of-mass frame.

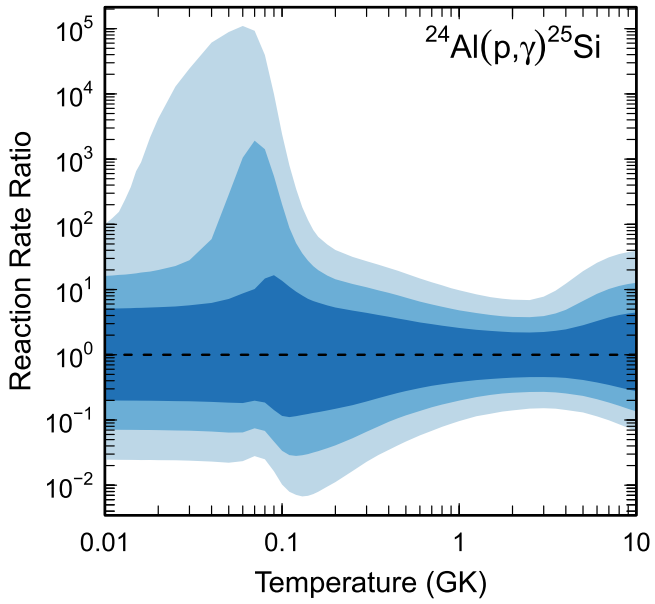

Figure 92. Reaction rate uncertainties versus temperature. The three different shades refer to coverage probabilities of 68%, 90%, and 98%.

Table 54
Total Laboratory Reaction Rates for ^{25}Al(p,γ)^{26}Si

T (GK)	Low	Median	High	*f.u.*	T (GK)	Low	Median	High	*f.u.*
0.001	5.726E-91	7.425E-91	9.670E-91	1.300E+00	0.140	1.380E-09	7.214E-09	4.149E-08	5.254E+00
0.002	2.389E-70	3.097E-70	4.034E-70	1.300E+00	0.150	3.798E-09	1.680E-08	9.311E-08	4.687E+00
0.003	2.441E-60	3.165E-60	4.123E-60	1.300E+00	0.160	1.208E-08	3.792E-08	1.908E-07	3.894E+00
0.004	5.047E-54	6.544E-54	8.524E-54	1.300E+00	0.180	1.489E-07	2.561E-07	7.251E-07	2.469E+00
0.005	1.570E-49	2.036E-49	2.652E-49	1.300E+00	0.200	1.429E-06	2.123E-06	3.543E-06	1.758E+00
0.006	4.200E-46	5.446E-46	7.093E-46	1.300E+00	0.250	1.038E-04	1.484E-04	2.137E-04	1.440E+00
0.007	2.304E-43	2.984E-43	3.885E-43	1.298E+00	0.300	1.893E-03	2.721E-03	3.930E-03	1.442E+00
0.008	4.174E-41	5.408E-41	7.039E-41	1.298E+00	0.350	1.481E-02	2.136E-02	3.096E-02	1.446E+00
0.009	3.383E-39	4.382E-39	5.704E-39	1.298E+00	0.400	6.773E-02	9.776E-02	1.419E-01	1.449E+00
0.010	1.490E-37	1.930E-37	2.513E-37	1.298E+00	0.450	2.166E-01	3.129E-01	4.548E-01	1.450E+00
0.011	4.079E-36	5.283E-36	6.877E-36	1.298E+00	0.500	5.403E-01	7.809E-01	1.136E+00	1.451E+00
0.012	7.632E-35	9.885E-35	1.287E-34	1.298E+00	0.600	2.056E+00	2.973E+00	4.326E+00	1.452E+00
0.013	1.047E-33	1.356E-33	1.766E-33	1.298E+00	0.700	5.175E+00	7.470E+00	1.087E+01	1.451E+00
0.014	1.111E-32	1.440E-32	1.874E-32	1.298E+00	0.800	1.011E+01	1.457E+01	2.117E+01	1.448E+00
0.015	9.505E-32	1.231E-31	1.602E-31	1.298E+00	0.900	1.681E+01	2.412E+01	3.495E+01	1.443E+00
0.016	6.764E-31	8.761E-31	1.140E-30	1.298E+00	1.000	2.500E+01	3.569E+01	5.151E+01	1.437E+00
0.018	2.178E-29	2.821E-29	3.671E-29	1.298E+00	1.250	5.013E+01	7.059E+01	1.004E+02	1.417E+00
0.020	4.331E-28	5.609E-28	7.299E-28	1.298E+00	1.500	7.902E+01	1.094E+02	1.532E+02	1.394E+00
0.025	1.726E-25	2.235E-25	2.909E-25	1.298E+00	1.750	1.089E+02	1.489E+02	2.049E+02	1.375E+00
0.030	1.658E-23	2.146E-23	2.792E-23	1.298E+00	2.000	1.382E+02	1.867E+02	2.540E+02	1.359E+00
0.040	1.305E-20	1.690E-20	2.205E-20	1.303E+00	2.500	1.929E+02	2.561E+02	3.422E+02	1.336E+00
0.050	1.930E-18	2.920E-18	6.928E-18	2.177E+00	3.000	2.418E+02	3.162E+02	4.169E+02	1.318E+00
0.060	1.314E-16	4.276E-16	2.179E-15	3.945E+00	3.500	2.868E+02	3.698E+02	4.819E+02	1.302E+00
0.070	5.600E-15	2.714E-14	1.538E-13	4.962E+00	4.000	3.296E+02	4.189E+02	5.395E+02	1.287E+00
0.080	1.186E-13	6.396E-13	3.701E-12	5.377E+00	5.000	(4.683E+02)	(6.492E+02)	(1.422E+03)	(1.788E+00)
0.090	1.329E-12	7.417E-12	4.317E-11	5.547E+00	6.000	(6.247E+02)	(1.046E+03)	(3.926E+03)	(2.714E+00)
0.100	9.199E-12	5.198E-11	3.035E-10	5.616E+00	7.000	(7.387E+02)	(1.563E+03)	(8.304E+03)	(3.715E+00)
0.110	4.452E-11	2.526E-10	1.474E-09	5.636E+00	8.000	(7.895E+02)	(2.265E+03)	(1.558E+04)	(4.873E+00)
0.120	1.651E-10	9.340E-10	5.445E-09	5.618E+00	9.000	(7.288E+02)	(3.250E+03)	(2.742E+04)	(6.449E+00)
0.130	5.047E-10	2.805E-09	1.630E-08	5.527E+00	10.000	(4.634E+02)	(4.634E+03)	(4.634E+04)	(1.000E+01)

Note. Observed resonances: none. Normalization: none. Unobserved resonances: J.-C. Thomas et al. (2004), P. N. Peplowski et al. (2009), D. Pérez-Loureiro et al. (2016), P. F. Liang et al. (2020), J. F. Perello et al. (2022), and E. Temanson et al. (2023). High-temperature rates (in parentheses): matching to statistical model rate above $T = 4.4$ GK. Previous rates: A. M. Laird et al. (2023). Other: values of C^2S were taken from mirror studies (M. Burlein et al. 1984; H. Arciszewski et al. 1984; C. B. Hamill et al. 2020). The γ-ray partial widths were estimated from the mirror-state lifetimes (F. Glatz et al. 1986; L. Canete et al. 2021). The branching ratio for the 5929 → 4188 keV transition has been adopted from C. Wrede (2009). Shell model calculations were taken from W. A. Richter et al. (2011). All energies are from M. Basunia & A. Hurst (2016).

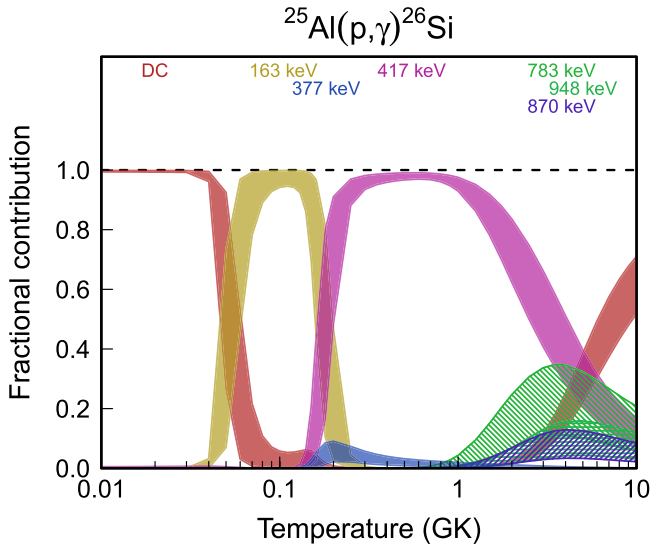

Figure 93. Fractional contributions to the total rate. "DC" refers to direct radiative capture. Resonance energies are given in the center-of-mass frame.

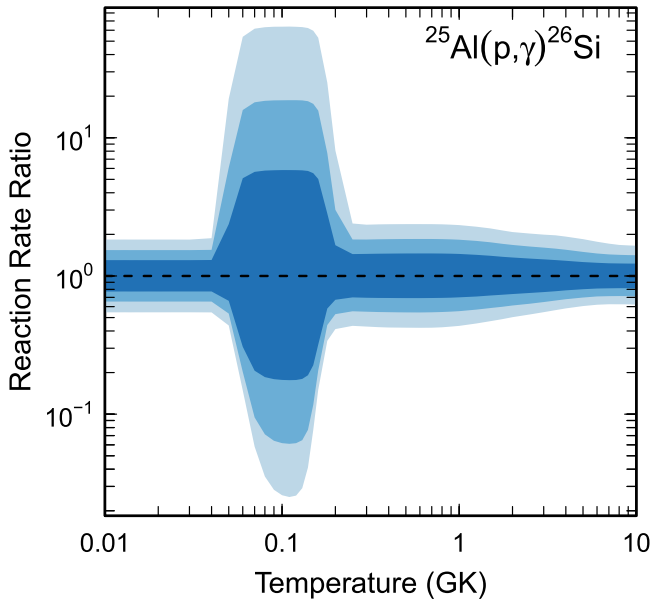

Figure 94. Reaction rate uncertainties versus temperature. The three different shades refer to coverage probabilities of 68%, 90%, and 98%.

Table 55
Total Laboratory Reaction Rates for ^{26}Al(p,γ)^{27}Si

T (GK)	Low	Median	High	*f.u.*	T (GK)	Low	Median	High	*f.u.*
0.001	2.650E-89	5.069E-88	5.712E-87	1.364E+01	0.140	1.905E-05	2.342E-05	2.948E-05	1.267E+00
0.002	4.537E-70	8.581E-70	8.902E-69	5.365E+00	0.150	4.939E-05	6.000E-05	7.404E-05	1.237E+00
0.003	3.574E-60	5.000E-60	6.999E-60	1.424E+00	0.160	1.154E-04	1.387E-04	1.684E-04	1.216E+00
0.004	7.388E-54	1.031E-53	1.437E-53	1.401E+00	0.180	4.967E-04	5.846E-04	6.924E-04	1.184E+00
0.005	2.310E-49	3.224E-49	4.493E-49	1.401E+00	0.200	1.700E-03	1.962E-03	2.277E-03	1.159E+00
0.006	6.205E-46	8.658E-46	1.207E-45	1.401E+00	0.250	1.945E-02	2.174E-02	2.439E-02	1.121E+00
0.007	3.399E-43	4.742E-43	6.610E-43	1.401E+00	0.300	1.219E-01	1.351E-01	1.499E-01	1.110E+00
0.008	6.175E-41	8.616E-41	1.201E-40	1.401E+00	0.350	5.040E-01	5.592E-01	6.204E-01	1.111E+00
0.009	5.015E-39	6.998E-39	9.754E-39	1.401E+00	0.400	1.529E+00	1.703E+00	1.899E+00	1.116E+00
0.010	2.213E-37	3.088E-37	4.304E-37	1.401E+00	0.450	3.679E+00	4.120E+00	4.623E+00	1.122E+00
0.011	6.070E-36	8.469E-36	1.180E-35	1.401E+00	0.500	7.458E+00	8.390E+00	9.459E+00	1.128E+00
0.012	1.144E-34	1.595E-34	2.219E-34	1.399E+00	0.600	2.140E+01	2.424E+01	2.752E+01	1.135E+00
0.013	1.636E-33	2.287E-33	3.199E-33	1.408E+00	0.700	4.488E+01	5.100E+01	5.816E+01	1.140E+00
0.014	1.958E-32	2.810E-32	4.303E-32	1.586E+00	0.800	7.743E+01	8.811E+01	1.006E+02	1.141E+00
0.015	2.062E-31	3.299E-31	7.488E-31	2.118E+00	0.900	1.178E+02	1.339E+02	1.529E+02	1.141E+00
0.016	1.996E-30	4.188E-30	1.528E-29	2.871E+00	1.000	1.646E+02	1.868E+02	2.129E+02	1.138E+00
0.018	1.781E-28	6.693E-28	3.181E-27	4.060E+00	1.250	3.042E+02	3.417E+02	3.858E+02	1.127E+00
0.020	1.222E-26	5.217E-26	2.466E-25	4.404E+00	1.500	4.674E+02	5.188E+02	5.786E+02	1.114E+00
0.025	4.627E-23	2.004E-22	8.787E-22	4.416E+00	1.750	6.441E+02	7.073E+02	7.802E+02	1.102E+00
0.030	1.515E-20	7.120E-20	3.662E-19	5.025E+00	2.000	(8.919E+02)	(9.967E+02)	(1.294E+03)	(1.208E+00)
0.040	7.199E-17	2.668E-16	1.569E-15	4.820E+00	2.500	(1.352E+03)	(1.600E+03)	(2.947E+03)	(1.513E+00)
0.050	3.525E-14	1.095E-13	4.001E-13	3.570E+00	3.000	(1.765E+03)	(2.218E+03)	(5.294E+03)	(1.822E+00)
0.060	2.764E-12	7.956E-12	2.390E-11	3.015E+00	3.500	(2.107E+03)	(2.825E+03)	(8.277E+03)	(2.135E+00)
0.070	7.080E-11	1.865E-10	5.173E-10	2.702E+00	4.000	(2.377E+03)	(3.414E+03)	(1.186E+04)	(2.455E+00)
0.080	1.010E-09	2.219E-09	5.639E-09	2.349E+00	5.000	(2.729E+03)	(4.573E+03)	(2.086E+04)	(3.119E+00)
0.090	1.032E-08	1.793E-08	3.935E-08	1.985E+00	6.000	(2.881E+03)	(5.791E+03)	(3.272E+04)	(3.830E+00)
0.100	7.767E-08	1.130E-07	2.055E-07	1.700E+00	7.000	(2.859E+03)	(7.183E+03)	(4.839E+04)	(4.625E+00)
0.110	4.313E-07	5.739E-07	8.821E-07	1.507E+00	8.000	(2.643E+03)	(8.849E+03)	(6.924E+04)	(5.586E+00)
0.120	1.851E-06	2.359E-06	3.250E-06	1.387E+00	9.000	(2.169E+03)	(1.088E+04)	(9.696E+04)	(6.964E+00)
0.130	6.454E-06	8.045E-06	1.044E-05	1.313E+00	10.000	(1.334E+03)	(1.334E+04)	(1.334E+05)	(1.000E+01)

Note. Observed resonances: L. Buchmann et al. (1984), R. B. Vogelaar (1989), and C. Ruiz et al. (2006). Normalization: L. Buchmann et al. (1984), R. B. Vogelaar (1989), and C. Ruiz et al. (2006). Unobserved resonances: R. B. Vogelaar et al. (1996), V. Margerin et al. (2015), and G. Lotay et al. (2020). High-temperature rates (in parentheses): matching to statistical model rate above $T = 1.8$ GK. Previous rates: C. Iliadis et al. (2010c). Other: as is the case for all other reactions presented in this evaluation, the results given in this table and Figures 95 and 96 correspond to the rate assuming the target, ^{26}Al, is in its ground state.

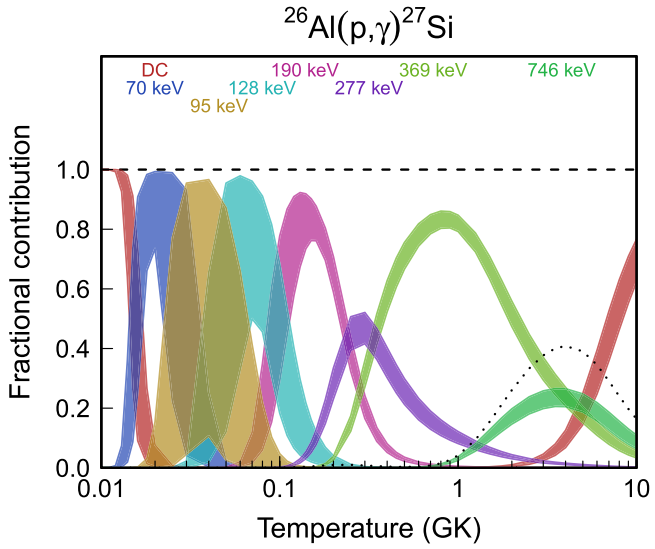

Figure 95. Fractional contributions to the total rate. "DC" refers to direct radiative capture. Resonance energies are given in the center-of-mass frame.

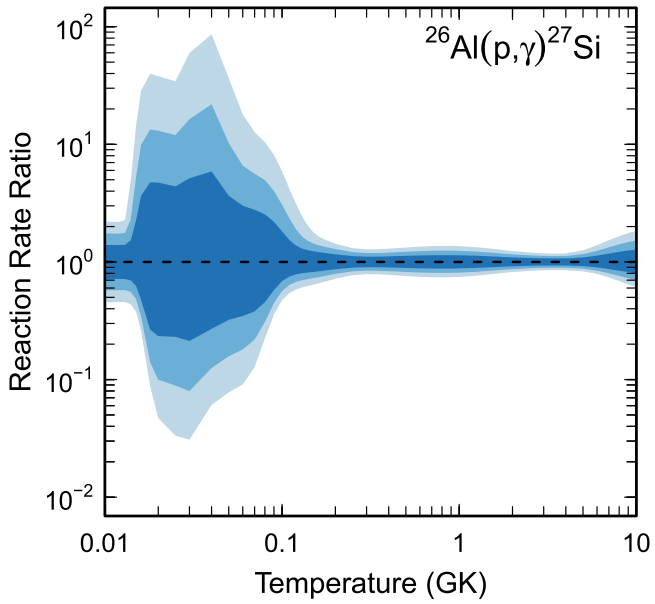

Figure 96. Reaction rate uncertainties versus temperature. The three different shades refer to coverage probabilities of 68%, 90%, and 98%.

Table 56
Total Laboratory Reaction Rates for ^{27}Al(p,γ)^{28}Si

T (GK)	Low	Median	High	*f.u.*	T (GK)	Low	Median	High	*f.u.*
0.001	1.186E-90	2.012E-90	3.396E-90	1.698E+00	0.140	4.493E-06	5.031E-06	5.734E-06	1.163E+00
0.002	5.180E-70	8.786E-70	1.483E-69	1.698E+00	0.150	1.268E-05	1.417E-05	1.610E-05	1.157E+00
0.003	5.411E-60	9.178E-60	1.549E-59	1.698E+00	0.160	3.146E-05	3.509E-05	3.977E-05	1.153E+00
0.004	1.134E-53	1.924E-53	3.247E-53	1.698E+00	0.180	1.444E-04	1.605E-04	1.807E-04	1.143E+00
0.005	3.563E-49	6.044E-49	1.020E-48	1.698E+00	0.200	4.983E-04	5.512E-04	6.176E-04	1.134E+00
0.006	9.603E-46	1.629E-45	2.749E-45	1.698E+00	0.250	5.146E-03	5.637E-03	6.251E-03	1.120E+00
0.007	5.325E-43	9.002E-43	1.515E-42	1.692E+00	0.300	2.826E-02	3.082E-02	3.422E-02	1.131E+00
0.008	9.700E-41	1.640E-40	2.759E-40	1.692E+00	0.350	1.073E-01	1.169E-01	1.307E-01	1.151E+00
0.009	7.896E-39	1.334E-38	2.245E-38	1.691E+00	0.400	3.194E-01	3.474E-01	3.911E-01	1.164E+00
0.010	3.492E-37	5.899E-37	9.926E-37	1.691E+00	0.450	7.984E-01	8.671E-01	9.759E-01	1.166E+00
0.011	9.592E-36	1.620E-35	2.725E-35	1.691E+00	0.500	1.754E+00	1.902E+00	2.131E+00	1.161E+00
0.012	1.802E-34	3.042E-34	5.115E-34	1.690E+00	0.600	6.409E+00	6.914E+00	7.635E+00	1.139E+00
0.013	2.507E-33	4.221E-33	7.072E-33	1.684E+00	0.700	1.793E+01	1.927E+01	2.100E+01	1.116E+00
0.014	2.859E-32	4.746E-32	7.875E-32	1.669E+00	0.800	4.137E+01	4.431E+01	4.786E+01	1.098E+00
0.015	2.924E-31	4.908E-31	8.523E-31	1.761E+00	0.900	8.249E+01	8.811E+01	9.468E+01	1.085E+00
0.016	2.775E-30	5.073E-30	1.103E-29	2.149E+00	1.000	1.469E+02	1.567E+02	1.677E+02	1.077E+00
0.018	2.131E-28	6.102E-28	2.368E-27	3.299E+00	1.250	4.398E+02	4.679E+02	4.986E+02	1.067E+00
0.020	1.363E-26	5.131E-26	2.202E-25	3.904E+00	1.500	9.565E+02	1.017E+03	1.081E+03	1.064E+00
0.025	5.323E-23	1.895E-22	7.820E-22	3.900E+00	1.750	1.713E+03	1.820E+03	1.934E+03	1.063E+00
0.030	1.465E-20	5.083E-20	1.794E-19	3.654E+00	2.000	2.700E+03	2.867E+03	3.046E+03	1.062E+00
0.040	1.610E-17	5.949E-17	1.743E-16	3.446E+00	2.500	5.250E+03	5.572E+03	5.916E+03	1.062E+00
0.050	1.046E-15	4.043E-15	1.273E-14	3.458E+00	3.000	8.314E+03	8.826E+03	9.373E+03	1.062E+00
0.060	2.136E-14	7.155E-14	2.275E-13	3.002E+00	3.500	1.161E+04	1.232E+04	1.309E+04	1.062E+00
0.070	9.666E-13	1.401E-12	2.635E-12	1.633E+00	4.000	1.491E+04	1.584E+04	1.683E+04	1.063E+00
0.080	3.911E-11	4.611E-11	5.589E-11	1.231E+00	5.000	2.104E+04	2.239E+04	2.386E+04	1.065E+00
0.090	7.804E-10	8.947E-10	1.049E-09	1.203E+00	6.000	2.619E+04	2.796E+04	2.994E+04	1.070E+00
0.100	8.803E-09	1.002E-08	1.164E-08	1.192E+00	7.000	3.029E+04	3.247E+04	3.502E+04	1.078E+00
0.110	6.415E-08	7.259E-08	8.381E-08	1.183E+00	8.000	3.342E+04	3.600E+04	3.914E+04	1.087E+00
0.120	3.354E-07	3.778E-07	4.338E-07	1.175E+00	9.000	3.573E+04	3.869E+04	4.248E+04	1.097E+00
0.130	1.357E-06	1.523E-06	1.742E-06	1.168E+00	10.000	3.737E+04	4.069E+04	4.514E+04	1.107E+00

Note. Observed resonances: P. M. Endt (1990) and S. Harissopulos et al. (2000). Normalization: see Table 2. Unobserved resonances: A. Champagne et al. (1986, 1988). High-temperature rates (in parentheses): no matching to statistical model rates is needed over the listed temperature range. Previous rates: S. Harissopulos et al. (2000) and C. Iliadis et al. (2010c). Other: for the resonances at $E_r^{c.m.} = 73$ and 86 keV, the proton widths have been obtained from a reanalysis of the transfer data reported by A. Champagne et al. (1986); see comments in C. Iliadis et al. (2001).

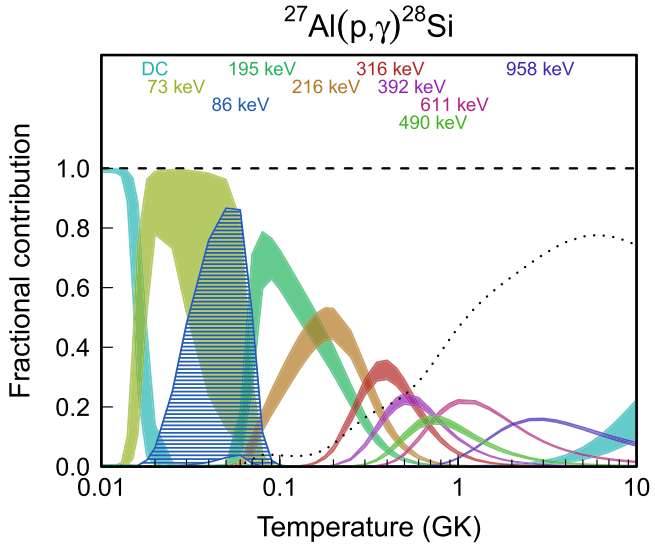

Figure 97. Fractional contributions to the total rate. "DC" refers to direct radiative capture. Resonance energies are given in the center-of-mass frame.

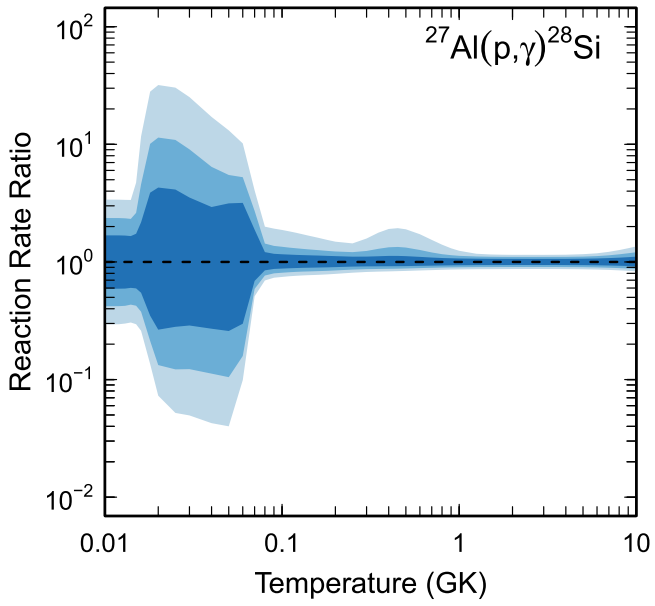

Figure 98. Reaction rate uncertainties versus temperature. The three different shades refer to coverage probabilities of 68%, 90%, and 98%.

Table 57
Total Laboratory Reaction Rates for ^{27}Al(p,α)^{24}Mg

T (GK)	Low	Median	High	*f.u.*	T (GK)	Low	Median	High	*f.u.*
0.001	1.213E-94	2.429E-94	4.807E-94	2.002E+00	0.140	5.294E-10	1.181E-09	2.910E-09	2.474E+00
0.002	5.702E-74	1.142E-73	2.259E-73	2.002E+00	0.150	1.571E-09	3.485E-09	8.745E-09	2.445E+00
0.003	6.313E-64	1.264E-63	2.501E-63	2.002E+00	0.160	4.631E-09	1.039E-08	2.581E-08	2.406E+00
0.004	1.390E-57	2.784E-57	5.509E-57	2.002E+00	0.180	3.769E-08	8.097E-08	1.913E-07	2.251E+00
0.005	4.561E-53	9.133E-53	1.807E-52	2.002E+00	0.200	2.800E-07	5.215E-07	1.113E-06	2.005E+00
0.006	1.278E-49	2.559E-49	5.065E-49	2.002E+00	0.250	2.311E-05	3.128E-05	4.648E-05	1.469E+00
0.007	4.780E-46	1.159E-45	3.502E-45	2.805E+00	0.300	6.039E-04	7.709E-04	9.913E-04	1.293E+00
0.008	9.250E-44	2.246E-43	6.805E-43	2.806E+00	0.350	6.645E-03	8.352E-03	1.050E-02	1.259E+00
0.009	8.034E-42	1.960E-41	5.963E-41	2.820E+00	0.400	4.095E-02	5.116E-02	6.393E-02	1.250E+00
0.010	3.810E-40	9.365E-40	2.874E-39	2.844E+00	0.450	1.703E-01	2.114E-01	2.628E-01	1.243E+00
0.011	1.141E-38	2.838E-38	8.851E-38	2.882E+00	0.500	5.371E-01	6.617E-01	8.176E-01	1.234E+00
0.012	2.933E-37	7.784E-37	2.640E-36	3.064E+00	0.600	3.080E+00	3.729E+00	4.537E+00	1.215E+00
0.013	1.348E-35	4.776E-35	1.943E-34	3.759E+00	0.700	1.111E+01	1.322E+01	1.583E+01	1.195E+00
0.014	9.142E-34	3.799E-33	1.620E-32	4.206E+00	0.800	3.042E+01	3.564E+01	4.197E+01	1.176E+00
0.015	4.509E-32	1.919E-31	8.204E-31	4.307E+00	0.900	7.049E+01	8.127E+01	9.418E+01	1.158E+00
0.016	1.407E-30	6.005E-30	2.560E-29	4.317E+00	1.000	1.466E+02	1.669E+02	1.907E+02	1.142E+00
0.018	4.347E-28	1.846E-27	7.833E-27	4.296E+00	1.250	6.829E+02	7.644E+02	8.564E+02	1.121E+00
0.020	4.229E-26	1.782E-25	7.527E-25	4.258E+00	1.500	2.363E+03	2.638E+03	2.947E+03	1.118E+00
0.025	1.589E-22	6.384E-22	2.668E-21	4.108E+00	1.750	6.499E+03	7.239E+03	8.076E+03	1.116E+00
0.030	3.967E-20	1.454E-19	5.925E-19	3.924E+00	2.000	1.488E+04	1.654E+04	1.840E+04	1.113E+00
0.040	3.918E-17	1.307E-16	4.747E-16	3.620E+00	2.500	5.239E+04	5.791E+04	6.403E+04	1.106E+00
0.050	2.363E-15	7.947E-15	2.524E-14	3.452E+00	3.000	1.291E+05	1.421E+05	1.564E+05	1.101E+00
0.060	3.490E-14	1.204E-13	3.547E-13	3.375E+00	3.500	2.527E+05	2.776E+05	3.047E+05	1.099E+00
0.070	2.334E-13	8.207E-13	2.382E-12	3.344E+00	4.000	(4.236E+05)	(4.653E+05)	(5.179E+05)	(1.106E+00)
0.080	9.611E-13	3.410E-12	9.931E-12	3.307E+00	5.000	(9.472E+05)	(1.222E+06)	(3.169E+06)	(1.942E+00)
0.090	3.028E-12	1.042E-11	3.007E-11	3.188E+00	6.000	(1.632E+06)	(2.549E+06)	(1.039E+07)	(2.819E+00)
0.100	8.520E-12	2.721E-11	7.518E-11	2.981E+00	7.000	(2.284E+06)	(4.522E+06)	(2.512E+07)	(3.768E+00)
0.110	2.297E-11	6.742E-11	1.753E-10	2.771E+00	8.000	(2.637E+06)	(7.124E+06)	(5.014E+07)	(4.870E+00)
0.120	6.208E-11	1.663E-10	4.116E-10	2.618E+00	9.000	(2.416E+06)	(1.028E+07)	(8.755E+07)	(6.387E+00)
0.130	1.780E-10	4.288E-10	1.034E-09	2.523E+00	10.000	(1.386E+06)	(1.386E+07)	(1.386E+08)	(1.000E+01)

Note. Observed resonances: P. M. Endt (1998). Normalization: none. A carefully determined standard-strength resonance has not been measured. Unobserved resonances: A. Champagne et al. (1986, 1988). High-temperature rates (in parentheses): matching to statistical model rate above $T = 3.9$ GK. Previous rates: C. Iliadis et al. (2010c). Other: we assumed unnatural parity for the following levels with ambiguous J^{π} values (based on shell-model assignments): E_x = 11,799.8, 11,933.5, 11,986, and 12,015.8 keV ($E_r^{c.m.}$ = 216, 350, 402, and 432 keV, respectively).

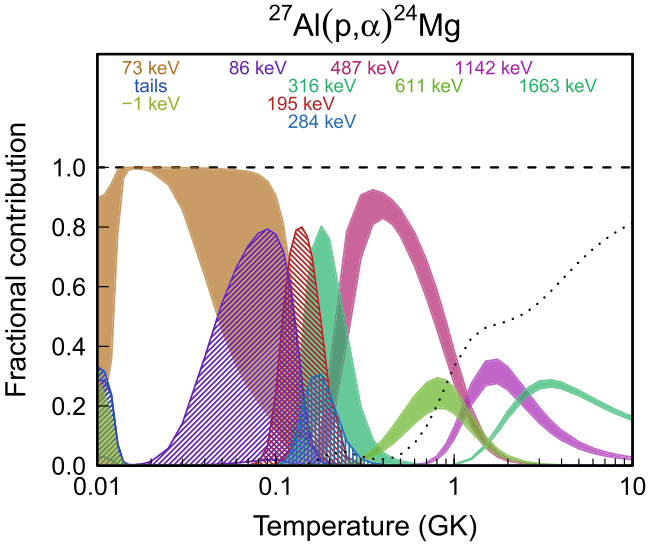

Figure 99. Fractional contributions to the total rate. "Tails" refers to low-energy tails of broad resonances. Resonance energies are given in the center-of-mass frame.

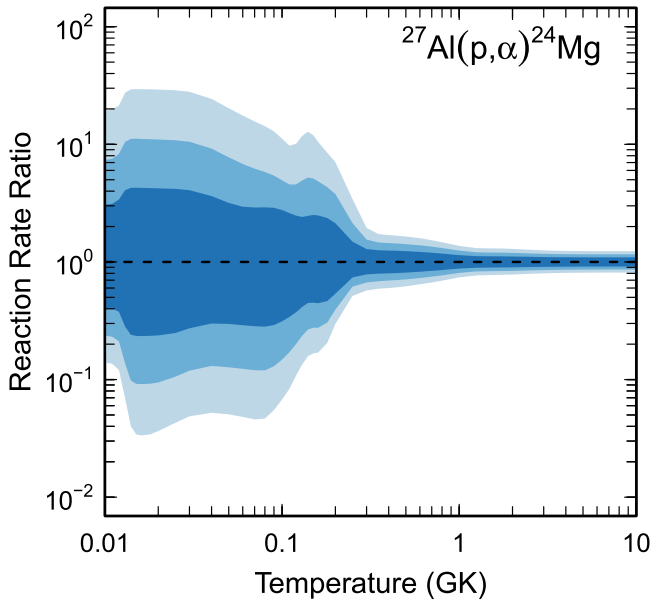

Figure 100. Reaction rate uncertainties versus temperature. The three different shades refer to coverage probabilities of 68%, 90%, and 98%.

Table 58
Total Laboratory Reaction Rates for ^{26}Si(p,γ)^{27}P

T (GK)	Low	Median	High	*f.u.*	T (GK)	Low	Median	High	*f.u.*
0.001	5.654E-96	9.631E-96	1.630E-95	1.699E+00	0.140	5.900E-09	1.311E-08	2.745E-08	2.163E+00
0.002	2.736E-74	4.661E-74	7.887E-74	1.699E+00	0.150	3.209E-08	6.909E-08	1.399E-07	2.098E+00
0.003	9.205E-64	1.568E-63	2.653E-63	1.699E+00	0.160	1.398E-07	2.944E-07	5.799E-07	2.044E+00
0.004	4.038E-57	6.879E-57	1.164E-56	1.699E+00	0.180	1.604E-06	3.244E-06	6.104E-06	1.962E+00
0.005	2.146E-52	3.656E-52	6.185E-52	1.699E+00	0.200	1.108E-05	2.169E-05	3.963E-05	1.903E+00
0.006	8.639E-49	1.471E-48	2.490E-48	1.699E+00	0.250	3.388E-04	6.323E-04	1.102E-03	1.816E+00
0.007	6.537E-46	1.114E-45	1.884E-45	1.699E+00	0.300	3.131E-03	5.676E-03	9.665E-03	1.770E+00
0.008	1.551E-43	2.641E-43	4.469E-43	1.699E+00	0.350	1.477E-02	2.633E-02	4.414E-02	1.745E+00
0.009	1.578E-41	2.688E-41	4.548E-41	1.699E+00	0.400	4.583E-02	8.089E-02	1.347E-01	1.729E+00
0.010	8.457E-40	1.440E-39	2.437E-39	1.699E+00	0.450	1.081E-01	1.895E-01	3.140E-01	1.719E+00
0.011	2.747E-38	4.680E-38	7.918E-38	1.699E+00	0.500	2.116E-01	3.684E-01	6.093E-01	1.713E+00
0.012	5.983E-37	1.019E-36	1.724E-36	1.699E+00	0.600	5.575E-01	9.626E-01	1.588E+00	1.705E+00
0.013	9.402E-36	1.601E-35	2.710E-35	1.699E+00	0.700	1.073E+00	1.846E+00	3.042E+00	1.701E+00
0.014	1.128E-34	1.921E-34	3.250E-34	1.699E+00	0.800	(1.732E+00)	(2.979E+00)	(4.960E+00)	(1.693E+00)
0.015	1.078E-33	1.835E-33	3.106E-33	1.699E+00	0.900	(2.645E+00)	(4.592E+00)	(8.059E+00)	(1.746E+00)
0.016	8.488E-33	1.446E-32	2.446E-32	1.699E+00	1.000	(3.730E+00)	(6.535E+00)	(1.206E+01)	(1.799E+00)
0.018	3.271E-31	5.572E-31	9.427E-31	1.699E+00	1.250	(6.328E+00)	(1.135E+01)	(2.352E+01)	(1.933E+00)
0.020	7.591E-30	1.293E-29	2.188E-29	1.699E+00	1.500	(1.073E+01)	(1.970E+01)	(4.528E+01)	(2.068E+00)
0.025	4.122E-27	7.021E-27	1.188E-26	1.699E+00	1.750	(1.409E+01)	(2.651E+01)	(6.694E+01)	(2.203E+00)
0.030	5.007E-25	8.528E-25	1.443E-24	1.699E+00	2.000	(1.849E+01)	(3.566E+01)	(9.813E+01)	(2.340E+00)
0.040	5.424E-22	9.240E-22	1.563E-21	1.699E+00	2.500	(2.588E+01)	(5.257E+01)	(1.685E+02)	(2.618E+00)
0.050	7.760E-20	1.322E-19	2.236E-19	1.699E+00	3.000	(3.265E+01)	(7.003E+01)	(2.562E+02)	(2.902E+00)
0.060	3.403E-18	5.796E-18	9.807E-18	1.699E+00	3.500	(3.880E+01)	(8.818E+01)	(3.625E+02)	(3.192E+00)
0.070	6.970E-17	1.185E-16	2.004E-16	1.696E+00	4.000	(4.431E+01)	(1.071E+02)	(4.887E+02)	(3.490E+00)
0.080	9.459E-16	1.557E-15	2.568E-15	1.651E+00	5.000	(5.318E+01)	(1.471E+02)	(8.046E+02)	(4.118E+00)
0.090	1.420E-14	2.451E-14	4.515E-14	1.823E+00	6.000	(5.848E+01)	(1.891E+02)	(1.206E+03)	(4.805E+00)
0.100	2.777E-13	6.271E-13	1.499E-12	2.290E+00	7.000	(5.970E+01)	(2.324E+02)	(1.692E+03)	(5.587E+00)
0.110	5.755E-12	1.410E-11	3.359E-11	2.397E+00	8.000	(5.668E+01)	(2.770E+02)	(2.268E+03)	(6.538E+00)
0.120	8.424E-11	2.010E-10	4.575E-10	2.330E+00	9.000	(4.948E+01)	(3.249E+02)	(2.955E+03)	(7.830E+00)
0.130	8.312E-10	1.912E-09	4.167E-09	2.241E+00	10.000	(3.784E+01)	(3.784E+02)	(3.784E+03)	(1.000E+01)

Note. Observed resonances: none. Normalization: none. Unobserved resonances: A. Gade et al. (2008), B. Longfellow et al. (2019), and L. J. Sun et al. (2019). High-temperature rates (in parentheses): matching to statistical model rate above $T = 0.78$ GK. Previous rates: L. J. Sun et al. (2019). Other: the proton partial widths and direct-capture S factor were estimated using experimental spectroscopic factors given in P. M. Endt (1977) and G. D'Agata et al. (2021). The γ-ray partial widths were calculated from the measured lifetimes of the ^{27}Mg mirror states (ENSDF 2010).

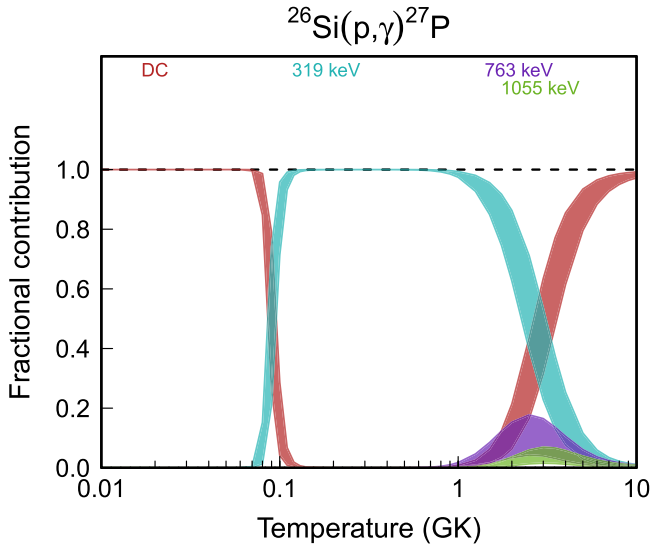

Figure 101. Fractional contributions to the total rate. "DC" refers to direct radiative capture. Resonance energies are given in the center-of-mass frame.

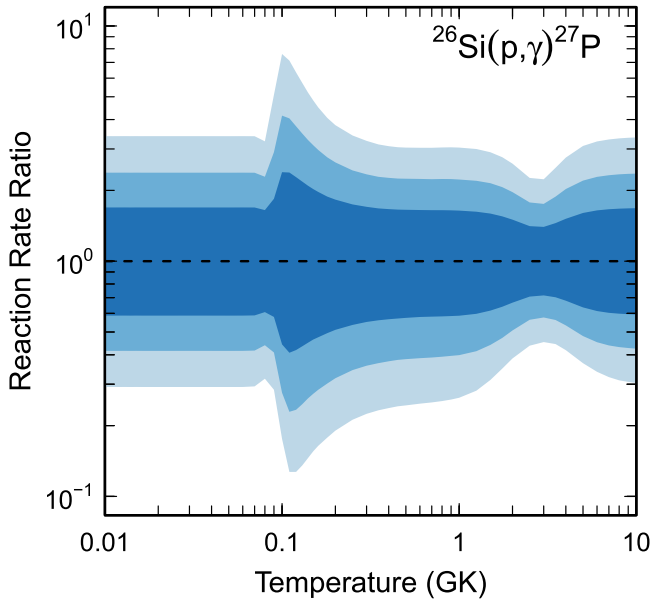

Figure 102. Reaction rate uncertainties versus temperature. The three different shades refer to coverage probabilities of 68%, 90%, and 98%.

Table 59
Total Laboratory Reaction Rates for $^{27}Si(p,\gamma)^{28}P$

T (GK)	Low	Median	High	*f.u.*	T (GK)	Low	Median	High	*f.u.*
0.001	4.630E-96	7.870E-96	1.338E-95	1.702E+00	0.140	1.899E-07	3.782E-07	7.535E-07	1.998E+00
0.002	2.297E-74	3.905E-74	6.641E-74	1.702E+00	0.150	4.285E-07	8.546E-07	1.703E-06	1.996E+00
0.003	7.828E-64	1.331E-63	2.263E-63	1.702E+00	0.160	8.872E-07	1.750E-06	3.484E-06	1.981E+00
0.004	3.464E-57	5.888E-57	1.001E-56	1.702E+00	0.180	3.302E-06	6.113E-06	1.171E-05	1.887E+00
0.005	1.853E-52	3.149E-52	5.355E-52	1.702E+00	0.200	1.140E-05	1.941E-05	3.401E-05	1.743E+00
0.006	7.496E-49	1.274E-48	2.167E-48	1.702E+00	0.250	1.823E-04	3.002E-04	4.919E-04	1.646E+00
0.007	1.443E-45	2.514E-45	4.782E-45	1.855E+00	0.300	1.639E-03	2.821E-03	4.844E-03	1.720E+00
0.008	9.736E-43	2.710E-42	9.596E-42	3.123E+00	0.350	8.793E-03	1.532E-02	2.657E-02	1.736E+00
0.009	2.291E-39	8.388E-39	3.017E-38	3.616E+00	0.400	3.179E-02	5.497E-02	9.459E-02	1.723E+00
0.010	2.105E-36	6.652E-36	2.062E-35	3.138E+00	0.450	8.696E-02	1.480E-01	2.521E-01	1.700E+00
0.011	5.573E-34	1.559E-33	4.297E-33	2.780E+00	0.500	1.957E-01	3.259E-01	5.478E-01	1.672E+00
0.012	5.720E-32	1.460E-31	3.659E-31	2.533E+00	0.600	6.653E-01	1.064E+00	1.731E+00	1.616E+00
0.013	2.818E-30	6.702E-30	1.565E-29	2.360E+00	0.700	1.605E+00	2.484E+00	3.922E+00	1.569E+00
0.014	7.836E-29	1.764E-28	3.908E-28	2.238E+00	0.800	3.114E+00	4.721E+00	7.259E+00	1.534E+00
0.015	1.378E-27	2.986E-27	6.358E-27	2.152E+00	0.900	5.203E+00	7.800E+00	1.179E+01	1.511E+00
0.016	1.674E-26	3.528E-26	7.301E-26	2.092E+00	1.000	7.850E+00	1.164E+01	1.745E+01	1.496E+00
0.018	1.047E-24	2.129E-24	4.274E-24	2.025E+00	1.250	1.646E+01	2.405E+01	3.563E+01	1.478E+00
0.020	2.788E-23	5.576E-23	1.105E-22	2.001E+00	1.500	2.717E+01	3.917E+01	5.777E+01	1.465E+00
0.025	9.396E-21	1.889E-20	3.801E-20	2.025E+00	1.750	3.972E+01	5.616E+01	8.193E+01	1.447E+00
0.030	4.279E-19	8.835E-19	1.823E-18	2.072E+00	2.000	5.390E+01	7.476E+01	1.074E+02	1.424E+00
0.040	7.313E-17	1.342E-16	2.558E-16	1.884E+00	2.500	8.702E+01	1.163E+02	1.618E+02	1.377E+00
0.050	3.610E-15	6.324E-15	1.117E-14	1.766E+00	3.000	1.260E+02	1.646E+02	2.223E+02	1.341E+00
0.060	8.349E-14	1.488E-13	2.728E-13	1.819E+00	3.500	1.702E+02	2.209E+02	2.939E+02	1.321E+00
0.070	1.552E-12	2.723E-12	4.796E-12	1.766E+00	4.000	2.199E+02	2.866E+02	3.802E+02	1.320E+00
0.080	2.200E-11	3.980E-11	7.308E-11	1.839E+00	5.000	(2.779E+02)	(4.143E+02)	(1.058E+03)	(2.022E+00)
0.090	2.111E-10	4.004E-10	7.705E-10	1.914E+00	6.000	(3.063E+02)	(5.503E+02)	(2.225E+03)	(2.920E+00)
0.100	1.402E-09	2.719E-09	5.303E-09	1.952E+00	7.000	(3.109E+02)	(7.026E+02)	(3.887E+03)	(3.896E+00)
0.110	6.718E-09	1.314E-08	2.589E-08	1.970E+00	8.000	(2.872E+02)	(8.749E+02)	(6.143E+03)	(5.034E+00)
0.120	2.478E-08	4.883E-08	9.667E-08	1.983E+00	9.000	(2.295E+02)	(1.072E+03)	(9.121E+03)	(6.590E+00)
0.130	7.432E-08	1.476E-07	2.924E-07	1.992E+00	10.000	(1.298E+02)	(1.298E+03)	(1.298E+04)	(1.000E+01)

Note. Observed resonances: none. Normalization: none. Unobserved resonances: P. M. Endt (1977), P. M. Endt & C. van der Leun (1978), P. M. Endt (1990), P. M. Endt (1998), and C. Iliadis et al. (1999). High-temperature rates (in parentheses): matching to statistical model rate above $T = 4.2$ GK. Previous rates: C. Iliadis et al. (1999, 2010c). Other: none.

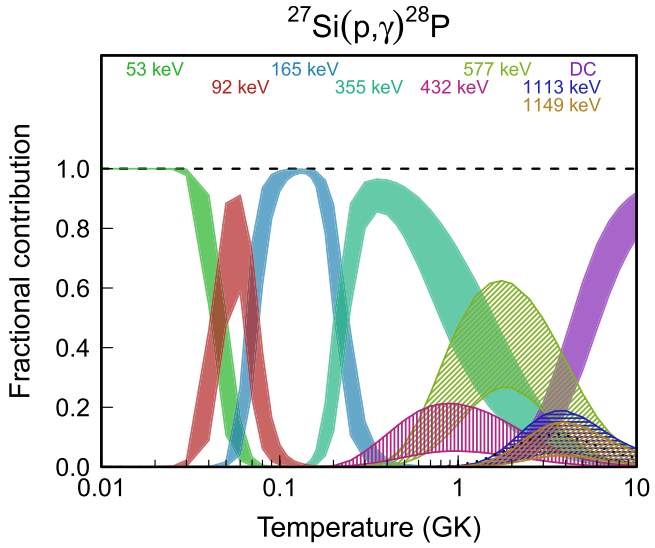

Figure 103. Fractional contributions to the total rate. "DC" refers to direct radiative capture. Resonance energies are given in the center-of-mass frame.

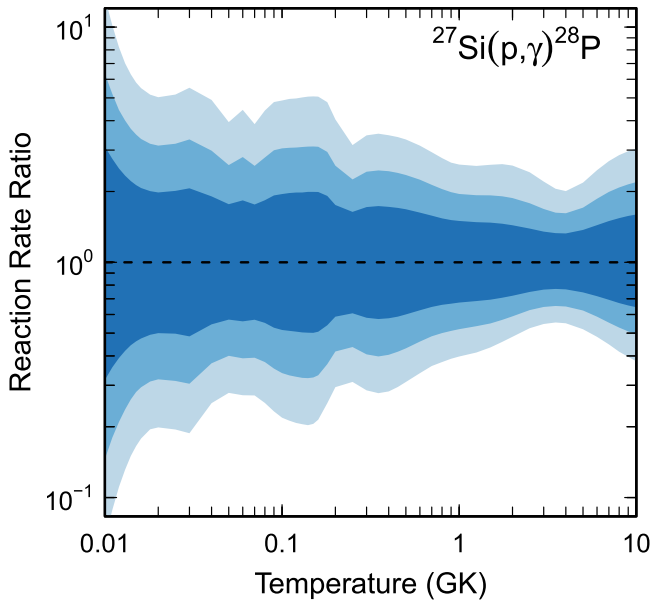

Figure 104. Reaction rate uncertainties versus temperature. The three different shades refer to coverage probabilities of 68%, 90%, and 98%.

Table 60
Total Laboratory Reaction Rates for ^{28}Si(p,γ)^{29}P

T (GK)	Low	Median	High	*f.u.*	T (GK)	Low	Median	High	*f.u.*
0.001	7.339E-96	9.555E-96	1.241E-95	1.302E+00	0.140	5.646E-10	6.996E-10	8.699E-10	1.242E+00
0.002	3.722E-74	4.846E-74	6.296E-74	1.302E+00	0.150	3.613E-09	4.495E-09	5.606E-09	1.246E+00
0.003	1.282E-63	1.669E-63	2.169E-63	1.302E+00	0.160	1.841E-08	2.293E-08	2.863E-08	1.247E+00
0.004	5.712E-57	7.437E-57	9.662E-57	1.302E+00	0.180	2.757E-07	3.435E-07	4.289E-07	1.248E+00
0.005	3.070E-52	3.997E-52	5.193E-52	1.302E+00	0.200	2.369E-06	2.951E-06	3.684E-06	1.247E+00
0.006	1.247E-48	1.623E-48	2.109E-48	1.302E+00	0.250	1.084E-04	1.349E-04	1.684E-04	1.247E+00
0.007	9.634E-46	1.250E-45	1.621E-45	1.298E+00	0.300	1.320E-03	1.641E-03	2.048E-03	1.246E+00
0.008	2.300E-43	2.985E-43	3.869E-43	1.298E+00	0.350	7.589E-03	9.434E-03	1.177E-02	1.246E+00
0.009	2.353E-41	3.054E-41	3.958E-41	1.298E+00	0.400	2.742E-02	3.410E-02	4.252E-02	1.246E+00
0.010	1.267E-39	1.645E-39	2.132E-39	1.298E+00	0.450	7.297E-02	9.071E-02	1.131E-01	1.246E+00
0.011	4.136E-38	5.367E-38	6.956E-38	1.298E+00	0.500	1.570E-01	1.952E-01	2.432E-01	1.246E+00
0.012	9.042E-37	1.174E-36	1.521E-36	1.298E+00	0.600	4.779E-01	5.940E-01	7.402E-01	1.245E+00
0.013	1.426E-35	1.851E-35	2.399E-35	1.298E+00	0.700	1.022E+00	1.270E+00	1.582E+00	1.245E+00
0.014	1.717E-34	2.228E-34	2.887E-34	1.298E+00	0.800	1.761E+00	2.188E+00	2.724E+00	1.245E+00
0.015	1.646E-33	2.136E-33	2.768E-33	1.298E+00	0.900	2.639E+00	3.276E+00	4.077E+00	1.244E+00
0.016	1.300E-32	1.687E-32	2.187E-32	1.298E+00	1.000	3.598E+00	4.460E+00	5.548E+00	1.243E+00
0.018	5.039E-31	6.539E-31	8.473E-31	1.298E+00	1.250	6.179E+00	7.595E+00	9.386E+00	1.234E+00
0.020	1.175E-29	1.525E-29	1.976E-29	1.298E+00	1.500	9.492E+00	1.139E+01	1.378E+01	1.206E+00
0.025	6.451E-27	8.370E-27	1.085E-26	1.298E+00	1.750	1.556E+01	1.797E+01	2.089E+01	1.160E+00
0.030	7.908E-25	1.026E-24	1.330E-24	1.298E+00	2.000	2.757E+01	3.099E+01	3.493E+01	1.127E+00
0.040	8.701E-22	1.129E-21	1.463E-21	1.297E+00	2.500	8.213E+01	9.219E+01	1.037E+02	1.124E+00
0.050	1.261E-19	1.635E-19	2.119E-19	1.297E+00	3.000	1.940E+02	2.194E+02	2.487E+02	1.133E+00
0.060	5.587E-18	7.248E-18	9.390E-18	1.297E+00	3.500	3.703E+02	4.200E+02	4.775E+02	1.137E+00
0.070	1.151E-16	1.493E-16	1.934E-16	1.297E+00	4.000	6.061E+02	6.885E+02	7.830E+02	1.138E+00
0.080	1.393E-15	1.807E-15	2.340E-15	1.297E+00	5.000	1.215E+03	1.381E+03	1.571E+03	1.138E+00
0.090	1.154E-14	1.493E-14	1.931E-14	1.295E+00	6.000	1.936E+03	2.201E+03	2.504E+03	1.139E+00
0.100	7.803E-14	9.894E-14	1.259E-13	1.270E+00	7.000	2.694E+03	3.067E+03	3.493E+03	1.140E+00
0.110	6.265E-13	7.482E-13	8.975E-13	1.198E+00	8.000	(3.051E+03)	(3.714E+03)	(6.608E+03)	(1.498E+00)
0.120	6.629E-12	7.931E-12	9.543E-12	1.201E+00	9.000	(1.424E+03)	(3.091E+03)	(1.820E+04)	(4.030E+00)
0.130	6.836E-11	8.385E-11	1.033E-10	1.230E+00	10.000	(2.186E+02)	(2.186E+03)	(2.186E+04)	(1.000E+01)

Note. Observed resonances: P. M. Endt (1990) and S. Graff et al. (1990). Normalization: see Table 2. Unobserved resonances: all expected resonances above the proton threshold have been observed. High-temperature rates (in parentheses): matching to statistical model rate above $T = 7.8$ GK. Previous rates: C. Iliadis et al. (2010c). Other: the tails of subthreshold resonances and the resonance at $E_r^{c.m.} = 358$ keV are unimportant for the total rate.

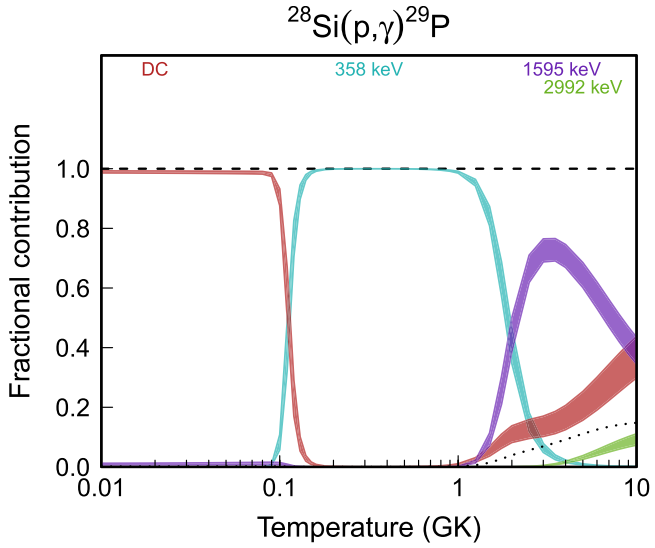

Figure 105. Fractional contributions to the total rate. "DC" refers to direct radiative capture. Resonance energies are given in the center-of-mass frame.

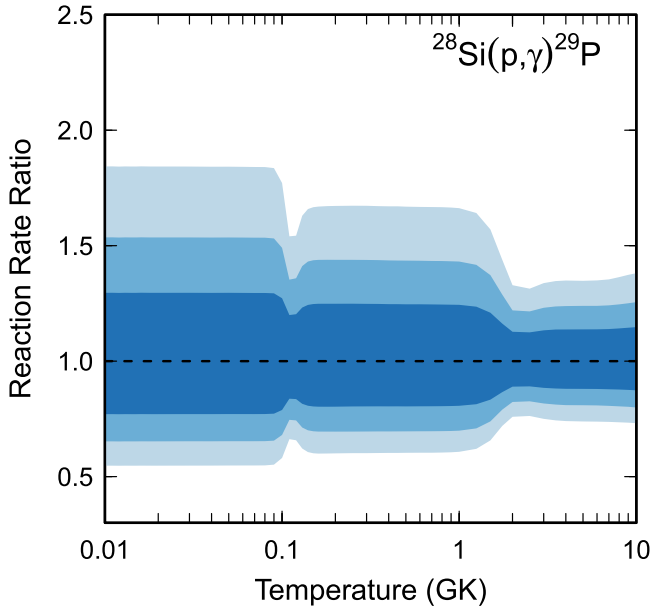

Figure 106. Reaction rate uncertainties versus temperature. The three different shades refer to coverage probabilities of 68%, 90%, and 98%.

Table 61
Total Laboratory Reaction Rates for $^{28}Si(\alpha,\gamma)^{32}S$

T (GK)	Low	Median	High	*f.u.*	T (GK)	Low	Median	High	*f.u.*
0.001	0.000E+00	0.000E+00	0.000E+00	1.000E+00	0.140	1.598E-29	1.462E-28	1.414E-27	9.057E+00
0.002	0.000E+00	0.000E+00	0.000E+00	1.000E+00	0.150	2.226E-28	1.974E-27	1.907E-26	8.851E+00
0.003	0.000E+00	0.000E+00	0.000E+00	1.000E+00	0.160	2.238E-27	1.915E-26	1.845E-25	8.633E+00
0.004	0.000E+00	0.000E+00	0.000E+00	1.000E+00	0.180	1.080E-25	8.374E-25	7.999E-24	8.179E+00
0.005	0.000E+00	0.000E+00	0.000E+00	1.000E+00	0.200	2.476E-24	1.708E-23	1.606E-22	7.718E+00
0.006	0.000E+00	0.000E+00	0.000E+00	1.000E+00	0.250	7.858E-22	3.972E-21	3.394E-20	6.537E+00
0.007	0.000E+00	0.000E+00	0.000E+00	1.000E+00	0.300	4.655E-20	1.695E-19	1.166E-18	5.251E+00
0.008	0.000E+00	0.000E+00	0.000E+00	1.000E+00	0.350	1.424E-18	3.676E-18	1.538E-17	3.721E+00
0.009	0.000E+00	0.000E+00	0.000E+00	1.000E+00	0.400	7.763E-17	1.169E-16	2.214E-16	1.978E+00
0.010	0.000E+00	0.000E+00	0.000E+00	1.000E+00	0.450	6.091E-15	7.340E-15	9.196E-15	1.285E+00
0.011	0.000E+00	0.000E+00	0.000E+00	1.000E+00	0.500	2.555E-13	2.995E-13	3.531E-13	1.183E+00
0.012	4.155E-98	1.528E-97	6.542E-97	3.920E+00	0.600	7.546E-11	8.757E-11	1.019E-10	1.163E+00
0.013	3.700E-95	1.360E-94	5.825E-94	3.917E+00	0.700	4.379E-09	5.065E-09	5.874E-09	1.159E+00
0.014	1.705E-92	6.247E-92	2.669E-91	3.909E+00	0.800	9.097E-08	1.050E-07	1.214E-07	1.156E+00
0.015	4.971E-90	1.697E-89	7.056E-89	3.746E+00	0.900	9.560E-07	1.099E-06	1.267E-06	1.152E+00
0.016	1.451E-87	4.493E-87	1.440E-86	3.252E+00	1.000	6.252E-06	7.159E-06	8.225E-06	1.148E+00
0.018	8.628E-83	5.424E-82	2.456E-81	5.128E+00	1.250	1.858E-04	2.100E-04	2.382E-04	1.133E+00
0.020	2.172E-78	2.342E-77	1.165E-76	7.591E+00	1.500	1.880E-03	2.087E-03	2.329E-03	1.114E+00
0.025	5.460E-70	6.351E-69	3.111E-68	9.208E+00	1.750	1.056E-02	1.153E-02	1.263E-02	1.094E+00
0.030	2.196E-64	2.531E-63	1.237E-62	9.380E+00	2.000	4.125E-02	4.438E-02	4.794E-02	1.079E+00
0.040	2.019E-57	2.316E-56	1.131E-55	9.121E+00	2.500	3.162E-01	3.356E-01	3.569E-01	1.063E+00
0.050	2.896E-53	3.227E-52	1.583E-51	7.956E+00	3.000	1.354E+00	1.432E+00	1.516E+00	1.058E+00
0.060	3.405E-50	2.120E-49	9.339E-49	5.093E+00	3.500	4.014E+00	4.247E+00	4.494E+00	1.059E+00
0.070	1.608E-46	1.076E-45	9.954E-45	7.678E+00	4.000	9.281E+00	9.837E+00	1.043E+01	1.061E+00
0.080	2.131E-42	2.088E-41	2.042E-40	9.743E+00	5.000	(2.842E+01)	(3.248E+01)	(5.705E+01)	(1.450E+00)
0.090	4.754E-39	4.648E-38	4.536E-37	9.751E+00	6.000	(5.315E+01)	(7.381E+01)	(2.513E+02)	(2.397E+00)
0.100	2.249E-36	2.179E-35	2.125E-34	9.666E+00	7.000	(7.753E+01)	(1.372E+02)	(6.934E+02)	(3.412E+00)
0.110	3.420E-34	3.297E-33	3.211E-32	9.552E+00	8.000	(9.206E+01)	(2.245E+02)	(1.505E+03)	(4.571E+00)
0.120	2.242E-32	2.131E-31	2.071E-30	9.411E+00	9.000	(8.591E+01)	(3.369E+02)	(2.813E+03)	(6.136E+00)
0.130	7.707E-31	7.197E-30	6.985E-29	9.245E+00	10.000	(4.751E+01)	(4.751E+02)	(4.751E+03)	(1.000E+01)

Note. Observed resonances: J. W. Toevs (1971), P. M. Endt & C. van der Leun (1978), and M. Babilon et al. (2002). Normalization: none. Unobserved resonances: T. Tanabe et al. (1981), A. Kangasmäki et al. (1998), and T. Madhusoodhanan et al. (1999). High-temperature rates (in parentheses): matching to statistical model rate above $T = 4.6$ GK. Previous rates: none. Other: the direct-capture contribution has been estimated using the experimental α-particle spectroscopic factors listed in Table 2 of T. Madhusoodhanan et al. (1999).

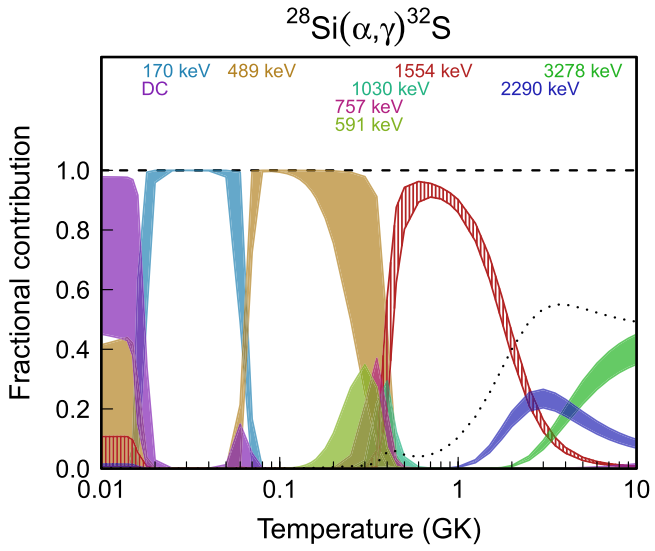

Figure 107. Fractional contributions to the total rate. "DC" refers to direct radiative capture. Resonance energies are given in the center-of-mass frame.

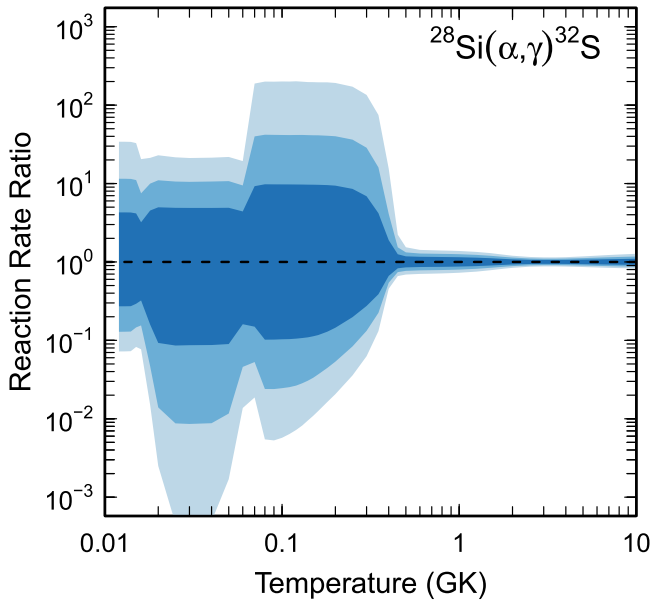

Figure 108. Reaction rate uncertainties versus temperature. The three different shades refer to coverage probabilities of 68%, 90%, and 98%.

Table 62
Total Laboratory Reaction Rates for ^{29}Si(p,γ)^{30}P

T (GK)	Low	Median	High	*f.u.*	T (GK)	Low	Median	High	*f.u.*
0.001	1.079E-95	1.403E-95	1.819E-95	1.300E+00	0.140	2.918E-07	3.339E-07	3.824E-07	1.146E+00
0.002	5.580E-74	7.258E-74	9.407E-74	1.300E+00	0.150	1.452E-06	1.659E-06	1.900E-06	1.144E+00
0.003	1.940E-63	2.523E-63	3.270E-63	1.300E+00	0.160	5.967E-06	6.817E-06	7.806E-06	1.144E+00
0.004	8.693E-57	1.131E-56	1.466E-56	1.300E+00	0.180	6.331E-05	7.225E-05	8.264E-05	1.143E+00
0.005	4.691E-52	6.102E-52	7.909E-52	1.300E+00	0.200	4.193E-04	4.775E-04	5.456E-04	1.141E+00
0.006	1.911E-48	2.486E-48	3.222E-48	1.300E+00	0.250	1.271E-02	1.441E-02	1.640E-02	1.137E+00
0.007	1.462E-45	1.900E-45	2.463E-45	1.300E+00	0.300	1.262E-01	1.426E-01	1.616E-01	1.132E+00
0.008	3.496E-43	4.546E-43	5.891E-43	1.300E+00	0.350	6.620E-01	7.457E-01	8.426E-01	1.129E+00
0.009	3.583E-41	4.658E-41	6.037E-41	1.300E+00	0.400	2.314E+00	2.602E+00	2.935E+00	1.127E+00
0.010	1.932E-39	2.512E-39	3.255E-39	1.300E+00	0.450	6.139E+00	6.895E+00	7.766E+00	1.125E+00
0.011	6.312E-38	8.205E-38	1.064E-37	1.300E+00	0.500	1.337E+01	1.501E+01	1.689E+01	1.124E+00
0.012	1.381E-36	1.796E-36	2.328E-36	1.300E+00	0.600	4.257E+01	4.773E+01	5.364E+01	1.123E+00
0.013	2.181E-35	2.835E-35	3.675E-35	1.300E+00	0.700	9.585E+01	1.074E+02	1.206E+02	1.122E+00
0.014	2.627E-34	3.414E-34	4.426E-34	1.300E+00	0.800	1.738E+02	1.947E+02	2.186E+02	1.122E+00
0.015	2.520E-33	3.275E-33	4.246E-33	1.300E+00	0.900	2.732E+02	3.060E+02	3.434E+02	1.121E+00
0.016	1.992E-32	2.590E-32	3.357E-32	1.300E+00	1.000	3.891E+02	4.358E+02	4.891E+02	1.121E+00
0.018	7.735E-31	1.005E-30	1.303E-30	1.300E+00	1.250	7.190E+02	8.055E+02	9.043E+02	1.121E+00
0.020	1.856E-29	2.402E-29	3.103E-29	1.295E+00	1.500	1.063E+03	1.192E+03	1.339E+03	1.122E+00
0.025	1.697E-26	5.819E-26	2.715E-25	3.299E+00	1.750	1.394E+03	1.565E+03	1.760E+03	1.124E+00
0.030	1.133E-23	1.464E-22	8.370E-22	6.995E+00	2.000	1.711E+03	1.922E+03	2.164E+03	1.125E+00
0.040	2.186E-19	3.224E-18	1.862E-17	9.498E+00	2.500	2.327E+03	2.617E+03	2.950E+03	1.126E+00
0.050	8.214E-17	1.215E-15	7.025E-15	9.949E+00	3.000	2.976E+03	3.349E+03	3.775E+03	1.126E+00
0.060	4.079E-15	6.026E-14	3.486E-13	9.835E+00	3.500	3.694E+03	4.154E+03	4.680E+03	1.125E+00
0.070	6.530E-14	9.457E-13	5.472E-12	8.886E+00	4.000	4.490E+03	5.042E+03	5.671E+03	1.124E+00
0.080	5.714E-13	7.327E-12	4.207E-11	7.157E+00	5.000	6.259E+03	7.003E+03	7.856E+03	1.121E+00
0.090	4.672E-12	3.684E-11	2.028E-10	5.150E+00	6.000	(6.927E+03)	(9.119E+03)	(2.395E+04)	(1.972E+00)
0.100	4.730E-11	1.594E-10	7.288E-10	3.267E+00	7.000	(6.691E+03)	(1.125E+04)	(5.029E+04)	(3.076E+00)
0.110	5.556E-10	9.058E-10	2.425E-09	1.953E+00	8.000	(5.755E+03)	(1.339E+04)	(8.454E+04)	(4.320E+00)
0.120	5.818E-09	7.238E-09	1.057E-08	1.341E+00	9.000	(4.116E+03)	(1.554E+04)	(1.267E+05)	(5.966E+00)
0.130	4.695E-08	5.465E-08	6.408E-08	1.169E+00	10.000	(1.771E+03)	(1.771E+04)	(1.771E+05)	(1.000E+01)

Note. Observed resonances: P. M. Endt (1998), L. N. Downen et al. (2022b), and Z. Mátyus et al. (2024). Normalization: see Table 2. Unobserved resonances: see Section IV.D in L. N. Downen et al. (2022b). High-temperature rates (in parentheses): matching to statistical model rate above $T = 5.2$ GK. Previous rates: C. Iliadis et al. (2010c). Other: the small differences, below $T = 0.1$ GK, between the numerical values listed here and those given in L. N. Downen et al. (2022b) are caused by an incorrect sampling for upper-limit resonances in the previous versions of RatesMC (see Section 5.2).

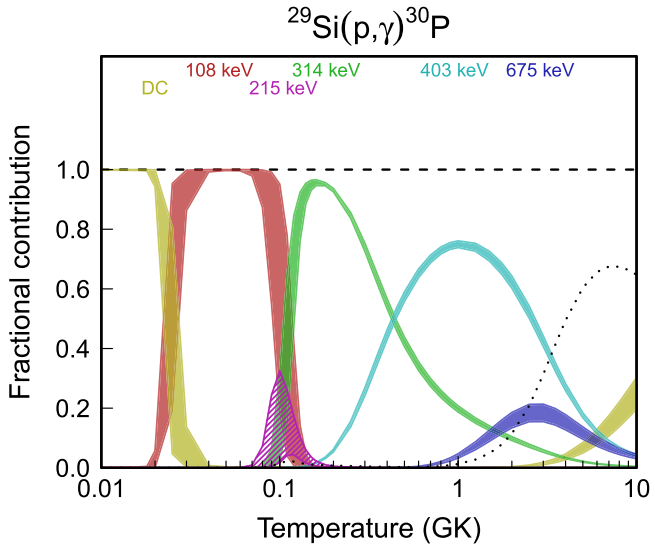

Figure 109. Fractional contributions to the total rate. "DC" refers to direct radiative capture. Resonance energies are given in the center-of-mass frame.

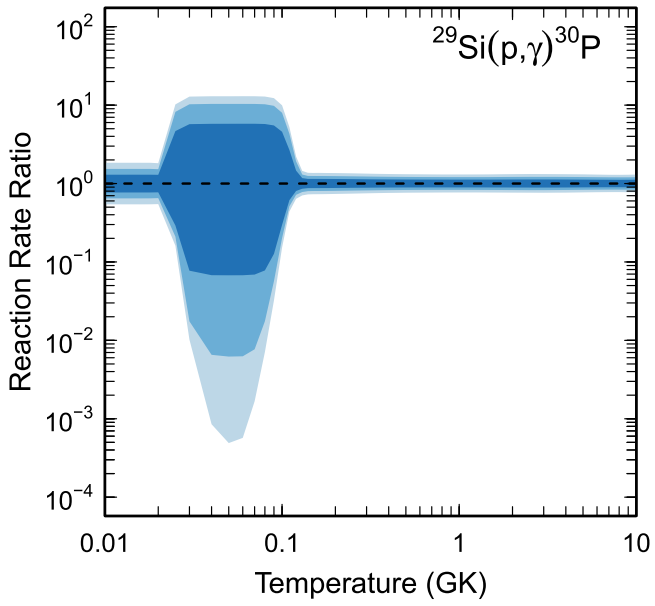

Figure 110. Reaction rate uncertainties versus temperature. The three different shades refer to coverage probabilities of 68%, 90%, and 98%.

Table 63
Total Laboratory Reaction Rates for ^{30}Si(p,γ)^{31}P

T (GK)	Low	Median	High	*f.u.*	T (GK)	Low	Median	High	*f.u.*
0.001	1.785E-95	2.317E-95	3.027E-95	1.450E+00	0.140	4.625E-11	5.873E-11	7.482E-11	1.275E+00
0.002	9.826E-74	1.322E-73	2.194E-73	2.779E+00	0.150	1.519E-10	1.865E-10	2.309E-10	1.236E+00
0.003	2.141E-62	1.033E-61	2.872E-61	3.552E+00	0.160	5.866E-10	6.793E-10	7.950E-10	1.167E+00
0.004	5.925E-55	3.291E-54	9.288E-54	3.889E+00	0.180	1.236E-08	1.348E-08	1.474E-08	1.093E+00
0.005	2.579E-50	1.295E-49	3.572E-49	3.671E+00	0.200	2.080E-07	2.263E-07	2.467E-07	1.090E+00
0.006	3.928E-47	1.721E-46	4.360E-46	3.328E+00	0.250	4.030E-05	4.367E-05	4.739E-05	1.085E+00
0.007	9.019E-45	3.402E-44	8.818E-44	2.981E+00	0.300	1.378E-03	1.486E-03	1.604E-03	1.079E+00
0.008	1.055E-42	2.268E-42	6.302E-42	2.574E+00	0.350	1.740E-02	1.867E-02	2.007E-02	1.074E+00
0.009	8.554E-41	1.233E-40	2.538E-40	2.133E+00	0.400	1.182E-01	1.264E-01	1.353E-01	1.070E+00
0.010	5.138E-39	7.606E-39	1.487E-38	1.890E+00	0.450	5.309E-01	5.659E-01	6.035E-01	1.066E+00
0.011	2.598E-37	5.045E-37	1.280E-36	2.235E+00	0.500	1.779E+00	1.891E+00	2.011E+00	1.064E+00
0.012	1.111E-35	2.775E-35	7.988E-35	2.633E+00	0.600	1.100E+01	1.165E+01	1.235E+01	1.060E+00
0.013	3.504E-34	9.679E-34	2.885E-33	2.831E+00	0.700	4.040E+01	4.272E+01	4.520E+01	1.058E+00
0.014	7.376E-33	2.110E-32	6.314E-32	2.907E+00	0.800	1.066E+02	1.126E+02	1.190E+02	1.057E+00
0.015	1.061E-31	3.080E-31	9.159E-31	2.933E+00	0.900	2.254E+02	2.379E+02	2.512E+02	1.056E+00
0.016	1.101E-30	3.203E-30	9.512E-30	2.941E+00	1.000	4.076E+02	4.300E+02	4.538E+02	1.055E+00
0.018	5.387E-29	1.568E-28	4.655E-28	2.941E+00	1.250	1.161E+03	1.225E+03	1.292E+03	1.055E+00
0.020	1.200E-27	3.488E-27	1.033E-26	2.935E+00	1.500	2.294E+03	2.419E+03	2.553E+03	1.055E+00
0.025	3.127E-25	8.892E-25	2.616E-24	2.883E+00	1.750	3.699E+03	3.903E+03	4.121E+03	1.056E+00
0.030	1.375E-23	3.575E-23	1.023E-22	2.693E+00	2.000	5.282E+03	5.577E+03	5.893E+03	1.057E+00
0.040	3.925E-21	6.112E-21	1.197E-20	1.819E+00	2.500	8.744E+03	9.245E+03	9.783E+03	1.058E+00
0.050	3.853E-19	5.022E-19	6.647E-19	1.332E+00	3.000	1.241E+04	1.314E+04	1.393E+04	1.060E+00
0.060	1.550E-17	2.001E-17	2.590E-17	1.296E+00	3.500	1.620E+04	1.717E+04	1.821E+04	1.061E+00
0.070	3.186E-16	4.113E-16	5.319E-16	1.295E+00	4.000	2.004E+04	2.127E+04	2.257E+04	1.062E+00
0.080	3.959E-15	5.089E-15	6.558E-15	1.292E+00	5.000	2.773E+04	2.945E+04	3.128E+04	1.063E+00
0.090	3.332E-14	4.283E-14	5.508E-14	1.290E+00	6.000	(3.264E+04)	(3.960E+04)	(9.140E+04)	(1.761E+00)
0.100	2.073E-13	2.669E-13	3.431E-13	1.290E+00	7.000	(3.318E+04)	(5.160E+04)	(2.183E+05)	(2.893E+00)
0.110	1.016E-12	1.309E-12	1.683E-12	1.291E+00	8.000	(2.966E+04)	(6.419E+04)	(3.950E+05)	(4.159E+00)
0.120	4.118E-12	5.304E-12	6.816E-12	1.290E+00	9.000	(2.169E+04)	(7.717E+04)	(6.233E+05)	(5.818E+00)
0.130	1.442E-11	1.852E-11	2.376E-11	1.288E+00	10.000	(9.039E+03)	(9.039E+04)	(9.039E+05)	(1.000E+01)

Note. Observed resonances: from C. Ouellet & B. Singh (2013) and J. Dermigny et al. (2020). Normalization: see Table 2. Unobserved resonances: from J. Dermigny et al. (2020), D. S. Harrouz et al. (2022), and D. Gribble et al. (2025). High-temperature rates (in parentheses): matching to statistical model rate above $T = 5.4$ GK. Previous rates: J. Dermigny et al. (2020) and D. S. Harrouz et al. (2022). Other: we assumed that near $E_x = 7.44$ MeV only a single level, with $J^\pi = 11/2^+$, contributes to the rates (see the justification in D. Gribble et al. 2025).

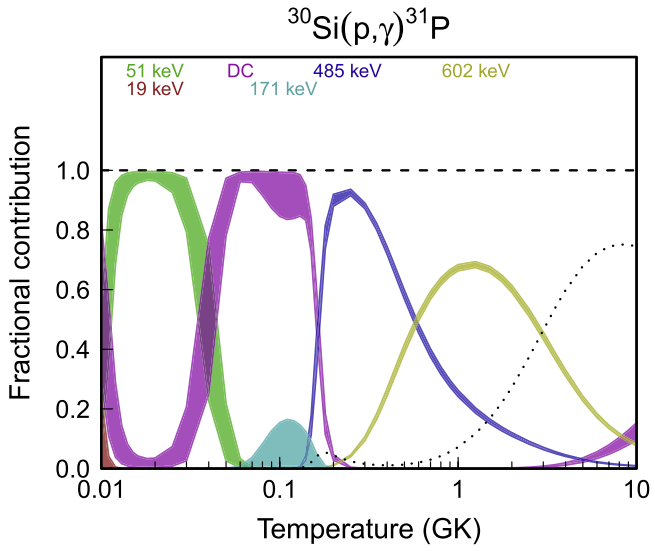

Figure 111. Fractional contributions to the total rate. "DC" refers to direct radiative capture. Resonance energies are given in the center-of-mass frame.

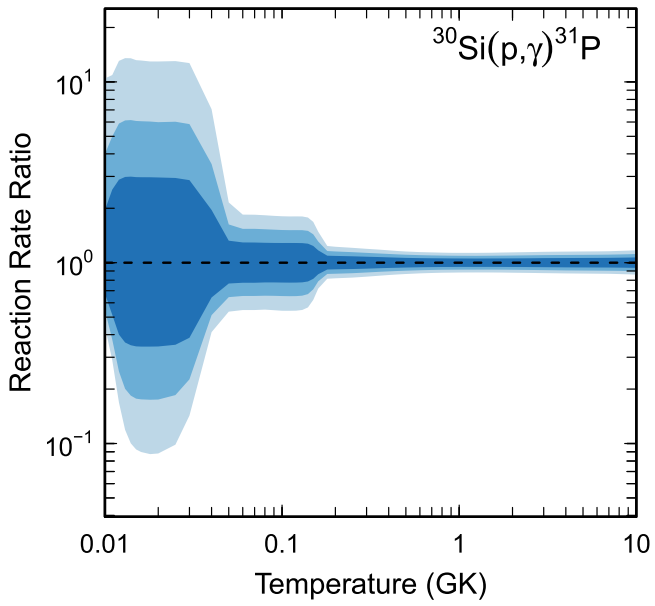

Figure 112. Reaction rate uncertainties versus temperature. The three different shades refer to coverage probabilities of 68%, 90%, and 98%.

Table 64
Total Laboratory Reaction Rates for $^{27}P(p,\gamma)^{28}S$

T (GK)	Low	Median	High	*f.u.*	T (GK)	Low	Median	High	*f.u.*
0.001	0.000E+00	0.000E+00	0.000E+00	1.000E+00	0.140	3.531E-13	7.010E-13	1.406E-12	2.019E+00
0.002	9.547E-79	1.893E-78	3.796E-78	1.998E+00	0.150	1.033E-12	2.052E-12	4.116E-12	2.024E+00
0.003	1.032E-67	2.047E-67	4.103E-67	1.998E+00	0.160	2.757E-12	5.475E-12	1.099E-11	2.028E+00
0.004	9.471E-61	1.878E-60	3.766E-60	1.998E+00	0.180	1.564E-11	3.106E-11	6.242E-11	2.039E+00
0.005	8.517E-56	1.689E-55	3.386E-55	1.998E+00	0.200	6.960E-11	1.383E-10	2.782E-10	2.051E+00
0.006	5.124E-52	1.016E-51	2.037E-51	1.998E+00	0.250	1.381E-09	2.749E-09	5.551E-09	2.087E+00
0.007	5.348E-49	1.061E-48	2.126E-48	1.998E+00	0.300	1.348E-08	2.686E-08	5.468E-08	2.125E+00
0.008	1.655E-46	3.281E-46	6.578E-46	1.998E+00	0.350	8.307E-08	1.661E-07	3.408E-07	2.163E+00
0.009	2.108E-44	4.181E-44	8.382E-44	1.998E+00	0.400	3.743E-07	7.491E-07	1.555E-06	2.196E+00
0.010	1.371E-42	2.720E-42	5.453E-42	1.998E+00	0.450	1.336E-06	2.682E-06	5.617E-06	2.221E+00
0.011	5.279E-41	1.047E-40	2.099E-40	1.998E+00	0.500	4.018E-06	8.065E-06	1.710E-05	2.234E+00
0.012	1.336E-39	2.650E-39	5.313E-39	1.998E+00	0.600	2.491E-05	5.010E-05	1.071E-04	2.229E+00
0.013	2.402E-38	4.765E-38	9.552E-38	1.998E+00	0.700	1.075E-04	2.152E-04	4.589E-04	2.188E+00
0.014	3.254E-37	6.453E-37	1.294E-36	1.998E+00	0.800	3.591E-04	7.126E-04	1.496E-03	2.126E+00
0.015	3.473E-36	6.888E-36	1.381E-35	1.998E+00	0.900	1.000E-03	1.949E-03	4.000E-03	2.052E+00
0.016	3.027E-35	6.004E-35	1.204E-34	1.998E+00	1.000	2.435E-03	4.633E-03	9.224E-03	1.975E+00
0.018	1.396E-33	2.768E-33	5.550E-33	1.998E+00	1.250	1.510E-02	2.679E-02	4.932E-02	1.811E+00
0.020	3.781E-32	7.500E-32	1.503E-31	1.998E+00	1.500	6.231E-02	1.064E-01	1.885E-01	1.749E+00
0.025	2.803E-29	5.559E-29	1.114E-28	1.998E+00	1.750	(7.296E-01)	(1.258E+00)	(2.414E+00)	(1.821E+00)
0.030	4.321E-27	8.570E-27	1.718E-26	1.998E+00	2.000	(2.398E+00)	(4.242E+00)	(9.176E+00)	(1.966E+00)
0.040	6.640E-24	1.317E-23	2.640E-23	1.998E+00	2.500	(7.601E+00)	(1.418E+01)	(3.761E+01)	(2.259E+00)
0.050	1.220E-21	2.420E-21	4.851E-21	1.998E+00	3.000	(1.498E+01)	(2.954E+01)	(9.285E+01)	(2.557E+00)
0.060	6.484E-20	1.286E-19	2.578E-19	1.999E+00	3.500	(2.393E+01)	(5.006E+01)	(1.818E+02)	(2.862E+00)
0.070	1.544E-18	3.061E-18	6.137E-18	2.000E+00	4.000	(3.386E+01)	(7.541E+01)	(3.109E+02)	(3.175E+00)
0.080	2.105E-17	4.176E-17	8.370E-17	2.002E+00	5.000	(5.454E+01)	(1.396E+02)	(7.120E+02)	(3.830E+00)
0.090	1.913E-16	3.795E-16	7.606E-16	2.004E+00	6.000	(7.328E+01)	(2.203E+02)	(1.340E+03)	(4.544E+00)
0.100	1.278E-15	2.535E-15	5.083E-15	2.006E+00	7.000	(8.698E+01)	(3.169E+02)	(2.238E+03)	(5.352E+00)
0.110	6.719E-15	1.333E-14	2.672E-14	2.009E+00	8.000	(9.292E+01)	(4.295E+02)	(3.454E+03)	(6.332E+00)
0.120	2.916E-14	5.786E-14	1.160E-13	2.012E+00	9.000	(8.855E+01)	(5.599E+02)	(5.050E+03)	(7.671E+00)
0.130	1.083E-13	2.148E-13	4.307E-13	2.015E+00	10.000	(7.115E+01)	(7.115E+02)	(7.115E+03)	(1.000E+01)

Note. Observed resonances: none. Normalization: none. Unobserved resonances: H. Herndl et al. (1995) and S. A. Gillespie et al. (2022). High-temperature rates (in parentheses): matching to statistical model rate above $T = 1.6$ GK. Previous rates: C. Iliadis et al. (2010c). Other: the direct-capture S factor was estimated using the shell-model spectroscopic factors of H. Herndl et al. (1995).

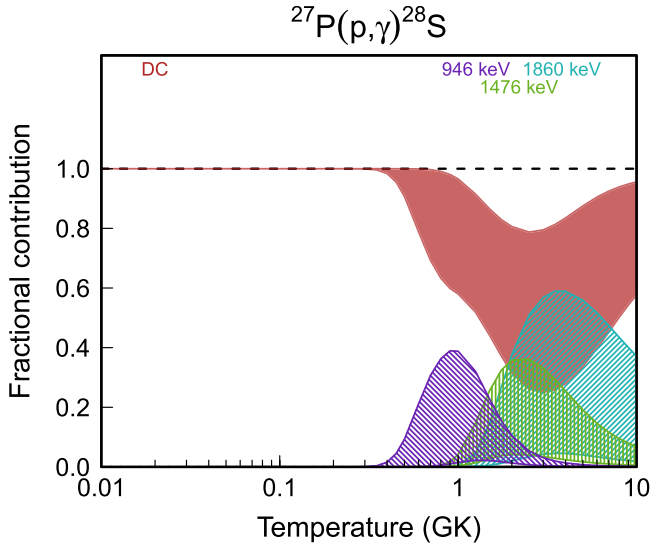

Figure 113. Fractional contributions to the total rate. "DC" refers to direct radiative capture. Resonance energies are given in the center-of-mass frame.

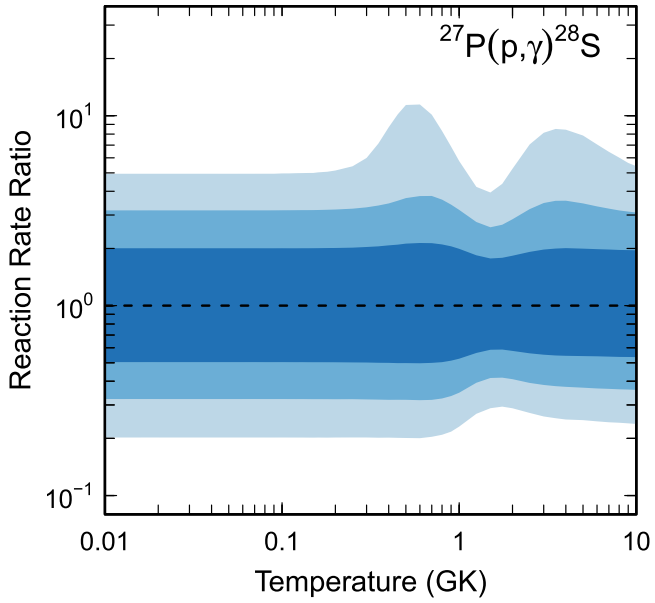

Figure 114. Reaction rate uncertainties versus temperature. The three different shades refer to coverage probabilities of 68%, 90%, and 98%.

Table 65
Total Laboratory Reaction Rates for ^{29}P(p,γ)^{30}S

T (GK)	Low	Median	High	*f.u.*	T (GK)	Low	Median	High	*f.u.*
0.001	0.000E+00	0.000E+00	0.000E+00	1.000E+00	0.140	1.413E-09	2.798E-09	5.519E-09	1.988E+00
0.002	3.784E-78	4.916E-78	6.380E-78	1.299E+00	0.150	6.499E-09	1.284E-08	2.529E-08	1.983E+00
0.003	4.176E-67	5.425E-67	7.040E-67	1.299E+00	0.160	2.470E-08	4.850E-08	9.533E-08	1.974E+00
0.004	3.883E-60	5.044E-60	6.546E-60	1.299E+00	0.180	2.293E-07	4.427E-07	8.622E-07	1.944E+00
0.005	3.523E-55	4.578E-55	5.940E-55	1.299E+00	0.200	1.389E-06	2.601E-06	4.994E-06	1.895E+00
0.006	2.135E-51	2.773E-51	3.599E-51	1.299E+00	0.250	4.075E-05	6.758E-05	1.194E-04	1.717E+00
0.007	2.240E-48	2.910E-48	3.777E-48	1.299E+00	0.300	4.504E-04	6.728E-04	1.065E-03	1.555E+00
0.008	6.962E-46	9.045E-46	1.174E-45	1.299E+00	0.350	2.664E-03	3.794E-03	5.556E-03	1.458E+00
0.009	8.904E-44	1.157E-43	1.501E-43	1.299E+00	0.400	1.030E-02	1.441E-02	2.024E-02	1.411E+00
0.010	5.811E-42	7.549E-42	9.797E-42	1.299E+00	0.450	2.958E-02	4.105E-02	5.688E-02	1.393E+00
0.011	2.243E-40	2.914E-40	3.782E-40	1.299E+00	0.500	6.857E-02	9.510E-02	1.312E-01	1.387E+00
0.012	5.692E-39	7.394E-39	9.595E-39	1.299E+00	0.600	2.387E-01	3.318E-01	4.594E-01	1.388E+00
0.013	1.026E-37	1.332E-37	1.729E-37	1.299E+00	0.700	5.735E-01	7.981E-01	1.108E+00	1.391E+00
0.014	1.392E-36	1.808E-36	2.346E-36	1.299E+00	0.800	1.098E+00	1.525E+00	2.117E+00	1.389E+00
0.015	1.488E-35	1.933E-35	2.509E-35	1.299E+00	0.900	1.824E+00	2.518E+00	3.479E+00	1.382E+00
0.016	1.299E-34	1.688E-34	2.190E-34	1.299E+00	1.000	2.759E+00	3.769E+00	5.166E+00	1.369E+00
0.018	6.007E-33	7.804E-33	1.013E-32	1.299E+00	1.250	6.179E+00	8.122E+00	1.078E+01	1.324E+00
0.020	1.631E-31	2.119E-31	2.750E-31	1.299E+00	1.500	(1.139E+01)	(1.458E+01)	(1.886E+01)	(1.287E+00)
0.025	1.214E-28	1.578E-28	2.047E-28	1.299E+00	1.750	(1.983E+01)	(2.605E+01)	(4.039E+01)	(1.432E+00)
0.030	1.878E-26	2.440E-26	3.167E-26	1.299E+00	2.000	(3.353E+01)	(4.524E+01)	(8.172E+01)	(1.578E+00)
0.040	2.900E-23	3.767E-23	4.888E-23	1.299E+00	2.500	(6.729E+01)	(9.597E+01)	(2.225E+02)	(1.872E+00)
0.050	5.344E-21	6.942E-21	9.009E-21	1.299E+00	3.000	(1.100E+02)	(1.664E+02)	(4.709E+02)	(2.172E+00)
0.060	2.847E-19	3.699E-19	4.799E-19	1.299E+00	3.500	(1.587E+02)	(2.555E+02)	(8.541E+02)	(2.476E+00)
0.070	7.044E-18	9.083E-18	1.170E-17	1.291E+00	4.000	(2.106E+02)	(3.626E+02)	(1.398E+03)	(2.788E+00)
0.080	1.514E-16	2.030E-16	2.833E-16	1.387E+00	5.000	(3.147E+02)	(6.285E+02)	(3.066E+03)	(3.438E+00)
0.090	4.724E-15	8.301E-15	1.533E-14	1.801E+00	6.000	(4.052E+02)	(9.634E+02)	(5.687E+03)	(4.140E+00)
0.100	1.437E-13	2.782E-13	5.433E-13	1.951E+00	7.000	(4.672E+02)	(1.372E+03)	(9.506E+03)	(4.932E+00)
0.110	2.661E-12	5.249E-12	1.035E-11	1.982E+00	8.000	(4.876E+02)	(1.873E+03)	(1.490E+04)	(5.897E+00)
0.120	3.066E-11	6.077E-11	1.200E-10	1.989E+00	9.000	(4.495E+02)	(2.495E+03)	(2.240E+04)	(7.263E+00)
0.130	2.419E-10	4.794E-10	9.466E-10	1.990E+00	10.000	(3.280E+02)	(3.280E+03)	(3.280E+04)	(1.000E+01)

Note. Observed resonances: none. Normalization: none. Unobserved resonances: P. M. Endt (1977; evaluated spectroscopic factors for mirror states); when no information was available, upper limit spectroscopic factors were assumed to be $C^2S < 0.01$. High-temperature rates (in parentheses): matching to statistical model rate above $T = 1.5$ GK. Previous rates: C. Iliadis et al. (2010c), S. Almaraz-Calderon et al. (2012), and K. Setoodehnia et al. (2013). Other: the γ-ray partial widths were calculated from the information evaluated for the mirror states (M. S. Basunia & A. Chakraborty 2024).

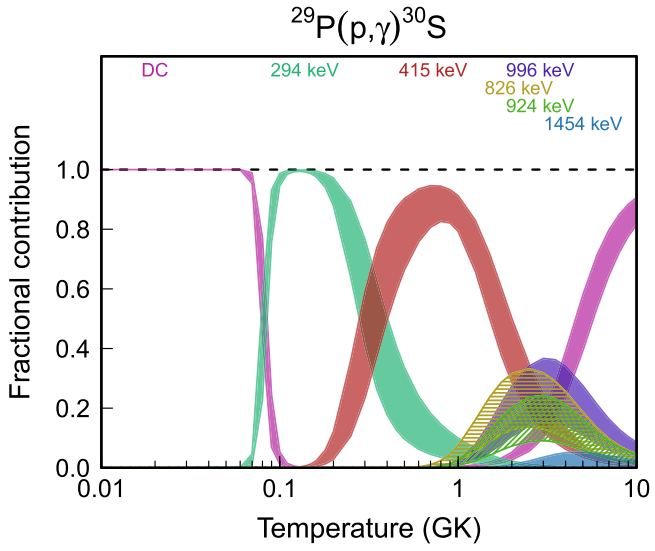

Figure 115. Fractional contributions to the total rate. "DC" refers to direct radiative capture. Resonance energies are given in the center-of-mass frame.

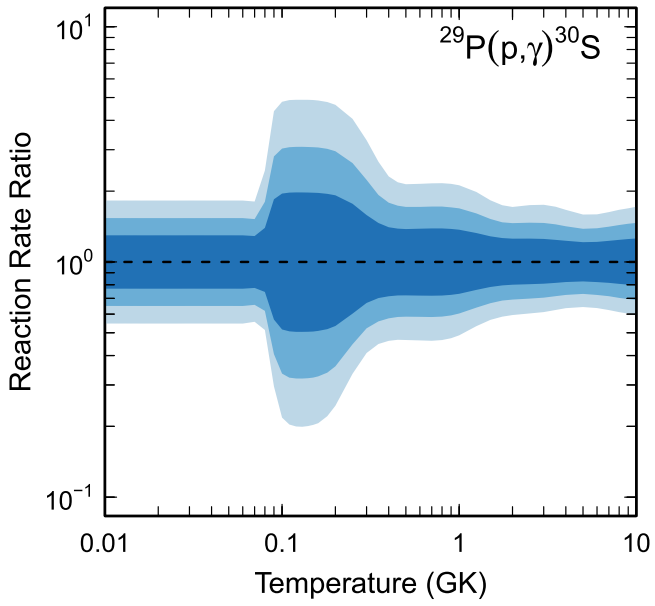

Figure 116. Reaction rate uncertainties versus temperature. The three different shades refer to coverage probabilities of 68%, 90%, and 98%.

Table 66
Total Laboratory Reaction Rates for $^{31}P(p,\gamma)^{32}S$

T (GK)	Low	Median	High	*f.u.*	T (GK)	Low	Median	High	*f.u.*
0.001	0.000E+00	0.000E+00	0.000E+00	1.000E+00	0.140	8.529E-08	1.210E-07	1.721E-07	1.419E+00
0.002	7.581E-78	1.296E-77	2.201E-77	1.704E+00	0.150	2.444E-07	3.395E-07	4.742E-07	1.391E+00
0.003	8.526E-67	1.457E-66	2.476E-66	1.704E+00	0.160	6.462E-07	8.697E-07	1.182E-06	1.352E+00
0.004	8.023E-60	1.371E-59	2.330E-59	1.704E+00	0.180	3.938E-06	4.914E-06	6.219E-06	1.259E+00
0.005	7.345E-55	1.255E-54	2.133E-54	1.704E+00	0.200	2.082E-05	2.467E-05	2.943E-05	1.191E+00
0.006	4.480E-51	7.657E-51	1.301E-50	1.704E+00	0.250	6.292E-04	7.265E-04	8.395E-04	1.157E+00
0.007	4.727E-48	8.079E-48	1.372E-47	1.704E+00	0.300	7.333E-03	8.411E-03	9.666E-03	1.149E+00
0.008	1.476E-45	2.522E-45	4.284E-45	1.704E+00	0.350	4.483E-02	5.101E-02	5.819E-02	1.140E+00
0.009	1.894E-43	3.238E-43	5.500E-43	1.704E+00	0.400	1.796E-01	2.029E-01	2.298E-01	1.132E+00
0.010	1.240E-41	2.120E-41	3.601E-41	1.704E+00	0.450	5.390E-01	6.058E-01	6.826E-01	1.126E+00
0.011	4.803E-40	8.208E-40	1.394E-39	1.704E+00	0.500	1.316E+00	1.475E+00	1.656E+00	1.123E+00
0.012	1.222E-38	2.088E-38	3.547E-38	1.704E+00	0.600	5.144E+00	5.755E+00	6.436E+00	1.119E+00
0.013	2.206E-37	3.771E-37	6.406E-37	1.704E+00	0.700	1.388E+01	1.552E+01	1.732E+01	1.118E+00
0.014	3.001E-36	5.129E-36	8.711E-36	1.704E+00	0.800	2.946E+01	3.296E+01	3.678E+01	1.118E+00
0.015	3.215E-35	5.494E-35	9.333E-35	1.704E+00	0.900	5.322E+01	5.953E+01	6.645E+01	1.118E+00
0.016	2.811E-34	4.805E-34	8.162E-34	1.704E+00	1.000	8.588E+01	9.595E+01	1.070E+02	1.117E+00
0.018	1.304E-32	2.229E-32	3.786E-32	1.704E+00	1.250	2.071E+02	2.306E+02	2.565E+02	1.113E+00
0.020	3.551E-31	6.070E-31	1.031E-30	1.704E+00	1.500	3.845E+02	4.258E+02	4.715E+02	1.108E+00
0.025	2.660E-28	4.546E-28	7.722E-28	1.704E+00	1.750	6.176E+02	6.807E+02	7.502E+02	1.103E+00
0.030	4.133E-26	7.064E-26	1.200E-25	1.704E+00	2.000	9.071E+02	9.961E+02	1.092E+03	1.098E+00
0.040	7.020E-23	1.164E-22	1.932E-22	1.661E+00	2.500	1.648E+03	1.800E+03	1.965E+03	1.093E+00
0.050	9.950E-20	1.541E-19	2.463E-19	1.584E+00	3.000	(2.558E+03)	(2.797E+03)	(3.145E+03)	(1.109E+00)
0.060	1.036E-16	1.658E-16	2.665E-16	1.609E+00	3.500	(3.413E+03)	(3.986E+03)	(7.009E+03)	(1.463E+00)
0.070	1.813E-14	2.841E-14	4.446E-14	1.570E+00	4.000	(4.220E+03)	(5.288E+03)	(1.265E+04)	(1.823E+00)
0.080	8.754E-13	1.343E-12	2.056E-12	1.535E+00	5.000	(5.548E+03)	(8.137E+03)	(2.978E+04)	(2.564E+00)
0.090	1.763E-11	2.657E-11	3.993E-11	1.508E+00	6.000	(6.341E+03)	(1.122E+04)	(5.527E+04)	(3.348E+00)
0.100	1.916E-10	2.853E-10	4.231E-10	1.487E+00	7.000	(6.503E+03)	(1.448E+04)	(8.972E+04)	(4.211E+00)
0.110	1.337E-09	1.968E-09	2.887E-09	1.470E+00	8.000	(5.972E+03)	(1.795E+04)	(1.340E+05)	(5.235E+00)
0.120	6.688E-09	9.759E-09	1.418E-08	1.455E+00	9.000	(4.685E+03)	(2.166E+04)	(1.891E+05)	(6.677E+00)
0.130	2.616E-08	3.772E-08	5.430E-08	1.440E+00	10.000	(2.569E+03)	(2.569E+04)	(2.569E+05)	(1.000E+01)

Note. Observed resonances: P. M. Endt (1990) and C. Iliadis et al. (1993b). Normalization: see Table 2. Unobserved resonances: J. Kalifa et al. (1978) and P. M. Endt (1990). High-temperature rates (in parentheses): matching to statistical model rate above $T = 2.9$ GK. Previous rates: C. Iliadis et al. (2010c). Other: the direct-capture contribution was estimated using experimental spectroscopic factors from J. Kalifa et al. (1978).

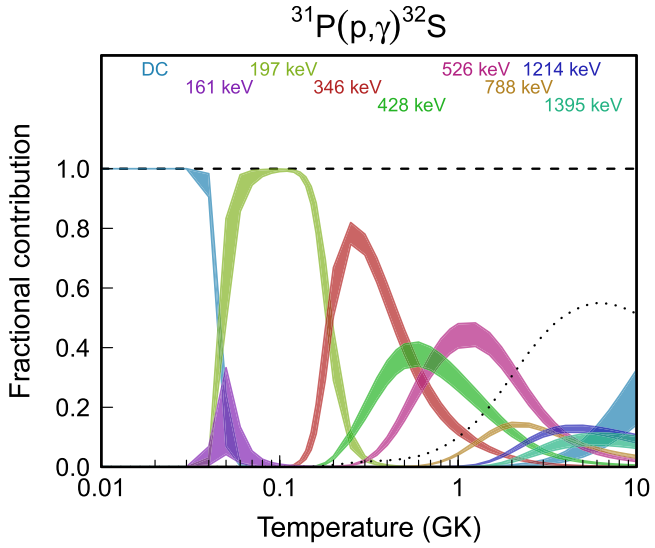

Figure 117. Fractional contributions to the total rate. "DC" refers to direct radiative capture. Resonance energies are given in the center-of-mass frame.

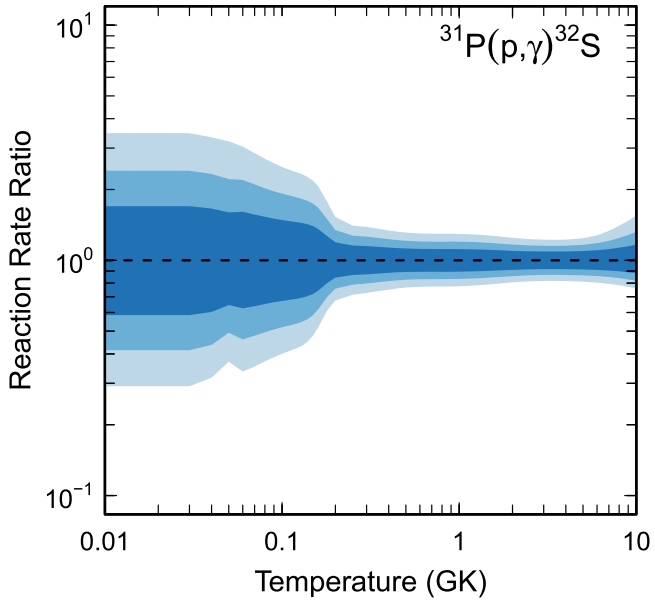

Figure 118. Reaction rate uncertainties versus temperature. The three different shades refer to coverage probabilities of 68%, 90%, and 98%.

Table 67
Total Laboratory Reaction Rates for $^{31}P(p,\alpha)^{28}Si$

T (GK)	Low	Median	High	*f.u.*	T (GK)	Low	Median	High	*f.u.*
0.001	0.000E+00	0.000E+00	0.000E+00	1.000E+00	0.140	3.101E-10	4.332E-10	7.024E-10	1.665E+00
0.002	0.000E+00	0.000E+00	0.000E+00	1.000E+00	0.150	1.877E-09	2.467E-09	3.386E-09	1.436E+00
0.003	0.000E+00	0.000E+00	0.000E+00	1.000E+00	0.160	9.603E-09	1.237E-08	1.621E-08	1.335E+00
0.004	0.000E+00	0.000E+00	0.000E+00	1.000E+00	0.180	1.543E-07	1.970E-07	2.523E-07	1.283E+00
0.005	0.000E+00	0.000E+00	0.000E+00	1.000E+00	0.200	1.444E-06	1.840E-06	2.345E-06	1.275E+00
0.006	0.000E+00	0.000E+00	0.000E+00	1.000E+00	0.250	7.897E-05	1.002E-04	1.273E-04	1.270E+00
0.007	1.269E-50	1.657E-50	2.181E-50	1.313E+00	0.300	1.111E-03	1.401E-03	1.770E-03	1.262E+00
0.008	4.078E-48	5.327E-48	7.014E-48	1.314E+00	0.350	7.566E-03	9.384E-03	1.168E-02	1.243E+00
0.009	5.386E-46	7.040E-46	9.278E-46	1.314E+00	0.400	3.486E-02	4.188E-02	5.079E-02	1.207E+00
0.010	3.626E-44	4.742E-44	6.256E-44	1.315E+00	0.450	1.280E-01	1.481E-01	1.732E-01	1.164E+00
0.011	1.443E-42	1.888E-42	2.492E-42	1.316E+00	0.500	3.986E-01	4.461E-01	5.041E-01	1.126E+00
0.012	3.772E-41	4.935E-41	6.516E-41	1.316E+00	0.600	2.534E+00	2.743E+00	2.975E+00	1.085E+00
0.013	6.994E-40	9.156E-40	1.210E-39	1.317E+00	0.700	1.032E+01	1.106E+01	1.184E+01	1.072E+00
0.014	9.760E-39	1.278E-38	1.690E-38	1.318E+00	0.800	3.085E+01	3.289E+01	3.511E+01	1.067E+00
0.015	1.073E-37	1.406E-37	1.859E-37	1.318E+00	0.900	7.493E+01	7.964E+01	8.470E+01	1.063E+00
0.016	9.625E-37	1.261E-36	1.669E-36	1.319E+00	1.000	1.588E+02	1.681E+02	1.782E+02	1.060E+00
0.018	4.690E-35	6.149E-35	8.147E-35	1.320E+00	1.250	7.468E+02	7.905E+02	8.378E+02	1.059E+00
0.020	1.340E-33	1.758E-33	2.332E-33	1.321E+00	1.500	2.723E+03	2.931E+03	3.170E+03	1.080E+00
0.025	1.126E-30	1.480E-30	1.967E-30	1.324E+00	1.750	8.198E+03	8.972E+03	9.880E+03	1.098E+00
0.030	1.960E-28	2.578E-28	3.433E-28	1.325E+00	2.000	2.057E+04	2.268E+04	2.518E+04	1.107E+00
0.040	9.069E-25	1.792E-24	4.645E-24	2.283E+00	2.500	8.226E+04	9.067E+04	1.006E+05	1.107E+00
0.050	3.408E-21	1.039E-20	3.226E-20	3.067E+00	3.000	2.147E+05	2.352E+05	2.592E+05	1.100E+00
0.060	1.372E-18	4.098E-18	1.230E-17	3.013E+00	3.500	4.279E+05	4.659E+05	5.097E+05	1.092E+00
0.070	1.020E-16	2.954E-16	8.607E-16	2.937E+00	4.000	7.152E+05	7.744E+05	8.423E+05	1.086E+00
0.080	2.582E-15	7.386E-15	2.127E-14	2.902E+00	5.000	1.445E+06	1.552E+06	1.672E+06	1.077E+00
0.090	3.197E-14	9.117E-14	2.631E-13	2.909E+00	6.000	(2.343E+06)	(2.834E+06)	(6.285E+06)	(1.714E+00)
0.100	2.404E-13	6.843E-13	1.994E-12	2.936E+00	7.000	(3.191E+06)	(4.947E+06)	(2.060E+07)	(2.857E+00)
0.110	1.317E-12	3.630E-12	1.072E-11	2.890E+00	8.000	(3.581E+06)	(7.726E+06)	(4.720E+07)	(4.133E+00)
0.120	6.909E-12	1.612E-11	4.514E-11	2.588E+00	9.000	(3.134E+06)	(1.113E+07)	(8.961E+07)	(5.802E+00)
0.130	4.497E-11	7.609E-11	1.720E-10	2.081E+00	10.000	(1.505E+06)	(1.505E+07)	(1.505E+08)	(1.000E+01)

Note. Observed resonances: P. M. Endt (1990), C. Iliadis et al. (1993b), and M. C. Moazen et al. (2011). Normalization: P. M. Endt (1990). Unobserved resonances: J. Kalifa et al. (1978) and J. G. Ross et al. (1995). High-temperature rates (in parentheses): matching to statistical model rate above $T = 5.4$ GK. Previous rates: C. Iliadis et al. (2010c). Other: none.

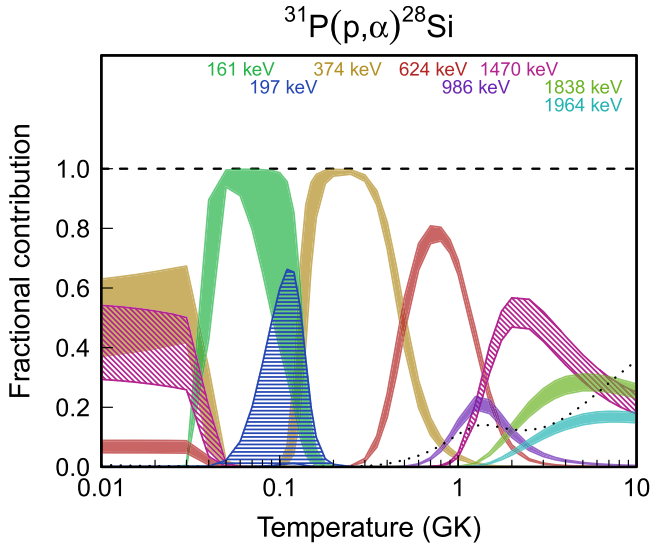

Figure 119. Fractional contributions to the total rate. Resonance energies are given in the center-of-mass frame.

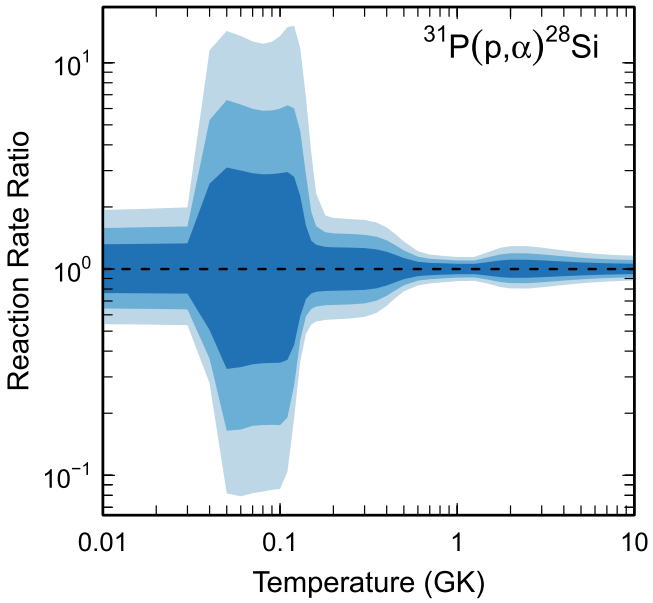

Figure 120. Reaction rate uncertainties versus temperature. The three different shades refer to coverage probabilities of 68%, 90%, and 98%.

Table 68
Total Laboratory Reaction Rates for $^{30}S(p,\gamma)^{31}Cl$

T (GK)	Low	Median	High	*f.u.*	T (GK)	Low	Median	High	*f.u.*
0.001	0.000E+00	0.000E+00	0.000E+00	1.000E+00	0.140	2.849E-14	4.886E-14	8.684E-14	1.840E+00
0.002	5.960E-83	1.014E-82	1.718E-82	1.700E+00	0.150	1.071E-13	1.930E-13	4.040E-13	2.151E+00
0.003	2.056E-71	3.497E-71	5.928E-71	1.700E+00	0.160	3.941E-13	7.917E-13	2.276E-12	2.601E+00
0.004	3.928E-64	6.681E-64	1.133E-63	1.700E+00	0.180	5.374E-12	1.584E-11	6.323E-11	3.388E+00
0.005	5.954E-59	1.013E-58	1.717E-58	1.700E+00	0.200	7.231E-11	2.551E-10	9.851E-10	3.612E+00
0.006	5.336E-55	9.077E-55	1.539E-54	1.700E+00	0.250	1.355E-08	4.327E-08	1.382E-07	3.208E+00
0.007	7.660E-52	1.303E-51	2.208E-51	1.700E+00	0.300	4.553E-07	1.286E-06	3.611E-06	2.832E+00
0.008	3.083E-49	5.243E-49	8.887E-49	1.700E+00	0.350	5.406E-06	1.402E-05	3.625E-05	2.597E+00
0.009	4.906E-47	8.344E-47	1.414E-46	1.700E+00	0.400	3.361E-05	8.195E-05	1.995E-04	2.445E+00
0.010	3.866E-45	6.575E-45	1.114E-44	1.700E+00	0.450	1.354E-04	3.167E-04	7.386E-04	2.342E+00
0.011	1.760E-43	2.993E-43	5.073E-43	1.700E+00	0.500	4.048E-04	9.171E-04	2.079E-03	2.269E+00
0.012	5.167E-42	8.787E-42	1.489E-41	1.700E+00	0.600	2.012E-03	4.368E-03	9.530E-03	2.174E+00
0.013	1.061E-40	1.804E-40	3.058E-40	1.700E+00	0.700	6.089E-03	1.289E-02	2.744E-02	2.118E+00
0.014	1.620E-39	2.755E-39	4.669E-39	1.700E+00	0.800	1.360E-02	2.826E-02	5.911E-02	2.082E+00
0.015	1.928E-38	3.278E-38	5.557E-38	1.700E+00	0.900	2.488E-02	5.095E-02	1.054E-01	2.055E+00
0.016	1.856E-37	3.157E-37	5.351E-37	1.700E+00	1.000	3.978E-02	8.049E-02	1.649E-01	2.033E+00
0.018	1.021E-35	1.736E-35	2.943E-35	1.700E+00	1.250	8.950E-02	1.764E-01	3.529E-01	1.983E+00
0.020	3.219E-34	5.475E-34	9.280E-34	1.700E+00	1.500	1.544E-01	2.913E-01	5.689E-01	1.917E+00
0.025	3.235E-31	5.502E-31	9.325E-31	1.700E+00	1.750	2.390E-01	4.240E-01	7.941E-01	1.826E+00
0.030	6.291E-29	1.070E-28	1.813E-28	1.700E+00	2.000	(4.828E-01)	(8.433E-01)	(1.659E+00)	(1.857E+00)
0.040	1.357E-25	2.307E-25	3.911E-25	1.700E+00	2.500	(1.579E+00)	(2.909E+00)	(7.180E+00)	(2.155E+00)
0.050	3.176E-23	5.401E-23	9.154E-23	1.700E+00	3.000	(3.367E+00)	(6.558E+00)	(1.948E+01)	(2.459E+00)
0.060	2.032E-21	3.456E-21	5.858E-21	1.700E+00	3.500	(5.843E+00)	(1.208E+01)	(4.194E+01)	(2.770E+00)
0.070	5.618E-20	9.551E-20	1.619E-19	1.700E+00	4.000	(8.972E+00)	(1.975E+01)	(7.849E+01)	(3.088E+00)
0.080	8.671E-19	1.474E-18	2.498E-18	1.700E+00	5.000	(1.692E+01)	(4.280E+01)	(2.131E+02)	(3.754E+00)
0.090	8.751E-18	1.488E-17	2.521E-17	1.700E+00	6.000	(2.636E+01)	(7.841E+01)	(4.691E+02)	(4.479E+00)
0.100	6.406E-17	1.089E-16	1.845E-16	1.699E+00	7.000	(3.584E+01)	(1.293E+02)	(9.035E+02)	(5.298E+00)
0.110	3.660E-16	6.212E-16	1.052E-15	1.698E+00	8.000	(4.327E+01)	(1.984E+02)	(1.586E+03)	(6.288E+00)
0.120	1.736E-15	2.939E-15	4.965E-15	1.695E+00	9.000	(4.598E+01)	(2.891E+02)	(2.601E+03)	(7.641E+00)
0.130	7.295E-15	1.233E-14	2.087E-14	1.714E+00	10.000	(4.059E+01)	(4.059E+02)	(4.059E+03)	(1.000E+01)

Note. Observed resonances: none. Normalization: none. Unobserved resonances: L. Axelsson et al. (1998), H. Fynbo et al. (2000), and C. Langer et al. (2014). High-temperature rates (in parentheses): matching to statistical model rate above $T = 1.9$ GK. Previous rates: C. Langer et al. (2014). Other: proton partial widths and the direct-capture S factor have been estimated using the experimental spectroscopic factors of the ^{31}Si mirror states (P. M. Endt 1990).

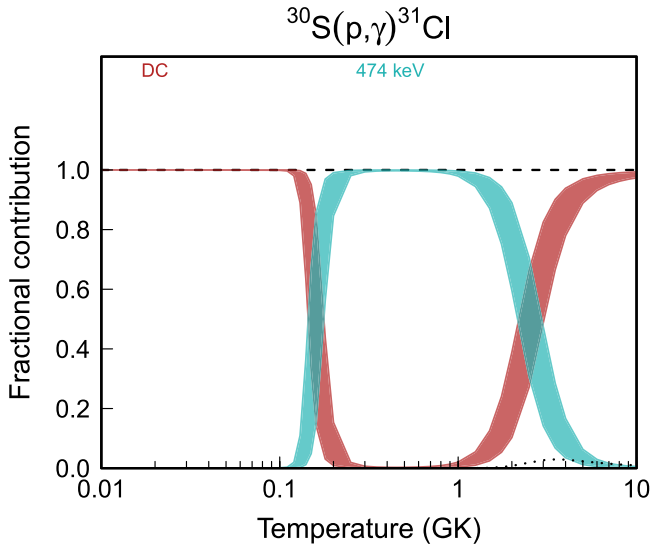

Figure 121. Fractional contributions to the total rate. "DC" refers to direct radiative capture. Resonance energies are given in the center-of-mass frame.

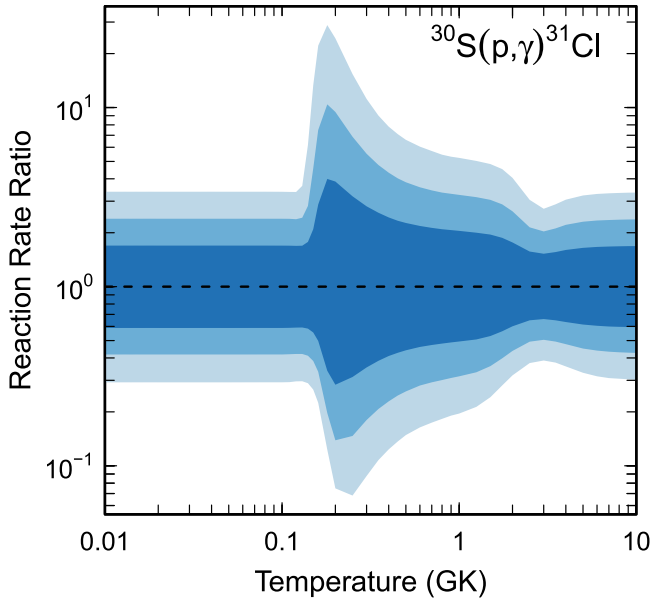

Figure 122. Reaction rate uncertainties versus temperature. The three different shades refer to coverage probabilities of 68%, 90%, and 98%.

Table 69
Total Laboratory Reaction Rates for $^{31}S(p,\gamma)^{32}Cl$

T (GK)	Low	Median	High	*f.u.*	T (GK)	Low	Median	High	*f.u.*
0.001	0.000E+00	0.000E+00	0.000E+00	1.000E+00	0.140	1.291E-11	3.773E-11	1.126E-10	2.958E+00
0.002	4.002E-82	6.790E-82	1.150E-81	1.701E+00	0.150	2.803E-11	8.133E-11	2.427E-10	2.942E+00
0.003	1.391E-70	2.361E-70	3.998E-70	1.701E+00	0.160	5.509E-11	1.588E-10	4.724E-10	2.919E+00
0.004	2.671E-63	4.531E-63	7.673E-63	1.701E+00	0.180	1.718E-10	4.820E-10	1.415E-09	2.847E+00
0.005	4.060E-58	6.889E-58	1.166E-57	1.701E+00	0.200	4.489E-10	1.181E-09	3.376E-09	2.711E+00
0.006	3.647E-54	6.188E-54	1.048E-53	1.701E+00	0.250	6.228E-09	1.097E-08	2.139E-08	1.906E+00
0.007	5.241E-51	8.894E-51	1.506E-50	1.701E+00	0.300	1.361E-07	2.377E-07	4.255E-07	1.765E+00
0.008	2.112E-48	3.583E-48	6.067E-48	1.701E+00	0.350	2.170E-06	3.928E-06	7.113E-06	1.808E+00
0.009	3.363E-46	5.707E-46	9.663E-46	1.701E+00	0.400	1.963E-05	3.520E-05	6.221E-05	1.781E+00
0.010	2.652E-44	4.500E-44	7.619E-44	1.701E+00	0.450	1.102E-04	1.946E-04	3.377E-04	1.752E+00
0.011	1.208E-42	2.049E-42	3.470E-42	1.701E+00	0.500	4.370E-04	7.615E-04	1.308E-03	1.729E+00
0.012	3.547E-41	6.018E-41	1.019E-40	1.701E+00	0.600	3.410E-03	5.805E-03	9.807E-03	1.699E+00
0.013	7.284E-40	1.236E-39	2.093E-39	1.701E+00	0.700	1.448E-02	2.430E-02	4.068E-02	1.680E+00
0.014	1.112E-38	1.887E-38	3.195E-38	1.701E+00	0.800	4.226E-02	7.003E-02	1.166E-01	1.665E+00
0.015	1.324E-37	2.246E-37	3.803E-37	1.701E+00	0.900	9.653E-02	1.578E-01	2.609E-01	1.650E+00
0.016	1.275E-36	2.163E-36	3.662E-36	1.701E+00	1.000	1.866E-01	3.004E-01	4.932E-01	1.633E+00
0.018	7.008E-35	1.189E-34	2.013E-34	1.701E+00	1.250	6.151E-01	9.517E-01	1.524E+00	1.581E+00
0.020	2.209E-33	3.749E-33	6.347E-33	1.701E+00	1.500	1.404E+00	2.081E+00	3.216E+00	1.525E+00
0.025	2.217E-30	3.762E-30	6.370E-30	1.701E+00	1.750	2.597E+00	3.717E+00	5.542E+00	1.472E+00
0.030	4.318E-28	7.317E-28	1.238E-27	1.699E+00	2.000	4.224E+00	5.877E+00	8.486E+00	1.428E+00
0.040	2.044E-24	3.635E-24	7.207E-24	1.947E+00	2.500	8.852E+00	1.192E+01	1.639E+01	1.367E+00
0.050	4.168E-21	1.163E-20	3.419E-20	2.846E+00	3.000	1.546E+01	2.062E+01	2.767E+01	1.342E+00
0.060	1.289E-18	3.779E-18	1.127E-17	2.968E+00	3.500	2.431E+01	3.258E+01	4.426E+01	1.350E+00
0.070	7.824E-17	2.306E-16	6.901E-16	2.983E+00	4.000	(4.316E+01)	(6.044E+01)	(1.050E+02)	(1.569E+00)
0.080	1.663E-15	4.905E-15	1.470E-14	2.986E+00	5.000	(1.067E+02)	(1.745E+02)	(5.434E+02)	(2.375E+00)
0.090	1.760E-14	5.191E-14	1.552E-13	2.986E+00	6.000	(1.770E+02)	(3.474E+02)	(1.561E+03)	(3.227E+00)
0.100	1.144E-13	3.371E-13	1.007E-12	2.984E+00	7.000	(2.371E+02)	(5.826E+02)	(3.419E+03)	(4.163E+00)
0.110	5.217E-13	1.538E-12	4.594E-12	2.981E+00	8.000	(2.691E+02)	(8.830E+02)	(6.398E+03)	(5.264E+00)
0.120	1.830E-12	5.386E-12	1.609E-11	2.977E+00	9.000	(2.539E+02)	(1.255E+03)	(1.082E+04)	(6.782E+00)
0.130	5.253E-12	1.541E-11	4.611E-11	2.969E+00	10.000	(1.703E+02)	(1.703E+03)	(1.703E+04)	(1.000E+01)

Note. Observed resonances: none. Normalization: none. Unobserved resonances: P. M. Endt (1977, 1990), P. M. Endt (1998), C. Wrede et al. (2010), M. Matoš et al. (2011), and L. Afanasieva et al. (2017). High-temperature rates (in parentheses): matching to statistical model rate above $T = 3.7$ GK. Previous rates: L. Afanasieva et al. (2017). Other: none.

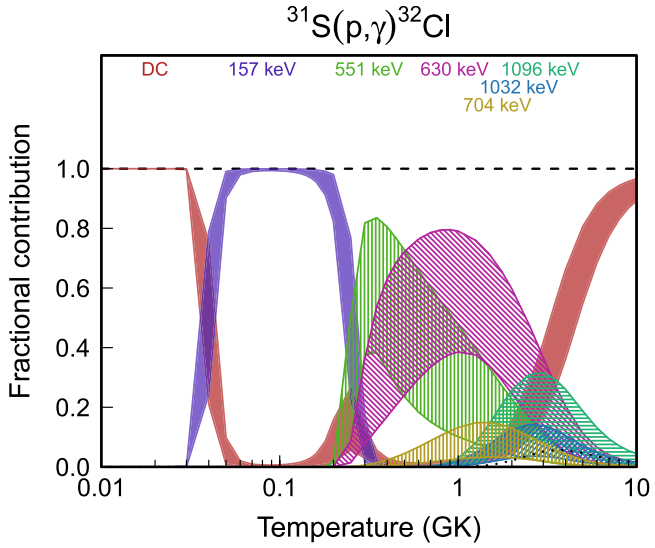

Figure 123. Fractional contributions to the total rate. "DC" refers to direct radiative capture. Resonance energies are given in the center-of-mass frame.

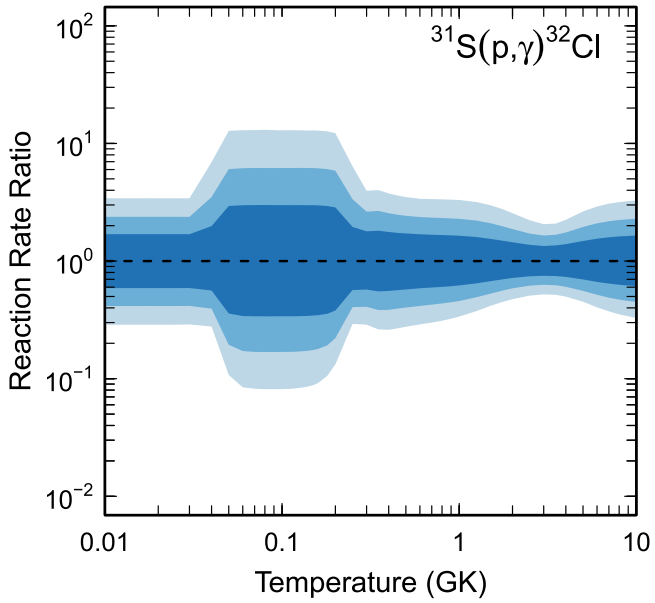

Figure 124. Reaction rate uncertainties versus temperature. The three different shades refer to coverage probabilities of 68%, 90%, and 98%.

Table 70
Total Laboratory Reaction Rates for $^{32}S(p,\gamma)^{33}Cl$

T (GK)	Low	Median	High	*f.u.*	T (GK)	Low	Median	High	*f.u.*
0.001	0.000E+00	0.000E+00	0.000E+00	1.000E+00	0.140	4.631E-13	5.690E-13	7.066E-13	1.243E+00
0.002	7.871E-82	9.847E-82	1.228E-81	1.250E+00	0.150	1.546E-12	1.839E-12	2.194E-12	1.194E+00
0.003	2.765E-70	3.459E-70	4.315E-70	1.250E+00	0.160	5.564E-12	6.502E-12	7.619E-12	1.172E+00
0.004	5.342E-63	6.683E-63	8.337E-63	1.250E+00	0.180	7.741E-11	9.089E-11	1.074E-10	1.177E+00
0.005	8.163E-58	1.021E-57	1.274E-57	1.250E+00	0.200	9.849E-10	1.142E-09	1.335E-09	1.165E+00
0.006	7.362E-54	9.210E-54	1.149E-53	1.250E+00	0.250	2.143E-07	2.377E-07	2.638E-07	1.110E+00
0.007	1.063E-50	1.329E-50	1.658E-50	1.250E+00	0.300	1.081E-05	1.199E-05	1.332E-05	1.111E+00
0.008	4.296E-48	5.372E-48	6.701E-48	1.250E+00	0.350	1.873E-04	2.083E-04	2.324E-04	1.115E+00
0.009	6.862E-46	8.580E-46	1.070E-45	1.250E+00	0.400	1.584E-03	1.765E-03	1.974E-03	1.117E+00
0.010	5.425E-44	6.783E-44	8.461E-44	1.250E+00	0.450	8.227E-03	9.174E-03	1.027E-02	1.118E+00
0.011	2.495E-42	3.115E-42	3.880E-42	1.248E+00	0.500	3.031E-02	3.381E-02	3.789E-02	1.119E+00
0.012	8.410E-41	1.045E-40	1.302E-40	1.248E+00	0.600	2.072E-01	2.314E-01	2.595E-01	1.120E+00
0.013	3.253E-39	4.801E-39	7.910E-39	1.577E+00	0.700	7.903E-01	8.829E-01	9.904E-01	1.120E+00
0.014	1.965E-37	3.729E-37	7.415E-37	1.935E+00	0.800	2.101E+00	2.348E+00	2.635E+00	1.121E+00
0.015	1.101E-35	2.210E-35	4.507E-35	2.023E+00	0.900	4.402E+00	4.920E+00	5.522E+00	1.121E+00
0.016	4.055E-34	8.163E-34	1.667E-33	2.031E+00	1.000	7.827E+00	8.749E+00	9.820E+00	1.121E+00
0.018	1.673E-31	3.355E-31	6.809E-31	2.020E+00	1.250	2.098E+01	2.346E+01	2.634E+01	1.121E+00
0.020	2.046E-29	4.077E-29	8.230E-29	2.009E+00	1.500	3.857E+01	4.312E+01	4.842E+01	1.121E+00
0.025	1.110E-25	2.193E-25	4.410E-25	1.997E+00	1.750	5.763E+01	6.443E+01	7.233E+01	1.121E+00
0.030	3.243E-23	6.407E-23	1.288E-22	1.993E+00	2.000	7.617E+01	8.511E+01	9.548E+01	1.120E+00
0.040	3.578E-20	7.069E-20	1.425E-19	1.994E+00	2.500	1.089E+02	1.214E+02	1.358E+02	1.117E+00
0.050	2.223E-18	4.393E-18	8.850E-18	1.998E+00	3.000	1.374E+02	1.522E+02	1.694E+02	1.111E+00
0.060	3.309E-17	6.551E-17	1.321E-16	2.001E+00	3.500	1.657E+02	1.826E+02	2.017E+02	1.104E+00
0.070	2.204E-16	4.363E-16	8.807E-16	2.002E+00	4.000	1.981E+02	2.174E+02	2.392E+02	1.099E+00
0.080	8.982E-16	1.770E-15	3.571E-15	1.993E+00	5.000	2.847E+02	3.144E+02	3.485E+02	1.107E+00
0.090	2.712E-15	5.239E-15	1.047E-14	1.959E+00	6.000	4.071E+02	4.586E+02	5.204E+02	1.132E+00
0.100	7.042E-15	1.288E-14	2.494E-14	1.871E+00	7.000	5.649E+02	6.495E+02	7.533E+02	1.156E+00
0.110	1.809E-14	2.962E-14	5.311E-14	1.710E+00	8.000	7.495E+02	8.767E+02	1.033E+03	1.174E+00
0.120	5.015E-14	7.150E-14	1.121E-13	1.510E+00	9.000	(7.570E+02)	(1.544E+03)	(8.391E+03)	(3.737E+00)
0.130	1.489E-13	1.926E-13	2.604E-13	1.343E+00	10.000	(2.449E+02)	(2.449E+03)	(2.449E+04)	(1.000E+01)

Note. Observed resonances: M. Aleonard et al. (1976) and C. Iliadis et al. (1992a). Normalization: see Table 2. Unobserved resonances: P. M. Endt (1977) and I. Lombardo et al. (2021). High-temperature rates (in parentheses): matching to statistical model rate above $T = 8.1$ GK. Previous rates: C. Iliadis et al. (2001, 2010c). Other: the strength of the $E_r^{c.m.} = 571$ keV resonance, listed in Table 1 of D. Sargood (1982), was used to normalize all measured resonance strengths. This assumption differs from previous work (C. Iliadis et al. 2001, 2010c).

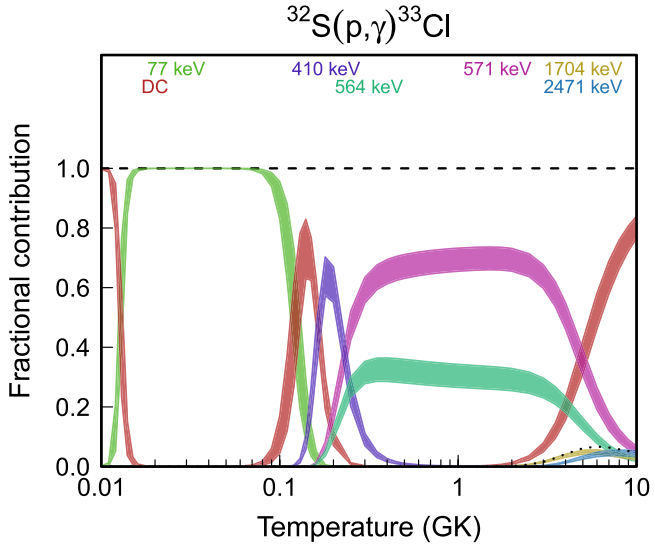

Figure 125. Fractional contributions to the total rate. "DC" refers to direct radiative capture. Resonance energies are given in the center-of-mass frame.

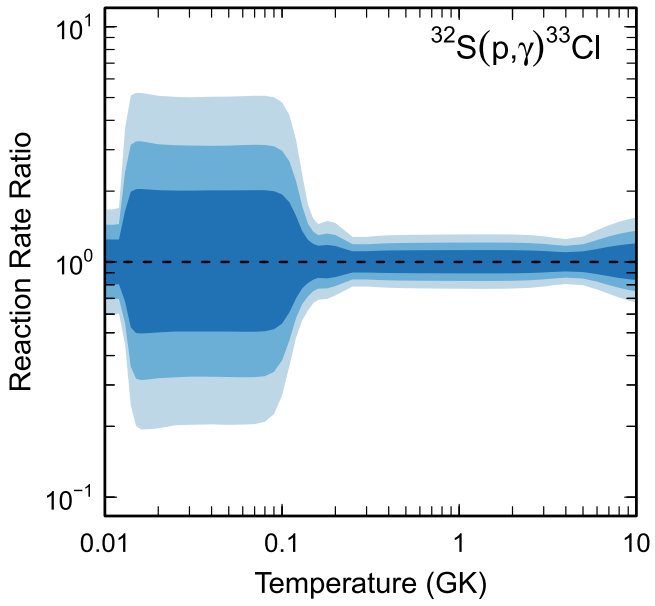

Figure 126. Reaction rate uncertainties versus temperature. The three different shades refer to coverage probabilities of 68%, 90%, and 98%.

Table 71
Total Laboratory Reaction Rates for $^{33}S(p,\gamma)^{34}Cl$

T (GK)	Low	Median	High	*f.u.*	T (GK)	Low	Median	High	*f.u.*
0.001	0.000E+00	0.000E+00	0.000E+00	1.000E+00	0.140	1.574E-08	2.763E-08	6.196E-08	2.109E+00
0.002	2.702E-81	3.102E-78	1.701E-76	9.789E+01	0.150	5.844E-08	9.474E-08	1.978E-07	1.971E+00
0.003	6.173E-70	4.391E-67	3.718E-65	1.097E+02	0.160	1.926E-07	2.930E-07	5.735E-07	1.863E+00
0.004	8.623E-63	1.295E-61	1.297E-58	8.088E+01	0.180	1.528E-06	2.155E-06	3.821E-06	1.721E+00
0.005	1.125E-57	2.742E-57	1.418E-54	3.712E+01	0.200	8.717E-06	1.177E-05	1.961E-05	1.637E+00
0.006	9.244E-54	1.828E-53	6.677E-52	1.593E+01	0.250	2.771E-04	3.433E-04	5.075E-04	1.488E+00
0.007	3.882E-48	1.967E-46	1.398E-45	2.260E+01	0.300	3.871E-03	4.575E-03	6.060E-03	1.367E+00
0.008	1.638E-45	6.227E-44	5.786E-43	1.482E+01	0.350	2.954E-02	3.424E-02	4.239E-02	1.288E+00
0.009	1.738E-43	5.321E-42	6.184E-41	1.491E+01	0.400	1.431E-01	1.642E-01	1.962E-01	1.239E+00
0.010	7.195E-42	1.772E-40	2.568E-39	1.492E+01	0.450	4.966E-01	5.671E-01	6.649E-01	1.209E+00
0.011	1.515E-40	3.509E-39	5.340E-38	1.483E+01	0.500	1.352E+00	1.537E+00	1.781E+00	1.189E+00
0.012	1.953E-39	4.225E-38	6.631E-37	1.452E+01	0.600	6.049E+00	6.851E+00	7.871E+00	1.167E+00
0.013	1.802E-38	3.359E-37	5.529E-36	1.383E+01	0.700	1.748E+01	1.976E+01	2.265E+01	1.157E+00
0.014	1.395E-37	2.192E-36	3.380E-35	1.246E+01	0.800	3.842E+01	4.342E+01	4.973E+01	1.152E+00
0.015	1.020E-36	1.597E-35	1.618E-34	1.021E+01	0.900	7.048E+01	7.967E+01	9.125E+01	1.150E+00
0.016	7.635E-36	1.148E-34	6.512E-34	7.491E+00	1.000	1.141E+02	1.290E+02	1.479E+02	1.148E+00
0.018	5.279E-34	4.034E-33	1.475E-32	5.016E+00	1.250	2.708E+02	3.065E+02	3.520E+02	1.147E+00
0.020	3.650E-32	2.095E-31	2.409E-30	7.710E+00	1.500	4.863E+02	5.509E+02	6.321E+02	1.145E+00
0.025	5.424E-28	5.903E-27	5.949E-26	9.675E+00	1.750	7.503E+02	8.501E+02	9.741E+02	1.144E+00
0.030	8.331E-25	6.453E-24	5.228E-23	7.526E+00	2.000	1.053E+03	1.194E+03	1.369E+03	1.143E+00
0.040	1.049E-20	5.628E-20	3.154E-19	5.385E+00	2.500	1.747E+03	1.988E+03	2.277E+03	1.143E+00
0.050	3.479E-18	1.696E-17	8.543E-17	4.807E+00	3.000	2.510E+03	2.863E+03	3.283E+03	1.145E+00
0.060	2.278E-16	9.103E-16	4.422E-15	4.310E+00	3.500	(3.225E+03)	(3.843E+03)	(6.014E+03)	(1.378E+00)
0.070	7.910E-15	2.321E-14	9.414E-14	3.521E+00	4.000	(3.826E+03)	(4.891E+03)	(1.083E+04)	(1.746E+00)
0.080	1.710E-13	4.238E-13	1.380E-12	2.973E+00	5.000	(4.686E+03)	(7.009E+03)	(2.461E+04)	(2.504E+00)
0.090	2.269E-12	5.452E-12	1.562E-11	2.754E+00	6.000	(5.053E+03)	(9.107E+03)	(4.380E+04)	(3.306E+00)
0.100	2.054E-11	4.858E-11	1.324E-10	2.670E+00	7.000	(4.923E+03)	(1.116E+04)	(6.815E+04)	(4.187E+00)
0.110	1.396E-10	3.172E-10	8.370E-10	2.579E+00	8.000	(4.306E+03)	(1.315E+04)	(9.737E+04)	(5.229E+00)
0.120	7.791E-10	1.651E-09	4.188E-09	2.440E+00	9.000	(3.220E+03)	(1.507E+04)	(1.311E+05)	(6.691E+00)
0.130	3.734E-09	7.218E-09	1.732E-08	2.273E+00	10.000	(1.690E+03)	(1.690E+04)	(1.690E+05)	(1.000E+01)

Note. Observed resonances: P. M. Endt (1990) and J. Fallis et al. (2013). Normalization: we renormalized the strengths of all resonances with $E_r^{c.m.} > 500$ keV to that of the $E_r^{lab} = 1211$ keV resonance in $^{34}S(p,\gamma)^{35}Cl$ (see Table 2). Unobserved resonances: A. Parikh et al. (2014). High-temperature rates (in parentheses): matching to statistical model rate above $T = 3.18$ GK. Previous rates: none. Other: none.

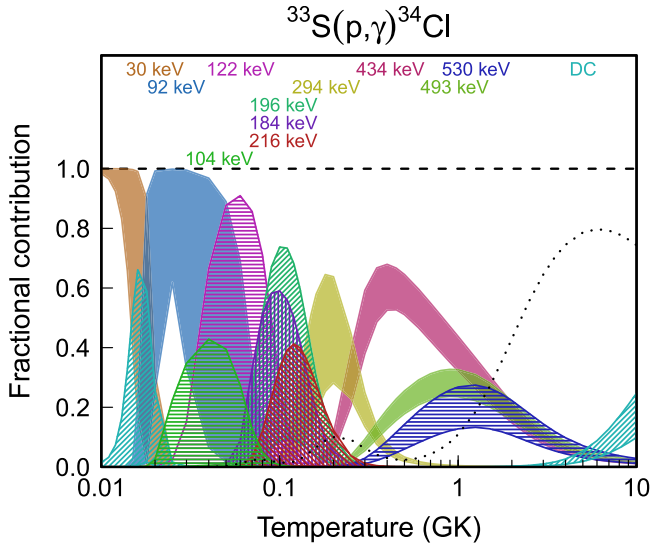

Figure 127. Fractional contributions to the total rate. "DC" refers to direct radiative capture. Resonance energies are given in the center-of-mass frame.

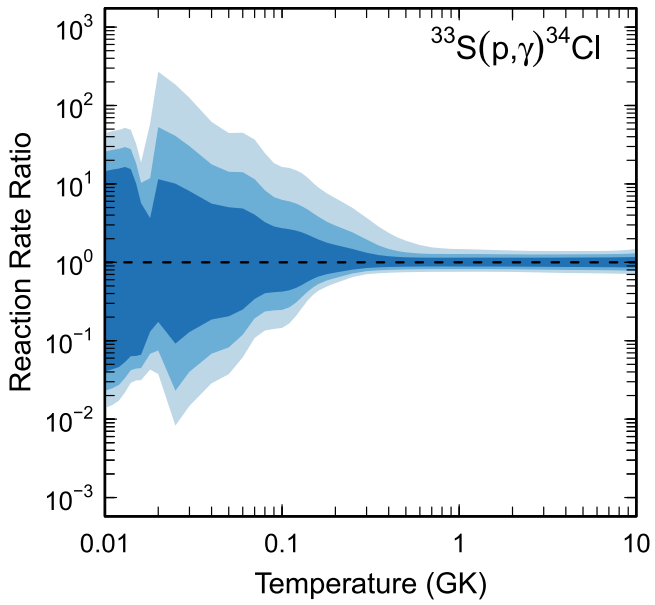

Figure 128. Reaction rate uncertainties versus temperature. The three different shades refer to coverage probabilities of 68%, 90%, and 98%.

Table 72
Total Laboratory Reaction Rates for $^{34}S(p,\gamma)^{35}Cl$

T (GK)	Low	Median	High	*f.u.*	T (GK)	Low	Median	High	*f.u.*
0.001	0.000E+00	0.000E+00	0.000E+00	1.000E+00	0.140	9.436E-09	1.550E-08	3.142E-08	1.881E+00
0.002	3.549E-80	2.858E-79	2.685E-78	7.202E+00	0.150	3.165E-08	4.842E-08	8.773E-08	1.731E+00
0.003	1.003E-69	2.432E-69	2.035E-68	4.591E+00	0.160	9.590E-08	1.409E-07	2.325E-07	1.616E+00
0.004	1.398E-62	2.472E-62	8.719E-62	4.936E+00	0.180	6.690E-07	9.405E-07	1.414E-06	1.495E+00
0.005	3.206E-57	2.092E-56	9.268E-55	1.423E+01	0.200	3.392E-06	4.728E-06	7.022E-06	1.478E+00
0.006	1.433E-52	4.600E-51	6.749E-50	1.514E+01	0.250	7.557E-05	1.097E-04	1.815E-04	1.598E+00
0.007	1.738E-48	3.216E-47	2.374E-46	1.093E+01	0.300	7.233E-04	1.107E-03	2.032E-03	1.715E+00
0.008	1.792E-45	2.497E-44	1.303E-43	8.977E+00	0.350	4.188E-03	6.502E-03	1.237E-02	1.758E+00
0.009	3.172E-43	4.382E-42	2.112E-41	8.776E+00	0.400	1.712E-02	2.606E-02	4.959E-02	1.747E+00
0.010	1.725E-41	2.692E-40	1.400E-39	9.358E+00	0.450	5.413E-02	7.971E-02	1.480E-01	1.709E+00
0.011	4.139E-40	7.574E-39	4.685E-38	9.851E+00	0.500	1.408E-01	2.003E-01	3.588E-01	1.659E+00
0.012	6.566E-39	1.214E-37	9.003E-37	9.370E+00	0.600	6.402E-01	8.497E-01	1.391E+00	1.549E+00
0.013	1.115E-37	1.298E-36	1.108E-35	7.798E+00	0.700	2.082E+00	2.605E+00	3.869E+00	1.440E+00
0.014	2.011E-36	1.130E-35	9.741E-35	5.909E+00	0.800	5.525E+00	6.600E+00	8.925E+00	1.343E+00
0.015	3.101E-35	1.041E-34	6.651E-34	4.371E+00	0.900	1.268E+01	1.468E+01	1.841E+01	1.265E+00
0.016	3.771E-34	9.847E-34	3.927E-33	3.344E+00	1.000	2.591E+01	2.950E+01	3.512E+01	1.209E+00
0.018	2.841E-32	6.007E-32	1.393E-31	2.341E+00	1.250	1.056E+02	1.185E+02	1.345E+02	1.141E+00
0.020	1.128E-30	2.253E-30	4.612E-30	2.062E+00	1.500	2.938E+02	3.285E+02	3.694E+02	1.124E+00
0.025	2.091E-27	1.268E-26	7.921E-26	5.120E+00	1.750	6.363E+02	7.109E+02	7.974E+02	1.120E+00
0.030	2.528E-24	2.518E-23	1.560E-22	6.030E+00	2.000	1.161E+03	1.297E+03	1.454E+03	1.119E+00
0.040	8.459E-20	3.703E-19	1.959E-18	4.048E+00	2.500	2.775E+03	3.100E+03	3.473E+03	1.119E+00
0.050	5.163E-17	1.415E-16	5.359E-16	2.978E+00	3.000	5.050E+03	5.640E+03	6.315E+03	1.119E+00
0.060	3.533E-15	8.410E-15	2.295E-14	2.475E+00	3.500	7.814E+03	8.726E+03	9.763E+03	1.118E+00
0.070	7.843E-14	1.702E-13	3.709E-13	2.182E+00	4.000	1.089E+04	1.216E+04	1.360E+04	1.118E+00
0.080	9.119E-13	1.858E-12	3.636E-12	2.020E+00	5.000	1.743E+04	1.945E+04	2.173E+04	1.117E+00
0.090	6.833E-12	1.363E-11	2.682E-11	2.018E+00	6.000	(2.243E+04)	(2.808E+04)	(6.196E+04)	(1.729E+00)
0.100	3.738E-11	7.521E-11	1.579E-10	2.111E+00	7.000	(2.427E+04)	(3.889E+04)	(1.616E+05)	(2.879E+00)
0.110	1.662E-10	3.375E-10	7.658E-10	2.185E+00	8.000	(2.287E+04)	(5.090E+04)	(3.106E+05)	(4.164E+00)
0.120	6.691E-10	1.314E-09	3.060E-09	2.161E+00	9.000	(1.755E+04)	(6.388E+04)	(5.143E+05)	(5.846E+00)
0.130	2.576E-09	4.661E-09	1.040E-08	2.041E+00	10.000	(7.767E+03)	(7.767E+04)	(7.767E+05)	(1.000E+01)

Note. Observed resonances: P. M. Endt (1990) and M. Lovely et al. (2021). Normalization: see Table 2. Unobserved resonances: K. Setoodehnia et al. (2019) and S. A. Gillespie et al. (2017). High-temperature rates (in parentheses): matching to statistical model rate above $T = 5.44$ GK. Previous rates: K. Setoodehnia et al. (2019). Other: none.

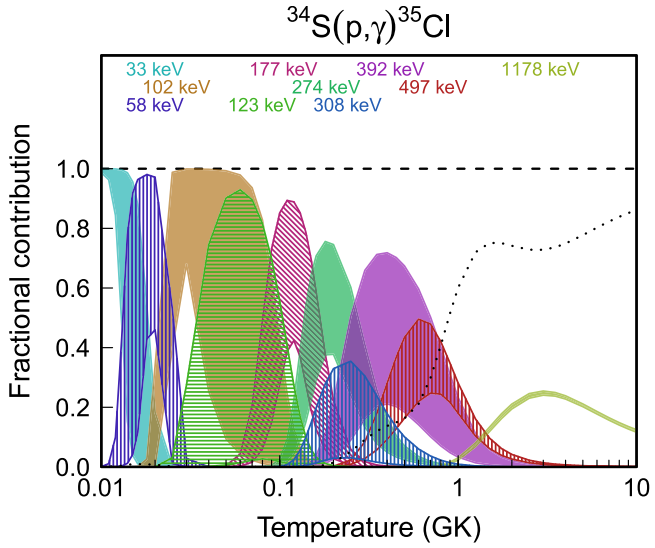

Figure 129. Fractional contributions to the total rate. Resonance energies are given in the center-of-mass frame.

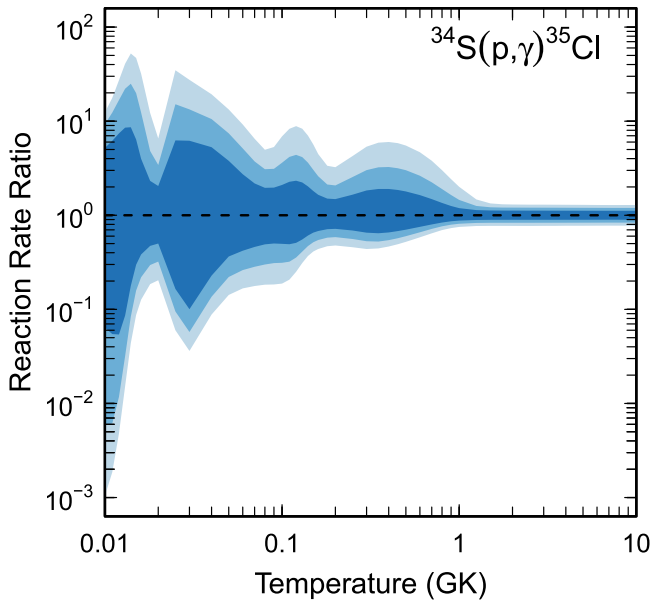

Figure 130. Reaction rate uncertainties versus temperature. The three different shades refer to coverage probabilities of 68%, 90%, and 98%.

Table 73
Total Laboratory Reaction Rates for ^{31}Cl(p,γ)^{32}Ar

T (GK)	Low	Median	High	*f.u.*	T (GK)	Low	Median	High	*f.u.*
0.001	0.000E+00	0.000E+00	0.000E+00	1.000E+00	0.140	1.772E-15	5.246E-15	1.561E-14	2.988E+00
0.002	5.591E-87	1.655E-86	4.925E-86	2.988E+00	0.150	5.731E-15	1.697E-14	5.049E-14	2.988E+00
0.003	5.896E-75	1.746E-74	5.193E-74	2.988E+00	0.160	1.676E-14	4.963E-14	1.476E-13	2.988E+00
0.004	2.282E-67	6.758E-67	2.010E-66	2.988E+00	0.180	1.118E-13	3.310E-13	9.847E-13	2.988E+00
0.005	5.721E-62	1.694E-61	5.039E-61	2.988E+00	0.200	5.722E-13	1.694E-12	5.041E-12	2.988E+00
0.006	7.530E-58	2.230E-57	6.633E-57	2.988E+00	0.250	1.501E-11	4.444E-11	1.322E-10	2.988E+00
0.007	1.469E-54	4.351E-54	1.294E-53	2.988E+00	0.300	1.805E-10	5.344E-10	1.590E-09	2.988E+00
0.008	7.621E-52	2.257E-51	6.713E-51	2.988E+00	0.350	1.311E-09	3.881E-09	1.155E-08	2.988E+00
0.009	1.503E-49	4.452E-49	1.324E-48	2.988E+00	0.400	6.713E-09	1.988E-08	5.913E-08	2.988E+00
0.010	1.425E-47	4.221E-47	1.256E-46	2.988E+00	0.450	2.666E-08	7.894E-08	2.348E-07	2.988E+00
0.011	7.629E-46	2.259E-45	6.720E-45	2.988E+00	0.500	8.735E-08	2.586E-07	7.692E-07	2.987E+00
0.012	2.585E-44	7.656E-44	2.277E-43	2.988E+00	0.600	6.160E-07	1.823E-06	5.423E-06	2.986E+00
0.013	6.036E-43	1.787E-42	5.317E-42	2.988E+00	0.700	2.928E-06	8.657E-06	2.572E-05	2.982E+00
0.014	1.035E-41	3.064E-41	9.114E-41	2.988E+00	0.800	1.063E-05	3.134E-05	9.286E-05	2.972E+00
0.015	1.368E-40	4.051E-40	1.205E-39	2.988E+00	0.900	3.179E-05	9.299E-05	2.747E-04	2.955E+00
0.016	1.451E-39	4.296E-39	1.278E-38	2.988E+00	1.000	8.217E-05	2.379E-04	6.996E-04	2.933E+00
0.018	9.464E-38	2.802E-37	8.337E-37	2.988E+00	1.250	5.593E-04	1.579E-03	4.565E-03	2.870E+00
0.020	3.458E-36	1.024E-35	3.046E-35	2.988E+00	1.500	2.430E-03	6.699E-03	1.906E-02	2.817E+00
0.025	4.669E-33	1.383E-32	4.113E-32	2.988E+00	1.750	7.793E-03	2.120E-02	5.949E-02	2.782E+00
0.030	1.138E-30	3.370E-30	1.002E-29	2.988E+00	2.000	2.009E-02	5.420E-02	1.511E-01	2.764E+00
0.040	3.414E-27	1.011E-26	3.007E-26	2.988E+00	2.500	8.583E-02	2.312E-01	6.437E-01	2.759E+00
0.050	1.011E-24	2.992E-24	8.902E-24	2.988E+00	3.000	2.519E-01	6.846E-01	1.927E+00	2.778E+00
0.060	7.733E-23	2.290E-22	6.812E-22	2.988E+00	3.500	5.840E-01	1.608E+00	4.579E+00	2.805E+00
0.070	2.465E-21	7.299E-21	2.171E-20	2.988E+00	4.000	1.154E+00	3.213E+00	9.223E+00	2.833E+00
0.080	4.279E-20	1.267E-19	3.769E-19	2.988E+00	5.000	3.229E+00	9.149E+00	2.661E+01	2.877E+00
0.090	4.769E-19	1.412E-18	4.201E-18	2.988E+00	6.000	6.680E+00	1.915E+01	5.611E+01	2.906E+00
0.100	3.800E-18	1.125E-17	3.347E-17	2.988E+00	7.000	1.137E+01	3.278E+01	9.653E+01	2.926E+00
0.110	2.330E-17	6.901E-17	2.053E-16	2.988E+00	8.000	1.686E+01	4.892E+01	1.444E+02	2.938E+00
0.120	1.159E-16	3.433E-16	1.021E-15	2.988E+00	9.000	2.280E+01	6.630E+01	1.961E+02	2.947E+00
0.130	4.864E-16	1.440E-15	4.284E-15	2.988E+00	10.000	2.870E+01	8.383E+01	2.482E+02	2.953E+00

Note. Observed resonances: none. Normalization: none. Unobserved resonances: H. Herndl et al. (1995). High-temperature rates (in parentheses): the total rate is dominated, at all temperatures, by the direct-capture process, and no corrections for higher-lying resonances have been applied. Previous rates: C. Iliadis et al. (2010c). Other: the resonance energy corresponding to the 2_2^+ level in ^{32}Ar was estimated from the Coulomb shift calculation of H. Herndl et al. (1995). This resonance makes only a minor contribution to the total rate; see Figure 131. The direct-capture S factor was also estimated using the shell-model spectroscopic factors given in H. Herndl et al. (1995).

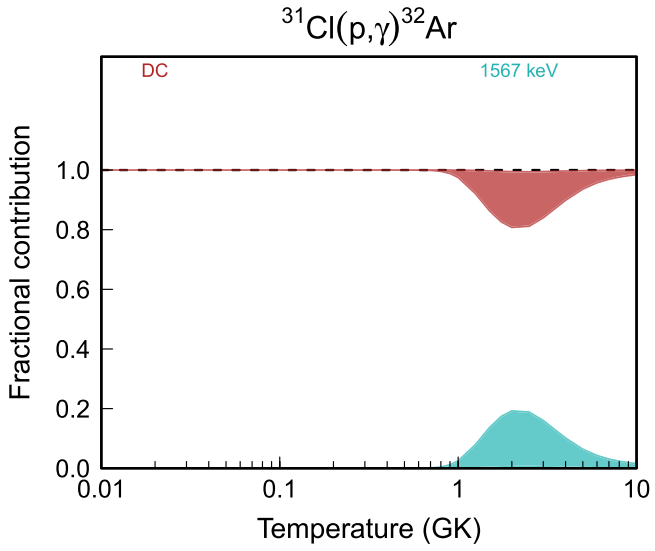

Figure 131. Fractional contributions to the total rate. "DC" refers to direct radiative capture. Resonance energies are given in the center-of-mass frame.

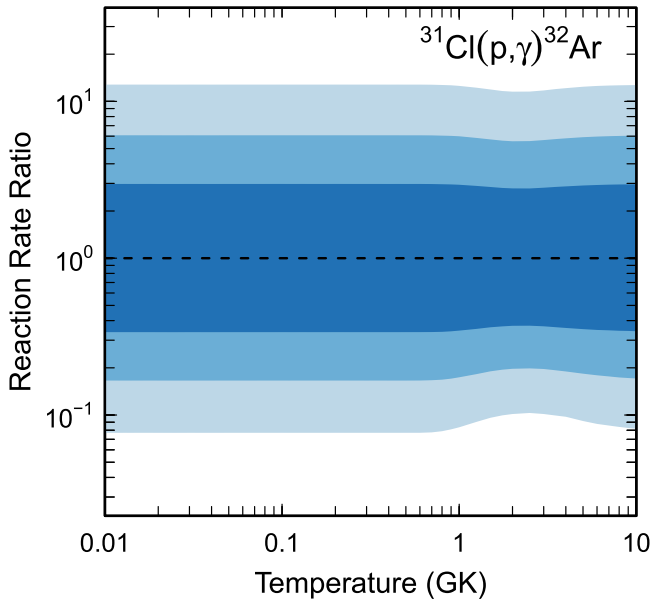

Figure 132. Reaction rate uncertainties versus temperature. The three different shades refer to coverage probabilities of 68%, 90%, and 98%.

Table 74
Total Laboratory Reaction Rates for $^{35}Cl(p,\gamma)^{36}Ar$

T (GK)	Low	Median	High	*f.u.*	T (GK)	Low	Median	High	*f.u.*
0.001	0.000E+00	0.000E+00	0.000E+00	1.000E+00	0.140	7.310E-10	1.547E-09	3.031E-09	1.962E+00
0.002	2.014E-85	4.005E-85	7.996E-85	2.003E+00	0.150	3.151E-09	5.266E-09	8.792E-09	1.665E+00
0.003	2.193E-73	4.361E-73	8.707E-73	2.003E+00	0.160	1.158E-08	1.713E-08	2.551E-08	1.493E+00
0.004	8.661E-66	1.722E-65	3.438E-65	2.003E+00	0.180	1.100E-07	1.475E-07	1.986E-07	1.349E+00
0.005	2.202E-60	4.378E-60	8.740E-60	2.003E+00	0.200	7.686E-07	9.846E-07	1.274E-06	1.291E+00
0.006	3.059E-56	5.975E-56	1.179E-55	1.972E+00	0.250	3.874E-05	4.744E-05	5.829E-05	1.228E+00
0.007	3.252E-52	7.726E-52	2.117E-51	2.557E+00	0.300	6.856E-04	8.357E-04	1.023E-03	1.223E+00
0.008	7.521E-48	2.043E-47	5.560E-47	2.729E+00	0.350	5.834E-03	7.101E-03	8.683E-03	1.222E+00
0.009	2.665E-44	6.552E-44	1.598E-43	2.457E+00	0.400	3.009E-02	3.648E-02	4.443E-02	1.217E+00
0.010	1.807E-41	4.115E-41	9.301E-41	2.277E+00	0.450	1.096E-01	1.322E-01	1.602E-01	1.210E+00
0.011	3.659E-39	7.889E-39	1.700E-38	2.162E+00	0.500	3.116E-01	3.738E-01	4.504E-01	1.204E+00
0.012	2.990E-37	6.232E-37	1.297E-36	2.089E+00	0.600	1.532E+00	1.821E+00	2.169E+00	1.191E+00
0.013	1.224E-35	2.492E-35	5.077E-35	2.044E+00	0.700	4.931E+00	5.811E+00	6.864E+00	1.181E+00
0.014	2.905E-34	5.825E-34	1.176E-33	2.018E+00	0.800	1.222E+01	1.432E+01	1.678E+01	1.173E+00
0.015	4.462E-33	8.909E-33	1.788E-32	2.004E+00	0.900	2.545E+01	2.967E+01	3.460E+01	1.167E+00
0.016	4.825E-32	9.609E-32	1.927E-31	2.000E+00	1.000	4.677E+01	5.436E+01	6.318E+01	1.163E+00
0.018	2.495E-30	4.990E-30	1.004E-29	2.008E+00	1.250	1.481E+02	1.713E+02	1.983E+02	1.158E+00
0.020	5.742E-29	1.158E-28	2.351E-28	2.028E+00	1.500	3.328E+02	3.843E+02	4.438E+02	1.156E+00
0.025	1.510E-26	3.152E-26	6.589E-26	2.094E+00	1.750	6.048E+02	6.978E+02	8.054E+02	1.155E+00
0.030	5.878E-25	1.261E-24	2.716E-24	2.157E+00	2.000	9.566E+02	1.103E+03	1.272E+03	1.154E+00
0.040	6.259E-23	1.286E-22	2.735E-22	2.101E+00	2.500	1.857E+03	2.140E+03	2.469E+03	1.154E+00
0.050	9.847E-21	6.386E-20	1.804E-19	3.677E+00	3.000	2.952E+03	3.403E+03	3.927E+03	1.154E+00
0.060	3.484E-18	3.045E-17	8.361E-17	4.194E+00	3.500	4.180E+03	4.818E+03	5.560E+03	1.154E+00
0.070	2.763E-16	2.461E-15	6.568E-15	4.169E+00	4.000	5.485E+03	6.324E+03	7.302E+03	1.155E+00
0.080	7.177E-15	6.423E-14	1.691E-13	4.147E+00	5.000	(8.083E+03)	(9.450E+03)	(1.219E+04)	(1.229E+00)
0.090	8.976E-14	7.968E-13	2.078E-12	4.109E+00	6.000	(9.287E+03)	(1.319E+04)	(3.998E+04)	(2.226E+00)
0.100	7.016E-13	5.895E-12	1.527E-11	3.968E+00	7.000	(9.514E+03)	(1.720E+04)	(8.210E+04)	(3.291E+00)
0.110	4.326E-12	3.049E-11	7.787E-11	3.595E+00	8.000	(8.651E+03)	(2.151E+04)	(1.402E+05)	(4.501E+00)
0.120	2.558E-11	1.244E-10	3.060E-10	3.011E+00	9.000	(6.578E+03)	(2.620E+04)	(2.164E+05)	(6.120E+00)
0.130	1.447E-10	4.490E-10	1.011E-09	2.418E+00	10.000	(3.135E+03)	(3.135E+04)	(3.135E+05)	(1.000E+01)

Note. Observed resonances: P. Johnson et al. (1974), P. M. Endt & C. van der Leun (1978), and C. Iliadis et al. (1994). Normalization: see Table 2. Unobserved resonances: C. Iliadis et al. (1994) and J. G. Ross et al. (1995). High-temperature rates (in parentheses): matching to statistical model rate above $T = 4.9$ GK. Previous rates: C. Iliadis et al. (2010c). Other: the direct-capture contribution was calculated using experimental spectroscopic factors of P. M. Endt (1977), P. M. Endt & C. van der Leun (1978), and C. Iliadis et al. (1994).

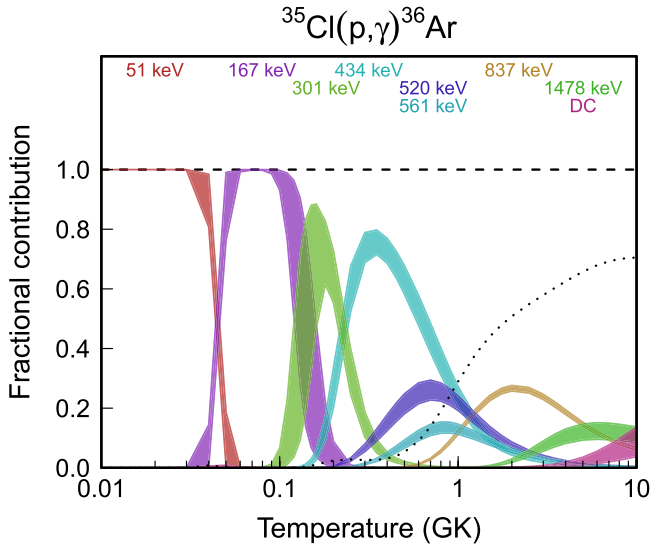

Figure 133. Fractional contributions to the total rate. "DC" refers to direct radiative capture. Resonance energies are given in the center-of-mass frame.

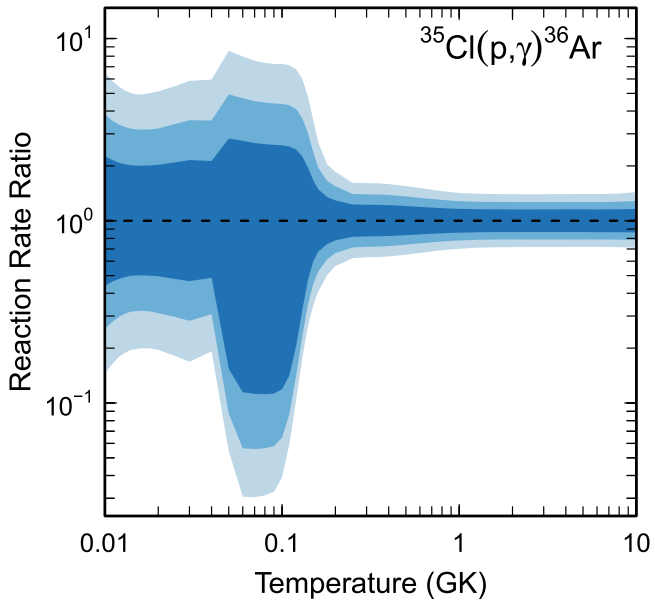

Figure 134. Reaction rate uncertainties versus temperature. The three different shades refer to coverage probabilities of 68%, 90%, and 98%.

Table 75
Total Laboratory Reaction Rates for $^{35}Cl(p,\alpha)^{32}S$

T (GK)	Low	Median	High	*f.u.*	T (GK)	Low	Median	High	*f.u.*
0.001	0.000E+00	0.000E+00	0.000E+00	1.000E+00	0.140	2.956E-12	1.486E-11	4.846E-11	4.131E+00
0.002	7.965E-92	1.592E-91	3.184E-91	2.002E+00	0.150	1.414E-11	6.060E-11	1.880E-10	3.671E+00
0.003	9.848E-80	1.969E-79	3.937E-79	2.002E+00	0.160	5.878E-11	2.209E-10	6.638E-10	3.377E+00
0.004	4.305E-72	8.607E-72	1.721E-71	2.002E+00	0.180	7.099E-10	2.317E-09	6.369E-09	3.002E+00
0.005	1.202E-66	2.397E-66	4.779E-66	1.996E+00	0.200	6.028E-09	1.772E-08	4.477E-08	2.736E+00
0.006	6.382E-62	3.493E-61	2.721E-60	5.978E+00	0.250	3.969E-07	9.224E-07	1.996E-06	2.315E+00
0.007	2.464E-56	3.435E-55	2.578E-54	1.083E+01	0.300	8.040E-06	1.698E-05	3.295E-05	2.090E+00
0.008	8.762E-52	1.156E-50	7.918E-50	1.170E+01	0.350	8.086E-05	1.610E-04	2.966E-04	1.927E+00
0.009	2.997E-48	3.763E-47	2.419E-46	1.146E+01	0.400	5.211E-04	9.718E-04	1.744E-03	1.795E+00
0.010	1.934E-45	2.398E-44	1.471E-43	1.122E+01	0.450	2.482E-03	4.254E-03	7.442E-03	1.690E+00
0.011	3.810E-43	4.652E-42	2.774E-41	1.105E+01	0.500	9.364E-03	1.488E-02	2.509E-02	1.606E+00
0.012	3.020E-41	3.697E-40	2.164E-39	1.093E+01	0.600	8.100E-02	1.145E-01	1.767E-01	1.477E+00
0.013	1.212E-39	1.480E-38	8.579E-38	1.086E+01	0.700	4.388E-01	5.777E-01	8.166E-01	1.390E+00
0.014	2.857E-38	3.476E-37	1.998E-36	1.082E+01	0.800	1.684E+00	2.130E+00	2.833E+00	1.334E+00
0.015	4.338E-37	5.323E-36	3.038E-35	1.080E+01	0.900	4.998E+00	6.187E+00	7.957E+00	1.297E+00
0.016	4.677E-36	5.742E-35	3.265E-34	1.079E+01	1.000	1.226E+01	1.496E+01	1.888E+01	1.269E+00
0.018	2.428E-34	2.964E-33	1.695E-32	1.080E+01	1.250	6.699E+01	7.935E+01	9.662E+01	1.217E+00
0.020	5.612E-33	6.863E-32	3.943E-31	1.082E+01	1.500	2.321E+02	2.674E+02	3.141E+02	1.172E+00
0.025	1.512E-30	1.864E-29	1.089E-28	1.089E+01	1.750	6.253E+02	7.023E+02	7.983E+02	1.136E+00
0.030	5.992E-29	7.401E-28	4.394E-27	1.076E+01	2.000	1.424E+03	1.570E+03	1.744E+03	1.110E+00
0.040	1.845E-26	1.279E-25	5.562E-25	6.556E+00	2.500	(5.209E+03)	(5.663E+03)	(6.366E+03)	(1.106E+00)
0.050	1.998E-24	7.161E-23	1.270E-21	1.948E+01	3.000	(1.465E+04)	(1.693E+04)	(2.905E+04)	(1.436E+00)
0.060	2.147E-22	3.275E-20	6.097E-19	3.739E+01	3.500	(3.374E+04)	(4.162E+04)	(9.605E+04)	(1.771E+00)
0.070	1.597E-20	2.628E-18	4.843E-17	3.872E+01	4.000	(6.677E+04)	(8.832E+04)	(2.561E+05)	(2.111E+00)
0.080	7.056E-19	6.860E-17	1.258E-15	2.928E+01	5.000	(1.875E+05)	(2.900E+05)	(1.184E+06)	(2.815E+00)
0.090	2.454E-17	8.758E-16	1.562E-14	1.941E+01	6.000	(3.825E+05)	(7.120E+05)	(3.749E+06)	(3.564E+00)
0.100	5.380E-16	7.900E-15	1.157E-13	1.262E+01	7.000	(6.169E+05)	(1.442E+06)	(9.297E+06)	(4.393E+00)
0.110	7.821E-15	7.139E-14	6.040E-13	8.571E+00	8.000	(8.134E+05)	(2.553E+06)	(1.949E+07)	(5.386E+00)
0.120	7.499E-14	5.362E-13	2.635E-12	6.243E+00	9.000	(8.585E+05)	(4.101E+06)	(3.616E+07)	(6.797E+00)
0.130	5.249E-13	3.128E-12	1.151E-11	4.905E+00	10.000	(6.127E+05)	(6.127E+06)	(6.127E+07)	(1.000E+01)

Note. Observed resonances: B. Bošnjaković et al. (1968), P. M. Endt & C. van der Leun (1978), and M. C. Moazen et al. (2011). Normalization: none. Unobserved resonances: C. Iliadis et al. (1994) and J. G. Ross et al. (1995). High-temperature rates (in parentheses): matching to statistical model rate above $T = 2.5$ GK. Previous rates: C. Iliadis et al. (2010c). Other: the contribution of low-energy tails of resonances in the $E_r^{c.m.} = 1231-2194$ keV region have been estimated using the information listed in P. M. Endt & C. van der Leun (1978).

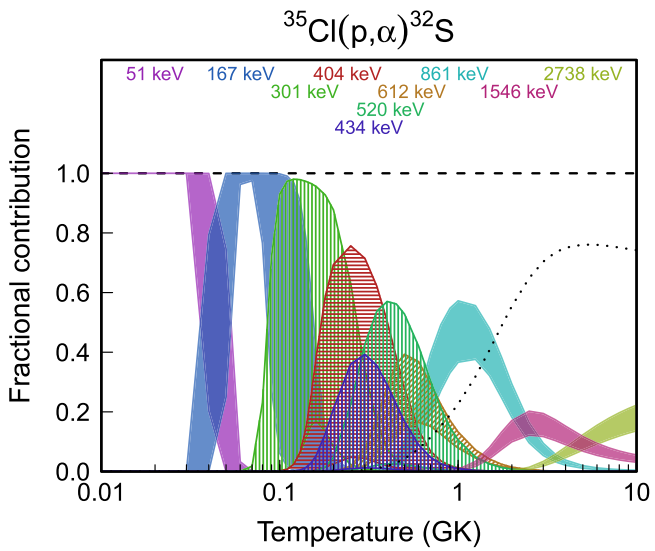

Figure 135. Fractional contributions to the total rate. Resonance energies are given in the center-of-mass frame.

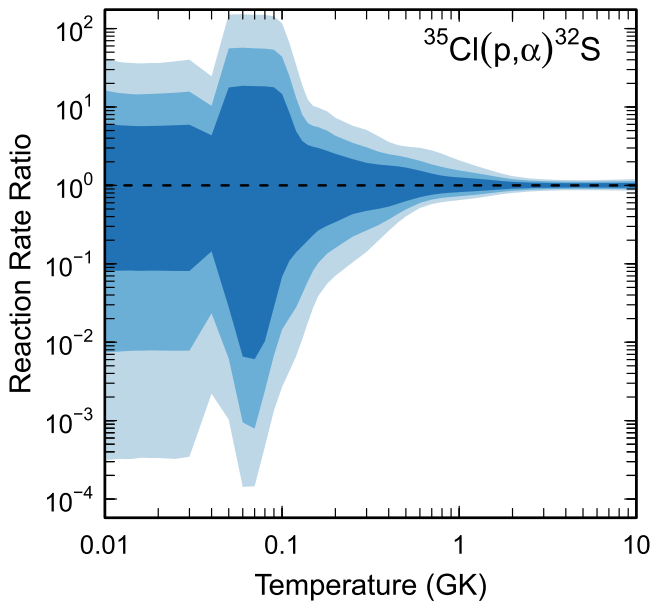

Figure 136. Reaction rate uncertainties versus temperature. The three different shades refer to coverage probabilities of 68%, 90%, and 98%.

Table 76
Total Laboratory Reaction Rates for ^{34}Ar(p,γ)^{35}K

T (GK)	Low	Median	High	*f.u.*	T (GK)	Low	Median	High	*f.u.*
0.001	0.000E+00	0.000E+00	0.000E+00	1.000E+00	0.140	3.672E-16	6.261E-16	1.069E-15	1.704E+00
0.002	1.717E-90	2.928E-90	4.998E-90	1.704E+00	0.150	1.246E-15	2.124E-15	3.626E-15	1.704E+00
0.003	5.483E-78	9.348E-78	1.596E-77	1.704E+00	0.160	3.807E-15	6.491E-15	1.108E-14	1.704E+00
0.004	4.268E-70	7.277E-70	1.242E-69	1.704E+00	0.180	2.746E-14	4.681E-14	7.991E-14	1.704E+00
0.005	1.758E-64	2.997E-64	5.117E-64	1.704E+00	0.200	1.504E-13	2.565E-13	4.378E-13	1.704E+00
0.006	3.379E-60	5.761E-60	9.834E-60	1.704E+00	0.250	4.532E-12	7.726E-12	1.319E-11	1.704E+00
0.007	8.918E-57	1.520E-56	2.595E-56	1.704E+00	0.300	6.071E-11	1.035E-10	1.767E-10	1.704E+00
0.008	5.933E-54	1.011E-53	1.727E-53	1.704E+00	0.350	4.814E-10	8.208E-10	1.401E-09	1.704E+00
0.009	1.444E-51	2.461E-51	4.202E-51	1.704E+00	0.400	2.654E-09	4.525E-09	7.724E-09	1.704E+00
0.010	1.640E-49	2.796E-49	4.773E-49	1.704E+00	0.450	1.123E-08	1.914E-08	3.267E-08	1.704E+00
0.011	1.028E-47	1.752E-47	2.991E-47	1.704E+00	0.500	3.886E-08	6.624E-08	1.131E-07	1.704E+00
0.012	4.004E-46	6.827E-46	1.165E-45	1.704E+00	0.600	3.004E-07	5.120E-07	8.740E-07	1.704E+00
0.013	1.059E-44	1.805E-44	3.081E-44	1.704E+00	0.700	1.537E-06	2.620E-06	4.471E-06	1.703E+00
0.014	2.030E-43	3.462E-43	5.909E-43	1.704E+00	0.800	5.927E-06	1.008E-05	1.718E-05	1.701E+00
0.015	2.972E-42	5.067E-42	8.650E-42	1.704E+00	0.900	1.862E-05	3.156E-05	5.369E-05	1.696E+00
0.016	3.458E-41	5.896E-41	1.006E-40	1.704E+00	1.000	5.028E-05	8.469E-05	1.435E-04	1.688E+00
0.018	2.658E-39	4.531E-39	7.735E-39	1.704E+00	1.250	3.755E-04	6.199E-04	1.037E-03	1.659E+00
0.020	1.118E-37	1.905E-37	3.253E-37	1.704E+00	1.500	1.753E-03	2.846E-03	4.701E-03	1.636E+00
0.025	1.997E-34	3.404E-34	5.811E-34	1.704E+00	1.750	5.914E-03	9.519E-03	1.563E-02	1.624E+00
0.030	6.013E-32	1.025E-31	1.750E-31	1.704E+00	2.000	1.587E-02	2.551E-02	4.181E-02	1.621E+00
0.040	2.449E-28	4.175E-28	7.127E-28	1.704E+00	2.500	7.251E-02	1.174E-01	1.936E-01	1.632E+00
0.050	9.026E-26	1.539E-25	2.627E-25	1.704E+00	3.000	2.259E-01	3.697E-01	6.142E-01	1.647E+00
0.060	8.185E-24	1.395E-23	2.382E-23	1.704E+00	3.500	5.503E-01	9.100E-01	1.524E+00	1.661E+00
0.070	2.990E-22	5.097E-22	8.701E-22	1.704E+00	4.000	1.130E+00	1.881E+00	3.166E+00	1.672E+00
0.080	5.809E-21	9.903E-21	1.690E-20	1.704E+00	5.000	3.306E+00	5.558E+00	9.410E+00	1.685E+00
0.090	7.121E-20	1.214E-19	2.072E-19	1.704E+00	6.000	6.980E+00	1.179E+01	2.002E+01	1.692E+00
0.100	6.160E-19	1.050E-18	1.793E-18	1.704E+00	7.000	1.193E+01	2.020E+01	3.437E+01	1.695E+00
0.110	4.060E-18	6.921E-18	1.181E-17	1.704E+00	8.000	1.770E+01	3.003E+01	5.111E+01	1.698E+00
0.120	2.153E-17	3.671E-17	6.267E-17	1.704E+00	9.000	2.382E+01	4.045E+01	6.888E+01	1.699E+00
0.130	9.569E-17	1.631E-16	2.785E-16	1.704E+00	10.000	2.991E+01	5.081E+01	8.655E+01	1.700E+00

Note. Observed resonances: none. Normalization: none. Unobserved resonances: P. M. Endt (1977; evaluated spectroscopic factors for mirror states). High-temperature rates (in parentheses): no matching to statistical model rates is needed over the listed temperature range. Previous rates: C. Iliadis et al. (2010c). Other: the resonance energy of $E_r^{c.m.} = 1471 \pm 5$ keV is based on the evaluation of J. Chen et al. (2011) from W. Benenson et al. (1976) and W. Trinder et al. (1999). The direct-capture contribution was calculated using experimental spectroscopic factor of P. M. Endt (1977) for the ground state of ^{35}K. The γ-ray partial width for the 1471 keV resonance was computed based on the evaluated information provided in J. Chen et al. (2011) for the mirror state in ^{35}S.

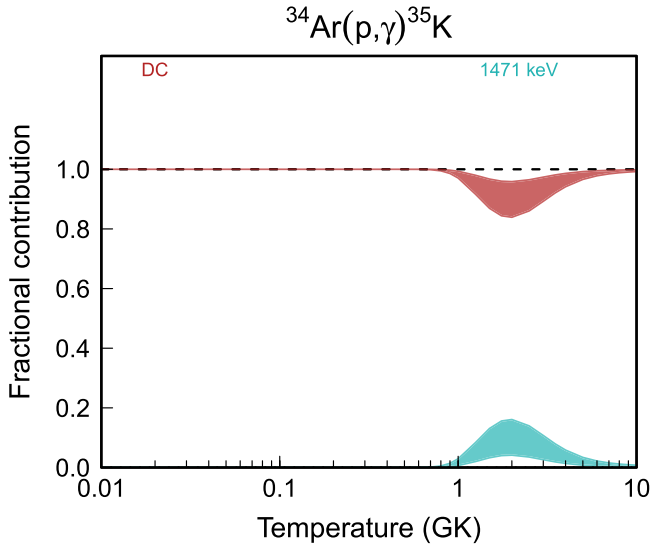

Figure 137. Fractional contributions to the total rate. "DC" refers to direct radiative capture. Resonance energies are given in the center-of-mass frame.

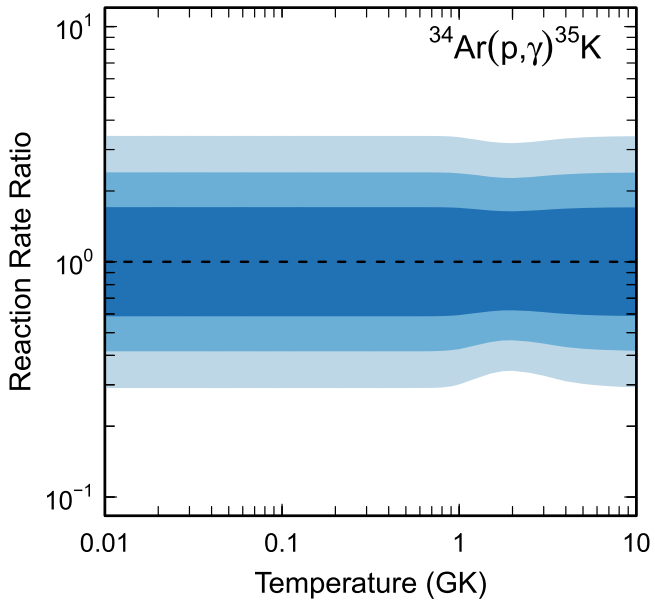

Figure 138. Reaction rate uncertainties versus temperature. The three different shades refer to coverage probabilities of 68%, 90%, and 98%.

Table 77
Total Laboratory Reaction Rates for ^{35}Ar(p,γ)^{36}K

T (GK)	Low	Median	High	*f.u.*	T (GK)	Low	Median	High	*f.u.*
0.001	0.000E+00	0.000E+00	0.000E+00	1.000E+00	0.140	2.209E-09	4.387E-09	8.690E-09	1.989E+00
0.002	7.392E-90	2.209E-89	6.570E-89	2.996E+00	0.150	8.433E-09	1.673E-08	3.314E-08	1.989E+00
0.003	2.378E-77	7.104E-77	2.113E-76	2.996E+00	0.160	2.704E-08	5.364E-08	1.063E-07	1.989E+00
0.004	1.859E-69	5.555E-69	1.652E-68	2.996E+00	0.180	1.859E-07	3.684E-07	7.296E-07	1.989E+00
0.005	7.682E-64	2.295E-63	6.827E-63	2.996E+00	0.200	8.544E-07	1.692E-06	3.354E-06	1.989E+00
0.006	1.480E-59	4.422E-59	1.315E-58	2.996E+00	0.250	1.265E-05	2.504E-05	4.966E-05	1.989E+00
0.007	4.358E-54	1.871E-53	7.525E-53	5.593E+00	0.300	7.286E-05	1.437E-04	2.848E-04	1.985E+00
0.008	1.324E-49	4.734E-49	1.711E-48	3.614E+00	0.350	2.497E-04	4.878E-04	9.619E-04	1.968E+00
0.009	3.733E-46	1.240E-45	4.123E-45	3.355E+00	0.400	6.367E-04	1.214E-03	2.355E-03	1.927E+00
0.010	2.081E-43	6.582E-43	2.086E-42	3.199E+00	0.450	1.380E-03	2.511E-03	4.743E-03	1.860E+00
0.011	3.597E-41	1.112E-40	3.404E-40	3.106E+00	0.500	2.712E-03	4.697E-03	8.473E-03	1.779E+00
0.012	2.591E-39	7.863E-39	2.371E-38	3.052E+00	0.600	8.725E-03	1.393E-02	2.300E-02	1.634E+00
0.013	9.545E-38	2.859E-37	8.505E-37	3.023E+00	0.700	2.423E-02	3.676E-02	5.702E-02	1.542E+00
0.014	2.068E-36	6.177E-36	1.830E-35	3.010E+00	0.800	(6.129E-02)	(9.362E-02)	(1.531E-01)	(1.581E+00)
0.015	2.948E-35	8.771E-35	2.606E-34	3.008E+00	0.900	(1.304E-01)	(2.010E-01)	(3.469E-01)	(1.634E+00)
0.016	2.991E-34	8.907E-34	2.644E-33	3.013E+00	1.000	(2.441E-01)	(3.798E-01)	(6.900E-01)	(1.686E+00)
0.018	1.393E-32	4.175E-32	1.248E-31	3.035E+00	1.250	(6.835E-01)	(1.089E+00)	(2.226E+00)	(1.819E+00)
0.020	2.947E-31	8.898E-31	2.684E-30	3.066E+00	1.500	(1.874E+00)	(3.059E+00)	(6.948E+00)	(1.952E+00)
0.025	6.741E-29	2.097E-28	6.515E-28	3.150E+00	1.750	(3.350E+00)	(5.607E+00)	(1.401E+01)	(2.086E+00)
0.030	2.372E-27	7.599E-27	2.427E-26	3.225E+00	2.000	(5.909E+00)	(1.015E+01)	(2.766E+01)	(2.222E+00)
0.040	1.915E-25	6.235E-25	2.046E-24	3.279E+00	2.500	(1.258E+01)	(2.279E+01)	(7.248E+01)	(2.496E+00)
0.050	4.282E-24	1.067E-23	3.021E-23	2.678E+00	3.000	(2.168E+01)	(4.153E+01)	(1.510E+02)	(2.775E+00)
0.060	2.571E-21	4.938E-21	9.628E-21	1.934E+00	3.500	(3.286E+01)	(6.680E+01)	(2.732E+02)	(3.061E+00)
0.070	2.496E-18	5.002E-18	9.978E-18	2.001E+00	4.000	(4.563E+01)	(9.883E+01)	(4.491E+02)	(3.355E+00)
0.080	4.568E-16	9.132E-16	1.817E-15	1.998E+00	5.000	(7.413E+01)	(1.847E+02)	(1.007E+03)	(3.972E+00)
0.090	2.575E-14	5.132E-14	1.019E-13	1.995E+00	6.000	(1.030E+02)	(3.018E+02)	(1.920E+03)	(4.647E+00)
0.100	6.369E-13	1.268E-12	2.518E-12	1.993E+00	7.000	(1.273E+02)	(4.532E+02)	(3.296E+03)	(5.416E+00)
0.110	8.672E-12	1.727E-11	3.423E-11	1.991E+00	8.000	(1.417E+02)	(6.424E+02)	(5.255E+03)	(6.357E+00)
0.120	7.550E-11	1.503E-10	2.977E-10	1.990E+00	9.000	(1.400E+02)	(8.732E+02)	(7.938E+03)	(7.665E+00)
0.130	4.673E-10	9.284E-10	1.841E-09	1.990E+00	10.000	(1.150E+02)	(1.150E+03)	(1.150E+04)	(1.000E+01)

Note. Observed resonances: none. Normalization: none. Unobserved resonances: P. M. Endt (1990) and C. Wrede et al. (2010). High-temperature rates (in parentheses): matching to statistical model rate above $T = 0.7$ GK. Previous rates: C. Iliadis et al. (2001, 2010c). Other: the ^{36}K $-^{36}$Cl mirror state assignments are partially based on C. Wrede et al. (2010) and W. A. Richter & B. A. Brown (2012).

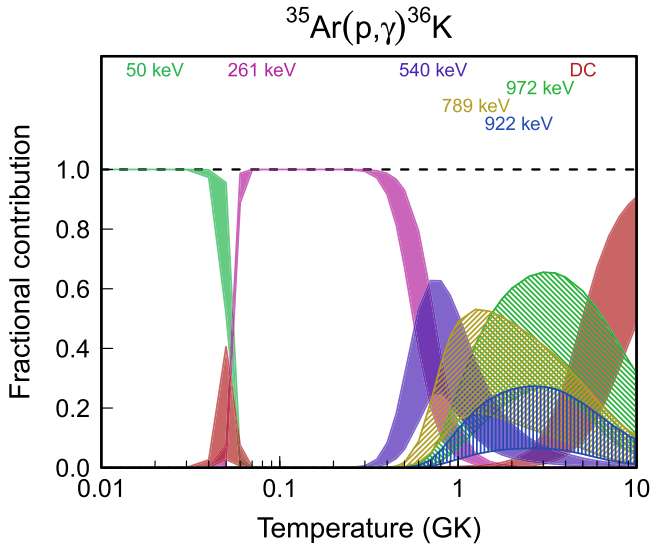

Figure 139. Fractional contributions to the total rate. "DC" refers to direct radiative capture. Resonance energies are given in the center-of-mass frame.

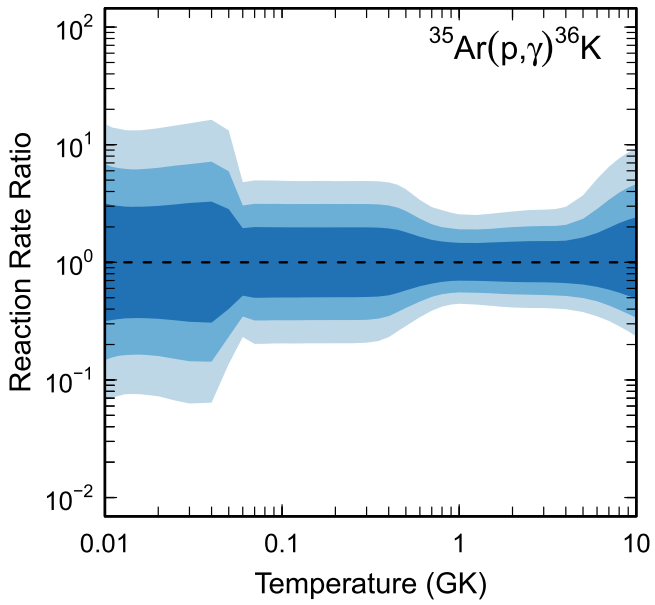

Figure 140. Reaction rate uncertainties versus temperature. The three different shades refer to coverage probabilities of 68%, 90%, and 98%.

Table 78
Total Laboratory Reaction Rates for $^{36}Ar(p,\gamma)^{37}K$

T (GK)	Low	Median	High	*f.u.*	T (GK)	Low	Median	High	*f.u.*
0.001	0.000E+00	0.000E+00	0.000E+00	1.000E+00	0.140	8.461E-09	1.062E-08	1.330E-08	1.255E+00
0.002	1.787E-89	2.847E-89	4.565E-89	1.605E+00	0.150	4.339E-08	5.447E-08	6.821E-08	1.255E+00
0.003	5.806E-77	9.250E-77	1.483E-76	1.605E+00	0.160	1.802E-07	2.263E-07	2.833E-07	1.255E+00
0.004	4.573E-69	7.286E-69	1.168E-68	1.605E+00	0.180	1.906E-06	2.392E-06	2.995E-06	1.255E+00
0.005	1.900E-63	3.028E-63	4.855E-63	1.605E+00	0.200	1.236E-05	1.552E-05	1.943E-05	1.255E+00
0.006	3.678E-59	5.860E-59	9.398E-59	1.605E+00	0.250	3.405E-04	4.273E-04	5.349E-04	1.255E+00
0.007	9.766E-56	1.556E-55	2.495E-55	1.605E+00	0.300	2.952E-03	3.705E-03	4.637E-03	1.255E+00
0.008	6.530E-53	1.040E-52	1.668E-52	1.605E+00	0.350	1.332E-02	1.672E-02	2.093E-02	1.255E+00
0.009	1.596E-50	2.543E-50	4.078E-50	1.605E+00	0.400	4.016E-02	5.039E-02	6.309E-02	1.255E+00
0.010	1.821E-48	2.901E-48	4.652E-48	1.605E+00	0.450	9.278E-02	1.164E-01	1.457E-01	1.255E+00
0.011	1.145E-46	1.825E-46	2.926E-46	1.605E+00	0.500	1.784E-01	2.238E-01	2.801E-01	1.254E+00
0.012	4.477E-45	7.133E-45	1.144E-44	1.605E+00	0.600	4.605E-01	5.772E-01	7.218E-01	1.253E+00
0.013	1.188E-43	1.892E-43	3.034E-43	1.605E+00	0.700	8.908E-01	1.113E+00	1.387E+00	1.249E+00
0.014	2.284E-42	3.639E-42	5.836E-42	1.605E+00	0.800	1.488E+00	1.840E+00	2.275E+00	1.237E+00
0.015	3.353E-41	5.342E-41	8.567E-41	1.605E+00	0.900	2.342E+00	2.846E+00	3.462E+00	1.216E+00
0.016	3.912E-40	6.232E-40	9.994E-40	1.605E+00	1.000	3.638E+00	4.317E+00	5.134E+00	1.189E+00
0.018	3.021E-38	4.813E-38	7.719E-38	1.605E+00	1.250	1.046E+01	1.180E+01	1.335E+01	1.130E+00
0.020	1.276E-36	2.033E-36	3.261E-36	1.605E+00	1.500	2.507E+01	2.776E+01	3.071E+01	1.107E+00
0.025	2.303E-33	3.670E-33	5.885E-33	1.605E+00	1.750	4.877E+01	5.371E+01	5.908E+01	1.101E+00
0.030	6.998E-31	1.115E-30	1.788E-30	1.605E+00	2.000	8.056E+01	8.857E+01	9.724E+01	1.099E+00
0.040	2.889E-27	4.602E-27	7.380E-27	1.605E+00	2.500	1.591E+02	1.747E+02	1.915E+02	1.098E+00
0.050	1.072E-24	1.708E-24	2.738E-24	1.605E+00	3.000	2.436E+02	2.672E+02	2.929E+02	1.097E+00
0.060	1.278E-22	1.863E-22	2.803E-22	1.482E+00	3.500	3.247E+02	3.559E+02	3.899E+02	1.096E+00
0.070	1.199E-19	1.492E-19	1.855E-19	1.246E+00	4.000	4.001E+02	4.384E+02	4.803E+02	1.096E+00
0.080	6.313E-17	7.928E-17	9.932E-17	1.256E+00	5.000	5.386E+02	5.915E+02	6.491E+02	1.098E+00
0.090	8.404E-15	1.056E-14	1.323E-14	1.256E+00	6.000	6.712E+02	7.410E+02	8.191E+02	1.106E+00
0.100	4.141E-13	5.203E-13	6.518E-13	1.256E+00	7.000	8.013E+02	8.924E+02	9.984E+02	1.119E+00
0.110	9.914E-12	1.245E-11	1.560E-11	1.255E+00	8.000	9.266E+02	1.042E+03	1.183E+03	1.134E+00
0.120	1.382E-10	1.736E-10	2.174E-10	1.255E+00	9.000	1.044E+03	1.186E+03	1.366E+03	1.149E+00
0.130	1.272E-09	1.598E-09	2.001E-09	1.255E+00	10.000	(2.187E+02)	(2.187E+03)	(2.187E+04)	(1.000E+01)

Note. Observed resonances: P. M. Endt & C. van der Leun (1978) and C. Iliadis et al. (1992b, 1993a). Normalization: see Table 2. Unobserved resonances: none. High-temperature rates (in parentheses): matching to statistical model rate above $T = 9.2$ GK. Previous rates: C. Iliadis et al. (2001, 2010c). Other: the direct-capture contribution was estimated using spectroscopic factors from P. M. Endt (1977).

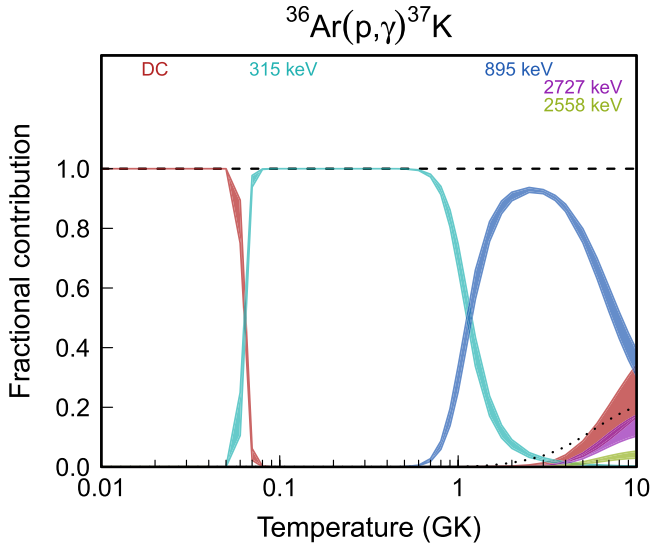

Figure 141. Fractional contributions to the total rate. "DC" refers to direct radiative capture. Resonance energies are given in the center-of-mass frame.

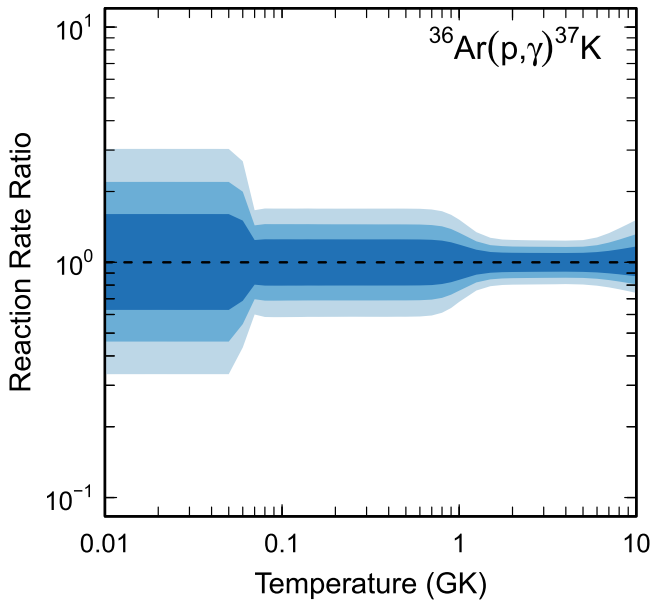

Figure 142. Reaction rate uncertainties versus temperature. The three different shades refer to coverage probabilities of 68%, 90%, and 98%.

Table 79
Total Laboratory Reaction Rates for ^{38}Ar(p,γ)^{39}K

T (GK)	Low	Median	High	*f.u.*	T (GK)	Low	Median	High	*f.u.*
0.001	0.000E+00	0.000E+00	0.000E+00	1.000E+00	0.140	4.128E-11	1.251E-10	5.208E-10	3.582E+00
0.002	3.759E-87	3.811E-85	1.374E-83	4.590E+01	0.150	1.269E-10	4.218E-10	1.923E-09	3.900E+00
0.003	6.365E-73	1.487E-71	1.795E-70	1.940E+01	0.160	3.682E-10	1.327E-09	6.506E-09	4.218E+00
0.004	5.869E-66	1.552E-64	2.808E-63	2.086E+01	0.180	2.714E-09	1.076E-08	5.703E-08	4.623E+00
0.005	6.054E-60	8.455E-59	9.067E-58	1.275E+01	0.200	1.658E-08	6.754E-08	3.543E-07	4.691E+00
0.006	3.758E-55	5.682E-54	5.954E-53	1.361E+01	0.250	6.526E-07	2.578E-06	1.181E-05	4.332E+00
0.007	1.473E-51	2.394E-50	2.329E-49	1.421E+01	0.300	9.682E-06	3.559E-05	1.491E-04	3.944E+00
0.008	7.329E-49	1.243E-47	1.248E-46	1.484E+01	0.350	8.038E-05	2.651E-04	1.022E-03	3.603E+00
0.009	8.747E-47	1.573E-45	1.706E-44	1.555E+01	0.400	4.562E-04	1.355E-03	4.748E-03	3.302E+00
0.010	3.851E-45	7.464E-44	8.762E-43	1.615E+01	0.450	1.958E-03	5.362E-03	1.708E-02	3.051E+00
0.011	8.289E-44	1.730E-42	2.222E-41	1.640E+01	0.500	6.757E-03	1.750E-02	5.168E-02	2.852E+00
0.012	1.112E-42	2.385E-41	3.273E-40	1.579E+01	0.600	5.010E-02	1.193E-01	3.178E-01	2.578E+00
0.013	1.377E-41	2.247E-40	3.196E-39	1.341E+01	0.700	2.364E-01	5.284E-01	1.324E+00	2.400E+00
0.014	2.253E-40	2.105E-39	2.441E-38	9.748E+00	0.800	8.093E-01	1.710E+00	4.096E+00	2.268E+00
0.015	4.223E-39	2.939E-38	2.283E-37	7.198E+00	0.900	2.226E+00	4.420E+00	1.018E+01	2.159E+00
0.016	8.038E-38	5.304E-37	3.623E-36	6.607E+00	1.000	5.175E+00	9.696E+00	2.147E+01	2.066E+00
0.018	2.246E-35	1.712E-34	1.326E-33	7.663E+00	1.250	2.582E+01	4.239E+01	8.578E+01	1.874E+00
0.020	3.347E-33	2.815E-32	2.137E-31	8.144E+00	1.500	8.091E+01	1.205E+02	2.212E+02	1.728E+00
0.025	3.597E-29	3.048E-28	2.131E-27	8.047E+00	1.750	1.895E+02	2.647E+02	4.449E+02	1.617E+00
0.030	1.731E-26	1.455E-25	1.001E-24	7.826E+00	2.000	3.673E+02	4.918E+02	7.659E+02	1.531E+00
0.040	6.251E-23	3.618E-22	2.196E-21	5.970E+00	2.500	9.575E+02	1.224E+03	1.709E+03	1.413E+00
0.050	2.234E-20	9.639E-20	4.244E-19	4.366E+00	3.000	1.853E+03	2.317E+03	3.043E+03	1.342E+00
0.060	2.204E-18	8.090E-18	3.971E-17	4.285E+00	3.500	(2.991E+03)	(3.728E+03)	(5.048E+03)	(1.300E+00)
0.070	8.912E-17	2.875E-16	1.610E-15	4.328E+00	4.000	(4.321E+03)	(5.774E+03)	(1.166E+04)	(1.678E+00)
0.080	1.720E-15	5.071E-15	2.843E-14	4.199E+00	5.000	(7.388E+03)	(1.154E+04)	(3.865E+04)	(2.456E+00)
0.090	1.859E-14	5.100E-14	2.681E-13	3.986E+00	6.000	(1.046E+04)	(1.966E+04)	(9.200E+04)	(3.279E+00)
0.100	1.342E-13	3.455E-13	1.628E-12	3.720E+00	7.000	(1.281E+04)	(3.021E+04)	(1.815E+05)	(4.184E+00)
0.110	7.332E-13	1.837E-12	7.553E-12	3.454E+00	8.000	(1.364E+04)	(4.315E+04)	(3.167E+05)	(5.252E+00)
0.120	3.252E-12	8.408E-12	3.225E-11	3.307E+00	9.000	(1.215E+04)	(5.841E+04)	(5.064E+05)	(6.738E+00)
0.130	1.230E-11	3.411E-11	1.322E-10	3.356E+00	10.000	(7.587E+03)	(7.587E+04)	(7.587E+05)	(1.000E+01)

Note. Observed resonances: R. Hänninen (1984). Normalization: R. Hänninen (1984). Unobserved resonances: K. Knöpfle et al. (1974). High-temperature rates (in parentheses): matching to statistical model rate above $T = 3.4$ GK. Previous rates: A. L. Sallaska et al. (2013). Other: the rate depends on a single normalization experiment for the $E_r^{\rm lab} = 1394$ keV resonance (R. Hänninen 1984).

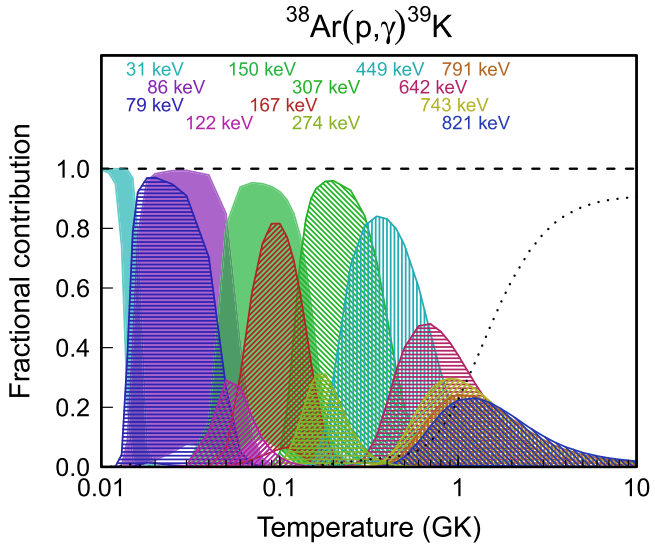

Figure 143. Fractional contributions to the total rate. Resonance energies are given in the center-of-mass frame.

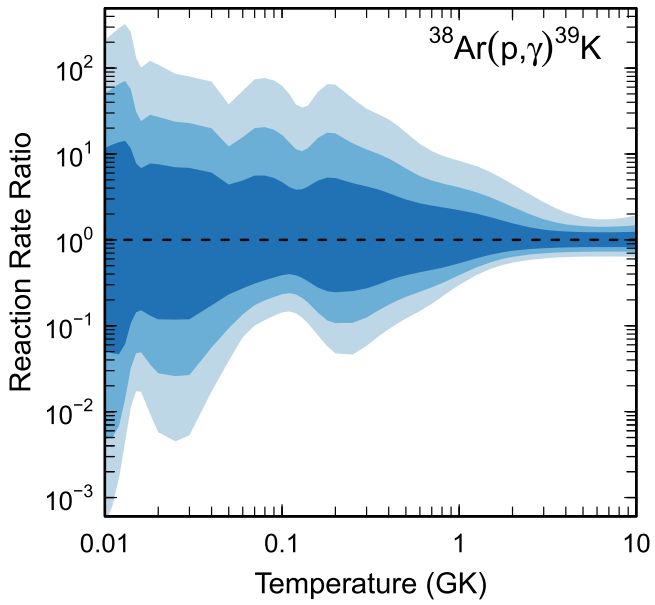

Figure 144. Reaction rate uncertainties versus temperature. The three different shades refer to coverage probabilities of 68%, 90%, and 98%.

Table 80
Total Laboratory Reaction Rates for ^{35}K(p,γ)^{36}Ca

T (GK)	Low	Median	High	*f.u.*	T (GK)	Low	Median	High	*f.u.*
0.001	0.000E+00	0.000E+00	0.000E+00	1.000E+00	0.140	4.597E-14	6.631E-14	9.597E-14	1.457E+00
0.002	1.073E-94	1.055E-93	1.031E-92	1.006E+01	0.150	5.014E-13	7.010E-13	9.816E-13	1.404E+00
0.003	1.009E-81	9.925E-81	9.693E-80	1.006E+01	0.160	4.050E-12	5.525E-12	7.548E-12	1.367E+00
0.004	1.557E-73	1.531E-72	1.495E-71	1.006E+01	0.180	1.303E-10	1.707E-10	2.238E-10	1.312E+00
0.005	1.045E-67	1.028E-66	1.004E-65	1.006E+01	0.200	2.057E-09	2.614E-09	3.323E-09	1.274E+00
0.006	2.918E-63	2.870E-62	2.803E-61	1.006E+01	0.250	2.791E-07	3.386E-07	4.115E-07	1.216E+00
0.007	1.065E-59	1.029E-58	9.988E-58	9.869E+00	0.300	6.946E-06	8.244E-06	9.799E-06	1.189E+00
0.008	9.081E-57	8.767E-56	8.512E-55	9.856E+00	0.350	6.615E-05	7.784E-05	9.156E-05	1.178E+00
0.009	2.726E-54	2.632E-53	2.555E-52	9.855E+00	0.400	3.476E-04	4.083E-04	4.784E-04	1.175E+00
0.010	3.713E-52	3.584E-51	3.480E-50	9.854E+00	0.450	1.234E-03	1.452E-03	1.700E-03	1.175E+00
0.011	2.728E-50	2.633E-49	2.556E-48	9.853E+00	0.500	3.338E-03	3.936E-03	4.618E-03	1.177E+00
0.012	1.224E-48	1.181E-47	1.147E-46	9.852E+00	0.600	1.429E-02	1.695E-02	2.001E-02	1.184E+00
0.013	3.673E-47	3.544E-46	3.441E-45	9.850E+00	0.700	3.888E-02	4.642E-02	5.510E-02	1.191E+00
0.014	7.896E-46	7.621E-45	7.399E-44	9.849E+00	0.800	8.014E-02	9.616E-02	1.147E-01	1.197E+00
0.015	1.283E-44	1.238E-43	1.202E-42	9.848E+00	0.900	1.378E-01	1.661E-01	1.990E-01	1.203E+00
0.016	1.642E-43	1.585E-42	1.539E-41	9.847E+00	1.000	2.093E-01	2.532E-01	3.045E-01	1.208E+00
0.018	1.496E-41	1.444E-40	1.401E-39	9.845E+00	1.250	4.271E-01	5.216E-01	6.350E-01	1.230E+00
0.020	7.287E-40	7.032E-39	6.825E-38	9.843E+00	1.500	6.726E-01	8.337E-01	1.053E+00	1.328E+00
0.025	1.752E-36	1.691E-35	1.641E-34	9.838E+00	1.750	9.285E-01	1.186E+00	1.684E+00	1.561E+00
0.030	6.638E-34	6.402E-33	6.214E-32	9.832E+00	2.000	1.195E+00	1.609E+00	3.030E+00	1.895E+00
0.040	3.791E-30	3.654E-29	3.546E-28	9.825E+00	2.500	1.789E+00	3.088E+00	1.037E+01	2.661E+00
0.050	1.776E-27	1.710E-26	1.660E-25	9.813E+00	3.000	2.619E+00	6.410E+00	2.775E+01	3.324E+00
0.060	1.931E-25	1.857E-24	1.802E-23	9.802E+00	3.500	3.897E+00	1.230E+01	5.823E+01	3.791E+00
0.070	8.151E-24	7.830E-23	7.595E-22	9.789E+00	4.000	5.772E+00	2.100E+01	1.022E+02	4.094E+00
0.080	1.785E-22	1.713E-21	1.661E-20	9.764E+00	5.000	1.111E+01	4.576E+01	2.239E+02	4.419E+00
0.090	2.588E-21	2.336E-20	2.252E-19	8.992E+00	6.000	1.792E+01	7.708E+01	3.764E+02	4.578E+00
0.100	6.725E-20	2.632E-19	2.164E-18	5.681E+00	7.000	2.525E+01	1.106E+02	5.397E+02	4.677E+00
0.110	3.380E-18	6.408E-18	1.975E-17	2.920E+00	8.000	3.243E+01	1.429E+02	7.003E+02	4.750E+00
0.120	1.252E-16	2.004E-16	3.443E-16	1.880E+00	9.000	3.887E+01	1.731E+02	8.491E+02	4.811E+00
0.130	2.947E-15	4.433E-15	6.727E-15	1.563E+00	10.000	4.429E+01	1.987E+02	9.843E+02	4.864E+00

Note. Observed resonances: none. Normalization: none. Unobserved resonances: A. Buerger et al. (2007), P. Doornenbal et al. (2007), A. M. Amthor (2009), L. Lalanne et al. (2021, 2022), and N. Dronchi et al. (2023). High-temperature rates (in parentheses): no matching to statistical model rates is needed over the listed temperature range. Previous rates: C. Iliadis et al. (2001, 2010a) and L. Lalanne et al. (2021). Other: for the proton spectroscopic factor of the ground state of ^{36}Ca, see shell model calculation of H. Herndl et al. (1995). For the proton spectroscopic factors corresponding to the resonances, and proton and γ-ray partial widths, see N. Dronchi et al. (2023). These partial widths have only been measured for the 448 keV resonance. For other resonances, they were scaled from the shell model calculations of N. Dronchi et al. (2023).

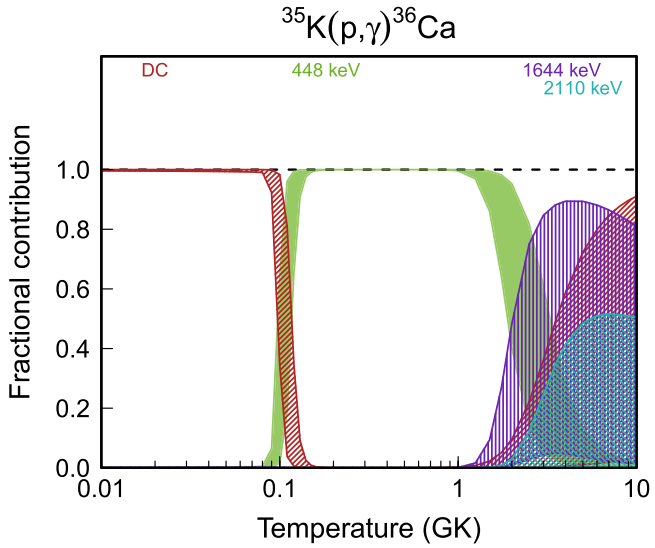

Figure 145. Fractional contributions to the total rate. "DC" refers to direct radiative capture. Resonance energies are given in the center-of-mass frame.

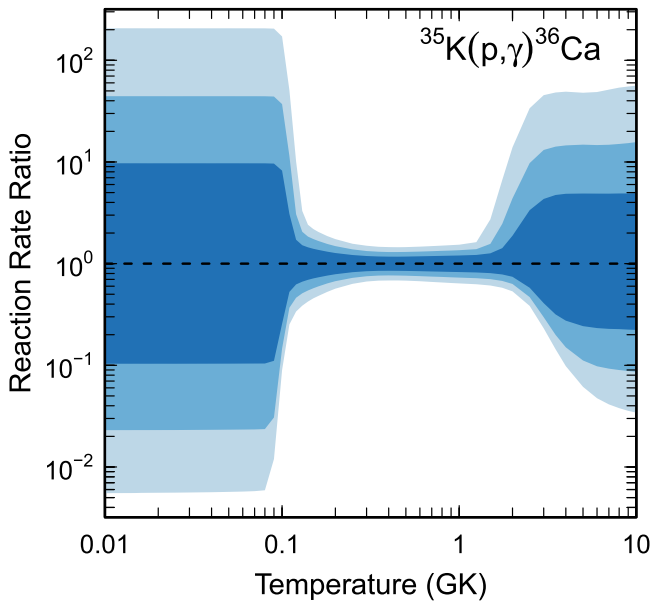

Figure 146. Reaction rate uncertainties versus temperature. The three different shades refer to coverage probabilities of 68%, 90%, and 98%.

Table 81
Total Laboratory Reaction Rates for ^{39}K(p,γ)^{40}Ca

T (GK)	Low	Median	High	*f.u.*	T (GK)	Low	Median	High	*f.u.*
0.001	0.000E+00	0.000E+00	0.000E+00	1.000E+00	0.140	7.102E-11	1.571E-10	4.500E-10	2.621E+00
0.002	4.731E-89	7.845E-88	8.030E-87	1.527E+01	0.150	2.706E-10	6.187E-10	1.720E-09	2.614E+00
0.003	5.250E-79	5.002E-78	5.718E-77	9.001E+00	0.160	9.366E-10	2.180E-09	5.855E-09	2.580E+00
0.004	2.325E-71	4.645E-71	1.990E-70	7.675E+00	0.180	8.385E-09	1.963E-08	5.004E-08	2.491E+00
0.005	2.264E-65	1.426E-64	2.246E-62	2.796E+01	0.200	5.355E-08	1.225E-07	3.009E-07	2.408E+00
0.006	2.611E-60	1.949E-58	7.567E-57	3.378E+01	0.250	1.859E-06	3.962E-06	9.097E-06	2.235E+00
0.007	7.886E-52	1.566E-51	3.124E-51	2.049E+00	0.300	2.364E-05	4.769E-05	1.033E-04	2.110E+00
0.008	6.016E-49	1.195E-48	2.387E-48	2.003E+00	0.350	1.643E-04	3.161E-04	6.602E-04	2.022E+00
0.009	1.045E-46	2.101E-46	4.305E-46	2.060E+00	0.400	7.845E-04	1.425E-03	2.886E-03	1.944E+00
0.010	6.640E-45	1.359E-44	2.919E-44	2.175E+00	0.450	2.937E-03	4.964E-03	9.633E-03	1.862E+00
0.011	2.046E-43	4.370E-43	1.011E-42	2.369E+00	0.500	9.102E-03	1.431E-02	2.653E-02	1.778E+00
0.012	3.723E-42	8.494E-42	2.237E-41	2.679E+00	0.600	5.756E-02	7.967E-02	1.336E-01	1.624E+00
0.013	4.557E-41	1.141E-40	3.669E-40	3.117E+00	0.700	2.384E-01	3.050E-01	4.601E-01	1.501E+00
0.014	4.066E-40	1.150E-39	4.743E-39	3.662E+00	0.800	7.314E-01	8.942E-01	1.239E+00	1.408E+00
0.015	2.828E-39	9.251E-39	4.819E-38	4.272E+00	0.900	1.816E+00	2.167E+00	2.818E+00	1.338E+00
0.016	1.600E-38	6.239E-38	3.774E-37	4.870E+00	1.000	3.870E+00	4.550E+00	5.670E+00	1.284E+00
0.018	6.657E-37	2.339E-36	1.297E-35	4.494E+00	1.250	1.668E+01	1.924E+01	2.266E+01	1.201E+00
0.020	8.298E-35	2.295E-34	6.688E-34	2.937E+00	1.500	4.879E+01	5.579E+01	6.416E+01	1.161E+00
0.025	3.234E-30	9.448E-30	2.791E-29	2.963E+00	1.750	1.117E+02	1.270E+02	1.446E+02	1.143E+00
0.030	5.036E-27	1.480E-26	4.375E-26	2.977E+00	2.000	2.155E+02	2.442E+02	2.770E+02	1.136E+00
0.040	4.653E-23	1.352E-22	3.969E-22	2.942E+00	2.500	5.714E+02	6.457E+02	7.300E+02	1.131E+00
0.050	1.466E-20	3.476E-20	9.190E-20	2.510E+00	3.000	1.142E+03	1.288E+03	1.453E+03	1.129E+00
0.060	1.476E-18	2.747E-18	5.257E-18	1.925E+00	3.500	1.925E+03	2.166E+03	2.440E+03	1.127E+00
0.070	5.906E-17	1.072E-16	1.962E-16	1.831E+00	4.000	(2.832E+03)	(3.255E+03)	(4.379E+03)	(1.247E+00)
0.080	1.168E-15	2.150E-15	4.087E-15	1.878E+00	5.000	(4.512E+03)	(6.085E+03)	(1.696E+04)	(2.068E+00)
0.090	1.393E-14	2.590E-14	5.035E-14	1.943E+00	6.000	(6.035E+03)	(9.840E+03)	(4.162E+04)	(2.930E+00)
0.100	1.143E-13	2.163E-13	4.441E-13	2.071E+00	7.000	(7.085E+03)	(1.461E+04)	(8.288E+04)	(3.867E+00)
0.110	7.114E-13	1.387E-12	3.208E-12	2.261E+00	8.000	(7.312E+03)	(2.050E+04)	(1.459E+05)	(4.960E+00)
0.120	3.699E-12	7.487E-12	1.977E-11	2.449E+00	9.000	(6.317E+03)	(2.767E+04)	(2.368E+05)	(6.469E+00)
0.130	1.697E-11	3.593E-11	1.018E-10	2.573E+00	10.000	(3.628E+03)	(3.628E+04)	(3.628E+05)	(1.000E+01)

Note. Observed resonances: C.-W. Cheng et al. (1981), S. Kikstra et al. (1990), and P. Scholz et al. (2023). Normalization: see Table 2. Unobserved resonances: W. Fox et al. (2024). High-temperature rates (in parentheses): matching to statistical model rate above $T = 3.8$ GK. Previous rates: R. Longland et al. (2018). Other: none.

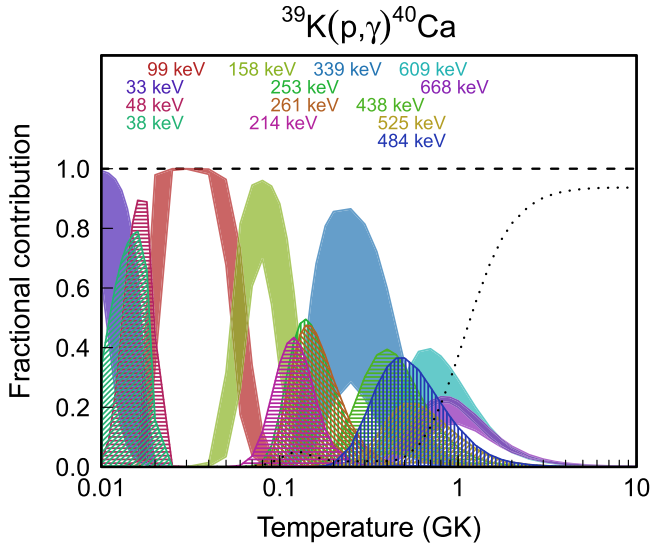

Figure 147. Fractional contributions to the total rate. Resonance energies are given in the center-of-mass frame.

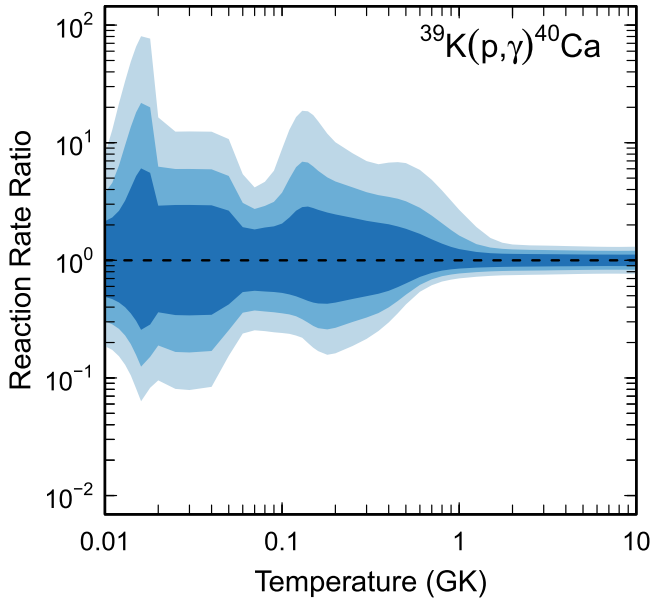

Figure 148. Reaction rate uncertainties versus temperature. The three different shades refer to coverage probabilities of 68%, 90%, and 98%.

Table 82
Total Laboratory Reaction Rates for $^{39}Ca(p,\gamma)^{40}Sc$

T (GK)	Low	Median	High	*f.u.*	T (GK)	Low	Median	High	*f.u.*
0.001	0.000E+00	0.000E+00	0.000E+00	1.000E+00	0.140	7.755E-12	2.273E-11	6.828E-11	2.953E+00
0.002	7.430E-98	2.204E-97	6.537E-97	2.987E+00	0.150	2.780E-11	8.012E-11	2.384E-10	2.907E+00
0.003	2.050E-84	6.083E-84	1.804E-83	2.987E+00	0.160	8.598E-11	2.415E-10	7.109E-10	2.842E+00
0.004	6.242E-76	1.852E-75	5.492E-75	2.987E+00	0.180	5.982E-10	1.537E-09	4.374E-09	2.662E+00
0.005	6.796E-70	2.016E-69	5.979E-69	2.987E+00	0.200	3.089E-09	7.008E-09	1.875E-08	2.445E+00
0.006	2.745E-65	8.143E-65	2.415E-64	2.987E+00	0.250	7.574E-08	1.339E-07	2.787E-07	1.975E+00
0.007	1.316E-61	3.895E-61	1.155E-60	2.984E+00	0.300	7.166E-07	1.159E-06	2.009E-06	1.724E+00
0.008	1.431E-58	4.233E-58	1.255E-57	2.983E+00	0.350	3.650E-06	5.745E-06	9.274E-06	1.618E+00
0.009	5.275E-56	1.561E-55	4.627E-55	2.983E+00	0.400	1.240E-05	1.930E-05	3.033E-05	1.579E+00
0.010	8.575E-54	2.537E-53	7.521E-53	2.983E+00	0.450	3.190E-05	4.954E-05	7.729E-05	1.567E+00
0.011	7.356E-52	2.176E-51	6.451E-51	2.982E+00	0.500	6.758E-05	1.047E-04	1.633E-04	1.563E+00
0.012	3.784E-50	1.120E-49	3.319E-49	2.982E+00	0.600	2.098E-04	3.227E-04	5.021E-04	1.553E+00
0.013	1.284E-48	3.797E-48	1.125E-47	2.982E+00	0.700	5.028E-04	7.614E-04	1.169E-03	1.533E+00
0.014	3.083E-47	9.118E-47	2.702E-46	2.982E+00	0.800	1.074E-03	1.622E-03	2.488E-03	1.535E+00
0.015	5.537E-46	1.638E-45	4.853E-45	2.982E+00	0.900	2.186E-03	3.343E-03	5.289E-03	1.580E+00
0.016	7.768E-45	2.298E-44	6.809E-44	2.981E+00	1.000	4.371E-03	6.739E-03	1.124E-02	1.632E+00
0.018	8.319E-43	2.461E-42	7.291E-42	2.981E+00	1.250	(3.621E-02)	(5.724E-02)	(1.051E-01)	(1.709E+00)
0.020	4.659E-41	1.378E-40	4.083E-40	2.980E+00	1.500	(2.046E-01)	(3.314E-01)	(6.859E-01)	(1.845E+00)
0.025	1.481E-37	4.379E-37	1.297E-36	2.979E+00	1.750	(5.299E-01)	(8.802E-01)	(2.027E+00)	(1.982E+00)
0.030	6.946E-35	2.051E-34	6.074E-34	2.977E+00	2.000	(1.204E+00)	(2.051E+00)	(5.201E+00)	(2.120E+00)
0.040	5.708E-31	1.628E-30	4.751E-30	2.893E+00	2.500	(3.555E+00)	(6.388E+00)	(1.918E+01)	(2.400E+00)
0.050	5.829E-27	1.627E-26	4.994E-26	2.939E+00	3.000	(7.588E+00)	(1.443E+01)	(5.004E+01)	(2.685E+00)
0.060	4.519E-23	1.418E-22	4.536E-22	3.183E+00	3.500	(1.341E+01)	(2.706E+01)	(1.065E+02)	(2.977E+00)
0.070	3.170E-20	9.787E-20	3.040E-19	3.114E+00	4.000	(2.098E+01)	(4.511E+01)	(1.986E+02)	(3.276E+00)
0.080	4.188E-18	1.275E-17	3.935E-17	3.070E+00	5.000	(4.062E+01)	(1.005E+02)	(5.361E+02)	(3.904E+00)
0.090	1.831E-16	5.536E-16	1.693E-15	3.043E+00	6.000	(6.413E+01)	(1.867E+02)	(1.170E+03)	(4.590E+00)
0.100	3.699E-15	1.111E-14	3.376E-14	3.026E+00	7.000	(8.763E+01)	(3.101E+02)	(2.233E+03)	(5.370E+00)
0.110	4.264E-14	1.278E-13	3.865E-13	3.014E+00	8.000	(1.057E+02)	(4.766E+02)	(3.877E+03)	(6.322E+00)
0.120	3.244E-13	9.655E-13	2.918E-12	3.001E+00	9.000	(1.113E+02)	(6.918E+02)	(6.273E+03)	(7.642E+00)
0.130	1.791E-12	5.306E-12	1.598E-11	2.982E+00	10.000	(9.604E+01)	(9.604E+02)	(9.604E+03)	(1.000E+01)

Note. Observed resonances: none. Normalization: none. Unobserved resonances: C. Fink & J. Schiffer (1974), P. M. Endt (1977), and V. Y. Hansper et al. (2000). High-temperature rates (in parentheses): matching to statistical model rate above $T = 1.1$ GK. Previous rates: P. Descouvemont (2000) and C. Iliadis et al. (2010c). Other: the rates of P. Descouvemont (2000) exceed the present results by factors of 10−100, because their spectroscopic factors of the first and second excited states, calculated from the microscopic model, differ significantly from the measured values (C. Fink & J. Schiffer 1974) adopted in the present work.

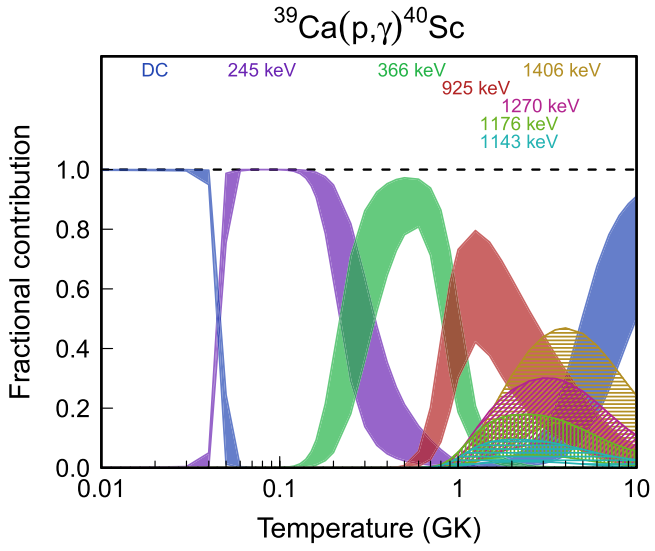

Figure 149. Fractional contributions to the total rate. "DC" refers to direct radiative capture. Resonance energies are given in the center-of-mass frame.

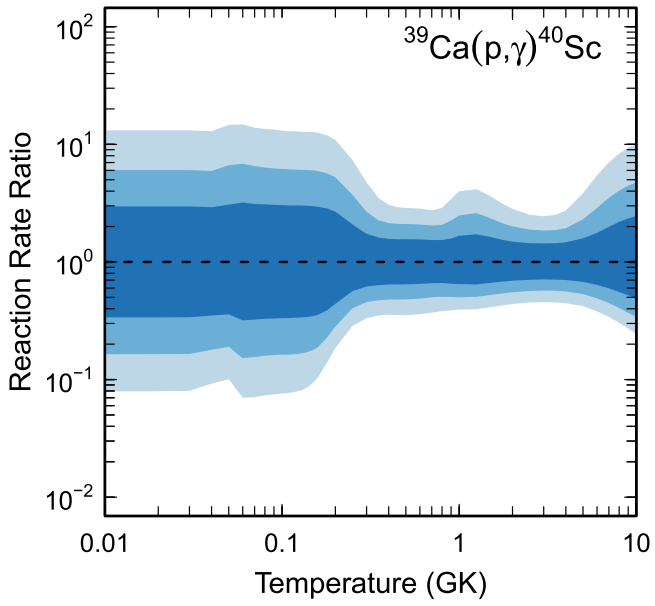

Figure 150. Reaction rate uncertainties versus temperature. The three different shades refer to coverage probabilities of 68%, 90%, and 98%.

Table 83
Total Laboratory Reaction Rates for ^{40}Ca(p,γ)^{41}Sc

T (GK)	Low	Median	High	*f.u.*	T (GK)	Low	Median	High	*f.u.*
0.001	0.000E+00	0.000E+00	0.000E+00	1.000E+00	0.140	1.350E-17	1.682E-17	2.100E-17	1.248E+00
0.002	1.117E-97	1.396E-97	1.747E-97	1.250E+00	0.150	5.271E-17	6.523E-17	8.099E-17	1.239E+00
0.003	3.118E-84	3.896E-84	4.874E-84	1.250E+00	0.160	2.120E-16	2.558E-16	3.104E-16	1.210E+00
0.004	9.571E-76	1.196E-75	1.496E-75	1.250E+00	0.180	6.183E-15	7.735E-15	9.774E-15	1.258E+00
0.005	1.049E-69	1.311E-69	1.640E-69	1.250E+00	0.200	2.344E-13	3.107E-13	4.120E-13	1.326E+00
0.006	4.262E-65	5.324E-65	6.662E-65	1.250E+00	0.250	2.501E-10	3.353E-10	4.488E-10	1.340E+00
0.007	2.049E-61	2.559E-61	3.202E-61	1.250E+00	0.300	2.561E-08	3.434E-08	4.598E-08	1.341E+00
0.008	2.239E-58	2.797E-58	3.498E-58	1.250E+00	0.350	6.747E-07	9.047E-07	1.211E-06	1.341E+00
0.009	8.292E-56	1.036E-55	1.295E-55	1.250E+00	0.400	7.638E-06	1.024E-05	1.371E-05	1.341E+00
0.010	1.353E-53	1.690E-53	2.114E-53	1.250E+00	0.450	4.938E-05	6.623E-05	8.865E-05	1.341E+00
0.011	1.165E-51	1.455E-51	1.820E-51	1.250E+00	0.500	2.162E-04	2.899E-04	3.881E-04	1.341E+00
0.012	6.015E-50	7.513E-50	9.397E-50	1.250E+00	0.600	1.909E-03	2.561E-03	3.429E-03	1.341E+00
0.013	2.047E-48	2.557E-48	3.198E-48	1.250E+00	0.700	8.732E-03	1.171E-02	1.568E-02	1.341E+00
0.014	4.931E-47	6.159E-47	7.703E-47	1.250E+00	0.800	2.658E-02	3.565E-02	4.772E-02	1.341E+00
0.015	8.885E-46	1.110E-45	1.388E-45	1.250E+00	0.900	6.190E-02	8.298E-02	1.111E-01	1.341E+00
0.016	1.250E-44	1.562E-44	1.953E-44	1.250E+00	1.000	1.197E-01	1.605E-01	2.148E-01	1.341E+00
0.018	1.347E-42	1.682E-42	2.104E-42	1.250E+00	1.250	3.753E-01	5.022E-01	6.716E-01	1.339E+00
0.020	7.585E-41	9.473E-41	1.185E-40	1.250E+00	1.500	7.809E-01	1.039E+00	1.382E+00	1.331E+00
0.025	2.441E-37	3.049E-37	3.813E-37	1.250E+00	1.750	1.337E+00	1.749E+00	2.299E+00	1.312E+00
0.030	1.156E-34	1.444E-34	1.806E-34	1.250E+00	2.000	2.110E+00	2.682E+00	3.445E+00	1.278E+00
0.040	9.169E-31	1.145E-30	1.432E-30	1.250E+00	2.500	4.901E+00	5.792E+00	6.954E+00	1.193E+00
0.050	5.434E-28	6.786E-28	8.485E-28	1.250E+00	3.000	(1.052E+01)	(1.211E+01)	(1.558E+01)	(1.219E+00)
0.060	7.074E-26	8.834E-26	1.104E-25	1.250E+00	3.500	(1.983E+01)	(2.437E+01)	(4.651E+01)	(1.569E+00)
0.070	3.452E-24	4.310E-24	5.388E-24	1.250E+00	4.000	(3.284E+01)	(4.328E+01)	(1.096E+02)	(1.925E+00)
0.080	8.526E-23	1.065E-22	1.331E-22	1.250E+00	5.000	(6.999E+01)	(1.079E+02)	(4.073E+02)	(2.658E+00)
0.090	1.282E-21	1.601E-21	2.001E-21	1.250E+00	6.000	(1.195E+02)	(2.216E+02)	(1.113E+03)	(3.438E+00)
0.100	1.324E-20	1.652E-20	2.066E-20	1.249E+00	7.000	(1.727E+02)	(4.022E+02)	(2.520E+03)	(4.297E+00)
0.110	1.019E-19	1.272E-19	1.590E-19	1.249E+00	8.000	(2.137E+02)	(6.688E+02)	(5.023E+03)	(5.320E+00)
0.120	6.209E-19	7.748E-19	9.684E-19	1.249E+00	9.000	(2.181E+02)	(1.040E+03)	(9.103E+03)	(6.761E+00)
0.130	3.126E-18	3.900E-18	4.874E-18	1.249E+00	10.000	(1.535E+02)	(1.535E+03)	(1.535E+04)	(1.000E+01)

Note. Observed resonances: F. Zijderhand et al. (1987) and P. M. Endt (1990). Normalization: see Table 2. Unobserved resonances: none. High-temperature rates (in parentheses): matching to statistical model rate above $T = 2.9$ GK. Previous rates: C. Iliadis et al. (2001, 2010c). Other: the direct-capture contribution was estimated using experimental C^2S values of P. M. Endt (1977), P. M. Endt & C. van der Leun (1978), and J. Guillot et al. (1991).

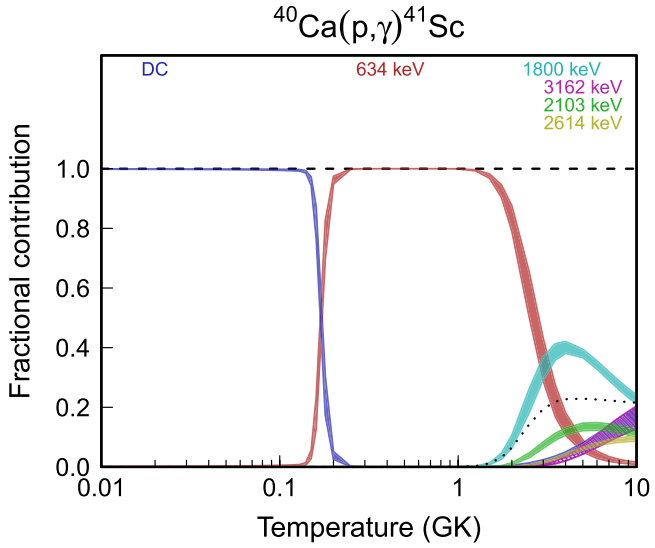

Figure 151. Fractional contributions to the total rate. "DC" refers to direct radiative capture. Resonance energies are given in the center-of-mass frame.

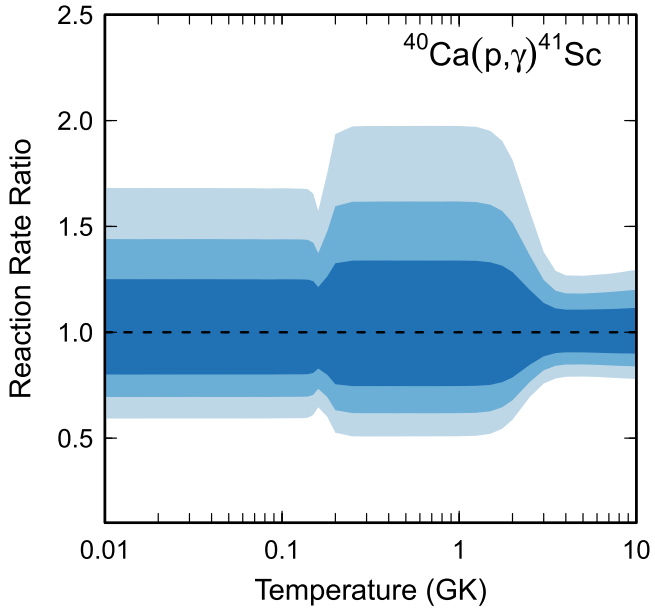

Figure 152. Reaction rate uncertainties versus temperature. The three different shades refer to coverage probabilities of 68%, 90%, and 98%.

Appendix F
Comparison to Previous Monte Carlo–based Reaction Rates

Figures 153–159 provide a comparison of our new rates (blue) with the Monte Carlo–based rates from 2010 (gray; C. Iliadis et al. 2010c; ETR10). Three reactions were not included in the 2010 evaluation: for ^{18}Ne(α,p)^{21}Mg, we compare to P. Mohr et al. (2014), for ^{38}Ar(p,γ)^{39}K, we compare to A. L. Sallaska et al. (2013), and for ^{39}K(p,γ)^{40}Ca, we compare to R. Longland et al. (2018). In each panel, the two bands represent 68% coverage probabilities,[13] and all rates are normalized to our newly recommended values. The solid black line depicts the ratio of previous to present rates.

A visual inspection of the panels reveals not only how much the recommended rates (solid black lines) differ from previous estimates but also how the associated uncertainties have changed. Most differences arise from newly available nuclear-physics input (e.g., updated excitation and resonance energies, resonance strengths, spectroscopic factors, and revised spin–parity assignments). Additional changes reflect updated procedural choices relative to the 2010 evaluation (ETR10), as discussed in Section 6.

Beyond these general reasons, two systematic features stand out. First, for several capture reactions (e.g., ^{14}N(α,γ)^{18}F, ^{16}O(α,γ)^{20}Ne, and ^{23}Mg(p,γ)^{24}Al), the uncertainties of the new rates exceed the previous ones at the lowest temperatures. This mainly results from our adoption of larger uncertainties for the bound-state spectroscopic factors, which directly scale the direct capture cross section (Section 9).

Second, when high-temperature matching is required, the new rates generally exhibit larger uncertainties than those reported in 2010. This difference stems from a fundamental change in methodology. In ETR10, the Monte Carlo median, low, and high rates were extended beyond the matching temperature by scaling the TALYS curve. The entire TALYS rate curve up to 10 GK was multiplied by a single scale factor determined at the matching temperature: one factor for the median rate, another for the low rate, and another for the high rate. Each factor was the ratio between the corresponding Monte Carlo value and the TALYS value at the matching point. This produced extrapolated curves that followed the TALYS temperature dependence but were shifted to agree with the Monte Carlo results at the matching temperature. As a result, the rate uncertainty remained relatively small and essentially fixed (i.e., equal to the Monte Carlo uncertainty at the matching temperature) throughout the extrapolated region.

In the present evaluation, we adopted a different approach (Section 10). We assumed the unscaled TALYS value at 10 GK to be correct within a factor-of-10 uncertainty and constructed smooth connections between this 10 GK anchor point and the Monte Carlo low, median, and high rates at the matching temperature. Although we cannot conclusively state that one extrapolation scheme is superior, we regard the present method as more conservative and therefore preferable for representing realistic high-temperature uncertainties.

[13] Note that, above the matching temperature, the rate uncertainties shown in the figures below agree with the numerical values listed in the tables of Appendix E.3, but not with the uncertainty figures that accompany each table. The latter figures display the unmatched high-temperature rates, whereas the tables list the matched values.

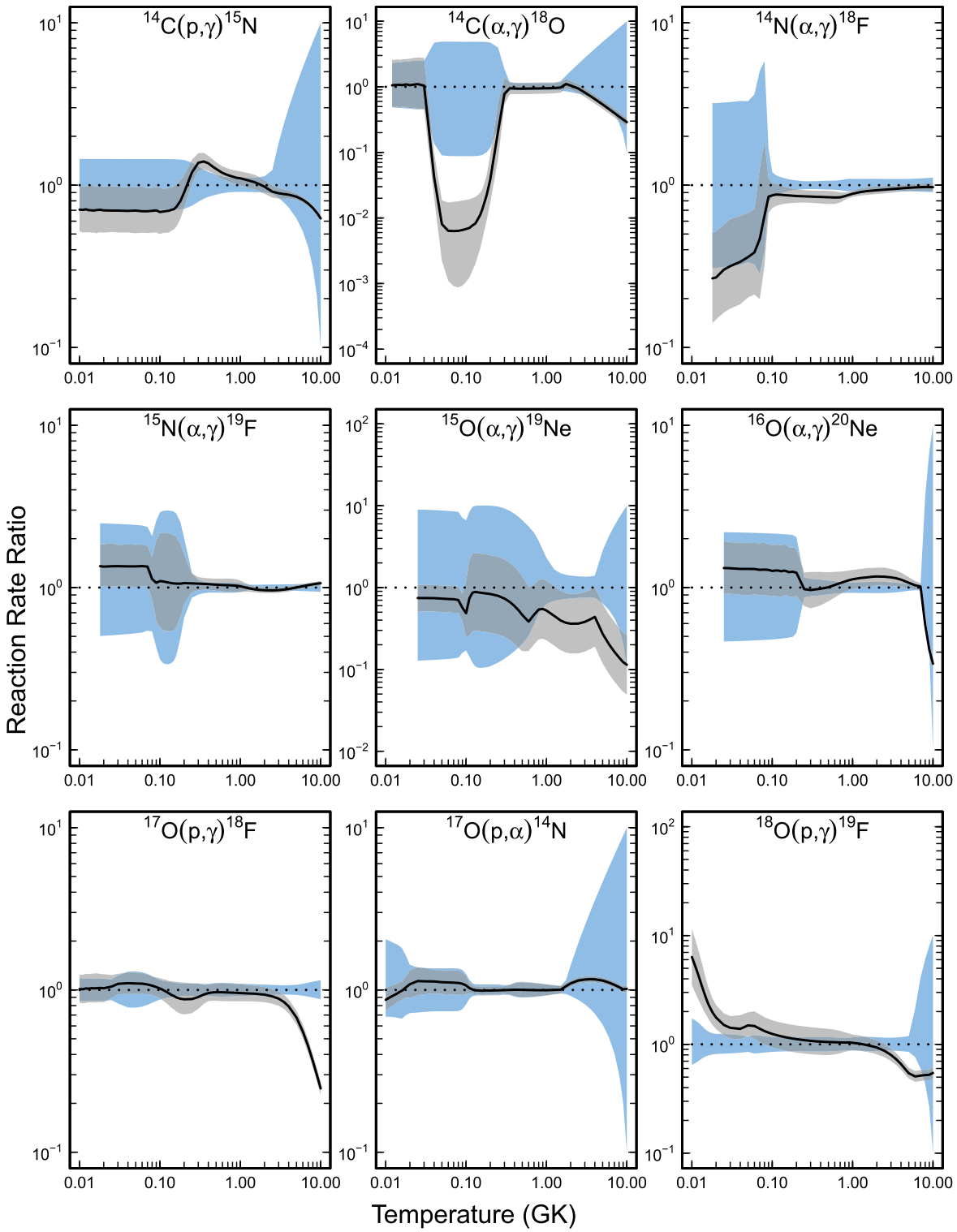

Figure 153. Comparison of our new rates (blue) with previous Monte Carlo rates (gray; C. Iliadis et al. 2010c). In each panel, the two bands show 68% coverage, and rates are normalized to our new recommended values; the solid black line depicts the ratio of previous to present rates.

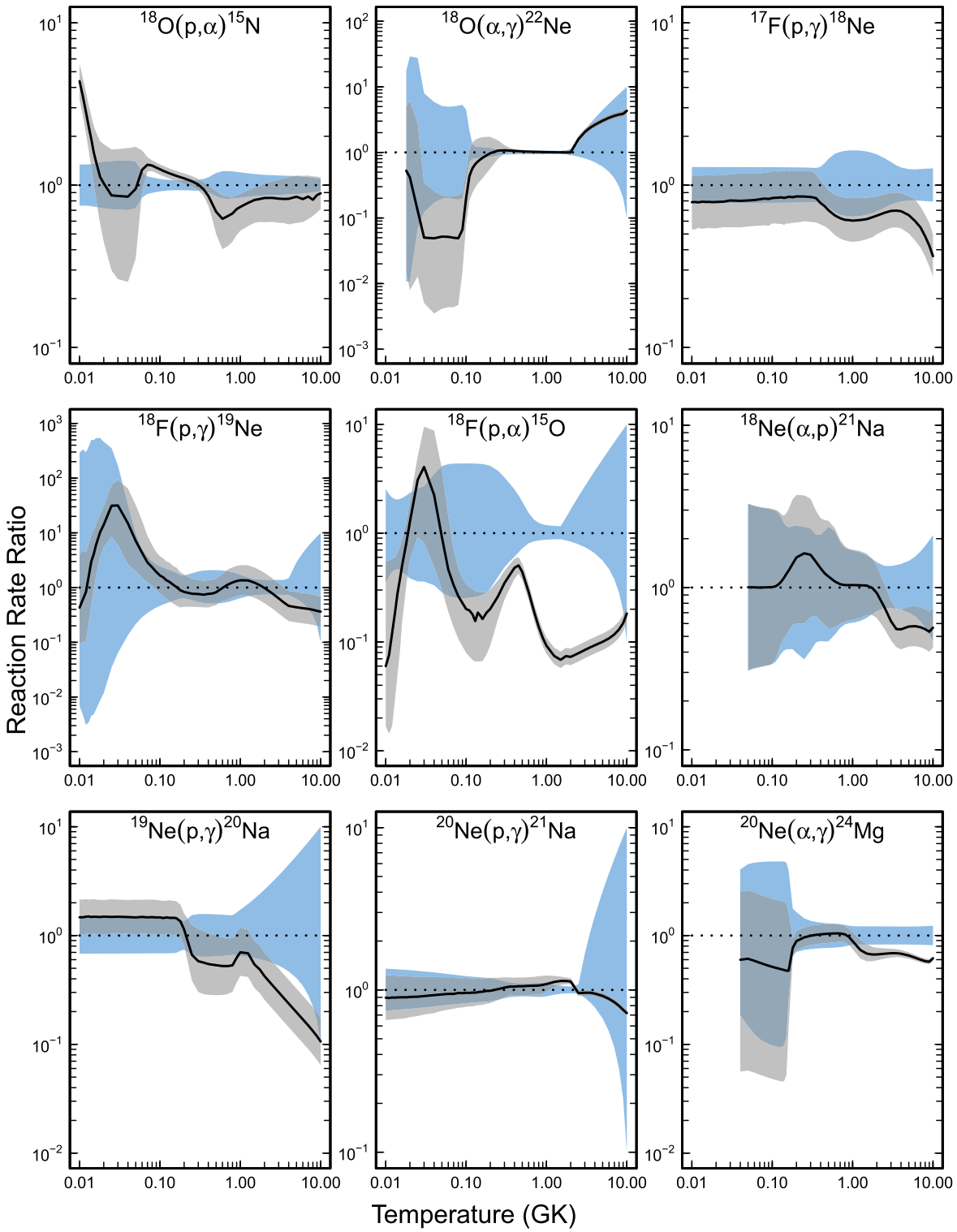

Figure 154. Comparison of our new rates (blue) with previous Monte Carlo rates (gray; C. Iliadis et al. 2010c; P. Mohr et al. 2014). In each panel, the two bands show 68% coverage, and rates are normalized to our new recommended values; the solid black line depicts the ratio of previous to present rates.

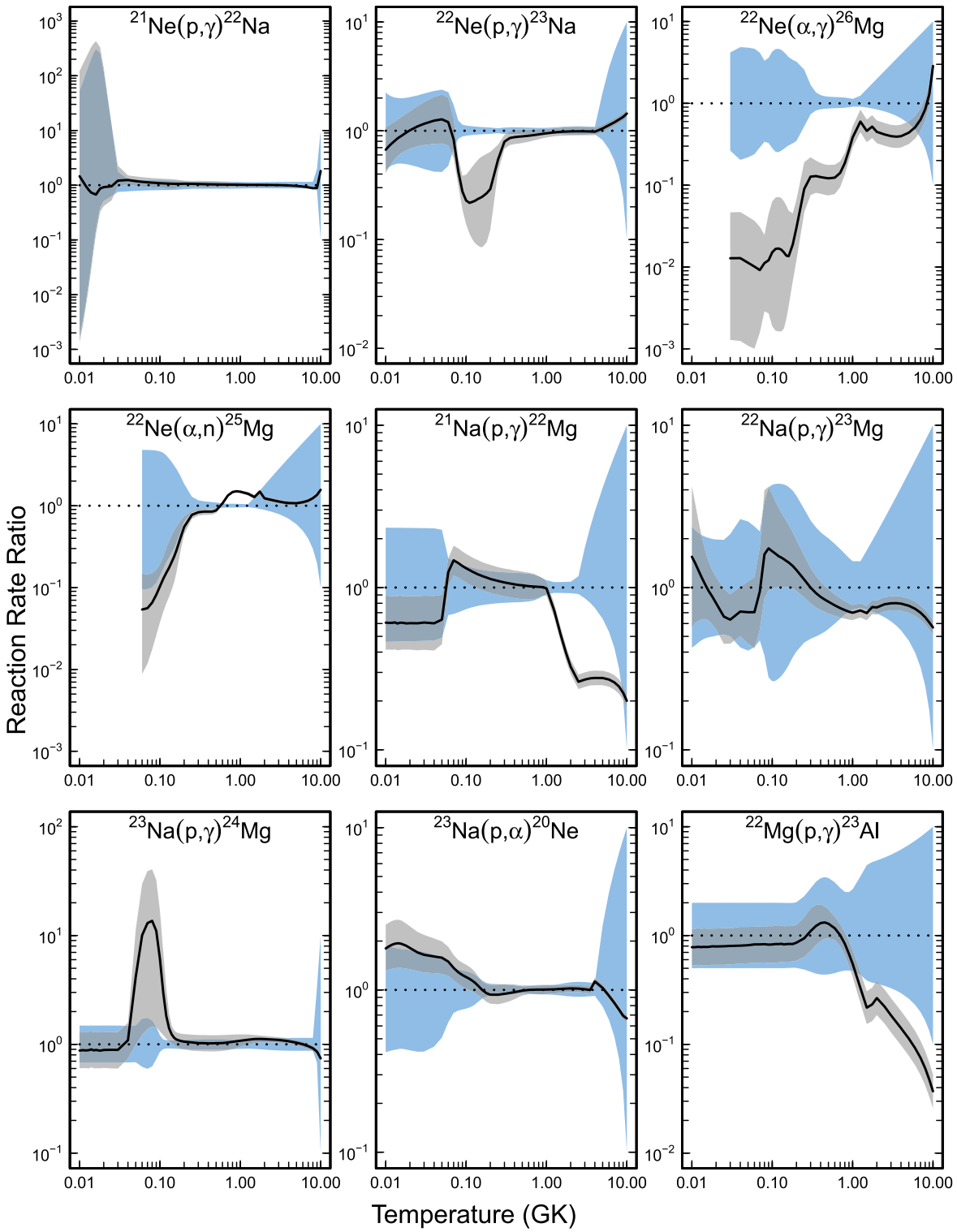

Figure 155. Comparison of our new rates (blue) with previous Monte Carlo rates (gray; C. Iliadis et al. 2010c). In each panel, the two bands show 68% coverage, and rates are normalized to our new recommended values; the solid black line depicts the ratio of previous to present rates.

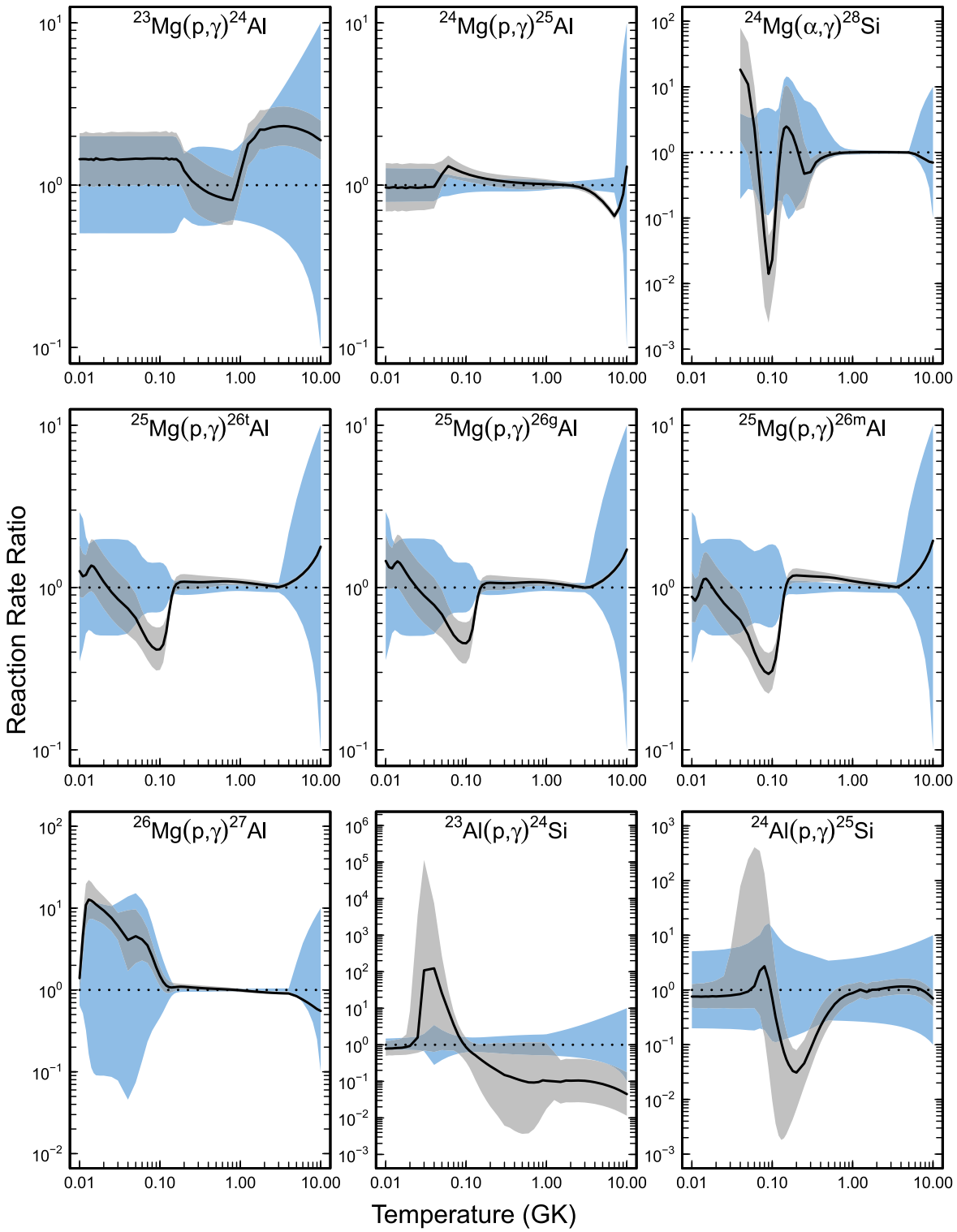

Figure 156. Comparison of our new rates (blue) with previous Monte Carlo rates (gray; C. Iliadis et al. 2010c). In each panel, the two bands show 68% coverage, and rates are normalized to our new recommended values; the solid black line depicts the ratio of previous to present rates.

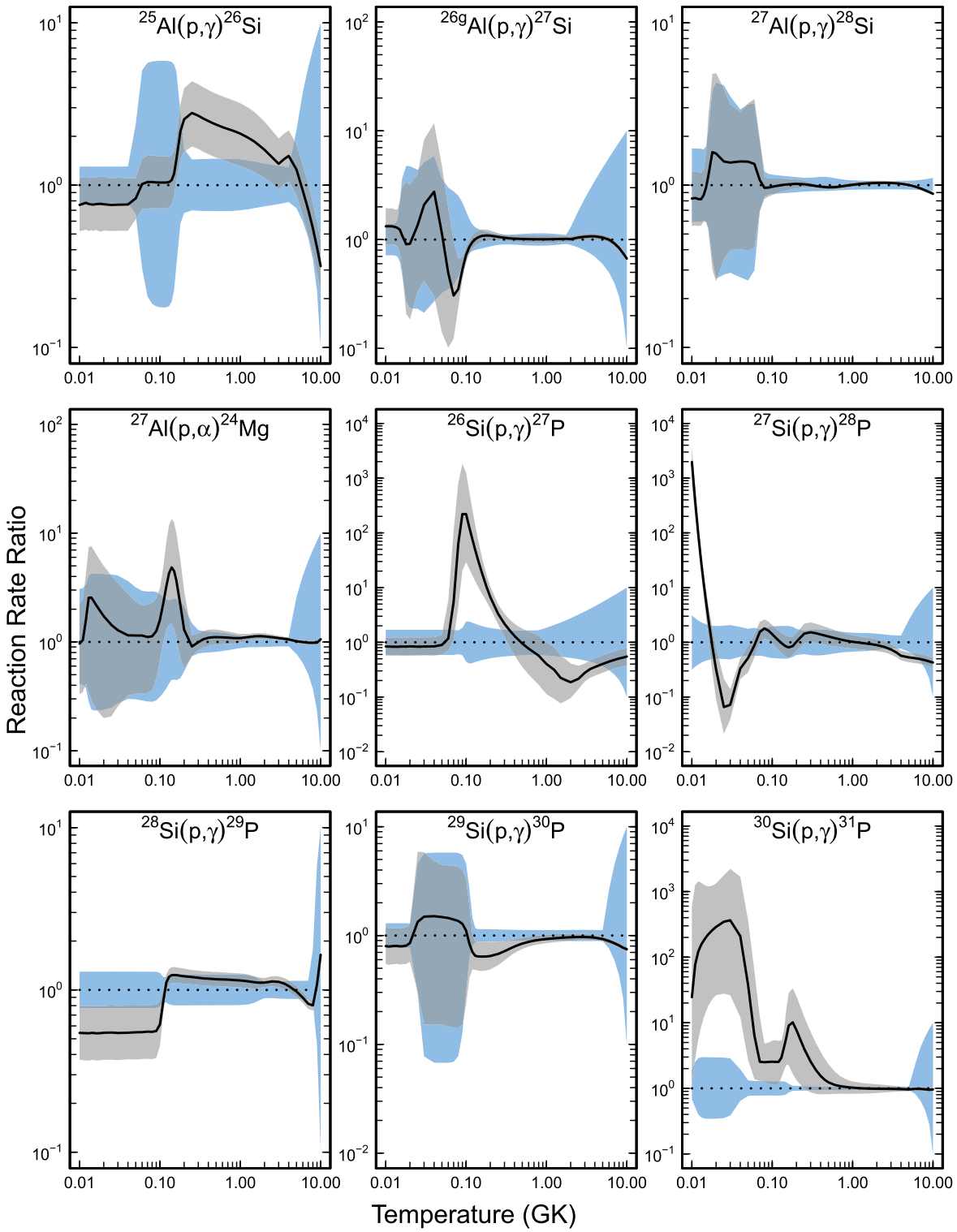

Figure 157. Comparison of our new rates (blue) with previous Monte Carlo rates (gray; C. Iliadis et al. 2010c). In each panel, the two bands show 68% coverage, and rates are normalized to our new recommended values; the solid black line depicts the ratio of previous to present rates.

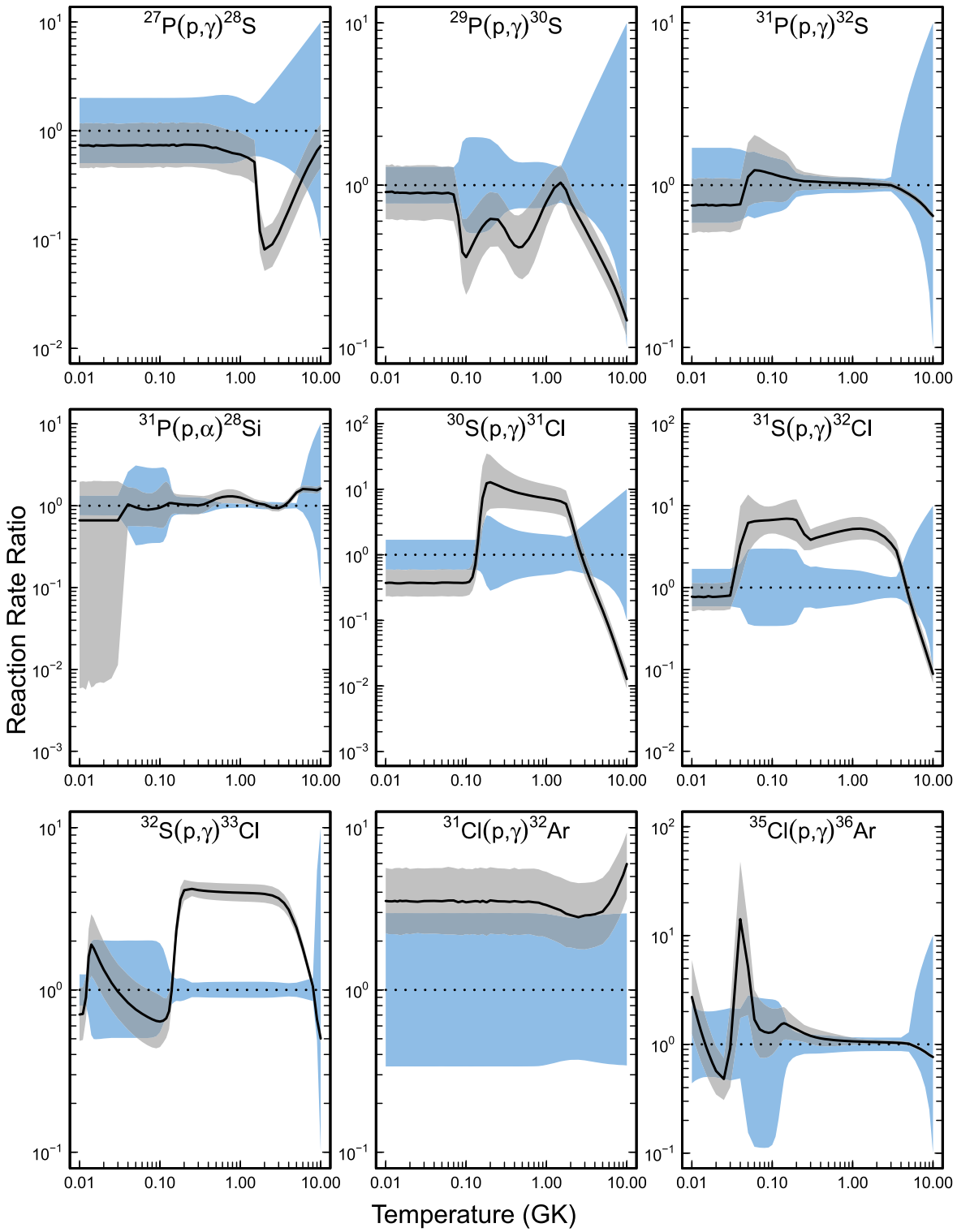

Figure 158. Comparison of our new rates (blue) with previous Monte Carlo rates (gray; C. Iliadis et al. 2010c). In each panel, the two bands show 68% coverage, and rates are normalized to our new recommended values; the solid black line depicts the ratio of previous to present rates.

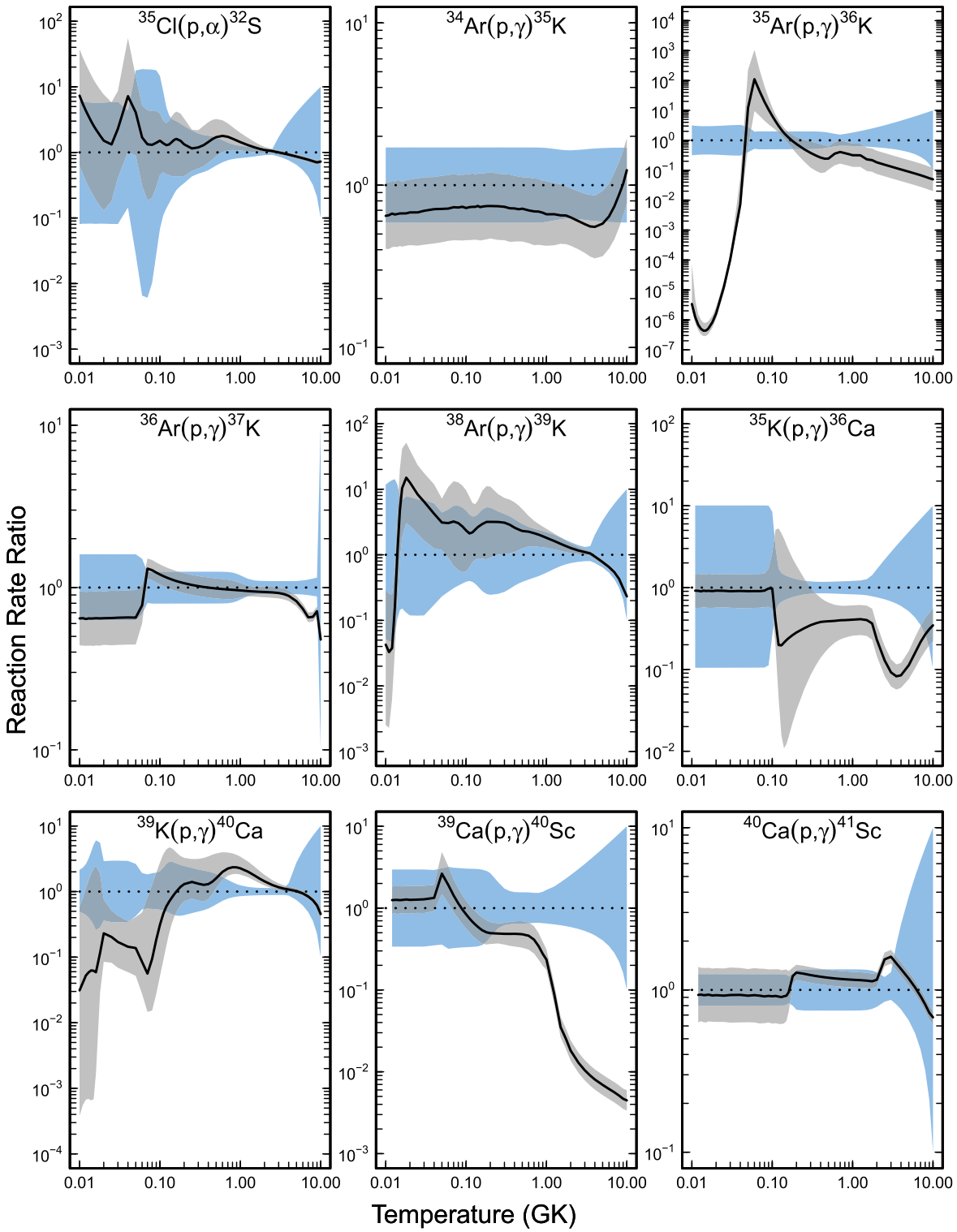

Figure 159. Comparison of our new rates (blue) with previous Monte Carlo rates (gray; C. Iliadis et al. 2010c; A. L. Sallaska et al. 2013; R. Longland et al. 2018). In each panel, the two bands show 68% coverage, and rates are normalized to our new recommended values; the solid black line depicts the ratio of previous to present rates.

ORCID iDs

Christian Iliadis https://orcid.org/0000-0003-2381-0412
Richard Longland https://orcid.org/0000-0001-7731-580X
Kiana Setoodehnia https://orcid.org/0000-0002-2149-5060
Caleb Marshall https://orcid.org/0000-0002-1194-2920
Peter Mohr https://orcid.org/0000-0002-6695-9359
Athanasios Psaltis https://orcid.org/0000-0003-2197-0797

References

Adekola, A. S., Brune, C. R., Bardayan, D. W., et al. 2011, PhRvC, 84, 054611
Adekola, A. S., Brune, C. R., Bardayan, D. W., et al. 2012, PhRvC, 85, 037601
Adelberger, E. G., García, A., Robertson, R. G. H., et al. 2011, RvMP, 83, 195
Adsley, P., Battino, U., Best, A., et al. 2021a, PhRvC, 103, 015805
Adsley, P., Brümmer, J. W., Faestermann, T., et al. 2018, PhRvC, 97, 045807
Adsley, P., Laird, A. M., & Meisel, Z. 2020, PhRvC, 102, 015801
Adsley, P., Nesterenko, V. O., Kimura, M., et al. 2021b, PhRvC, 103, 044315
Afanasieva, L., Blackmon, J. C., Deibel, C. M., et al. 2017, PhRvC, 96, 035801
Aitken, J., Litherland, A., Dixon, W., & Storey, R. 1969, PhLB, 30, 473
Aitken, J. H., Azuma, R. E., Litherland, A. E., et al. 1970, CaJPh, 48, 1617
Akers, C., Laird, A. M., Fulton, B. R., et al. 2016, PhRvC, 94, 065803
Aleonard, M., Hubert, P., Sarger, L., & Mennrath, P. 1976, NuPhA, 257, 490
Aliotta, M., & Langanke, K. 2022, FrP, 10, 942726
Almaraz-Calderon, S., Tan, W. P., Aprahamian, A., et al. 2012, PhRvC, 86, 065805
Amthor, A. M. 2009, PhD thesis, Michigan State Univ.
Anantaraman, N., Gove, H., Tōke, J., & Draayer, J. 1977, NuPhA, 279, 474
Anantaraman, N., Gove, H. E., Lindgren, R. A., et al. 1979, NuPhA, 313, 445
Anderson, M., Kennett, S., Mitchell, L., & Sargood, D. 1980, NuPhA, 349, 154
Andreon, S., & Weaver, B. 2015, Bayesian Methods for the Physical Sciences: Learning from Examples in Astronomy and Physics (Springer)
Angulo, C., Arnould, M., Rayet, M., et al. 1999, NuPhA, 656, 3
Arciszewski, H., Bakkum, E., Van Engelen, C., Endt, P., & Kamermans, R. 1984, NuPhA, 430, 234
Assenbaum, H. J., Langanke, K., & Rolfs, C. 1987, ZPhyA, 327, 461
Axelsson, L., Äystö, J., Borge, M., et al. 1998, NuPhA, 634, 475
Babilon, M., Bayer, W., Galaviz, D., et al. 2002, PhRvC, 66, 028801
Bailey, G., Griffiths, G., & Donnelly, T. 1967, NuPhA, 94, 502
Bair, J. K., & Haas, F. X. 1973, PhRvC, 7, 1356
Bair, J. K., & Willard, H. B. 1962, PhRv, 128, 299
Banu, A., Trache, L., Carstoiu, F., et al. 2011, PhRvC, 84, 015803
Bardayan, D. W., Batchelder, J. C., Blackmon, J. C., et al. 2002, PhRvL, 89, 262501
Bardayan, D. W., Blackmon, J. C., Brune, C. R., et al. 2000, PhRvC, 62, 055804
Basunia, M., & Hurst, A. 2016, NDS, 134, 1
Basunia, M. S., & Chakraborty, A. 2022, NDS, 186, 3
Basunia, M. S., & Chakraborty, A. 2024, NDS, 197, 1
Becker, H. W., Bahr, M., Berheide, M., et al. 1995, ZPhyA, 351, 453
Becker, H. W., Kieser, W. E., Rolfs, C., Trautvetter, H. P., & Wiescher, M. 1982, ZPhyA, 305, 319
Benenson, W., Guichard, A., Kashy, E., Mueller, D., & Nann, H. 1976, PhRvC, 13, 1479
Berg, U. E. P., Ackermann, K., & Bangert, K. 1984, PhLB, 140, 191
Bertone, P. F., Champagne, A. E., Boswell, M., et al. 2002, PhRvC, 66, 055804
Best, A., Beard, M., Görres, J., et al. 2013, PhRvC, 87, 045805
Best, A., Pantaleo, F., Boeltzig, A., et al. 2019, PhLB, 797, 134900
Blackmon, J. C., Champagne, A. E., Hofstee, M. A., et al. 1995, PhRvL, 74, 2642
Boeltzig, A., Best, A., Pantaleo, F., et al. 2019, PhLB, 795, 122
Boeltzig, A., deBoer, R. J., Chen, Y., et al. 2022, PhRvC, 106, 045801
Bommer, J., Ekpo, M., Fuchs, H., Grabisch, K., & Kluge, H. 1975, NuPhA, 251, 246
Bosch, H. S., & Hale, G. 1993, NucFu, 33, 1919
Bošnjaković, B., Bouwmeester, J., Van Best, J., & Pruys, H. 1968, NuPhA, 110, 17
Bragg, W. H., & Kleeman, R. 1905, LEDPM, 10, 318
Brown, R. E., Jarmie, N., & Hale, G. E. 1987, PhRvC, 35, 1999
Bruno, C. G., Scott, D. A., Aliotta, M., et al. 2016, PhRvL, 117, 142502
Brussaard, P. J., & Glaudemans, P. W. M. 1977, Shell-Model Applications in Nuclear Spectroscopy (North-Holland), 1
Buchmann, L., D'Auria, J. M., & McCorquodale, P. 1988, ApJ, 324, 953
Buchmann, L., Hilgemeier, M., Krauss, A., et al. 1984, NuPhA, 415, 93
Buckner, M. Q., Iliadis, C., Cesaratto, J. M., et al. 2012, PhRvC, 86, 065804
Buckner, M. Q., Iliadis, C., Kelly, K. J., et al. 2015, PhRvC, 91, 015812
Buerger, A., Azaiez, F., Stanoiu, M., et al. 2007, AcPPB, 38, 1353
Burlein, M., Dhuga, K. S., & Fortune, H. T. 1984, PhRvC, 29, 2013
Caggiano, J. A., Bazin, D., Benenson, W., et al. 2001, PhRvC, 64, 025802
Canete, L., Lotay, G., Christian, G., et al. 2021, PhRvC, 104, L022802
Carey, T. A., Roos, P. G., Chant, N. S., Nadasen, A., & Chen, H. L. 1984, PhRvC, 29, 1273
Casella, C., Costantini, H., Lemut, A., et al. 2002, NuPhA, 706, 203
Casella, G., & George, E. I. 1992, Am. Stat., 46, 167
Caughlan, G. R., & Fowler, W. A. 1988, ADNDT, 40, 283
Cesaratto, J. M., Champagne, A. E., Buckner, M. Q., et al. 2013, PhRvC, 88, 065806
Chafa, A., Tatischeff, V., Aguer, P., et al. 2005, PhRvL, 95, 031101
Chafa, A., Tatischeff, V., Aguer, P., et al. 2007, PhRvC, 75, 035810
Champagne, A., Cella, C., Kouzes, R., et al. 1988, NuPhA, 487, 433
Champagne, A., Magnus, P., Smith, M., & Howard, A. 1990, NuPhA, 512, 317
Champagne, A., & Pitt, M. 1986, NuPhA, 457, 367
Champagne, A., Pitt, M., Zhang, P., Lee, L., & Levine, M. 1986, NuPhA, 459, 239
Chen, J., Cameron, J., & Singh, B. 2011, NDS, 112, 2715
Chen, Y., Berg, G. P. A., deBoer, R. J., et al. 2021, PhRvC, 103, 035809
Cheng, C.-W., Saha, S. K., Keinonen, J., Mak, H.-B., & McLatchie, W. 1981, CaJPh, 59, 238
Chipps, K. A., Bardayan, D. W., Blackmon, J. C., et al. 2009, PhRvL, 102, 152502
Chouraqui, G., Muller, T., Port, M., & Thirion, J. 1970, JPhys, 31, 249
Christian, G., Hutcheon, D., Akers, C., et al. 2013, PhRvC, 88, 038801
Christy, R., & Duck, I. 1961, NucPh, 24, 89
Coc, A., Petitjean, P., Uzan, J.-P., et al. 2015, PhRvD, 92, 123526
Coc, A., Uzan, J.-P., & Vangioni, E. 2014, JCAP, 2014, 050
Cooper, S. G. 1986, JPhG, 12, 869
Cooper, S. G., Huby, R., & Mines, J. R. 1982, JPhG, 8, 559
Costantini, H., Bemmerer, D., Confortola, F., et al. 2008, NuPhA, 814, 144
Costantini, H., deBoer, R. J., Azuma, R. E., et al. 2010, PhRvC, 82, 035802
Coszach, R., Cogneau, M., Bain, C. R., et al. 1995, PhLB, 353, 184
Coszach, R., Delbar, T., Galster, W., et al. 1994, PhRvC, 50, 1695
Couch, R., Spinka, H., Tombrello, T., & Weaver, T. 1971, NuPhA, 175, 300
Cover, T. M., & Thomas, J. A. 2006, Elements of Information Theory (Wiley-Interscience)
Crawley, G. M., Djalali, C., Marty, N., et al. 1989, PhRvC, 39, 311
Cunsolo, A., Foti, A., Immè, G., et al. 1981, PhRvC, 24, 476
Dababneh, S., Heil, M., Käppeler, F., et al. 2003, PhRvC, 68, 025801
D'Agata, G., Kilic, A. I., Burjan, V., et al. 2021, PhRvC, 103, 015806
Daigle, S., Kelly, K. J., Champagne, A. E., et al. 2016, PhRvC, 94, 025803
Damone, L., Barbagallo, M., Mastromarco, M., et al. 2018, PhRvL, 121, 042701
D'Auria, J. M., Azuma, R. E., Bishop, S., et al. 2004, PhRvC, 69, 065803
Davids, B., Cyburt, R. H., José, J., & Mythili, S. 2011, ApJ, 735, 40
Davids, B., van den Berg, A. M., Dendooven, P., et al. 2003, PhRvC, 67, 012801
deBoer, R. J., Görres, J., Smith, K., et al. 2014, PhRvC, 90, 035804
deBoer, R. J., Görres, J., Wiescher, M., et al. 2017, RvMP, 89, 035007
deBoer, R. J., Wiescher, M., Görres, J., et al. 2010, PhRvC, 82, 025802
de Oliveira, F., Coc, A., Aguer, P., et al. 1996, NuPhA, 597, 231
Depalo, R., Cavanna, F., Aliotta, M., et al. 2016, PhRvC, 94, 055804
Dermigny, J., Iliadis, C., Buckner, M., & Kelly, K. 2016, NIMPA, 830, 427
Dermigny, J., Iliadis, C., Champagne, A., & Longland, R. 2020, PhRvC, 102, 014609
Dermigny, J. R., & Iliadis, C. 2017, ApJ, 848, 14
Descouvemont, P. 2000, ApJ, 543, 425
Descouvemont, P., Adahchour, A., Angulo, C., Coc, A., & Vangioni-Flam, E. 2004, ADNDT, 88, 203
Descouvemont, P., & Baye, D. 2010, RPPh, 73, 036301
de Souza, R. S., Boston, S. R., Coc, A., & Iliadis, C. 2019a, PhRvC, 99, 014619
de Souza, R. S., Iliadis, C., & Coc, A. 2019b, ApJ, 872, 75
de Souza, R. S., Kiat, T. H., Coc, A., & Iliadis, C. 2020, ApJ, 894, 134
de Valpine, P., Turek, D., Paciorek, C. J., et al. 2017, J. Comput. Graph. Stat., 26, 403
Di Leva, A., Scott, D. A., Caciolli, A., et al. 2014, PhRvC, 89, 015803
Di Leva, A., Imbriani, G., Buompane, R., et al. 2017, PhRvC, 95, 045803

Dixon, W., & Storey, R. 1977, NuPhA, 284, 97
Dixon, W. R., & Storey, R. S. 1971, CaJPh, 49, 1714
Dixon, W. R., Storey, R. S., Aitken, J. H., Litherland, A. E., & Rogers, D. W. O. 1971, PhRvL, 27, 1460
Dombos, A. C., Robertson, D., Simon, A., et al. 2022, PhRvL, 128, 162701
Doornenbal, P., Reiter, P., Grawe, H., et al. 2007, PhLB, 647, 237
Downen, L., Iliadis, C., Champagne, A., et al. 2022a, ApJ, 928, 128
Downen, L. N., Iliadis, C., Champagne, A. E., et al. 2022b, PhRvC, 105, 055804
Dronchi, N., Weisshaar, D., Brown, B. A., et al. 2023, PhRvC, 107, 034306
Drotleff, H. W., Denker, A., Knee, H., et al. 1993, ApJ, 414, 735
Dufour, M., Descouvemont, P., & Baye, D. 1994, PhRvC, 50, 795
Endt, P. M. 1977, ADNDT, 19, 23
Endt, P. M. 1990, NuPhA, 521, 1
Endt, P. M. 1998, NuPhA, 633, 1
Endt, P. M., & van dèr Leun, C. 1973, NuPhA, 214, 1
Endt, P. M., & van der Leun, C. 1978, NuPhA, 310, 1
Engel, S., Hutcheon, D., Bishop, S., et al. 2005, NIMPA, 553, 491
Engelbertink, G., & Endt, P. M. 1966, NucPh, 88, 12
Erikson, L., Ruiz, C., Ames, F., et al. 2010, PhRvC, 81, 045808
Fallis, J., Parikh, A., Bertone, P. F., et al. 2013, PhRvC, 88, 045801
Fang, R., Görres, J., deBoer, R. J., et al. 2024, PhRvC, 110, 025806
Ferraro, F., Takács, M. P., Piatti, D., et al. 2018, PhRvL, 121, 172701
Fienberg, S. E. 2006, BayAn, 1, 1
Fink, C., & Schiffer, J. 1974, NuPhA, 225, 93
Fisher, T. R., & Whaling, W. 1963, PhRv, 131, 1723
Flack, F. C., Rutherglen, J. G., & Grant, P. J. 1954, PPSA, 67, 973
Flavigny, F., Keeley, N., Gillibert, A., & Obertelli, A. 2018, PhRvC, 97, 034601
Foreman-Mackey, D., Hogg, D. W., Lang, D., & Goodman, J. 2013, PASP, 125, 306
Fortune, H. T. 2003, PhRvC, 68, 034317
Fortune, H. T., & Betts, R. R. 1974, PhRvC, 10, 1292
Fortune, H. T., Lacaze, A., & Sherr, R. 2010, PhRvC, 82, 034312
Fortune, H. T., & Lacaze, A. G. 2003, PhRvC, 67, 064305
Fougères, C., de Oliveira Santos, F., José, J., et al. 2023, NatCo, 14, 4536
Fowler, W. A., Caughlan, G. R., & Zimmerman, B. A. 1967, ARA&A, 5, 525
Fowler, W. A., Caughlan, G. R., & Zimmerman, B. A. 1975, ARA&A, 13, 69
Fox, C., Iliadis, C., Champagne, A. E., et al. 2005, PhRvC, 71, 055801
Fox, W., Longland, R., Marshall, C., & Chaves, F. P. 2024, PhRvL, 132, 062701
Freer, M., Achouri, N. L., Angulo, C., et al. 2012, PhRvC, 85, 014304
Funck, C., & Langanke, K. 1989, ApJ, 344, 46
Fynbo, H., Borge, M., Axelsson, L., et al. 2000, NuPhA, 677, 38
Gade, A., Adrich, P., Bazin, D., et al. 2008, PhRvC, 77, 044306
Gai, M. 1992, PhRvC, 45, R2548
Gai, M., Keddy, R., Bromley, D. A., Olness, J. W., & Warburton, E. K. 1987, PhRvC, 36, 1256
García, A., Adelberger, E. G., Magnus, P. V., et al. 1991, PhRvC, 43, 2012
Garrett, J. D., Fortune, H. T., Middleton, R., & Scholz, W. 1978, PhRvC, 18, 2032
Gelman, A., Simpson, D., & Betancourt, M. 2017, Entrp, 19, 555
Giesen, U., Browne, C. P., Görres, J., et al. 1993, NuPhA, 561, 95
Gillespie, S. A., Brown, K. W., Charity, R. J., et al. 2022, PhRvC, 105, 044321
Gillespie, S. A., Parikh, A., Barton, C. J., et al. 2017, PhRvC, 96, 025801
Glatz, F., Norbert, S., Bitterwolf, E., et al. 1986, Phy, 324, 187
Glatz, F., Norbert, S., Bitterwolf, E., et al. 1986, ZPhyA, 324, 187
Glaudemans, P., & Endt, P. M. 1962, NucPh, 30, 30
Glendenning, N. K. 1983, Direct Nuclear Reactions (Academic), 24
Goldberg, E., Haeberli, W., Galonsky, A. I., & Douglas, R. A. 1954, PhRv, 93, 799
Gómez Iñesta, A., Iliadis, C., & Coc, A. 2017, ApJ, 849, 134
Gorodetzky, S., Freeman, R. M., Gallmann, A., Haas, F., & Heusch, B. 1967, PhRv, 155, 1119
Görres, J., Arlandini, C., Giesen, U., et al. 2000, PhRvC, 62, 055801
Görres, J., Becker, H., Buchmann, L., et al. 1983, NuPhA, 408, 372
Görres, J., Graff, S., Wiescher, M., et al. 1990, NuPhA, 517, 329
Görres, J., Graff, S., Wiescher, M., et al. 1992, NuPhA, 548, 414
Görres, J., Wiescher, M., & Rolfs, C. 1989, ApJ, 343, 365
Graff, J., Chouraqui, G., Port, M., et al. 1968, JPhys, 29, 141
Graff, S., Görres, J., Wiescher, M., et al. 1990, NuPhA, 510, 346
Graulich, J. S., Binon, F., Bradfield-Smith, W., et al. 1997, NuPhA, 626, 751
Gribble, D., Iliadis, C., Janssens, R. V. F., et al. 2025, PhRvC, 112, 025804
Guillot, J., Langevin-Joliot, H., van de Wiele, J., et al. 1991, PhLB, 258, 271
Hager, U., Brown, J. R., Buchmann, L., et al. 2011, PhRvC, 84, 022801
Hager, U., Buchmann, L., Davids, B., et al. 2012, PhRvC, 86, 055802
Hahn, K. I., García, A., Adelberger, E. G., et al. 1996, PhRvC, 54, 1999
Hale, S. E., Champagne, A. E., Iliadis, C., et al. 2001, PhRvC, 65, 015801
Hale, S. E., Champagne, A. E., Iliadis, C., et al. 2004, PhRvC, 70, 045802
Hall, M. R., Bardayan, D. W., Baugher, T., et al. 2020, PhRvC, 102, 045802
Hamill, C. B., Woods, P. J., Kahl, D., et al. 2020, EPJA, 56, 36
Hänninen, R. 1984, NuPhA, 420, 351
Hansen, L. F., Anderson, J. D., McClure, J. W., et al. 1967, NuPhA, 98, 25
Hansper, V. Y., Champagne, A. E., Hale, S. E., Iliadis, C., & Powell, D. C. 2000, PhRvC, 61, 028801
Hardie, G., Filippone, B. W., Elwyn, A. J., Wiescher, M., & Segel, R. E. 1984, PhRvC, 29, 1199
Harissopulos, S., Chronidou, C., Spyrou, K., et al. 2000, EPJA, 9, 479
Harms, V., Kratz, K.-L., & Wiescher, M. 1991, PhRvC, 43, 2849
Harrouz, D. S., de Séréville, N., Adsley, P., et al. 2022, PhRvC, 105, 015805
Hartos, M., Bertulani, C. A., Shubhchintak, Mukhamedzhanov, A. M., & Hou, S. 2018, ApJ, 862, 62
Hashimoto, M. A., Nomoto, K. I., Arai, K., & Kaminisi, K. 1986, ApJ, 307, 687
Hebbard, D., & Robson, B. 1963, NucPh, 42, 563
Heinrich, J., & Lyons, L. 2007, ARNPS, 57, 145
Herndl, H., Fantini, M., Iliadis, C., Endt, P. M., & Oberhummer, H. 1998, PhRvC, 58, 1798
Herndl, H., Görres, J., Wiescher, M., Brown, B. A., & Van Wormer, L. 1995, PhRvC, 52, 1078
Highland, G., & Thwaites, T. 1968, NuPhA, 109, 163
Hilbe, J. M., de Souza, R. S., & Ishida, E. E. O. 2017, Bayesian Models for Astrophysical Data Using R, JAGS, Python, and Stan (Cambridge Univ. Press)
Huang, K. N., Aoyagi, M., Chen, M. H., Crasemann, B., & Mark, H. 1976, ADNDT, 18, 243
Hunt, S., Iliadis, C., Champagne, A., Downen, L., & Cooper, A. 2019, PhRvC, 99, 045804
Iliadis, C. 1997, NuPhA, 618, 166
Iliadis, C. 2015, Nuclear Physics of Stars (2nd ed.; Wiley-VCH)
Iliadis, C. 2019, PhRvC, 99, 065809
Iliadis, C. 2023, PhRvC, 107, 044610
Iliadis, C., Anderson, K. S., Coc, A., Timmes, F. X., & Starrfield, S. 2016, ApJ, 831, 107
Iliadis, C., Angulo, C., Descouvemont, P., Lugaro, M., & Mohr, P. 2008, PhRvC, 77, 045802
Iliadis, C., Buchmann, L., Endt, P. M., Herndl, H., & Wiescher, M. 1996, PhRvC, 53, 475
Iliadis, C., & Coc, A. 2020, ApJ, 901, 127
Iliadis, C., D'Auria, J. M., Starrfield, S., Thompson, W. J., & Wiescher, M. 2001, ApJS, 134, 151
Iliadis, C., Downen, L. N., José, J., Nittler, L. R., & Starrfield, S. 2018, ApJ, 855, 76
Iliadis, C., Endt, P. M., Prantzos, N., & Thompson, W. J. 1999, ApJ, 524, 434
Iliadis, C., Giesen, U., Görres, J., et al. 1992a, NuPhA, 539, 97
Iliadis, C., Görres, J., Ross, J., et al. 1993b, NuPhA, 559, 83
Iliadis, C., Görres, J., Ross, J., et al. 1994, NuPhA, 571, 132
Iliadis, C., Höhne, J., Käppeler, F., et al. 1993a, PhRvC, 48, R1479
Iliadis, C., Longland, R., Champagne, A., & Coc, A. 2010a, NuPhA, 841, 251
Iliadis, C., Longland, R., Champagne, A., & Coc, A. 2010b, NuPhA, 841, 323
Iliadis, C., Longland, R., Champagne, A., Coc, A., & Fitzgerald, R. 2010c, NuPhA, 841, 31
Iliadis, C., Longland, R., Coc, A., Timmes, F. X., & Champagne, A. E. 2015, JPhG, 42, 034007
Iliadis, C., Longland, R., Setoodehnia, K., et al. 2025, Data for the 2025 Evaluation of Experimental Reaction Rates (ETR25), vETR25, Zenodo, doi:10.5281/zenodo.17610211
Iliadis, C., Palanivelrajan, V., & de Souza, R. S. 2022, PhRvC, 106, 055802
Iliadis, C., Ross, J. G., Görres, J., et al. 1992b, PhRvC, 45, 2989
Iliadis, C., Schange, T., Rolfs, C., et al. 1990, NuPhA, 512, 509
Iliadis, C., & Wiescher, M. 2004, PhRvC, 69, 064305
Jaeger, M., Kunz, R., Mayer, A., et al. 2001, PhRvL, 87, 202501
Jayatissa, H., Avila, M. L., Rehm, K. E., et al. 2022, PhRvC, 105, L042802
Jayatissa, H., Rogachev, G., Goldberg, V., et al. 2020, PhLB, 802, 135267
Johnson, P., Meyer, M., & Reitmann, D. 1974, NuPhA, 218, 333
Kahl, D., José, J., & Woods, J. 2021, A&A, 653, A64
Kalifa, J., Vernotte, J., Deschamps, Y., et al. 1978, PhRvC, 17, 1961
Kangasmäki, A., Tikkanen, P., Keinonen, J., et al. 1998, PhRvC, 58, 699
Keinonen, J., Riihonen, M., & Anttila, A. 1977, PhRvC, 15, 579
Kelly, K. J., Champagne, A. E., Downen, L. N., et al. 2017, PhRvC, 95, 015806

Kelly, K. J., Champagne, A. E., Longland, R., & Buckner, M. Q. 2015, PhRvC, 92, 035805
Kieser, W., Azuma, R., & Jackson, K. 1979, NuPhA, 331, 155
Kikstra, S., Van Der Leun, C., Endt, P., et al. 1990, NuPhA, 512, 425
Kim, K. H., Park, M. H., & Kim, B. T. 1987, PhRvC, 35, 363
King, G. B., Lovell, A. E., & Nunes, F. M. 2018, PhRvC, 98, 044623
Knee, H. 1995, PhD thesis, Univ. Stuttgart
Knöpfle, K., Doll, P., Mairle, G., & Wagner, G. 1974, NuPhA, 233, 317
Koehler, P. E. 2002, PhRvC, 66, 055805
Koning, A., Hilaire, S., & Goriely, S. 2023, EPJA, 59, 131
Kontos, A., Görres, J., Best, A., et al. 2012, PhRvC, 86, 055801
Kontos, A., Uberseder, E., deBoer, R., et al. 2013, PhRvC, 87, 065804
Kozub, R. L., Bardayan, D. W., Batchelder, J. C., et al. 2005, PhRvC, 71, 032801
Kozub, R. L., Bardayan, D. W., Batchelder, J. C., et al. 2006, PhRvC, 73, 044307
Kraushaar, J. J., Fujiwara, M., Hosono, K., et al. 1986, PhRvC, 34, 1530
Krausmann, E., Balogh, W., Oberhummer, H., et al. 1996, PhRvC, 53, 469
Kuperus, J., Glaudemans, P., & Endt, P. 1963, Phy, 29, 1281
Kuvin, S. A., Belarge, J., Baby, L. T., et al. 2017, PhRvC, 96, 045812
La Cognata, M., Spitaleri, C., & Mukhamedzhanov, A. M. 2010, ApJ, 723, 1512
La Cognata, M., Spitaleri, C., Mukhamedzhanov, A. M., et al. 2008, PhRvL, 101, 152501
Laird, A. M., Cherubini, S., Ostrowski, A. N., et al. 2002, PhRvC, 66, 048801
Laird, A. M., Lugaro, M., Kankainen, A., et al. 2023, JPhG, 50, 033002
Lalanne, L., Sorlin, O., Assié, M., et al. 2021, PhRvC, 103, 055809
Lalanne, L., Sorlin, O., Poves, A., et al. 2022, PhRvL, 129, 122501
Landre, V., Aguer, P., Bogaert, G., et al. 1989, PhRvC, 40, 1972
Lane, A. M. 1960, RvMP, 32, 519
Lane, A. M., & Thomas, R. G. 1958, RvMP, 30, 257
Langanke, K. 1984, ZPhyA, 317, 325
Langer, C., Lepyoshkina, O., Aksyutina, Y., et al. 2014, PhRvC, 89, 035806
Lees, E. W., Johnston, A., Brain, S. W., et al. 1974, JPhA, 7, 936
Li, T. K., Dehnhard, D., Brown, R. E., & Ellis, P. J. 1976, PhRvC, 13, 55
Liang, P. F., Sun, L. J., Lee, J., et al. 2020, PhRvC, 101, 024305
Limata, B., Strieder, F., Formicola, A., et al. 2010, PhRvC, 82, 015801
Linfoot, E. H. 1957, Inform. Control, 1, 85
Lombardo, I., Dell'Aquila, D., Cinausero, M., et al. 2021, JPhG, 48, 065101
Longfellow, B., Gade, A., Brown, B. A., et al. 2018, PhRvC, 97, 054307
Longfellow, B., Gade, A., Brown, B. A., et al. 2019, PhRvC, 99, 064330
Longland, R. 2017, A&A, 604, A34
Longland, R. 2025, RatesMC: Monte Carlo Reaction Rate Code, v2.3, Zenodo, doi:10.5281/zenodo.17516449
Longland, R., Dermigny, J., & Marshall, C. 2018, PhRvC, 98, 025802
Longland, R., & de Séréville, N. 2020, A&A, 642, A41
Longland, R., Iliadis, C., Champagne, A. E., et al. 2010, NuPhA, 841, 1
Longland, R., Iliadis, C., & Karakas, A. I. 2012, PhRvC, 85, 065809
Longland, R., Iliadis, C., Rusev, G., et al. 2009, PhRvC, 80, 055803
Lorenz-Wirzba, H., Schmalbrock, P., Trautvetter, H., et al. 1979, NuPhA, 313, 346
Lotay, G., Woods, P. J., Seweryniak, D., et al. 2008, PhRvC, 77, 042802
Lotay, G., Doherty, D. T., Seweryniak, D., et al. 2019, EPJA, 55, 109
Lotay, G., Henderson, J., Catford, W., et al. 2022, PhLB, 833, 137361
Lotay, G., Woods, P. J., Moukaddam, M., et al. 2020, EPJA, 56, 3
Lovell, A. E., Nunes, F. M., Sarich, J., & Wild, S. M. 2017, PhRvC, 95, 024611
Lovely, M., Lennarz, A., Connolly, D., et al. 2021, PhRvC, 103, 055801
Lugaro, M., Ugalde, C., Karakas, A. I., et al. 2004, ApJ, 615, 934
Lunney, D., Pearson, J. M., & Thibault, C. 2003, RvMP, 75, 1021
Luukko, A., Anttila, A., Bister, M., & Piiparinen, M. 1970, PhyS, 2, 159
Lyons, S., Görres, J., deBoer, R. J., et al. 2018, PhRvC, 97, 065802
Ma, L., Karwowski, H. J., Brune, C. R., et al. 1997, PhRvC, 55, 588
Madhusoodhanan, T., Mandal, S., Shyam, R., et al. 1999, JPhG, 25, 1897
Magnus, P. V., Smith, M. S., Howard, A. J., Parker, P. D., & Champagne, A. E. 1990, NuPhA., 506, 332
Mak, H.-B., Ewan, G., Evans, H., et al. 1980, NuPhA, 343, 79
Mao, Z. Q., Fortune, H. T., & Lacaze, A. G. 1996, PhRvC, 53, 1197
Margerin, V., Lotay, G., Woods, P. J., et al. 2015, PhRvL, 115, 062701
Marshall, C., Morfouace, P., de Séréville, N., & Longland, R. 2020, PhRvC, 102, 024609
Marshall, C., Setoodehnia, K., Cinquegrana, G. C., et al. 2023, PhRvC, 107, 035806
Masha, E., Barbieri, L., Skowronski, J., et al. 2023, PhRvC, 108, L052801
Massimi, C., Koehler, P., Bisterzo, S., et al. 2012, PhRvC, 85, 044615
Matoš, M., Blackmon, J. C., Linhardt, L. E., et al. 2011, PhRvC, 84, 055806
Mátyus, Z., Csedreki, L., Fülöp, Z., et al. 2024, EPJA, 60, 218
Mayer, A. 2001, PhD thesis, Univ. Stuttgart
Meyer, A., de Séréville, N., Laird, A. M., et al. 2020, PhRvC, 102, 035803
Moazen, M. C., Bardayan, D. W., et al. 2011, EPJA, 47, 66
Mohr, P. 2005, PhRvC, 72, 035803
Mohr, P., Longland, R., & Iliadis, C. 2014, PhRvC, 90, 065806
Mohr, P., Oberhummer, H., Gyürky, G., et al. 1999, PhRvC, 59, 1790
Moscoso, J., de Souza, R. S., Coc, A., & Iliadis, C. 2021, ApJ, 923, 49
Moshinsky, M. 1959, NucPh, 13, 104
Mosley, C. A., & Fortune, H. T. 1977, PhRvC, 16, 1697
Moss, C. E. 1976, NuPhA, 269, 429
Mossa, V., Stöckel, K., Cavanna, F., et al. 2020, Natur, 587, 210
Mountford, D. J., Murphy, A. S. J., Achouri, N. L., et al. 2012, PhRvC, 85, 022801
Mukhamedzhanov, A. M., Bém, P., Burjan, V., et al. 2006, PhRvC, 73, 035806
Mukhamedzhanov, A. M., Gagliardi, C. A., & Tribble, R. E. 2001, PhRvC, 63, 024612
Murphy, A. S. J., Laird, A. M., Angulo, C., et al. 2009, PhRvC, 79, 058801
Neogy, P., Middleton, R., & Scholz, W. 1972, PhRvC, 6, 885
Newton, J. R., Longland, R., & Iliadis, C. 2008, PhRvC, 78, 025805
Odell, D., Brune, C. R., & Phillips, D. R. 2022a, PhRvC, 105, 014625
Odell, D., Brune, C. R., Phillips, D. R., deBoer, R. J., & Paneru, S. N. 2022b, FrP, 10, 888476
Ostrowski, A. N., Laird, A. M., Shotter, A. C., et al. 2002, NuPhA, 701, 621
Ouellet, C., & Singh, B. 2013, NDS, 114, 209
Paine, B., & Sargood, D. 1979, NuPhA, 331, 389
Pantaleo, F. R., Boeltzig, A., Best, A., et al. 2021, PhRvC, 104, 025802
Parikh, A., Wimmer, K., Faestermann, T., et al. 2014, PhLB, 737, 314
Parker, P. D. 1968, PhRv, 173, 1021
Parpottas, Y., Grimes, S. M., Al-Quraishi, S., et al. 2005, PhRvC, 72, 025802
Peplowski, P. N., Baby, L. T., Wiedenhöver, I., et al. 2009, PhRvC, 79, 032801
Perello, J. F., Almaraz-Calderon, S., Asher, B. W., et al. 2022, PhRvC, 105, 035805
Pérez-Loureiro, D., Wrede, C., Bennett, M. B., et al. 2016, PhRvC, 93, 064320
Pisanti, O., Mangano, G., Miele, G., & Mazzella, P. 2021, JCAP, 2021, 020
Plummer, M. 2003, Proc. of the 3rd Int. Workshop on Distributed Statistical Computing, ed. K. Hornik et al. https://www.r-project.org/conferences/DSC-2003/Proceedings/
Pogrebnyak, I., Howard, C., Iliadis, C., Longland, R., & Mitchell, G. E. 2013, PhRvC, 88, 015808
Polsky, L. M., Holbrow, C. H., & Middleton, R. 1969, PhRv, 186, 966
Porter, C. E., & Thomas, R. G. 1956, PhRv, 104, 483
Powell, D., Iliadis, C., Champagne, A., et al. 1998, NuPhA, 644, 263
Powell, D., Iliadis, C., Champagne, A., et al. 1999, NuPhA, 660, 349
Powers, J. R., Fortune, H. T., Middleton, R., & Hansen, O. 1971, PhRvC, 4, 2030
Psaltis, A., Chen, A. A., Longland, R., et al. 2022a, PhRvL, 129, 162701
Psaltis, A., Chen, A. A., Longland, R., et al. 2022b, PhRvC, 106, 045805
Psaltis, A., José, J., Longland, R., & Iliadis, C. 2025, ApJ, 987, 88
Puentes, D., Meisel, Z., Bollen, G., et al. 2022, PhRvC, 106, L012801
Rapagnani, D., Straniero, O., Imbriani, G., et al. 2025, PhRvC, 111, 025805
Rauscher, T., & Thielemann, F.-K. 2000, ADNDT, 75, 1
Richter, W. A., & Brown, B. A. 2012, PhRvC, 85, 045806
Richter, W. A., Brown, B. A., Signoracci, A., & Wiescher, M. 2011, PhRvC, 83, 065803
Rogers, D. W. O., Aitken, J. H., & Litherland, A. E. 1972a, CaJPh, 50, 268
Rogers, D. W. O., Beukens, R. P., & Diamond, W. T. 1972b, CaJPh, 50, 2428
Rogers, D. W. O., Carter, A. L., Symons, T. J. M., et al. 1976, CaJPh, 54, 938
Rogers, D. W. O., Dixon, W. R., & Storey, R. S. 1973, CaJPh, 51, 1
Rolfs, C. 1973, NuPhA, 217, 29
Rolfs, C., Berka, I., & Azuma, R. 1973a, NuPhA, 199, 306
Rolfs, C., Charlesworth, A., & Azuma, R. 1973b, NuPhA, 199, 257
Rolfs, C., Rodne, W., Shapiro, M., & Winkler, H. 1975, NuPhA, 241, 460
Rolfs, C., Trautvetter, H., Azuma, R., & Litherland, A. 1973c, NuPhA, 199, 289
Ross, J. G., Görres, J., Iliadis, C., et al. 1995, PhRvC, 52, 1681
Rowland, C., Iliadis, C., Champagne, A. E., & Mosher, J. 2002, PhRvC, 65, 064609
Ruiz, C., Parikh, A., José, J., et al. 2006, PhRvL, 96, 252501
Ruziev, E. T., Artemov, S. V., & Tojiboev, O. R. 2024, IJMPE, 33, 2450024
Salisbury, S. R., Hardie, G., Oppliger, L., & Dangle, R. 1962, PhRv, 126, 2143
Salisbury, S. R., & Richards, H. T. 1962, PhRv, 126, 2147
Sallaska, A. L., Iliadis, C., Champange, A. E., et al. 2013, ApJS, 207, 18
Sallaska, A. L., Wrede, C., García, A., et al. 2011, PhRvC, 83, 034611

Sargood, D. 1982, PhR, 93, 61
Schmalbrock, P., Becker, H., Buchmann, L., et al. 1983, NuPhA, 398, 279
Schmid, G. J., Chasteler, R. M., Laymon, C. M., et al. 1995, PhRvC, 52, R1732
Schmidt, S., Rolfs, C., Schulte, W., et al. 1995, NuPhA, 591, 227
Scholz, P., deBoer, R. J., Görres, J., et al. 2023, PhRvC, 107, 065806
Sercely, R., Peterson, R., Smith, P., & Flynn, E. 1979, NuPhA, 324, 53
Sergi, M. L., Spitaleri, C., La Cognata, M., et al. 2015, PhRvC, 91, 065803
Setoodehnia, K., Chen, A. A., Kahl, D., et al. 2013, PhRvC, 87, 065801
Setoodehnia, K., Kelly, J. H., & Sheu, C. G. 2025, arXiv:2511.07635
Setoodehnia, K., Kelley, J. H., Marshall, C., Portillo Chaves, F., & Longland, R. 2019, PhRvC, 99, 055812
Seuthe, S., Rolfs, C., Schröder, U., et al. 1990, NuPhA, 514, 471
Shahina, G. J., Robertson, D., et al. 2022, PhRvC, 106, 025805
Sharma, S. 2017, ARA&A, 55, 213
Smotrich, H., Jones, K. W., McDermott, L. C., & Benenson, R. E. 1961, PhRv, 122, 232
Smulders, P. 1965, Phy, 31, 973
Stegmüller, F., Rolfs, C., Schmidt, S., et al. 1996, NuPhA, 601, 168
Strandberg, E., Beard, M., Couder, M., et al. 2008, PhRvC, 77, 055801
Strieder, F., Limata, B., Formicola, A., et al. 2012, PhLB, 707, 60
Sun, L. J., Xu, X. X., Lin, C. J., et al. 2019, PhRvC, 99, 064312
Surbrook, J., Bollen, G., Brodeur, M., et al. 2021, PhRvC, 103, 014323
Switkowski, Z. E., O'Brien, R., Smith, A. K., & Sargood, D. G. 1975, AuJPh, 28, 141
Symons, T. J. M., Fifield, L. K., Hurst, M. J., et al. 1978, JPhG, 4, 411
Szücs, T., & Mohr, P. 2015, PhRvC, 92, 044328
Talwar, R., Adachi, T., Berg, G. P. A., et al. 2016, PhRvC, 93, 055803
Tan, W. P., Görres, J., Beard, M., et al. 2009, PhRvC, 79, 055805
Tanabe, T., Haga, K., Yasue, M., et al. 1983, NuPhA, 399, 241
Tanabe, T., Yasue, M., Sato, K., et al. 1981, PhRvC, 24, 2556
Temanson, E., Baker, J., Baby, L. T., et al. 2023, PhRvC, 108, 065804
ter Braak, C. J. F., & Vrugt, J. A. 2008, Stat. Comput., 18, 435
Thomas, J.-C., Achouri, L., Äystö, J., et al. 2004, EPJA, 21, 419
Thomas, R. G. 1951, PhRv, 81, 148
Thompson, I. J. 1988, CoPhR, 7, 167
Thompson, W. J., & Iliadis, C. 1999, NuPhA, 647, 259
Tilley, D., Cheves, C., Kelley, J., Raman, S., & Weller, H. 1998, NuPhA, 636, 249
Tilley, D., Weller, H., & Cheves, C. 1993, NuPhA, 564, 1
Tišma, I., Lipoglavšek, M., Mihovilovič, M., et al. 2019, EPJA, 55, 137
Toevs, J. W. 1971, NuPhA, 172, 589
Tomandl, I., Novák, J., Burjan, V., et al. 2004, PhRvC, 69, 014312
Torres-Sánchez, P., Praena, J., Porras, I., et al. 2023, PhRvC, 107, 064617
Trautvetter, H. P. 1975, NuPhA, 243, 37
Trautvetter, H. P., & Rolfs, C. 1975, NuPhA, 242, 519
Trautvetter, H. P., Wiescher, M., Kettner, K. U., Rolfs, C., & Hammer, J. W. 1978, NuPhA, 297, 489
Trinder, W., Angélique, J. C., Anne, R., et al. 1999, PhLB, 459, 67
Turkat, S., Hammer, S., Masha, E., et al. 2021, PhRvC, 103, 045805
Ugalde, C., Champagne, A. E., Daigle, S., et al. 2007, PhRvC, 76, 025802
Underwood, B., Wormald, M., Anyas-Weiss, N., Jelley, N., & Allen, K. 1974, NuPhA, 225, 253
Vanhoy, J. R., Bilpuch, E. G., Westerfeldt, C. R., & Mitchell, G. E. 1987, PhRvC, 36, 920
Vermeer, W., Pringle, D., & Wright, I. 1988, NuPhA, 485, 380
Vincent, C. M., & Fortune, H. T. 1970, PhRvC, 2, 782
Visser, D. W., Caggiano, J. A., Lewis, R., et al. 2004, PhRvC, 69, 048801
Visser, D. W., Wrede, C., Caggiano, J. A., et al. 2007, PhRvC, 76, 065803
Visser, D. W., Wrede, C., Caggiano, J. A., et al. 2008, PhRvC, 78, 028802
Vogelaar, R. B. 1989, PhD thesis, California Institute of Technology
Vogelaar, R. B., Mitchell, L. W., Kavanagh, R. W., et al. 1996, PhRvC, 53, 1945
Vogelaar, R. B., Wang, T. R., Kellogg, S. E., & Kavanagh, R. W. 1990, PhRvC, 42, 753
Volya, A., Goldberg, V. Z., Nurmukhanbetova, A. K., Nauruzbayev, D. K., & Rogachev, G. V. 2022, PhRvC, 105, 014614
Walkiewicz, T. A., Raman, S., Jurney, E. T., Starner, J. W., & Lynn, J. E. 1992, PhRvC, 45, 1597
Wallace, E., Iliadis, C., & Starrfield, S. 2025, ApJ, 991, 200
Wang, L., Su, J., Shen, Y., et al. 2023, PhRvL, 130, 092701
Wang, M., Huang, W., Kondev, F., Audi, G., & Naimi, S. 2021, ChPhC, 45, 030003
Wapstra, A., Audi, G., & Thibault, C. 2003, NuPhA, 729, 129
Ward, L., Iliadis, C., Bose, M., et al. 2025, ApJ, 986, 109
Warren, J. B., Erdman, K. L., Robertson, L. P., Axen, D. A., & MacDonald, J. R. 1963, PhRv, 132, 1691
Weidenmüller, H. A., & Mitchell, G. E. 2009, RvMP, 81, 539
Weigmann, H., Macklin, R. L., & Harvey, J. A. 1976, PhRvC, 14, 1328
Wiescher, M., Becker, H., Görres, J., et al. 1980, NuPhA, 349, 165
Wiescher, M., Boyd, R. N., Blatt, S. L., et al. 1983, PhRvC, 28, 1431
Wiescher, M., deBoer, R. J., & Görres, J. 2023, EPJA, 59, 11
Wilkinson, R., Lotay, G., Lennarz, A., et al. 2017, PhRvL, 119, 242701
Williams, M., Lennarz, A., Laird, A. M., et al. 2020, PhRvC, 102, 035801
Wilmes, S., Wilmes, V., Staudt, G., Mohr, P., & Hammer, J. W. 2002, PhRvC, 66, 065802
Wolf, C., Langer, C., Montes, F., et al. 2019, PhRvL, 122, 232701
Wolke, K., Becker, H. W., Rolfs, C., et al. 1989, ZPhyA, 334, 491
Wrede, C. 2009, PhRvC, 79, 035803
Wrede, C., Clark, J. A., Deibel, C. M., et al. 2010, PhRvC, 82, 035805
Xu, Y., Takahashi, K., Goriely, S., et al. 2013, NuPhA, 918, 61
Yasue, M., Ogawa, K., Niizeki, T., et al. 1990, PhRvC, 42, 1279
Yeh, T.-H., Olive, K. A., & Fields, B. D. 2021, JCAP, 2021, 046
Zerkin, V., & Pritychenko, B. 2018, NIMPA, 888, 31
Zhang, H., Li, Z.-H., Su, J., et al. 2021, ChPhC, 45, 084108
Zhang, H., Su, J., Li, Z. H., et al. 2023, PhRvC, 107, 065801
Zhang, L. Y., He, J. J., Parikh, A., et al. 2014, PhRvC, 89, 015804
Zhang, L. Y., Su, J., He, J. J., et al. 2022, PhRvC, 106, 055803
Zhang, X., Nollett, K. M., Phillips, D. R., et al. 2020, JPhG, 47, 054002
Ziegler, J. F., Ziegler, M., & Biersack, J. 2010, NIMPB, 268, 1818
Zijderhand, F., Makkus, R., & Van Der Leun, C. 1987, NuPhA, 466, 280
Zyskind, J., Rios, M., & Rolfs, C. 1981, ApJL, 243, L53